CORA Cork Open Research Archive
Cartlann Taighde Oscailte Chorcaí

Title	Photosynthetic biogas upgrading: technological advancements and integration into a circular economy
Authors	Bose, Archishman
Publication date	2021-12-15
Original Citation	Bose, A. 2021. Photosynthetic biogas upgrading: technological advancements and integration into a circular economy. PhD Thesis, University College Cork.
Type of publication	Doctoral thesis
Rights	© 2021, Archishman Bose. - https://creativecommons.org/licenses/by-nc-nd/4.0/
Download date	2026-10-31 03:13:01
Item downloaded from	https://hdl.handle.net/10468/12477



UCC
University College Cork, Ireland
Coláiste na hOllscoile Corcaigh

Ollscoil na hÉireann, Corcaigh

National University of Ireland, Cork



Photosynthetic Biogas Upgrading: Technological Advancements and Integration into a Circular Economy

Thesis submitted by

Archishman Bose, BE, MSc

[ORCID ID: 56234727200]

for the degree of

Doctor of Philosophy in Energy Engineering

School of Engineering and Architecture

University College Cork

Head of School: Prof. Jorge Oliveira

Academic Supervisors: Prof. Jerry D. Murphy & Dr. Richard O'Shea

Academic Advisor: Dr. Richen Lin

December 2021

For actions urgent and immediate,

To tackle our rapidly changing climate,

Is presented in this thesis,

A technology that can tackle this crisis.

By exploring in detail, both wider and deeper,

Bioproducts made both greener and cheaper,

Assisting transition to an economy circular,

Enabling thus a future, better.

A Thesis in Sum

Archihsman Bose,

10.09.2021

Cork, Ireland

Table of contents

Table of contents i

List of figures x

List of tables xxi

Declaration xxvii

Acknowledgement xxviii

Abstract xxx

Thesis output xxxii

General nomenclature xxxiv

1 Introduction 1

1.1 Background to the thesis 2

1.1.1 Climate targets, climate action plans and sustainable development goals (SDGs) 2

1.1.2 Circular bioeconomy for sustainable development and climate action plans 3

1.1.3 Biofuels in the future circular bioeconomy 3

1.1.4 Biomethane: A renewable biofuel 4

1.1.5 Novel biogas upgrading technologies to reduce GHG emissions in biomethane production 5

1.1.6 Photosynthetic biogas upgrading 5

1.1.7 Biorefinery for a sustainable and circular bioeconomy 6

1.2 Rationale behind the thesis 6

1.3 Thesis objectives and scope 7

1.4 Thesis outline and the link between chapters 9

1.4.1 Chapter 2: How to optimise photosynthetic biogas upgrading: a perspective on system design and microalgae selection (*Review*) 9

1.4.2 Chapter 3: Design, commissioning and performance assessment of a lab-scale bubble column reactor for photosynthetic biogas upgrading with Spirulina platensis (*Original Research*) 10

1.4.3 Chapter 4: A comparative evaluation of design factors on bubble column operation in photosynthetic biogas upgrading (*Original Research*) 10

1.4.4 Chapter 5: Optimisation and performance prediction of photosynthetic biogas upgrading using a bubble column (*Original Research*) 10

1.4.5 Chapter 6: A perspective on novel cascading algal biomethane biorefinery systems (*Review*) 11

1.4.6 Chapter 7: Producing biofuel with food and biofertiliser in a circular economy system (*Original Research*) 11

1.4.7 Chapter 8: A profitable low carbon process to co-produce biomethane, food and biofertiliser (*Original Research*) 12

1.5 References 13

2 How to optimise photosynthetic biogas upgrading: a perspective on system design and microalgae selection 18

2.1 Introduction 20

2.1.1 Biogas and biomethane 20

2.1.2 Innovative biogas upgrading technologies including carbon capture and reuse 20

2.1.3 Photosynthetic biogas upgrading 23

2.1.4 Novelty and objectives 23

2.2 Biological carbon uptake and influence of microalgae choice 24

2.2.1 Carbon assimilation pathways in microalgae 24

2.2.2 Carbon partitioning 27

2.3 Biogas upgrading and influence on microalgae choice 28

2.3.1 Carbonic Anhydrase (CA) promoted CO_2 removal in an alkaline environment 28

2.3.2 Carbonate/bicarbonate cycle for CO_2 capture 29

2.3.3 H_2S removal and impact on Oxygen in biomethane 30

2.3.4 Impacts of other trace gases on microalgae growth.....31

2.3.5 Microalgae selection to enhance biogas upgrading.....32

2.4 Bio-fixation of absorbed CO_2 by microalgae cultivation.....33

2.4.1 Impact of CO_2 concentration in biogas on microalgae growth.....33

2.4.2 Impact of bicarbonate concentration on microalgae growth.....33

2.4.3 Carbon balance during bio-fixation of CO_2.....34

2.5 System design for biogas upgrading by microalgae.....41

2.5.1 Absorption column.....41

2.5.2 Photobioreactor design.....46

2.5.3 Microalgae harvesting.....58

2.6 Discussion and perspectives.....59

2.6.1 Selection of microalgae species.....59

2.6.2 Industrial scale application.....61

2.7 Conclusions.....64

2.8 Acknowledgement.....64

2.9 References.....66

3 Design, commissioning and performance assessment of a lab-scale bubble column reactor for photosynthetic biogas upgrading with *Spirulina platensis*.....88

Nomenclature.....90

3.1 Introduction.....91

3.1.1 Photosynthetic biogas upgrading.....91

3.1.2 Significance of operation and design of the bubble column.....91

3.1.3 Current trends in bubble column design for photosynthetic biogas upgrading 93

3.1.4 Objective.....97

3.2 Design and evaluation of bubble column for photosynthetic biogas upgrading 98

3.2.1 Working range and operating medium.....98

3.2.2 Working principle for CO_2 absorption.....98

3.2.3 Design and configuration of the lab-scale bubble column 99
3.2.4 Performance evaluation 102
3.3 Experiments and methods 107
3.3.1 Microorganisms and culture conditions 107
3.3.2 Commissioning and performance evaluation of the bubble column operations... 108
3.3.3 Analytical procedures 109
3.3.4 Statistical analysis 110
3.4 Start-up and design modifications 111
3.4.1 External oxygen ingression into upgraded biomethane 111
3.4.2 Condensation 112
3.4.3 Foaming 112
3.4.4 Clogging 113
3.4.5 Stability of bubble column operation 113
3.5 Results 116
3.5.1 Impact of design changes on system performance 116
3.5.2 CO_2 removal efficiency 118
3.5.3 Rate of CO_2 absorption 119
3.5.4 O_2 stripping 121
3.5.5 Carbon balance 124
3.6 Discussion 125
3.6.1 Validation and scale-up perspective of the bubble column set-up 125
3.6.2 Impact of algal concentration and photosynthetic activity 127
3.6.3 Integration with microalgae cultivation 128
3.6.4 Oxygen stripping and H_2S 128
3.7 Conclusions 129
3.8 Acknowledgement 130

3.9 References....131

4 A comparative evaluation of design factors on bubble column operation in photosynthetic biogas upgrading....139

Nomenclature....141

4.1 Introduction....142

4.1.1 Microalgal (photosynthetic) biogas upgrading....142

4.1.2 Need for a focussed approach to photosynthetic biogas upgrading....142

4.1.3 Objective and novelty....146

4.2 Materials and methods....147

4.2.1 Microorganisms and culture conditions....147

4.2.2 Experimental setup....147

4.2.3 Experimental design....149

4.2.4 Analytical procedures....159

4.3 Results and discussions....161

4.3.1 Validation of the bubble column operation....161

4.3.2 Adequacy of the experimental design....165

4.3.3 Results of the screening design of experiments....166

4.3.4 Comparison between design factors and significant interactions....178

4.3.5 Significance of results....184

4.4 Conclusions and future directions....186

4.5 Acknowledgement....188

4.6 References....189

5 Optimisation and performance prediction of photosynthetic biogas upgrading using a bubble column....198

Nomenclature....200

5.1 Introduction....201

5.1.1 Photosynthetic (microalgal) biogas upgrading....201

5.1.2 Need for optimisation of biogas upgrading in the bubble column....202

5.1.3 Objective and novelty 203
5.2 Materials and methods 205
5.2.1 Microorganisms and culture conditions 205
5.2.2 Experimental setup 205
5.2.3 Process responses for optimisation of bubble column 207
5.2.4 Experimental design and assessment 207
5.2.5 Analytical procedures 212
5.2.6 Statistical analysis 213
5.3 Results and discussions 213
5.3.1 Validation of the bubble column operations 213
5.3.2 Model fitting and statistical assessments 214
5.3.3 Verification of response surface models 220
5.3.4 Analysis of design factors 221
5.3.5 Optimisation of bubble column operations 225
5.3.6 Significance of results 231
5.4 Conclusions 237
5.5 Acknowledgement 238
5.6 Supplementary to Chapter 5 239
5.7 References 244
6 A perspective on novel cascading algal biomethane biorefinery systems 252
6.1 Introduction 254
6.1.1 Biofuels in the future bioeconomy 254
6.1.2 Biomethane: a renewable biofuel 254
6.1.3 Advances in biogas upgrading to biomethane using microalgae 254
6.1.4 Cascading algal biomethane biorefinery system (CABBS) in a circular bioeconomy 255
6.2 Microalgae in biogas and biomethane systems 256

6.2.1 Biogas generation from microalgae 256
6.2.2 Biogas upgrading by microalgae 261
6.2.3 Digestate treatment by microalgae 263
6.2.4 Combined biogas upgrading and digestate treatment by microalgae 263
6.3 Further opportunities from microalgae bioresource 264
6.3.1 Bioproducts from microalgae 264
6.3.2 Economic considerations of microalgae bio-products 265
6.3.3 The dilemma of microalgal use 266
6.3.4 Decision tree for selecting microalgae biorefinery pathway 270
6.4 Cascading Algal Biomethane Biorefinery System (CABBS) 273
6.4.1 Composition-based biorefinery 273
6.5 Environmental, economic and practical challenges and prospects 276
6.5.1 Environmental perspectives 276
6.5.2 Techno-economic perspectives 279
6.5.3 Practical challenges and perspectives 279
6.6 Conclusions 280
6.7 Acknowledgement 281
6.8 Appendix for Chapter 6 284
6.9 References 287
7 Producing biofuel with food and biofertiliser in a circular economy system . 302
7.1 Introduction 305
7.2 Methods 310
7.2.1 Feedstock, resources and process outputs 310
7.2.2 Process description and scenarios for performance assessment 311
7.2.3 Process modelling 314
7.2.4 Process performance assessment 324
7.2.5 Estimation of energy, land and water footprints 326

7.2.6 Allocation principles....328
7.2.7 Product performance assessment and functional units....328
7.2.8 Estimation of GHG emissions....330
7.2.9 Sensitivity analysis....335
7.3 Results....336
7.3.1 Mass balance and model validation....336
7.3.2 Energy balance and GHG emissions....341
7.3.3 Process performance....347
7.3.4 Product performance....349
7.3.5 Sensitivity analysis of process parameters of photosynthetic biogas upgrading....356
7.4 Legislative challenges and implications of economic allocation....357
7.5 Conclusions and strategies to improve process performance....361
7.6 Acknowledgement....362
7.7 Supplementary to Chapter 7....364
7.8 References....368
8 A profitable low carbon process to co-produce biomethane, food and biofertiliser....385
8.1 Introduction....388
8.2 Methods....391
8.2.1 Feedstock, resources and process outputs....391
8.2.2 Process description....393
8.2.3 Scenarios for process assessment....395
8.2.4 Economic analysis....400
8.2.5 LCOA or MAC....408
8.2.6 Sensitivity Assessment....411
8.3 Results....412
8.3.1 Technical analyses....412

8.3.2 Economic assessments....416
8.3.3 LCOA (Marginal abatement cost)....424
8.3.4 Sensitivity assessment....430
8.3.5 Operations with financial benefits to biomethane....433
8.4 Discussion....435
8.5 Conclusions....437
8.6 Acknowledgement....439
8.7 Supplementary to Chapter 8....440
8.8 References....448
9 Conclusions and Recommendations....466
9.1 Chapter overview....467
9.2 Conclusions to the thesis objectives....467
9.2.1 Objective 1: Identify the areas where photosynthetic biogas requires the most improvement and establish a framework for selecting suitable microalgae species. 468
9.2.2 Objective 2: Perform robust optimisation using a systems approach to advance the overall photosynthetic biogas upgrading technology.....469
9.2.3 Objective 3: Identify strategies to integrate photosynthetic biogas upgrading based biomethane systems in a circular bioeconomy system. 472
9.2.4 Objective 4: Propose and apply methods to assess the energetic, environmental and economic performances of a polygeneration system using photosynthetic biogas upgrading and compare it with state-of-the-art biogas upgrading technologies. 474
9.3 Impact on policy, industry and society....477
9.3.1 Policy implications....477
9.3.2 Industry implications....479
9.3.3 Social implications....480
9.4 Recommendations and future research....481
9.5 Final Remarks....483
9.6 References....484

List of figures

Figure 1-1 Schematic representation of a possible integrated Anaerobic Digestion (AD)-biorefinery system utilising microalgae in a future circular bio-economy system [44] 7

Figure 2-1 Process flow diagram and system configuration for biogas upgrading with microalgae where DIC: dissolved inorganic content; CA: Carbonic anhydrase..... 22

Figure 2-2 Simplistic schematic representation for inorganic and organic carbon transport for CO_2 accumulation and partitioning pathways in a microalgal cell along with nitrogen fixation pathways [7,24] 25

Figure 2-3 Biogas upgrading by microalgae in an alkaline (carbonate) algal solution via carbonate/bicarbonate cycle (The number of markings of each chemical species are indicative only to their relative quantity and not in absolute terms. 31

Figure 2-4 Schematic representation of overall biogas upgrading process with microalgae Indicating flow of inorganic carbon for mass balance within the system. 35

Figure 2-5 Influence of pH and L/G ratio on the mass transfer performance of the absorber column. 43

Figure 2-6 Simplistic schematic representation of closed photobioreactors, (a) Horizontal Tubular photobioreactor; (b) Plastic Bag photobioreactor; (c) Air-lift Bubble Column photobioreactor; (d) Flat Plate photobioreactor. 49

Figure 3-1 Process flow diagram and design details of the lab-scale bubble column for photosynthetic biogas upgrading (Not to scale) 100

Figure 3-2 Pictorial representation of the experimental setup for photosynthetic biogas upgrading with (a) the overall bubble column reactor setup within a temperature and light controlled housing; (b) detail of the gas-liquid separator with a U-loop to prevent emptying by syphoning and also adjust the outlet liquid flow rate as per the inlet flow rate; (c) example of foaming observed during operation with high algae concentration; (d) representation of homogeneous flow regime characterised by uniform bubble size under low algal concentration; and (e) detail of the control panel with the condensate trap placed within an ice bath (bottom of the figure). Additional details marked in

figure (a) represent (i) the bubble column (additional tapping points for future experiments); (ii) the gas-liquid separator; (iii) control panel with gas flow controllers, mass flow meter, manometer gauge, and the switches for temperature control; (iv) the heater; and (v) the peristaltic pump.....101

Figure 3-3 Recorded biomethane mass flow profiles at similar L/G ratio (0.3) (a) without (low algal concentrations) and (b) with foaming (high algal concentrations). 114

Figure 3-4 Variation in outlet biomethane flow and liquid pH before reaching steady-state. The examples chosen are (a) L/G 0.1 and (b) L/G 0.3 for experiment LON. It is to be noted that, the initial pH for (a) was 8.113, while for (b) it was 8.16 from respective preceding experiments. The data are from the pre-modified setup, chosen for better representation. 115

Figure 3-5 CO_2 content (a) and removal efficiency (b) of the bubble column operated under different L/G ratios at higher and lower algal concentrations; where LON: Low concentration with lights on; HON: High concentration with lights on. 119

Figure 3-6 Effect of L/G ratio and algal concentration on the (a) absorption rate of CO_2 alongside mean carbonate concentration in solution and (b) overall mass transfer coefficient ($k_{G_{CO_2}}a$). 121

Figure 3-7 Effect of the L/G ratio and the algal concentration on (a) the theoretical and measured oxygen outflow rates (mL_n/min) and (b) the overall mass transfer coefficient for oxygen ($k_{l_{O_2}}a$) [s^{-1}]. It is to be noted that $k_{l_{O_2}}a$ for HON has not been evaluated as the results are confounded with the photosynthetic activity of the algae and would not depict the actual hydrodynamic performance of the bubble column. 122

Figure 3-8 Oxygen concentration in the upgraded biomethane under different operating conditions in the lab-scale bubble column.....124

Figure 3-9 Variation in the rate of carbon addition with respect to the L/G ratio ...125

Figure 4-1 Diagrammatic representation of the two-step bubble column-photobioreactor photosynthetic biogas upgrading system using the carbonate bicarbonate cycle for the production of biomethane and microalgae for high-value products and/or biofuels. 143

Figure 4-2 Diagrammatic representation (not to scale) of the experimental setup for the screening design of experiments where (a) is the primary bubble column, (b) is the gas-liquid separator and (c) is the gas diffuser.....148

Figure 4-3 Outline of the Taguchi Screening design of experiments using orthogonal arrays.....150

Figure 4-4 Comparison between expected and measured values of (a) O_2 and (b) N_2 to validate the bubble column operations and measurement techniques utilised.....162

Figure 4-5 Analysis plots for the relative influence of design factors on CO_2 removal efficiency: (a) Main effects plot with mean; (b) Main effects plots with S/N ratio. The rank of each design factor is included in parenthesis; (c) Contribution of each design factor and interactions on the overall system outcome; and (d) Half normal probability plot with the relative contribution of major effects highlighted in brackets. 167

Figure 4-6 Interactive effects between (a) pH and L/G ratio; (b) superficial gas velocity (u_G) and pH; and (c) superficial gas velocity (u_G) and L/G ratio on CO_2 removal efficiency.....169

Figure 4-7 Analysis plots for the relative influence of design factors on mean steady state rate of CO_2 absorption: (a) Main effects plot with means; (b) Main effects plots with S/N ratio. The rank of each design factor is included in parenthesis; (c) Contribution of each design factor and interactions on the overall system outcome; and (d) Half normal probability plot with the relative contribution of major effects highlighted in brackets. 171

Figure 4-8 Analysis plots for the relative influence of design factors on the gas side volumetric mass transfer coefficient for CO_2: (a) Main effects plot with means; (b) Main effects plots with S/N ratio. The rank of each design factor is included in parenthesis; (c) Contribution of each design factor and interactions on the overall system outcome; and (d) Half normal probability plot with the relative contribution of major effects highlighted in brackets. 173

Figure 4-9 Analysis plots for relative influence of design factors on O_2 concentration in biomethane: (a) Main effects plot with mean; (b) Main effects plots with S/N ratio. The rank of each design factor is included in parenthesis; (c) Contribution of each design factor and interactions on the overall system outcome; and (d) Half normal

probability plot with the relative contribution of major effects highlighted in brackets. 175

Figure 4-10 Interaction between L/G ratio and algal concentration (C_{alg}) for (a) O_2 concentration in outlet biomethane and (b) O_2 outflow rate within upgraded biomethane. 176

Figure 4-11 Analysis plots for the relative influence of design factors on O_2 flow rate in biomethane: (a) Main effects plot with mean; (b) Main effects plots with S/N ratio. The rank of each design factor is included in parenthesis; (c) Contribution of each design factor and interactions on the overall system outcome; and (d) Half normal probability plot with the relative contribution of major effects highlighted in brackets. 178

Figure 4-12 Comparison of regression model and experimental data along with 95% Confidence Interval and 95% Prediction Interval for the S/N ratios of (a) $R_{eff,\ CO_2}$ and (b) $O_{2,BM}$ 183

Figure 4-13 Prediction of biomethane composition at (a) u_G 0.06 cm/s (c. 0.98 L/hr) and (b) u_G 0.2 cm/s (c. 3.29 L/hr). The constant setting of other design factors are as follows: Alk 2.5gIC/L; T_{col} 20°C; C_{alg} 0.05gDW/L; and EBRT 6 mins. The acceptable region of operation is indicated in white 184

Figure 5-1 Concept diagram of the two-step bubble column-photobioreactor photosynthetic biogas upgrading system using the carbonate bicarbonate cycle for the production of biomethane and microalgae. 202

Figure 5-2 Schematic representation of the experimental setup for the optimisation of the bubble column performance (not to scale) in which (a) represents the bubble column, (b) represents the gas-liquid separator and (c) represents the gas diffuser. Adapted from Bose et al. (2021) [8] 206

Figure 5-3 Predicted vs actual plot of the regression models for (a) $Eff_{RE_CO_2}$; (b) $K_{CO_2}a$; (c) $C_{O_2,BM}$; and (d) pH_{out}. The circular dots indicate the experimental data while the lines indicate the trend for ideally fit data. 219

Figure 5-4 Main effects plot of the mean responses of $Eff_{RE_CO_2}$, $K_{CO_2}a$, $C_{O_2,BM}$ and pH_{out} against the four independent design factors, namely, liquid inlet pH, superficial gas velocity, L/G ratio and liquid inlet alkalinity. Except for the factor that is being

varied, all the other factors are placed at their centre points, namely, pH at 9.8; u_G at 0.45 cm/s, L/G at 0.55 and Alk at 1.7 gIC/L.....223

Figure 5-5 Interactive effects between (a) pH and L/G ratio on $Eff_{RE_CO_2}$; (b) pH and alkalinity on $Eff_{RE_CO_2}$; (c) pH and L/G ratio on $K_{CO_2}a$; and (d) pH and alkalinity on $C_{O_2,BM}$. Except for the factors that are being varied, all the other factors are placed at their centre points, namely, pH at 9.8; u_G at 0.45 cm/s, L/G at 0.55 and Alk at 1.7 gIC/L 225

Figure 5-6 Two dimensional contour plots of CO_2 removal efficiency ($Eff_{RE_CO_2}$) versus pH and L/G ratio at different superficial gas velocities and alkalinity. The contour lines correspond to the values indicated in the legend.....227

Figure 5-7 Two dimensional contour plots of mass transfer coefficient of CO_2 ($K_{CO_2}a$) a) versus pH and L/G ratio for at different superficial gas velocities and alkalinity. The contour lines correspond to the values indicated in the legend.....227

Figure 5-8 Two dimensional contour plots of the impact of inlet pH and L/G ratio on liquid outlet pH from the bubble column (pH_{out}) at different alkalinity. The effect of superficial gas velocity has been omitted due to its low statistical significance on pH_{out} ($P > 0.05$). The contour lines correspond to the values indicated in the legend. 228

Figure 5-9 Two dimensional contour plot of superficial gas velocity (u_G) versus L/G ratio on O_2 concentration in the bubble column ($C_{O_2,BM}$). The effects of pH and alkalinity have not been depicted due to their low statistical significance on $C_{O_2,BM}$ ($P > 0.05$). The contour lines correspond to the values indicated in the legend.....229

Figure 5-10 Overlaid contour plots to identify the optimal operating region of the bubble column for photosynthetic biogas upgrading for liquid inlet pH and alkalinity (Alk) ranging between 10 and 10.2 and 1.7 gIC/L and 2.1 gIC/L respectively. The un-shaded area indicates the optimal operating regions to achieve a CO_2 removal efficiency above 97% and oxygen concentration in biomethane less than 0.8%.....230

Figure S5-1 Box Cox Power Transformation plot for (a) $Eff_{RE_CO_2}$; (b) $K_{CO_2}a$; (c) $C_{O_2,BM}$; and (d) pH_{out}.....240

Figure S5-2 Normal probability plot of residuals for the selected regression models developed for (a) $Eff_{RE_CO_2}$; (b) $K_{CO_2}a$; (c) $C_{O_2,BM}$; and (d) pH_{out}. The colour code indicates the maximum and minimum value of the respective process response…..242

Figure S5-3 Half-Normal probability plot of the terms included in the selected regression models developed for (a) $Eff_{RE_CO_2}$; (b) $K_{CO_2}a$; (c) $C_{O_2,BM}$; and (d) pH_{out}. The points farthest away from the straight (45°) line has the highest influence on the process response. 243

Figure 6-1 Schematic representation of a cascading algae biomethane biorefinery system with a summary of different microalgae bio-products and possible applications in food, feed and energy; F&F: Food and Feed; FF: Functional Food 257

Figure 6-2 Schematic of photosynthetic biogas upgrading in an alkaline (carbonate) algal solution via carbonate/bicarbonate cycle followed by microalgae harvesting (The number of markings of each chemical species are indicative only to their relative quantity and not in absolute terms [8].....262

Figure 6-3 Evaluation of market opportunity and economic possibilities with respect to the current market sale price of some common bio-products from microalgae, considering (a) the speculated global market value and market growth up to 2024-26, in which, the bubble size and hatching style represents the compound annual growth rate (CAGR) of each product and (b) the equivalent selling price of corresponding bio-products respectively. The bubble sizes in (b) indicate the maximum fraction of microalgae utilisable for the corresponding bio-product considering maximum conversion. All references are explained and included in detail in Table A6.1 in the appendix. 267

Figure 6-4 Decision-making algorithm for microalgae application in a biorefinery approach from the perspective of microalgae composition. 272

Figure 6-5 Cascading Algal Biomethane Biorefinery System (CABBS) (a) with protein-rich microalgae for photosynthetic biogas upgrading; (b) with lipid-rich microalgae for photosynthetic biogas upgrading; (c) integrating pyrolysis with AD systems and photosynthetic biogas upgrading 274

Figure 6-6 Comparison of net CO_2 flow in (a) state-of-the-art grass/energy crop based AD plant with physicochemical biogas upgrading and (b) proposed CABBS layout

with the production of selected chemicals from microalgae to be regarded as a potential Bioenergy with Carbon Capture and storage (BECCS) system. 278

Figure 7-1 Concept layout of cascading algal biomethane-biorefinery systems (CABBS) with agricultural wastes using anaerobic digestion and photosynthetic biogas upgrading 308

Figure 7-2 General process flow diagram of biomethane and dietary protein production as food-grade Spirulina platensis alongside biofertiliser as digestate using agricultural feedstock and photosynthetic biogas upgrading 309

Figure 7-3 Graphical representation of the scenarios assessed to study its performance. The acronyms EC and EN refer to economic and energy allocation respectively. BASE represents the Base case scenario, RED refers to the scenario replicating the recommendations of the EU Renewable Energy Directive (Recast) (RED-II), i.e., excluding digestate as a valuable product, ALLOC-EN allows for an energy allocation method whilst considering digestate as a valuable product and FPCULT refers to the scenario where flat plate photobioreactors were used to cultivate the microalgae. .313

Figure 7-4 Simulated model details of the anaerobic digestion section.....318

Figure 7-5 Simulated model details of the photosynthetic biogas upgrading section including biomethane injection into the gas grid 318

Figure 7-6 Simulated model of the microalgae cultivation section including the inoculum reactor and accessories. The air compressor for circulating air would be necessary only when closed photobioreactors are concerned. However, it has been included in the general model to maintain generality. 322

Figure 7-7 Simulated model of the microalgae harvesting and processing section towards obtaining dry *Spirulina*.....322

Figure 7-8 Simulated model of the recirculation adjustment section 323

Figure 7-9 Mass flow diagram for co-generation of biomethane and *Spirulina* powder in a cascading polygeneration system utilising photosynthetic biogas upgrading for the base case scenario (BASE-EC) 337

Figure 7-10 Hourly mass balance of the proposed polygeneration plant producing biomethane, Spirulina powder and digestate for (a) scenarios BASE-EC, RED-EN, RED-EC and ALLOC-EN, (b) scenario FPCULT-EC 342

Figure 7-11 Energy balance of the proposed polygeneration plant producing biomethane, *Spirulina* powder and digestate for each scenario where (a) represents the overall direct energy consumption of the plant (final energy basis), (b) represents the contribution of the different plant components towards the overall energy consumption of the plant when either an open pond or a flat plate photobioreactor (PBR) is used. 343

Figure 7-12 (a) GHG emissions and emission savings per Nm^3 biogas produced from the proposed polygeneration process under each scenario assessed; (b) the contribution to emissions when either an open pond or a flat plate photobioreactor (PBR) is used. 344

Figure 7-13 Results and sensitivities of (a & b) standard energy return on investment (S-EROI); (c & d) cost utilization factor (CUF); (e & f) carbon emission factor (CEF) of the proposed polygeneration process. The "curve" lines in figures (a), (c) and (e) signify the uncertainty distribution of S-EROI, CUF and CEF respectively. For details of the uncertainty assessment, refer to section 7.2.9. 348

Figure 7-14 (a) Allocation and performance of biomethane based on (b) Specific energy consumed [kWh/Nm^3-biomethane]; (c) Specific GHG emissions [$gCO_{2\text{-}eq}$/MJ]; (d) Specific land footprint [m^2/Nm^3-biomethane]; and (e) Specific water footprint [L/MJ]. The values of specific water footprint for the production of conventional and renewable energies shown in (e) were compiled from Mekonnen et al. (2015) [135]. 350

Figure 7-15 (a) Allocation and performance of dietary protein (*Spirulina* powder) based on (b) Specific energy consumed [kWh/100 grams protein]; (c) Specific GHG emissions [$kgCO_{2\text{-}eq}$/100 grams protein and $kgCO_{2\text{-}eq}$/100 $NDS_{NRF9.3}$ score]; (d) Specific land footprint [m^2/100 grams protein and m^2/100 $NDS_{NRF9.3}$ score]; and (e) Specific water footprint [L/100 grams protein and L/100 $NDS_{NRF9.3}$ score]. The specific energy consumption of protein from conventional sources has been compiled from Pimentel et al. (2003) [137]. The $NDS_{NRF9.3}$ values, together with the GHG Emissions, land and water footprints of the conventional protein sources are compiled in Table S7-2. 352

Figure 7-16 Performance of biofertiliser or digestate production (equivalent N) based on (a) Specific GHG emissions; (b) Specific energy consumption, land and water

footprints. The GHG emissions in the production of conventional fertilisers have been compiled from Hoxha and Christensen (2018) for the EU average scenario [93]...353

Figure 7-17 Sensitivity Analysis of process variables and product selling prices on the specific GHG emissions of (a) Biomethane, (b) *Spirulina* powder, (c) *Spirulina* powder as a protein supplement, (d) *Spirulina* powder as a complete food using the $NRF_{9.3}$ nutrient profile and (e) digestate (equivalent N) as a substitute of inorganic nitrogenous fertilisers.....354

Figure 7-18 Results of the Monte Carlo uncertainty assessment on the specific GHG emissions of each co-product from the proposed integrated polygeneration process. IQR signifies the interquartile range.....355

Figure 7-19 Sensitivity of the process and product performance from the variations of (a) Makeup water pH; (b) L/G ratio; (c) Microalgae productivity; and (d) Makeup water alkalinity.....356

Figure 7-20 Specific emissions of biomethane from the proposed process with the annual energy demand for heating the greenhouse (climatic conditions) and the electricity emission factors (grid electricity) for the following scenarios (a) RED-EN, (b) BASE-EC with the biomethane selling price of 7 c€/kWh and (c) BASE-EC with the biomethane selling price of 15 c€/kWh. The country-specific electricity grid emission factors were obtained from multiple pieces of literature [114,136] while the annual energy demands were estimated from the results of Mariani et al. (2016) [46]. It is to be noted that the country-specific energy requirements have been based on the average climatic conditions of a country. The results might vary based on location-specific climatic fluctuations.....359

Figure 7-21 Variation of the selling prices of *Spirulina* powder required to produce biomethane which satisfies the sustainable criteria for (a) transport and (b) heat according to RED-II from the proposed polygeneration system with variation in the heat demand of the greenhouse, electricity grid emission factor and the biomethane selling price while (c) shows the minimum selling price of *Spirulina* powder against the biomethane selling price and the heat required in the greenhouse to ensure a Cost Utilisation Factor (CUF) greater than 1. 360

Figure 8-1 Concept layout of cascading biomethane-biorefinery with agricultural feedstock using anaerobic digestion and photosynthetic biogas upgrading.....389

Figure 8-2 General process flow diagram of biomethane and dietary protein production as food-grade *Spirulina* platensis using agricultural feedstock and photosynthetic biogas upgrading.....394

Figure 8-3 Annual mass balances of the polygeneration process under each of the scenarios assessed. Scenario 64IBP-R was not shown, as it is similar to 64IBP without the digestate as per RED-II guidelines.....413

Figure 8-4 Overall and specific energy demand of the proposed polygeneration process under the fifteen scenarios. 415

Figure 8-5 Annualised discounted costs, revenues, and net profit from the proposed polygeneration system without any incentives or subsidies towards the process or the products specific to 1 Nm^3/hr of biogas flow.....417

Figure 8-6 Breakdown of (a) CAPEX and (b) OPEX of the proposed polygeneration process for each scenario assessed.....418

Figure 8-7 Discounted cash flow of each of the fifteen scenarios of the proposed polygeneration plant studied in this work. 420

Figure 8-8 Net present value (NPV), internal rate of return (IRR) and discounted payback (DPBP) of the proposed polygeneration plant under each scenario assessed. 421

Figure 8-9 Levelised cost of (a) biomethane; (b) *Spirulina* powder and *Spirulina* protein; (c) digestate from the proposed polygeneration plant under each scenario. The levelised cost of biomethane from other technologies was obtained from Vo et al. (2018) [28]. The feed-in tariffs were compiled from various literature [14,129,130]. The *Spirulina* price at the plant gate was obtained from Benemann et al. (2019) [54], while the wholesale price of *Spirulina* was sourced from Araujo et al. (2021) [131]. Wholesale prices of other protein sources are compiled in Table S8-3 in the supplementary. The price of solid manure was sourced from Teagasc (2021) [128] while the prices of inorganic fertilisers were obtained from Walsh (2021) [132]. The nitrogen content of the inorganic fertilisers was evaluated using the results in Hoxha and Christensen (2018) [125].....423

Figure 8-10 Greenhouse emissions and savings from the proposed polygeneration plant for (a) scenarios 82IBP, 82IBF, 82IMP, 82IMF, 82ICP, 82ICF, 82ITP and

82ITF, (b) 82IBP-R, (c) 82MBP and 82MBF, (d) 82SBP and 82SBF, (e) 64IBP and (f) 64IBP-R. In the figures, CCS refers to carbon capture and storage, CCR refers to carbon capture and replacement. 425

Figure 8-11 Contribution of the co-products towards the overall emissions in each of the fifteen scenarios 427

Figure 8-12 Levelised cost of GHG abatement (LCOA) or marginal abatement cost (MAC) of the proposed polygeneration plant under each of the fifteen scenarios assessed along with the current cost CO_2 and the MACs of a few alternatives to biomethane. The current (2020) and the future prices of CO_2 were obtained from data from the Government of Ireland [134] and projections of Ireland's GHG emissions by EPA (2021) [135] respectively. The MACs of the alternative technologies were obtained from various sources of literature [136–139] 429

Figure 8-13 Sensitivity assessments of the different variables including the prices of biomethane and *Spirulina* powder on the NPV, IRR, LCOA and the levelised cost of each co-product for the base case scenario (scenario 82IBP) 431

Figure 8-14 Monte Carlo simulations to determine the most probable (a) NPV and (b) LCOA or marginal abatement cost of the proposed technology for the base case scenario (82IBP). * 10% cost variation indicates a variation of ± 10% of the individual cost components of the OPEX including the cost for the nutrient medium for microalgae cultivation. 432

Figure 8-15 Impact of selling price of biomethane on (a) NPV and IRR of the 82IBP (&F) scenarios, (b) NPV and IRR of the 82MBP (&F) scenarios and (c) levelised cost of Spirulina powder of the 82IBP (&F), 82MBP (&F) and 82SBP (&F) scenarios. 434

Figure 8-16 Variation in the minimum price of *Spirulina* powder with the price of biomethane to ensure the profitability of the medium (82MBP and 82MBF) and the small-scale (82SBP and 82SBF) scenarios (NPV > 0) 437

List of tables

Table 2-1 CO_2 metabolism pathways for microalgae species/genera. 27

Table 2-2 High-CO_2-tolerant species of microalgae reported in the literature. 34

Table 2-3 Summary of CO_2 bio-fixation and losses reported in recent experiments.37

Table 2-4 Details of absorption columns used in experiments for biogas upgrading with microalgae. 44

Table 2-5 Comparative summary of closed photobioreactors for mass cultivation [123,124,135-138]. 50

Table 2-6 Summary of photobioreactors types and operational details for microalgae cultivation with simultaneous biogas upgrading. 54

Table 2-7 Evaluation of 15 common microalgae species with regards to defined microalgae selection criteria for biogas upgrading compiled based on the following references [23,28,52,64,78,81,160–184].....60

Table 3-1 Scale and design factors of bubble columns applied for photosynthetic biogas upgrading in recent literature.....94

Table 3-2 Effect of design changes on the mass flow rates of CO_2, O_2 and N_2 contained in upgraded biomethane in comparison to the inlet flows for operation under low algal concentration indicating the adequacy of the design changes and measurement techniques adopted during commissioning the bubble column setup. The molar masses of CO_2, N_2 and O_2 assumed were 44 gram/mol, 28 gram/mol and 32 gram/mol respectively. 117

Table 4-1 Variables affecting bubble column operations in photosynthetic biogas upgrading including those selected in the present study for comparative assessment. The current and limiting/ industrial level values have been compiled from multiple literature sources [4,7,9,11,13,16,18,19,25–30].....145

Table 4-2 Design factors and corresponding levels. 152

Table 4-3 L_{16} Taguchi Orthogonal array for screening design of experiments (L_{16}) with seven factors (A-G) at two levels (2^7).....153

Table 4-4 Results from the 16 experimental runs in triplicates performed on the L_{16} Taguchi Orthogonal Array along with the S/N ratios of the responses selected for factors screening studies 163

Table 4-5 Results of ANOVA for each process response considering each replicate as a separate experimental trial as an adequacy test of the designed screening experiment. 165

Table 4-6 Results of ANOVA assessment for CO_2 removal efficiency with main effects and interaction contributing over 95% towards the output response.*Denotes the statistically significant ($P < 0.05$) source (factors).....168

Table 4-7 Results of ANOVA assessment for mean steady state absorption rate of CO_2 with main effects and interaction contributing over 95% towards the output response.*Denotes the statistically significant ($P < 0.05$) source (factors). 171

Table 4-8 Results of ANOVA assessment for mean overall CO_2 mass transfer coefficient with main effects and interaction contributing over 95% towards the output response. *Denotes the statistically significant ($P < 0.05$) source (factors). 173

Table 4-9 Results of ANOVA assessment for O_2 content in the upgraded biomethane with main effects and interaction contributing over 95% towards the output response. *Denotes the statistically significant ($P < 0.05$) source (factors). 176

Table 4-10 Results of ANOVA assessment for O_2 outflow with biomethane with main effects and interaction contributing over 90% towards the output response. *Denotes the statistically significant ($P < 0.05$) source (factors).....178

Table 4-11 Comparison and primary conclusions about the design factors affecting the studied process responses to assess the performance of the bubble column in photosynthetic biogas upgrading for both CO_2 removal and O_2 stripping. The values in brackets indicate the rank of the design factors based on S/N ratios for the respective response.....180

Table 4-12 Statistical characteristics of the models for predicting CO_2 removal efficiency and O_2 flow rate in upgraded biomethane to predict the biomethane composition.....182

Table 4-13 Impact of pH and L/G ratio on the inorganic carbon added to the algal liquid from biogas with the corresponding CO_2 removal efficiency in brackets. CO_2

removal efficiencies are based on the predicted values obtained using Eq. 4.15 and Eq. 4.10 in order. 186

Table 5-1 Ranges and experimental levels of the independent variables for optimising the bubble column performance of photosynthetic biogas upgrading 208

Table 5-2 Results of the process responses against each setting of operating condition designed using the central composite design for optimisation and prediction of bubble column operations in photosynthetic biogas upgrading.....215

Table 5-3 Statistical summaries of the models chosen to describe the behaviour of the four process responses selected to describe the performance of the bubble column operations in photosynthetic biogas upgrading. 216

Table 5-4 Summary of the pooled ANOVA assessment of the fitted quadratic models for the four process responses selected to describe the bubble column performance for photosynthetic biogas upgrading.....217

Table 5-5 Results of the confirmatory experiments and their comparison with the predicted values at two different L/G ratios for a liquid inlet pH of 10.1, superficial gas velocity of 0.3 cm/s and, alkalinity of 2 gIC/L. 221

Table 5-6 Estimation of the number of bubble columns required to upgrade 478 Nm^3/hr of biogas (equivalent to $1MW_e$ biogas based electric plant) based on the bubble column size between 5-200 m^3 and superficial gas velocities between 0.4-0.6 cm/s. The bubble column is assumed to operate at NTP (20 °C and 1 atm) 232

Table 5-7 Influence of L/G ratio and algal productivity on the design and sizing of a flat plate photobioreactor system under optimal operations of the bubble column for upgrading 478 Nm^3/hr of biogas (equivalent to that produced in a $1MW_e$ biogas based electricity plant [6]).....234

Table S5-1 Summary of the thirty experimental trials developed using the central composite design (CCD) to study the impact of inlet liquid pH (pH), superficial gas velocity (u_G), liquid to gas flow rate ratio (L/G) and inlet liquid alkalinity (Alk) on the process responses of a bubble column for photosynthetic biogas upgrading……....239

Table S5-2 Statistical summary of the models chosen to describe the behaviour of the four process responses selected to describe the performance of the bubble column operations in photosynthetic biogas upgrading…….....241

Table 6-1 Theoretical and actual specific methane yield (SMY) in batch tests without pre-treatment, after pre-treatment and following fraction (lipid and protein) extraction of multiple microalgae species reported in the literature 258

Table 6-2 Comparison of the present review article and recent review papers (since 2015) focussing on the use of microalgae in AD systems and the development of microalgae biorefinery 282

Table A6-1 References for product content in microalgae and economics (sale price, compound annual growth rate and speculated market value) of bio-products…...…284

Table 7-1 Characteristics of co-digestion substrates used in this study along with their respective costs as adapted from [21,30–35] 310

Table 7-2 Summary of the major inputs to the process and their corresponding costs 311

Table 7-3 Process parameters utilised to simulate the biogas section in SuperPro .316

Table 7-4 Specific energy consumption of the individual components of the Anaerobic Digestion section, the Biogas Upgrading section, the Microalgae Cultivation section and the Microalgae Harvesting and Processing Section. The values without references are default values of the components in the SuperPro Designer library. 317

Table 7-5 Energy consumption details of the demineralisation plant and other auxiliary units considered within the system boundary of the proposed polygeneration unit 324

Table 7-6 Nutrient value in *Spirulina* powder along with the recommended and the maximum daily values of each of the corresponding nutrients. The nutrient values in *Spirulina* were obtained from [102,106], while the recommended daily value (RDV) and the maximum daily value (MDV) were compiled from [104,107,108]. 330

Table 7-7 Specific emissions under the different emission categories required to evaluate the overall GHG emissions of the proposed polygeneration plant as per the RED-II.....333

Table 7-8 Model validation of biogas production via anaerobic co-digestion of grass silage and cattle slurry.....338

Table 7-9 Model validation of biogas upgrading in photosynthetic biogas upgrading 339

Table 7-10 Model validation of microalgae cultivation and harvesting in photosynthetic biogas upgrading.....340

Table 7-11 Validation of methane, carbon and water losses for the proposed polygeneration system.....341

Table 7-12 Summary of allocation of resources and emissions to the co-products under each scenario. 349

Table S7-1 Summary of the major outputs to the process and their corresponding unit prices/ costs 364

Table S7-2 $NRF_{9.3}$ scores and specific emissions of other protein-based foods compared with *Spirulina*. The data has been compiled from multiple literature [104,108,146–149].....365

Table 8-1 Characteristics of co-digestion substrates used in this study along with their respective costs as adapted from [10,28–33] 391

Table 8-2 Summary of the major inputs to the process and their corresponding costs 392

Table 8-3 Description of the scenarios assessed towards studying the techno-economic and the LCOA (MAC) of the polygeneration system coproducing biomethane and Spirulina powder as a protein supplement. 396

Table 8-4 Values of process variables assumed for different scenarios. † Similar assumptions to be used for scenarios 82IBF, 82IMP, 82IMF, 82ICP, 82ICF, 82ITP, 82ITF, 82IBP-R and 64IBP-R.....398

Table 8-5 Reference capital cost of each equipment included in the model of the proposed polygeneration plant. 401

Table 8-6 Annual labour costs for each scale of operation.....406

Table 8-7 Generalised assumptions for techno-economic analysis 406

Table 8-8 Specific emissions under the different emission categories required to evaluate the overall GHG emissions of the proposed polygeneration plant as per the EU Renewable Energy Directive II (Recast) (RED-II).....409

Table 8-9 Specific emissions from reference components to be replaced by the co-products produced in the proposed polygeneration plant 411

Table 8-10 Technical parameters of the polygeneration plant under different scenarios 414

Table 8-11 Specific GHG emissions from each co-product and the overall lifetime GHG emission savings of the proposed polygeneration plant for each of the fifteen scenarios assessed. 426

Table S8-1 Summary of the major outputs to the process and their corresponding unit prices/ costs 440

Table S8-2 Nutrient value in *Spirulina* powder along with the recommended and the maximum daily values of each of the corresponding nutrients. The nutrient values in Spirulina were obtained from [110,151], while the recommended daily value (RDV) and the maximum daily value (MDV) were compiled from [65,152,153].....441

Table S8-3 $NRF_{9.3}$ scores, wholesale prices and specific emissions of the four protein-based foods compared with *Spirulina*, namely, beef, milk, chicken and tofu (soybeans).....441

Table S8-4 Bare erected cost and the corresponding sizing of each equipment within the individual scenarios assessed. All costs are in 2020 Euros.....443

Table S8-5 Breakdown of the operational costs of the polygeneration process for each scenario. All costs are in ’000 Euros and are calculated for the base year (2020).....447

Declaration

I hereby declare that this thesis is my own work and that it has not been submitted for another degree, either at University College Cork or elsewhere. Where other sources of information have been used, they have been acknowledged. I have read and understood the regulations of University College Cork concerning plagiarism.

Signed: 

[Archishman Bose]

Date: 10th September 2021

Acknowledgement

I would like to start by sincerely thanking my supervisor, Prof. Jerry D. Murphy for; firstly, the opportunity to research in the Circular Economy Energy and Environmental Systems (CEEES) research area in the MaREI Centre for Energy Climate and Marine, based at the Environmental Research Institute (ERI), University College Cork and secondly, for his endless support, guidance, ideas, advice and motivation towards completion of this work. Although extremely busy, he was always there, whenever I ran into trouble or required a chat about my research or writing. His support during the COVID-19 pandemic, especially in organising laboratory and workspace and keeping the team together was a guiding light for this work. His optimism, passion and enthusiasm provided the valuable impetus to complete the work, navigating setbacks and delays throughout this three-year journey.

Next, I would like to mention my grateful indebtedness to my co-supervisor Dr. Richard O'Shea, without whose support, this work wouldn't have been complete. Not only was he always there to guide me in the right direction but was also always there as a colleague. This led to a constant interchange of ideas and group work that increasingly enhanced the output of the thesis. Also, in times of struggle during the thesis and especially after lockdown due to the COVID-19 pandemic, I am eternally grateful for the brainstorming sessions we had about everything from experiments to analyses of results and simulations. His advice, feedbacks and words of motivation provided the necessary driving force required to complete this work.

I would also like to acknowledge Dr. Richen Lin, my PhD thesis advisor. I am most obliged for his constant support and consultations, as well as his very valuable comments on each work, especially experiments and this thesis. I would be failing in my duty if I do not thank Dr. Karthik Rajendran, my initial PhD co-supervisor for easing me into this journey with valuable guidance, advice and of course, assurances.

I would like to take this opportunity to thank my current and former fellow researchers and friends in the CEEES research group, Davis, Xihui, Benteng, Shane, Aoife, Xue, Anga, Nathan, Donal and Daniel for allowing me to share my thoughts and providing me with feedback, ideas and support through shared discussions over cups of coffee (often virtually). I would also like to thank Dr. David Wall and Dr.

Chen Deng of the CEEES research group for their valuable time, advice and support whenever I needed them. Also, I would like to say special thanks to Tara Reddington and Aoife Dunne for their constant support and assistance with all administrative work throughout this research.

I must express my very profound gratitude to my parents and the almighty for providing me with unfailing support and continuous encouragement throughout my years of study and through the process of researching and writing this thesis.

Thank you Nayani, my fiancé for coming into my life during this arduous journey and making it enjoyable through constant support, inspiration and motivation. Thank you for tolerating me through stressful times and sleepless nights. I look up to you for all the positive energy that I needed to complete this work.

I would also be failing in my duty if I do not thank my friends and the UCC Cricket Club for giving me the space to enjoy life beyond this work. A special thanks to Suvaprasad, Sutapa, Rajannya, Tanmay, Aritra, Kankana, Arindam and Debapriya for tolerating me through these years, giving me a chance to laugh and tasting my first-try recipes.

Lastly, I would like to thank my PhD funders, Gas Networks Ireland, Science Foundation Ireland (SFI) and the MaREI Centre for Energy, Climate and Marine. Saying so, I would like to stress that the research presented reflects only my views and the funders cannot be held responsible for any use, which may be made of the information contained therein.

Thank you all
Archishman Bose
10.09.2021
Cork, Ireland

Abstract

Biomethane is a viable alternative to natural gas and diesel and its use has significant applications in decarbonising the hard to abate sectors of industry, heavy transport, and agriculture. Yet, commercial technologies for upgrading biogas from anaerobic digestion (AD) to biomethane (such as amine and water scrubbing) bring high costs and significant energy demand.

In this research, photosynthetic biogas upgrading was studied as an alternative to conventional biogas upgrading. The two-step bubble column photobioreactor setup was established as the suitable technological configuration. Five criteria were developed to select favourable microalgae species for photosynthetic biogas upgrading; *Spirulina platensis* was evaluated as optimal amongst common microalgae species.

Following a systems approach, the bubble column (the least optimised component of photosynthetic biogas upgrading) was interrogated in detail through design of experiments to advance the understanding of the overall technology. Findings concluded that the liquid inlet pH, the liquid to gas flow (L/G) ratio and their interactions are major factors for bubble column operations. A lower algal concentration would ensure both a higher CO_2 removal efficiency and a lower O_2 concentration in biomethane. Regression equations, developed from experiments, were found to adequately predict CO_2 removal efficiency, overall CO_2 mass transfer coefficient, O_2 concentration in biomethane and pH of the outlet algal medium for bubble column operations at liquid inlet pHs between 9.4 and 10.2, alkalinities between 1.3 g-inorganic carbon (IC)/L and 2.1 gIC/L, superficial gas velocities (u_G) between 0.3 cm/s and 0.6 cm/s and L/G ratios between 0.3 and 0.8.

A minimum pH of 10, alkalinity of 1.7 gIC/L with L/G ratios between 0.6 and 0.7 and u_G between 0.5 and 0.6 cm/s were found sufficient to achieve grid quality biomethane (CO_2 and O_2 less than 2.5%$_{vol}$ and 0.8%$_{vol}$ respectively) at a CO_2 mass transfer coefficient above 150 hr^{-1}. These optimal conditions were also favourable for the growth of *Spirulina platensis* in a connected photobioreactor.

Following technological optimisation, several strategies were developed to integrate photosynthetic biogas upgrading into a circular economy system using a Cascading Algal Biomethane Biorefinery System (CABBS). A microalgae composition-based decision tree was proposed to facilitate the maximisation of the profitability of these integrated biorefineries.

A detailed model of a fuel (biomethane), food (*Spirulina* powder), biofertiliser (digestate) polygeneration process was developed. Through a multi-criteria performance assessment, the economic and the environmental benefits of the process were shown. Contrary to the energy allocation approach of the Recast EU Renewable Energy Directive (RED-II) methodology, the energy, emissions, land, and water footprints of each co-product from the polygeneration system were found to be best represented by economic allocation while allowing cost-competitiveness with market available alternatives for food and fertiliser. Using the carbon intensity of electricity grids and the individual market price of each co-product, an economic allocation was found to facilitate the production of sustainable biomethane (as defined by carbon intensity of less than 14.4 $gCO_{2\text{-}eq}$/MJ for biomethane for use in heat as per RED-II). *Spirulina* powder and biofertiliser were also assessed to have lower emissions than meat protein and synthetic nitrogenous fertilisers respectively.

The conditions for the profitability of the polygeneration plant was shown at industrial, medium and small scales while selling biomethane at the price of natural gas (3 c€/kWh). A negative marginal abatement cost established the industrial-scale process as a profitable technology comparing very favourably to conventional biomethane production processes. Future lower carbon intensity of electricity grids and trading of biomethane in the EU emission trading scheme should facilitate financial viability of smaller-scale processes by 2030.

Thesis output

The following chapters are either published as peer-review journal papers or are currently under review with journals or currently being prepared for submission to an international journal. For these papers, I was the first author, preparing the original draft and responsible for the decision making in the approach of the study. I was also responsible for the experimental and study design, laboratory and simulation works and data analysis and interpretation performed to arrive at the conclusions included therein. The supervisors greatly helped improve the quality of the work by providing constant mentorship, feedback and criticism during the conceptualisation of the works, design of experiments or simulations and during analyses of results. The supervisors were also responsible for reviewing and editing the original draft, especially concerning the clarity of the text and enhancing the language quality. Additionally, the supervisors provided considerable support to set up the experimental rig especially during procurement of equipment and materials and during construction and commissioning of the experimental rig itself.

Chapter 2

Bose, A., Lin, R., Rajendran, K., O'Shea, R., Xia, A., Murphy, J.D. (2019) "How to optimise photosynthetic biogas upgrading: a perspective on system design and microalgae selection". Biotechnology Advances, Volume 37, Issue 8, December 2019, 107444, 10.1016/j.biotechadv.2019.107444

Chapter 3

Bose, A., O'Shea, R., Lin, R., Murphy, J.D. (2021) "Design, Commissioning, and Performance Assessment of a Lab-Scale Bubble Column Reactor for Photosynthetic Biogas Upgrading with *Spirulina platensis*". I&EC Research, Volume 60, Issue 15, 5688–5704, 10.1021/acs.iecr.0c05974

Chapter 4

Bose, A., O'Shea, R., Lin, R., Murphy, J.D. (2021) "A comparative evaluation of design factors on bubble column operation in photosynthetic biogas upgrading".

Biofuel Research Journal, Volume 8, Issue 2, June 2021, 1351-1373, 10.18331/BRJ2021.8.2.2

Chapter 5

Bose, A., O'Shea, R., Lin, R., Murphy, J.D. (2021) "Optimisation and performance prediction of photosynthetic biogas upgrading using a bubble column". Chemical Engineering Journal (*Revisions submitted*)

Chapter 6

Bose, A., O'Shea, R., Lin, R., Murphy, J.D. (2020) "A perspective on novel cascading algal biomethane biorefinery systems". Bioresource Technology, Volume 304, May 2020, 123027, 10.1016/j.biortech.2020.123027

Chapter 7

Bose, A., O'Shea, R., Lin, R., Long, A., Rajendran, K., Wall, D., De, S., Murphy, J.D. (2021) "Producing biofuel with food and fertiliser in a circular economy" Energy and Environmental Science (*Under Review*)

Chapter 8

Bose, A., O'Shea, R., Lin, R., Long, A., Rajendran, K., Wall, D., De, S., Murphy, J.D. (2021) "A biomethane-food-fertiliser polygeneration plant as a profitable strategy for GHG reductions" (*Manuscript to be submitted*)

General nomenclature

A list of nomenclature used in this thesis is outlined below, unless otherwise explicitly mentioned as different in the individual chapter's nomenclature (if provided). All chemical symbols are used according to the standard nomenclature by the International Union of Pure and Applied Chemistry (IUPAC) and hence are not separately mentioned in the list below.

Symbols	Descriptions
AD	Anaerobic digestion
Alloc	Allocation
ANOVA	Analysis of Variance
atm	atmosphere
BEC	Bare erected cost [€]
BECCS	Bioenergy with carbon capture and storage
BMC	Base module cost [€]
BMP	Biomethane potential
c	Cents
c.	Approximately
CA	Carbonic Anhydrase (enzyme)
CABBS	Cascading Algal Biomethane Biorefinery System
CAGR	Compound annual growth rate [%]
CAPEX	Capital expenditure [€]
CCD	Central composite design
CEF	Carbon emission factor
CI	Confidence Interval
C:N	Carbon to Nitrogen ratio
$CO_{2\text{-eq}}$	Equivalent carbon dioxide
COD	Chemical oxygen demand [mgO_2/L]
COP	Coefficient of performance
CUF	Carbon utilisation factor
Depr	Depriciation cost [€]
DIC	Dissolved Inorganic Carbon [g/L]
DO	Dissolved oxygen [mg/L]

Symbols	Descriptions
DoE	Design of experiments
DoF	Degree(s) of freedom
DPBP	Discounted payback period [years]
DS	Dry solids [kg]
DW	Dry weight [kg]
€	Euro
EBRT	Empty bed residence time [mins]
EPCC	Engineering, procurement and construction cost [€]
ESP	Equivalent selling price [€/kg-whole dry microalgae]
EU	The European Union
Eq.	Equation
FFC	Fossil fuel comparator
FiTs	Feed-in tariffs
FW	Fresh weight [kg]
GC	Gas chromatograph
GHG	Greenhouse gases [$CO_{2\text{-}eq}$]
H	Henry's Constant [L.atm/mol]
ha	hectares [ha]
hr	hour(s)
H/D	Height to diameter ratio of bubble column (Aspect Ratio)
HRT	Hydraulic retention time [days or hours]
i	Discount rate [%]
IEA	International Energy Agency
IC	Inorganic carbon
IPCC	Intergovernmental Panel for Climate Change
IRR	Internal rate of return [%]
k_La	Volumetric mass transfer coefficient [s^{-1} or hr^{-1}]
kWh	kilowatt hours [kWh]
LCA	Life cycle analysis
LCOA	Levelised cost of CO_2 abatement [€/tonne-$CO_{2\text{-}eq}$]
L/G	Liquid to gas flow rate (ratio)
L_n	Litres at NTP
LHV	Lower heating value [MJ/kg]
MAC	Marginal abatement cost [€/tonne-$CO_{2\text{-}eq}$]

Symbols	Descriptions
MJ	mega joules [MJ]
MSP	Minimum selling price
Nm^3	Normal metre cube [volume at normal conditions of 20 °C and 1 atmosphere]
NPV	Net present value [€]
NRF	Nutrient Rich Food (Index)
OA	Orthogonal Array
OECD	Organisation for Economic Co-operation and Development
OPEX	Operational expenditure [€]
OLR	Organic loading rating [$kgVS/m^3$]
%	Percentage (volume basis)
£	Pound (British currency)
PBU	Photosynthetic biogas upgrading
PI	Prediction Interval
ppm	Parts per million
PUFA	Polyunsaturated fatty acids
R	Universal Gas Constant (8.314 kJ/mol.K)
RED-II	Renewable Energy Directive (Recast)
RSM	Response Surface Method
s	seconds
SDGs	Sustainable Development Goal(s)
S-EROI	Standard energy return on investment
SMY	Specific methane yield [$LCH_4/kg\text{-}VS$]
S/N	Signal to noise (ratio)
t	tonne(s)
TAN	Total ammoniacal nitrogen
TEA	Technoeconomic assessment
TBEC	Total bare erected cost [€]
TDPC	Total direct plant cost [€]
TOPC	Total overnight plant cost [€]
TPC	Total project cost [€]
TRL	Technology readiness level
TSS	Total suspended solids [g/L]
u_G	Superficial gas velocity [cm/s]

Symbols	Descriptions
UN	United Nations
USD	United States Dollars
VFA	Volatile fatty acids
VS	Volatile solids [kg]
yr	year

1 Introduction

1.1 Background to the thesis

1.1.1 Climate targets, climate action plans and sustainable development goals (SDGs)

For humanity to avoid the severe risks of climate change, both the Paris Agreement of 2015 and the Glasgow Climate Pact of 2021 agree that the global temperature rise must be limited to 1.5 °C above pre-industrial levels [1,2]. Achieving this target while allowing the increase in the production of food, energy and materials to meet the demands of the modern world would require a '*rapid and unprecedented'* societal and industrial transition [3].

To accelerate this transition, stringent national and international targets are being set to decarbonise industry and society. For example, the EU has now set into law the goal of achieving net-zero by 2050, legally binding the member states to decarbonise society and economy as a whole within that time frame [4]. As a mid-term target, it also aims to reduce its greenhouse gas (GHG) emissions by 55% as compared to 1990 levels by 2030 [4]. Aligning with these targets, within the EU, each country has developed its own climate action plan, timeline and roadmap to achieve carbon neutrality. For example, while Iceland and Austria have set targets to achieve zero carbon emissions by 2040, Germany and Sweden's climate action plans have aimed at 2045 to achieve the same [5]. In Ireland, the Irish government has brought in the Climate Action and Low Carbon Development (Amendment) Bill 2021, making it a binding requirement for the state to achieve a climate-neutral economy before 2050 [6]. Besides the EU, countries such as the USA, China and India have all pledged to reduce their GHG emissions to zero, latest by 2070 [5].

Besides the climate action plans, most countries have unanimously adopted the United Nation's 17 sustainable development goals (SDGs) to enable a fair, peaceful and prosperous society by 2030 [7]. Thus, the climate action and transition to a decarbonised world must be synergistic with the UN SDGs, ensuring, besides carbon neutrality, eradication of energy poverty and hunger, development of healthier environment and sustainable communities and increasing opportunities for education and jobs [8,9].

1.1.2 Circular bioeconomy for sustainable development and climate action plans

There is an acknowledgement that to sustainably decarbonise society as a whole, the environmental impacts including GHG emissions must be reduced for the production of food, energy and material through simultaneous transitions from

1) a linear "take, make and dispose" economy to a circular economy [10]; and
2) a traditional fossil-based economy to a renewable bioeconomy [11].

While the circular economy aims to enhance the use of available resources and close the resource-loop by both reducing and re-using wastes, and decreasing the need for raw materials, [12], a bioeconomy focuses on forming renewable biological resources, the basis for the production of energy, material and chemicals [13]. Each of the two principles has received wide research interest as pathways to achieve effective and sustainable decarbonisation to meet the national and international climate action plans. However, a fully developed bioeconomy, able to replace over 90 per cent of the present fossil-oil based products [14], would require vast resources to supply the needs of the present-day economy. Not only would this require considerable changes to the present socio-political and technological framework [14] but would need critical assessment to diminish increased impacts on the environment and existing ecosystems, solely relying on biological resources [15]. The use of palm oil as biofuel leading to increased deforestation in Indonesia, and the subsequent negative impacts on the SDGs is a major practical example [16]. However, by synergistic usage of the concepts of circular and bioeconomy, recent literature has revealed the feasibility of establishing "circular bioeconomy" as a major and essential element to achieve sustainable and long-term decarbonisation of the society and the economy [17–19].

1.1.3 Biofuels in the future circular bioeconomy

Recent studies reveal that significant progress has been made in achieving sustainability in multiple aspects of bioeconomy including agriculture, forestry, fisheries and biotechnology and energy industries [19]. Among the different bio-products making progress, the generation of biofuels as a substitute for liquid and gaseous fossil fuels is an essential element of decarbonising society and energy usage in particular [20,21]. Biofuels are especially being considered to address

decarbonisation of hard-to-abate sectors such as agriculture, heavy transport and industries requiring high-temperature heat (such as food and beverage industries) due to their heavy reliance on fossil fuels and limited opportunity to electrify [21–24]. Nonetheless, to maximise the emission savings from biofuel systems and ensure their long-term sustainability, suitable choices of resources and production and processing with minimal environmental and economic burdens are crucial.

1.1.4 Biomethane: A renewable biofuel

Biogas produced via anaerobic digestion (AD) of biodegradable organic materials has multiple advantages in both processing and use. These include: *i)* The possibility for the high biomass utilisation; *ii)* low capital and operational costs; *iii)* ability to incorporate a wide variety of feedstocks; as well as *iv)* scope for nutrient recycling [25,26]. Even though each substrate, together with the conditions existing inside the digester results in a different composition of the biogas generated, a typical generic composition of biogas from AD can be summarized to comprise primarily of CH_4: 45-70% and CO_2: 20-55% [27–29]. Besides methane, all the other gases or contaminants (such as hydrogen sulphide, ammonia, siloxanes and chlorine) either lower the calorific value of biogas and/or cause environmental pollution from their use. Thus, to enhance biogas properties including its calorific value and its utility in the energy sector, the CO_2 from biogas is often removed in a process termed “biogas upgrading”; the ensuing product is termed biomethane [27,28].

Biomethane is considered a versatile renewable biofuel with higher GHG savings than liquid biofuels [30]. Comprising mostly (above 93%) of CH_4, it is, therefore, an effective substitute for fossil natural gas and may be applied in complex energy systems including applications in heat, electricity and transport; biogas as such is a bioenergy vector with considerable advantages over solid biofuels for example woodchips [22,24] and as such a comparison of these two bioenergy systems on the basis of €/kWh is unhelpful. In the accounting of greenhouse gas emissions, biomethane provides emissions savings outside the EU emissions trading system (EU-ETS) and as such facilitates countries in meeting their binding annual greenhouse gas emissions targets in the hard to abate sectors of agriculture and transport [11].

1.1.5 Novel biogas upgrading technologies to reduce GHG emissions in biomethane production

By 2026, in the EU, biomethane must effect a GHG emissions reduction of 65% as compared to the fossil fuel comparator (FFC) to be deemed sustainable as a biofuel in the transport sector [31]. The corresponding reduction in the heat sector must be above 80% [31]. Thus, besides innovation in feedstock selection (the primary contributor towards the overall emissions), emissions and energy use in biogas upgrading needs to be reduced [32]. Traditional upgrading technologies employing physicochemical techniques, viz., membrane separation, chemical adsorption and pressure swing adsorption have a significant energy penalty (3-6% of the energy content of biogas processed) and a high cost (up to 30% of the total cost of upgraded biogas) [27,33]. Biogas conversion to biomethane with carbon capture and sequestration or re-use of CO_2 can effect a reduced carbon footprint for a number of systems (including for food, fertiliser and fuel). Biological biogas upgrading systems, which integrates microalgae cultivation and the production of value-added products (biofuels, food and/or feed and chemicals) are a potential solution for cost-efficient upgrading in an optimised system providing direct CO_2 capture and reuse on or near-site [34,35]; it can also improve the energy balance through added financial and environmental benefits beyond biomethane production.

1.1.6 Photosynthetic biogas upgrading

Photosynthetic biogas upgrading using microalgae may overcome the economic and environmental drawbacks associated with traditional biogas upgrading [36]. In this process, CO_2 is removed from biogas by a carbonate-rich solution generating bicarbonate. The bicarbonates rich solution is used as an inorganic carbon source for microalgae cultivation at a relatively high pH. Higher areal productivity of microalgae compared to terrestrial plants and seaweeds, rapid CO_2 fixation, and the ability of microalgae to grow in a wide range of environments [37] could potentially increase the sustainability of photosynthetic biogas upgrading.

Optimised photosynthetic biogas upgrading must enable both, continuous production of gas grid quality biomethane (defined here as less than 2.5% CO_2 and 1% O_2 (by volume) [38,39]) and rapid and efficient uptake of the absorbed CO_2 by the

microalgae. Although research towards optimising the performance of photosynthetic biogas upgrading is ongoing, as a novel technology, the choice of operational parameters and the microalgae species for optimal performance has not yet been definitively agreed upon or standardised. This has led to considerable variabilities and uncertainties in reported results, presenting significant uncertainty for industrial-scale implementation of photosynthetic biogas upgrading.

1.1.7 Biorefinery for a sustainable and circular bioeconomy

Co-production of multiple outputs including biofuels, chemicals and heat or electricity through the integration of suitable technologies is an effective strategy to maximise the use of biomass resources [40]. Working similar to a traditional refinery, except using biomass as a feedstock, this essentially forms the core principle of a biorefinery [41,42]. Lignocellulosic feedstock (non-edible crops, agricultural residues and wastes including food waste and sewage sludge) are most commonly considered as the building blocks of a biorefinery at present [42]. Bolstered by innovative policies, as well as the ability to offset significant emissions by bio-products, significant efforts are being made worldwide by chemical producing companies like Dow-Dupont, Brasken and Granbio among others to advance the biorefinery industry [14,42]. Photosynthetic biogas upgrading, by co-producing biomethane with other bio-products (with associated revenue) could therefore provide a novel biorefinery approach for cost-efficient upgrading of biogas. It also presents the opportunity for direct CO_2 sequestration on or near-site [34,35] while potentially improving the resource utilisation, process performance and flexibility of operation of the novel process over standalone conventional biomethane production facilities.

1.2 Rationale behind the thesis

To develop novel biogas upgrading technologies and ensure sustainable biomethane both in terms of carbon and finance in a future circular bioeconomy, this thesis was set out to explore and advance upon photosynthetic biogas upgrading technology. Microalgae are one of the most efficient natural bio-factories [43]. This informed the rationale of the thesis to integrate efficient and sustainable biogas systems in the production of biomethane with co-production of high value and/or bulk products such as food and/or feed (microalgae), fuel and chemicals from a microalgae

biorefinery. Accordingly, both process optimisation and effective incorporation of photosynthetic biogas upgrading in a circular bioeconomy framework including market perspectives were investigated in the thesis. The concept, with photosynthetic biogas upgrading as the enabler for the circular economy system is represented in Figure 1-1.

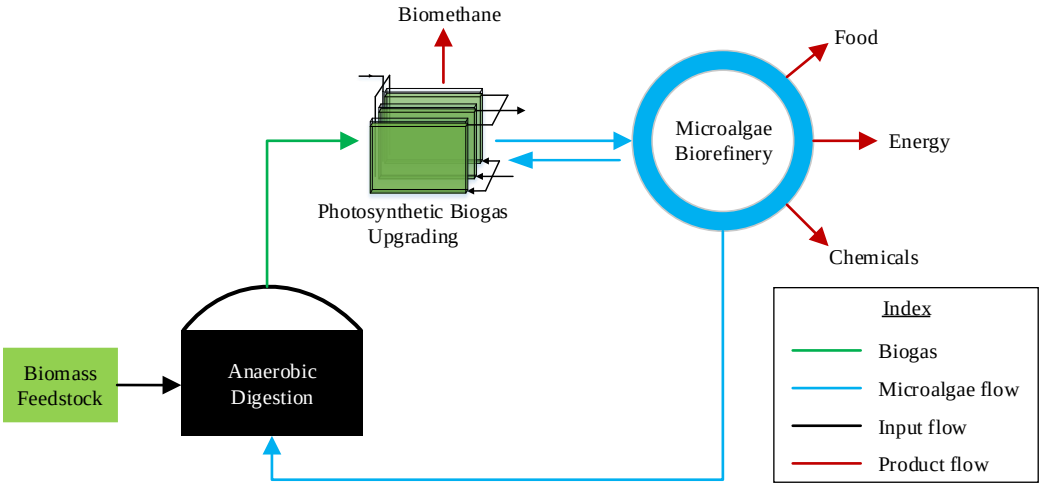


Figure 1-1 Schematic representation of a possible integrated Anaerobic Digestion (AD)-biorefinery system utilising microalgae in a future circular bio-economy system [44]

1.3 Thesis objectives and scope

The binding thread or narrative of the thesis aims to reduce the uncertainty and variabilities of an optimised photosynthetic biogas upgrading system and its incorporation in a circular bioeconomy system. Accordingly, the technology was studied both on its own and within a broader circular economy context to address four high-level objectives and corresponding sub-objectives as follows:

- Identify the areas where photosynthetic biogas requires the most improvement and establish a framework for selecting suitable microalgae species.

  → Develop a systems approach to divide the entire photosynthetic biogas upgrading technology into constituent sub-systems and hence analyse their roles and optimisation with respect to the overall process.

  → Identify the major sources of variabilities in process output and determine the sub-system that is most lacking in optimisation.

  → Develop criteria to select the most suitable microalgae species for photosynthetic biogas upgrading.

- Perform robust optimisation using a systems approach to advance the overall photosynthetic biogas upgrading technology.

  → Design and commission an experimental setup focusing on the sub-system which exhibited the least optimisation relative to other sub-systems.
  → Compare the impact of controllable designed factors on the investigated sub-system and select the most critical factors.
  → Perform optimisation and performance prediction of the investigated sub-system to maximise process yield and robustness of operation.
  → Develop a perspective of robust operations of photosynthetic biogas upgrading using the optimised subsystem with other subsystems.

- Identify strategies to integrate photosynthetic biogas upgrading based biomethane systems in a circular bioeconomy system.

  → Investigate opportunities to incorporate photosynthetic biogas upgrading in a circular bioeconomy framework.
  → Develop robust strategies to integrate AD and photosynthetic biogas upgrading with microalgae biorefinery for co-production of energy (biomethane), food and/or feed, chemicals and/or energy (biofuels).
  → Assess the sustainability potential of the biomethane-biorefinery systems and their possibility to be negative emission or low carbon technologies.

- Propose and apply methods to assess the energetic, environmental and economic performances of a polygeneration system using photosynthetic biogas upgrading and compare it with state-of-the-art biogas upgrading technologies.

  → Develop and simulate a cascading biomethane-biorefinery system including for photosynthetic biogas upgrading.
  → Perform techno-economic and sustainability assessments of the simulated model.
  → Compare the economic and environmental characteristics of biomethane and co-products produced in the integrated system with corresponding products produced using commercial technologies in standalone systems.

→ Discuss policy implications and assess possible modifications to enable implementations of such integrated systems in the future circular bioeconomy framework.

1.4 Thesis outline and the link between chapters

This nine-chapter thesis presented as a thesis by publication investigates photosynthetic biogas upgrading from both technological aspects and the perspective of its incorporation within a circular bioeconomy framework. Except Chapter 1 (Introduction) and Chapter 9 (Conclusion), each chapter corresponds to a paper and can be read independently with corresponding appendices and references.

At the time of production of this thesis (December 2021) chapters 2, 3, 4 and 6 are published in international journals following peer-review while chapters 5 and 7 are currently under review. The manuscript for chapter 8 will be submitted later in the year. Accordingly, each chapter in this thesis closely resembles the published or submitted manuscripts bar some minor modifications including harmonising abbreviations and reducing repetition to improve the reading experience. The link between each chapter and a summary of chapters 2 to 8 are given as follows:

1.4.1 Chapter 2: How to optimise photosynthetic biogas upgrading: a perspective on system design and microalgae selection (*Review*)

This chapter aims to develop a comprehensive understanding of photosynthetic biogas upgrading and provide the reader with a suitable background to the thesis. This chapter includes both an in-depth study of the fundamental concepts as well as a detailed review of the relevant literature. To simplify the assessment, this chapter undertakes a systems approach to break down the complete technology into individual sub-systems. Perspectives on the factors affecting the performance of the individual sub-systems and the research gaps are developed. These provide the background for further investigations documented in the following chapters. The chapter develops a framework of five criteria to identify the most suitable microalgae species for the optimal operation of photosynthetic biogas upgrading.

1.4.2 Chapter 3: Design, commissioning and performance assessment of a lab-scale bubble column reactor for photosynthetic biogas upgrading with *Spirulina platensis* (*Original Research*)

Chapter 3 introduces the need for a focussed investigation of bubble column performance for biogas upgrading within the context of the overall optimisation of photosynthetic biogas upgrading. The chapter outlines the development of the lab-scale experimental bubble column setup which is used for all subsequent experiments. The design, commissioning and validation of the operations of the bubble column setup is thoroughly described along with the operational and analytical challenges associated with its start-up and regular operations. Perspectives on such challenges under industrial operations are also discussed. The potential for commercialisation of the process is explored to identify the operating regime of biogas upgrading to ensure scalable results.

1.4.3 Chapter 4: A comparative evaluation of design factors on bubble column operation in photosynthetic biogas upgrading (*Original Research*)

Using the knowledge developed in Chapter 2 and the initial experimental outcomes of Chapter 3, Chapter 4 documents the identification and ranking of the most significant factors which affect the performance of biogas upgrading in the bubble column. The main effects of, and interactions between, the selected factors are assessed using the Taguchi orthogonal array as a screening design of experiments. The chapter also provides the operating setpoints of the selected factors to ensure robust biogas upgrading and the composition of the corresponding upgraded biomethane.

1.4.4 Chapter 5: Optimisation and performance prediction of photosynthetic biogas upgrading using a bubble column (*Original Research*)

Based on the critical factors identified in Chapter 4, Chapter 5 documents the process to optimise the bubble column performance in photosynthetic biogas upgrading. The Central Composite Design (CCD) within the Response Surface

Methodology (RSM) is used as the design of experiment. Performance of bubble column operations and biomethane composition is predicted within the suitable operational domain. Suitable operating conditions for continuous and robust production of grid quality biomethane (CO_2 < 2.5% and O_2 < 1%) are identified. Industrial-scale integration of the optimised bubble column with a suitable photobioreactor is evaluated to assess the overall optimal performance of the photosynthetic biogas upgrading technology.

1.4.5 Chapter 6: A perspective on novel cascading algal biomethane biorefinery systems (*Review*)

Chapter 6 describes the investigation of the applicability of photosynthetic biogas upgrading within a circular bioeconomy framework through investigation of the role of microalgae in AD systems and biorefineries for both economic and environmental value addition to the biomethane produced. A decision-making strategy for effective integration of anaerobic digestion, photosynthetic biogas upgrading and a microalgae biorefinery starting from the microalgae composition is proposed. Multiple configurations of a Cascading Algal Biomethane Biorefinery Systems (CABBS) are provided. Perspectives of corresponding techno-economic and environmental sustainability and practical challenges of such integrated systems are developed.

1.4.6 Chapter 7: Producing biofuel with food and biofertiliser in a circular economy system (*Original Research*)

Based on the opportunities presented in Chapter 6, a biomethane, *Spirulina* powder (protein supplement) and digestate (biofertiliser) polygeneration plant is proposed in Chapter 7. A detailed process simulation is developed to assess the performance of the process and its products using literature data and the results of experiments described in Chapter 5. A multi-criteria performance assessment is adopted to assess the comprehensive performance of the overall polygeneration process. Energy and economic allocations are used to compare and contrast the specific energy, greenhouse gas emissions, and land and water footprint of each co-product with other market-available alternatives. *Spirulina* is assessed based on both its protein content and extended nutrition profile. The feasibility of the proposed

technology under the current RED-II is evaluated. Possible modifications to the RED-II methodologies are discussed to enhance the evidence base for the sustainability of the polygeneration processes.

1.4.7 Chapter 8: A profitable low carbon process to co-produce biomethane, food and biofertiliser (*Original Research*)

Chapter 8 describes the detailed techno-economic and enviro-economic analysis of the proposed polygeneration process generating biomethane, S*pirulina* protein and biofertiliser. Multiple scales, feedstock composition and allocation principles are assessed along with the impact of replacing different protein sources with *Spirulina* protein. The results are compiled to establish the Marginal Abatement Cost (MAC) of the technology and compare it with the MAC of other biomethane and low carbon technologies. Combined with the previous chapter, this chapter enables the complete quantification of the benefits and challenges of the proposed integrated polygeneration plant using an optimised photosynthetic biogas upgrading technology.

1.5 References

[1] United Nations Framework Convention on Climate Change (UNFCCC). Glasgow Climate Pact. Conf. Parties Serv. as Meet. Parties to Paris Agreem., Glasgow: United Nations; 2021.

[2] UNFCCC. Paris Agreement. Conf Parties Its Twenty-First Sess 2015:32. doi:FCCC/CP/2015/L.9/Rev.1.

[3] IPCC. Global warming of 1.5°C. In: Masson-Delmotte V, Zhai P, Pörtner H-O, Roberts D, Skea J, Shukla PR, et al., editors. An IPCC Spec. Rep. impacts Glob. Warm. 1.5°C above pre-industrial levels Relat. Glob. Greenh. gas Emiss. pathways, Context Strength. Glob. response to Threat Clim. Chang. Sustain. Dev., 2018.

[4] European Commission. Regulation (EU) 2021/1119 of the European Parliament and of the council establishing the framework for achieving climate neutrality and amending Regulations (EC) No 401/2009 and (EU) 2018/1999 ('European Climate Law'). vol. 2021. European Union; 2021.

[5] Energy and Climate Intelligence Unit. Net Zero Scorecard 2021. https://eciu.net/netzerotracker. (date accessed: 07.12.2021)

[6] Department of the Environment Climate and Communications. 2021 Climate Action and Low Carbon Development (Amendment) Bill 2021. Dublin: Department of the Environment Climate and Communications; 2021.

[7] UN General Assembly. Transforming our world : the 2030 Agenda for Sustainable Development. United Nations; 2015.

[8] Fuso Nerini F, Sovacool B, Hughes N, Cozzi L, Cosgrave E, Howells M, et al. Connecting climate action with other Sustainable Development Goals. Nat Sustain 2019;2:674–80. doi:10.1038/s41893-019-0334-y.

[9] Soergel B, Kriegler E, Weindl I, Rauner S, Dirnaichner A, Ruhe C, et al. A sustainable development pathway for climate action within the UN 2030 Agenda. Nat Clim Chang 2021;11:656–64. doi:10.1038/s41558-021-01098-3.

[10] McDowall W, Geng Y, Huang B, Barteková E, Bleischwitz R, Türkeli S, et al. Circular Economy policies in China and Europe. J Ind Ecol 2017;21:651–61. doi:10.1111/jiec.12597.

[11] Sanz-Hernández A, Esteban E, Garrido P. Transition to a bioeconomy: Perspectives from social sciences. J Clean Prod 2019;224:107–19. doi:10.1016/j.jclepro.2019.03.168.

[12] Prieto-Sandoval V, Jaca C, Ormazabal M. Towards a consensus on the circular economy. J Clean Prod 2018;179:605–15. doi:10.1016/j.jclepro.2017.12.224.

[13] Barsanti L, Gualtieri P. Is exploitation of microalgae economically and energetically sustainable? Algal Res 2018;31:107–15. doi:10.1016/j.algal.2018.02.001.

[14] Borgström S, Mauerhofer V. Developing law for the bioeconomy. J Energy Nat Resour Law 2016;34:373–406. doi:10.1080/02646811.2016.1200349.

[15] European Commission. A sustainable bioeconomy for Europe: Strengthening the connection between economy, society and the environment. 2018. doi:10.2777/478385.

[16] Austin KG, Mosnier A, Pirker J, McCallum I, Fritz S, Kasibhatla PS. Shifting patterns of oil palm driven deforestation in Indonesia and implications for zero-deforestation commitments. Land Use Policy 2017;69:41–8. doi:10.1016/j.landusepol.2017.08.036.

[17] D'Amato D, Droste N, Allen B, Kettunen M, Lähtinen K, Korhonen J, et al. Green, circular, bio economy: A comparative analysis of sustainability avenues. J Clean Prod 2017;168:716–34. doi:10.1016/j.jclepro.2017.09.053.

[18] D'Amato D, Korhonen J. Integrating the green economy, circular economy and bioeconomy in a strategic sustainability framework. Ecol Econ 2021;188:107143. doi:10.1016/j.ecolecon.2021.107143.

[19] Kelleher L, Henchion M, O'Neill E. Framing the circular bioeconomy in Ireland's broadsheet media, 2004–2019. Environ Commun 2021;15:678–98.

doi:10.1080/17524032.2021.1889632.

[20] Danielis R, Scorrano M, Giansoldati M. Decarbonising transport in Europe: Trends, goals, policies and passenger car scenarios. Res Transp Econ 2021:101068. doi:10.1016/j.retrec.2021.101068.

[21] Gray N, Mcdonagh S, Shea RO, Smyth B, Murphy JD. Decarbonising ships, planes and trucks : An analysis of suitable low-carbon fuels for the maritime, aviation and haulage sectors. Adv Appl Energy 2021;1:100008. doi:10.1016/j.adapen.2021.100008.

[22] Rajendran K, O'Gallachoir B, Murphy JD. The combined role of policy and incentives in promoting cost efficient decarbonisation of energy: A case study for biomethane. J Clean Prod 2019;219:278–90. doi:10.1016/j.jclepro.2019.01.298.

[23] O'Shea R, Lin R, Wall DM, Browne JD, Murphy JD. Using biogas to reduce natural gas consumption and greenhouse gas emissions at a large distillery. Appl Energy 2020;279:115812. doi:10.1016/j.apenergy.2020.115812.

[24] Wall DM, McDonagh S, Murphy JD. Cascading biomethane energy systems for sustainable green gas production in a circular economy. Bioresour Technol 2017;243:1207–15. doi:10.1016/j.biortech.2017.07.115.

[25] Ahern EP, Deane P, Persson T, Ó Gallachóir B, Murphy JD. A perspective on the potential role of renewable gas in a smart energy island system. Renew Energy 2015;78:648–56. doi:10.1016/j.renene.2015.01.048.

[26] Wall DM, Dumont M, Murphy JD. Green gas: Facilitating a future green gas grid through the production of renewable gas. 2018.

[27] Angelidaki I, Treu L, Tsapekos P, Luo G, Campanaro S, Wenzel H, et al. Biogas upgrading and utilization: Current status and perspectives. Biotechnol Adv 2018;36:452–66. doi:10.1016/j.biotechadv.2018.01.011.

[28] Ullah Khan I, Hafiz Dzarfan Othman M, Hashim H, Matsuura T, Ismail AF, Rezaei-DashtArzhandi M, et al. Biogas as a renewable energy fuel – A review

of biogas upgrading, utilisation and storage. Energy Convers Manag 2017;150:277–94. doi:10.1016/j.enconman.2017.08.035.

[29] Awe OW, Zhao Y, Nzihou A, Minh DP, Lyczko N. A Review of biogas utilisation, purification and upgrading technologies. Waste and Biomass Valorization 2017;8:267–83. doi:10.1007/s12649-016-9826-4.

[30] Xia A, Cheng J, Murphy JD. Innovation in biological production and upgrading of methane and hydrogen for use as gaseous transport biofuel. Biotechnol Adv 2016;34:451–72. doi:10.1016/j.biotechadv.2015.12.009.

[31] European Parliament and the Council of the European Union. Directive (EU) 2018/2001 of the European Parliament and of the Council on the promotion of the use of energy from renewable sources. 2018.

[32] Valli L, Rossi L, Fabbri C, Sibilla F, Gattoni P, Dale BE, et al. Greenhouse gas emissions of electricity and biomethane produced using the Biogasdoneright™ system: four case studies from Italy. Biofuels, Bioprod Biorefining 2017;11:847–60. doi:10.1002/bbb.1789.

[33] Xia A, Herrmann C, Murphy JD. How do we optimize third-generation algal biofuels ? Biofuels, Bioprod Biorefining 2015;9:358–67. doi:10.1002/bbb.1550.

[34] Farrelly DJ, Everard CD, Fagan CC, McDonnell KP. Carbon sequestration and the role of biological carbon mitigation: A review. Renew Sustain Energy Rev 2013;21:712–27. doi:10.1016/j.rser.2012.12.038.

[35] Zhou W, Wang J, Chen P, Ji C, Kang Q, Lu B, et al. Bio-mitigation of carbon dioxide using microalgal systems: Advances and perspectives. Renew Sustain Energy Rev 2017;76:1163–75. doi:10.1016/j.rser.2017.03.065.

[36] Toledo-Cervantes A, Estrada JM, Lebrero R, Muñoz R. A comparative analysis of biogas upgrading technologies: Photosynthetic vs physical/chemical processes. Algal Res 2017;25:237–43. doi:10.1016/j.algal.2017.05.006.

[37] Jankowska E, Sahu AK, Oleskowicz-Popiel P. Biogas from microalgae:

Review on microalgae's cultivation, harvesting and pretreatment for anaerobic digestion. Renew Sustain Energy Rev 2017;75:692–709. doi:10.1016/j.rser.2016.11.045.

[38] CEN. CEN/TC 234 Gases from non-conventional sources — Injection into natural gas grids — Requirements and recommendations. 2011.

[39] Meier L, Barros P, Torres A, Vilchez C, Jeison D. Photosynthetic biogas upgrading using microalgae: Effect of light/dark photoperiod. Renew Energy 2017;106:17–23. doi:10.1016/j.renene.2017.01.009.

[40] Sarma SJ, Ayadi M, Brar SK. Biorefinery: General Overview. Platf. Chem. Biorefinery, 2016, p. 21–32. doi:10.1007/s00253-003-1383-7.

[41] Cherubini F. The biorefinery concept: Using biomass instead of oil for producing energy and chemicals. Energy Convers Manag 2010;51:1412–21. doi:10.1016/j.enconman.2010.01.015.

[42] Chandel AK, Garlapati VK, Singh AK, Antunes FAF, da Silva SS. The path forward for lignocellulose biorefineries: Bottlenecks, solutions, and perspective on commercialization. Bioresour Technol 2018;264:370–81. doi:10.1016/j.biortech.2018.06.004.

[43] 't Lam GP, Vermuë MH, Eppink MHM, Wijffels RH, van den Berg C. Multi-product microalgae biorefineries: From concept towards reality. Trends Biotechnol 2018;36:216–27. doi:10.1016/j.tibtech.2017.10.011.

[44] Bose A, O'Shea R, Lin R, Murphy JD. A perspective on novel cascading algal biomethane biorefinery systems. Bioresour Technol 2020;304:123027. doi:10.1016/j.biortech.2020.123027.

[45] Bose A, Lin R, Rajendran K, Xia A, O'Shea R, Murphy JD. How to optimize photosynthetic biogas upgrading: a perspective on system design and microalgae selection. Biotechnol Adv 2019;37. doi:10.1016/j.biotechadv.2019.107444.

2 How to optimise photosynthetic biogas upgrading: a perspective on system design and microalgae selection

How to optimise photosynthetic biogas upgrading: a perspective on system design and microalgae selection

Archishman Bose[a,b], Richen Lin[a,b], Karthik Rajendran[c], Richard O'Shea[a,b], Ao Xia[d], Jerry D. Murphy[a,b]

[a]Environmental Research Institute, MaREI Centre, University College Cork, Cork, T23 XE10, Ireland

[b]Department of Civil, Structural and Environmental Engineering, School of Engineering and Architecture, University College Cork, Cork, T12 K8AF, Ireland.

[c] Department of Environmental Science, SRM University-AP, Andhra Pradesh, 522 240, India

[d]Key Laboratory of Low-grade Energy Utilization Technologies and Systems, Chongqing University, Chongqing 400044, China

Abstract

Photosynthetic biogas upgrading using microalgae provides a promising alternative to commercial upgrading processes as it allows for carbon capture and re-use, improving the sustainability of the process in a circular economy system. A two-step absorption column-photobioreactor system employing alkaline carbonate solution and flat plate photobioreactors is proposed. Together with process optimisation, the choice of microalgae species is vital to ensure continuous performance with optimal efficiency. In this paper, in addition to critically assessing the system design and operation conditions for optimisation, five criteria are selected for choosing optimal microalgae species for biogas upgrading. These include the ability for mixotrophic growth; high pH tolerance; external carbonic anhydrase activity; high CO_2 tolerance; and ease of harvesting. Based on such criteria, five common microalgae species were identified as potential candidates. Of these, *Spirulina platensis* is deemed the most favourable species. An industrial perspective of the technology further reveals the significant challenges for successful commercial application of microalgal upgrading of biogas, including a significant land footprint; the need for decreasing microalgae solution recirculation rate; and selecting preferable microalgae utilisation pathway.

2.1 Introduction

2.1.1 Biogas and biomethane

Biogas derived from anaerobic digestion of wet organic materials is a renewable source of energy, with significant importance in future energy systems to reduce greenhouse gas (GHG) emissions from industry, transportation and domestic sectors amongst others [1,2]. Biogas typically comprises 45-70% CH_4, 20-55% CO_2, and other gases, namely, N_2 (0-3%), O_2 (0-1%), water vapour (1-10%), hydrogen sulphide (0-10,000 ppm), ammonia (0-100 ppm), and traces of hydrocarbons, siloxanes and chlorine [3–6]. All gases except methane either lower the calorific value of biogas and/or are considered environmental pollutants, leading to unwanted emissions from their use. Subsequent to a primary cleaning of biogas for the removal of H_2S and other trace compounds, its calorific value can be enhanced by the removal of CO_2, a process termed "biogas upgrading" [5]. The resulting cleaned and upgraded gas is known as biomethane [3,5].

2.1.2 Innovative biogas upgrading technologies including carbon capture and reuse

Strategies for biogas upgrading traditionally entail physicochemical removal of CO_2 [5]. While chemical methods include absorption of CO_2 with solvents or mineral carbonation, CO_2 can be physically separated from biogas by membrane separation, pressure swing adsorption, cryogenic separation among others [7]. Most of these technologies, even though commercialized, continue to suffer from a significant energy penalty (3-6% of the energy content of biogas) and a high cost (up to 30% of the total cost of upgraded biogas) [5,8]. Negative emission technologies are seen as an *essential requirement to allow humanity to meet the Paris and Glasgow Agreements' targets of limiting global temperature rise to 1.5 °C above pre-industrial levels, thus avoiding dangerous climate change* [9,10]. Bioenergy with carbon capture and sequestration (CCS) such as in deep saline aquifers can reduce the CO_2 footprint of biogas systems [11]. However, major limitations of implementing this technology lie in the requirement of high pressures for CO_2 compression (up to 110 bar) and then transportation to the storage site [12,13]. Such elaborate processing often drives up the cost of geological storage of CO_2. In addition, uncertainties including the impact of

geological CO_2 storage on the surrounding water and marine life quality and possibilities of sudden CO_2 release with fatal consequences to marine or terrestrial life are major bottlenecks to the commercialisation of this technology [13,14]. As an alternative, the recycling and reuse of the captured CO_2 are gaining significant focus of the scientific community [15,16]. Numerous pathways are being proposed to use CO_2, either directly, or by conversion to valuable products through chemical conversion processes [17]. In this work, biological biogas upgrading systems integrating microalgae cultivation and production of value-added products has been studied as a potential future solution for cost-efficient upgrading of biomethane. If optimised, it can not only result in an optimised system providing direct CO_2 sequestration on or near-site [7,18], but can also potentially improve the resource utilisation, process performance and flexibility of operation of the overall process over standalone facilities through the integration of suitable technologies [19].

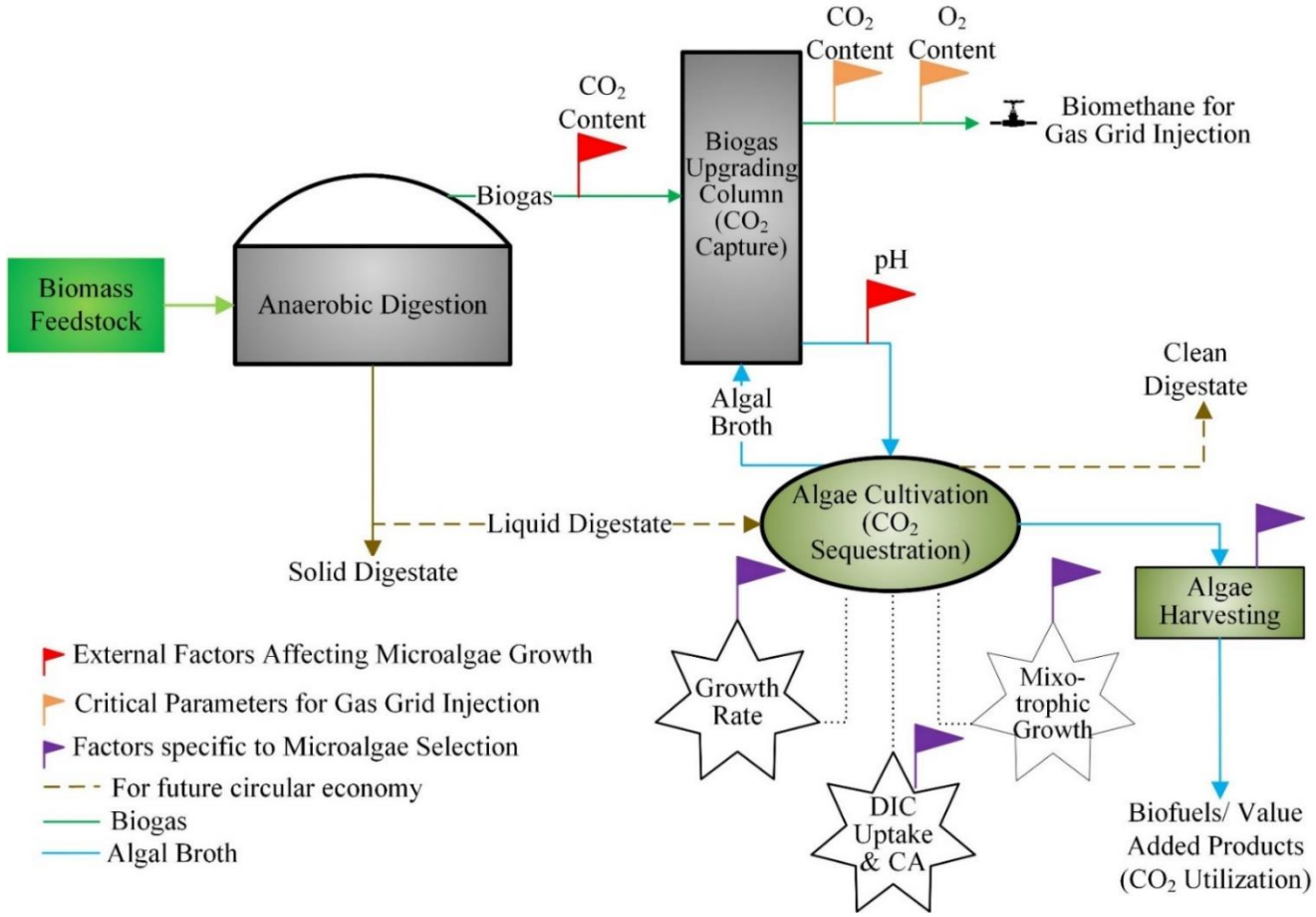


Figure 2-1 Process flow diagram and system configuration for biogas upgrading with microalgae where DIC: dissolved inorganic content; CA: Carbonic anhydrase

2.1.3 Photosynthetic biogas upgrading

A commercial photosynthetic biogas upgrading system must be able to operate continuously while maintaining a CO_2 concentration in the range of 2-6% and an O_2 concentration of lower than 1% in the upgraded biomethane [20]. Low oxygen content is essential to prevent a potentially explosive environment. Nonetheless, oxygen generated during photosynthesis, causing a rise in the O_2 levels in the upgraded biomethane continues to be a major challenge for this biological biogas upgrading process. In addition, other challenges including *1)* low CO_2 mass transfer; *2)* lack of effective control of process parameters including gas and liquid flow rates and pH; *3)* diurnal variability in operations due to photo-autotrophy (absorption of carbon by microalgae, assisted by chlorophyll only in the presence of light); and *4)* intermittent operations from seasonal temperature fluctuations affecting microalgae growth, are significant.

A two-step photosynthetic biogas upgrading process with separate microalgae harvesting step (Figure 2-1) allows each step: *i) Biogas Upgrading* for CO_2 removal to grid injection standards, *ii) CO_2 Sequestration* by fixing the captured CO_2 by microalgae and *iii) CO_2 utilisation* by harvesting microalgae for use in biofuels or chemicals to have its optimisation strategies. In addition, through the selection of microalgae species with specific properties, there can be the opportunity for further optimisation of the system. However, to the best of the knowledge of the authors, simultaneous considerations of both microalgae strain selection and system parameter optimisation for photosynthetic biogas upgrading is rare in the literature.

2.1.4 Novelty and objectives

This paper aims to fill a significant knowledge gap within the photosynthetic biogas upgrading technology. In a novel approach, a perspective on overcoming the identified challenges by optimising different process parameters and selecting the optimal microalgae species considering the intrinsic interlinks with system parameters have been provided. In this regard, the technology of biogas upgrading with microalgae cultivation has been systematically reviewed with an emphasis on the following knowledge, currently limited in literature:

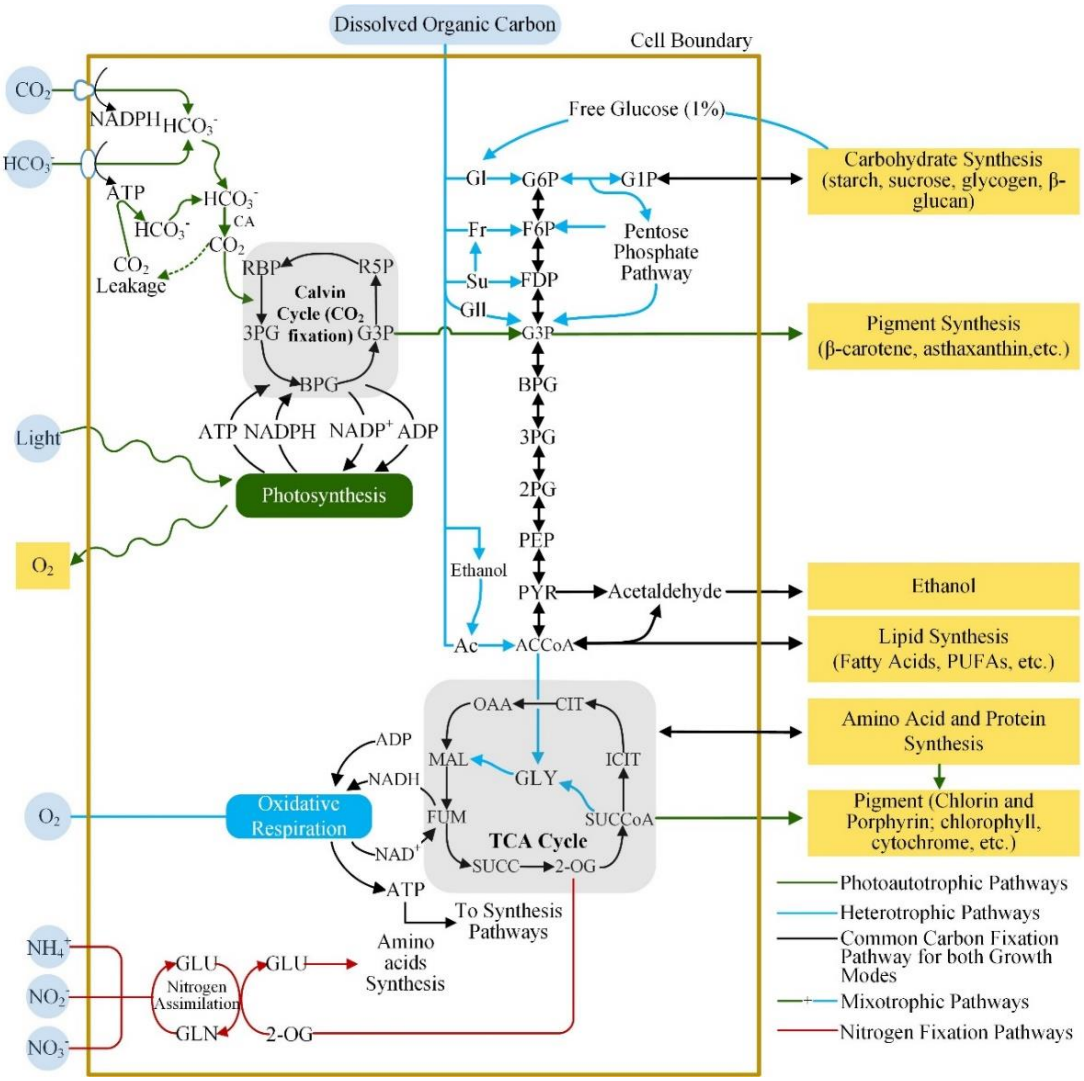
- The crucial factors affecting system performance.

- The essential criteria for selecting the microalgae species.
- Identification of a few common microalgae species suitable for biogas upgrading.
- A broad scale-up perspective of such systems.

2.2 Biological carbon uptake and influence of microalgae choice

2.2.1 Carbon assimilation pathways in microalgae

Microalgal species favouring rapid carbon uptake provide effective carbon fixation via either photo-autotrophic (accept inorganic carbon in the presence of light), heterotrophic (accept organic carbon in presence or absence of light) or mixotrophic (accept inorganic and organic carbon) pathways. Three primary photosynthetic carbon uptake strategies by microalgae can be synthesised as follows: *i)* direct uptake of CO_2 through the plasmatic membrane; *ii)* assimilation of bicarbonates through active transporters on the plasma membrane; and *iii)* using extracellular carbonic anhydrase or CA (a zinc metalloproteinase enzyme associated with the external cell surface of some microalgae) for enhanced conversion of bicarbonates into intracellular CO_2 [21]. The form of dissolved inorganic carbon (DIC) is governed by the pH of the aqueous medium, viz., CO_2 (pH<5); Carbonic Acid (5<pH<7); Bicarbonate ions (7<pH<9); and Carbonate ions (pH>9) [22,23]. Therefore, based on the CO_2 uptake strategy, the native environment of microalgae (freshwater (pH 7), marine (pH 8 to 8.2) and soda lakes (with a high content of sodium salts and a pH of 9.5 and above)), as well as the presence/ absence of external CA and the respective tolerable and desired pH ranges of individual microalgae species can be identified.



Compound abbreviations are summarized as follows: ***2-OG****: 2-oxoglutarate;* ***2PG****: 2-phosphoglycerate;* ***3PG****: 3-phosphoglycerate;* ***R5P****: ribulose-5 phosphate;* ***ACCoA****: acetyl-Coenzyme A;* ***ADP****: adenosine-diphosphate;,* ***ATP****: adenosine-triphosphate;* ***BPG****: 1,3-biphosphoglycerate;* ***CIT****: citrate;* ***F6P****: fructose-6 phosphate;* ***FDP****: Fructose 1,6-biphosphate;* ***FUM****: fumarate;* ***G1P****: glucose-1 phosphate;* ***G3P****: glyceraldehyde-3 phosphate:* ***G6P****: glucose-6 phosphate;* ***GLN****: glutamine;* ***GLU****: glutamate;* ***ICIT****: isocitrate;* ***MAL****: malate;* ***NAD$^+$****: nicotinamide adenine dinucleotide (oxidized);* ***NADH****: nicotinamide adenine dinucleotide (reduced);* ***NADP$^+$****: nicotinamide adenine dinucleotide phosphate (oxidized);* ***NADPH****: nicotinamide adenine dinucleotide phosphate (reduced);* ***OAA****: oxaloacetate;* ***OXA****: oxalosuccinate;* ***PEP****: phosphoenolpyruvate;* ***PYR****: pyruvate;,* ***RBP:*** *ribulose-1,5 biphosphate;* ***SUCC****: succinate;* ***SUCCCoA****: succinyl-Coenzyme;* ***Gl****: Glucose;* ***Fr****: Fructose;* ***Su****: Sucrose;* ***Gll****: Glycerol;* ***Ac****: Acetate*

Figure 2-2 Simplistic schematic representation for inorganic and organic carbon transport for CO_2 accumulation and partitioning pathways in a microalgal cell along with nitrogen fixation pathways [7,24]

In a typical photo-autotrophic mechanism, for species favouring direct CO_2 uptake, carbon fixation occurs via a three-step regenerative cycle, (the Calvin-Benson Cycle) using Adenosine Triphosphate (ATP) (Figure 2-2) [25,26]. For such species, like *Chlorella vulgaris*, a highly alkaline environment would require bicarbonate

uptake using ATP. This in turn would lower its availability for carbon assimilation, and hence decrease both the carbon uptake capacity and growth rate [27]. Extreme alkaliphilic microalgae, on the other hand, are well adapted to grow at a pH >10 with HCO_3^- as the primary inorganic carbon source. Converting bicarbonate to CO_2 by carbon concentrating mechanisms (CCMs) within the cell [28], these species can subsequently fix carbon via the Calvin-Benson cycle. High alkalinity also provides an increased carbon supply, through the rapid scavenging of CO_2 from the atmosphere enabling high growth and carbon fixation rates for most naturally occurring alkaliphilic microalgae [28,29].

Alternate to photosynthesis, some microalgae can assimilate organic carbon, viz., glucose, acetate, etc. both in the presence and in absence of sunlight via the heterotrophic mechanism. However, the uptake of only organic carbon along with the release of CO_2 during dissimilation of organic carbon [30] would limit the application of heterotrophic growth when aiming for CO_2 removal. Mixotrophic organisms can alternate between photo-autotrophic and heterotrophic pathways (Figure 2-2) [21,25]. This not only allows for greater flexibility of carbon assimilation but potentially results in greater carbon uptake and microalgae yield, along with lower photo-inhibition and photo-limitation [25,31]. However, only the genera of *Anabaena*, *Spirulina* and *Synechococcus* (cyanobacteria) along with specific species of other genera have been reported to show mixotrophic growth, as listed in Table 2-1.

2.2.1.1 Microalgae selection criteria 1: Mixotrophic growth

Genera/species able to grow in mixotrophic conditions can provide a significant advantage over other species, especially when wastewater or digestate treatment is combined with biogas upgrading, facilitating the development of circular economy systems. This can be argued from a range of perspectives including; high microalgae growth rate, the economic viability of microalgae biofuel, ability to work well with wastewater or liquid anaerobic digestates (in circular economy system), and the ability to maintain productivity and cell density in the algal culture even during the dark phase. Although CO_2 release during heterotrophic growth would seem non-ideal while removing CO_2 from biogas, operating in a highly alkaline solution would provide considerable buffer capacity by dissolving CO_2 to counteract this effect. This is discussed in detail in the following sections. Indeed, if no wastewater or digestate

treatment is intended, adherence to the criteria would not be essential for microalgae selection.

Table 2-1 CO_2 metabolism pathways for microalgae species/genera.

Autotrophic microalgae genera	**Heterotrophic microalgae genera[*] [35,36]**	**Mixotrophic microalgae genera/ species[#] [37–40]**
Almost all species can grow autotrophically.	*Amphora* *Anabaena* *Ankistrodesmus* *Chlamydomonas* *Chlorella* *Chlorococcum* *Crypthecodinium* *Cyclotella* *Dunaliella* *Euglena* *Nannochloropsis* *Nitzschia* *Ochromonas* *Spirulina* *Synechococcus* *Tetraselmis*	*Anabaena* *Brachiomonas submarina* *Chlorella* spp. *Chlorococcum* sp. *Cyclotella cryptica* *Dunaliella salina* *Euglena gracilis* *Haematococcus pluvialis* *Nannochloropsis* spp. *Neochloris oleubundans* *Navicula saprophila* *Nitzschia* sp. *Ochromonas minima* *Phaeodactylum tricornutum* *Rhodomonas reticulate* *Scenedesmus obliquus* *Spirulina* *Synechococcus*

[*]*Genera refers to the family of organisms below which specific species or sub-species are grouped, usually comprising at least 2 species*
[#]*Species is one particular organism within the family or organisms or genera*

2.2.2 Carbon partitioning

Based on the carbon assimilation pathway and favourable growth conditions, most microalgae exhibit default distribution mechanisms of the photosynthetic and metabolic products such as starch, lipids, proteins, and pigments. This results in distinct and predictive cellular composition, as shown in Figure 2-2 [8,32,33]. However, under variable environments, or so-called stressed conditions, individual species show either dramatically different behaviour (acclimation response) or continue to maintain balanced cell composition (homeostatic response) [21,34]. During biogas upgrading the effect of specific stress conditions on the microalgae

species including exposure to a high CO_2 and/or HCO_3^- concentration need to be studied in detail after a suitable strain selection.

2.3 Biogas upgrading and influence on microalgae choice

A decrease in contact time between the algal solution and the unprocessed biogas is essential to lower methane loss and oxygen contamination of biomethane during biogas upgrading. Direct bubbling of the unprocessed biogas into algal cultures requires significant contact time with the algae solution to ensure sufficient removal of CO_2. Consequently, the oxygen concentration in the biomethane ensuing from such systems was reported to be between 10-24% [41,42]. Alternatively, in a bubble column-photobioreactor configuration (indirect biogas upgrading), as shown in Figure 2-1, the biogas upgrading and microalgae growth can be optimised as two separate processes. This can significantly decrease the contact time between the recirculated algal solution and the biogas. Indirect biogas upgrading can result in a CO_2 and O_2 content in the upgraded biomethane of less than or equal to 6% and 5% as compared to 13% and 32% respectively for direct bubbling of biogas in algae cultivation under similar conditions [43]. Henceforth, only the indirect photosynthetic biogas upgrading process was considered in this paper and further, in this thesis.

2.3.1 Carbonic Anhydrase (CA) promoted CO_2 removal in an alkaline environment

The use of carbonate-rich solutions at pH>9 in a bubble column allows CO_2 to be transferred into the aqueous medium in the form of bicarbonate as shown in Eq. 2.1. Notwithstanding the benefit of the higher dissolution of CO_2 in an alkaline solution, the reaction continues to be relatively slow, with the reaction rate constant (k_{CA}) varying between 2×10^3 and 3×10^5 m^3/kmol-s at temperatures between 293-373 K (20-100 °C) [44,45]. In addition, there are other disadvantages to using a highly alkaline solution for CO_2 absorption, especially when applied to a photosynthetic biogas upgrading system. The overall mass transfer coefficient for oxygen and nitrogen increases with pH [46], leading to increased O_2 content in the resulting biomethane. Furthermore, a high pH also results in phosphorus deposition as phosphates, causing nutrient deficiency in microalgae cultivation [47,48]. Low

nutrients leading to lower growth rates of microalgae would then imply lower carbon fixation, diminishing the sustainability of a photosynthetic biogas upgrading system.

$$CO_2 + H_2O + CO_3^{2-} \rightarrow 2HCO_3 \quad \Delta G \approx -50 \text{ kJ/mol} \ (300K) \qquad (2.1)$$

Enhancing the rate of absorption of CO_2 in an alkaline medium by the application of promoters [49,50] could provide distinct benefits. Not only would this lower the contact time between the biogas and algal solution to reduce the O_2 stripping, but also potentially allow lower pH levels to be employed with similar benefits. Carbonic anhydrase (CA) has recently gained much research interest as an organic promoter due to its *i)* ability to catalyse the reversible CO_2 hydration reaction (Eq. 2.1) in an environmentally friendly way; *ii)* limited influence on the CO_2 vapour-liquid equilibrium and heat of absorption; *iii)* compatibility with conventional CO_2 absorbing substrates including carbonates, amines, as well as with membrane separation processes [51]. Of the different isoforms of the CA enzyme, viz., α, β, γ, δ and ζ, [52] the most widely reported α-CA has a typical k_{CA} value between 1.1×10^8 and 3.5×10^8 m^3/kmol-s [45,53]. CO_2 absorption rates would therefore be significantly increased with the addition of CA. An alkaline algal solution containing microalgae species with external CA activity in lieu of a stand-alone alkaline carbonate solution can thus be hypothesised to enhance CO_2 absorption rates. Indeed, the absence of external CA would require cell rupturing to release internal CA, decreasing the effectiveness of the overall process.

Unfortunately, most of the enzymes are reported to suffer drastic degradation at high temperatures and sustained operation at high pH [51,54]. Moreover, limited literature is available on β and γ-CA, mostly present in microalgae [23]. Most of the experiments have been performed considering pure CA enzymes, with a considerable lack of studies under actual conditions [45]. Therefore, significant research is needed to develop and further the understanding of the catalytic influence and performance of microalgal CA on CO_2 absorption in alkaline carbonate solutions.

2.3.2 Carbonate/bicarbonate cycle for CO_2 capture

CO_2 absorption in the alkaline (carbonate-rich) solution, followed by the transfer of the bicarbonate rich solution for microalgae cultivation is graphically represented

in Figure 2-3. For microalgae uptaking bicarbonate (HCO_3^-) and showing external CA activity, the bicarbonate is incorporated within the cell as CO_2 through dehydration, thus releasing hydroxide represented in Eq. 2.2. The released hydroxide, subsequently increases the pH, allowing carbonate (CO_3^{2-}) regeneration as per Eq. 2.3. The formation of bicarbonate by CO_2 absorption and subsequent regeneration of carbonate from algal activity thus leads to both natural maintenance of the carbonate/bicarbonate cycle and pH regulation. This saves the need for costly equipment and large energy expense for carbonate regeneration.

$$HCO_3^- \xrightarrow{CA} CO_2 + OH^- \quad (2.2)$$

$$HCO_3^- + OH^- \rightarrow CO_3^2 + H_2O \quad (2.3)$$

Dosing with alkanolamines can further enhance the effectiveness of CO_2 removal through additional bicarbonate formation and maintenance of the carbonate/bicarbonate cycle [55]. Nevertheless, the addition of too high concentrations of alkanolamines can inhibit the growth of microalgae. Therefore optimisation between CO_2 capture efficiency and microalgae growth is necessary to employ alkanolamine dosing effectively in photosynthetic biogas upgrading.

2.3.3 H_2S removal and impact on Oxygen in biomethane

Another important contaminant in biogas, H_2S, being acidic, is removed similar to CO_2 by the carbonate-rich solution. At the working pH between 9 and 11, aided by high dissolved oxygen (DO) concentration due to photosynthetic activity, fast sulphate precipitation occurs even in the absence of sulphur oxidising bacteria [56,57] as per the following Eq. 2.4. This additionally prevents the inhibition of algal growth from excess H_2S [42,57].

$$2HS^- + 4O_2 \rightarrow 2H^+ + 2SO_4^{2-} \quad (2.4)$$

Depending on the volume of H_2S in the unprocessed biogas, a fraction of the oxygen would thus be also removed by sulphate precipitation. Indeed, as reported by Bahr et al., (2014) [58], the presence of 1,000 ppm of H_2S in simulated biogas yielded biomethane with 0.5 ± 0.3% O_2, in comparison to 0.7 ± 0.3% O_2 with 500 ppm H_2S.

Therefore, the fraction of H_2S in the unprocessed biogas plays a crucial role in determining the quality of biogas in terms of oxygen content.

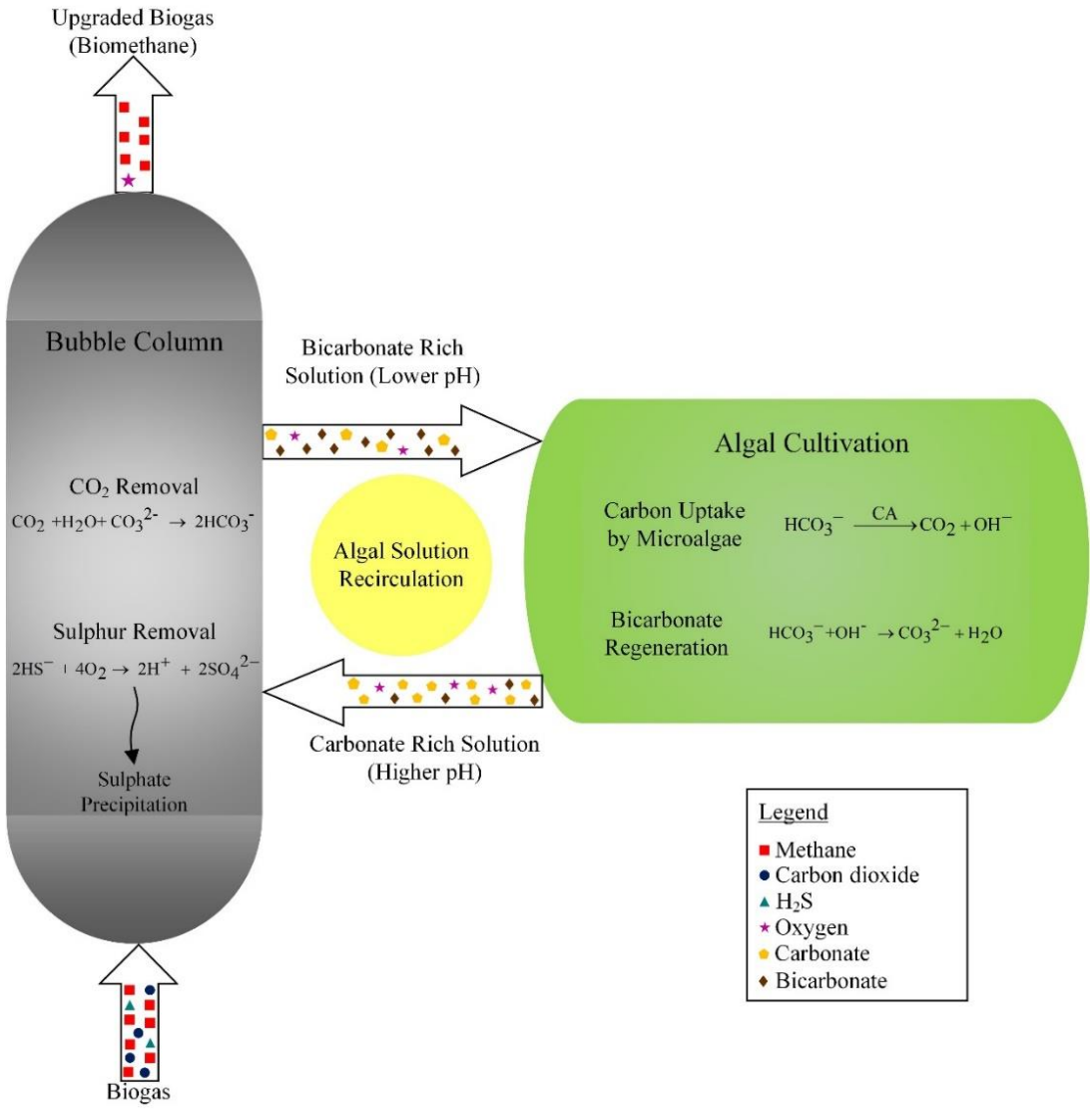


Figure 2-3 Biogas upgrading by microalgae in an alkaline (carbonate) algal solution via carbonate/bicarbonate cycle (The number of markings of each chemical species are indicative only to their relative quantity and not in absolute terms.

2.3.4 Impacts of other trace gases on microalgae growth

No inhibitory impact of methane on microalgae growth has been reported in the literature [59,60]. Nitrogen and hydrogen have limited solubility in water [61], and therefore do not impose a significant stress factor on the overall microalgae growth conditions. Other trace gases (such as siloxanes, ammonia, and chlorine) in biogas are of significantly low quantity to be assumed to have minimal influence on the growth

of microalgae. Indeed, to the best of the authors' knowledge, no study has reported the influence of trace gases on this system of biogas upgrading and microalgae growth.

2.3.5 Microalgae selection to enhance biogas upgrading

2.3.5.1 Microalgae selection criteria 2: High pH tolerance

To withstand a carbonate solution with pH above 9, alkaliphilic microalgae strains uptaking bicarbonates as the primary DIC would be ideal. Alkalihalophilic cyanobacteria, such as *Spirulina* and *Euhalothece* (strongly alkaliphilic), *Synechococcus* and *Anabaena,* (moderately alkaliphilic) are preferable [23,62]. Within the chlorophyte genera species, several strains have recently been identified, which grow well even at pH 10. Most of these strains are native to soda lakes such as *Chlorella sorokiniana* SLA-04 [28], a mutant strain of *Chlorella* sp. AT1 [63] and *Dunaliella salina* NIES-2257 [62]. Alternatively, some freshwater species like *Scenedesmus obliquus* can also tolerate a high pH of 10.6 [64], allowing it to be the dominant species in a mixed culture system for biogas upgrading at a pH of 9.37 [65]. However, the interaction of each species with other cultivation conditions besides pH must be studied in detail to establish the dominant species in a shifting microalgae community [65,66].

2.3.5.2 Microalgae selection criteria 3: External carbonic anhydrase activity

The hypothesised catalytic effect of microalgae species exhibiting external CA activity towards CO_2 absorption in a carbonate solution could significantly improve the overall CO_2 capture efficiency. Thus, either or both the operational pH and the contact time between the biogas and the alkaline solution in the bubble column can be reduced to decrease the oxygen content in the resulting biomethane, while ensuring sufficient CO_2 removal. All cyanobacterium species possess external CA activity, though of different variants of CA strains. Of the chlorophyte genera, *Chlamydomonas reinhardtii*, *Chlorella vulgaris*, *Chlorella sorokiniana* and *Scenedesmus obliquus* among others, display external CA activity.

2.4 Bio-fixation of absorbed CO_2 by microalgae cultivation

2.4.1 Impact of CO_2 concentration in biogas on microalgae growth

To utilise the bio-catalytic effect of microalgae with external CA activity, the species would come in direct contact with biogas near the inlet of the upgrading column as shown in Figure 2-3. Due to the limited contact time, the ability of the species to survive under high CO_2 concentration forms the limiting factor, as opposed to the relative drop in growth in a high CO_2 environment, seen in Table 2-2. *Spirulina*, *Anabaena* and *Synechococcus* can tolerate a 100% CO_2 environment with or without pH control [67,68]. Of the chlorophyte species, *Scenedesmus obliquus* can tolerate up to 80% CO_2, while *Chlorella vulgaris* is completely inhibited at CO_2 concertation beyond 60% [69]. *Chlorella* genera are one of the most versatile in tolerating a high range of CO_2 concentrations with a typical limit of around 40% CO_2 [70,71]. CO_2 acclimatisation can further improve the CO_2 tolerance of microalgae [72,73].

2.4.1.1 Microalgae selection criteria 4: High CO_2 tolerance

The CO_2 concentration in biogas ranges from about 20% to 55%. As such, a high CO_2 tolerating microalgae strain is desirable. Although most CO_2 tolerant species continue to maintain respectable growth under high CO_2 concentrations, external CA activity is inhibited. This leads to a preference for direct uptake of CO_2. Even though this might increase the overall carbon uptake efficiency for strains favouring CO_2, it would be undesirable according to *Criteria 3* (external CA activity).

2.4.2 Impact of bicarbonate concentration on microalgae growth

A pH of 10 could lead to a high bicarbonate ion concentration of up to 1.0 M [8], suitable for alkalihalophilic microalgae. de Farias Silva et al., (2016) [83] reported high productivity of the moderately alkaliphilic cyanobacterium, *Synechococcus* sp. (PCC 7002) of 1.12 g/L/day in a batch process with a bicarbonate concentration of 88 g/L (1.05M), and a pH of 8.5 controlled by HCl addition. Sodium bicarbonate in the range 2-4 g/L (0.02-0.05 M) was found to be optimal for the growth of *Spirulina platensis*, even though, no significant differences were noticed at a concentration of 13.5 g/L [84]. In another study, Kishi and Toda, (2018) [62] reported an optimal bicarbonate concentration of 0.23M (19.3 g/L) for *Spirulina platensis*, a result similar to that reported by Zhu et al., (2018a) [85]. *Dunaliella salina* on the other hand

exhibited optimal growth at a bicarbonate concentration of 0.5M (42 g/L), while *Euhalothece* sp. preferred 1.1M (92.4 g/L) $NaHCO_3$. For the alkali tolerant mutant strain, *Chlorella* sp. STI, high specific biomass productivity of 0.726 g/L/day was recorded at pH 10. For neutrophilic microalgae (species favouring pH between 7.0-8.0), the presence of bicarbonate has been shown to significantly improve the growth rate, and affect the chemical composition, however, at a controlled pH [86,87]. Therefore, the impact of growth and carbon partitioning mechanisms of each species under high bicarbonate and pH conditions would provide essential knowledge on the effective bio-fixation of the captured CO_2 from biogas upgrading.

Table 2-2 High-CO_2-tolerant species of microalgae reported in the literature.

Species	Maximum CO_2 tolerance	Culture concentration at maximum CO_2	Optimum CO_2 level	Culture concentration at optimum CO_2	Reference
Anabaena sp.	100%	NR*	12%	3 g/L after 8 days	[67,74]
Chlorella sp. *(ZY-1)*	70%	0.776 g/L after 6 days	10%	5.772 g/L after 6 days	[75]
Chlorella vulgaris	60%	0.05 g/L after 8 days	5-20%	0.8 g/L after 8 days	[69,76]
Chlorococcum littorale	50%	0.5 g/L after 12 days	5%	c. 84 g/L after 25 days	[77,78]
Euglena graciliis	40%	c. $5x10^6$ cells/ml after 7 days	5%	c. $15x10^6$ cells/ml after 7 days	[79]
Scenedesmus obliquus	80%	c. 0.04 g/L after 8 days	12-15%	0.85 g/L after 14 days; 2 g/L after 20 days	[69,80,81]
Spirulina platensis	100% (with 8.4g/L NaOH)	1.83 g/L after 4 days	12%	c. 4g/L after 20 days	[68,81]
Synechococcus sp	100%	NR	5%	NR	[67,82]

**NR: Not reported*

2.4.3 Carbon balance during bio-fixation of CO_2

Eq. 2.5 is a mass balance of carbon across the closed system starting from biogas upgrading (without digestate treatment). The primary source of inorganic carbon entering the system is the CO_2 in biogas ($M_{C_{BG,in}}$). The right side of the equation

includes inorganic carbon in treated biogas ($M_{C_{BG,out}}$), carbon leaving the system through the liquid effluent ($M_{C_{effl}}$), and carbon lost via stripping or desorption ($M_{C_{stripping}}$). Microalgae sequester a significant portion of the inorganic carbon during the light phase through photosynthesis ($M_{C_{Biom}}$), while a fraction is lost through respiration during the dark phase ($M_{C_{Resp}}$). In addition, carbon can also be accumulated in the liquid phase as DIC, included as $M_{C_{L,acc}}$. Accordingly, an elemental inorganic carbon balance can be developed as shown in Figure 2-4.

$$M_{C_{BG,in}} = M_{C_{BG,out}} + M_{C_{Biom}} + M_{C_{Resp}} + M_{C_{effl}} + M_{C_{stripping}} + M_{C_{L,acc}} \qquad (2.5)$$

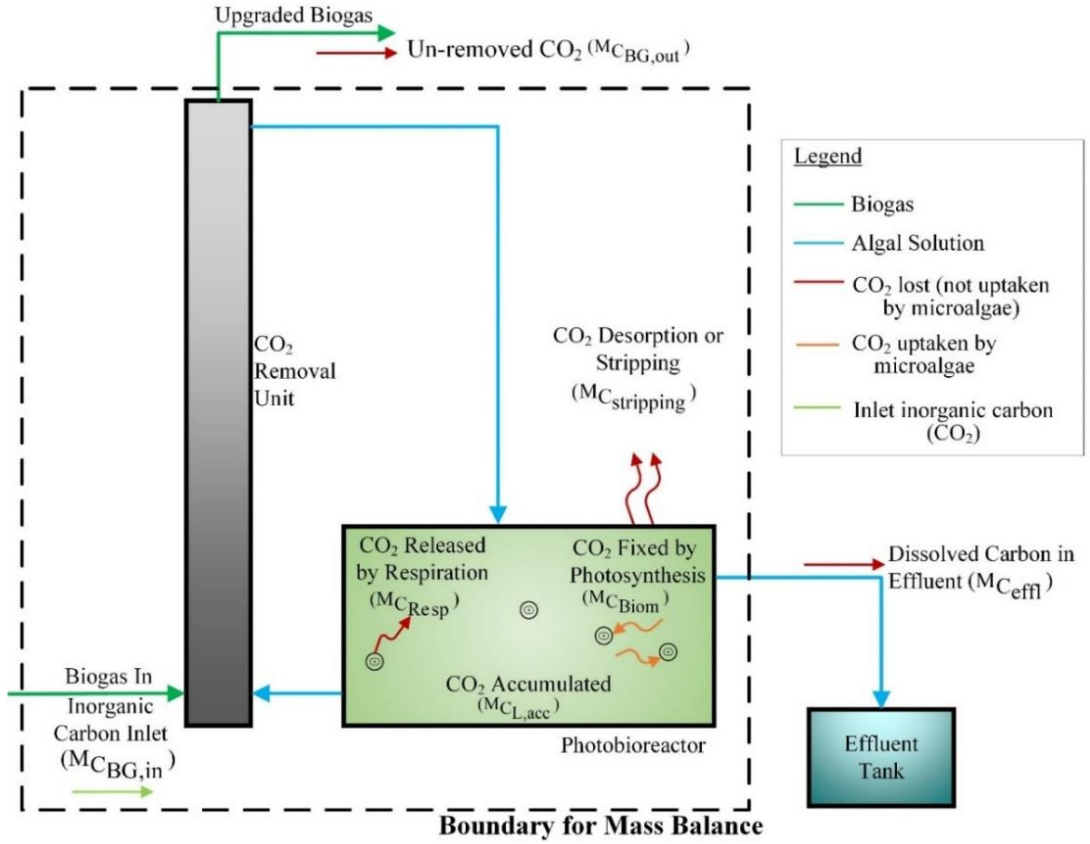


Figure 2-4 Schematic representation of overall biogas upgrading process with microalgae Indicating flow of inorganic carbon for mass balance within the system.

Each of the components can be further represented as a percentage of the total source of CO_2, a review of the values of which is summarized in Table 2-3. On reviewing Table 2-3, for open pond cultivation, desorption or stripping can be concluded to be a prominent contributor to carbon loss. Both the dissolved carbon content and the pH of the medium are important factors in this context. Therefore, except for CO_2 concentrations below 2-5% in the feed gas, high CO_2 uptake by

microalgae is seldom reached. However, the use of closed photobioreactors (PBRs) decreases the CO_2 stripping rate considerably. Unlike other researchers, Marín et al., (2018) [66] reported a complete CO_2 fixation in an open pond environment at an average temperature of 23-24 $^{\circ}$C and a high pH of 9.3-9.7 using a mixed cyanobacteria-chlorophyte culture. However, the results from a similar set-up continued to show low CO_2 fixation rates [88].

A high pH can significantly lower the carbon loss by desorption due to the presence of bicarbonates and also inhibit bacterial and parasitic growth, improving carbon uptake of the microalgae culture [8,89]. However, for open systems with pH higher than the saturation pH corresponding to the dissolved bicarbonate, scavenging of atmospheric CO_2 occurs. Especially at lower bicarbonate concentrations, this leads to an additional supply of inorganic carbon to boost the carbon uptake, although the overall biomass productivity would be lower. This phenomenon was reported by Zhu et al., (2018b) [90], where, increasing the bicarbonate concentration from 0.1 M to 0.7 M caused the carbon uptake efficiency to drop from almost 90% to 40% for the microalgae *Neochloris oleoabundans*. Nonetheless, in absence of desorption, DIC loss through effluent can also be significant. Up to 60-70% of the DIC was found to be lost through the effluent by Meier et al., (2017) [91].

Multiple pathways have been proposed to increase the carbon uptake efficiency of microalgae. By adding 5 mM Triethylamine (TrEAm), the CO_2 fixation rate improved by 39.3% [92]. However, the growth of *Scenedesmus* sp. was hindered at higher TrEAm concentrations. Cheng et al., (2013a) [93] proposed sequential bioreactors in addition to adjusting illumination intensity and nutrient content. The use of such a sequence of reactors increased the CO_2 residence time, also referred to as the empty bed residence time, within the bioreactor. Consequently, a CO_2 fixation efficiency of up to 70.5% was attained while supplying the algal solution with air containing 15% CO_2. Through intermittent lighting at a 10s/10s cycle, a 95% carbon uptake efficiency was obtained as opposed to 56% under continuously illuminated conditions [94]. Nevertheless, such measures are often discrete, requiring further research for industrial applications.

Table 2-3 Summary of CO_2 bio-fixation and losses reported in recent experiments

Microalgae species	CO_2 % in feed gas, $M_{C_{BG,in}}$	Type of reactor and pH	Light/ dark period [h]	% C Uptake by microalgae, $M_{C_{Biom}}$	% C in Biomethane, $M_{C_{BG,out}}$	% Inorganic C lost				Reference
						In effluent $M_{C_{eff}}$	Desorption $M_{C_{Stripping}}$	Respiration $M_{C_{resp}}$	Accumulated $M_{C_{L,acc}}$	
Phaeodactylum tricornutum	100 to 40	Airlift Photobioreactor and pH of 7.6-8.2	10:14	60	NA			NR		[95]
Synechococcus sp.	5	NR	NR	<5%	NA		NR		c. 4%	[96]
Spirulina Platensis	0.04 to 18	Erlenmeyer Flask with pH of 8.26 ± 0.45 to 9.88 ± 0.35	12:12	74 for 0.04% CO_2, 5.52 for 6% CO_2, 1.13 for 18% CO_2	NA			NR		[86]
		Vertical Tubular Photobioreactor, 2 L at pH of 6.83 ± 0.53 to 9.04 ± 0.72		96.8 for 0.04% CO_2, 9.30 for 6% CO_2, 2.48 for 18% CO_2				NR		
		Vertical Tubular Photobioreactor, 4 vL and pH of 6.83 ± 0.53 to 9.04 ± 0.72		99.9 for 0.04% CO_2, 9.15 for 6% CO_2, 3.48 to 18% CO_2				NR		
Scenedesmus accuminatus	5%	1L Erlenmeyer Flasks with pH of 7.4-7.6	24:0	5.71% without TEA	NA			NR		[92]
				7.18% at 5mM TEA addition				NR		
	4%			10.57% at 5mM TEA addition				NR		

Microalgae species	CO_2 % in feed gas, $M_{C_{BG,in}}$	Type of reactor and pH	Light/ dark period [h]	% C Uptake by microalgae, $M_{C_{Biom}}$	% C in Biomethane, $M_{C_{BG,out}}$	% Inorganic C lost				Reference
						In effluent $M_{C_{eff}}$	Desorption $M_{C_{Stripping}}$	Respiration $M_{C_{resp}}$	Accumulated $M_{C_{L,acc}}$	
Scenedesmus obliquus	30-50%	5.3 L Translucent cylindrical plastic tank, at pH of 6.5-8	16:8 average	7.1%	NA			NR		[97]
	15%	Open Cylindrical Glass Tube Photobioreactor	14:10	10.23% at 12 hours CO_2 supply 2.57% at 24 hours CO_2 supply	NA			NR		[98]
Nannochloropsis Oculata	12±2	High Rate Algal Pond with pH between 6 and 7.8	12:00	71.4 to 35.6%	NA			NR		[99]
	Air	Bubble Column Photobioreactor at pH of 7-8	12:12	30-55%	NA			NR		[100]
Neochloris oleoabundans	HCO_3^- Medium, 0.1-0.7M	Erlenmeyer flask and variable pH	24:0	c. 88% at 0.1 M of HCO_3 (pH 9.5); c. 40% at 0.1 M (pH 10.1);	NA			NR		[90]
Chlorella vulgaris	15%	Closed raceway pond with paddle wheel and pH between 6.18 ± 0.14 and 7.22 ± 0.05	24:0	56% with Continuous gas sparging	NA			NR		[94]
				95% with intermittent gas sparging of 10s at an interval of 10s	NA			NR		

Microalgae species	CO_2 % in feed gas, $M_{C_{BG,in}}$	Type of reactor and pH	Light/ dark period [h]	% C Uptake by microalgae, $M_{C_{Biom}}$	% C in Biomethane, $M_{C_{BG,out}}$	% Inorganic C lost				Reference
						In effluent $M_{C_{eff}}$	Desorption $M_{C_{Stripping}}$	Respiration $M_{C_{resp}}$	Accumulated $M_{C_{L,acc}}$	
	4%	Airlift Photobioreactor at pH of 7.0	12:12	13.8- 4% as per gas inlet velocity	NA			NR		[101]
	15%	Perforated inverted arc trough (PIAT) inserted into flat plate Photobioreactor	NR	Fixation rate of 36.6 $mgCO_2\,L^{-1}\,h^{-1}$, an increase of 26.2% over conventional flat plate Photobioreactor	NA			NA		[102]
Chlorella sp.	2%	Cylindrical glass Photobioreactor at pH of 6.4		58%	NA			NR		[1033]
	15%			16%	NA			NR		
	5%	Bubble Column Photobioreactor and pH of 5.6	24:0	28 ± 1.2%	NA			NR		[104]
Chlorella PY-ZU1	15%	Sequential Bubble Column Photobioreactor and pH between 5.5 and 7	24:0	50.31% at 10 min empty bed residence time	NA			NR		[93]
				70.48% at 140 min empty bed residence time	NA			NR		
Chlorella sorokiniana	32.0 ± 1.9%	Photobioreactor connected to bubble	Light phase	19%	11%	13%	57%	NA	NA	[91]

Microalgae species	CO_2 % in feed gas, $M_{C_{BG,in}}$	Type of reactor and pH	Light/ dark period [h]	% C Uptake by microalgae, $M_{C_{Biom}}$	% C in Biomethane, $M_{C_{BG,out}}$	% Inorganic C lost				Reference
						In effluent $M_{C_{eff}}$	Desorption $M_{C_{Stripping}}$	Respiration $M_{C_{resp}}$	Accumulated $M_{C_{L,acc}}$	
		column at average pH between 7.3-7.4	Dark Phase	0%	7%	-	60%	3%	30%	
Picochlorum sp. and *Halospirulina* sp. mixed culture	29.50%	High Rate Algal Pond connected to absorption column (AC) at pH between 9.3-9.7	12:12	7%	6%	71%	5%	NR	11%	[88]
			24:0	27%	11%	52%	4%	NA	6%	
Phormidium sp. (71%), *Oocystis* (20%) and *Microspora* sp. (9%) Mixed Culture	30%	Indoor HRAP connected to absorption column (AC) at pH between 8.1 ± 0.1	24:0	9 ± 2%	40%	1%	49 ± 5%	NR	NR	[105]
Nannochloropsis gaditana.	28 ± 2%	Indoor HRAP connected to absorption column (AC) and pH between 7.5 and 8	24:0	81%	6%	14%		NA		[43]
Mixed Cyanobacteria-Chlorophyta culture including *Leptolyngbya lagerheimii* (54%) and *Chlorella vulgaris* (28%)	29.5%	Outdoor HRAP connected to absorption column and pH between 9.4-.6	14:10	47 ± 2% at an average temperature of 15.3 ± 7.3ºC	NR	NR	53%	NR	NR	[66]
			12:12	100% at an average temperature of 23.4 ± 3.8ºC			NA			

NA: Not Applicable; NR: Not Reported

2.5 System design for biogas upgrading by microalgae

The complete photosynthetic biogas upgrading system (as illustrated in Figure 2-1 with detail in Figure 2-3) can be divided into four fundamental components, namely (1) the *Absorption Column* for biogas upgrading, (2) the *Bioreactor* for microalgae cultivation followed by (3) the *Microalgae Harvesting System* and (4) *Accessories dedicated to the above three systems including pumps and automation systems*.

2.5.1 Absorption column

2.5.1.1 Gas-sparged bubble column

Conventional removal of CO_2 in alkaline or amine solution commonly employs packed columns in a counter-current mode. However, while utilising algal solutions directly for biogas upgrading, the packed bed column may suffer from clogging [46], resulting in high operation and maintenance costs. A similar performance is achieved by the gas-sparged multi-phase bubble column without any packing [58]. Typically, the alkaline algal liquid acts as the dispersed medium, with biogas sparged from the bottom of the column. This results in a high mass transfer rate through efficient mixing removing the requirement for moving parts [59,106].

The homogeneous flow regime provides preferential operating conditions for CO_2 absorption. More uniform flow and smaller bubbles developed in this regime allow for a larger surface area and improved performance [106,107]. For a homogeneous flow regime, assuming similarity with air-water systems, the superficial gas velocity should always be below 4 cm/s at ambient temperature and pressure [108,109]. This minimises the influence of the sparger design, [110] and reduces bubble coalescence, breakage and collision [111]. The presence of microalgae as the solid phase inside the bubble column improves the CO_2 absorption rates further by increasing the gas hold-up and mass transfer rates [112]. This is due to the increased specific contact area of bubbles through the modification in surface tension and bubble breakage from the collision between the gas and the dispersed phase [108,112].

2.5.1.2 Comments on absorber column design and research gaps

Reported studies for indirect CO_2 removal by microalgae in an external column are summarized in Table 2-4. As can be seen, most columns have been operated at a superficial gas velocity well below 4 cm/s together with a liquid velocity much below 4 cm/s. As for the flow configuration, despite favouring higher gas hold-up, the counter-current configuration was reported to suffer significant drawbacks. A drop in pH from 10.2 to 9.5 led to lower microalgae growth and associated CO_2 removal. In combination with the clogging of gas spargers from sulphur deposition, biomass accumulation was observed at the top of the column. In addition, growth of invasive non-photosynthetic cyanobacteria at the bottom of the column and greater stripping of the dissolved oxygen due to increased gas hold-up has been observed for the counter-current mode operation [59]. Thus, the co-current configuration has generally been preferred.

Significant increase in CO_2 removal alongside ensuring a lower O_2 content in the upgraded biomethane can be achieved by optimising the pH of the recirculating liquid (algal solution) and the liquid to gas flow (L/G) ratio. As can be observed from the results of previous studies, compiled in Figure 2-5, CO_2 removal is significantly improved above pH 9, irrespective of the L/G ratio. As high as 98% CO_2 removal efficiency was obtained at a constant pH of 10.2. However, this fell to 96% at a pH of 9.5 [59]. Similar CO_2 removal rates of 95-96% were reported between pH 9.3-9.7 [66,88,113,114]. In contrast, for lower pH ranges, an L/G ratio of greater than 15 was required to ensure a CO_2 removal efficiency of over 90% [115]. H_2S removal in most cases has been reported to be almost 100% at a pH over 9 irrespective of the L/G ratio [59,88,116].

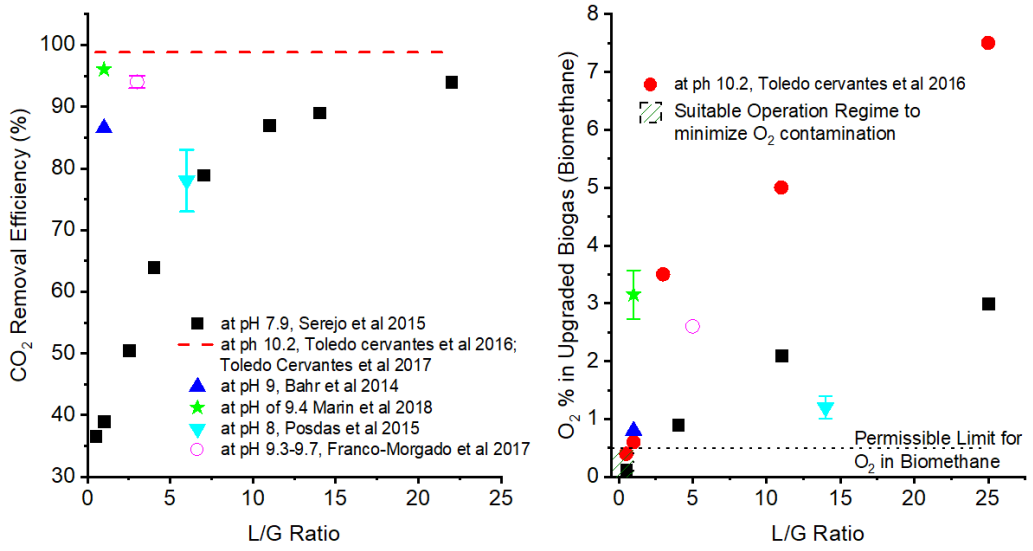


Figure 2-5 Influence of pH and L/G ratio on the mass transfer performance of the absorber column.

A higher L/G ratio causes greater O_2 stripping into the upgraded biomethane, with this effect amplified at higher pH. Therefore, for the same L/G ratio, O_2 content in the biomethane can be observed to be much higher at a pH of 10.2 than at a pH of 7.9 (Figure 2-5). Toledo-Cervantes et al., (2017b) [59] advised the use of an L/G ratio lower than 1 to ensure oxygen content in biomethane meets grid injection standards at a high pH of 10.2 (Figure 2-5). However, using the same L/G ratio of 1, Marín et al., (2018) [66] reported an O_2 concentration of 3.15 ± 0.42% in the upgraded biomethane during year-round operations with an open algal pond. Interestingly, unlike the L/G ratio, which was the same for both the studies, a higher liquid flow rate, as well as different microalgae species were used. In a similar study, at a much lower pH (c. 6.5) and ~~an~~ at an L/G ratio of 5, Meier et al., (2017) [91] reported the O_2 content of lower than 1% in the upgraded biogas while the corresponding CO_2 varied between 2 and 4% respectively during light and dark cycles.

Research gaps for absorption column design can be identified as follows:

- **Impact of pH at a constant L/G ratio, but variable liquid and gas flow rates** have not been reported in any literature for the biogas upgrading purposes by algal liquid.

Table 2-4 Details of absorption columns used in experiments for biogas upgrading with microalgae.

Column Type	Column dimensions				Liquid Flow		Gas Flow				Sparger					
	H_c [cm]	D_c [cm]	H_c/D_c	V_c [L]	Flow rate, L [ml/s]	u_L [cm/s]	Flow rate, G [ml/s]	u_G [cm/s]	L/G	Mode	Type	d_0 [mm]	pH	CO_2 in supplied biogas	CO_2 in upgraded biomethane	Reference
Bubble Column	NR	NR	NR	2.5	0.833	NR	0.833	NR	1	C	MD	NR	9.1-9.9	29.5%	< 2% at higher pH	[114]
	NR	NR	NR	2.5	0.416	NR	0.833	NR	0.5	C	MD	NR	10	29.5%	0.6% - 1%	[113]
	NR	NR	NR	150	31.778-268.333	NR	39.722-116.667	NR	0.8-2.3	CC	PP	NR	9.05-9.50	31.5 ± 1.1%	2.7 ± 0.1% (pH 9.5) to 12 ± 0.0% (pH 9.05) for L/G ratio 0.8;	[117]
	NR	NR	NR	2.5	≤1.1	NR	1-3.6	NR	≤1.1	C	MD	NR	8.5-10	29.5%	1.5% at the highest gas flow rate	[118]
	NR	NR	NR	150	91.33-446.25	NR	76.111-127.5	NR	1.2-3.5	CC	PP	NR	7.3-8.9	32.7 ± 2.8	0.3 at L/G 3.5	[119]
	165	4.4	37.5	2.5	0.68	0.045	1.361	0.089	0.5	C	NR	NR	7.5-11	29.5%	0.3±0.1% to 23±0.9% from high to low pH	[120]
	165	4.4	37.5	2.5	0.867	0.057	0.867	0.057	1	C			9.4	29.5%	0.7% to 11.9%	[66]
	165	4.4	37.5	2.5	1.734	0.114	0.867	0.057	2	C	MD	0.002	8.8-9.8	29.5%	1.5% to 14.25% from high to low pH	[121]
	165	4.4	37.5	2.5	Varies	Varies	0.667	0.044	0.3-1	C			10.2 ± 0.5	29.5%	0.35%	[59]
	3000	1.2	250	NR	0.347	0.307	0.579	0.512	0.6	CC	NR	NR	7.3	32.0 ± 1.9%	2-4% between light and dark cycles respectively	[91]
	80	1.9	42.1	NR	1.274	0.449	0.2545	0.089	5	C	PS	NR	9.5	30%	1.5% to 4.5%	[88]
	NR	1.9	NR	0.35	0.031	0.011	0.181	0.064	8.43	CC	NR	NR	9.37	30%	NR	[65]

Column Type	Column dimensions				Liquid Flow		Gas Flow				Sparger		pH	CO_2 in supplied biogas	CO_2 in upgraded biomethane	Reference
	H_c [cm]	D_c [cm]	H_c/D_c	V_c [L]	Flow rate, L [ml/s]	u_L [cm/s]	Flow rate, G [ml/s]	u_G [cm/s]	L/G	Mode	Type	d_0 [mm]				
Packed Column	165	4.4	37.5	2.5	Varies	Varies	Varies	Varies	0.05-60	C			10 ± 0.3	29.5%	0.3% to 0.4%	[46]
	165	4.4	37.5	2.5	5.499	0.362	0.514	0.034	10.7	C	MD	0.002	8	29.5%	5% to 7.4%	[122]
	165	4.4	37.5	2.5	Varies	Varies	Varies	Varies	0.5-67	C			7.9	29.5-30%	Varies between 3% and 18%	[115]
	220	2	110	0.7	0.055	0.014	0.024	0.006	2.33	CC	NR	NR	7.7 ± 0.2	30%	13% CO2	[43]
	50	4.5	11.1	0.8		0.027 - 0.106	0.833	0.052	0.4-1.6	CC	NR	NR	7-10	30%	24% to lower than 0.5% at pH 10	
	50	4.5	11.1	0.8		0.027 - 0.106	0.833	0.052	0.4-1.6	CC	NR	NR	7-10	30%	No removal at pH 7 to lower than 0.5% at pH 10	[58]

H_c: Bubble Column Height; D_c: Bubble Column Diameter; V_c: Bubble Column Volume; u_L: Liquid Superficial Velocity; u_G: Superficial gas velocity; d_0: sparger diameter; C: Co-current flow; CC: Counter-current flow; MD: Metallic Diffuser; PP: Polypropylene diffuser; PS: Porous Stone

- **Impact of gas/liquid velocity at a constant L/G ratio:** Even for a constant L/G ratio, a higher gas velocity would be required for industrial scale-up of the present technology. This is essential to maintain sufficient residence time at a considerable column height. Based on recent experiments, a low gas flow rate of c. 0.05 cm/s would require an extremely high volume of bubble columns and be a severe limitation, unless optimised. There is a need to decrease the empty bed residence time (time required by gas to rise through the column in case of no liquid) to around 3-6 minutes, typical values similar to those for aerobic or anoxic biotrickling filters [58], allowing industrial scale-up.

- **Impact of photosynthetic activity and algae concentration** on the overall biogas upgrading remains to be studied as a potential optimisation strategy. A higher photosynthetic activity results in higher dissolved oxygen, which, in turn, has shown to increase the oxygen content in the upgraded biogas [82]. It should also be noted that in most of the studies, algae solution after harvesting is recirculated into the bubble column, and hence the effect of the presence of microalgae on CO_2 removal could seldom be established.

- **Influence of CO_2 content in the biogas** on determining the overall system operations has also been scarcely reported.

2.5.2 Photobioreactor design

To optimise the sequestration of the captured carbon, an ideal photobioreactor should be able to provide a sufficient residence time of the dissolved carbon through the matching of microalgae growth parameters with the CO_2 absorption rate [108]. This can be achieved by controlling multiple factors, widely reviewed in the literature [123-125]. Simultaneous optimisation of both light intensity and frequency of light and dark cycles for each microalgae species is crucial to improve its growth rate [124,126]. Minimisation of the light path by a superior surface to volume ratio, preventing a significant drop in light intensity, would further aid algal growth [127]. The adequate light intensity can be further controlled by maintaining the culture concentration of microalgae, thus preventing increased light scattering and the creation of dead zones [123]. This, in turn, would enable optimal uptake of carbon and nutrients from the medium [123]. In addition, each species has a preferable

temperature and pH domain [123], as well as the requirement of essential nutrients including macro-elements (such as C, N, P, S and Cl), mineral elements (K, Ca, Mg, Na), micro-elements (Fe, Mn, Zn, Cu, B, Mo, Si, Se, V, Co, Ni and I) and/or other additives to ensure effective growth rates [7,128].

For photosynthetic biogas upgrading, a highly alkaline solution with a high bicarbonate concentration would result. This would therefore lead to significant loss of ammonia by stripping [47,129] and phosphorus through deposition of salts of calcium and magnesium [47,48]. Indeed, as high as 17% of nitrogen was reported to be lost through stripping at a pH of 10 from a high rate algal pond [47]. In other studies, Marin et al. (2021) [114] observed nitrogen and phosphorus fixations of less than 50% at pHs above 9.8. Franco-Morgado et al., (2017) [88] reported fixation of c. 50% of nitrogen and only c. 15% of phosphorus by biomass while operating a continuously lit photobioreactor. However, this fell to 13% and 4% respectively while operating the bioreactor over a 12-hour light/dark cycle. Such optimisation is possible by effective mixing, often performed via mechanical agitation by impeller or static mixer in a predominantly bicarbonate medium [109]. Efficient mixing would also ensure uniform pH, nutrient distribution, temperature gradient, necessary DIC and DO concentration and adequate mass transfer rates throughout the medium. In addition, cell clumping and sedimentation, the formation of dead zones, and the attachment of microalgae to the photobioreactor walls could also be avoided [124,130]. Nonetheless, care must be taken to prevent cell damage from excessive mechanical stress on the fragile microalgae from excessive mixing [124,131].

2.5.2.1 Raceway ponds

Artificial open ponds, often referred to as High Rate Algal Ponds (HRAP) are a low-cost, easy to operate and highly effective technology for large scale cultivation of microalgae [124,132]. CO_2 from biogas captured as bicarbonate in the highly alkaline solution means that a separate CO_2 sparging system into the open pond may not be necessary. This can further ease the design and operation of open ponds for microalgae cultivation along with biogas upgrading. However, there are significant disadvantages. These include a high land footprint; difficulty to maintain optimum operation conditions; contamination from invasive species, bacteria and viruses [7,132]. Even though a higher pH can lower the CO_2 desorption rate, as well as contamination by

invasive species, the increased loss of nitrogen would continue to be considerable limitations for coupling HRAP with biogas upgrading.

2.5.2.2 Photobioreactors

As a substitute to raceway ponds, PBRs allow for significant improvement in culture conditions and microalgal biomass density; up to 5-6 times higher than that of open raceway ponds [125]. Yearlong operation at optimised conditions could thus be achieved. Traditionally, four PBR configurations have been recommended for scalability and suitability for mass cultivation [124,133], simplistic sketches of which are provided in Figure 2-6. Recently, the Bicarbonate-based Integrated Carbon Capture and Algae Production System on Ocean (BICCAPSO) using horizontal floating PBRs have been proposed as a low-cost alternative for large scale microalgae cultivation [76]. The waves and the surrounding water would provide necessary mixing and cooling, while aqueous bicarbonate solution could be economically supplied via ships or water pipelines [76,134]. Indeed, the use of bicarbonate and alkaliphilic microalgae would benefit the integration of the BICCAPSO technology with photosynthetic biogas upgrading. However, mixing and temperature control due to variable wave characteristics, as well as fouling inside and outside the PBR are major challenges [134]. Further drawbacks include lower ocean temperatures in colder climates inhibiting microalgae growth and the need for significant logistics for continuous transport of aqueous bicarbonates over long distances; these must be overcome to allow successful application of the BICCAPSO technology with photosynthetic biogas upgrading.

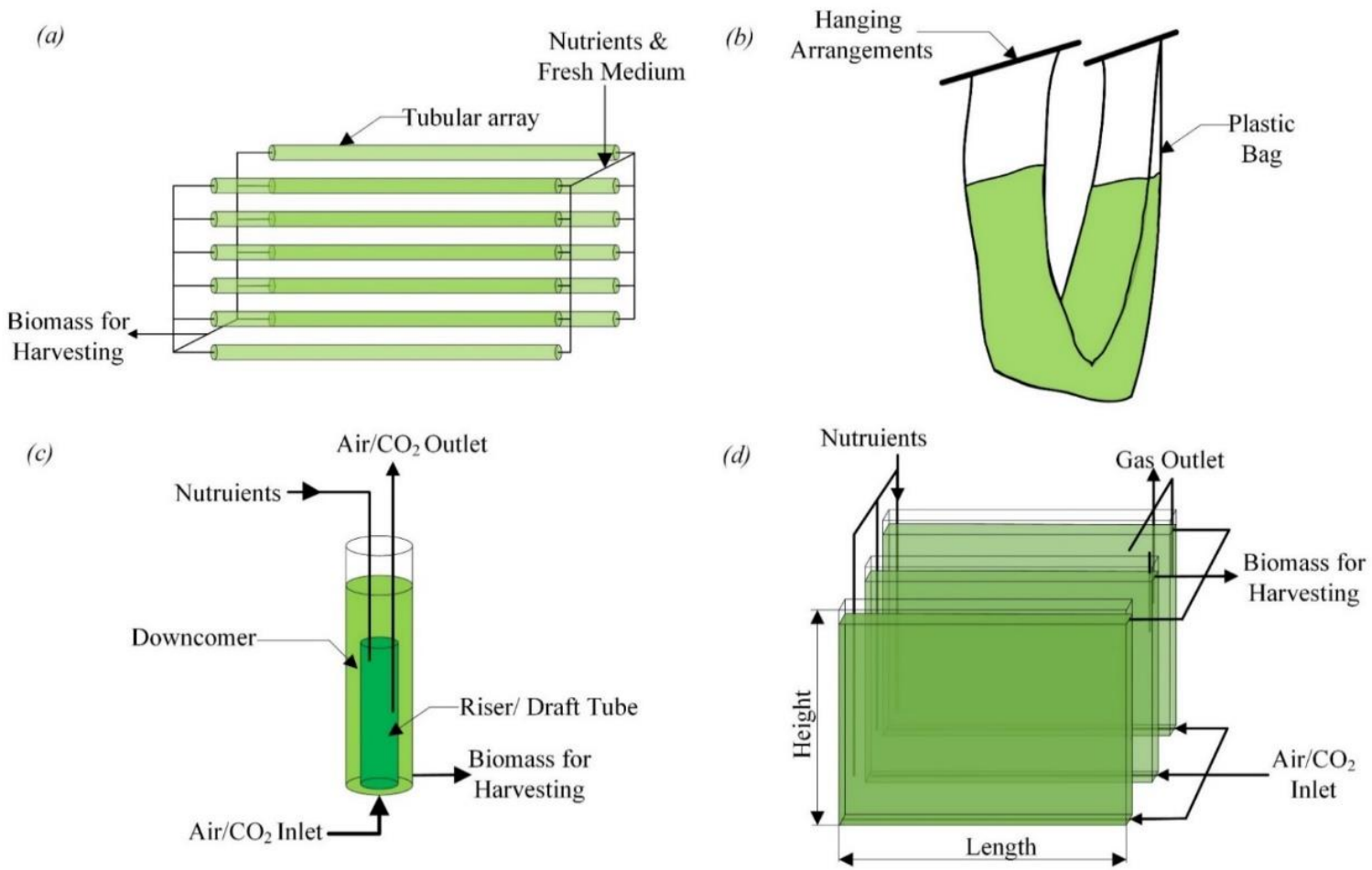


Figure 2-6 Simplistic schematic representation of closed photobioreactors, (a) Horizontal Tubular photobioreactor; (b) Plastic Bag photobioreactor; (c) Air-lift Bubble Column photobioreactor; (d) Flat Plate photobioreactor.

Table 2-5 Comparative summary of closed photobioreactors for mass cultivation [123,124,135-138].

Points of comparison	**Types of photobioreactors**			
	Tubular PBR	**Plastic Bag PBR**	**Column Airlift PBR**	**Flat Plate PBR**
Temperature Control	Low-temperature control; difficulty in cooling during summer.	Depending on the size of the bag, effective control of temperature may or may not be obtained.	Effective temperature control can be achieved with proper design.	Ease of temperature control by water spraying in summer or immersion in a water bath and through internal heat exchangers in winter
Light Control	Photo-limitation is a common phenomenon, especially for larger diameter tubes.	Photo-limitation is a major problem due to the distortion of bags.	Optimisation of column diameter is needed to ensure adequate light control across the cross-section of the reactor and prevention shading	High surface to volume ratios, leading to high light intensity control. However, needs to be optimally placed to avoid shading.
Effective Mixing and Mass Transfer	Reactors with long tubes encounter mass transfer and mixing problems.	Inadequate mixing, requiring an aerator.	Efficient mixing and mass transfer at low shear stress on the cells.	Efficient mass transfer and mixing at low shear stress on the cells.
pH control	Difficult due to poor mixing	Difficult due to poor mixing	Good pH control	Effective control of pH is achieved.
Surface to Volume Ratio (Illuminated)	High	Low	Moderate	High
Robustness	A robust system that can be operated both indoors and outdoors.	Frail, prone to leakage and has a short lifespan.	Robust design, however within material limits.	Extremely robust in design
Materials of Construction	Glass or plastic tubes are the most common materials.	Plastic bags, usually polyethene.	Mostly glass.	Both glass and plastic can be used.
Capital Costs	High	Low	High	High (with glass).
Operational Costs and primary issues	Cleaning is the major challenge, especially the inner walls of the	Frail systems and poor mixing result in high recurring costs.	Difficulty in cleaning leads to a higher operating cost.	Low operational cost. The cost of cleaning can be significantly

Points of comparison	Types of photobioreactors			
	Tubular PBR	**Plastic Bag PBR**	**Column Airlift PBR**	**Flat Plate PBR**
	tube, raising the operating cost.	The disposal of plastic bags is also a major issue.		reduced based on effective design
Power Requirements	Power requirement is high	Low power requirements.	Low Power Requirement	Low power requirement, however, is based on the type of cooling.
Present industrial applications	Industrial application for high-value products, but with limited application for CO_2 capture and fuel production	Widely used and limited to small-scale cultivation and pilot-scale projects.	Presently confined in lab scale, up to 300L due to difficulty in scalability.	Both academic and industrial-scale applications have been widely performed

Among the four traditional PBRs shown in Figure 2-6, and compared in Table 2-5, plastic bag PBRs are the least favoured for large-scale cultivation. Both the tubular and the bubble column PBRs are major candidates for wide-scale industrial application, however, subject to significant challenges, as summarised in Table 2-5. Currently, only tubular and flat-plate photobioreactors are used for the commercial cultivation of algae for the production of high-value chemicals in facilities in Germany and Israel and the Czech Republic respectively [139]. Column air-lift photobioreactors, although yet to be commercialised are being subjected to large-scale experiments in China [139]. Flat plate photobioreactors show several advantages including a high surface to volume ratio, superior efficiency, easy operation, and robustness. This, added with a low reactor thickness results in 5 to 20 times more yield than other closed PBR systems [125]. Novel configurations like the Thin-film Flat Plate PBR are being developed to further lower the cost and improve the scalability of the Flat Plate PBRs further [140]. However, the need for use of costly materials, together with the requirement of optimally spacing the flat plates to minimise shading between the reactors increases the cost and land footprint, thus limiting the cost-benefit and scale-up of such reactors.

2.5.2.3 Hybrid configurations

To incorporate the relative advantages of both closed photobioreactors and open ponds, and hence improve the PBR performance, several hybrid photobioreactor configurations have been proposed. A multi-layered stacked hybrid bioreactor [141] has been studied to provide a large cultivation area within a small footprint while maintaining most other beneficial operation parameters for photobioreactors. However, no large-scale system of such configuration has yet been reported. Jesus and Filho, (2017) [142] proposed a concentric draft tube stirred airlift photobioreactor. The stirring speed was suggested as a major factor to influence the growth and composition of the microalgae. García-Galán et al., (2018) [143] developed a full-scale hybrid HRAP– tubular photobioreactor system in Tarragona, Spain, where horizontal arrays of tubular PBRs were connected between two HRAPs on either end. Even though batch tests showed culture productivity of 68.1-82.9 mg/L/d for a retention time of 4 days, the continuous experiments in a full scale resulted in only 13.8 mg/L/d in winter, and 74.4 mg/L/d in summer for a retention time of 16 days. Hence both the design and operation optimisation of such reactors are necessary to ensure the full potential of such hybrid systems.

2.5.2.4 Comments on bioreactor design and research gaps

Of the different photobioreactor designs employed in cultivating microalgae after carbon capture from biogas, HRAPs are the most preferred (Table 2-6). All the studies reported so far have been on a lab scale, highlighting the low technology readiness (TRL) of the present technology. In fact, Marín et al., (2018) [66] and (2021) [114] conducting experiments in Valladolid, Spain, reported no biomass growth during the winter period at an average temperature of 9 ºC. This caused a much lower concentration of biomass (around 55 mg Total Suspended Solids (TSS)/L) a clear decrease from the inoculated concentration of 210 mg TSS/L [66]. In both the studies, the CO_2 removal efficiency correspondingly dropped from over 96% in summer (average temperature 24 ºC) to less than 90% in winter (average temperature 9 ºC). The mean daily productivity in open ponds did not significantly vary between experiments. Nevertheless, based on the type of microalgae, a significant variation in culture density was obtained (Table 2-6), with the highest 2.6 g dry weight (DW)/L from *Mychonastes homosphaera* [144]. A lower average cell density obtained from

Spirulina cultivation was reported at 1.2 gDW/L by Bahr et al (2014) [58] while using a light intensity of 80 µmol/m^2-s. Indeed, this indicates scope for optimisation of culture conditions. As an example, Kebede and Ahlgren, (1996) [145] reported photo-inhibition of *Spirulina* at a light intensity of around 300 µmol/m^2-s while it was found to be 432 µmol/m^2-s by Toor et al., (2013) [146]. Based on the above considerations, the following can be identified as the significant research gaps concerning photobioreactor design for the present technology:

- **Selecting microalgae and optimising culture conditions:** Only a few studies [58,59,66] have used cyanobacteria species favouring high pH for assessment of their optimal growth. In contrast, most other studies have either utilised freshwater chlorophyte species (*Chlorella* sp.) or a consortium of microalgae and cyanobacteria favouring a neutral pH [56,88,91,115]. However, even for those, the optimisation of culture conditions has not been critically considered, leading to a considerable research scope in future.

- **Choice of Photobioreactor:** With the exception of Meier et al., (2017) [91], open HRAP was selected as the bioreactor, either indoors or outdoors. Indeed, a comparison of results in Table 2-6 reveals cell density decreases significantly in outdoor culture, even with similar mean daily productivity and similar inoculation. None of the potential closed PBRs discussed above or a hybrid system has so far been applied to microalgal biogas upgrading. Indeed, the evaluation of the closed PBRs under a controlled environment for yearlong operation, especially in colder climates is urgently needed to expand the applicability of microalgal biogas upgrading worldwide.

Table 2-6 Summary of Photobioreactors types and operational details for microalgae cultivation with simultaneous biogas upgrading.

PBR Type	PBR Details			Operation Details						Biomass Productivity			References
	V_R (L); A_{lll} [m^2]	Dim. [cm]	Mode	T_R [°C]	L.I. [µmol/m^2-s]	L:D	W_{comp} [L/d]	[DO] [mg/L]	pH	Inoculation [mg TSS/L]	r_{evap} [L/m^2/d]	B_{mean} [g/m^2/d]	X_{avg} [mg/L]	
Outdoor HRAP	180 and 1.2	15x82 x170	C	-4 °C - 40 °C in different stages	c. 150 (winter days); 600-900 (summer days)	Natural cycle	NR	7.7-10.6 (morning); 7.3-12.8 (afternoon)	9.1-9.9	*Mychonastes homosphaera* (82%), *Pseudanabaena* sp. (17%) and *Scenedesmus* sp. (1%)	< 2 in winter; > 5 in summer	0-15	0.3 (winter) 1.34 in (summer)	[114]
				24.2 ± 2.0	25.5 ± 1.3 MJ/m^2/day	Natural cycle	NR	NR	9.05-9.5		NR	NR	NR	[117]
Outdoor HRAP	9,600 and 32	Depth 30 cm	C	18.8-23.5	Outdoor	Natural cycle	NR	8.3 ± 2.8 (23.5°C) 9.4 ± 1.4 (18.8 °C)	7.3 ± 0.2 (23.5°C) 8.9 ± 0.3 (18.8 °C)		14.7 ± 18.7 (23.5°C) −0.1 ± 0.6 (18.8 °C)	NR	0.33-0.56	[119]
				28.2 ± 1.3	1,240 ± 512	24:0	6.9 ± 0.7	4.4 ± 1.2 (low X_{avg}) to 12.8 ± 1.9 (high X_{avg})	9.7-9.8	Consortium of cyanobacteria/ microalgae and bacteria	6.9 ± 0.7	3.4-15.5	0.4-1.38	[113]
Indoor HRAP	180 and 1.2	15x67 x202	C	15 and 35 during different stages	c. 1,350	24:0	NR	NR	10		NR	NR	NR	[118]
				12 and 35 during	1,350 ± 660	12:12	NR	10.1- 16.6 (light phase);	7.5-11		15.9 ± 1.2 at 35 °C;	7.5	400-500	[120]

PBR Type	PBR Details			Operation Details						Biomass Productivity			References
	V_R (L); A_{ill} [m^2]	Dim. [cm]	Mode	T_R [°C]	L.I. [µmol/m^2-s]	L:D	W_{comp} [L/d]	[DO] [mg/L]	pH	Inoculation [mg TSS/L]	r_{evap} [L/m^2/d]	B_{mean} [g/m^2/d]	X_{avg} [mg/L]	
Outdoor HRAP	180 and 1.2	Depth 15 cm	C	different stages				1.3-10 (dark phase)			1.9 ± 0.4 at 12 °C			[66]
				9.1 ± 4.1	679 ± 420	10:14	NA	6.0-10.9	9.2-9.4	210 [*Leptolyngbya lagerheimii* (54%), *Chlorella vulgaris* (28%), *Parachlorella kessleri* (9%), *Tetradesmus obliquus* (5%) & *Mychonastes homosphaera* (2%)]	-1.2	0	55-314	
				15.3 ± 7.3	1,587 ± 150	14:10	3.9± 3.2 (TW)	7.5-10.6	9.3-9.6		2.0-6.2	7.5	447.5	
				24.4 ± 5.8	1,626 ± 60	15:9	7.7± 2.0 (TW)	6.8-7.9	9.4		6.7 ± 4.9	15	519-571	
				23.4 ± 3.8	1,326 ± 71	12:12	5.9± 2.4 (TW)	5.3-6.4	9.6-9.8		5.9 ± 3.4	22.5	625-514	
				18.4 ± 7.0	820 ± 0	10:14	2.0± 1.8 (TW)	6	9.6		3.2 ± 2.1	15	424	
Outdoor HRAP				23.8 ± 6.7	1,427 ± 65	12:12	0.6± 0.4 (TW)	1.4 - 15.6	8.3 ± 0.33	210 [*Chlorella sp*]	7 ± 2	15	660 ± 17	[121]
				23.5 ± 6.4	1,258 ± 140	11:13	0.8± 0.4 (TW)	1.3 - 16.7	9.9 ±0.09		9 ± 1	15	1078 ± 84	
				20.0 ± 6.7	946 ± 174	9:15	NA	0.9 - 13.2	10.06 ±0.13		3 ± 2	15	665 ± 79	
Indoor HRAP				NR	1,500 ± 600	14:10	NR (TW)	15.9 ± 1.6	10.2	NR [*Mychonastes homosphaera*]	NR	15	2600 ± 300	[59]

PBR Type	PBR Details			Operation Details						Inoculation [mg TSS/L]	Biomass Productivity			References
	V_R (L); A_{ill} [m^2]	Dim. [cm]	Mode	T_R [°C]	L.I. [µmol/m^2-s]	L:D	W_{comp} [L/d]	[DO] [mg/L]	pH		r_{evap} [L/m^2/d]	B_{mean} [g/m^2/d]	X_{avg} [mg/L]	
Indoor PBR (Glass Vessel)	50 and 0.87	15x50 x67		20-28	4 steps up to 100	12:12	NR	8.5	7.1-7.4	NR [*Chlorella srooknina*]	NR	0.06 g/L/d	600	[91]
				NR	500	12:12	DW	11.4 ± 0.5 /2.8 ± 0.1 (Light/dark)	9.71 / 9.39 (Light/dark)	120 [*Picochlorum* sp. & *Halospirulina sp*]	NR	0.023 ± 0.001 g/L/d	230 ± 50	[88]
Indoor HRAP	25 and 0.28	125x 25x14	C (HRT: 9.5 days)							$4.8*10^8$ cells/ml [dominated by *Picochlorum* sp. & *Scenedesmus* sp.]				
				20-25	500	24:0	NR	NR	>9		NR	120.2*	1230	[65]
				22 ± 3				5.4 ± 0.8	9.1 ± 0.1	NR [*Geitlerinema* sp. (61.5%), *Staurosira* sp. (1.5%) & *Stigeoclonium tenue* (37%)]		2.2 ± 1.4	1600 ± 100	
			C	25 ± 2	420 ± 105	16:8	NR (TW)	7.5 ± 1.4	9.6 ± 0.3		NR	4.4 ± 1.5	1200 ± 400	[46]
Indoor HRAP	180 and 1.2	Depth 15 cm		28 ± 1				9.6 ± 0.4	10.6 ± 0.1			7.5 ± 0.1	900 ± 100	
			C (HRT: 7.4 ± 0.2 d)	24 ± 1	104 ± 25	16:8	NR	7 ± 1 (max)	≈8	910 [*Planktolynga brevicellularis* (81%), *Stigeoclonium*	4.4 ± 1.4 - 7.3 ± 0.2	11.4±1.8 to 13.5±2.2	933 ± 49 to 1228 ± 36	[122]

PBR Type	PBR Details		Operation Details							Biomass Productivity			References
	V_R (L); A_{ill} [m^2]	Dim. [cm]	Mode	T_R [°C]	L.I. [µmol/m^2-s]	L:D	W_{comp} [L/d]	[DO] [mg/L]	pH	Inoculation [mg TSS/L]	r_{evap} [L/m^2/d]	B_{mean} [g/m^2/d]	X_{avg} [mg/L]	
										tenue (14%) & *Limnothrix planktonica* (5%)]				
			C (HRT: 7.4 ± 0.3 d)	26 ± 2	104 ± 25	16:8	NR	4.2 ± 0.5 -8.2 ± 0.9)	≈7.9	600 [*Chlorella vulgaris*]	NR	12 ± 1	130 ± 70	[115]
Indoor PBR (Glass Vessel)	75 and 0.525	15x50 x100	C	25 ± 1	100 ± 20	24:0	NR	Around 7	≈8	NR [*Nannochloropsis gaditana*]	NR	0.03 g/L/d	450 ± 30	[43]
Indoor HRAP	180 and 1.2	Depth 15 cm	C (HRT : 2 d)	26 ± 1	80	NR	NR	≈ 10	9.4 7	NR [*Spirulina Platensis*]	6	NR	1200 ± 100 600 ± 20	[58]

V_R: Bioreactor Volume; A_{ill}: Illuminated Area; Dim: Dimensions; C: Continuous; T_R: Reactor Temperature; L.I.: Light Intensity; L:D: Light to Dark Ratio; W_{comp} : Water Consumption; [DO] : Concentration of dissolved oxygen; r_{evap} : Rate of Evaporation; B_{mean}: Mean Biomass Yield; X_{avg}: Average biomass concentration.; HRT: Hydraulic Retention Time; d: days; TW: Tap water; DW: Distilled water

[*] *Considering each gram of algal biomass is produced by sequestering 1.8 grams of CO_2 [147]*

2.5.3 Microalgae harvesting

Algae harvesting is usually referred to as the technique to increase the total solid content up to 10-25% TSS from a dilute algal broth [148,149]. Screening is the first step for microalgae harvesting. Even though mesh sizes in micro-strainers of as low as 1 μm are available, the harvesting efficiency continues to be low by screening [150]. Only filamentous species, for example, *Spirulina* sp., with a filament length varying between 50 and 500 μm [151] can be relatively easily screened with higher screen size and at a higher flow rate, significantly decreasing the process economics. Vibrating or stationary screens have been shown to be more efficient, which in fact, is the current commercial process for harvesting *Spirulina*, resulting in a recovery of 8-10% TSS [151].

2.5.3.1 Algae harvesting techniques

For most microalgae, the initial thickening of algal broth via gravity sedimentation is accelerated by the addition of flocculants as the most common harvesting technology [152,153]. However, the requirement for a low working pH (5-6), together with the necessity of large quantities of corrosive inorganic chemical flocculants such as metallic salts (which contaminates the growth medium) are severe limitations [148,149]. Increasing the pH to enhance flocculation, or auto-flocculation has received considerable success at the lab scale. This reduces the cost and energy needs of the harvesting process and is non-toxic. Up to 95% recovery of the total biomass content within 30 mins for *Chlorella vulgaris* at a pH of 10.5 was reported by García-pérez et al., (2014) [154]; reports of more than 90% recovery of the total biomass content for freshwater species (*Chlorella vulgaris, Scenedesmus* sp. *and Chlorococcum* sp.), as well as marine algae (*Nannochloropsis Oculata, Phaeodactylum tricornutum*) at a pH of around 10.6 [155], are encouraging. However, the exact mechanism behind auto-flocculation is uncertain; and the significant unreliability of this technique is still a major bottleneck to its large-scale commercial application [148].

Further to thickening, filtration is one of the most promising dewatering techniques. By this technique, the microalgae are strained off from the liquid by being forced through a membrane at a pressure gradient [149]. However, clogging is a major

drawback, especially for harvesting high-density cultures [148]. For a scale handling more than 20 m^3/d of liquid flow, centrifugation provides the fastest alternative but is hindered by high cost and energy demand [156]. Hence, its applicability is justified only when high-value products are extracted from microalgae, such as unsaturated fatty acids, pharmaceuticals, or cosmetic products [152,153].

Decoupling harvesting from cultivation by the use of a separate settling tank has been mostly applied while upgrading biogas with microalgae. This suggests the use of gravity separation as the preferred harvesting technology. Toledo-Cervantes et al., (2017b) [59] used an organic flocculant or polyelectrolyte, polyacrylamide-based flocculant solution, (due to its low cost for a higher sludge volume) in an external stirred tank to harvest *Mychonastes homosphaera*. Such limited reports available in the literature, therefore, leave significant research gaps to understand the coupling of commercial harvesting techniques with biogas upgrading by microalgae including the further understanding of auto-flocculation technology.

2.5.3.2 Microalgae selection criteria 5: Ease of harvesting

Ease of harvesting can provide a significant advantage by improving the overall energetic and economic balance of the biogas upgrading system. Harvesting filamentous species like *Anabaena* and *Spirulina* [157] through screening provides the easiest of all harvesting techniques. On the other hand, unicellular microalgae like *Chlorella* sp. or *Chlorella vulgaris* or *Scenedesmus obliquus* are extremely hard to harvest. In such cases, flocculation, followed by gravity separation or centrifugation, based on the downstream application would be the most techno-economic option.

2.6 Discussion and perspectives

2.6.1 Selection of microalgae species

Microalgae selection for effective biogas upgrading and system operation is intrinsically interlinked with system parameters. This work suggests five criteria for microalgae selection and assesses these for 15 common microalgae species in Table 2-7. Green tabs represent a beneficial response of the species; red a detrimental response. The cyanobacteria species of genera *Anabaena* and *Spirulina* are suggested as the most suitable for biogas upgrading. Of the *Chlorella* genera, specific strains of

Chlorella sorokiniana and *Scenedesmus obliquus* are the most preferable, while the preference of *Chlorella vulgaris* for uptake of CO_2 at high pH might decrease its effectiveness. Any species, showing two or more red tabs would hence be difficult to be considered suitable for biogas upgrading.

Table 2-7 Evaluation of 15 common microalgae species with regards to defined microalgae selection criteria for biogas upgrading compiled based on the following references [23,28,52,64,78,81,158–182].

Species	Genera	Criteria				
		Mixotrophy	High pH tolerance (above 9)	External CA activity	CO_2 tolerance	Ease of harvesting
Chlamydomonas reinhardtii	*Chlamydomonas*	No	No	Yes	17%	No, Unicellular
Chlorella vulgaris	*Chlorella*	Yes	Up to10 (Free CO_2 Preferable)	Yes	60%	No, Unicellular
Chlorella sorokiniana	*Chlorella*	Yes	Yes	Yes	40%	No, Unicellular
Chlorococcum littorale	*Chlorococcum*	Yes	Up to 10	No	60%	No, Unicellular
Desmodesmus sp.	*Desmodesmus*	No	Up to 11	Yes	Reported up to 20%	No, Unicellular
Dunaliella salina	*Dunaliella*	Yes	9-11	Yes	12%	No, Unicellular
Neochloris oleobundans	*Neochloris*	Yes	Up to 10.2	Yes	Reported up to 6%	No, Unicellular
Scenedesmus obliquus	*Scenedesmus*	Yes	Maximum 10.6	Yes	80%	No, Unicellular
Tetraselmis suecica	*Tetraselmis*	No	Not Reported	Yes	14%	No, Unicellular
Phaeodactylum tricornutum	*Phaeodactylum*	No	Maximum 10.3	Yes/No	100%	No, Diatom
Emiliania huxleyi	*Emiliania*	No	No	Yes/No	Very Low	No, Unicellular
Nannochloropsis gaditana	*Nannochloropsis*	No	No	No	15%	No, Unicellular
Euglena gracilis	*Euglena*	Yes	No	No	40%	No, Unicellular Flagellate
Anabaena cylindrica	*Anabaena*	Yes	Moderately Alkaliphilic	Yes	50%	Yes, Filamentous
Spirulina platensis	*Arthrospira*	Yes	Strongly Alkaliphilic	Yes	100%	Yes, Filamentous
Synechococcus sp	*Synechococcus*	Yes	Moderately Alkaliphilic	Yes	100%	No, Unicellular

2.6.2 Industrial scale application

Based on the above design conditions an overall system sizing for an industrial scale microalgal biogas upgrading system can be estimated. Assuming the culture liquid drawn for harvesting to be half of the liquid recirculated in the bubble column, 0.75 m^3 of algal liquid would be necessary for each cubic metre of biogas upgraded for an L/G ratio of 0.5. This implies a requirement of 1.5 m^3 of algae cultivation for a flat plate PBR system, while 11.25 m^2 of open pond system would be required for a 0.2 m deep pond with HRT of 2 and 3 days respectively [183,184]. A detailed calculation is summarised in *BOX 2.1*. This result is comparable to the assumption of Toledo-Cervantes et al., (2017a) [144], whereby 4.84 m^2 of open pond was proposed for each m^3 of biogas upgraded for an L/G ratio of 0.5 without separate withdrawal of culture for harvesting and a lower hydraulic retention time.

The number and dimensions of bubble columns would depend on multiple factors. Superficial gas velocity, column diameter, temperature and pressure of operation are of considerable significance in this regard. Indeed, Toledo-Cervantes et al., (2017a) [144], estimates 1.2 m^3 of effective column volume per m^3 of biogas upgraded per hour at a gas superficial velocity of 0.05 cm/s. However, this could be significantly reduced to 60 L per m^3 of biogas upgraded per hour for a gas superficial velocity of 1 cm/s. Therefore, optimisation s of biogas flow velocity, together with other operational parameters are urgently required to avoid severe limitations to practical applications of such designs.

Parasitic consumption would vary significantly depending on the type of harvesting system, whereby up to 54% of the overall energy consumption for biogas upgrading has been calculated to be expended [144]. Electricity consumption of 0.14 kWh/m^3 of biogas with 30% CO_2 for open pond systems was calculated for outdoor cultivation in open ponds without harvesting [66], lower than most of the commercial physicochemical methods. A total parasitic loss of 2.5% can thus be envisaged. However, for a flat plate PBR, the electricity consumption of 53 W/m^3 [135], can significantly modify the overall performance of the upgrading system.

BOX 2.1: Calculation for Industrial Scale Perspective of Photosynthetic Biogas Upgrading

1MW electricity plant with an electrical efficiency of 35% on continuous operation. Assuming the Lower Heating Value of methane as 35.8 MJ/m^3 and biogas contains 60% methane:

➔ Energy input = $\frac{1000 \times 24}{0.35} = 68{,}571.43 \frac{kWh}{day} \approx 246.86 \times 10^3$ MJ/day

➔ Biogas Generated (G_d) = $\frac{246.86 \times 10^3}{35.8 \times 0.6} = 11{,}492.4$ m^3/day

Assuming L/G ratio as 0.5 as per the current technological trend observed in Table 2-4,

➔ Algal broth circulated in bubble column (L_d) = $11{,}492.4 \times 0.5 = 5{,}746.2$ m^3/day

Algae Cultivation System

Algal broth drawn separately for harvesting is assumed as 0.5 times that circulated in the bubble column. A 3 day hydraulic retention time (HRT) is recommended for open pond cultivations [158]. For flat plate PBRs, HRT $2\mu^{-1}$ is advised, μ being the specific growth rate (day^{-1}) [159]. For *Scenedesmus obliquus* with an average growth rate of 0.94 ± 0.08 day^{-1} [159], an HRT of 2 days would be sufficient.

➔ Open pond volume = $(L_d + 0.5L_d) \times HRT_{pond} = 1.5 \times 5{,}746.2 \times 3 = 25{,}857.94$ m^3

➔ Flat Plate PBR volume =
$(L_d + 0.5L_d) \times HRT_{PBR} = 1.5 \times 5{,}746.2 \times 2 = 17{,}238.63$ m^3

➔ Open pond area (with 0.2m depth) = $\frac{25{,}857.94}{0.2 \times 10{,}000} = 12.93$ ha

➔ Flat Plate PBR (2.5mX1.5mX0.07m) = $\frac{17{,}238.63 \times S}{10 \times 10{,}000} = 4.93$ ha

When,

➔ Surface to Volume ratio of Flat Plate PBR (S) $\approx \frac{2 \times (2.5 \times 1.5)}{2.5 \times 1.5 \times 0.07} = 28.57$ m^2/m^3

and assuming the need of a tenth of the surface area of the reactors as a land requirement of the flat plate PBRs [185].

Economies of scale and the flow rates of biogas are significant factors in assessing the cost of biomethane [5]. For a 300 Nm^3/hr biogas flow, a specific capital expenditure (CAPEX) of 6,034 €/(Nm^3/hr-biogas) was predicted for photosynthetic biogas upgrading using an open pond for algae cultivation [144]. This was 1.6 times higher than a traditional activated carbon-water scrubbing based upgrading technology. The corresponding operational expenditure (OPEX) of the photosynthetic biogas upgrading system was 0.03 €/Nm^3 of biogas treated. These costs are applicable for a 1MW_e biogas power plant (generating around 479 Nm^3/hr biogas or 10GJ/hr). For a flat plate PBR system, although less land would be required than an open pond system, the high cost of the PBRs would lead to an increased CAPEX [186]. Notwithstanding the increased energy demand from pumping, the lower cost of labour and requirement of less energy-intensive harvesting techniques due to a higher concentration of biomass systems could lower its corresponding OPEX [186].

The final usage of the microalgae is crucial towards the economic viability of the photosynthetic upgrading system. Toledo-Cervantes et al., (2017a) [144] calculated a payback of 5 years while selling biomethane at natural gas prices without incentives through the added revenue generated from microalgae sales. Indeed, extraction of high-value products based on the microalgae composition [187] or the production of bioproducts or biofuels could provide added economic benefits towards the commercialisation of the photosynthetic biogas upgrading system. Indeed, a higher economic benefit from a flat Plate PBR over an open pond system can be envisaged only when a high-value product is aimed for from the produced microalgae [188].

The presence of oxygen in the upgraded biomethane could lead to a significant economic penalty to the photosynthetic biogas upgrading system. Physicochemical O_2 scavenging via adsorption with activated carbon/ molecular sieves, or catalytic reduction using hydrazine, sodium sulphite or pyrogallol is commercially feasible [189]. However, this would not only raise the CAPEX, but the OPEX as well, due to the requirement for high temperature and pressure differentials to carry out the same [189]. Therefore, minimisation of the O_2 content in biomethane must be aimed for. For this, the most important strategies highlighted in the paper include: *1)* lowering the contact time between the unprocessed biogas and algae solution, *2)* reducing the pH of the working media and *3)* optimising the relative biogas and algal solution

recirculation flow rate, or the L/G ratio *4)* suitably selecting microalgae species to benefit the first three strategies. However, although the parameters and strategies for lowering the O_2 content in the biomethane are well understood, a lack of agreement regarding their exact values to achieve grid quality biomethane needs to be overcome for the techno-economic viability of this technology on an industrial scale.

2.7 Conclusions

Biogas upgrading with microalgae is a novel technology, allowing the unique opportunity for on-site CO_2 removal, sequestration and use. In this work, the fundamental principles governing biogas upgrading with microalgae have been identified and critically analysed for possible optimisation strategies.

- Five criteria affecting the selection of microalgae have been identified; the ability for mixotrophic growth, high pH tolerance, external CA activity, high CO_2 tolerance and ease of harvesting. Five common microalgae species have been identified to fit best for biogas upgrading, namely: *Anabaena cylindrica, Chlorella sorokiniana, Scenedesmus obliquus, Spirulina platensis and Synechococcus* sp.
- The gas-sparged bubble absorption column coupled to flat plate photobioreactors is the most promising technological configuration for biogas upgrading and microalgae cultivation although the open pond is the most commercially feasible technology at present. Working parameters needing optimisation have also been identified.
- A 1 MW electric biogas plant was estimated to require 12.9 hectares of open pond or 4.9 hectares of flat plate PBRs with an L/G ratio of 0.5 and using *Scenedesmus obliquus* as the microalgae at the present technological level.

2.8 Acknowledgement

This work was funded by Science Foundation Ireland (SFI) through the Centre for Marine and Renewable Energy (MaREI) under Grant Number 12/RC/2302 and 16/SP/3829 with industrial funding from Gas Networks Ireland through The Green Gas Innovation Group and by ERVIA. This work was also supported by the European Union’s Horizon 2020 research and innovation programme under the Marie

Skłodowska-Curie grant (No. 797259). This work was also supported by the European Union's Horizon 2020 research and innovation programme under the Marie Skłodowska-Curie grant (No. 797259) and the Environmental Protection Agency – Ireland (2018-RE-MS-13).

2.9 References

[1] Scarlat N, Dallemand JF, Fahl F. Biogas: Developments and perspectives in Europe. Renew Energy 2018;129:457–72. doi:10.1016/j.renene.2018.03.006.

[2] Wall DM, McDonagh S, Murphy JD. Cascading biomethane energy systems for sustainable green gas production in a circular economy. Bioresour Technol 2017;243:1207–15. doi:10.1016/j.biortech.2017.07.115.

[3] Ullah Khan I, Hafiz Dzarfan Othman M, Hashim H, Matsuura T, Ismail AF, Rezaei-DashtArzhandi M, et al. Biogas as a renewable energy fuel – A review of biogas upgrading, utilisation and storage. Energy Convers Manag 2017;150:277–94. doi:10.1016/j.enconman.2017.08.035.

[4] Awe OW, Zhao Y, Nzihou A, Minh DP, Lyczko N. A Review of Biogas utilisation, purification and upgrading technologies. Waste and Biomass Valorization 2017;8:267–83. doi:10.1007/s12649-016-9826-4.

[5] Angelidaki I, Treu L, Tsapekos P, Luo G, Campanaro S, Wenzel H, et al. Biogas upgrading and utilization: Current status and perspectives. Biotechnol Adv 2018;36:452–66. doi:10.1016/j.biotechadv.2018.01.011.

[6] Muñoz R, Meier L, Diaz I, Jeison D. A review on the state-of-the-art of physical/chemical and biological technologies for biogas upgrading. Rev Environ Sci Biotechnol 2015;14:727–59. doi:10.1007/s11157-015-9379-1.

[7] Zhou W, Wang J, Chen P, Ji C, Kang Q, Lu B, et al. Bio-mitigation of carbon dioxide using microalgal systems: Advances and perspectives. Renew Sustain Energy Rev 2017;76:1163–75. doi:10.1016/j.rser.2017.03.065.

[8] Xia A, Herrmann C, Murphy JD. How do we optimise third-generation algal biofuels ? Biofuels, Bioprod Biorefining 2015;9:358–67. doi:10.1002/bbb.1550.

[9] UNFCCC. Paris Agreement. Conf Parties Its Twenty-First Sess 2015:32. doi:FCCC/CP/2015/L.9/Rev.1.

[10] United Nations Framework Convention on Climate Change (UNFCCC). Glasgow Climate Pact. Conf. Parties Serv. as Meet. Parties to Paris Agreem., Glasgow: United Nations; 2021.

[11] Yue X, Deane JP, O'Gallachoir B, Rogan F. Identifying decarbonisation opportunities using marginal abatement cost curves and energy system scenario ensembles. Appl Energy 2020;276:115456. doi:10.1016/j.apenergy.2020.115456.

[12] Cabral RP, Mac Dowell N. A novel methodological approach for achieving £/MWh cost reduction of CO_2 capture and storage (CCS) processes. Appl Energy 2017;205:529–39. doi:10.1016/j.apenergy.2017.08.003.

[13] Raza A, Gholami R, Rezaee R, Rasouli V, Rabiei M. Significant aspects of carbon capture and storage – A review. Petroleum 2019;5:335–40. doi:10.1016/j.petlm.2018.12.007.

[14] Pham LHHP, Rusli R, Keong LK. Consequence Study of CO_2 Leakage from Ocean Storage. Procedia Eng 2016;148:1081–8. doi:10.1016/j.proeng.2016.06.597.

[15] Farooqui A, Bose A, Ferrero D, Lorca J, Santarelli M. Simulation of two-step redox recycling of non-stoichiometric ceria with thermochemical dissociation of CO_2/H_2O in moving bed reactors - Part 1: Model development with redox kinetics and sensitivity analysis. Chem Eng Sci n.d.

[16] Cuéllar-Franca RM, Azapagic A. Carbon capture, storage and utilisation technologies: A critical analysis and comparison of their life cycle environmental impacts. J CO2 Util 2015;9:82–102. doi:10.1016/j.jcou.2014.12.001.

[17] Koytsoumpa EI, Bergins C, Kakaras E. The CO_2 economy: Review of CO_2 capture and reuse technologies. J Supercrit Fluids 2018;132:3–16. doi:10.1016/j.supflu.2017.07.029.

[18] Farrelly DJ, Everard CD, Fagan CC, McDonnell KP. Carbon sequestration and the role of biological carbon mitigation: A review. Renew Sustain Energy Rev 2013;21:712–27. doi:10.1016/j.rser.2012.12.038.

[19] Jana K, Ray A, Mansouri M, Assadi M, De S. Polygeneration as a future sustainable energy solution – A comprehensive review. Appl Energy 2017;202:88–111. doi:10.1016/j.apenergy.2017.05.129.

[20] Maggioni L, Pieroni C. Report on the biomethane injection into national gas grid. 2016.

[21] Vuppaladadiyam AK, Yao JG, Florin N, George A, Wang X, Labeeuw L, et al. Impact of flue gas compounds on microalgae and mechanisms for carbon assimilation and utilization. ChemSusChem 2018;11:334–55. doi:10.1002/cssc.201701611.

[22] Fan LH, Zhang YT, Zhang L, Chen HL. Evaluation of a membrane-sparged helical tubular photobioreactor for carbon dioxide biofixation by *Chlorella vulgaris*. J Memb Sci 2008;325:336–45. doi:10.1016/j.memsci.2008.07.044.

[23] Klanchui A, Cheevadhanarak S, Prommeenate P, Meechai A. Exploring Components of the CO_2-concentrating mechanism in alkaliphilic cyanobacteria through genome-based analysis. Comput Struct Biotechnol J 2017;15:340–50. doi:10.1016/j.csbj.2017.05.001.

[24] Venkata Mohan S, Rohit M V, Chiranjeevi P, Chandra R, Navaneeth B. Heterotrophic microalgae cultivation to synergize biodiesel production with waste remediation: Progress and perspectives. Bioresour Technol 2015;184:169–78. doi:10.1016/j.biortech.2014.10.056.

[25] Calvin M. Forty years of photosynthesis and related activities. Photosynth Res 1989;21:3–16. doi:10.1007/BF00047170.

[26] Huang Y, Cheng J, Lu H, He Y, Zhou J, Cen K. Transcriptome and key genes expression related to carbon fixation pathways in *Chlorella* PY-ZU1 cells and their growth under high concentrations of CO_2. Biotechnol Biofuels 2017;10:1–10. doi:10.1186/s13068-017-0868-z.

[27] Vadlamani A, Viamajala S, Pendyala B, Varanasi S. Cultivation of microalgae at extreme alkaline pH conditions: A novel approach for biofuel production. ACS Sustain Chem Eng 2017;5:7284–94. doi:10.1021/acssuschemeng.7b01534.

[28] Canon-Rubio KA, Sharp CE, Bergerson J, Strous M, De la Hoz Siegler H. Use of highly alkaline conditions to improve cost-effectiveness of algal biotechnology. Appl Microbiol Biotechnol 2016;100:1611–22. doi:10.1007/s00253-015-7208-7.

[29] Perez-Garcia O, Escalante FME, de-Bashan LE, Bashan Y. Heterotrophic cultures of microalgae: metabolism and potential products. Water Res 2011;45:11–36. doi:10.1016/j.watres.2010.08.037.

[30] Smetana S, Sandmann M, Rohn S, Pleissner D, Heinz V. Autotrophic and heterotrophic microalgae and cyanobacteria cultivation for food and feed: life cycle assessment. Bioresour Technol 2017;245:162–70. doi:10.1016/j.biortech.2017.08.113.

[31] Wang J, Yang H, Wang F. Mixotrophic cultivation of microalgae for biodiesel production: Status and prospects. Appl Biochem Biotechnol 2014;172:3307–29. doi:10.1007/s12010-014-0729-1.

[32] Geider RJ, Osborne BA. Respiration and microalgal growth. A review of the quantitative relationship between dark respiration and growth. New Phytol 1989;112:327–41.doi: 10.1111/j.1469-8137.1989.tb00321.x

[33] Behrens PW. Photobioreactors and Fermentors: The light and dark sides of growing algae. In: Anderson RA, editor. Algal Cult. Tech. 1st ed., Burlington: Elsevier Academic Press; 2005, p. 189–203.

[34] Kang R, Wang J, Shi D, Cong W, Cai Z, Ouyang F. Interactions between organic and inorganic carbon sources during mixotrophic cultivation of *Synechococcus* sp. Biotechnol Lett 2004;26:1429–32. doi:10.1023/B:BILE.0000045646.23832.a5.

[35] Abu Hajar HA, Riefler RG, Stuart BJ. Cultivation of the microalga *Neochloris oleoabundans* for biofuels production and other industrial applications (a review). Appl Biochem Microbiol 2017;53:640–53. doi:10.1134/S0003683817060096.

[36] Kadkhodaei S, Abbasiliasi S, Shun TJ, Fard Masoumi HR, Mohamed MS, Movahedi A, et al. Enhancement of protein production by microalgae *Dunaliella*

salina under mixotrophic conditions using response surface methodology. RSC Adv 2015;5:38141–51. doi:10.1039/c5ra04546k.

[37] Cecchin M, Benfatto S, Griggio F, Mori A, Cazzaniga S, Vitulo N, et al. Molecular basis of autotrophic vs mixotrophic growth in *Chlorella sorokiniana*. Sci Rep 2018;8:1–13. doi:10.1038/s41598-018-24979-8.

[38] Sialve B, Bernet N, Bernard O. Anaerobic digestion of microalgae as a necessary step to make microalgal biodiesel sustainable. Biotechnol Adv 2009;27:409–16. doi:10.1016/j.biotechadv.2010.10.005.

[39] Perez-Garcia O, Bashan Y. Microalgal heterotrophic and mixotrophic culturing for bio-refining: from metabolic routes to techno-economics. In: A. P, R. B, M. Z, editors. Algal Biorefineries, Springer; 2015, p. 61–131. doi:https://doi.org/10.1007/978-3-319-20200-6_3.

[40] Montechiaro F, Hirschmugl CJ, Raven JA, Giordano M. Homeostasis of cell composition during prolonged darkness. Plant, Cell Environ 2006;29:2198–204. doi:10.1111/j.1365-3040.2006.01593.x.

[41] Converti A, Oliveira RPS, Torres BR, Lodi A, Zilli M. Biogas production and valorization by means of a two-step biological process. Bioresour Technol 2009;100:5771–6. doi:10.1016/j.biortech.2009.05.072.

[42] Prandini JM, da Silva MLB, Mezzari MP, Pirolli M, Michelon W, Soares HM. Enhancement of nutrient removal from swine wastewater digestate coupled to biogas purification by microalgae *Scenedesmus* spp. Bioresour Technol 2016;202:67–75. doi:10.1016/j.biortech.2015.11.082.

[43] Meier L, Pérez R, Azócar L, Rivas M, Jeison D. Photosynthetic CO_2 uptake by microalgae: An attractive tool for biogas upgrading. Biomass and Bioenergy 2015;73:102–9. doi:10.1016/j.biombioe.2014.10.032.

[44] Borhani TNG, Azarpour A, Akbari V, Wan Alwi SR, Manan ZA. CO_2 capture with potassium carbonate solutions: A state-of-the-art review. Int J Greenh Gas Control 2015;41:142–62. doi:10.1016/j.ijggc.2015.06.026.

[45] Ye X, Lu Y. CO_2 absorption into catalyzed potassium carbonate-bicarbonate solutions: Kinetics and stability of the enzyme carbonic anhydrase as a biocatalyst. Chem Eng Sci 2014;116:567–75. doi:10.1016/j.ces.2014.05.040.

[46] Toledo-Cervantes A, Serejo ML, Blanco S, Pérez R, Lebrero R, Muñoz R. Photosynthetic biogas upgrading to bio-methane: Boosting nutrient recovery via biomass productivity control. Algal Res 2016;17:46–52. doi:10.1016/j.algal.2016.04.017.

[47] Delgadillo-mirquez L, Lopes F, Taidi B, Pareau D. Nitrogen and phosphate removal from wastewater with a mixed microalgae and bacteria culture. Biotechnol Reports 2016;11:18–26. doi:10.1016/j.btre.2016.04.003.

[48] Larsdotter K, Jansen J la our, Dalhammar G. Phosphorus removal from wastewater by microalgae in Sweden – a year-round perspective. Environ Technol 2010;31:117–123. doi:10.1080/09593330903382815.

[49] Dutcher B, Fan M, Russell AG. Amine-based CO_2 capture technology development from the beginning of 2013 - A review. ACS Appl Mater Interfaces 2015;7:2137–48. doi:10.1021/am507465f.

[50] Imle M, Kumelan J, Speyer D, Mccann N, Maurer G, Hasse H. Solubility of carbon dioxide in activated potash solutions in the low and high gas loading regions. Ind Eng Chem Res 2013; 52(37):13477–13489. doi:10.1021/ie401835x

[51] Hu G, Nicholas NJ, Smith KH, Mumford KA, Kentish SE, Stevens GW. Carbon dioxide absorption into promoted potassium carbonate solutions: A review. Int J Greenh Gas Control 2016;53:28–40. doi:10.1016/j.ijggc.2016.07.020.

[52] Ores J da C, Amarante MCA De, Fernandes SS, Kalil SJ. Production of carbonic anhydrase by marine and freshwater microalgae. Biocatal Biotransformation 2016;34:57–65. doi:10.1080/10242422.2016.1227793.

[53] Luca V De, Vullo D, Scozzafava A, Carginale V, Rossi M, Supuran CT, et al. An α-carbonic anhydrase from the thermophilic bacterium *Sulphurihydrogenibium azorense* is the fastest enzyme known for the CO_2 hydration reaction. Bioorganic Med Chem 2013;21:1465–9. doi:10.1016/j.bmc.2012.09.047.

[54] Thee H, Smith KH, Silva G, Kentish SE, Stevens GW. Carbonic anhydrase promoted absorption of CO_2 into potassium carbonate solutions 2015;114:108–14. doi:10.1002/ghg.

[55] Behr P, Maun A, Deutgen K, Tunnat A, Oeljeklaus G, Görner K. Kinetic study on promoted potassium carbonate solutions for CO_2 capture from flue gas. Energy Procedia 2011;4:85–92. doi:10.1016/j.egypro.2011.01.027.

[56] Posadas E, Morales M del M, Gomez C, Acién FG, Muñoz R. Influence of pH and CO_2 source on the performance of microalgae-based secondary domestic wastewater treatment in outdoors pilot raceways. Chem Eng J 2015;265:239–48. doi:10.1016/j.cej.2014.12.059.

[57] Meier L, Stará D, Bartacek J, Jeison D. Removal of H_2S by a continuous microalgae-based photosynthetic biogas upgrading process. Process Saf Environ Prot 2018;119:65–8. doi:10.1016/j.psep.2018.07.014.

[58] Bahr M, Díaz I, Dominguez A, González Sánchez A, Muñoz R. Microalgal-biotechnology as a platform for an integral biogas upgrading and nutrient removal from anaerobic effluents. Environ Sci Technol 2014;48:573–81. doi:10.1021/es403596m.

[59] Toledo-Cervantes A, Madrid-Chirinos C, Cantera S, Lebrero R, Muñoz R. Influence of the gas-liquid flow configuration in the absorption column on photosynthetic biogas upgrading in algal-bacterial photobioreactors. Bioresour Technol 2017;225:336–42. doi:10.1016/j.biortech.2016.11.087.

[60] Kao CY, Chiu SY, Huang TT, Dai L, Wang GH, Tseng CP, et al. A mutant strain of microalga *Chlorella* sp. for the carbon dioxide capture from biogas. Biomass and Bioenergy 2012;36:132–40. doi:10.1016/j.biombioe.2011.10.046.

[61] Schmidt U. The solubility of carbon monoxide and hydrogen in water and sea-water at partial pressures of about 10^{-5} atmospheres. Tellus 1979;31:68–74. doi:10.1111/j.2153-3490.1979.tb00883.x.

[62] Kishi M, Toda T. Carbon fixation properties of three alkalihalophilic microalgal strains under high alkalinity. J Appl Phycol 2018;30:401–10. doi:10.1007/s10811-017-1226-z.

[63] Kuo CM, Lin TH, Yang YC, Zhang WX, Lai JT, Wu HT, et al. Ability of an alkali-tolerant mutant strain of the microalga *Chlorella* sp. AT1 to capture carbon dioxide for increasing carbon dioxide utilization efficiency. Bioresour Technol 2017;244:243–51. doi:10.1016/j.biortech.2017.07.096.

[64] Goldman JC, Azov Y, Riley CB, Dennett MR. The effect of pH in intensive microalgal cultures. I. Biomass regulation. J Exp Mar Bio Ecol 1982;57:1–13. doi:10.1016/0022-0981(82)90140-X.

[65] Granada-Moreno CI, Aburto-Medina A, de los Cobos Vasconcelos D, González-Sánchez A. Microalgae community shifts during the biogas upgrading in an alkaline open photobioreactor. J Appl Microbiol 2017;123:903–15. doi:10.1111/jam.13552.

[66] Marín D, Posadas E, Cano P, Pérez V, Blanco S, Lebrero R, et al. Seasonal variation of biogas upgrading coupled with digestate treatment in an outdoors pilot-scale algal-bacterial photobioreactor. Bioresour Technol 2018;263:58–66. doi:10.1016/j.biortech.2018.04.117.

[67] Thomas DJ, Sullivan SL, Price AL, Zimmermann SM. Common freshwater cyanobacteria grow in 100% CO_2. Astrobiology 2005;5:58–64. doi:10.13343/j.cnki.wsxb.2011.02.006.

[68] Kumari A, Kumar A, Pathak AK, Guria C. Carbon dioxide assisted *Spirulina platensis* cultivation using NPK-10:26:26 complex fertilizer in sintered disk chromatographic glass bubble column. J CO2 Util 2014;8:49–59. doi:10.1016/j.jcou.2014.07.001.

[69] Hanagata N, Takeuchi T, Fukuju Y, Barnes DJ, Karube I. Tolerance of microalgae to high CO_2 and high temperature. Phytochemistry 1992;31:3345–8. doi:10.1016/0031-9422(92)83682-O.

[70] Maeda K, Owadai M, Kimura NK, Karubd I. CO_2 fixation from the flue gas on coal-fired thermal power plant by microalgae to screen microalgae which arc suitable for direct CO_2 fixation, microalgae were sampled from. Energy Convers Manag 1995;36:717–20.

[71] Sung K, Lee J, Shin C, Park S. Isolation of a new highly CO_2 tolerant freshwater Microalga *Chlorella* sp. KR-1. Korean J Chem Eng 1998;15:449–50.

[72] Miyachi S, Iwasaki I, Shiraiwa Y. Historical perspective on microalgal and cyanobacterial acclimation to low- and extremely high-CO_2 conditions. Photosynth Res 2003;77:139–53. doi:10.1023/A:1025817616865.

[73] Yun Y, Lee SB, Park JM, Lee C, Yang J. Carbon dioxide fixation by algal cultivation using wastewater nutrients. J Chem Technol Biotechnol 1997;69:451–5. doi:10.1002/(sici)1097-4660(199708)69:4<451::aid-jctb733>3.3.co;2-d.

[74] De Farias Silva CE, Grisa B, Sforza E, Rocca N La, Bertucco A. Effects of sodium bicarbonate on biomass and carbohydrate production in *Synechococcus PCC* 7002. Chem Eng Trans 2016;49:241–6. doi:10.3303/CET1649041.

[75] El-Kassas HY, Heneash AMM, Hussein NR. Cultivation of *Arthrospira (Spirulina) platensis* using confectionary wastes for aquaculture feeding. J Genet Eng Biotechnol 2015;13:145–55. doi:10.1016/j.jgeb.2015.08.003.

[76] Zhu C, Zhai X, Wang J, Han D, Li Y, Xi Y, et al. Large-scale cultivation of *Spirulina* in a floating horizontal photobioreactor without aeration or an agitation device. Appl Microbiol Biotechnol 2018;102:8979–87. doi:10.1007/s00253-018-9258-0.

[77] Mokashi K, Shetty V, George SA, Sibi G. Sodium bicarbonate as inorganic carbon source for higher biomass and lipid production integrated carbon capture in *Chlorella vulgaris*. Achiev Life Sci 2016;10:111–7. doi:10.1016/j.als.2016.05.011.

[78] White DA, Pagarette A, Rooks P, Ali ST. The effect of sodium bicarbonate supplementation on growth and biochemical composition of marine microalgae cultures. J Appl Phycol 2013;25:153–65. doi:10.1007/s10811-012-9849-6.

[79] Yoon JH, Shin JH, Park TH. Characterization of factors influencing the growth of *Anabaena variabilis* in a bubble column reactor. Bioresour Technol 2008;99:1204–10. doi:10.1016/j.biortech.2007.02.012.

[80] Yue L, Chen W. Isolation and determination of cultural characteristics of a new highly CO_2 tolerant freshwater microalgae. Energy Convers Manag 2005;46:1868–76. doi:10.1016/j.enconman.2004.10.010.

[81] Lam MK, Lee KT. Effect of carbon source towards the growth of *Chlorella vulgaris* for CO_2 bio-mitigation and biodiesel production. Int J Greenh Gas Control 2013;14:169–76. doi:10.1016/j.ijggc.2013.01.016.

[82] Hu Q, Kurano N, Kawachi M, Iwasaki I, Miyachi S. Ultrahigh-cell-density culture of a marine green alga *Chlorococcum littorale* in a flat-plate photobioreactor. Appl Microbiol Biotechnol 1998;49:655–62. doi:10.1007/s002530051228.

[83] Ota M, Kato Y, Watanabe H, Watanabe M, Sato Y, Jr RLS, et al. Fatty acid production from a highly CO_2 tolerant alga, *Chlorocuccum littorale*, in the presence of inorganic carbon and nitrate. Bioresour Technol 2009;100:5237–42. doi:10.1016/j.biortech.2009.05.048.

[84] Nakano Y, Miyatake K, Okuno H, Hamazaki K, Takenaka S, Honami N, et al. Growth of photosynthetic algae *Euglena* in high CO_2 conditions and its photosynthetic characteristics. Acta Hortic 1996. doi:10.17660/ActaHortic.1996.440.9.

[85] Patil L, Kaliwal B. Effect of CO_2 concentration on growth and biochemical composition of newly isolated indigenous microalga *Scenedesmus bajacalifornicus* BBKLP-07. Appl Biochem Biotechnol 2017;182:335–48. doi:10.1007/s12010-016-2330-2.

[86] De Morais MG, Costa JAV. Carbon dioxide fixation by *Chlorella kessleri*, *C. vulgaris*, *Scenedesmus obliquus* and *Spirulina* sp. cultivated in flasks and vertical tubular photobioreactors. Biotechnol Lett 2007;29:1349–52. doi:10.1007/s10529-007-9394-6.

[87] Miyari S. CO_2 assimilation in thermophilic cyanobacterium. Energy Convers Manag 1995;36:763–6. doi:10.1016/0196-8904(95)00116-U.

[88] Franco-Morgado M, Alcántara C, Noyola A, Muñoz R, González-Sánchez A. A study of photosynthetic biogas upgrading based on a high rate algal pond under alkaline conditions: Influence of the illumination regime. Sci Total Environ 2017;592:419–25. doi:10.1016/j.scitotenv.2017.03.077.

[89] Chi Z, O'Fallon J V, Chen S. Bicarbonate produced from carbon capture for algae culture. Trends Biotechnol 2011;29:537–41. doi:10.1016/j.tibtech.2011.06.006.

[90] Zhu C, Zhang R, Cheng L, Chi Z. A recycling culture of *Neochloris oleoabundans* in a bicarbonate-based integrated carbon capture and algae production system with harvesting by auto-flocculation. Biotechnol Biofuels 2018;11:1–11. doi:10.1186/s13068-018-1197-6.

[91] Meier L, Barros P, Torres A, Vilchez C, Jeison D. Photosynthetic biogas upgrading using microalgae: Effect of light/dark photoperiod. Renew Energy 2017;106:17–23. doi:10.1016/j.renene.2017.01.009.

[92] Kim G, Choi W, Lee CH, Lee K. Enhancement of dissolved inorganic carbon and carbon fixation by green alga Scenedesmus sp. in the presence of alkanolamine CO2 absorbents. Biochem Eng J 2013;78:18–23. doi:10.1016/j.bej.2013.02.010.

[93] Cheng J, Huang Y, Feng J, Sun J, Zhou J, Cen K. Improving CO_2 fixation efficiency by optimizing Chlorella PY-ZU1 culture conditions in sequential bioreactors. Bioresour Technol 2013;144:321–7. doi:10.1016/j.biortech.2013.06.122.

[94] Li S, Luo S, Guo R. Efficiency of CO_2 fixation by microalgae in a closed raceway pond. Bioresour Technol 2013;136:267–72. doi:10.1016/j.biortech.2013.03.025.

[95] Sobczuk TM, Camacho FG, Rubio FC, Fernández FGA, Molina Grima E. Carbon dioxide uptake efficiency by outdoor microalgal cultures in tubular airlift photobioreactors. Biotechnol Bioeng 2000;67:465–75.

[96] Fukuzawa H, Suzuki E, Komukai Y, Miyachi S. A gene homologous to chloroplast carbonic anhydrase (icfA) is essential to photosynthetic carbon dioxide fixation by *Synechococcus PCC7942*. Proc Natl Acad Sci 1992;89:4437–41. doi:10.1073/pnas.89.10.4437.

[97] Thiansathit W, Keener TC, Khang SJ, Ratpukdi T, Hovichitr P. The kinetics of *Scenedesmus obliquus* microalgae growth utilizing carbon dioxide gas from biogas. Biomass and Bioenergy 2015;76:79–85. doi:10.1016/j.biombioe.2015.03.012.

[98] Basu S, Sarma Roy A, Ghoshal AK, Mohanty K. Operational strategies for maximizing CO_2 utilization efficiency by the novel microalga *Scenedesmus obliquus* SA1 cultivated in lab-scale photobioreactor. Algal Res 2015;12:249–57. doi:10.1016/j.algal.2015.09.010.

[99] Cheng J, Yang Z, Zhou J, Cen K. Improving the CO_2 fixation rate by increasing flow rate of the flue gas from microalgae in a raceway pond. Korean J Chem Eng 2018;35:498–502. doi:10.1007/s11814-017-0300-1.

[100] Valdés FJ, Hernández MR, Catalá L, Marcilla A. Estimation of CO_2 stripping/ CO_2 microalgae consumption ratios in a bubble column photobioreactor using the analysis of the pH profiles. Application to *Nannochloropsis oculata* microalgae culture. Bioresour Technol 2012;119:1–6. doi:10.1016/j.biortech.2012.05.120.

[101] Hulatt CJ, Thomas DN. Productivity, carbon dioxide uptake and net energy return of microalgal bubble column photobioreactors. Bioresour Technol 2011;102:5775–87. doi:10.1016/j.biortech.2011.02.025.

[102] Xia A, Hu Z, Liao Q, Huang Y, Zhu X, Ye W, et al. Enhancement of CO_2 transfer and microalgae growth by perforated inverted arc trough internals in a flat plate photobioreactor. Bioresour Technol 2018;269:292–9. doi:10.1016/j.biortech.2018.08.110.

[103] Chiu SY, Kao CY, Chen CH, Kuan TC, Ong SC, Lin CS. Reduction of CO_2 by a high-density culture of *Chlorella* sp. in a semicontinuous photobioreactor. Bioresour Technol 2008;99:3389–96. doi:10.1016/j.biortech.2007.08.013.

[104] Vo HNP, Bui XT, Nguyen TT, Nguyen DD, Dao TS, Cao NDT, et al. Effects of nutrient ratios and carbon dioxide bio-sequestration on biomass growth of *Chlorella* sp. in bubble column photobioreactor. J Environ Manage 2018;219:1–8. doi:10.1016/j.jenvman.2018.04.109.

[105] Alcántara C, García-Encina PA, Muñoz R. Evaluation of the simultaneous biogas upgrading and treatment of centrates in a high-rate algal pond through C, N and P mass balances. Water Sci Technol 2015;72:150–7. doi:10.2166/wst.2015.198.

[106] Leonard C, Ferrasse JH, Boutin O, Lefevre S, Viand A. Bubble column reactors for high pressures and high temperatures operation. vol. 100. Institution of Chemical Engineers; 2015. doi:10.1016/j.cherd.2015.05.013.

[107] Cheng L, Li T, Keener TC, Lee JY. A mass transfer model of absorption of carbon dioxide in a bubble column reactor by using magnesium hydroxide slurry. Int J Greenh Gas Control 2013;17:240–9. doi:10.1016/j.ijggc.2013.05.018.

[108] Kantarci N, Borak F, Ulgen KO. Bubble column reactors. Process Biochem 2005;40:2263–83. doi:10.1016/j.procbio.2004.10.004.

[109] Rollbusch P, Bothe M, Becker M, Ludwig M, Grünewald M, Schlüter M, et al. Bubble columns operated under industrially relevant conditions - Current understanding of design parameters. Chem Eng Sci 2015;126:660–78. doi:10.1016/j.ces.2014.11.061.

[110] Götz M, Lefebvre J, Mörs F, Ortloff F, Reimert R, Bajohr S, et al. Novel gas holdup correlation for slurry bubble column reactors operated in the homogeneous regime. Chem Eng J 2017;308:1209–24. doi:10.1016/j.cej.2016.09.101.

[111] Pourtousi M, Ganesan P, Sahu JN. Effect of bubble diameter size on prediction of flow pattern in Euler-Euler simulation of homogeneous bubble column regime. Meas J Int Meas Confed 2015;76:255–70. doi:10.1016/j.measurement.2015.08.018.

[112] Manjrekar ON, Sun Y, He L, Tang YJ, Dudukovic MP. Hydrodynamics and mass transfer coefficients in a bubble column photo-bioreactor. Chem Eng Sci 2017;168:55–66. doi:10.1016/j.ces.2017.04.016.

[113] Rodero M del R, Severi CA, Rocher-Rivas R, Quijano G, Muñoz R. Long-term influence of high alkalinity on the performance of photosynthetic biogas upgrading. Fuel 2020;281:118804. doi:10.1016/j.fuel.2020.118804.

[114] Marín D, Carmona-Martínez AA, Blanco S, Lebrero R, Muñoz R. Innovative operational strategies in photosynthetic biogas upgrading in an outdoors pilot scale algal-bacterial photobioreactor. Chemosphere 2021;264. doi:10.1016/j.chemosphere.2020.128470.

[115] Serejo ML, Posadas E, Boncz MA, Blanco S, García-Encina P, Muñoz R. Influence of biogas flow rate on biomass composition during the optimization of biogas upgrading in microalgal-bacterial processes. Environ Sci Technol 2015;49:3228–36. doi:10.1021/es5056116.

[116] Posadas E, Szpak D, Lombó F, Domínguez A, Díaz I, Blanco S, et al. Feasibility study of biogas upgrading coupled with nutrient removal from anaerobic effluents using microalgae-based processes. J Appl Phycol 2016;28:2147–57. doi:10.1007/s10811-015-0758-3.

[117] Rodero M del R, Carvajal A, Arbib Z, Lara E, de Prada C, Lebrero R, et al. Performance evaluation of a control strategy for photosynthetic biogas upgrading in a semi-industrial scale photobioreactor. Bioresour Technol 2020;307:123207. doi:10.1016/j.biortech.2020.123207.

[118] Rodero M del R, Carvajal A, Castro V, Navia D, de Prada C, Lebrero R, et al. Development of a control strategy to cope with biogas flowrate variations during photosynthetic biogas upgrading. Biomass and Bioenergy 2019;131. doi:10.1016/j.biombioe.2019.105414.

[119] Rodero M del R, Lebrero R, Serrano E, Lara E, Arbib Z. Technology validation of photosynthetic biogas upgrading in a semi- industrial scale algal-bacterial photobioreactor. Bioresour Technol 2019;279:43–9. doi:10.1016/j.biortech.2019.01.110.

[120] Rodero M del R, Posadas E, Toledo-Cervantes A, Lebrero R, Muñoz R. Influence of alkalinity and temperature on photosynthetic biogas upgrading efficiency in high rate algal ponds. Algal Res 2018;33:284–90. doi:10.1016/j.algal.2018.06.001.

[121] Posadas E, Marín D, Blanco S, Lebrero R, Muñoz R. Simultaneous biogas upgrading and centrate treatment in an outdoors pilot scale high rate algal pond. Bioresour Technol 2017;232:133–41. doi:10.1016/j.biortech.2017.01.071.

[122] Posadas E, Serejo ML, Blanco S, Pérez R, García-Encina PA, Muñoz R. Minimization of biomethane oxygen concentration during biogas upgrading in algal-bacterial photobioreactors. Algal Res 2015;12:221–9. doi:10.1016/j.algal.2015.09.002.

[123] Vasumathi KK, Premalatha M, Subramanian P. Parameters influencing the design of photobioreactor for the growth of microalgae. Renew Sustain Energy Rev 2012;16:5443–50. doi:10.1016/j.rser.2012.06.013.

[124] Huang Q, Jiang F, Wang L, Yang C. Design of Photobioreactors for mass cultivation of photosynthetic organisms. Engineering 2017;3:318–29. doi:10.1016/J.ENG.2017.03.020.

[125] Vo HNP, Ngo HH, Guo W, Nguyen TMH, Liu Y, Liu Y, et al. A critical review on designs and applications of microalgae-based photobioreactors for pollutants treatment. Sci Total Environ 2019;651:1549–68. doi:10.1016/j.scitotenv.2018.09.282.

[126] Sforza E, Simionato D, Giacometti GM, Bertucco A, Morosinotto T. Adjusted light and dark cycles can optimize photosynthetic efficiency in algae growing in photobioreactors. PLoS One 2012;7. doi:10.1371/journal.pone.0038975.

[127] Shang H, Scott JA, Shepherd SH, Ross GM. A dynamic thermal model for heating microalgae incubator ponds using off-gas. Chem Eng Sci 2010;65:4591–7. doi:10.1016/j.ces.2010.04.042.

[128] Radzun KA, Wolf J, Jakob G, Zhang E, Stephens E, Ross I, et al. Automated nutrient screening system enables high-throughput optimisation of microalgae production conditions. Biotechnol Biofuels 2015;8(65):1–17. doi:10.1186/s13068-015-0238-7.

[129] Idelovitch E, Michail M. Nitrogen removal by free ammonia stripping from high. Water Pollut Control Fed 1987;53:1391–401.

[130] Carvalho AP, Meireles LA, Malcata FX. Microalgal reactors: A review of enclosed system designs and performances. Biotechnol Prog 2006;22:1490–506. doi:10.1021/bp060065r.

[131] Posten C. Design principles of photo-bioreactors for cultivation of microalgae. Eng Life Sci 2009;9:165–77. doi:10.1002/elsc.200900003.

[132] Goli A, Shamiri A, Talaiekhozani A, Eshtiaghi N, Aghamohammadi N, Kheireddine M. An overview of biological processes and their potential for CO_2 capture. J Environ Manage 2016;183:41–58. doi:10.1016/j.jenvman.2016.08.054.

[133] Ugwu CU, Aoyagi H, Uchiyama H. Photobioreactors for mass cultivation of algae. Bioresour Technol 2008;99:4021–8. doi:10.1016/j.biortech.2007.01.046.

[134] Zhu C, Zhu H, Cheng L, Chi Z. Bicarbonate-based carbon capture and algal production system on ocean with floating inflatable-membrane photobioreactor. J Appl Phycol 2018;30:875–85. doi:10.1007/s10811-017-1285-1.

[135] Sierra E, Acien FG, Fernandez JM, Garcia JL, Gonzalez C, Molina E. Characterization of a flat plate photobioreactor for the production of microalgae. Chem Eng J 2008;138:136–47. doi:10.1016/j.cej.2007.06.004.

[136] Dasgupta CN, Jose Gilbert J, Lindblad P, Heidorn T, Borgvang SA, Skjanes K, et al. Recent trends on the development of photobiological processes and photobioreactors for the improvement of hydrogen production. Int J Hydrogen Energy 2010;35:10218–38. doi:10.1016/j.ijhydene.2010.06.029.

[137] Endres CH, Roth A, Brück TB. Modelling microalgae productivity in industrial-scale vertical flat panel photobioreactors. Environ Sci Technol 2018;52:5490–8. doi:10.1021/acs.est.7b05545.

[138] Guo Y, Yuan Z, Xu J, Wang Z, Yuan T, Zhou W, et al. Metabolic acclimation mechanism in microalgae developed for CO_2 capture from industrial flue gas. Algal Res 2017;26:225–33. doi:10.1016/j.algal.2017.07.029.

[139] Tan J Sen, Lee SY, Chew KW, Lam MK, Lim JW, Ho SH, et al. A review on microalgae cultivation and harvesting, and their biomass extraction processing using ionic liquids. Bioengineered 2020;11:116–29. doi:10.1080/21655979.2020.1711626.

[140] Yan C, Zhang Q, Xue S, Sun Z, Wu X, Wang Z, et al. A novel low-cost thin-film flat plate photobioreactor for microalgae cultivation. Biotechnol Bioprocess Eng 2016;21:103–9. doi:10.1007/s12257-015-0327-2.

[141] Zhou W, Chen P, Min M, Ma X, Wang J, Griffith R, et al. Environment-enhancing algal biofuel production using wastewaters. Renew Sustain Energy Rev 2014;36:256–69. doi:10.1016/j.rser.2014.04.073.

[142] de Jesus SS, Maciel Filho R. Potential of algal biofuel production in a hybrid photobioreactor. Chem Eng Sci 2017;171:282–92. doi:10.1016/j.ces.2017.05.041.

[143] García-Galán MJ, Gutiérrez R, Uggetti E, Matamoros V, García J, Ferrer I. Use of full-scale hybrid horizontal tubular photobioreactors to process agricultural runoff. Biosyst Eng 2018;166:138–49. doi:10.1016/j.biosystemseng.2017.11.016.

[144] Toledo-Cervantes A, Estrada JM, Lebrero R, Muñoz R. A comparative analysis of biogas upgrading technologies: Photosynthetic vs physical/chemical processes. Algal Res 2017;25:237–43. doi:10.1016/j.algal.2017.05.006.

[145] Kebede E, Ahlgren G. Optimum growth conditions and light utilization efficiency of Spirulina. Hydrobiologia 1996:99–109.

[146] Toor SS, Reddy H, Deng S, Hoffmann J, Spangsmark D, Madsen LB, et al. Hydrothermal liquefaction of *Spirulina* and *Nannochloropsis salina* under subcritical and supercritical water conditions. Bioresour Technol 2013;131:413–9. doi:10.1016/j.biortech.2012.12.144.

[147] Chisti Y. Biodiesel from microalgae. Biotechnol Adv 2007;25:294–306. doi:10.1016/j.biotechadv.2007.02.001.

[148] Singh G, Patidar SK. Microalgae harvesting techniques: A review. J Environ Manage 2018;217:499–508. doi:10.1016/j.jenvman.2018.04.010.

[149] Barros AI, Gonçalves AL, Simões M, Pires JCM. Harvesting techniques applied to microalgae: A review. Renew Sustain Energy Rev 2015;41:1489–500. doi:10.1016/j.rser.2014.09.037.

[150] Show K, Lee D. Chapter 5 - Algal Biomass Harvesting. Biofuels from Algae, Elsevier B.V.; 2014, p. 85–110. doi:10.1016/B978-0-444-59558-4.00005-X.

[151] Habib MAB, Parvin M, Huntington TC, Hasan MR. A Review on culture, production and use of *Spirulina* as food for humans and feeds for domestic animals and Fish. vol. 1034. Rome: 2008.

[152] Christenson L, Sims R. Production and harvesting of microalgae for wastewater treatment, biofuels, and bioproducts. Biotechnol Adv 2011;29:686–702. doi:10.1016/j.biotechadv.2011.05.015.

[153] Rawat I, Ranjith Kumar R, Mutanda T, Bux F. Dual role of microalgae: Phycoremediation of domestic wastewater and biomass production for sustainable biofuels production. Appl Energy 2011;88:3411–24. doi:10.1016/j.apenergy.2010.11.025.

[154] García-Pérez JS, Beuckels A, Vandamme D, Depraetere O, Foubert I, Parra R, et al. Influence of magnesium concentration, biomass concentration and pH on flocculation of Chlorella vulgaris. Algal Res 2014;3:24–9. doi:10.1016/j.algal.2013.11.016.

[155] Wu Z, Zhu Y, Huang W, Zhang C, Li T, Zhang Y, et al. Evaluation of flocculation induced by pH increase for harvesting microalgae and reuse of flocculated medium. Bioresour Technol 2012;110:496–502. doi:10.1016/j.biortech.2012.01.101.

[156] Molina Grima E, Belarbi EH, Acién Fernández FG, Robles Medina A, Chisti Y. Recovery of microalgal biomass and metabolites: Process options and economics. Biotechnol Adv 2003;20:491–515. doi:10.1016/S0734-9750(02)00050-2.

[157] Komárek J, Johansen JR. Filamentous Cyanobacteria. Freshw. Algae North Am. Ecol. Classif., 2015, p. 135–235. doi:10.1016/B978-0-12-385876-4.00004-9.

[158] Elzenga JTM, Prins HBA, Stefels J. carbonic anhydrase activity in inorganic carbon utilization of *Phaeocystis globose* (Prymnesiophyceae): A comparison with other marine algae using the isotopic. Limnol Oceanogr 2000;45:372–80. doi:10.2307/2670491.

[159] Rocha JMS, Garcia JEC, Henriques MHF. Growth aspects of the marine microalga *Nannochloropsis gaditana*. Biomol Eng 2003;20:237–42. doi:10.1016/S1389-0344(03)00061-3.

[160] Huertas IE, Lubian LM. Comparative study of dissolved inorganic carbon utilization and photosynthetic responses in *Nannochloris* (Chlorophyceae) and *Nannochloropsis* (Eustigmatophyceae) species. Can J Bot Can Bot 1998;76:1104–8. doi:10.1139/cjb-76-6-1104.

[161] Emma Huertas I, Colman B, Espie GS, Lubian LM. Active transport of CO_2 by three species of marine microalgae. J Phycol 2000;36:314–20. doi:10.1046/j.1529-8817.2000.99142.x.

[162] Danilov RA, Ekelund NGA. Effects of pH on the growth rate, mobility and photosynthesis in *Euglena gracilis*. Folia Microbiol (Praha) 2001;46:549–54. doi:10.1007/BF02818001.

[163] Colman B, Balkos KD. Mechanisms of inorganic carbon acquisition in two *Euglena* species. Can J Bot Can Bot 2005;83:865–71. doi:10.1139/b05-072.

[164] Giraldez-Ruiz N, Bonilla I, Fernadez-Piñas F. The relationship between intracellular pH, growth characteristics and calcium in the cyanobacterium *Anabaena* sp. strain PCC7120 exposed to low pH. New Phytol 1999;137:599–605. doi:10.1046/j.1469-8137.1997.00864.x.

[165] Ferriols VMEN, Saclauso CA, Fortes NR, Toledo NA, Pahila IG. Effect of Elevated carbon dioxide and phosphorus levels on nitrogen uptake, lipid content and growth of *Tetraselmis* sp. J Fish Aquat Sci 2013;8:659–72. doi:10.3923/jfas.2013.659.672.

[166] Jeon H, Jeong J, Baek K, McKie-Krisberg Z, Polle JEW, Jin ES. Identification of the carbonic anhydrases from the unicellular green alga *Dunaliella salina* strain CCAP 19/18. Algal Res 2016;19:12–20. doi:10.1016/j.algal.2016.07.010.

[167] Dhaka P, Pal Singh G. Effect of pH on growth and biopigment accumulation of green alga *Dunaliella salina*. Int J Pharm Sci Res 2018;9:271–6. doi:10.13040/IJPSR.0975-8232.9(1).271-76.

[168] Peng L, Zhang Z, Lan CQ, Basak A, Bond N, Ding X, et al. Alleviation of oxygen stress on *Neochloris oleoabundans*: effects of bicarbonate and pH. J Appl Phycol 2017;29:143–52. doi:10.1007/s10811-016-0931-3.

[169] Santos AM, Janssen M, Lamers PP, Evers WAC, Wijffels RH. Growth of oil accumulating microalga *Neochloris oleoabundans* under alkaline-saline conditions. Bioresour Technol 2012;104:593–9. doi:10.1016/j.biortech.2011.10.084.

[170] Palmqvist K, Ogren E, Lernmark U. The CO_2-concentrating mechanism is absent in the green-alga *Coccomyxa* - a comparative study of photosynthetic CO_2 and light responses of *Coccomyxa*, *Chlamydomonas reinhardtii* and barley protoplasts. Plant Cell Environ 1994;17:65–72. doi:10.1111/j.1365-3040.1994.tb00266.x.

[171] Yang J, Tang H, Zhang X, Zhu X, Huang Y, Yang Z. High temperature and pH favor *Microcystis aeruginosa* to outcompete *Scenedesmus obliquus*. Environ Sci Pollut Res 2018;25:4794–802. doi:10.1007/s11356-017-0887-0.

[172] Sultemeyer DF, Miller AG, Espie GS, Fock HP, Canvin DT. Active CO_2 transport by the green alga *Chlamydomonas reinhardtii*. Plant Physiol 1989;89:1213–9. doi:10.1104/pp.89.4.1213.

[173] Dhaliwal G, Lee T, Talwar D, Wang O. Effect of varying pH adjusted media on the growth rate of. Exped UBC 2017;7:1–14.

[174] Swarnalatha G V., Hegde NS, Chauhan VS, Sarada R. The effect of carbon dioxide rich environment on carbonic anhydrase activity, growth and metabolite production in indigenous freshwater microalgae. Algal Res 2015;9:151–9. doi:10.1016/j.algal.2015.02.014.

[175] Schnackenberg J, Ikemoto H, Miyachi S. Photosynthesis and hydrogen evolution under stress conditions in a CO_2-tolerant marine green alga, *Chlorococcum littorale*. J Photochem Photobiol B Biol 1996;34:59–62. doi:10.1016/1011-1344(95)07270-5.

[176] Satoh A, Kurano N, Miyachi S. Inhibition of photosynthesis by intracellular carbonic anhydrase in microalgae under excess concentrations of CO_2. Photosynth Res 2001;68:215–24. doi:10.1023/A:1012980223847.

[177] Ota M, Takenaka M, Sato Y, Lee Smith R, Inomata H. Effects of light intensity and temperature on photoautotrophic growth of a green microalga, *Chlorococcum littorale*. Biotechnol Reports 2015;7:24–9. doi:10.1016/j.btre.2015.05.001.

[178] Usharani G, Saranraj P, Kanchana D. *Spirulina* Cultivation: A Review. Int J Pharm Biol Arch 2012;3:1327–41.

[179] Qiao H, Cong C, Sun C, Li B, Wang J, Zhang L. Effect of culture conditions on growth, fatty acid composition and DHA/EPA ratio of *Phaeodactylum tricornutum*. Aquaculture 2016;452:311–7. doi:10.1016/j.aquaculture.2015.11.011.

[180] Rotatore C, Colman B, Kuzma M. the Active uptake of carbon dioxide by the marine diatoms *Phaeodactylum tricornutum* and *Cyclotella* sp. Plant Cell Environ 1995;18:913–8. doi:10.1111/j.1365-3040.1995.tb00600.x.

[181] Perrin L, Probert I, Langer G, Aloisi G. Growth of the coccolithophore *Emiliania huxleyi* in light and nutrient-limited batch reactors: Relevance for the BIOSOPE deep ecological niche of coccolithophores. Biogeosciences 2016;13:5983–6001. doi:10.5194/bg-13-5983-2016.

[182] Moheimani NR, Borowitzka MA. Increased CO_2 and the effect of pH on growth and calcification of *Pleurochrysis carterae* and *Emiliania huxleyi* (Haptophyta) in semicontinuous cultures. Appl Microbiol Biotechnol 2011;90:1399–407. doi:10.1007/s00253-011-3174-x.

[183] Takabe Y, Hidaka T, Tsumori J, Minamiyama M. Effects of hydraulic retention time on cultivation of indigenous microalgae as a renewable energy source

using secondary effluent. Bioresour Technol 2016;207:399–408. doi:10.1016/j.biortech.2016.01.132.

[184] Ruiz J, Álvarez-Díaz PD, Arbib Z, Garrido-Pérez C, Barragán J, Perales JA. Performance of a flat panel reactor in the continuous culture of microalgae in urban wastewater: Prediction from a batch experiment. Bioresour Technol 2013;127:456–63. doi:10.1016/j.biortech.2012.09.103.

[185] Płaczek M, Patyna A, Witczak S. Technical evaluation of photobioreactors for microalgae cultivation. E3S Web Conf 2017;19:1–10. doi:10.1051/e3sconf/20171902032.

[186] Richardson JW, Johnson MD, Zhang X, Zemke P, Chen W, Hu Q. A financial assessment of two alternative cultivation systems and their contributions to algae biofuel economic viability. Algal Res 2014;4:96–104. doi:10.1016/j.algal.2013.12.003.

[187] Borowitzka MA. High-value products from microalgae-their development and commercialisation. J Appl Phycol 2013;25:743–56. doi:10.1007/s10811-013-9983-9.

[188] Gifuni I, Pollio A, Safi C, Marzocchella A, Olivieri G. Current bottlenecks and challenges of the microalgal biorefinery. Trends Biotechnol 2019;37:242–52. doi:10.1016/j.tibtech.2018.09.006.

[189] Peppel T, Seeburg D, Fulda G, Kraus M, Trommler U, Roland U, et al. Methods for the trace oxygen removal from methane-rich gas streams. Chem Eng Technol 2017;40:153–61. doi:10.1002/ceat.201600171.

3 Design, commissioning and performance assessment of a lab-scale bubble column reactor for photosynthetic biogas upgrading with *Spirulina platensis*

Design, commissioning and performance assessment of a lab-scale bubble column reactor for photosynthetic biogas upgrading with *Spirulina platensis*

Archishman Bose[a,b], Richard O'Shea[a,b], Richen Lin[a,b], Jerry D Murphy[a,b]

[a]Environmental Research Institute, MaREI Centre, University College Cork, Cork, T23 XE10, Ireland

[b]Department of Civil, Structural and Environmental Engineering, School of Engineering and Architecture, University College Cork, Cork, T12 K8AF, Ireland.

Abstract

The two-step bubble column-photobioreactor photosynthetic biogas upgrading system can enable the simultaneous production of biomethane and value-added products from microalgae. However, due to the influence of a large number of variables, including downstream processes and the presence of microalgae, no unanimity has been reached regarding the performance of bubble column reactors in photosynthetic biogas upgrading. To investigate this further, the present work documents in detail, the design and commissioning of a lab-scale bubble column reactor capable of treating up to 16.3 L_n/hr of biogas while being scalable. The performance of the bubble column was assessed at a pH of 9.35 with different algal densities of *Spirulina platensis* at 20°C in the presence of light (3-5 klux or 40.5-67.5 $\mu molm^{-2}s^{-1}$). A liquid/gas flow (L/G) ratio of 0.5 allowed consistent CO_2 removal of over 98% irrespective of algal density or its photosynthetic activity. For lower concentrations of algae, volumetric O_2 concentration in the upgraded biomethane varied between 0.05-0.52%, thus providing grid quality biomethane. However, for higher algal concentrations, increased oxygen content in the upgraded biomethane both due to enhanced O_2 stripping and the photosynthetic activity of the microalgae, as well as clogging and foaming posed severe operational challenges.

Nomenclature

Symbols/Acronyms	Descriptions
Alk	Alkalinity [g-IC/L]
ANOVA	Analysis of Variance
DW	Dry weight
EBRT	Empty bed residence Time [mins]
G	Biogas flow rate [mL_n/s]
H_{O_2}	Henry' Law Constant for oxygen [L.atm/mol]
IC	Inorganic carbon
$K_{G_{CO_2}}a$	Mean overall CO_2 mass transfer coefficient [hr^{-1}]
$k_{l_{O_2}}a$	Volumetric mass transfer coefficient for O_2 [hr^{-1} or s^{-1}]
L/G	Liquid to gas flow rate (L/G) ratio
mL_n	millilitres normal
N	Molar flow rate [mol/s]
$r_{A_{CO_2}}$	Mean steady state CO_2 absorption rate [mol/L/s]
RE_CO_2	CO_2 removal efficiency [%]
$r_{S_{O_2}}$	Rate of oxygen stripping [mol/L/s]]
TRL	Technology readiness level
Subscripts	**Descriptions**
BC	Bubble column
BG	Biogas
BM	Biomethane

3.1 Introduction

3.1.1 Photosynthetic biogas upgrading

Conventional physicochemical biogas upgrading technologies such as water scrubbing and pressure swing absorption continue to consume a significant amount of energy (up to 6% of the energy content in biogas) [1]. In addition, it also results in a high cost of biomethane necessitating incentives to achieve financial sustainability [2]. As an alternative, biological biogas upgrading technologies are being investigated to increase the sustainability of biomethane derived from biogas by reducing costs and energy demands [1]. Photosynthetic biogas upgrading is a novel biogas upgrading technology that can be employed to remove the CO_2 and H_2S in biogas by absorption in a carbonate-bicarbonate based alkaline algal medium [3,4]. The absorbed CO_2 would allow the cultivation of microalgae for food, feed and/or energy [5]. As a consequence, the resulting biomethane could be both economically and environmentally more beneficial than that obtained through traditional biogas upgrading systems [5,6]. The two-step bubble column-photobioreactor photosynthetic biogas upgrading configuration is currently under assessment by the scientific community for optimisation of both; biogas upgrading in a bubble column and growth of microalgae in a photobioreactor [7,8].

3.1.2 Significance of operation and design of the bubble column

Effective bubble column operation in photosynthetic biogas upgrading must achieve continuous grid quality biomethane; this typically requires biomethane with CO_2 and O_2 concentrations below 2.5% and 1% on a volume basis, respectively [9,10]. Photobioreactors (PBRs) should then ensure rapid and effective CO_2 utilisation by microalgae to achieve a sustainable biogas upgrading facility utilising microalgae. Optimisation studies for CO_2 removal in bubble column reactors with carbonate-bicarbonate solutions in the absence of microalgae are available in literature as a stand-alone setup [11,12]. However such optimal operational conditions in the bubble column may not be ideal for microalgae cultivation. For example, the requirement of a high temperature (above 50°C) [13] and a high pH (12 and above) [14] is fatal to most microalgae species [8]. At a temperature and pH below 35 °C and 10 respectively, CO_2 absorption rates drop significantly [14]. Therefore, the bubble

columns for photosynthetic biogas upgrading are usually of a large aspect ratio (ratio of height to diameter, also termed length to diameter or L/D ratio) and employ low gas flow rates. This in turn results in high empty bed residence time or EBRT [mins] (signifying the time taken by the gas to traverse the length of the bubble column in absence of any liquid medium), typically ranging between 15 and 90 mins (Table 3-1). Typical EBRT for industrial applications are in the range of 3-6 mins [15], and as such, this would potentially somewhat limit the scale-up and industrial application of not only the bubble column but also the photosynthetic biogas upgrading technology. In addition, although present in minor quantities (<1%), the H_2S in biogas could affect the performance of CO_2 absorption in inadequately designed bubble columns for photosynthetic biogas upgrading. To highlight this, Meier et al. (2018) [3] observed no significant change in CO_2 removal efficiency (98%) in the presence (1,800-3,500 ppm_v) and absence of H_2S in the biogas when the bubble column pH was maintained around 8.7. However, Bahr et al. (2014) [15], controlling the bubble column inlet pH at 8.5, noticed a drop in the CO_2 removal efficiency from 95% ± 3% to 89% ± 5% when the H_2S content in the biogas was increased from 0 to 500 ppm_v. However, when it was further increased to 1,500 ppm_v no further drop in the CO_2 removal efficiency was noticed. In both the studies, an almost complete H_2S removal was recorded. Therefore, ensuring conditions in the bubble column for sufficient CO_2 removal is required to allow simultaneous H_2S removal with a minor influence on the absorption of CO_2 and bubble column performance. The absorbed H_2S in the form of sulphates, besides providing valuable nutrient supplements, was found to not influence the growth rates of microalgae and the design of photobioreactors [3].

Stripping of dissolved oxygen (DO) from the algal liquid during biogas upgrading is also a major concern. Often, this leads to the O_2 concentration in the upgraded biomethane beyond permissible limits for grid injection [8,16]. Additional technological bottlenecks, such as the fluctuation in biomethane composition due to the diurnal [9] and seasonal [17] variations in the PBR, especially open ponds must also be overcome to achieve practical applications of photosynthetic biogas upgrading. On the contrary, although the scope for improvements in the microalgae cultivation and harvesting techniques have been highlighted by Bose et al. (2019) [8], unlike that for the bubble column, these improvements are not technological bottlenecks for photosynthetic biogas upgrading. Especially with the adequate selection of microalgae

species, the cultivation and harvesting of microalgae can be further simplified [8]. For example, selecting filamentous microalgae *Spirulina platensis* would enable simple harvesting with the use of inclined screens [8]. Thus, optimisation and robust operation of the bubble column for biogas upgrading in conjunction with photosynthetic biogas upgrading requires further analysis and research.

Optimisation of bubble columns for industrial applications is often carried out in a lab-scale setup with a corresponding scale-up strategy [18,19]. The primary challenge for such studies is the effective prediction of the scaled-up performance of the bubble column. This is due to the difference in either/or *i)* heat and mass transfer characteristics; *(ii)* mixing and flow characteristics; *(iii)* chemical kinetics of the reacting system for the two separate scales (i.e., laboratory and industrial) [18,19]. Therefore, despite the simplistic design of the bubble column, the choice of different design parameters needs to be validated and appropriate scale-up criteria must be chosen to predict the industrial operation of the bubble column. In addition, the chosen design factors must also be robust and allow for flexibility in operation, apart from providing essential information on techno-economic and environmental aspects [17] of the operation of the bubble column.

3.1.3 Current trends in bubble column design for photosynthetic biogas upgrading

Photosynthetic biogas upgrading utilising a separate bubble column depends on multiple factors such as; biogas composition, pH, gas and liquid flow rates, the concentration of the algae, temperature and alkalinity, as well as the microalgae species and cultivation conditions [8,16,20]. Numerous studies have been undertaken to advance the aforementioned technology, however, results and conclusions have varied significantly. This can be attributed to the large variability in design factors, operation parameters and system configurations selected in the studies, summarised in Table 3-1.

Table 3-1 Scale and design factors of bubble columns applied for photosynthetic biogas upgrading in recent literature

References	Scale	Column Dimensions				Gas flow rate [LPH]	Operation Parameters								Optimal Biomethane Composition (%)	
		Diameter [cm]	Aspect ratio[§]	Volume [L]	Mode		L/G ratio	Superficial gas velocity [m/s]	EBRT [mins]	pH	Alkalinity [mgIC/L]	Temperature [°C]	X_{algae} [g/L]	Light	CO_2 [%]	O_2 [%]
Rodero et al. (2020) [23]	L	NR	NR	2.5	C	3	0.5	NR	NR	10	3,152-3,814	28±2	Varies	CLD	0.6-1	0.1 ± 0.1
Rodero et al. (2020) [21]	SI	NR	NR	150	CC	143-420	0.8-2.3	NR	NR	9.05-9.50	1,907 ±109	24.2±2	NR*	OP	2.4	≤ 1
Rodero et al. (2019) [24]	L	NR	NR	2.5	C	3.6-9	≤1.1	NR	NR	8.5-10	100-1,500	15 and 35	NR*	NR	1.5 (3.6 LPH gas flow)	≤ 1
Rodero et al. (2019) [25]	SI	SI	SI	150	CC	274-459	1.2-3.5	NR	NR	7.3-8.9	NR	12.4-23.5	NR*	OP	0.3 (L/G 3.5)	7.4 ± 0.4 (L/G 3.5)
Marin et al. (2018) [17]	P	4.4	37.5	2.5	C	3.12	1	0.057	48.25	9.4	1,663-4,138	9.1-24.4	NR*	OP	0.7-11.9	0 - 3.4
Rodero et al. (2018) [20]	L	4.4	37.5	2.5	C	4.9	0.5	0.089	30.89	7.2-11.5	100-1,500	15 and 35	NR*	CLD	At pH 10.5: 0.9±0.3 (1467±115 gIC/L)	0 - 0.2

References	Scale	Column Dimensions				Gas flow rate [LPH]	Operation Parameters								Optimal Biomethane Composition (%)	
		Diameter [cm]	Aspect ratio[§]	Volume [L]	Mode		L/G ratio	Superficial gas velocity [m/s]	EBRT [mins]	pH	Alkalinity [mgIC/L]	Temperature [°C]	X_{algae} [g/L]	Light	CO_2 [%]	O_2 [%]
															18.4±1 (505±57gIC/L)	
Posadas et al. (2017) [26]	P	4.4	37.5	2.5	C	3.12	0.5-5	0.057	48.25	8.8-9.8	267-2,660	20-23.8	NR*	OP	8.8	0.7-1.1
Toledo-Cervantes et al. (2017) [16]	L	4.4	37.5	2.5	C/CC	2.4	0.3-1	0.044	62.5	10.2±0.5	1,500±168	23.8±1.7	NR*	CLD	0.4±0.3 (C)	0.7 ± 0.4 (C)
Meier et al. (2017) [9]	L	1.2	2500	NR	CC	2.08	0.6	0.512	97.66	7.3	660-880	20-28	Varies	CLD	2-4.5	≤1
Franco-Morgado et al. (2017) [27]	L	1.9	NR	0.35	CC	0.65	5	NR	NR	9.3-9.7	1,130±0.09	16-28	NR*	CLD	0-0.3	2.6
Posadas et al. (2015) [28]	L	4.4	37.5	2.5	C	1.85±0.07	10.7±0.4	0.034±0.001	c. 80	7.9	66-126	23±1	NR*	CLD	6.6±0.7	≤1.2

References	Scale	Column Dimensions				Gas flow rate [LPH]	Operation Parameters								Optimal Biomethane Composition (%)	
		Diameter [cm]	Aspect ratio[§]	Volume [L]	Mode		L/G ratio	Superficial gas velocity [m/s]	EBRT [mins]	pH	Alkalinity [mgIC/L]	Temperature [°C]	X_{algae} [g/L]	Light	CO_2 [%]	O_2 [%]
Serejo et al. (2015) [29]	L	4.4	37.5	2.5	C	0.5-67	Varies	0.006-0.033	83.33-458.33	7.9	63-82	20.9-26.4	NR[*]	CLD	0.9-2.1 (L/G ≥ 15)	3 ± 1 (L/G ≥ 15)
Meier et al. (2015) [4]	L	2	110	0.7	C	0.09	2.33	0.055	66.67	7.7± 0.2	88-176	20±2	Varies	CLD	1.9	1.2

The acronyms are as follows: L: laboratory-scale; P: Pilot-scale; SI: Semi-industrial scale; NR: Not reported; C: Co-current; CC: Countercurrent; LPH: Litres per hour; IC: Inorganic Carbon; X_{algae}: Algae concentration; OP: Open Pond; CLD: Controlled Light and dark cycles

[*]Algal concentration although not explicitly reported, the algae was circulated in the bubble column after harvesting

[§]Aspect ratio signifies the height to diameter ratio of the bubble column

For instance, while Toledo-Cervantes et al., (2017) [16] concluded that a liquid to gas flow rate (L/G ratio) ratio of less than 1 is essential to achieve grid quality biomethane, Rodero et al., (2020) [21] reported 14.1% CO_2 concentration in upgraded biomethane at an L/G ratio of 0.8. The aim to minimise both CO_2 and O_2 simultaneously has also led to contradicting values of process parameters. For example, while a pH greater than 9 is essential to ensure adequate CO_2 removal, higher pH also seems to increase O_2 stripping into the biomethane [8]. In another instance, increasing algal concentration has been shown to improve bubble column hydrodynamics [22]. This could enhance both CO_2 removal and O_2 stripping. In fact, the presence of photosynthesising microalgae could increase the O_2 content in the upgraded biomethane further. However, in a recent study, Rodero et al. (2020) [23] obtained no statistically significant difference in CO_2 removal rate with increasing algal concentration in the bubble column. The impact on O_2 stripping was also not reported. A focused assessment of bubble column operations could therefore be considered essential to optimise biogas upgrading, which in turn would assist in advancing the overall photosynthetic biogas upgrading technology.

3.1.4 Objective

To study in detail the performance and hence, the opportunity to optimise photosynthetic biogas upgrading, a lab-scale bubble column unit was designed and commissioned. In the present work, rather than optimising the bubble column performance, its design and commissioning have been studied and documented. The performance of the bubble column has been evaluated under different operating conditions with the following objectives:

i. validate the design and performance of a lab-scale bubble column reactor for photosynthetic biogas upgrading.

ii. identify and resolve challenges to operating and assessing the performance of such facilities both on the laboratory and industrial scale.

iii. study the impacts of algal concentration and photosynthetic activity on reactor performance.

iv. develop a scale-up perspective and integration with microalgae cultivation systems.

3.2 Design and evaluation of bubble column for photosynthetic biogas upgrading

3.2.1 Working range and operating medium

A bubble column for photosynthetic biogas upgrading should be able to operate with a CO_2 and H_2S content in the inlet biogas between 20% to 50% and 0 to 10,000 ppm_v, respectively. A homogeneous flow regime, characterised by uniform flow and smaller bubbles (c. 3 mm diameter [30]) is preferable for CO_2 absorption due to the availability of a larger surface area and improved hydrodynamic and hydraulic performance [12,31] *Spirulina platensis* would be one of the most favourable microalgae species of choice for biogas upgrading as discussed in the previous work by the authors [8]. As such, the maximum working pH and temperature of the bubble column should be limited to 11 and 37 °C to avoid fatal consequences for *Spirulina platensis* [32]. Finally, the bubble column was operated near atmospheric pressures for ease of operation and to facilitate integration with open pond and closed photobioreactors alike.

3.2.2 Working principle for CO_2 absorption

In a carbonate-bicarbonate buffer solution, the carbonate ions dissociate in water to locally form hydroxyl ions, via the following Eq. 3.1 [33].

$$CO_3^{2-} + H_2O \Leftrightarrow HCO_3^- + OH^- \quad (3.1)$$

CO_2 absorption in such a solution (typically above pH 8) can then be described in two steps; the irreversible hydration equation (Eq. 3.2) producing bicarbonates and the instantaneous reversible proton transfer reaction (Eq. 3.3) yielding back carbonates [33,34]. The hydration equation, driven by locally formed hydroxyl ions is usually considered the rate-determining step for the CO_2 absorption process [34,35].

$$CO_2 + OH^- \rightarrow HCO_3^- \quad (3.2)$$

$$HCO_3^- + OH^- \Leftrightarrow CO_3^{2-} + H_2O \quad (3.3)$$

The overall absorption of CO_2 in sodium carbonate-bicarbonate buffer solution can thus be described as a combination of Eq. 3.1 and Eq. 3.2 as per the following Eq. 3.4 [33,35].

$$CO_2 + CO_3^{2-} + H_2O \Leftrightarrow 2HCO_3^- \quad \Delta G \cong -50 \text{ kJ/mol at } 300K \text{ [8]} \qquad (3.4)$$

3.2.3 Design and configuration of the lab-scale bubble column

3.2.3.1 Description of the overall setup

A lab-scale bubble column measuring 24 mm inner diameter (D_{BC}) and 2 m high was built using a clear acrylic tube. The co-current flow configuration was selected as per recommendations published by Toledo-Cervantes et al., (2017) [16]. A cylindrical diffuser (25 mm long; 18 mm diameter) was vertically mounted at the bottom of the column to sparge gas into the bubble column. All liquid heights were measured from the top of the sparger. Similar to recently studied lab-scale bubble columns for photosynthetic biogas upgrading [16,17], the column height (H_{BC}) selected for start-up and commissioning was 540 mm (aspect ratio or H/D ratio 22.5). This was implemented by tapping a liquid outlet at the desired height as indicated in Figure 3-1.

The entire setup was housed in a temperature-controlled cabinet, capable of operating between 20 °C and 35 °C. Heating and cooling was provided by an electric heater and an extractor fan respectively, that were connected to thermostatic controllers with temperature probes placed near the bubble column. The cabinet was also fitted with two cool white fluorescent lights to provide illumination between 2 to 6 klux (27-81 $\mu molm^{-2}s^{-1}$). A pictorial representation of the experimental setup is shown in Figure 3-2a.

3.2.3.2 Inlet configuration

Co-current operations mandated both the biogas and the liquid (alkaline algal solution) to be injected from the bottom of the bubble column. Liquid circulation into the bubble column at the desired flow rates was obtained using a VWR AU-UPC-EZ programmable peristaltic pump (2-70 ml/min with 1.6 mm (internal diameter) tube). The tube on the suction side of the pump was fitted with a fine mesh cloth at its mouth to prevent algal clumps from flowing into the bubble column. The mesh cloth provided a fair replication of a foot valve, widely used in the industry at the mouth of the suction

line of a liquid circulating pump to screen dirt, clumps and other particles. The gas supply was controlled by separate N_2 and CO_2 flow controllers (Red-y smart controller GSC, Vögtlin Instruments GmbH). This follows the recommendations of Serejo et al., (2015) [29] where N_2 was used to replace methane to avoid explosion hazards in experimental setups. To prevent backflow of liquid into the inlet air lines, the topmost point of the air line was located above the maximum possible liquid level in the bubble column, as shown in Figure 3-1. As an asphyxiant and potentially an explosive gas, H_2S was omitted due to health and safety concerns to minimise risks to personnel.

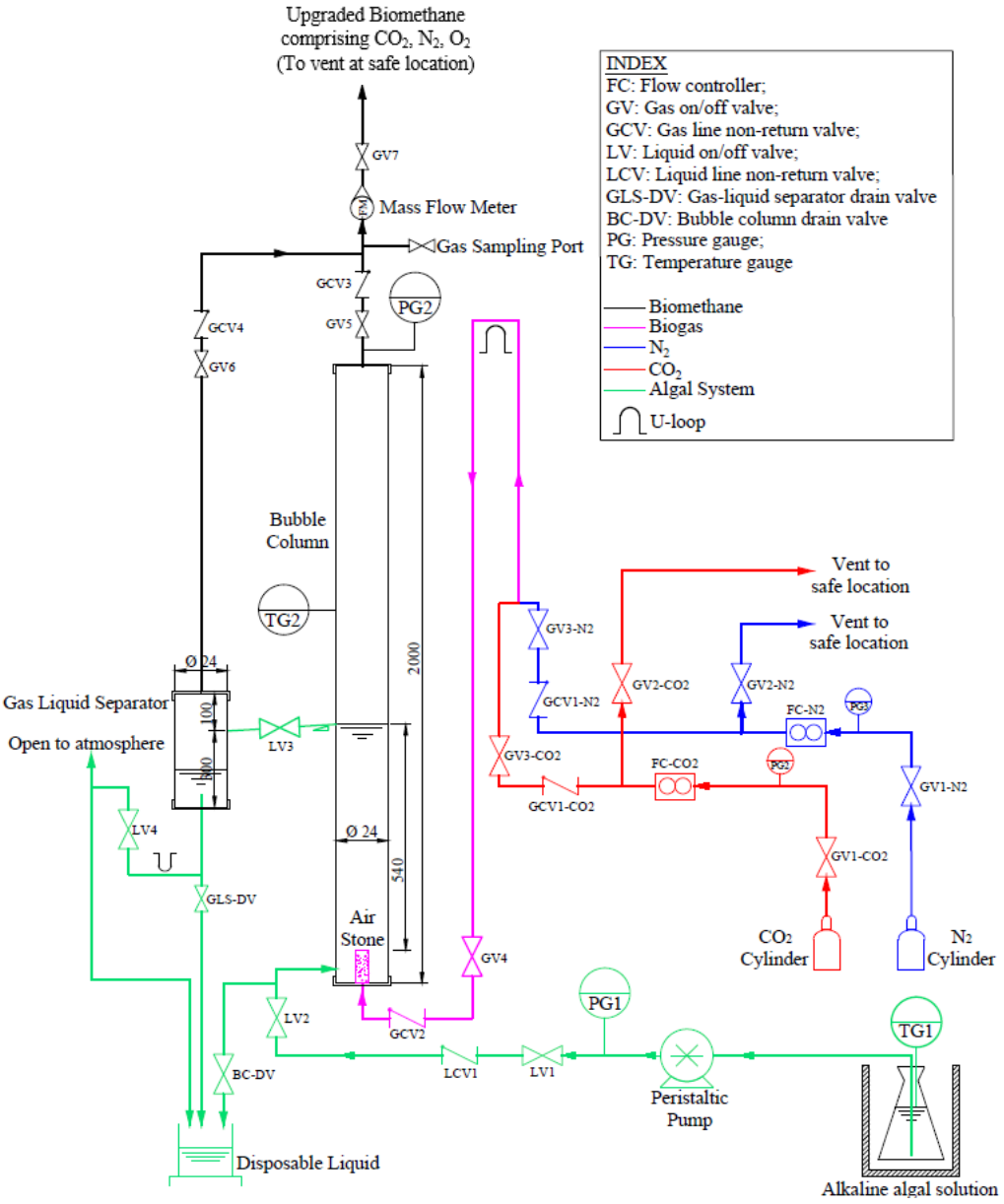


Figure 3-1 Process flow diagram and design details of the lab-scale bubble column for photosynthetic biogas upgrading (Not to scale)

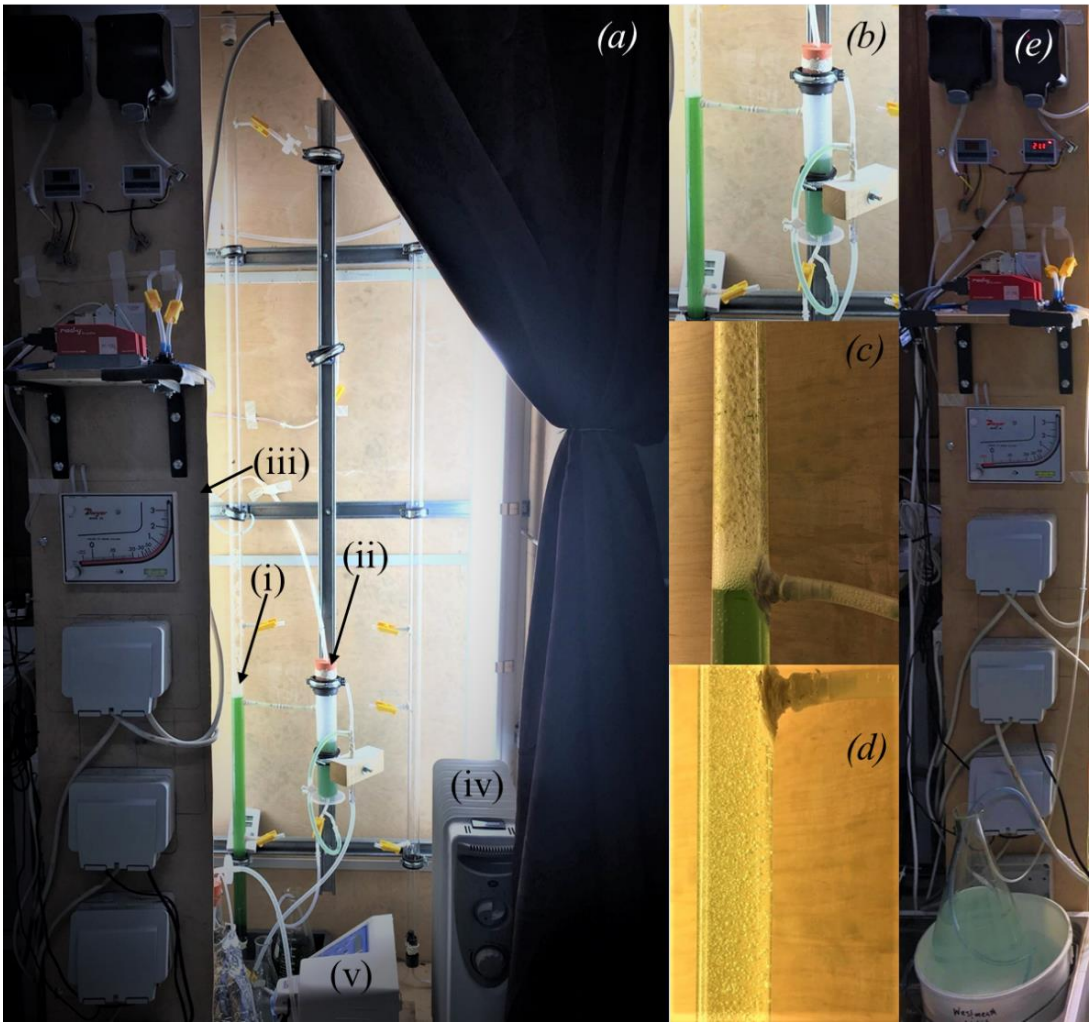


Figure 3-2 Pictorial representation of the experimental setup for photosynthetic biogas upgrading with (a) the overall bubble column reactor setup within a temperature and light controlled housing; (b) detail of the gas-liquid separator with a U-loop to prevent emptying by syphoning and also adjust the outlet liquid flow rate as per the inlet flow rate; (c) example of foaming observed during operation with high algae concentration; (d) representation of homogeneous flow regime characterised by uniform bubble size under low algal concentration; and (e) detail of the control panel with the condensate trap placed within an ice bath (bottom of the figure).
Additional details marked in figure (a) represent (i) the bubble column (additional tapping points for future experiments); (ii) the gas-liquid separator; (iii) control panel with gas flow controllers, mass flow meter, manometer gauge, and the switches for temperature control; (iv) the heater; and (v) the peristaltic pump

3.2.3.3 Outlet configuration

The liquid outlet from the bubble column was routed to a 300 mm high and 24 mm diameter gas-liquid separator. The connecting line from the bubble column outlet to the gas-liquid separator was gently sloped to prevent airlock formation and minimise fluctuations in the flow. From the gas-liquid separator, the liquid was routed through a U-tube configuration to a position higher than the bottom of the separator. This ensured that a minimum liquid level was maintained in the separator. As can be seen from Figure 3-1, at the higher location, one end of the liquid outlet from the gas-

liquid separator was kept open to the atmosphere using a tee connection. This avoided siphonic emptying of the gas-liquid separator. The system then became self-adjusting from a liquid flowrate perspective, whereby the liquid outlet flow rate would match the liquid inlet flow. The spent algal solution was collected and disposed of following safety guidelines.

The gas from the gas-liquid separator was connected to the upgraded biomethane exiting the top of the bubble column. The combined gas flow passed through a mass flow meter (Bronkhorst® F101D Low-ΔP-Flow Thermal Mass Meter) to vent at a safe location, as shown in Figure 3-1. A gas sampling point was also added before the flow meter to measure gas composition with minimal errors. A detailed discussion for such a setup is provided in Section 3.3.3. A differential pressure gauge was fitted to the gas outlet from the bubble column to measure the pressure in the entire set-up during continuous operation.

3.2.3.4 Process control and measurements

All operations were manually monitored and controlled, except the temperature controls. The inlet pH, alkalinity and DO of the algal solution were measured and controlled as necessary, described in Section 3.3.3. Constant pressure was maintained at the gas outlet from the bubble column during the entire duration of the experiments by adjusting the constriction of the downstream gas line tubing. The pH of the liquid at the outlet of the gas-liquid separator was monitored at regular intervals. The gas flow rate was logged continuously. When both the gas flow rate and the pH of the outlet liquid became constant simultaneously (less than 5% variation in both the gas flow rate and the pH was achieved over 120 seconds), the gas was collected for content analysis (specifically, the volumetric composition of CO_2, N_2 and O_2) by gas chromatography. Subsequently, the individual volumetric flow rates of the respective gases at a steady-state were obtained to allow evaluation of the performance of the bubble column.

3.2.4 Performance evaluation

The performance of the bubble column reactor was evaluated based on the CO_2 and O_2 content of the ensuing biomethane. The obtained values were compared with

existing literature to validate the design and operations of the bubble column setup for photosynthetic biogas upgrading.

3.2.4.1 CO_2 absorption

CO_2 absorption in a bubble column is typically analysed in terms of the absorption reaction rate and overall mass transfer coefficient [14]. The mean steady-state absorption rate of CO_2 ($r_{A_{CO_2}}$) [mol/L/s] can be described by the shell material balance in terms of the molar flow [mol/s] of CO_2 in the biogas entering the column ($N_{CO_2,BG}$); the molar flow of CO_2 in biomethane ($N_{CO_2,BM}$); and the volume [L] of the liquid in the column (V_{BC}) [14]. This requires several assumptions. Ideally, the presence of microalgae in the alkaline water as a solid phase would require the current system to be evaluated as a slurry bubble column. However, even with microalgae concentration up to 1 gDW/L, that would represent less than 0.1% total solids in the liquid. At such low solid concentrations, the impact of the solid phase can be neglected [36,37] and the overall system can be assumed to be well represented by the two-film theory [11,38]. Additional assumptions include:

i. assuming a thoroughly mixed gas and liquid phase in plug flow under isothermal conditions [14];

ii. minimal absorption of nitrogen [14];

iii. applicability of ideal gas laws;

iv. N_2, CO_2 and O_2 are the primary gas phase components resulting in a ternary system; and,

v. fast chemical reactions typically above pH 8 [35].

From the assumption of the insolubility of N_2 and minimal N_2 stripping from the algal solution, the total molar flow of N_2 must be constant at the inlet ($N_{N_2,BG}$) and exit ($N_{N_2,BM}$) of the column [14]. Thus, $N_{CO_2,BM}$ can be expressed in terms of $N_{CO_2,BG}$, the molar fraction of CO_2 at the inlet ($y_{CO_2,BG}$) and the molar fractions of CO_2 and O_2 at the exit of the bubble column ($y_{CO_2,BM}$ and $y_{O_2,BM}$ respectively), as shown in the following Eq. 3.5.

$$N_{CO_2,BM} = \frac{1 - y_{CO_2,BG}}{y_{CO_2,BG}} \cdot \frac{y_{CO_2,BM}}{1 - y_{CO_2,BM} - y_{O_2,BM}} \cdot N_{CO_2,BG} \quad (3.5)$$

Consequently the absorption rate of CO_2, $r_{A_{CO_2}}$ [mol/L/s] can be written as per Eq. 3.6 [14], which can then be expanded to Eq. 3.7 using Eq. 3.5 and $N_{CO_2,BG} = \frac{G.P.y_{CO_2,BG}}{RT}$ following ideal gas laws.

$$r_{A_{CO_2}} = \frac{N_{CO_2,BG} - N_{CO_2,BM}}{V_{BC}} \quad (3.6)$$

$$r_{A_{CO_2}} = \frac{N_{CO_2,BG}}{V_{BC}} \cdot \left(1 - \frac{1 - y_{CO_2,BG}}{y_{CO_2,BG}} \cdot \frac{y_{CO_2,BM}}{1 - y_{CO_2,BM} - y_{O_2,BM}}\right) = \frac{1}{V_{BC}} \cdot \frac{G.P.y_{CO_2,BG}}{RT} \cdot \left(1 - \frac{1 - y_{CO_2,BG}}{y_{CO_2,BG}} \cdot \frac{y_{CO_2,BM}}{1 - y_{CO_2,BM} - y_{O_2,BM}}\right) \quad (3.7)$$

where, G is the biogas flow rate into the bubble column [m^3/s]; P is the absolute pressure of the gas phase; R is the universal gas constant [8.314 J/mol/K]; T is the temperature [K].

The overall mass transfer coefficient $K_{G_{CO_2}}a$ [s^{-1}] for CO_2 absorption accounting for both the gaseous side and liquid side mass transfer coefficient was estimated via a lumped approach as shown in Eq. 3.8 [11,39].

$$K_{G_{CO_2}}a = \frac{G}{V_{BC}} \cdot \ln \frac{N_{CO_2,BG}}{N_{CO_2,BM}} = \frac{G}{V_{BC}} \cdot \ln \frac{y_{CO_2,BG}}{y_{CO_2,BM}} \quad (3.8)$$

The CO_2 removal efficiency (RE_CO_2) is a widely used parameter to evaluate the performance of a bubble column for CO_2 removal from biogas. Knowing the CO_2 flow rates in and out of the bubble column RE_CO_2 [%] can thus be evaluated as per Eq 3.9.

$$RE_CO_2 = \frac{N_{CO_2,BG} - N_{CO_2,BM}}{N_{CO_2,BG}} \times 100 \quad (3.9)$$

3.2.4.2 O_2 stripping

Stripping of dissolved oxygen from the liquid phase is governed by the volumetric mass transfer coefficient from the liquid to the gaseous phase, represented as $k_{l_{O_2}}a$ [s^{-1}] [40]. As described by Franco-Morgado et al., (2017) [27], the rate of the

oxygen stripping ($r_{S_{O_2}}$) [mol/L/s] can be calculated from the mass balance at the gas-liquid interface, by using the two-film theory as per Eq. 3.10.

$$r_{S_{O_2}} = k_{l_{O_2}} a \left(DO - \frac{P.y_{O_2}}{H_{O_2}} \right) \quad (3.10)$$

in which, DO represents the instantaneous dissolved oxygen concentration [mol/L] in the bulk liquid; y_{O_2} is the instantaneous O_2 concentration in the gas flow; P is the absolute pressure of the gas phase and H_{O_2} is the Henry's Law constant for oxygen (635 L.atm/mol at 20 °C [41]).

On the gas side, the rate of O_2 leaving the column could be given as a difference in the molar flow of oxygen entering ($N_{O_2,BG}$) and exiting ($N_{O_2,BM}$) the column per its unit volume. Considering the shell material mass balance, under steady-state, as suggested by Jin et al., (2001) [42], $k_{l_{O_2}} a$ can thus be estimated at the entry of the bubble column photobioreactor as per Eq. 3.11.

$$k_{l_{O_2}} a = \frac{1}{\left(DO_{in} - \frac{P.y_{O_2}}{H_{O_2}} \right)} \cdot \frac{N_{O_2,BM}}{V_{BC}} \approx \frac{1}{(DO_{in})} \cdot \frac{N_{O_2,BM}}{V_{BC}} \quad (3.11)$$

where, the term $\frac{P.y_{O_2}}{H_{O_2}}$ can be neglected due to negligible O_2 concentration in the feed biogas.

Alternatively, numerous correlations are also available to estimate $k_{l_{O_2}} a$. However, results vary significantly due to the type of gas-liquid system, column diameter, as well as sparger design (especially for smaller diameter columns and lower gas superficial velocities). As an approximation, the correlations by Shah et (1982) [43] for cross nozzle spargers were considered for cross-validation of the bubble column performance. The correlation, as depicted in Eq. 3.12, describes $k_{l_{O_2}} a$ in terms of the superficial gas velocity, u_G as shown below.

$$k_{l_{O_2}} a \approx 0.467 u_G^{0.82} \quad (3.12)$$

3.2.4.3 pH, alkalinity and carbon mass balance

Under steady-state operations, the CO_2 removed from the biogas would be absorbed into the liquid as sodium bicarbonate following Eq. 3.4 with a corresponding drop in pH. Assuming minimal algal growth within the bubble column, the carbon mass balance (in terms of molar flow rates) between the inlet and outlet of the bubble column could be written as per Eq. 3.13

$$N_{C,BG} + N_{IC,in,L} = N_{C,BM} + N_{IC,out,L} \quad (3.13)$$

in which, $N_{C,BG}$ and $N_{C,BM}$ are the mole flow rates of carbon [mol/L-C] in the biogas and upgraded biomethane respectively, while the respective molar flow rates of inorganic carbon on the liquid inlet and outlet are denoted as $N_{IC,in,L}$ and $N_{IC,out,L}$. Consequently, following from Eq 3.5, the dissolved inorganic carbon loading in the bubble column (ΔDIC_{BC}) [mol/L-C] relative to the liquid flow rate (L) [m^3/s] in the bubble column can be described by Eq. 3.14 as

$$\Delta DIC_{BC} = \frac{(N_{CO_2,BG} - N_{CO_2,BM})}{L} \quad (3.14)$$

In photosynthetic biogas upgrading using inorganic media only for microalgae growth, the IC concentration can be interchangeably used for alkalinity [20]. This is since, at a pH above 8, the primary forms of IC in solution are [HCO_3^-] and [CO_3^{2-}]. Thus, the increase in the inorganic carbon (IC) concentration due to the absorption of CO_2 in the solution can be equated to the rise in total alkalinity. Correspondingly, the carbon mass balance between the entry (i) and exit (o) of the column could be re-arranged from Eq. 3.13 to Eq. 3.15

$$([CO_3]^{2-})^i + ([HCO_3]^-)^i + \Delta DIC_{BC} = ([CO_3]^{2-})^o + ([HCO_3]^-)^o \quad (3.15)$$

in which, the instantaneous concentrations of [HCO_3^-] and [CO_3^{2-}] can be determined after Kishi et al., (2019) [44] via Eq. 3.16 and Eq. 3.17 in terms of corresponding pH and alkalinity as

$$[HCO_3^-] = \frac{Alk}{1 + \frac{[H^+]}{K_1} + \frac{K_2}{[H^+]}} \quad (3.16)$$

$$\left[CO_3^{2-}\right] = \frac{Alk}{1 + \frac{[H^+]}{K_2} + \frac{[H^+]^2}{K_1 K_2}} \quad (3.17)$$

where K_1 and K_2 are the stoichiometric constants for bicarbonate and carbonate respectively; pH can be determined as -log[H^+]; and Alk represents the alkalinity [mol/L-C]. K_1 and K_2 can be estimated in terms of pK_1 and pK_2, by the following Eq. 3.18 [45].

$$pK_i = pK_i^0 + A_0 + A_1/T_{BC} + A_2 \ln T_{BC} \quad (3.18)$$

where pK_i is $-\log_{10} K_i$; pK_i^0 is the dissociation constants in pure water accounting for the impact of temperature for i = 1,2. The values of pK_1^0 and pK_2^0 can be estimated from Eq. 3.19 and Eq. 3.20 according to Millero et al. (2006) [45]. On the other hand, the values of the adjustable parameters A_0, A_1, and A_2 accounting for the impact of salinity were directly obtained from Millero et al. (2006) [45].

$$pK_1 = -126.34 + 6320.81/T_{BC} + 19.57 \ln T_{BC} \quad (3.19)$$

$$pK_2 = -90.18 + 5143.69/T_{BC} + 14.613 \ln T_{BC} \quad (3.20)$$

3.3 Experiments and methods

3.3.1 Microorganisms and culture conditions

All operations and experiments were performed with non-axenic strain of *Arthrospira* (*Spirulina) platensis* SAG 85.79, procured from Sammlung von Algenkulturen Goettingen (SAG), Germany. The microalgae were batch cultivated in 5 L Erlenmeyer Flasks using the modified Zarrouk's media after Madkour et al., (2012) [46] comprising [gL^{-1} of distilled water]: 16.80 $NaHCO_3$; 0.50 K_2HPO_4; 2.50 $NaNO_3$; 1.00 K_2SO_4; 1.00 NaCl; 0.2 $MgSO_4 \cdot 7H_2O$; 0.04 $CaCl_2 \cdot 2H_2O$; 0.01 $FeSO_4 \cdot 2H_2O$; 0.08 EDTA-Na; and 1mL micronutrient solution. The micronutrient solution was made up with 2.86 g/L H_3BO_3; 1.810g/L $MnCl_2 \cdot 4H_2O$; 0.222 g/L $ZnSO_4 \cdot 7H_2O$; 0.0177 g/L Na_2MoO_4; 0.079 g/L $CuSO_4 \cdot 5H_2O$. All batches were inoculated with 0.15 gDW/L of algae. The temperature was kept constant at 20 ± 1 °C and illumination was programmed to provide 16:8 hours of light: dark cycles using cool white fluorescent lamps at an intensity of 5-6 klux (75 ± 5 $\mu molm^{-2}s^{-1}$). The algae

were continuously agitated with air to ensure adequate mixing and promotion of algae growth. The strain was maintained in 50 mL batches inside 100 mL sterilised Erlenmeyer Flasks, using modified Zarrouk's medium at 20 ± 1 °C, a pH between 9 and 10 and shaking twice daily manually. Illumination was maintained at 2.5 klux (33.75µmol$m^{-2}s^{-1}$) with a 16:8 light: dark period and the cultures were transferred to a new medium every 3 weeks.

3.3.2 Commissioning and performance evaluation of the bubble column operations

In accordance with the primary objective of the work, the experimental design was not only aimed at evaluating the performance of the bubble column, but also at identifying the potential challenges towards its operation and evaluation procedures. Corresponding to each challenge, design modifications were implemented with a focus on both the laboratory and the commercial-scale operation of such systems. For this, simplistic experiments were performed with synthetic biogas containing 40% CO_2 and balance N_2. The flow rate was kept constant at 54.83 mL_n/min (corresponding to a u_G of 0.2 cm/s) typical to the upper limits of current experimental values. The resultant EBRT was 4.5 mins, corresponding to those typically used in industrial bubble columns [15]. On the other hand, the liquid flow rate, and hence, the L/G ratio was varied until no statistically significant change in the biomethane CO_2 composition was noticed. Accordingly, the L/G ratio was increased in steps of 0.1 from an initial value of 0.1 (corresponding to the lower limit of the peristaltic pump operations).

In the two-step bubble column photobioreactor configuration, the culture medium can be circulated into the bubble column from the photobioreactor either before harvesting or post-harvesting. All commissioning and troubleshooting was performed with a liquid of low algal concentration of 0.05 gDW/L, typical of those obtained post-harvesting of microalgae. On successful completion of all low algal concentration trials, the algae concentration was increased to 0.75 gDW/L to evaluate the effects of higher algal concentration on the bubble column operation. The higher concentration value was in accordance with those achievable in open ponds and closed photobioreactors alike before harvesting [47,48]. Additionally, to evaluate any potential impact of photosynthesis on biogas upgrading, experiments were performed under continuous illumination between 3-5 klux (40.5-67.5 µmol$m^{-2}s^{-1}$) (similar to

those used for *Spirulina* cultivation). For ease of following the paper, from this point forward, all low algal concentration experiments will be denoted as LON and all those with high algal concentration as HON.

The alkaline algal liquid for biogas upgrading was prepared by diluting 2-3 gDW/L live *Spirulina platensis* cultures with distilled water. The pH of the algal solution was maintained at 9.35 ± 0.05 for all experiments by addition of sodium carbonate/ bicarbonate wherever applicable, or by purging with CO_2 within the optimal range of *Spirulina platensis* (pH 9 to 11) [32]. The alkalinity was controlled at 2.8 ± 1 gIC/L by the addition of sodium carbonate/ bicarbonate, or by diluting with distilled water and subsequent adjustment of the algal density. All bubble column experiments were performed at a temperature of 21 ± 2 °C; the DO of the algal solution varied between 7-10 mgO_2/L (90% ± 10% saturation value) as per those recorded during batch cultivation of algae. Each experiment was performed in triplicate.

3.3.3 Analytical procedures

Algal density in solution was measured as optical density in a VWR® V-3000 PC manual spectrophotometer, calibrated against the microalgae dry weight. For this, the dry weight of microalgae was determined by filtering 2 mL of a sample through pre-washed and dried Whatman filter papers (47 mm diameter and nominal pore size 0.45 μm). Each filtered sample was washed thrice with distilled water to remove residual salts; dried in an oven at 80 °C for 4 hours; and cooled in a desiccator to obtain the corresponding dry weight [46]. λ 530 nm was selected after multiple wavelength screening to calibrate the spectrophotometer optical density to the standard microalgae dry weight. Both pH and DO were measured using a handheld pH meter (VWR® MD 8000H Multi Parameter Meter) fitted with interchangeable pHenomenal VWR® pH / ORP and pHenomenal VWR® OPOX 11-3 sensors respectively. Alkalinity was determined by titrating the sample in the Titronic® Universal Titrator with 0.1 N H_2SO_4 up to an endpoint pH of 4.5 as per the basic methodology described in Method No. 2320B of APHA [49]. Salinity (parts per thousand) due to carbonate and bicarbonate salts can be estimated in terms of the amount of their respective oxides per kg of water [50]. Assuming all other salts to be negligible due to the use of distilled water, the salinity of the medium was thus estimated from the theoretical amount of

sodium oxide per litre of water. For this, the complete oxidation of added amounts of sodium carbonate and sodium bicarbonate were considered according to Eq. 3.21

$$2NaHCO_3 \leftrightarrow Na_2CO_3 + H_2O + CO_2 \leftrightarrow Na_2O + 2CO_2 + H_2O \quad (3.21)$$

The upgraded biomethane flow rate was measured in terms of equivalent N_2 flow [$mlnN_2$/min] by a thermal mass flow meter (Bronkhorst® F101D Low-ΔP-Flow Thermal Mass Meter). The corresponding steady-state composition was measured using Agilent® 7890B Gas Chromatograph (USA) equipped with a thermal conductivity detector and a 5A column and calibrated with 2% O_2 and 30% CO_2 (balance N_2) from Buse Gases Ltd®, UK. Subsequently, an online gas Converter tool by Fluidat® (Bronkhorst®) was used to record the actual flow rates of the component gases at the bubble column outlet.

3.3.4 Statistical analysis

The spectrophotometer standard curve for measuring algal density was estimated by fitting a linear curve using Origin® 8.5 software. As the error distribution for a linear model is usually normally distributed [51], the Root Mean Square Prediction Error (RMSE) was used as an adequate metric to compare the predicted and the experimental values and determine the accuracy of the linear fit [52]. This method is also a widely used numerical metric to measure the error in mathematical predictions [53]. Statistical analyses of the performance of photosynthetic biogas upgrading were conducted using Minitab® version 19 (Minitab LLC., Pennsylvania, USA). A one-way analysis of variance (ANOVA) was performed to evaluate if the means of two or more groups of an independent variable (L/G ratio and presence or absence of light) resulted in a statistically significant outcome. The two way ANOVA was used to evaluate if the effect of the two independent variables (light and L/G ratio) were statistically significant.

To assess if two groups of an independent variable are statistically significantly different, the Tukey honestly significant difference (HSD) post hoc test was used as suggested in previous literature [54,55]. In this test, a q statistic is first generated as a single statistical value employing a studentised t-test and using 95% confidence interval ($P < 0.05$). Any pairwise difference that was lower than the q-statistic was

considered to have no statistically significant difference between their means and vice versa [55].

3.4 Start-up and design modifications

3.4.1 External oxygen ingression into upgraded biomethane

At the start of operations, the O_2 concentrations in the upgraded biomethane ranged between 3% and 4%. Although the values were similar to those reported in the literature [17,29], a feasibility check for the results was performed nonetheless. For this, the $k_{l_{O_2}}a$ was estimated for the experimental trials as described via Eq. 3.11 and compared to the empirical value obtained through Eq. 3.12. The experimental values were at least 4.5 times that of the empirical value of 0.0029 s^{-1}. A mass balance based on the assumptions discussed in Section 3.2.4, was further conducted considering the O_2 in the biomethane to be derived solely from the DO of the circulating low algal concentration liquid. Assuming the DO in the inlet liquid to be 10 mg/L and that it was completely stripped from the liquid by biomethane, theoretical maximum oxygen content in the biomethane was obtained. However, the observed O_2 concentrations in the upgraded biomethane were at least 10 times that of the theoretical maximum. This indicated significant O_2 ingression in the system, requiring substantial design modifications.

To understand the source of O_2 ingression, the O_2 concentration was measured at different locations of the experimental set-up with only N_2 gas flowing through the system. From the results, the high permeability of silicone tubing used in the system was recognised as the major factor affecting O_2 concentrations in the upgraded biomethane followed by the use of gas bags for sampling biomethane. However, industrial settings operating with impermeable steel pipelines would seldom face gas ingression issues. Thus, to enable accurate measurement and replication of industrial operations in the current experimental setup, the following modifications in system design were implemented. The results before and after the modification are discussed in Section 3.5.

- All gas line tubing was replaced with Tygon 3603® tubing having at least 50 times less permeability than silicone-based rubber tubes.

- The gas bag was replaced with a 10 mL plastic syringe for gas sampling.
- The gas collection point was shifted before the flow meter to minimise the measurement error.
- A much smaller outlet residual O_2 flow was still observed when N_2 gas was flowing through the system with the modified tubing. To further minimise this error, the residual flow of O_2 in the gas tubing was subtracted from the O_2 flow rates in the raw biomethane. Therefore, a two-point oxygen and nitrogen correction was applied to increase the measurement accuracy. For this, the outlet gas was measured for its composition and flow rate while flowing N_2 at 25 and 50 mL_n/min into the system, yielding an O_2 and N_2 correction factor. These correction factors were then subtracted from the respective gas flow rates in the upgraded biomethane for each experimental run to evaluate the corrected O_2 and N_2 concentrations in biomethane.

3.4.2 Condensation

Moisture condensation build-up within the gas tubing at the bubble column outlet was observed over time affecting the accuracy of measurements. Enhanced mass transfer to achieve higher CO_2 removal, resulting also in enhanced evaporation [56] caused considerable humidification of the biomethane. The issue was solved by immersing a length of a large diameter tube in an ice bath to act as the condensate trap as can be seen from Figure 3-2e. In an industrial setup, a condenser would thus be necessary to remove moisture from the upgraded biomethane to the required limit of downstream operation.

3.4.3 Foaming

Significant foaming was observed (Figure 3-2c) above the liquid column, especially during operation with higher algal concentrations similar to those reported by Besagni and Inzoli (2017) [57], while working with active organic compounds and aspect ratios greater than 10. Significant foaming properties of *Spirulina platensis* recently documented in detail by Buchmann et al. (2019) [58], further confirms the observed phenomenon. Over time, the foam rose to the top of both the bubble column and gas-liquid separator, coating the walls of the gas tubes (Figure 3-2c) and causing

significant spikes in the gas flow (Figure 3-3b). A 500 mL foam trap added between the bubble column and the gas flow meter prevented any foam overflow into the gas flow meter, although the oscillations in the gas flow readings remained. In addition, large foaming incidents increased the pressure in the system causing the gas to flow out through the liquid outlet in the gas-liquid separator, especially at higher liquid flow rates. Therefore, in industrial-scale bubble columns, mechanical foam breakers or the addition of anti-foam agents, based on their suitability of application could aid operations with a high algae concentration.

3.4.4 Clogging

Operation with higher algal concentration increased clogging in the U bend at the outlet of the gas-liquid separator. This restricted the outlet flow of the circulating liquid, causing the liquid in the bubble column to rise above its liquid outlet level. This in turn raised the pressure inside the bubble column due to the reduction in the gas headspace. The problem was solved by increasing the tubing diameter at the liquid outlet of the gas-liquid separator. In an industrial setting without an outflow pump, the liquid outlet pipe diameter could therefore be a critical design challenge.

3.4.5 Stability of bubble column operation

All measurements were performed at a steady state, characterised by both, a constant gas outflow rate and a constant pH of the outlet liquid. To achieve steady-state operations, both stability of the volumetric flow rate and pH were considered necessary and sufficient. As illustrated in Figure 3-4, the time required to reach steady-state was around 40 minutes for an L/G ratio of 0.4, governed by the stability of the pH. It is in close approximation to Chen et al., (2015) [14] who also obtained a stability time of 40 minutes for CO_2 removal with NaOH. However, the time to reach steady-state was much longer for a lower L/G ratio of 0.1 (Figure 3-4a). Thus, irrespective of a steady-state being attained before the indicated times, to increase robustness in the data obtained, a minimum time of 40 minutes was used for each run based on the approximation of gas line length, the gas flow rates and literature suggestion from Chen et al., (2015) [14].

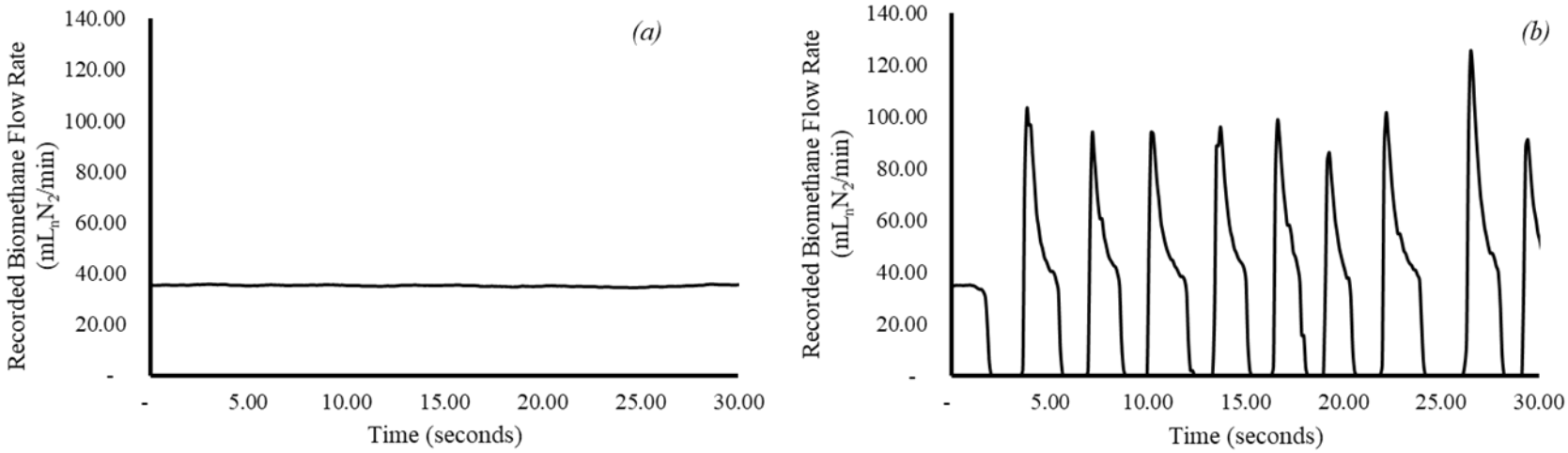


Figure 3-3 Recorded biomethane mass flow profiles at similar L/G ratio (0.3) (a) without (low algal concentrations) and (b) with foaming (high algal concentrations).

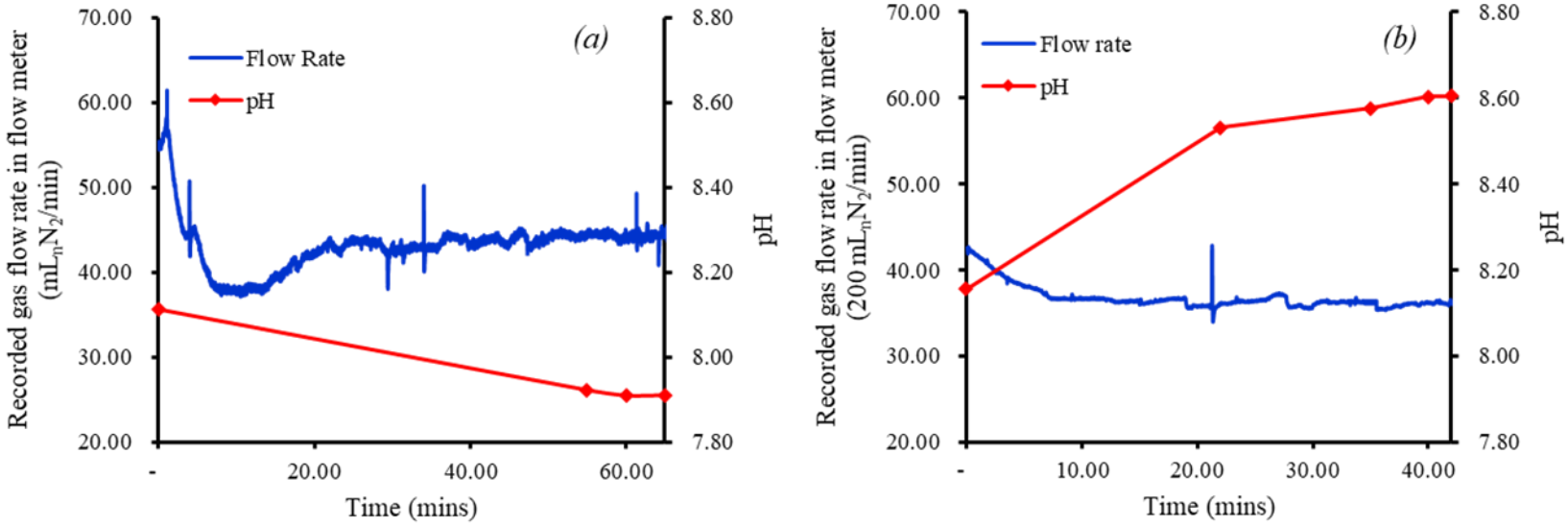


Figure 3-4 Variation in outlet biomethane flow and liquid pH before reaching steady-state. The examples chosen are (a) L/G 0.1 and (b) L/G 0.3 for experiment LON. It is to be noted that, the initial pH for (a) was 8.113, while for (b) it was 8.16 from respective preceding experiments. The data are from the pre-modified setup, chosen for better representation.

3.5 Results

All initial trials were performed with a low algal concentration (0.05 gDW/L) to establish a working bubble column setup for biogas upgrading with microalgae. For every assessment, therefore, the impact of the algal presence was neglected unless explicitly mentioned.

3.5.1 Impact of design changes on system performance

Comparable pH at the liquid outlet both before and after the changes to the gas tubing and gas sampling arrangements indicated a similar performance of the bubble column in both instances. However, as can be seen from Table 3-2, both the CO_2 and O_2 in the upgraded biomethane changed significantly after the modifications. The higher CO_2 content recorded after implementing respective design changes could be explained by the fact that due to the permeability of silicone tubing, CO_2 was lost through diffusion. The effect became more pronounced for trials with higher CO_2 flow rates in the ensuing biomethane making the selection of tubing a critical aspect in the design of such a laboratory-scale setup. It is to be understood here, that unlike the variation in the O_2 content in the biomethane, the variations in the result (in terms of percentage composition of biomethane) from the loss of CO_2 would be much less pronounced due to its higher flow rates. This is especially true for biomethane with low CO_2 content, due to the much lower atmospheric CO_2 concentrations, the CO_2 efflux would be minimal. Thus, a CO_2 correction step was omitted without the loss of generality.

Table 3-2 Effect of design changes on the mass flow rates of CO_2, O_2 and N_2 contained in upgraded biomethane in comparison to the inlet flows for operation under low algal concentration indicating the adequacy of the design changes and measurement techniques adopted during commissioning the bubble column setup. The molar masses of CO_2, N_2 and O_2 assumed were 44 gram/mol, 28 gram/mol and 32 gram/mol respectively.

L/G Ratio	Inlet biogas flow [mg/min]			Inlet liquid flow (mL_{in}/min)	Maximum inlet dissolved oxygen (DO) (mg/L)	O_2 flow in inlet liquid (mg/min)	pH of outlet liquid	Outlet biomethane flow [mg/min]					
								Initial setup			Modified and commissioned setup		
	CO_2	N_2	O_2					CO_2	N_2	O_2	CO_2	N_2	O_2
0.1				5.48		0.055	7.84	10.43 ± 0.90	39.29 ± 0.26	1.66 ± 0.01	22.02 ± 0.91	38.40 ± 0.31	0.031 ± 0.027
0.2				10.97		0.110	8.06	4.09 ± 0.38	38.48 ± 0.03	1.59 ± 0.11	8.43 ± 0.33	38.33 ± 0.31	0.126 ± 0.040
0.3	40.12 ± 0.20	38.30 ± 0.19	0.0 ± 0.0	16.45	10	0.164	8.47	1.61 ± 0.35	38.12 ± 0.09	1.65 ± 0.05	2.57 ± 0.26	38.34 ± 0.45	0.135 ± 0.067
0.4				21.93		0.219	8.74	0.8 ± 0.16	37.70 ± 0.40	1.68 ± 0.11	1.14 ± 0.13	38.33 ± 0.43	0.207 ± 0.013
0.5				27.42		0.274	8.92	0.42 ± 0.42	37.73 ± 0.43	1.60 ± 0.05	0.71 ± 0.07	38.30 ± 0.61	0.230 ± 0.040

The biggest change was observed in the O_2 content in the upgraded biomethane. From the mass balance, as can be seen from Table 3-2, the modified setup provided agreeable results to the theoretical maximum (corresponding to the inlet O_2 flow rate in liquid [mg/min] indicated in Table 3-2). The corresponding calculated $k_{l_{O_2}}a$ values ranged between 0.0013 s^{-1} for an L/G ratio of 0.1 to 0.0027 s^{-1} for an L/G ratio of 0.5. These values compare much better to both the empirical estimation (0.0029 s^{-1} from Shah et al (1982) [43]) as well as the experimental values obtained in a similar bubble column by Franco-Morgado et al (2017) (0.0016 s^{-1}) [27]. Indeed, beyond an L/G ratio of 0.4, where the CO_2 content was below 2.5%, this resulted in achieving a grid quality biomethane. The resulting corrected N_2 flow rate in the exiting biomethane of 38.33 ± 0.43 mg/min also indicated the adequacy of the methodology applied (N_2 inflow set at 32.9 mL_n/min or 38.30 mg/min). All subsequent results depicted are thus for the modified system setup.

3.5.2 CO_2 removal efficiency

The variations in CO_2 content in the outlet biomethane at different L/G ratios, under both the lower and higher algal concentrations, are shown in Figure 3-5a. For the higher concentration, the L/G ratio of 0.5 was not recorded as the experiments were deemed to provide non-conclusive evidence due to excessive foaming. A CO_2 concentration of around 25% was observed for all runs at the lowest L/G ratio of 0.1. A rapid drop in CO_2 content could be seen between an L/G ratio of 0.2 and 0.3. Above an L/G ratio of 0.4, CO_2 concentration levels suitable for grid injection (less than 2.5%) were consistently achieved. Indeed, between an L/G ratio of 0.4 and 0.5, no statistically significant decrease in the CO_2 content of the upgraded biomethane was observed. Statistical assessments also established that no significance of the algae concentration and the photosynthetic effect was exerted on the performance of CO_2 removal. A study of the corresponding liquid outlet pH from Table 3-2 provides further insight into the system performance. At an L/G ratio below 0.1, when the CO_2 removal was the lowest, the pH fell below 8. Subsequently, a steady rise in pH can be observed, with the highest pH recorded being 8.92 ± 0.02 at an L/G ratio of 0.5. Similar observations were made by Rodero et al., (2018) [20], who achieved a minimal drop in pH at alkalinity above 1,000 mgIC/L and L/G ratio of 0.5 with sufficient CO_2 removal.

In congruence with the CO_2 content in the upgraded biomethane, the CO_2 removal efficiencies (RE_CO_2) were found to vary from 42.5% ± 2.41% (L/G 0.1) to 98.15% ± 0.22% (L/G 0.5) respectively as plotted in Figure 3-5b. In comparison to Toledo-Cervantes et al., (2017) [16] who achieved a CO_2 removal efficiency of 70% ± 1% at an L/G ratio of 0.3, the present experiments yielded a higher RE_CO_2 of 93.29% ± 0.66%. This could be due to the higher inorganic carbon concentration in the algal solution chosen in the present study. However, for an L/G ratio of 0.5, the present results were replicable with both Toledo-Cervantes et al., (2017) [16] and Rodero et al., (2018) [20], who reported corresponding values of 97.3% ± 0.1% and 97.8% ± 0.8% respectively. Thus, for higher L/G ratios, the significance of alkalinity could be understood to be diminished, with pH being the primary factor determining the efficiency of CO_2 removal.

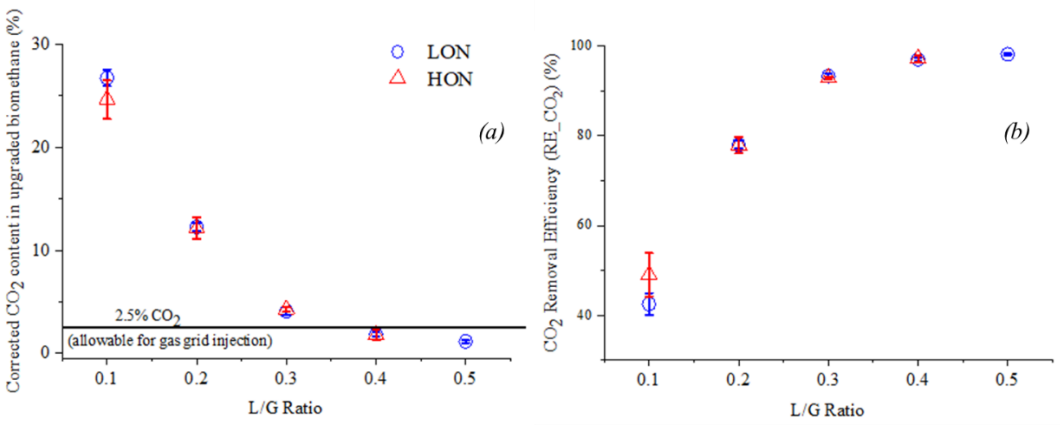


Figure 3-5 CO_2 content (a) and removal efficiency (b) of the bubble column operated under different L/G ratios at higher and lower algal concentrations; where LON: Low concentration with lights on; HON: High concentration with lights on.

3.5.3 Rate of CO_2 absorption

The mean CO_2 absorption rates along with the carbonate concentration in the liquid at the bubble column outlet are shown in Figure 3-6a. The values presented are for both the operations with higher and lower algal concentrations. Considering the inlet carbonate concentration to be 48.73% ± 0.56% (corresponding to pH 9.35 ± 0.05 and salinity 10.19 ± 0.36), no statistically significant improvement in the CO_2 absorption rates was noticed ($P > 0.05$) when the outlet carbonate concentration was above 20% (corresponding to a pH of 8.75 ± 0.02). On the contrary, a drastic reduction in the CO_2 removal rates was observed as the carbonate concentration fell below 5% (below L/G 0.2). This conclusion matches well with the results obtained by Knuutila

et al. (2010) [34] who reported a drop in the reaction rates of over 10 times as the carbonate concentration decreased from 20% to 5%. Thus, there is a requirement for the average carbonate concentration in the liquid to be around 20% to ensure sufficient CO_2 removal. The corresponding CO_2 absorption rates for LON were 0.576 ± 0.002 $\times 10^{-4}$ mol/L/s and 0.583 ± 0.001 $\times 10^{-4}$ mol/L/s (c. 14.15$\times 10^{-6}$ mol/s normalised by liquid volume of 0.244 L), at L/G ratios of 0.4 and 0.5 respectively. The absorption rates for LON compare well to the results of Chen et al. (2015) [14], who reported a CO_2 absorption rate of 1.03$\times 10^{-4}$mol/L/s at 25 °C and initial pH of 10 for CO_2 removal in a bubble column by sodium hydroxide. The lower rates could be explained by both a lower temperature and a lower pH used in the present experiments. The comparison can be supported by the fact that irrespective of the use of Na_2CO_3 or NaOH, the local reaction is driven by $[OH]^-$ as per Eq. 3.2 [34,35]. Indeed, below a pH of 8 due to the minimal presence of carbonates in the solution, Eq. 3.4 is replaced by the following carbonic acid formation reaction (Eq. 3.22) [35]. Thus, the absorption rates would drop rapidly and the present assumptions would not be valid to determine the kinetics of the system [35]. No significant change in CO_2 absorption rates was obtained when the algal concentration increased. This indicated that no impact of the algae was exerted on CO_2 absorption; the latter being primarily driven by the $[OH]^-$ ions in solution.

$$CO_2 + H_2O \Leftrightarrow H_2CO_3 \quad \Delta G \cong 14.75 \text{ kJ/mol}^1 \text{ at } 25°C \quad [54] \qquad (3.22)$$

[1] Calculated using the fundamental equation $\Delta G = -RT\ln K_{eq}$, where the equilibrium constant K_{eq} for the above Eq 3.19 is 2.6$\times 10^{-3}$ at 25°C [59]

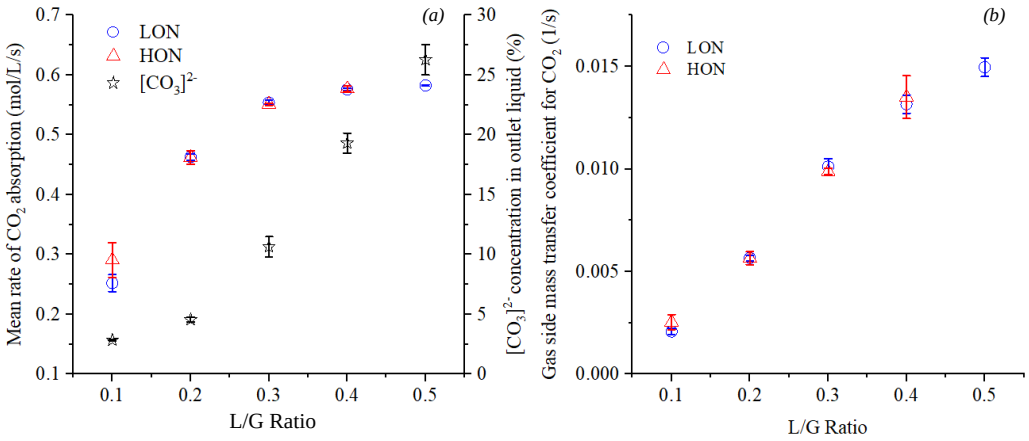


Figure 3-6 Effect of L/G ratio and algal concentration on the (a) absorption rate of CO_2 alongside mean carbonate concentration in solution and (b) overall mass transfer coefficient ($k_{G_{CO_2}}a$).

The overall mass transfer coefficient, $K_{G_{CO_2}}a$ was found to increase linearly from 0.0025 s^{-1} at L/G 0.1 to 0.015 s^{-1} at L/G 0.5 as shown in Figure 3-6b. An enhanced mass transfer coefficient at higher L/G ratios have been previously noted as well [33]. Indeed, although at lower L/G ratios, the mass transfer coefficient is significantly lower than that reported in the literature, for the trials with appreciable CO_2 removal rates (L/G 0.4 and 0.5), the results match well to that of Chen et al., (2015) [14], who reported $K_{G_{CO_2}}a$ of 0.015 s^{-1} at an inlet pH of 10 and 25°C. Similar to the absorption rates, no statistically significant influence of a higher algal content can be seen from the data presented in Figure 3-6b.

3.5.4 O_2 stripping

As can be seen from Figure 3-7a, as the L/G ratio increased from 0.1 to 0.5, the oxygen flow rates increased from 0.023 ± 0.016 mL_n/min to 0.173 ± 0.026 mL_n/min respectively for the operations with low algae concentration following the trend of the theoretical values. However, the corresponding O_2 flow rates while operating with a higher algal concentration were not only much higher but also showed higher variability. One possible explanation could be the non-uniform mixing because of the filamentous microalgae in the liquid solution. Similar observations of the improved mass transfer due to increased algal concentration in the liquid phase has been previously reported by Manjrekar et al. (2017) [22]. However, to explain the flow rates above the theoretical values, it can be speculated that this increase is from the high concentration of photosynthesising microalgae present in the system.

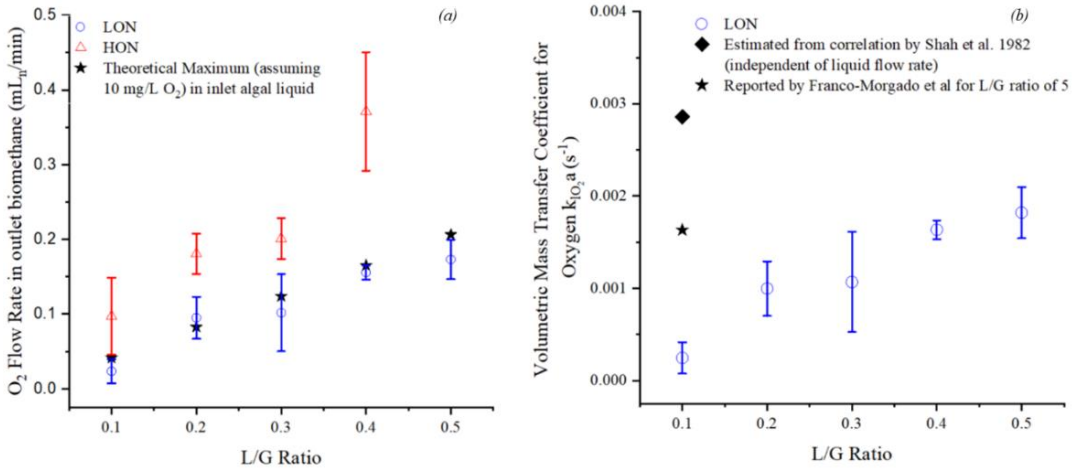


Figure 3-7 Effect of the L/G ratio and the algal concentration on (a) the theoretical and measured oxygen outflow rates [mL_n/min] and (b) the overall mass transfer coefficient for oxygen ($k_{l_{O_2}}a$) [s^{-1}]. It is to be noted that $k_{l_{O_2}}a$ for HON has not been evaluated as the results are confounded with the photosynthetic activity of the algae and would not depict the actual hydrodynamic performance of the bubble column.

To assess the hydrodynamic performance of the bubble column, the volumetric mass transfer coefficient is presented in Figure 3-7b and compared with the literature. In accordance with the above discussion, the $k_{l_{O_2}}a$ was not calculated for operations with higher algal volumes, as there was a significant probability of confounding the results with the oxygen produced via photosynthesis. Thus, there is good agreement between the predicted (0.0029 s^{-1}), literature (0.0016 s^{-1}) and the experimental results (varying between 0.0002 s^{-1} and 0.0018 s^{-1} at L/G ratios between 0.1 and 0.5 respectively). These results further compare well to multiple literature sources using similar column diameter and u_G, whereby a $k_{l_{O_2}}a$ of less than 0.01 s^{-1} can be seen, irrespective of operating conditions such as pH [55,56]. Nonetheless, the present results also indicate that the liquid flow rate would exert a relatively large influence on the volumetric mass transfer coefficient of oxygen. This is unlike most correlations for estimating $k_{l_{O_2}}a$ that neglects the impact of the liquid velocity. As explained by Besagni et al. (2018) [62], this occurs when the liquid and gas flow rates become comparable, which indeed is the case for the present operations. Increase in $k_{l_{O_2}}a$ has also been reported by Chaumat et al. (2007) [63] influenced by an increased liquid flow rate, although the gas superficial velocity is still the most significant factor affecting the same. Therefore, in the bubble column for photosynthetic biogas upgrading, the liquid flow rates would play a definitive role in determining the hydrodynamic performance of the bubble column, especially with relation to oxygen

stripping. This is supported by multiple literature sources that have claimed the L/G ratio to be a significant factor in controlling the O_2 concentration in the upgraded biomethane [16,28].

The corrected O_2 concentrations in the upgraded biomethane are depicted in Figure 3-8. During operation with a lower algae concentration, the O_2 content in the upgraded biomethane increased from 0.05% ± 0.04% at an L/G ratio of 0.1 to 0.52% ± 0.08% at an L/G of 0.5. In addition to the increased O_2 outflow, the higher CO_2 removal efficiency was also instrumental in increasing the O_2 content in the upgraded biomethane with the increase in L/G ratios. From the perspective of O_2 content in the biogas, the results match well with those in literature while working with lower algal concentration post-harvesting. For example, Toledo Cervantes et al. (2017) [16] reported an O_2 concentration of 0.1% ± 0.0% at an L/G ratio of 0.5 and pH of 10.2 ± 0.2 at the bubble column inlet. The low values were mostly due to the consumption of DO by H_2S in biogas. Similarly, Rodero et al. (2019) [24] also obtained O_2 concentration around 0.2% for an L/G ratio between 0.3 and 0.5 and pH 10 while operating with biogas containing 300 ppm_v H_2S. On the other hand, Marín et al., (2018) [17] found 0% to 3.4% O_2 variation in the upgraded biogas at an L/G of 1 and pH varying between 9.3 and 9.7.

In the present work, a less than 1% O_2 concentration has been achieved while working with low concentration algal liquids without H_2S in inlet biogas. This signifies the possibility to achieve grid quality oxygen limits in photosynthetic biogas upgrading even without requiring H_2S from biogas for oxygen removal. Combined with CO_2 concentrations below 2.5% at L/G ratios of 0.4 and 0.5, the ensuing biomethane in the present form would thus be suitable for gas grid injection. The corresponding oxygen content in the upgraded biomethane for operation with higher algal concentrations were 0.23% ± 0.12% for an L/G of 0.1 and 1.11% ± 0.24% at an L/G of 0.4. The higher O_2 flows from enhanced mixing and the presence of photosynthesising micro-organisms would therefore render the biomethane unsuitable for gas grid injection above an L/G ratio of 0.4 from the perspective of O_2. The operations with higher algal concentrations would therefore be detrimental to achieving grid quality biomethane, and hence, the applicability of the photosynthetic biogas upgrading system.

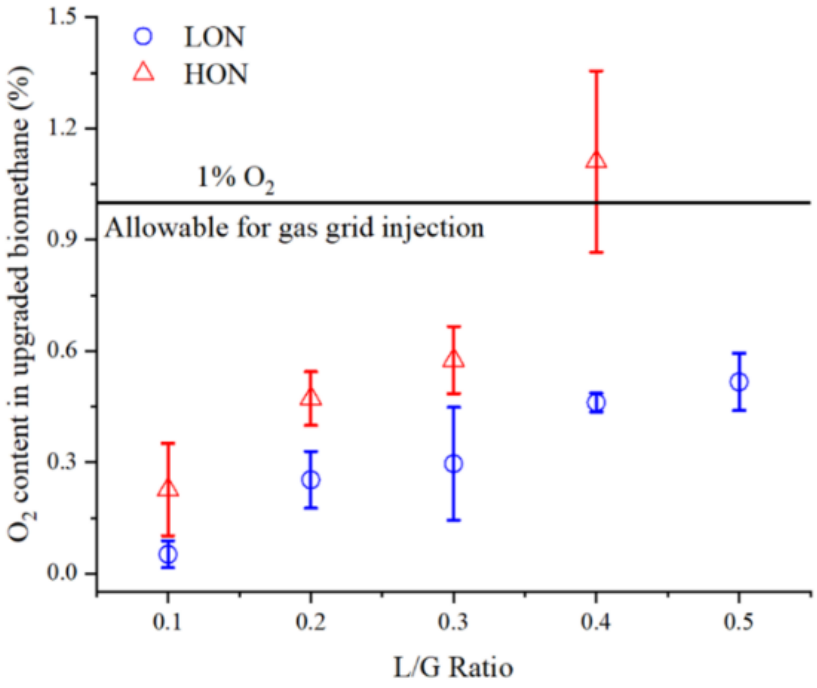


Figure 3-8 Oxygen concentration in the upgraded biomethane under different operating conditions in the lab-scale bubble column

3.5.5 Carbon balance

The effective inorganic carbon addition into the liquid medium from CO_2 absorption, as can be derived from Eq. 3.14, is produced in Figure 3-9. With the increase in the L/G ratio, signifying an increase in the liquid flow rate, the CO_2 absorption rate increases as well. However, the increased liquid flow rate results in a lesser quantity of CO_2 being absorbed per unit liquid flow rate. Thus, the DIC addition to the algal solution would decrease as the L/G ratio increases. As such, the carbon assimilation by bicarbonate formation in the circulating liquid drops from 0.067 ± 0.004 mol/L at L/G 0.1 to 0.031 mol/L at L/G 0.5. For microalgae subsequently grown using the inorganic nutrient medium, this reduction of carbon addition rate is thus of considerable significance for further integration and optimisation of the overall photosynthetic biogas upgrading technology.

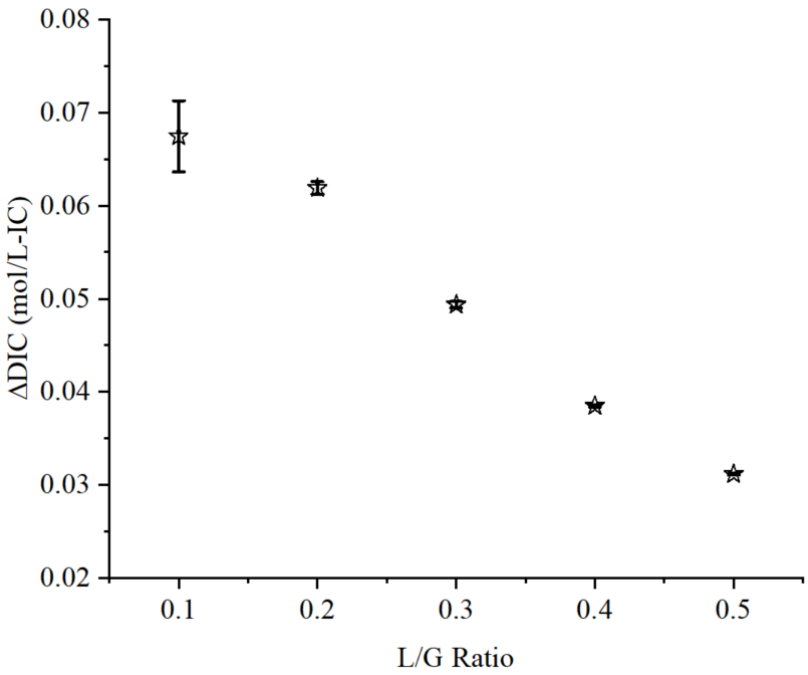


Figure 3-9 Variation in the rate of carbon addition with respect to the L/G ratio

3.6 Discussion

3.6.1 Validation and scale-up perspective of the bubble column set-up

The results from the initial experiments indicate both, the accuracy and reliability of obtained measurements and how well the designed bubble column configuration compares with those previously published research, hence validating the designed lab-scale set-up. The performance of the bubble column matches well to previous lab-scale experiments for photosynthetic biogas upgrading, in which an L/G ratio of 0.5 provided sufficient removal of CO_2 for grid injection of biomethane [16,20]. From the fundamental aspect of CO_2 mass transfer and absorption rates, the corrected results after necessary system modifications show proximity to previously published research [14]. As for the bubble column hydrodynamics, both the overall CO_2 mass transfer coefficient ($K_{G_{CO_2}}a$) and the volumetric liquid side O_2 mass transfer coefficient ($k_{l_{O_2}}a$) agree well with existing literature at a similar scale of bubble column and similar superficial gas velocities [14,64]. The differences obtained could be argued from the variation of column diameter, comparable liquid and gas flow rates, as well as the sparger design; the latter being shown to noticeably impact the bubble column performance especially at low superficial gas velocities (< 0.15 m/s) [65]. It

must be mentioned here that due to the use of nitrogen as a substitute for methane, nitrogen stripping from the liquid was not observed in the present experiments. However, as is evident from literature, a similar trend exists between the N_2 and O_2 stripping, resulting in comparable percentages of the respective gases in the upgraded biomethane [17,23,25]. For this, it can be speculated that a similar N_2 concentration (c. 0.5%) can be envisaged in the upgraded biomethane under similar operating conditions with actual biogas.

Beyond validating the design and operations of the lab-scale bubble column for photosynthetic biogas upgrading, the corresponding assessment for scale-up is crucial from an industrial perspective. Most often, similarity in global hydrodynamic parameters, such as the gas hold-up (signifying the ratio of the gassed volume of the bubble column with respect to the liquid volume before any gas flow) is used to predict dynamic similarities in bubble columns across scale [19]. For operations in the homogeneous regime, characterised by a uniform radial profile of gas hold up and limited interactions between bubbles, the similarity between gas holdup is necessary and sufficient to achieve dynamic similarity upon scale-up [66]. In the current experiments, no observable change in the liquid column height was noticed before and after initiating gas flows in the bubble column, indicating minimal gas hold-up. This is consistent with the observations by Majumder, (2016) [67] who reported a nominal gas hold-up at low superficial gas velocities. Mathematically, a theoretical estimate of the gas hold-up, ε_g was obtained to be 0.006 via Eq. 3.23 as given by Chisti (1989) [68], for bubble column bioreactors operating at $u_G<0.05$ m/s.

$$\varepsilon_g=2.47u_G^{0.97} \quad (3.23)$$

Improvements in sparger designs to decrease bubble diameter and hence increase in gas-liquid contact times could result in higher oxygen stripping. However, for such low gas holdup, scale-up of the bubble column reactor with minimal errors for similar sparger designs can be envisaged [66]. Indeed, for higher superficial gas velocities, especially beyond 0.01 m/s, the gas holdup would become significant (0.03 according to Eq. 3.23). In such a situation, the Wilkinson criteria (minimum 15 cm column diameter with a minimum aspect ratio of 5 and with a sparger pore diameter greater than 1-2 mm) would be essential for scale-up [69,70]. In addition, below 0.01 m/s, a minimal influence of pressure on the gas hold-up of the bubble column

irrespective of the superficial liquid velocity has been reported [69]. Being a necessary and sufficient condition to allow scale-up of a bubble column operation in the homogeneous regime [66], a similar gas hold-up would therefore allow results to be upscaled with negligible influence of the increased hydraulic pressure of a tall bubble column below 0.01 m/s. Accordingly, the present bubble column would remain scalable for biogas flow rates of up to 16.3 L_n/hr, or 271.43 mL_n/min, corresponding to a superficial gas velocity of 0.01 m/s (1 cm/s).

From the practicality of scale-up of the bubble column, operating under atmospheric conditions presents significant challenges. Usual operating conditions of high temperature and pressure would not be suitable while using microalgae. Although a grid quality biomethane has been achieved, the lower absorption rates of around 0.58×10^{-4} mol/L/s would thus require a bubble column with higher aspect ratios (present aspect ratio of 22.5 is significantly higher than aspect ratios of 3-10 usually used in industry [71]). This requirement of large column heights would not only limit the industrial scale-up of the bubble column but would also result in an increased level of O_2 stripping into the upgraded biomethane. Thus, improvement in the absorption rates of CO_2 within the permissible limits of photosynthetic biogas upgrading via modification in temperature, alkalinity, pH, L/G ratios and gas flow rates should be studied in detail.

3.6.2 Impact of algal concentration and photosynthetic activity

The external carbonic anhydrase enzyme of *Spirulina platensis* has been previously speculated to act as a biocatalyst for CO_2 absorption in carbonate solution [8]. However, the current experiments revealed no significant impact of the algal density and the corresponding photosynthetic activity on the CO_2 removal performance of the bubble column. This could be because of the low activity of *Spirulina platensis* at 20 °C [32]; in which case, experiments at higher temperatures (30 °C - 35 °C) must be performed to establish a definite understanding. However, the presence of microalgae significantly increased foaming and clogging, while also increasing the O_2 flow rates within the ensuing biomethane. Thus, unless a significant benefit can be established towards CO_2 removal from the higher presence of algae in the liquid phase, operations with lower algal density seem preferable.

3.6.3 Integration with microalgae cultivation

A continuous operation of the photobioreactor-bubble column system without accumulation or depletion of carbon would require maintenance of carbon balance throughout the carbonate bicarbonate cycle. Therefore, for operations with no organic carbon, the inorganic carbon added (ΔDIC) during biogas upgrading should account for the carbon uptake by the microalgae in the photobioreactor. As was seen from the experimental trials, an L/G ratio of 0.5 would be suitable for sufficient CO_2 removal. At this operating condition, as can be seen from Figure 3-9, the corresponding DIC addition to the circulating algal liquid would be 0.36 g-C/L (c. 0.31 mol/L). On the other hand, the productivity of *Spirulina platensis* at 20 °C is about 0.125 g/L/day, averaged over 15 days of cultivation [32]. Assuming the typical carbon content in *Spirulina platensis* is around 50% [72], this, therefore, signifies an average carbon uptake of 0.063 g-C/L/day (c. 0.005 mol/L/day) by *Spirulina platensis*. This indicates, that the maximum hydraulic retention time of 6 days would be possible and the resulting *Spirulina* concentration would not be higher than 0.75 gDW/L. On the other hand, for a lower L/G ratio, although the CO_2 removal is much less, the addition of 0.804 g-C/L would allow a maximum possible *Spirulina platensis* concentration of 1.6 gDW/L. The hydraulic retention time could be much higher, around 13 days. Therefore, to achieve grid quality biomethane, either hydraulic retention time or productivity has to be compromised, unless the L/G ratio can be lowered without decreasing the biomethane quality.

3.6.4 Oxygen stripping and H_2S

H_2S was not included in the synthetic biogas in the present study due to health and safety regulations. However, as discussed in the introduction, it is well established that for conditions enabling sufficient CO_2 removal (above pH 8.5), an appreciable H_2S removal by chemical absorption could be simultaneously achieved with CO_2 removal during photosynthetic biogas upgrading. In that condition, the effect of H_2S on CO_2 absorption and the bubble column performance would be negligible [3]. Indeed, in the present study, for L/G ratios of 0.4 and 0.5, which resulted in the liquid pH to remain above 8.5 and CO_2 content in biomethane to be below 2.5%, the results could be considered to remain valid even with the presence of H_2S. The absorbed H_2S

in the solution (as HS^-) at those operating pHs would then react with the DO, forming sulphates according to Eq. 3.24 [3].

$$2HS^- + 4O_2 \rightarrow 2H^+ + 2SO_4^{2-} \quad \text{when } DO \gg HS^- \tag{3.24}$$

Using the L/G ratio of 0.5 corresponding to sufficient CO_2 removal a DO concentration in the feed liquid of 10 mgO_2/L and 500 ppm_v H_2S in the feed biogas, $DO/_{HS^-}$ ratio would be greater than 7. In that case, almost 29% of the DO could be removed as sulphates, lowering the O_2 stripping into biomethane further. A similar reduction in O_2 content in the upgraded biomethane has been obtained by Bahr et al., (2014) [15] upon increasing the H_2S content in the inlet biogas.

3.7 Conclusions

The present research describes the design and commissioning of a small lab-scale bubble column reactor to upgrade biogas using *Spirulina platensis* algal solution. The setup would be able to treat up to 16.3 L_n/hr of biogas for scalable results. The primary focus in the present work is given on its design and commissioning, rather than optimisation. Selection of tubing and sampling arrangements were found to significantly affect the results and system performance especially with regards to a large oxygen ingress in the upgraded biomethane. Modification to system design, together with the implementation of correction factors to account for residual O_2 and N_2 resulted in achieving grid quality biomethane (CO_2 below 2% and O_2 below 0.55% by volume) above L/G ratios of 0.4 and low algal concentrations. At this condition, the corresponding CO_2 removal efficiency achieved was above 98%. The volumetric oxygen mass transfer coefficient ($k_{l_{O_2}}a$) varied between 0.0002 s^{-1} and 0.0018 s^{-1} at L/G ratios 0.1 and 0.5 respectively for lower concentrations of algae in the liquid phase. These results not only validated the performance of the bubble column when compared to literature but also indicated the adequacy of the measurement and data acquisition techniques employed in the current setup. No significant impact of the algal density and photosynthetic activity was found on the CO_2 removal performance of the bubble column. On the contrary, a higher algae concentration in the circulating liquid imparted practical challenges of foaming, clogging and increased oxygen concentrations in the upgraded biomethane Although to achieve grid quality biomethane a higher L/G ratio of 0.4 and above was necessary, the increased liquid

flow rate resulted in a drop in the inorganic carbon addition per unit volume into the alkaline algal liquid. In industrial-scale operations, this would not only lower the concentration of the cultivated microalgae but also impact the design of the photobioreactor in terms of its hydraulic retention time based on the algal productivity. Thus, further optimisation of the bubble column through the variation of gas and liquid flow rates, pH, alkalinity, temperature and residence times would increase its integration and practicality in photosynthetic biogas upgrading.

3.8 Acknowledgement

This work acknowledges the support from Science Foundation Ireland (SFI) through the Centre for Marine and Renewable Energy (MaREI) under Grant No. 12/RC/2302_P2 and 16/SP/3829, with industrial funding from Gas Networks Ireland through The Green Gas Innovation Group and by ERVIA and IDL Pernod Ricard. This work was also supported by the Environmental Protection Agency – Ireland (2018-RE-MS-13).

3.9 References

[1] Angelidaki I, Treu L, Tsapekos P, Luo G, Campanaro S, Wenzel H, et al. Biogas upgrading and utilization: Current status and perspectives. Biotechnol Adv 2018;36:452–66. doi:10.1016/j.biotechadv.2018.01.011.

[2] Rajendran K, O'Gallachoir B, Murphy JD. The combined role of policy and incentives in promoting cost efficient decarbonisation of energy: A case study for biomethane. J Clean Prod 2019;219:278–90. doi:10.1016/j.jclepro.2019.01.298.

[3] Meier L, Stará D, Bartacek J, Jeison D. Removal of H_2S by a continuous microalgae-based photosynthetic biogas upgrading process. Process Saf Environ Prot 2018;119:65–8. doi:10.1016/j.psep.2018.07.014.

[4] Meier L, Pérez R, Azócar L, Rivas M, Jeison D. Photosynthetic CO_2 uptake by microalgae: An attractive tool for biogas upgrading. Biomass and Bioenergy 2015;73:102–9. doi:10.1016/j.biombioe.2014.10.032.

[5] Bose A, O'Shea R, Lin R, Murphy JD. A perspective on novel cascading algal biomethane biorefinery systems. Bioresour Technol 2020;304:123027. doi:10.1016/j.biortech.2020.123027.

[6] Toledo-Cervantes A, Estrada JM, Lebrero R, Muñoz R. A comparative analysis of biogas upgrading technologies: Photosynthetic vs physical/chemical processes. Algal Res 2017;25:237–43. doi:10.1016/j.algal.2017.05.006.

[7] Muñoz R, Meier L, Diaz I, Jeison D. A review on the state-of-the-art of physical/chemical and biological technologies for biogas upgrading. Rev Environ Sci Biotechnol 2015;14:727–59. doi:10.1007/s11157-015-9379-1.

[8] Bose A, Lin R, Rajendran K, Xia A, O'Shea R, Murphy JD. How to optimise photosynthetic biogas upgrading: a perspective on system design and microalgae selection. Biotechnol Adv 2019;37. doi:10.1016/j.biotechadv.2019.107444.

[9] Meier L, Barros P, Torres A, Vilchez C, Jeison D. Photosynthetic biogas upgrading using microalgae: Effect of light/dark photoperiod. Renew Energy 2017;106:17–23. doi:10.1016/j.renene.2017.01.009.

[10] Gas Networks Ireland. Code of Operations, Part G. 2018.

[11] Chen PC, Lin S. Optimisation in the absorption and desorption of CO_2 using sodium glycinate solution. Appl Sci 2018;8:2041. doi:10.3390/app8112041.

[12] Cheng L, Li T, Keener TC, Lee JY. A mass transfer model of absorption of carbon dioxide in a bubble column reactor by using magnesium hydroxide slurry. Int J Greenh Gas Control 2013;17:240–9. doi:10.1016/j.ijggc.2013.05.018.

[13] Cents AHG, Brilman DWF, Versteeg GF. CO_2 absorption in carbonate/bicarbonate solutions: The Danckwerts-criterion revisited. Chem Eng Sci 2005;60:5830–5. doi:10.1016/j.ces.2005.05.020.

[14] Chen P, Huang C, Su T, Chen H, Yang M, Tsao J. Optimum conditions for the capture of carbon dioxide with a bubble-column scrubber. Int J Greenh Gas Control 2015;35:47–55. doi:10.1016/j.ijggc.2015.01.011.

[15] Bahr M, Díaz I, Dominguez A, González Sánchez A, Muñoz R. Microalgal-biotechnology as a platform for an integral biogas upgrading and nutrient removal from anaerobic effluents. Environ Sci Technol 2014;48:573–81. doi:10.1021/es403596m.

[16] Toledo-Cervantes A, Madrid-Chirinos C, Cantera S, Lebrero R, Muñoz R. Influence of the gas-liquid flow configuration in the absorption column on photosynthetic biogas upgrading in algal-bacterial photobioreactors. Bioresour Technol 2017;225:336–42. doi:10.1016/j.biortech.2016.11.087.

[17] Marín D, Posadas E, Cano P, Pérez V, Blanco S, Lebrero R, et al. Seasonal variation of biogas upgrading coupled with digestate treatment in an outdoors pilot scale algal-bacterial photobioreactor. Bioresour Technol 2018;263:58–66. doi:10.1016/j.biortech.2018.04.117.

[18] Kantarci N, Borak F, Ulgen KO. Bubble column reactors. Process Biochem 2005;40:2263–83. doi:10.1016/j.procbio.2004.10.004.

[19] Shaikh A, Al-Dahhan M. Scale-up of bubble column reactors: A review of current state-of-the-art. Ind Eng Chem Res 2013;52:8091–108. doi:10.1021/ie302080m.

[20] Rodero M del R, Posadas E, Toledo-cervantes A, Lebrero R. Influence of alkalinity and temperature on photosynthetic biogas upgrading efficiency in high rate algal ponds. Algal Res 2018;33:284–90. doi:10.1016/j.algal.2018.06.001.

[21] Rodero M del R, Carvajal A, Arbib Z, Lara E, de Prada C, Lebrero R, et al. Performance evaluation of a control strategy for photosynthetic biogas upgrading in a semi-industrial scale photobioreactor. Bioresour Technol 2020;307:123207. doi:10.1016/j.biortech.2020.123207.

[22] Manjrekar ON, Sun Y, He L, Tang YJ, Dudukovic MP. Hydrodynamics and mass transfer coefficients in a bubble column photo-bioreactor. Chem Eng Sci 2017;168:55–66. doi:10.1016/j.ces.2017.04.016.

[23] Rodero M del R, Severi CA, Rocher-Rivas R, Quijano G, Muñoz R. Long-term influence of high alkalinity on the performance of photosynthetic biogas upgrading. Fuel 2020;281:118804. doi:10.1016/j.fuel.2020.118804.

[24] Rodero M del R, Carvajal A, Castro V, Navia D, de Prada C, Lebrero R, et al. Development of a control strategy to cope with biogas flowrate variations during photosynthetic biogas upgrading. Biomass and Bioenergy 2019;131. doi:10.1016/j.biombioe.2019.105414.

[25] Rodero M del R, Lebrero R, Serrano E, Lara E, Arbib Z. Technology validation of photosynthetic biogas upgrading in a semi- industrial-scale algal-bacterial photobioreactor. Bioresour Technol 2019;279:43–9. doi:10.1016/j.biortech.2019.01.110.

[26] Posadas E, Marín D, Blanco S, Lebrero R, Muñoz R. Simultaneous biogas upgrading and centrate treatment in an outdoors pilot scale high rate algal pond. Bioresour Technol 2017;232:133–41. doi:10.1016/j.biortech.2017.01.071.

[27] Franco-Morgado M, Alcántara C, Noyola A, Muñoz R, González-Sánchez A. A study of photosynthetic biogas upgrading based on a high rate algal pond under

alkaline conditions: Influence of the illumination regime. Sci Total Environ 2017;592:419–25. doi:10.1016/j.scitotenv.2017.03.077.

[28] Posadas E, Serejo ML, Blanco S, Pérez R, García-Encina PA, Muñoz R. Minimization of biomethane oxygen concentration during biogas upgrading in algal-bacterial photobioreactors. Algal Res 2015;12:221–9. doi:10.1016/j.algal.2015.09.002.

[29] Serejo ML, Posadas E, Boncz MA, Blanco S, García-Encina P, Muñoz R. Influence of biogas flow rate on biomass composition during the optimisation of biogas upgrading in microalgal-bacterial processes. Environ Sci Technol 2015;49:3228–36. doi:10.1021/es5056116.

[30] Pourtousi M, Ganesan P, Sahu JN. Effect of bubble diameter size on prediction of flow pattern in Euler-Euler simulation of homogeneous bubble column regime. Meas J Int Meas Confed 2015;76:255–70. doi:10.1016/j.measurement.2015.08.018.

[31] Leonard C, Ferrasse JH, Boutin O, Lefevre S, Viand A. Bubble column reactors for high pressures and high temperatures operation. vol. 100. Institution of Chemical Engineers; 2015. doi:10.1016/j.cherd.2015.05.013.

[32] de Oliveira MACL, Monteiro MPC, Robbs PG, Leite SGF. Growth and chemical composition of *Spirulina maxima* and *Spirulina platensis* biomass at different temperatures. Aquac Int 1999;7:261–75. doi:10.1023/A:1009233230706.

[33] Hikita H, Asai S, Takatsuka T. Absorption of carbon dioxide into aqueous sodium hydroxide and sodium carbonate-bicarbonate solutions. Chem Eng J 1976;11:131–41. doi:10.1016/S0300-9467(76)80035-4.

[34] Knuutila H, Juliussen O, Svendsen HF. Kinetics of the reaction of carbon dioxide with aqueous sodium and potassium carbonate solutions. Chem Eng Sci 2010;65:6077–88. doi:10.1016/j.ces.2010.07.018.

[35] Borhani TNG, Azarpour A, Akbari V, Wan Alwi SR, Manan ZA. CO_2 capture with potassium carbonate solutions: A state-of-the-art review. Int J Greenh Gas Control 2015;41:142–62. doi:10.1016/j.ijggc.2015.06.026.

[36] Clark KN. The effect of high pressure and temperature on phase distributions in a bubble column. Chem Eng Sci 1990;45:2301–7. doi:10.1016/0009-2509(90)80109-R.

[37] Deckwer WD, Louisi Y, Zaidi A, Ralek M. Hydrodynamic properties of the Fischer-Tropsch slurry process. Ind Eng Chem Process Des Dev 1980;19:699–708. doi:10.1021/i260076a032.

[38] Fernández I, Guzmán JL, Berenguel M, Acién FG. Dynamic modeling of microalgal production in photobioreactors. In: Tripathi, Bhumi Nath, Kumar D, editor. Prospect. Challenges Algal Biotechnol., Springer; 2017, p. 49–86. doi:10.1007/978-981-10-1950-0.

[39] Lin CC, Liu WT, Tan CS. Removal of carbon dioxide by absorption in a rotating packed bed. Ind Eng Chem Res 2003;42:2381–6. doi:10.1021/ie020669+.

[40] Götz M, Lefebvre J, Mörs F, Ortloff F, Reimert R, Bajohr S, et al. Novel gas holdup correlation for slurry bubble column reactors operated in the homogeneous regime. Chem Eng J 2017;308:1209–24. doi:10.1016/j.cej.2016.09.101.

[41] Weiner ER. Applications of Environmental Chemistry. A Practical Guide for Environmental Professionals. 2nd ed. CRC Press; 2000.

[42] Jin B, Yu Q, Yan XQ, Van Leeuwen JH. Characterization and improvement of oxygen transfer in pilot plant external air-lift bioreactor for mycelial biomass production. World J Microbiol Biotechnol 2001;17:265–72. doi:10.1023/A:1016622413185.

[43] Shah YT, Kelkar BG, Godbole SP, Deckwer W -D. Design parameters estimations for bubble column reactors. AIChE J 1982;28:353–79. doi:10.1002/aic.690280302.

[44] Kishi M, Yamada Y, Katayama T, Matsuyama T. Carbon mass balance in *Arthrospira platensis* culture with medium recycle and high CO_2 supply. Appl Sci 2019;10:1–14. doi:10.3390/app10010228.

[45] Millero FJ, Graham TB, Huang F, Bustos-Serrano H, Pierrot D. Dissociation constants of carbonic acid in seawater as a function of salinity and temperature. Mar Chem 2006;100:80–94. doi:10.1016/j.marchem.2005.12.001.

[46] Madkour FF, Kamil AEW, Nasr HS. Production and nutritive value of *Spirulina platensis* in reduced cost media. Egypt J Aquat Res 2012;38:51–7. doi:10.1016/j.ejar.2012.09.003.

[47] Hu Q, Guterman H, Richmond A. A flat inclined modular photobioreactor for outdoor mass cultivation of photoautotrophs. Biotechnol Bioeng 1996;51:51–60. doi:10.1002/(sici)1097-0290(19960705)51:1<51::aid-bit6>3.0.co;2-%23.

[48] Costa JAV, Colla LM, Filho PD. *Spirulina platensis* growth in open raceway ponds using freshwater supplemented with carbon, nitrogen and metal ions. Zeitschrift Fur Naturforsch - Sect C J Biosci 2003;58:76–80. doi:10.1515/znc-2003-1-214.

[49] American Public Health Association (APHA). APHA Method 2320. Stand. Methods Exam. Water Wastewater. 18th ed., Washington, DC: American Public Health Association (APHA); 1992.

[50] Rich VI, Maier RM. Aquatic Environments. Elsevier Inc.; 2015. doi:10.1016/B978-0-12-394626-3.00006-5.

[51] Moosavi SM, Ghassabian S. Linearity of Calibration Curves for Analytical Methods: A Review of Criteria for Assessment of Method Reliability. In: Stauffer M, editor. Calibration Valid. Anal. Methods - A Sampl. Curr. Approaches, 2018. doi:10.5772/intechopen.72932.

[52] Chai T, Draxler RR. Root mean square error (RMSE) or mean absolute error (MAE)? -Arguments against avoiding RMSE in the literature. Geosci Model Dev 2014;7:1247–50. doi:10.5194/gmd-7-1247-2014.

[53] Neill SP, Hashemi MR. Ocean Modelling for resource characterization. In: Neill SP, Hashemi MR, editors. Fundam. Ocean Renew. Energy, Academic Press; 2018, p. 193–235. doi:10.1016/b978-0-12-810448-4.00008-2.

[54] Lee S, Lee DK. What is the proper way to apply the multiple comparison test? Korean J Anesthesiol 2018;71:353–60. doi:10.4097/kja.d.18.00242.

[55] Schlattmann P, Dirnagl U. Statistics in experimental cerebrovascular research: Comparison of more than two groups with a continuous outcome variable. J Cereb Blood Flow Metab 2010;30:1558–63. doi:10.1038/jcbfm.2010.95.

[56] Zimmerman WB, Al-Mashhadani MKH, Bandulasena HCH. Evaporation dynamics of microbubbles. Chem Eng Sci 2013;101:865–77. doi:10.1016/j.ces.2013.05.026.

[57] Besagni G, Inzoli F. The effect of liquid phase properties on bubble column fluid dynamics: Gas holdup, flow regime transition, bubble size distributions and shapes, interfacial areas and foaming phenomena. Chem Eng Sci 2017;170:270–96. doi:10.1016/j.ces.2017.03.043.

[58] Buchmann L, Bertsch P, Böcker L, Krähenmann U, Fischer P, Mathys A. Adsorption kinetics and foaming properties of soluble microalgae fractions at the air/water interface. Food Hydrocoll 2019;97:105182. doi:10.1016/j.foodhyd.2019.105182.

[59] Langmuir D. Aqueous Environmental Geochemistry. New Jersey: Prentice-Hall; 1997.

[60] Krishna R, Van Baten JM. Mass transfer in bubble columns. Catal Today 2003;79–80:67–75. doi:10.1016/S0920-5861(03)00046-4.

[61] Ferreira A, Cardoso P, Teixeira JA, Rocha F. PH influence on oxygen mass transfer coefficient in a bubble column. Individual characterization of kL and a. Chem Eng Sci 2013;100:145–52. doi:10.1016/j.ces.2013.02.020.

[62] Besagni G. Two-Phase bubble columns : A comprehensive review. ChemEngineering 2018;2:13. doi:10.3390/2020013.

[63] Chaumat H, Billet AM, Delmas H. Hydrodynamics and mass transfer in bubble column: Influence of liquid phase surface tension. Chem Eng Sci 2007;62:7378–90. doi:10.1016/j.ces.2007.08.077.

[64] Mineta R, Salehi Z, Yoshikawa H, Kawase Y. Oxygen transfer during aerobic biodegradation of pollutants in a dense activated sludge slurry bubble column: Actual volumetric oxygen transfer coefficient and oxygen uptake rate in p-nitrophenol degradation by acclimated waste activated sludge. Biochem Eng J 2011;53:266–74. doi:10.1016/j.bej.2010.11.006.

[65] Han L, Al-Dahhan MH. Gas-liquid mass transfer in a high pressure bubble column reactor with different sparger designs. Chem Eng Sci 2007;62:131–9. doi:10.1016/j.ces.2006.08.010.

[66] Shaikh A, Al-Dahhan M. A new methodology for hydraulic similarity in bubble columns. Can J Chem Eng 2010;88:503–17. doi:10.1002/cjce.20357.

[67] Majumder SK. Hydrodynamics and transport processes of inverse bubbly flow. Elsevier; 2016. doi:10.1016/C2014-0-01619-X.

[68] Chisti MY. Airlift Bioreactors. London: Elsevier Applied Science; 1989.

[69] Wilkinson PM, Spek AP, Dierendonck LL Van. Design parameters estimation for scale-up of high-pressure bubble columns. AIChE J 1992;38:544–54. doi:10.1002/aic.690380408.

[70] Besagni G, Gallazzini L, Inzoli F. On the scale-up criteria for bubble columns. Petroleum 2019;5:114–22. doi:10.1016/j.petlm.2017.12.005.

[71] Jakobsen HA. Bubble Column Reactors. Chem. React. Model. Multiph. React. Flows, Trondheim: Springer Berlin Heidelberg; 2009, p. 335–501.

[72] Binaghi L, Del Borghi A, Lodi A, Converti A, Del Borghi M. Batch and fed-batch uptake of carbon dioxide by *Spirulina platensis*. Process Biochem 2003;38:1341–6. doi:10.1016/S0032-9592(03)00003-7.

4 A comparative evaluation of design factors on bubble column operation in photosynthetic biogas upgrading

A comparative evaluation of design factors on bubble column operation in photosynthetic biogas upgrading

Archishman Bose[a,b,†], Richard O'Shea[a,b,*,†], Richen Lin[a,b,†], Jerry D Murphy[a,b,†]

[a]Environmental Research Institute, MaREI Centre, University College Cork, Cork, T23 XE10, Ireland

[b]Department of Civil, Structural and Environmental Engineering, School of Engineering and Architecture, University College Cork, Cork, T12 K8AF, Ireland.

Abstract

Studies attempting to optimise photosynthetic biogas upgrading by simultaneous investigation of the bubble column-photobioreactor setup have experienced considerable variability in results and conclusions. To identify the sources of such variation, this work quantitatively compared seven design factors (superficial gas velocity; liquid to gas flow rate (L/G) ratio; empty bed residence time; liquid inlet pH; liquid inlet alkalinity; temperature; and algal concentration) using the L_{16} Taguchi orthogonal array as a screening design of experiment. Assessments were performed using the signal to noise (S/N) ratio on the performance of CO_2 removal (CO_2 removal efficiency, CO_2 absorption rate and overall CO_2 mass transfer coefficient) and O_2 stripping (O_2 concentration in biomethane and O_2 flow rate in biomethane). Results show that pH and L/G ratio are the most critical design factors. Temperature and gas residence times had minimal impact on the biomethane composition. The interactive effect between pH and L/G ratio was the most impactful followed by the interactive effects between superficial gas velocity and L/G ratio and pH on CO_2 removal efficiency. The impact of L/G ratio, algal concentration and pH (in that order of impact) caused up to a 90% variation in oxygen content in biomethane. However, algal concentration had a diminishing role as the L/G ratio increased. Using only the statistically significant main effects and interactions, the biomethane composition (CO_2% and O_2%) was predicted with over 95% confidence through regression equations for superficial gas velocity up to 0.2 cm/s.

Nomenclature

Symbols/Acronyms	Descriptions
Adj	Adjusted
Alk	Alkalinity [g-IC/L]
ANOVA	Analysis of Variance
C_{alg}	Algae concentration [g-DW/L]
CI	Confidence nterval
DoF	Degree of Freedom
DW	Dry weight
EBRT	Empty bed residence Time [mins]
G	Biogas flow rate [mL_n/s]
hr	hour
IC	Inorganic carbon
k	kilo
$k_{G_{CO_2}}a$	Mean overall CO_2 mass transfer coefficient [hr^{-1}]
LB	Lower-the-better
L/G	Liquid to gas flow rate (L/G) ratio
mL_n	millilitres normal
MS	Mean squares
N	Molar flow rate (mol/s)
n_{ex}	Number of experiments
OA	Orthogonal Array
PI	Prediction Interval
R_{abs,CO_2}	Mean steady state CO_2 absorption rate [mol/L/s]
R_{eff,CO_2}	Efficiency of CO_2 removal from biogas [%]
s	seconds
SB	Smaller-the-better
S/N	Signal to noise
SS	Sum of squares
SSE	Sum of square errors
T_{col}	Temperature of bubble column [°C]
TRL	Technology readiness level
u_G	Superficial gas velocity [cm/s]

Subscripts	Descriptions
BC	Bubble column
BG	Biogas
BM	Biomethane

4.1 Introduction

4.1.1 Microalgal (photosynthetic) biogas upgrading

Biomethane from anaerobic digestion (AD) is a renewable and versatile biofuel [1,2]. As compared to conventional biogas upgrading technologies such as water scrubbing and pressure swing absorption, novel biogas upgrading technologies aim to increase the sustainability of biomethane derived from biogas by reducing costs and energy demands [3]. The two-step photosynthetic biogas upgrading process, employing CO_2 removal and subsequent utilisation of CO_2 by microalgae is considered a novel biogas upgrading technology [4,5]. In the first step, as shown in Figure 4-1, CO_2, as well as H_2S is absorbed in a bubble column by a carbonate-rich sodium carbonate-bicarbonate buffer solution (pH 9 and above) via the principle governing Eq. 4.1 [4], decreasing the pH. In the subsequent step, the bicarbonate uptake by the algae in a photobioreactor regenerates carbonate in the solution with a corresponding rise in pH (Eq. 4.2). The re-circulation of the regenerated carbonate-rich solution into the bubble column then continues the carbonate-bicarbonate cycle. In addition to the biomethane, the cultivated microalgae is a high-value product critical to improving both the economic benefits and sustainability of the biomethane produced [6].

Bubble Column: $$CO_2 + H_2O + CO_3^{2-} \rightarrow 2HCO_3^- \quad (4.1)$$

Photobioreactor: $$\left\{ \begin{array}{l} HCO_3^- \xrightarrow{Algae} CO_2 + OH^- \\ HCO_3^- + OH^- \xrightarrow{Medium} CO_3^{2-} + H_2O \end{array} \right\} \quad (4.2)$$

4.1.2 Need for a focussed approach to photosynthetic biogas upgrading

Ensuring continuous grid quality biomethane (CO_2 and O_2 less than 2.5% and 1% by volume respectively) [7,8] and adequate carbon uptake by microalgae are essential to maximise the economic and environmental benefits from the photosynthetic biogas upgrading system. To achieve this, the influence of multiple operational factors (compiled in Table 4-1) such as pH [4,9], gas and liquid flow velocities [4,10] and flow rates [11], temperature [12], alkalinity [12,13], biogas

composition [4], concentration of the algae [4,13], as well as the microalgae species and its cultivation conditions [4] must be simultaneously taken into account. Accordingly, the operations of the individual components such as the bubble column and the microalgae cultivation and harvesting in photosynthetic biogas upgrading could significantly deviate from those of optimised stand-alone setups. For example, when *Spirulina platensis* is chosen as the microalgae, the bubble column in the photosynthetic biogas upgrading system should operate below a pH of 11 and a temperature of 40 °C to prevent severe damage to the microalgae [14]. This is in contrast to operating conditions of pH above 11 and a temperature above 40 °C, commonly employed for CO_2 removal in an alkaline medium without the presence of microalgae [15]. In another example of differentiation between individual components and the integrated system, researchers aimed to achieve a carbon balance in the bubble column-photobioreactor system by fixing algal productivity [16]. The controlled values, varying between 7.5-15 g/m^2/day are much lower than the achievable productivity of 20-25 g/m^2/day in open pond systems [17].

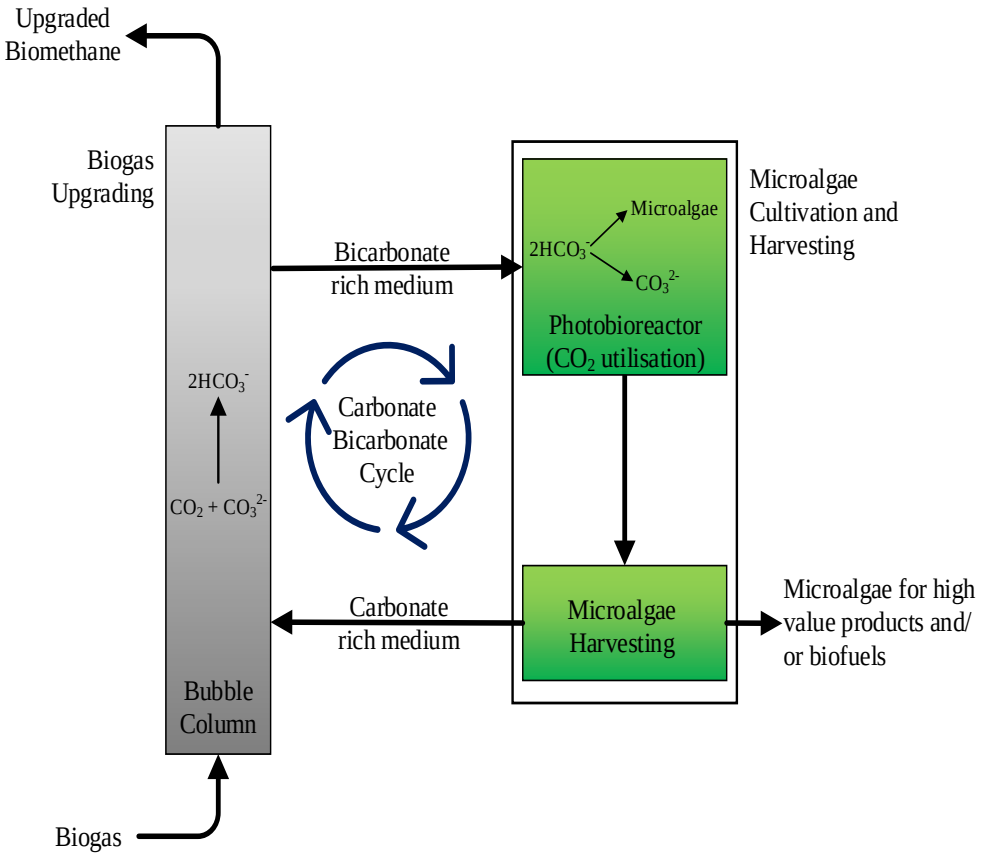


Figure 4-1 Diagrammatic representation of the two-step bubble column-photobioreactor photosynthetic biogas upgrading system using the carbonate bicarbonate cycle for the production of biomethane and microalgae for high-value products and/or biofuels.

The simultaneous influence of multiple design factors and their corresponding levels of operation on photosynthetic biogas upgrading (compiled in Table 4-1) has additionally caused considerable differences in conclusions on the system performance. For instance, Toledo-Cervantes et al., (2017) [11] suggested the use of co-current bubble column configuration and a liquid to gas flow rate (L/G) ratio of less than 1 to achieve grid quality biomethane. However, Rodero et al., (2020a) [18] employing a counter-current bubble column, reported 14.1% CO_2 concentration in upgraded biomethane at an L/G ratio of 0.8 in a pilot-scale facility. In a more recent study by the same research team, the CO_2 content in the biogas varied between 1.5% and 4.4% at an alkalinity of 1,200 mg/L-IC and inlet pH between 9.7 and 9.8 [13]. In contrast, Marin et al. (2021) [16] in a similar experimental range and using a similar setup, reported a much lower CO_2 content in biogas of 0.5%. Seasonal variations, especially with open pond microalgae cultivation caused CO_2 percentages in biomethane to vary from 0.7% during summer to 11.9% during winter; the corresponding O_2 concentration varied between 0% and 3.5% [19]. Diurnal variations between 2% and 4.5% in CO_2 content in the upgraded biomethane were reported by Meier et al. (2017) [7].

These variabilities and uncertainties arise not only from the different experimental conditions that exist in each study but also, from the probable interactive effects among operating factors that are seldom considered in these studies. Thus, although present Technology Readiness Levels (TRLs) would suggest viable knowledge for scale-up and industrial-scale implementation of photosynthetic biogas upgrading, it would still suffer from significant uncertainty. Therefore, rather than trying to optimise the overall photosynthetic biogas upgrading system, a focused look into individual sub-systems could be beneficial. It would allow optimisation of biogas upgrading and hence the selection of appropriate microalgae cultivation and harvesting techniques to maximise the overall system effectiveness and robustness.

Table 4-1 Variables affecting bubble column operations in photosynthetic biogas upgrading including those selected in the present study for comparative assessment. The current and limiting/ industrial level values have been compiled from multiple literature sources [4,7,9,11,13,16,18,19,25–30]

Variables	Description	Levels			Factor selection in current study
		Current	Limits/ Levels	Research need	
Superficial gas velocity [cm/s]	Inlet velocity of biogas to the bubble column	0.05 – 0.5	4	To be increased	Selected
Empty bed residence time [mins]	Time of biogas in an empty bubble column, indicating the height of the column.	10-90	3-6	To be reduced	Selected
Aspect ratio	Ratio of column height to diameter.	10-110	3-10 [31]	To be reduced	Not selected as confounded with the both the previous factors.
L/G Ratio	Ratio of liquid to gas flow rate	0.5-10	NA	To be optimised	Selected
Flow configuration	Co-current or counter-current gas-liquid flow configurations.	Co/Counter-current	NA	N/A	Co-current chosen after Toledo-Cervantes et al., (2017b) [11]
pH	pH of the algal solution at the bubble column inlet	7-10.5	8.5-11	To be optimised	Selected
Alkalinity [gIC/L]	Strength of a buffer solution, indicating the amount of dissolved inorganic carbon content in a solution	0.1-4.1	N/A	To be optimised	Selected
Temperature [°C]	Operating temperature of the bubble column.	10 - 28	20 - 40	To be optimised	Selected
Algae concentration [gDW/L]	Concentration of microalgae in the cultivation medium	Algae circulated after harvesting	Up to 10 [21]	To be optimised	Selected
Light [klux]	Cool white light affecting appreciable *Spirulina platensis* growth.	On/Off	As per those required by chosen algal species	Effect to be understood	Kept on at all times in the bubble column setup
Algae productivity [gDW/L/day]	Average daily growth rate of microalgae	0.06-0.1	0.175 [14]	To be maximised	Not considered as not directly linked to

Variables	Description	Levels			Factor selection in current study
		Current	Limits/ Levels	Research need	
					bubble column optimisation.
CO_2 in biogas [%]	CO_2 concentration in the influent biogas	NA	20-55	External Factor	Kept constant as an external factor
H_2S in biogas [ppm]	H_2S concentration in the influent biogas	NA	0-10,000	External Factor	
Dissolved oxygen (DO) concentration [mg/L]	The content of the dissolved oxygen in the inlet algal liquid	2-15	<100% air saturation level [32]	External Factor	Kept constant as an external factor

NA: Not Applicable; *IC*: Inorganic carbon; *DW*: Dry weight

4.1.3 Objective and novelty

Research on bubble columns for CO_2 absorption in sodium/potassium carbonate-bicarbonate solutions has primarily focused on performance improvement in either pure or catalysed solutions in the absence of microalgae [15,20]. On the contrary, microalgae cultivation [21,22] and harvesting [23,24], have been extensively studied and discussed in the literature under similar conditions suitable for photosynthetic biogas upgrading.

Thus, in a novel approach, rather than optimisation by varying a few factors, the present work aims to compare the main effects of, and interactions between, different design factors on the bubble column performance for biogas upgrading. The Taguchi orthogonal array as a screening design of experiment was selected as the statistical tool. Using this comparative assessment, the authors believe a significant knowledge gap in the operation of the bubble column and hence the overall photosynthetic biogas upgrading system could be overcome. Accordingly, experiments were conducted on a lab-scale bubble column to:

i. Determine and rank the factors according to their influence on the performance of the bubble column for photosynthetic biogas upgrading.
ii. Determine the most impactful interactive effects between the design factors to affect the bubble column operations.

iii. Identify the suitable operating setpoints of the design factors to ensure robust operation of the bubble column.

iv. Predict and analyse the operation of the bubble column with respect to product biomethane composition and its significance to photosynthetic biogas upgrading.

4.2 Materials and methods

4.2.1 Microorganisms and culture conditions

All experiments were performed with microalgae *Arthrospira* (*Spirulina*) *platensis* SAG 85.79, from Sammlung von Algenkulturen Goettingen (SAG), Germany. The microalgae were grown in 3 L batches within 5 L Erlenmeyer Flasks with continuous bubbling of air. Temperature and light were maintained at 20 ± 1 °C and 4,000 ± 500 lux with a 16:8 light/dark cycle. Modified Zarrouk's medium was used as the nutrient medium, the detailed composition of which can be found elsewhere [33]. The cultures were transferred to a new medium every three to four weeks to continue cultivation. Strains were maintained in 100 mL Erlenmeyer flasks, maintaining a pH between 9 and 10.

4.2.2 Experimental setup

Experiments were conducted in a 2 m high, 24 mm diameter absorption (bubble) column made from a clear acrylic tube. Multiple liquid outlets at desired heights were fitted to allow the study of variable gas flow rates and EBRT. A 24 mm diameter, 300 mm high gas-liquid separator was used to remove all trapped gas bubbles at the liquid outlet. The entire setup was housed in a cabinet capable of maintaining temperature and light intensities between 20 to 40 °C and 2,000 to 6,000 lux respectively. A schematic overview of the experimental setup is provided in Figure 4-2. The microalgae solution was pumped through the bottom of the column by a VWR® AU-UPC-EZ programmable peristaltic pump in a co-current configuration to the biogas. Synthetic biogas, at an absolute pressure of 1.2 bar was bubbled through a 25 mm long and 18 mm diameter air-stone diffuser placed at the bottom of the bubble column. Synthetic biogas comprising 40% CO_2 and the remainder N_2 (in lieu of CH_4) without any H_2S was chosen from safety considerations. N_2 in lieu of CH_4 has been previously used in the literature [27] due to its inertness and similar solubility (0.0019 g/100g

H_2O) to that of CH_4 (0.0023 g/100 g H_2O) [34] under atmospheric conditions. The individual N_2 and CO_2 flows were controlled by separate flow controllers (Red-y smart controller GSC, Vögtlin Instruments® GmbH). Differential pressure between the top of the bubble column and the atmosphere fluctuated between 0.01 ± 0.01 bar (g) measured by a manometer fitted to the outlet of the column**.**

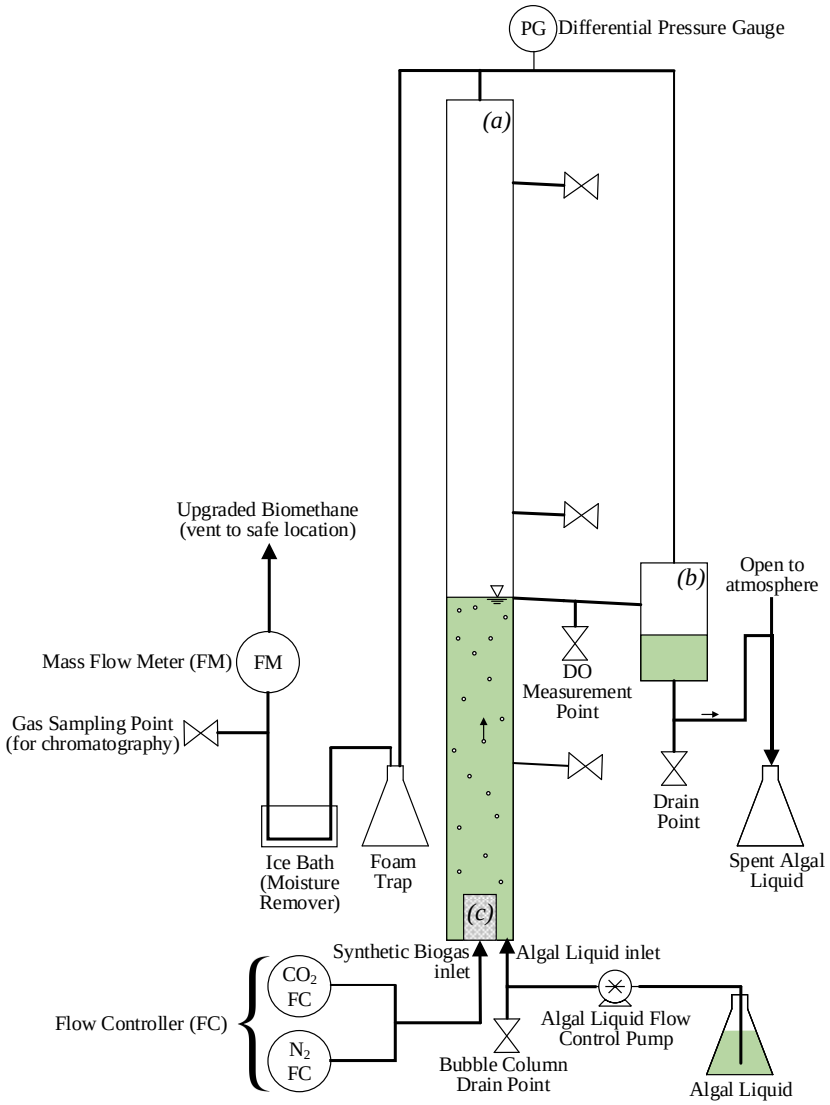


Figure 4-2 Diagrammatic representation (not to scale) of the experimental setup for the screening design of experiments where (a) is the primary bubble column, (b) is the gas-liquid separator and (c) is the gas diffuser

The liquid outlet from the gas/liquid separator was routed to a tee with one end open to the atmosphere via a U-shaped connection as shown in Figure 4-2. This prevented the syphoning out of the liquid from the gas-liquid separator, while allowing the outlet flow to match the inlet flow controlled by the peristaltic pump. The combined outlet gas from the bubble column and the gas-liquid separator was

sequentially routed through a foam trap and an ice bath to remove foam and moisture. Inside the ice bath, a larger diameter pipe was used as a condensate trap and was regularly drained after a few experiments to ensure its adequacy of operation. Flow and composition measurements were hence performed on a dry gas basis described in Section 4.2.4.

4.2.3 Experimental design

4.2.3.1 Screening design of experiments

The Taguchi orthogonal array (OA) as a screening design of experiments was used to quantitatively determine the most critical design factors and their corresponding settings at which both the desired output is achieved and the system resilience is maximised [35,36]. This method was selected as it provides a robust, balanced and unbiased technique to compare the main effects of the design factors independently of each other with a minimum number of experiments [35,37,38]. Additionally, a few interactions among the design factors can also be studied [35,39]. In this concept, each design factor is studied at two levels ("high" or "low" for quantitative factors or "on" or "off" for qualitative ones) to systematically record and rank their influences on the desired outcome [40]. Figure 4-3 outlines the step by step methodology of Taguchi experimental design used in the present study. A brief description of each step has been provided in the following sections, further details of which can be found in the literature and textbooks [35,41].

4.2.3.2 Selection of process responses as bubble column performance criteria

To prevent confounding and to develop a perspective on the bubble column design, cost and operations, system performance was assessed in terms of CO_2 removal and oxygen stripping from the microalgal medium into the biomethane. CO_2 removal efficiency ($R_{eff,\,CO_2}$) [%]; the mean steady-state absorption rate of CO_2 (R_{abs,CO_2}) [mol/L/s]; and the mean overall CO_2 mass transfer coefficient $k_{G_{CO_2}}a$ [hr^{-1}] were used to assess CO_2 removal [42]. To measure oxygen stripping, the O_2 concentration in the upgraded biomethane ($O_{2,\%,BM}$) [%], together with the flow rate of O_2 in the outlet biomethane ($O_{2,BM}$) [mL_n/min] were studied.

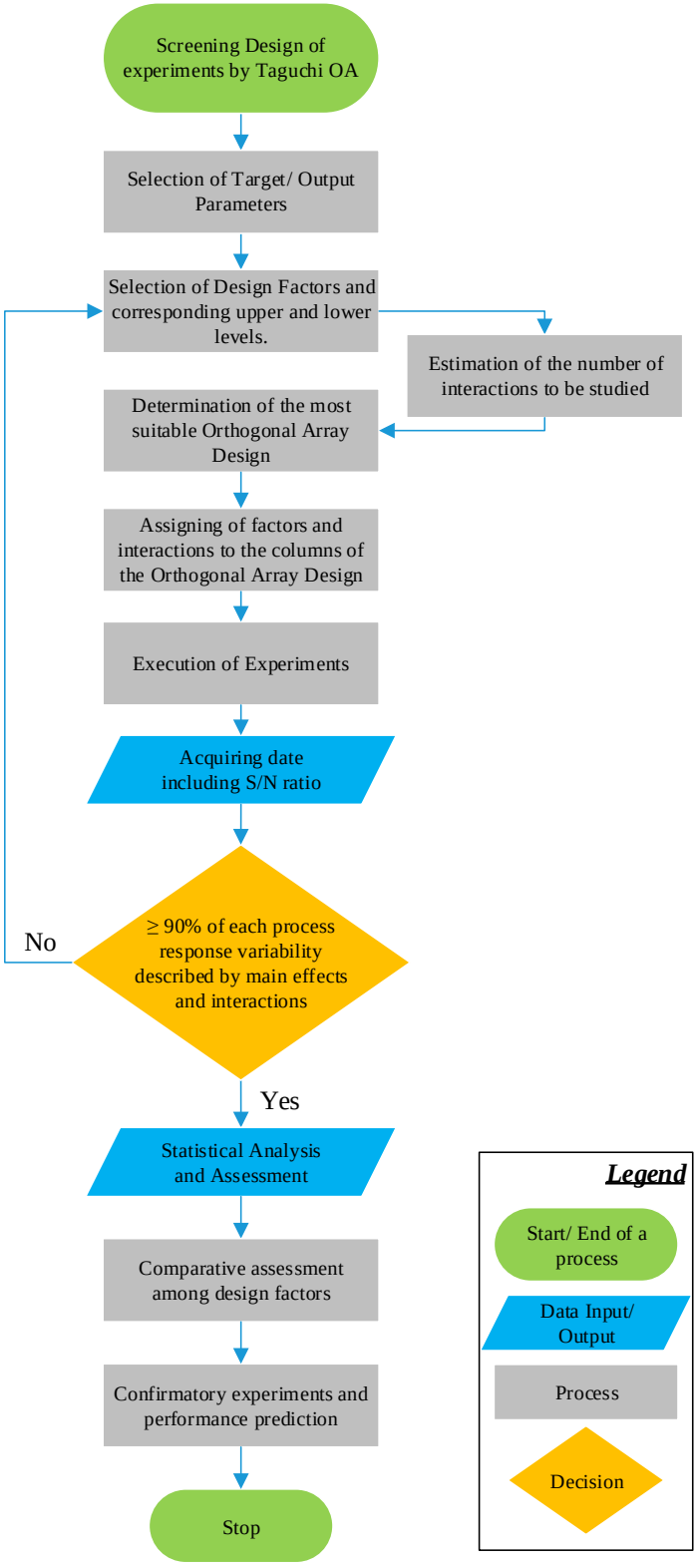


Figure 4-3 Outline of the Taguchi Screening design of experiments using orthogonal arrays

Assuming a closed system with no loss of gases, $R_{eff,\,CO_2}$ was calculated from the inlet molar flow rate of CO_2 in the biogas ($N_{CO_2,BG}$) and the outlet molar flowrate of CO_2 in the biomethane ($N_{CO_2,BM}$) [mol/min] according to Eq. 4.3. The

corresponding mean steady-state absorption rate of CO_2 (R_{abs,CO_2}) [mol/L/s] is described in Eq. 4.4 in which V_{BC} denotes the liquid volume in the bubble column in litres [42]. The following assumptions were made: i) a two-phase system with minimal influence of the solid phase [43,44]; ii) a thoroughly mixed homogeneous system that can be considered as a plug flow and can be well represented by the two-film theory [45,46]; iii) isothermal conditions conforming to the ideal gas laws; and iv) fast chemical reactions occurring above pH 8 [47]. Finally, the mean overall mass transfer coefficient for CO_2 absorption $k_{G_{CO_2}}a$ [hr^{-1}] was estimated after Chen and Lin, (2018) [45] via Eq. 4.5 where G represents the total gas flow rate in the influent biogas in mL_n/s.

$$R_{eff,\,CO_2} = \frac{N_{CO_2,BG} - N_{CO_2,BM}}{N_{CO_2,BG}} \times 100 \tag{4.3}$$

$$R_{abs,CO_2} = \frac{N_{CO_2,BG} - N_{CO_2,BM}}{V_{BC}} \tag{4.4}$$

$$k_{G_{CO_2}}a = \frac{G}{V_{BC}} \cdot \ln \frac{N_{CO_2,BG}}{N_{CO_2,BM}} \tag{4.5}$$

4.2.3.3 Selection of Design Factors and their levels

Seven controllable variables or design factors affecting the operation of the bubble column in photosynthetic biogas upgrading were selected for comparative assessment, namely: superficial gas velocity (u_G); the liquid to gas flow rate (L/G) ratio; empty bed residence time (EBRT); liquid inlet pH; liquid inlet alkalinity (Alk); temperature (T_{col}); and algal concentration in the liquid circulating in the bubble column (C_{alg}). As discussed in Section 4.1.2, and compiled in Table 4-1 all factors except algal concentration and EBRT have been separately investigated for their importance to the operations of the overall photosynthetic biogas upgrading system. While factors such as the pH and alkalinity would need to be optimised, understanding the relative importance of superficial gas velocity is important in order to increase the throughput of the bubble column. On the contrary, the influence of EBRT and algal concentration have only been evaluated explicitly by Bahr et al., (2014) [9] and Rodero et al., (2020b) [13] respectively. However, in a previous work by the authors [4], these factors were discussed to be of potentially considerable importance and hence are selected for assessment herein. Indeed, decreasing the EBRT to current industrial

levels is critical towards ensuring the use of state-of-the-art bubble columns for photosynthetic biogas upgrading, as this would reduce construction and operation costs. Other variables, such as the CO_2 and H_2S content in biogas and the dissolved oxygen in the circulating algal liquid, which affect the bubble column operation are exogenous to the bubble column design and hence not included in the design factors.

The upper and lower bound value of each design factor was selected by assessing current trends and future targets from literature as indicated in Table 4-2. However, for u_G and EBRT, the upper values were selected based on the limitation of the experimental set-up described in Section 4.2.2. Thus, the maximum u_G and EBRT was limited to 0.2 cm/s and 15 minutes respectively, although their maximum limits lie at 4 cm/s and 90 minutes respectively. Additionally, the maximum algal density was fixed at 0.75 gDW/L, limited by the foaming of the algae medium observed during pre-experiments [48]. However, it is still representative of the algal concentrations obtained in closed and open photobioreactors [49,50]. Similarly, the lower and upper temperature values correspond to the tolerable and ideal values for *Spirulina platensis* [14].

Table 4-2 Design factors and corresponding levels.

Factor	Design Factors	Notation	Level	
			Low (1)	High (2)
A	L/G ratio	L/G	0.2	1
B	Superficial gas velocity [cm/s]	u_G	0.06	0.2
C	Empty bed residence Time [mins]	EBRT	6	15
D	Inlet pH	pH	9	10.5
E	Inlet alkalinity [gIC/L]	Alk	1	2.5
F	Temperature [°C]	T_{col}	20	35
G	Algae concentration [gDW/L]	C_{alg}	0.05	0.75

4.2.3.4 Selection of Taguchi OA, interactions and experimental trials

The Taguchi Orthogonal Array (OA) comprising 16 experimental trials (L_{16}) was selected to quantitatively compare (screen) seven factors (tested at two levels, referred to as a "2^7"). Each design factor was assigned one column in the fifteen column L_{16} OA. The remaining eight columns were used to study two-factor interactions, namely: i) L/G vs pH; ii) L/G vs u_G; iii) u_G vs EBRT; iv) u_G vs pH; v) u_G

vs Alk; vi) u_G vs T_{col}; vii) pH vs Alk; and viii) T_{col} vs C_{alg}. Accordingly, the following Taguchi OA structure was generated as shown in Table 4-3. All higher-order interactions were neglected with fair confidence [36].

Table 4-3 L_{16} Taguchi Orthogonal array for screening design of experiments (L_{16}) with seven factors (A-G) at two levels (2^7)

	Taguchi L_{16} Columns														
	1	**2**	**3**	**4**	**5**	**6**	**7**	**8**	**9**	**10**	**11**	**12**	**13**	**14**	**15**
Run No.	**L/G (A)**	**Interaction**			**u_G [cm/s] (B)**	**EBRT [mins] (C)**	**Interaction**	**pH (D)**	**Interaction**	**Alk [gIC/L] (E)**	**T_{col} [°C] (F)**	**C_{alg} [g/DW/L] (G)**	**Interaction**		
		pH vs Alk	u_G vs EBRT	L/G vs u_G			T_{col} vs C_{alg}		L/G vs pH				u_G vs pH	u_G vs T_{col}	u_G vs Alk
1	0.2				0.06	6		9		1	20	0.05			
2	0.2				0.06	6		10.5		2.5	35	0.75			
3	0.2				0.2	15		9		1	20	0.75			
4	0.2				0.2	15		10.5		2.5	35	0.05			
5	0.2				0.06	15		9		2.5	35	0.05			
6	0.2				0.06	15		10.5		1	20	0.75			
7	0.2				0.2	6		9		2.5	35	0.75			
8	0.2				0.2	6		10.5		1	20	0.05			
9	1				0.2	6		9		1	35	0.05			
10	1				0.2	6		10.5		2.5	20	0.75			
11	1				0.06	15		9		1	35	0.75			
12	1				0.06	15		10.5		2.5	20	0.05			
13	1				0.2	15		9		2.5	20	0.05			
14	1				0.2	15		10.5		1	35	0.75			
15	1				0.06	6		9		2.5	20	0.75			
16	1				0.06	6		10.5		1	35	0.05			

Experiments were conducted using each row in the selected L_{16} OA (Table 4-3) as individual experimental runs. Columns 1, 5, 6, 8, 10, 11 and 12 represents the different settings of the design factors for the 16 experimental runs; the remaining columns accommodated the interactions. Each run was triplicated and randomised to minimise repeatable errors, also referred to as systematic bias [51] and to enable accurate estimation of the variations in the bubble column performance due to uncontrollable factors or noise.

4.2.3.5 Signal to noise (S/N) ratio

Each process response can be categorised as *i)* the signal or the intended response from the influence of the design factors and *ii)* unintended outcomes resulting from noise [52]. In the Taguchi method, to estimate the sensitivity of the main effects and interactions against the noise, the signal to noise (S/N) ratio is used as a qualitative metric [41]. A higher value of the S/N ratio is always desired, as, the higher the value of the S/N ratio, the more stable the process response is against the noise [41,53]. In addition, a process response might be required to be minimised or maximised. When a process response needs to be maximised ($R_{eff,\,CO_2}$, R_{abs,CO_2}, $k_{G_{CO_2}}a$), the S/N ratio is classified as the larger-the-better (LB) criterion, given by Eq. 4.6. Alternatively, when the process response is intended to be minimised ($O_{2,BM}$, $O_{2,\%,BM}$), the smaller-the-better (SB) S/N ratio is used, represented by Eq. 4.7 [54].

$$\left(S/N\right)_{LB} = -10\log_{10}\left[\frac{1}{n}\sum_{i}^{n}\frac{1}{y_{ij}^{2}}\right] \tag{4.6}$$

$$\left(S/N\right)_{SB} = -10\log_{10}\left[\frac{1}{n}\sum_{i}^{n}y_{ij}^{2}\right] \tag{4.7}$$

where y_{ij} refers to the i^{th} output signal (i = 1,2,3) of the process response j (e.g. $R_{eff,\,CO_2}$) among n replicates (n = 3).

4.2.3.6 Determining the adequacy of the experimental design

Prior to analyses of results, a statistical test was performed to check the adequacy of the chosen experimental design. A general linear model via analysis of variance (ANOVA) (summarised in Section 4.2.3.8) was fitted considering each replicate as a separate experiment [55]**.** If the experimental design is adequate, the fitted model should be able to describe the majority of the variabilities in the process responses using the fifteen factors (seven main effects and eight interactions) chosen in the experimental design.

4.2.3.7 Interpretation of the experimental results

Based on the results of the Taguchi OA, the influence of the design factors on the performance of CO_2 removal and O_2 stripping in the bubble column were compared using the following steps:

Step 1: A main effects plot showing the mean process response at each level (low (1) or high (2)) of the design factors was first plotted to graphically identify the influence of the design factors on the mean process responses. This also allowed the identification of the design factor settings to obtain the desired process responses. The slope of the plot additionally indicates the influence of each design factor on the response [56]; a positive slope shows an increase in response on increasing the design factor value and vice-versa.

Step 2: A similar main effects plot with the S/N ratio of the process response was then plotted. The design factor that caused the highest variation in the S/N ratio of the process response between its low and high setting was concluded to have the largest influence on the studied process response [56]. All other design factors were then ranked subsequently.

Step 3: A general linear model via the analysis of variance (ANOVA) was then fitted to the S/N ratios to obtain the percentage contributions of the design factors and the interactions towards the process response (described in Section 4.2.3.8).

Step 4: A half-normal probability plot was plotted to graphically compare the relative contribution of both the main effects of the design factors and the studied interactions on the process response [57].

Step 5: A confirmatory pooled ANOVA was performed using only the design factors and interactions having over 95% contribution towards the process response to determine the factors (main effects and interactions) that are statistically significant ($P < 0.05$). All other factors were pooled under the error term. The higher value of 95% was selected to minimise the possibility of falsely rejecting important design factors, also known as type II error in statistical terms [36,58]. Especially for screening experiments, such a false rejection affecting the omission of a major design factor from future detailed designs could severely limit the development of a product or process [58].

4.2.3.8 Analysis of variance (ANOVA)

Analysis of variance or ANOVA provides a statistical approach to quantify the variations in the process responses resulting from the main effects and interactions

[52]. Additionally, it also provides an estimation of the unexplained variations or errors resulting from noise, experimental limitations and assumptions [52]. The results of the multivariate ANOVA are typically represented as a table having the following entries (not in order): *i)* sources, signifying the design factors, interactions, errors and the cumulative total of variations *ii)* degree of freedom (DoF); *iii)* adjusted sum of squares (Adj SS); *iv)* adjusted mean squares (Adj MS); *v)* the Fischer's F distribution (F-value) *v)* P-value; and *vii)* contribution ($\%_{contrib}$) of each main effect, interaction and error term towards the process response calculated by Eq. 4.8.

$$\%_{contrib} = \frac{\text{AdJ MS}_{source}}{\text{AdJ MS}_{total}} \times 100 \qquad (4.8)$$

In the ANOVA table, the degrees of freedom of a source or a model signifies the number of independent inputs required to describe itself [36]. The F-value signifies the extent to which the variance due to a certain source compares with variance arising from the errors, i.e., how large or small the variations due to a certain source is with respect to the unexplained variations [59]. Irrespective of its value, to evaluate if the F value as obtained is true, the corresponding P-value is calculated as the probability of the F value being obtained by random chance [36,59]. Thus, a higher P-value indicates a greater probability of obtaining the F-value as a random chance and hence a lower statistical significance of the calculated F-value. Contrarily, a lower P-value indicates a lesser probability of obtaining the F-value as a chance and hence indicates a greater statistical significance of the calculated F-value. Additionally, for each general linear model, a model-F value is also generated by ANOVA that signifies the predictability of the model in comparison to a model that contains no independent variables. The model F-value must be higher than the value of the F statistic below which there exists a probability of α to mistakenly reject a true null hypothesis (i.e., the two variances are equal) [60], also known as the critical F-value (F_{crit}). F_{crit}, given in the form of $F_{\alpha(k-1,n_{ex}-k)}$ can be obtained from standard statistical handbooks, where k is the number of predictors in the model and n_{ex} is the total number of experimental trials. The respective model P-value signifies the probability that the model F-value was derived from the influence of noise, and hence, a lower P-value is always desired [52,59]. The details of each of these statistics can be further explored in multiple literature and textbooks [36,41].

4.2.3.9 Performance prediction and confirmatory experiment

Using the statistically significant ($P < 0.05$) main effects and interactions, the biomethane composition exiting the bubble column under different conditions was predicted by a general linear equation in the form expressed in Eq. 4.9.

$$\hat{Z} = A_0 + A_i X_i + A_{ij} X_i X_j \quad (4.9)$$

where A_0 represents the constant of the model, A_i is the coefficient of each design factor X_i and A_{ij} is the coefficient of each interaction between the design factors X_i and X_j. These coefficients are derived from the ANOVA analysis and also signify the relative quantitative influence of the main effect and interaction on the process response variable [40]. CO_2 removal efficiency ($R_{eff,\,CO_2}$) [%] and O_2 outflow rate ($O_{2,BM}$) [mL_n/min] were used as estimates for CO_2 and O_2 flow rates respectively from which their respective compositions in biomethane can then be derived. The goodness of fit of the model was assessed with regards to the regression coefficient R^2 (a measure of the agreement between predicted and actual values) and standard error of regression (S), signifying the average deviation of the observed data from the predicted model.

As the predictive regression equations were derived from ANOVA that utilises the S/N ratio statistic, Eq. 4.10 and Eq. 4.11 were used to convert the predictors back into actual responses for physical interpretation.

$$\hat{R}_{eff,\,CO_2} \cong \left[10^{(-(S/N)_{R_{eff,\,CO_2}}/10)}\right]^{-0.5} \quad (4.10)$$

$$\hat{O}_{2,BM} \cong \left[10^{(-(S/N)_{O_{2,BM}}/10)}\right]^{0.5} \quad (4.11)$$

where $\hat{R}_{eff,\,CO_2}$ and $\hat{O}_{2,BM}$ predicts for $R_{eff,\,CO_2}$ and $O_{2,BM}$ respectively. For each prediction, the 95% confidence interval ($CI_{95\%}$) was calculated by Eq. 4.12 [41].

$$CI_{95\%} = \hat{Z} \pm \sqrt{\frac{F_{0.05}(f_1,f_2) \times V_{error}}{n_{eq}}} \quad (4.12)$$

where $\hat{Z}$ ($\hat{R}_{eff,\,CO_2}$ and $\hat{O}_{2,BM}$) represents the predicted value and V_{error} represents the variance in the error term. $F_{0.05}(f_1,f_2)$ is the F-value for DoF f_1 and f_2 at a significance

level of 0.05 (confidence interval of 95%); where $f_1 = 1$, being the DoF of factors in the regression model and f_2 is the DoF of the error term. This value of F is obtained from the F-tables from any standard statistical handbook. n_{eq}= Number of trials$/(f_1+f_{factors})$ is known as the number of equivalent replications in which, $f_{factors}$ is the DoF of factors in the regression model, also equal to 1.

On the other hand, the 95% prediction interval ($PI_{95\%}$) for each prediction was calculated via Eq. 4.13 [61] to estimate the range within which 95% of the predicted values would lie with a confidence of 95%.

$$PI_{95\%} = \hat{Z} \pm t_{\alpha/2,(n-2)} \times \sqrt{\frac{SSE}{n-2}\left(1 + \frac{1}{n} + \frac{n\left(x^* - \bar{x}\right)^2}{n\sum_{i=1}^{n} x_i - \left(\sum_{i=1}^{n} x_i\right)^2}\right)} \qquad (4.13)$$

In the above equation, $t_{\alpha/2,(n-2)} = t_{0.05/2,(16-2)}$ is the $100(\alpha/2)^{th}$ percentile of the student's t-distribution with 14 degrees of freedom with the significance level (α) as 0.05 and n=16 from the 16 experimental runs. SSE denotes the sum of squared errors given as $\sum_{i=1}^{n}(x_i - \bar{x})^2$ where x_i is the value of the i^{th} observation and $\bar{x}$ indicates the value of the mean of all observations. x^* represents the value of the independent predictor for predicting the corresponding $\hat{Z}$.

A confirmatory experiment was performed at a chosen level of control (different from the sixteen Taguchi trial settings) based on the experimental trials and conclusions from the screening design of experiments. The mean from the triplicated experiment (Z_{actual}) was compared with the predicted output ($\hat{Z}$) with the following consideration (Eq. 4.14):

$$\hat{Z} - CI_{95\%} \leq Z_{actual} \leq \hat{Z} + CI_{95\%} \qquad (4.14)$$

Finally, using the predictive regression equations, the variation in biomethane composition was studied between the interval of pH 9 (factor level "1") and pH 10.5 (factor level "2") and L/G ratio 0.2 (factor level "1") and 1 (factor level "2"). For this, the superficial gas velocity was varied at two levels, namely 0.06 cm/s (factor level "1") and 0.2 cm/s (factor level "2"). All other design factors were fixed to maximise the S/N ratio.

4.2.4 Analytical procedures

4.2.4.1 Data acquisition

The steady-state criteria to acquire measurements and assess the system performance were defined as follows: *i)* a constant gas flow rate (less than 5% variation on average); and *ii)* less than 5% variation in the pH of the liquid at the outlet of the gas-liquid separator over a period of 120 seconds each. Gas was sampled for compositional assessment via chromatography from a tap placed between the ice bath and the mass flow meter as indicated in Figure 4-2. A 10 mL plastic syringe was used for this purpose. The dissolved oxygen (DO) content of the outlet liquid was measured near the bubble column outlet to prevent distortion of results from the ingression of oxygen.

4.2.4.2 Analytical procedures

The algal density was measured as optical density at a wavelength of 530 nm in a VWR® V-3000 PC manual spectrophotometer calibrated to the microalgae dry weight. All pH and DO measurements were performed using a handheld pH meter (VWR® MD 8000H Multi Parameter Meter) fitted with respective interchangeable probes (pHenomenal VWR® pH / ORP sensor/ pHenomenal VWR® OPOX 11-3 sensor). Alkalinity was measured using Titronic® Universal Titrator as per Method No. 2320 B of APHA [62] by titrating up to pH 4.5. Algal solution for photosynthetic biogas upgrading was prepared by diluting 2-3 gDW/L microalgae culture with distilled water to the algal concentration. In an actual photosynthetic biogas upgrading cycle, algae will be circulated after cultivation to ensure CO_2 uptake. As such, nutrient adjustment was not performed in order to resemble the nutrient replete medium after cultivation. The DO content in the inlet liquid varied between 6 to 10 mg/LO_2 as per those obtained during *Spirulina platensis* cultivation and are representative of those typically obtained in photobioreactors [63].

The volumetric gas flow rate was measured in terms of equivalent N_2 flow using a thermal mass flow meter (Bronkhorst® F101D Low-ΔP-Flow Thermal Mass Meter). CO_2, N_2 and O_2 content in the gas were analysed by a gas chromatograph (GC; Agilent® 7890B, USA) equipped with a thermal conductivity detector and a 5A column. The online gas Converter tool by Fluidat® (Bronkhorst®) was used to convert

the gas flow recorded to the actual volumetric as flow in terms of its constituents based on the composition obtained from the gas chromatograph. The actual gas flow rate and composition were obtained after a further correction step to the individual oxygen and nitrogen flow rates. This was done because noticeable air (N_2 and O_2) ingress by diffusion into the gas tubing used in the experiment was recorded during pre-experiments [48]. To obtain the correction terms needed to remove this interference from the recorded flowrates, N_2 was blown into the system at the same rate as that used in the subsequent experiments and the gas composition and flow rates were measured. The additional O_2 and N_2 flow rates that were obtained as correction factors were subtracted from the respective biomethane component flow rates to calculate the final biomethane composition and flow rate.

4.2.4.3 Statistical Analysis

All statistical analyses including the design and assessment of the Taguchi L_{16} orthogonal array were performed using Minitab® software version 19 (Minitab LLC., Pennsylvania, USA). Multiple literature have been published debating the selection of the confidence interval levels. Selecting a confidence interval of 99% ($P < 0.01$) or higher has often been suggested to minimise false detection of statistically non-significant effects [64]. However, for the screening design of experiments, typically used at the start of a product or process development care must also be taken to prevent false rejection of a statistically significant effect due to the selection of a very high confidence interval. Following the conventional and the most widely practised approach in the literature [64,65], a confidence level of 95% ($P < 0.05$) was selected for asserting statistical significance. However, as recommended in recent literature, all P-values are reported to enable unbiased interpretation of statistical analyses and allow future revisiting of data for detailed experimentation and process optimisation [64,66–68].

To compare the pairwise significant differences between the means of all possible groups, the Tukey honestly significant difference (HSD) post-hoc test was conducted. The Tukey test was selected as it performs best on balanced data such as the data from the Taguchi OA and when all possible pairwise comparisons are being performed [69,70]. In this test, a q statistic is first generated as a single statistical value employing a studentised t-test and using 95% confidence interval ($P < 0.05$). Any

pairwise difference that was lower than the q-statistic was considered to have no statistically significant difference between their means; contrarily, if the pairwise difference between the means of two groups were greater than the q-statistic, then the two groups were concluded to be statistically significantly different [70]. Further details of the Tukey HSD methodology can be read in the literature [69–71].

4.3 Results and discussions

4.3.1 Validation of the bubble column operation

The biomethane composition generated during each trial, together with the pH of the liquid at the bubble column outlet and the process responses (e.g. $R_{eff,\,CO_2}$ and R_{abs,CO_2}) are compiled in Table 4-4. Out of all the trials, grid quality biomethane was obtained only in Run 4 (L/G ratio of 0.2, pH 10.5 and values for other 5 variables); the respective CO_2 and O_2 in the outlet biomethane was 0% ± 0.00% and 0.23% ± 0.1%.

A mass balance approach was used to validate the outcomes of O_2 and N_2 in the upgraded biomethane. Investigative assessments were performed on four experimental runs (Runs 5, 8, 9 and 12 of the Taguchi OA) that use low algal concentration. This was to ensure that the O_2 in the biomethane is derived primarily from stripping of the DO of the circulating algal liquid with minimal influence of the O_2 released by the active photosynthesising microalgae. Considering no O_2 in the inlet biogas, a good agreement was found between the theoretical and the experimental values for oxygen in the outlet biomethane (Figure 4-4a). On the other hand, as can be seen in Figure 4-4b, the N_2 flow in the biogas generally matched closely with that in the biomethane confirming the assumption of minimal N_2 stripping.

CO_2 removal performance was validated by comparing the values of the evaluation metrics with data from the literature. As can be seen from Table 4-4, the CO_2 removal efficiencies varied between 19.29% and 100%; the corresponding absorption rates (R_{abs,CO_2}) ranged from 0.036×10^{-4} mol/L/s to 0.459×10^{-4} mol/L/s. The volumetric mass transfer coefficient ($k_{G_{CO_2}}a$) varied from 0.87 hr^{-1} (0.0002 s^{-1}) to 97.64 hr^{-1} (0.027 s^{-1}). The results are in close agreement with those reported by Chen et al., (2015) [42] who studied the behaviour of CO_2 removal with NaOH. Operating between pH of 10 and 11, temperatures of 25 °C and 35 °C and L/G ratios of 0.05 and

0.16, $k_{G_{CO_2}}a$ extended from 54 hr^{-1} to 154.8 hr^{-1}, while the lowest and the highest absorption rates were 1.03×10^{-4} mol/L/s and 2.13×10^{-4} mol/L/s respectively; the higher values recorded at higher pH and temperature. It must be mentioned here that as the CO_2 absorption reaction is primarily driven by carbonate derived $[OH]^-$ ions [15,72], the comparison with NaOH is reasonable. These comparisons were concluded as sufficient to validate the bubble column operations and measurement techniques for acceptable prediction of the experimental outcomes.

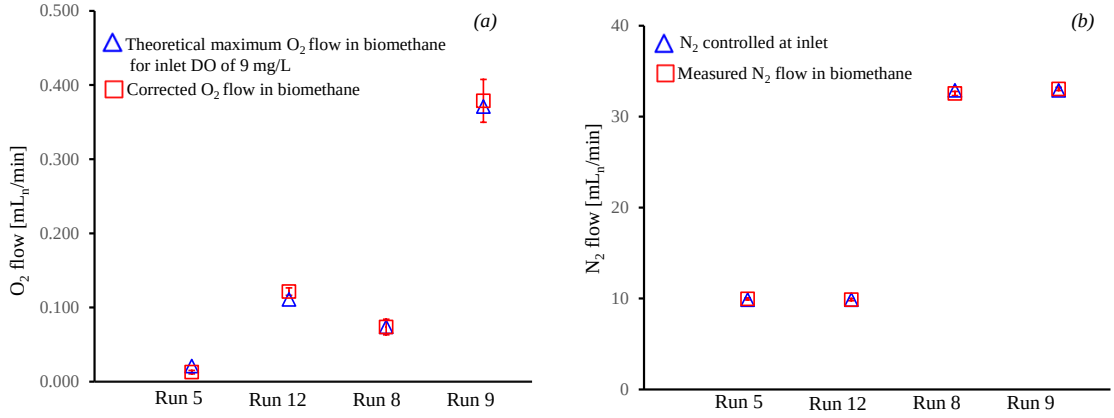


Figure 4-4 Comparison between expected and measured values of (a) O_2 and (b) N_2 to validate the bubble column operations and measurement techniques utilised.

Table 4-4 Results from the 16 experimental runs in triplicates performed on the L_{16} Taguchi Orthogonal Array along with the S/N ratios of the responses selected for factors screening studies

Run No.	Biomethane Composition		Liquid outlet pH	R_{eff,CO_2} [%]	R_{abs,CO_2} [mol/L/s]	$k_{G_{CO_2}}a$ [hr^{-1}]	$O_{2,BM}$ [mL_n/min]	S/N Ratio				
	CO_2 [%]	O_2 [%]						R_{eff,CO_2} ζ	R_{abs,CO_2} ζ	$k_{G_{CO_2}}a$ ζ	$O_{2,96,BM}$ §	$O_{2,BM}$ §
1	27.76 ± 0.07	0.16 ± 0.06	7.74 ± 0.04	40.44 ± 0.46	0.189 ± 0.002	5.23 ± 0.08	0.023 ± 0.008	-7.87	14.37	-14.48	55.32	32.33
2	6.47 ± 1.09	0.28 ± 0.13	9.68 ± 0.02	89.48 ± 1.87	0.418 ± 0.009	22.91 ± 1.83	0.030 ± 0.014	-0.97	27.12	-7.59	50.07	29.55
3	34.23 ± 1.71	0.51 ± 0.12	8.26 ± 0.01	19.29 ± 3.61	0.036 ± 0.007	0.87 ± 0.18	0.263 ± 0.062	-14.79	-1.83	-29.38	45.66	11.36
4	**0.00 ± 0.00***	**0.23 ± 0.01***	**9.49 ± 0.07**	**100.00 ± 0.00**	**0.187 ± 0.000**	**40.38 ± 0.00**	**0.078 ± 0.004**	**0.00**	**32.12**	**-14.58**	**52.56**	**22.16**
5	23.99 ± 0.47	0.09 ± 0.02	8.19 ± 0.07	52.11 ± 0.85	0.097 ± 0.002	9.92 ± 0.24	0.013 ± 0.002	-5.66	19.92	-20.24	60.01	37.63
6	7.69 ± 0.42	1.28 ± 0.24	9.18 ± 0.06	87.35 ± 0.74	0.163 ± 0.001	27.87 ± 0.78	0.139 ± 0.027	-1.18	28.89	-15.75	37.71	17.011
7	32.06 ± 0.09	0.39 ± 0.02	7.82 ± 0.07	29.57 ± 0.68	0.138 ± 0.003	1.06 ± 0.03	0.187 ± 0.013	-10.59	0.51	-17.21	48.21	14.55
8	13.21 ± 0.89	0.19 ± 0.03	7.94 ± 0.04	77.01 ± 1.66	0.359 ± 0.008	4.46 ± 0.22	0.074 ± 0.011	-2.28	12.96	-8.89	54.18	22.56
9	18.34 ± 0.93	0.94 ± 0.06	7.97 ± 0.04	66.25 ± 1.69	0.309 ± 0.008	3.29 ± 0.15	0.379 ± 0.029	-3.58	10.33	-10.20	40.54	8.41
10	1.06 ± 0.52	1.39 ± 0.04	10.15 ± 0.02	98.35 ± 0.84	0.459 ± 0.004	12.79 ± 1.42	0.471 ± 0.019	-0.14	21.96	-6.76	37.12	6.53
11	14.23 ± 0.55	0.82 ± 0.10	8.15 ± 0.02	75.07 ± 0.5	0.140 ± 0.001	18.71 ± 0.27	0.094 ± 0.011	-2.49	25.44	-17.07	41.70	20.48

Run No.	Biomethane Composition		Liquid outlet pH	R_{eff,CO_2} [%]	R_{abs,CO_2} [mol/L/s]	$k_{G_{CO_2}}a$ [hr^{-1}]	$O_{2,BM}$ [mL_n/min]	S/N Ratio				
	CO_2 [%]	O_2 [%]						R_{eff,CO_2} ζ	R_{abs,CO_2} ζ	$k_{G_{CO_2}}a$ ζ	$O_{2,\%BM}$ §	$O_{2,BM}$ §
12	0.33 ± 0.47	1.21 ± 0.04	10.09 ± 0.06	99.48 ± 0.73	0.186 ± 0.001	97.64 ± 29.35	0.121 ± 0.005	-0.04	38.14	-14.62	38.34	18.30
13	2.52 ± 0.18	0.88 ± 0.18	8.39 ± 0.04	96.06 ± 0.27	0.179 ± 0.001	13.07 ± 0.29	0.300 ± 0.066	-0.35	22.32	-14.93	40.96	10.29
14	0.00 ± 0.00	1.35 ± 0.2	9.84 ± 0.04	100.00 ± 0.00	0.187 ± 0.000	40.38 ± 0.00	0.450 ± 0.065	0.00	32.12	-14.58	37.28	6.85
15	10.13 ± 0.67	0.73 ± 0.25	8.54 ± 0.07	82.60 ± 1.42	0.386 ± 0.007	17.69 ± 0.85	0.082 ± 0.026	-1.66	24.93	-8.28	42.24	21.28
16	3.13 ± 1.04	0.89 ± 0.14	10.06 ± 0.05	95.10 ± 1.46	0.444 ± 0.007	31.01 ± 3.51	0.094 ± 0.019	-0.44	29.68	-7.06	40.94	20.39

**Denotes grid quality biomethane was achieved; ζDenotes process responses using larger-the-better criteria; § Denotes process responses using smaller--the-better criteria*

4.3.2 Adequacy of the experimental design

The result of the design adequacy test as explained in Section 4.2.3.6 is summarised in Table 4-5. For each process response, the chosen 15 factors (seven main effects and eight interactions) were able to account for at least over 90% of the variations in each process response. CO_2 removal efficiency and absorption rates were almost sufficiently described with an unknown variation of less than 0.5% in the outcome. However, to describe the hydrodynamic aspect of CO_2 absorption, a few other variables might be required to explain the remaining 9.22% of the system fluctuations. The chosen screening design was able to explain over 92% of the variations for O_2 stripping during biogas upgrading.

From a statistical perspective, the F values of the fit models were also much higher than the critical F-value ($F_{0.05(15,32)}$) (k = 16 including the constant and N = 48 from 16 triplicated experiments) of 1.99 at a 95% confidence level with a corresponding P-value less than 0.001. This indicates the statistical significance of the selected main effects and interactions to describe the bubble column performance in photosynthetic biogas upgrading [73].

Table 4-5 Results of ANOVA for each process response considering each replicate as a separate experimental trial as an adequacy test of the designed screening experiment.

Regression parameters	$\mathbf{R_{eff,\,CO_2}}$ **[%]**	$\mathbf{R_{abs,CO_2}}$ **[$\times 10^{-4}$ mol/L/s]**	$\mathbf{k_G a(CO_2)}$ **[hr^{-1}]**	$\mathbf{O_{2,\%,BM}}$ **[%]**	$\mathbf{O_{2,BM}}$ **[mL_n/min]**
Total DoF	47	47	47	47	47
Model DOF	15	15	15	15	15
Error DoF	32	32	32	32	32
Explained variations (Model Contribution) [%]	99.72	99.86	90.78	92.09	95.76
Unexplained variations [%]	0.28	0.14	9.22	7.91	4.24
Model F Value	762.26 (P < 0.001)	1520.37 (P < 0.001)	21.01 (P < 0.001)	25.02 (P < 0.001)	48.22 (P < 0.001)

4.3.3 Results of the screening design of experiments

The following section summarises the results from the Taguchi OA for each process response describing CO_2 removal and O_2 stripping in the bubble column.

4.3.3.1 CO_2 removal efficiency (R_{eff, CO_2})

Figure 4-5a shows the main effects plot with mean CO_2 removal efficiency (R_{eff, CO_2}). The highest variation in the mean response was obtained from the variation of pH, closely followed by that due to the L/G ratio. For both these factors, a higher setting increases the mean response, i.e., improves the CO_2 removal efficiency. Higher alkalinity and empty bed residence time were also found to increase the CO_2 removal efficiency signifying a lower average CO_2 content in the upgraded biomethane. Between 20 °C (factor level "1") and 35 °C (factor level "2"), temperature caused a negligible increase in R_{eff, CO_2}, closely resembling the results presented by Chen et al., (2015) [42]. On the other hand, an increase in superficial gas velocity and algal concentration decreased the CO_2 removal efficiency.

A study of the main effects plot of the S/N ratio in Figure 4-5b also reveals a similar trend for the design factors. Operations at a higher pH, L/G ratio, alkalinity and temperature setting would result in more robust operations (higher S/N ratios). The effect of EBRT on the system fluctuations was minimal (minimal variation in the S/N ratio). An increased superficial gas velocity and algal concentration would cause larger system variabilities (lower S/N ratios and negative slope of the main effects plot). Comparing variation of the S/N ratio corresponding to each main effect (Figure 4-5b), pH was found to be the most influential factor towards the efficiency of CO_2 removal from biogas followed by L/G ratio and alkalinity. These are followed by microalgae concentration and superficial gas velocity, however, as explained before, in a negative way. Temperature and EBRT were obtained as the two of the least affecting factors in the selected experimental regime to affect the removal efficiency of CO_2.

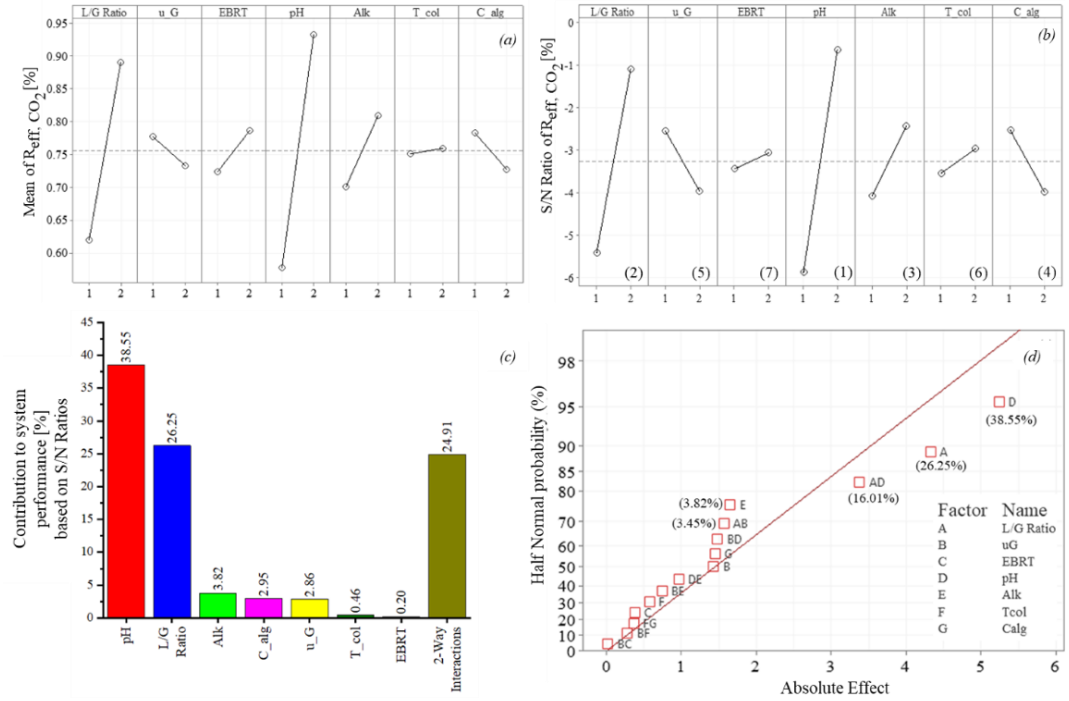


Figure 4-5 Analysis plots for the relative influence of design factors on CO_2 removal efficiency: (a) Main effects plot with mean; (b) Main effects plots with S/N ratio. The rank of each design factor is included in parenthesis; (c) Contribution of each design factor and interactions on the overall system outcome; and (d) Half normal probability plot with the relative contribution of major effects highlighted in brackets.

The quantification of the rankings and influences provided in Figure 4-5c shows the contribution of the different main effects and the two-way interactions (pooled together) towards the process response (CO_2 removal efficiency). Matching the observations from the main effects plots, pH was found to account for 38.55% of the variations in the CO_2 removal efficiencies followed by L/G ratio (26.25%) and alkalinity (3.82%). Interactions were found to play a major role, whereby they were responsible for almost 25% of the system variations. To obtain a further detailing of the results, a half normal probability (Figure 4-5d) was used to demonstrate the influence of the fifteen factors (seven main effects and eight interactions). In it, the factors having the highest influence on the process response and also being statistically significant ($P < 0.05$) usually lies further away from linearity, indicated by the straight line with a 45° slope [55,57]. As expected, the pH and L/G ratio can be seen to be located furthest away from the 45° linearity. Moreover, it can be interpreted, that of all the interactions, the interaction between pH and L/G ratio had the highest influence (above 16%) on the efficiency of CO_2 removal. Alkalinity and the interactions of superficial gas velocity with pH and L/G ratio could also be seen to deviate somewhat from linearity, indicating their possible influence on the process response. All other

factors being nearer to the 45° line could be concluded to have a minimal influence on the efficiency of CO_2 removal from biogas.

To confirm the above hypothesis, a pooled ANOVA was performed; the results are indicated in Table 4-6. As can be seen, all the main effects of pH, L/G ratio, alkalinity, superficial gas velocity and algal concentration were found to be statistically significant ($P < 0.05$). The statistically significant interactions to affect CO_2 removal efficiency were those between pH and L/G ratio and between superficial gas velocity and pH and L/G ratio.

*Table 4-6 Results of ANOVA assessment for CO_2 removal efficiency with main effects and interaction contributing over 95% towards the output response.*Denotes the statistically significant ($P < 0.05$) source (factors).*

Source	DoF	Adj SS	Adj MS	F-Value	P-Value	Contribution
pH*	1	110.024	110.024	88.92	<0.001	38.55%
L/G*	1	74.911	74.911	60.54	<0.001	26.25%
L/G vs pH*	1	45.692	45.692	36.93	0.001	16.01%
Alk*	1	10.893	10.893	8.8	0.021	3.82%
L/G vs u_G*	1	9.842	9.842	7.95	0.026	3.45%
u_G vs pH*	1	8.773	8.773	7.09	0.032	3.07%
C_{alg}*	1	8.425	8.425	6.81	0.035	2.95%
u_G*	1	8.159	8.159	6.59	0.037	2.86%
Pooled Error	7	8.661	1.237			3.03%
Cumulative Total	15	285.38				

Figure 4-6 shows the statistically significant ($P < 0.05$) interactions affecting CO_2 removal efficiency. For the interactive effect between L/G ratio and pH, depicted in Figure 4-6a, at lower pH levels (pH 9, factor level of "1"), the L/G ratio can be seen to have a greater influence on the performance of the CO_2 removal efficiency (higher variation in the S/N ratio). Accordingly, to reduce the operating pH, the L/G ratio must be increased to ensure effective CO_2 removal performance, i.e., ensure a higher S/N ratio. However, under high pH levels (pH 10.5, factor level of "2"), much more flexibility in operation with regards to the L/G ratio can be envisaged. Indeed, as can be seen from Figure 4-6a, even at a low L/G of 0.2 ratio (factor level "1"), a pH of 10.5 (factor level "2") would ensure a high CO_2 removal efficiency indicated by higher system robustness or S/N ratio. The subsequent increase in the system performance on increasing the L/G ratio to 1 (factor level "2") would hence be minimal.

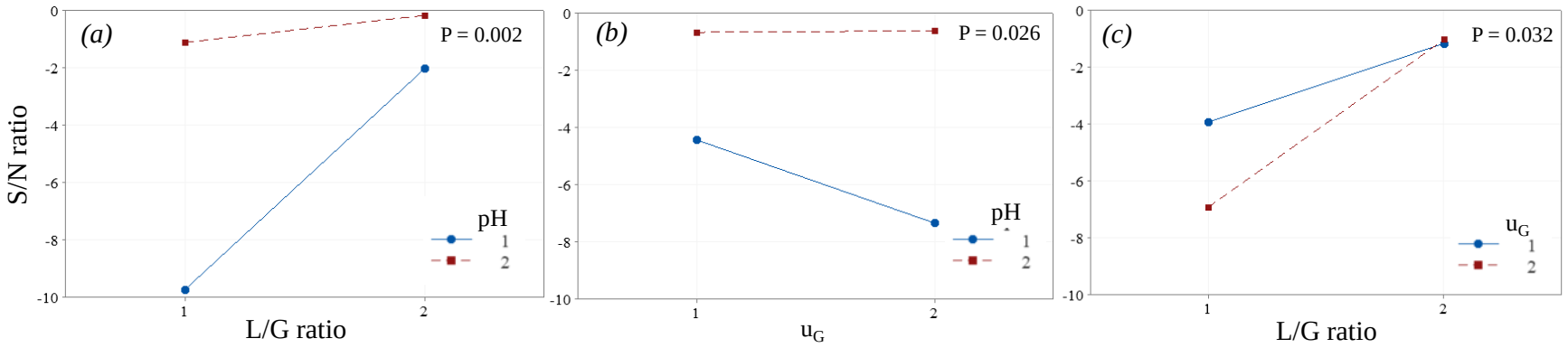


Figure 4-6 Interactive effects between (a) pH and L/G ratio; (b) superficial gas velocity (u_G) and pH; and (c) superficial gas velocity (u_G) and L/G ratio on CO_2 removal efficiency.

Respectively Figure 4-6b and Figure 4-6c reveal that both a high pH and a high L/G ratio would allow the superficial gas velocity and hence the gas flow rate to be increased without a substantial drop in CO_2 removal efficiency and hence the robustness of the bubble column operations. Of course, this is assuming the fact that all other effects not included in the interaction are set at the desirable set points that will maximise the S/N ratio (for example, alkalinity at 2.5 gIC/L and algal concentration at 0.05 gDW/L). In comparison, at lower pH and L/G ratios, the superficial gas velocity would cause larger fluctuations in the S/N ratio, lowering the CO_2 removal efficiency to the extent that grid quality biomethane might no longer be obtained.

4.3.3.2 Mean steady state CO_2 absorption rate (R_{abs,CO_2})

Similar to the discussion above, for the mean steady state CO_2 absorption rate (R_{abs,CO_2}), Figure 4-7a-d lead to the conclusion that EBRT is the most influential design factor. To understand this result, it must be understood that R_{abs,CO_2} signifies a lumped estimate of the kinetics of CO_2 absorption in the algal buffer solution. A large drop in the mean R_{abs,CO_2} at a higher EBRT, therefore, indicates a non-linear CO_2 absorption reaction along the length of the bubble column, with a rapid drop in the absorption rates along the length of the column. Correspondingly, the system also becomes more susceptible to uncontrollable variabilities, indicated by a drop in the S/N ratio (Figure 4-7b). Nonetheless, for a specific bubble column with a fixed height of the liquid column and hence a fixed EBRT, pH would have the largest positive influence followed by the L/G ratio on R_{abs,CO_2}. Similar to CO_2 removal efficiencies, a higher setting of these design factors would thus yield both better performance (Figure 4-7a, mean of response increases as the factor level increases) and more replicable responses (Figure 4-7b, S/N ratio increases as factor level increases). Figure 4-7c confirms the ranking of factors showing their percentage contributions towards the process response. Additionally, the half-normal probability plot in Figure 4-7d highlights the importance of the interaction between pH and L/G ratio on influencing the current process response. The confirmatory ANOVA test in Table 4-7 with factors affecting 95% of the variations in mean CO_2 absorption rate, revealed that EBRT, pH and L/G ratio and the interaction between pH and L/G ratio, were the only statistically

significant ($P < 0.05$) factors. Thus, to optimise R_{abs,CO_2} in a specific bubble column (fixed EBRT), pH and L/G ratio would be sufficient to describe the system kinetics.

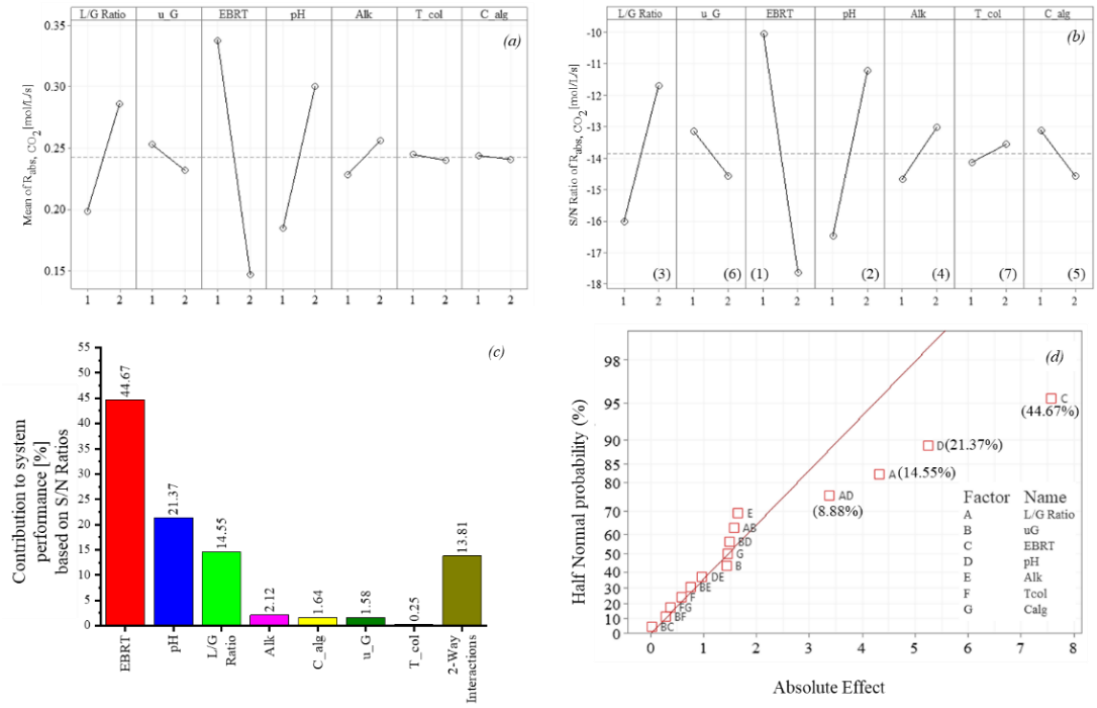


Figure 4-7 Analysis plots for the relative influence of design factors on mean steady state rate of CO_2 absorption: (a) Main effects plot with means; (b) Main effects plots with S/N ratio. The rank of each design factor is included in parenthesis; (c)Contribution of each design factor and interactions on the overall system outcome; and (d) Half normal probability plot with the relative contribution of major effects highlighted in brackets.

*Table 4-7 Results of ANOVA assessment for mean steady state absorption rate of CO_2 with main effects and interaction contributing over 95% towards the output response.*Denotes the statistically significant ($P < 0.05$) source (factors).*

Source	DF	Adj SS	Adj MS	F-Value	P-Value	Contribution
EBRT*	1	229.965	229.965	97.45	<0.001	44.67%
pH*	1	110.024	110.024	46.62	<0.001	21.37%
L/G*	1	74.911	74.911	31.74	0.001	14.55%
L/G vs pH*	1	45.692	45.692	19.36	0.003	8.88%
Alk	1	10.893	10.893	4.62	0.069	2.12%
L/G vs u_G	1	9.842	9.842	4.17	0.08	1.91%
u_G vs pH	1	8.773	8.773	3.72	0.095	1.70%
u_G	1	8.159	8.159	3.46	0.105	1.58%
Pooled Error	7	16.519	2.36			3.21%
Cumulative Total	15	514.778				100.00%

The only statistically significant ($P < 0.05$) interactive effect between pH and L/G ratio had a similar profile to that presented in Figure 4-6a for CO_2 removal

efficiency (and hence not shown). Therefore, for a lower operating pH, to increase R_{abs,CO_2}, L/G ratio must be high. However, a higher pH would ensure a high R_{abs,CO_2} irrespective of the influence of the L/G ratio varying between 0.2 (factor level "1") and 1 (factor level "2").

4.3.3.3 Mean overall CO_2 mass transfer coefficient ($k_{G_{CO_2}}a$)

Following similar arguments as discussed above, it can be concluded from Figure 4-8a-d that pH had the highest influence on the mean overall CO_2 mass transfer coefficient, a measure of the hydrodynamic performance of the CO_2 absorption in the alkaline algal medium. This is followed (in order) by superficial gas velocity, L/G ratio, EBRT and alkalinity which all showed substantial influences on both the mean response and the S/N ratio. However, unlike the rest, an increase in the superficial gas velocity was found to lower the hydrodynamic performance (a lower $k_{G_{CO_2}}a$, Figure 4-8a) and its corresponding resilience (a lower S/N ratio, Figure 4-8b). Figure 4-8c shows the relatively large contributions of pH (37.31%), superficial gas velocity (19.82%), L/G ratio (16.36%) and EBRT (9.55%) on the hydrodynamic parameter of $k_{G_{CO_2}}a$. However, although the contribution of alkalinity was substantial (over 4%, Figure 4-8c), the half-normal probability plot in Figure 4-8d indicated its weak influence on the mean overall CO_2 mass transfer coefficient (being located on the 45° line).

The pooled ANOVA presented in Table 4-8 nonetheless confirmed the statistical significance ($P < 0.05$) of the influence of alkalinity, alongside those of pH, superficial gas velocity, L/G ratio and EBRT on the bubble column hydrodynamics with respect to CO_2 absorption. None of the other main effects and interactions caused any statistically significant ($P < 0.05$) variation on the current process response.

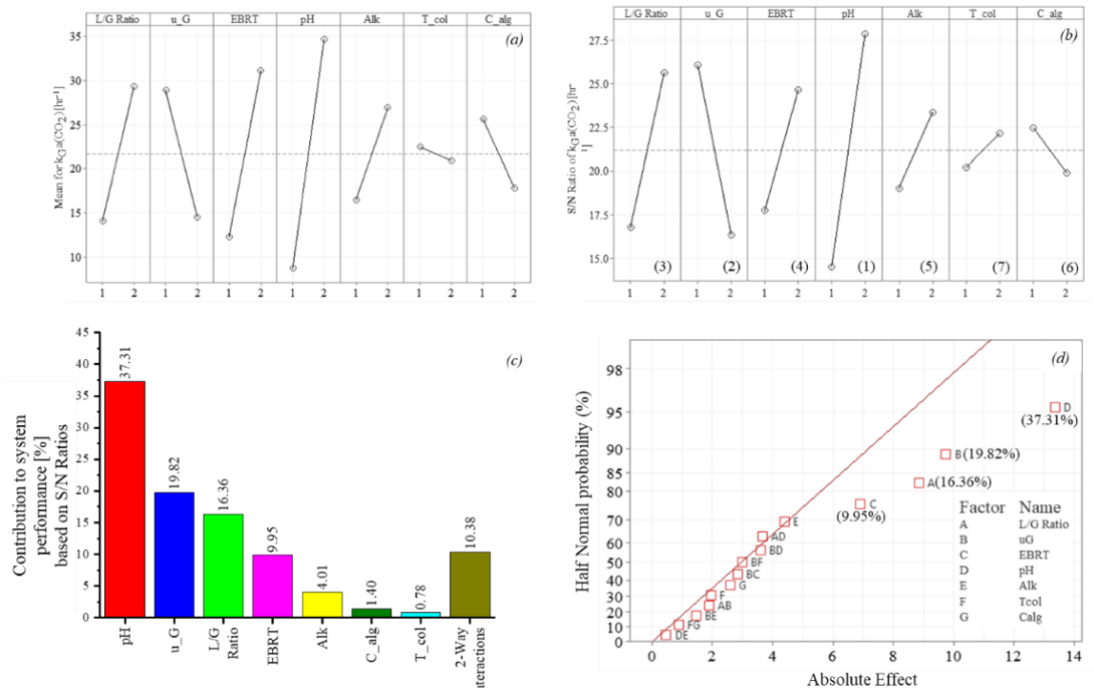


Figure 4-8 Analysis plots for the relative influence of design factors on the gas side volumetric mass transfer coefficient for CO_2: (a) Main effects plot with means; (b) Main effects plots with S/N ratio. The rank of each design factor is included in parenthesis; (c)Contribution of each design factor and interactions on the overall system outcome; and (d) Half normal probability plot with the relative contribution of major effects highlighted in brackets.

*Table 4-8 Results of ANOVA assessment for mean overall CO_2 mass transfer coefficient with main effects and interaction contributing over 95% towards the output response. *Denotes the statistically significant ($P < 0.05$) source (factors).*

Source	DoF	Adj SS	Adj MS	F-Value	P-Value	Contribution
pH*	1	715.65	715.65	67.08	<0.001	37.31%
u_G *	1	380.13	380.13	35.63	0.002	19.82%
L/G *	1	313.79	313.79	29.41	0.003	16.36%
EBRT*	1	190.91	190.91	17.89	0.008	9.95%
Alk*	1	76.89	76.89	7.21	0.044	4.01%
L/G vs pH	1	53.39	53.39	5	0.075	2.78%
u_G vs pH	1	51.36	51.36	4.81	0.08	2.68%
u_G vs T_{col}	1	35.59	35.59	3.34	0.127	1.86%
u_G vs EBRT	1	32.13	32.13	3.01	0.143	1.68%
T_{col}	1	15.01	15.01	1.41	0.289	0.78%
Pooled Error	5	53.34	10.67			2.78%
Cumulative Total	15	1918.19				100.00%

4.3.3.4 O_2 content in biomethane ($O_{2,\%,BM}$)

The L/G ratio had by far the largest influence among all other design factors on the O_2 content of the upgraded biomethane ($O_{2,\%,BM}$) (Figure 4-9a-d) whereby, a higher setting of L/G ratio led to the increase of $O_{2,\%,BM}$. Besides L/G ratio, pH, EBRT and algal concentration increased $O_{2,\%,BM}$ (a higher mean response, Figure 4-9a) when operated at the higher setting ("2"). On the contrary, both temperature and alkalinity were found to lower $O_{2,\%,BM}$ when increased. The increase of $O_{2,\%,BM}$ from an increased superficial gas velocity was minimal. To achieve grid quality biomethane the aim is to minimise oxygen stripping, however, an increase in the mean process response ($O_{2,\%,BM}$), would lower the robustness of operation. As a result, unlike the plots for CO_2, where the 'larger-the-better' response was desired, the main effects plot with S/N ratio for oxygen stripping had an opposite slope to that of the main effects plot with means. Accordingly, the factors such as the L/G ratio that raised the mean response on their increase, resulted in the drop of S/N ratio for the same and vice versa (Figure 4-9b). Following the L/G ratio, algal concentration was the second most influential design factor, followed by pH. Numerically, they accounted for 55.92%, 14.36% and 5.48% of the total variations in $O_{2,\%,BM}$ (Figure 4-9c). All interactions combined caused 16.76% of the variations in $O_{2,\%,BM}$ in biomethane.

On further investigation into the half-normal probability plot in Figure 4-9d, the interaction between superficial gas velocity and pH was obtained as the only major interaction (lying farthest from the 45° line). However, this is while the contribution of superficial gas velocity was not only low (0.75%, Figure 4-9c) but it can also be seen to be lying over the 45° line in Figure 4-9d, indicating its weak statistical significance. To confirm this phenomenon, the pooled ANOVA was performed including superficial gas velocity to maintain the hierarchy. As can be seen from Table 4-9, while the influence of pH on $O_{2,\%,BM}$ was statistically significant ($P = 0.014$), that of superficial gas velocity was not ($P = 0.252$). In contrast, their interaction showed a statistically significant effect ($P = 0.003$), contributing to over 11% in the variability of the current response (Figure 4-9d and Table 4-9). This can be explained from the alias structure of the designed L_{16} orthogonal array, whereby the interactions between L/G and algal concentration were found to be confounded with the interactions between superficial gas velocity and pH and between EBRT and the bubble column temperature. To solve this issue, the hierarchical model was adopted, whereby, the

aliased effect can be assigned to the interaction that had both the main effects as statistically significant ($P < 0.05$) [55]. Accordingly, the observed statistically significant ($P < 0.05$) interaction was concluded to be that between the two of the most impactful factors, L/G ratio and algal concentration ($P < 0.001$). The influence of temperature towards $O_{2,\%,BM}$ was also confirmed to be statistically significant ($P < 0.05$) via the pooled ANOVA (Table 4-9).

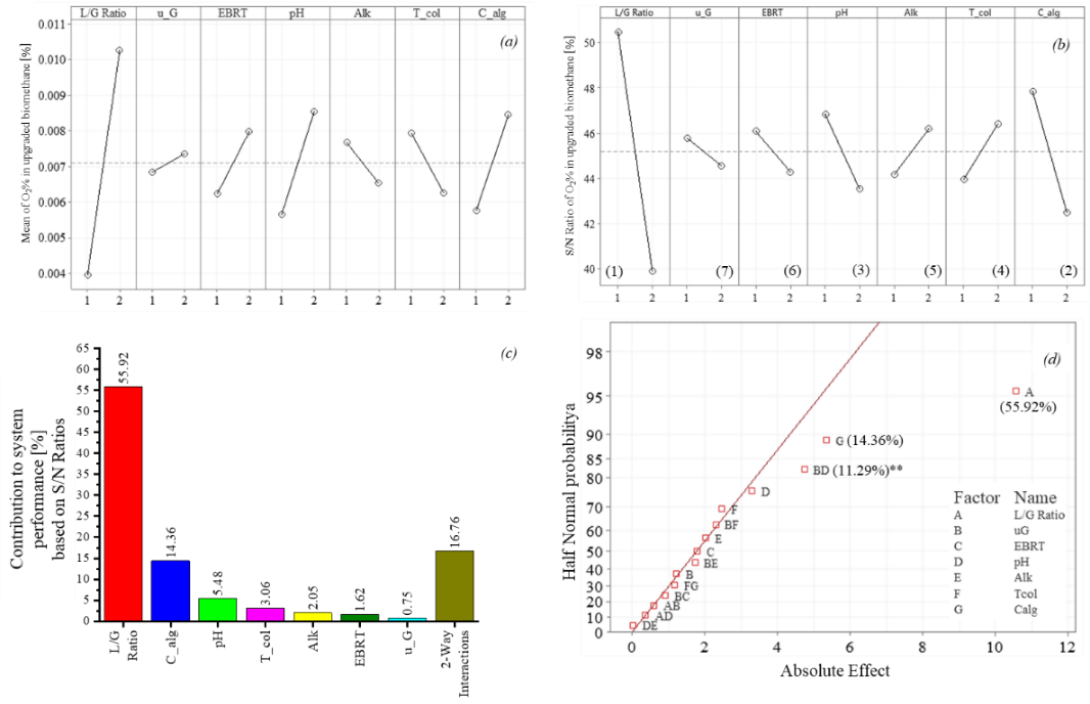


Figure 4-9 Analysis plots for relative influence of design factors on O_2 concentration in biomethane: (a) Main effects plot with mean; (b) Main effects plots with S/N ratio. The rank of each design factor is included in parenthesis; (c)Contribution of each design factor and interactions on the overall system outcome; and (d) Half normal probability plot with the relative contribution of major effects highlighted in brackets.

Figure 4-10a depicts the interactive effect between the L/G ratio and the algal concentration on the $O_{2,\%,BM}$. As can be followed from Figure 4-10a, at a lower algal concentration (factor level "1"), the L/G ratio is the primary influencer of oxygen stripping, with a higher L/G ratio signifying a higher $O_{2,\%,BM}$. At higher algal concentration (factor level "2"), however, the relative variation in oxygen stripping between the extreme L/G ratios are considerably reduced. Especially at lower L/G ratios (factor level "1"), the increased presence of algae plays a major role in oxygen stripping (Figure 4-10a) while at higher L/G ratios (factor level "2"), a comparable O_2 stripping, leading to similar $O_{2,\%,BM}$ can be noticed irrespective of the algal concentration. This indicates that although the hydrodynamics related to oxygen

stripping are greatly affected by the increased presence of algae at lower L/G ratios, the effect diminishes largely at higher L/G ratios. A plausible explanation could be the relatively large influence of superficial liquid velocities on the system hydrodynamics including bubble diameter and bubble rise velocity at higher liquid flow rates [66] (bubble column diameter being constant). Thus, at higher L/G ratios (factor level "2"), the ensuing biomethane would contain a high concentration of oxygen irrespective of the algal concentration in the circulating liquid.

*Table 4-9 Results of ANOVA assessment for O_2 content in the upgraded biomethane with main effects and interaction contributing over 95% towards the output response. *Denotes the statistically significant ($P < 0.05$) source (factors).*

Source	DoF	Adj SS	Adj MS	F-Value	p-Value	Contribution
L/G Ratio*	1	447.04	447.04	118.82	<0.001	55.92%
C_{alg}*	1	114.808	114.808	30.51	0.001	14.36%
u_G vs pH *	1	90.228	90.228	23.98	0.003	11.29%
pH*	1	43.779	43.779	11.64	0.014	5.48%
T_{col}*	1	24.457	24.457	6.5	0.044	3.06%
u_G vs T_{col}	1	21.215	21.215	5.64	0.055	2.65%
Alk	1	16.392	16.392	4.36	0.082	2.05%
EBRT	1	12.963	12.963	3.45	0.113	1.62%
u_G	1	6.031	6.031	1.6	0.252	0.75%
Pooled Error	6	22.575	3.762			2.82%
Cumulative Total	15	799.488				100.00%

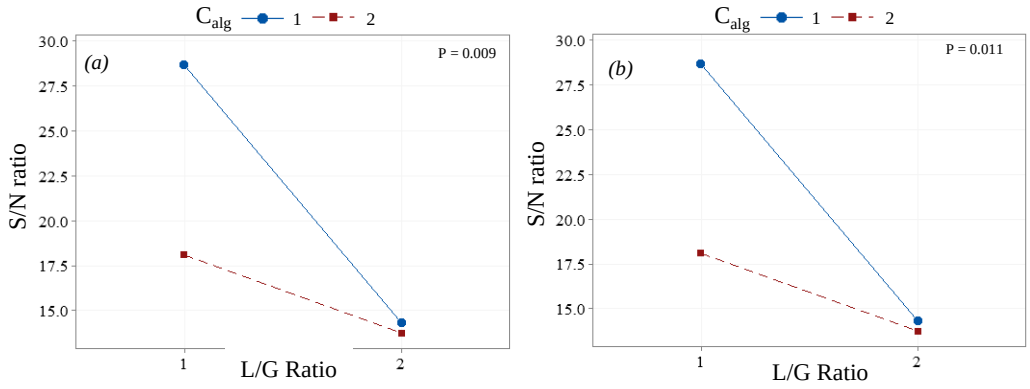


Figure 4-10 Interaction between L/G ratio and algal concentration (C_{alg}) for (a) O_2 concentration in outlet biomethane and (b) O_2 outflow rate within upgraded biomethane.

4.3.3.5 O_2 outflow within biomethane ($O_{2,BM}$)

Opposite to that observed for $O_{2,\%,BM}$, Figure 4-11a-d reveals that the superficial gas velocity has the strongest proportional influence on the volume of O_2 stripped into

the biogas per unit time ($O_{2,BM}$). The resulting increase of oxygen stripping would inherently cause a decreased performance of the bubble column, indicated by a corresponding drop in the S/N ratio on increasing the superficial gas velocity (Figure 4-11b). This is followed in order by the influence of the L/G ratio and algal concentration. EBRT and pH, on the other hand, were seen to only slightly increase the O_2 stripping, while alkalinity and temperature resulted in the lowering of the same (Figure 4-11a). On the aspect of contribution, therefore, only superficial gas velocity (44.78%), L/G ratio (28.03%) and algal concentration (9.97%) affected O_2 stripping by more than 5% (Figure 4-11c).

The confirmatory pooled ANOVA established the statistical significance ($P < 0.05$) of the three major design factors (superficial gas velocity, L/G ratio and algal concentration in order) to impact on $O_{2,BM}$. Similar to $O_{2,\%,BM}$, a statistically significant ($P = 0.004$) interaction between superficial gas velocity and pH was obtained (seen as interaction BD, lying away from the 45° line in the half-normal probability plot in Figure 4-11d and also confirmed by pooled ANOVA in Table 4-10). pH, however, had no statistically significant main effect ($P = 0.231$). By the hierarchical principle adopted above, the interaction was thus concluded to be that of the aliased interaction between the two statistically significant main effects, L/G ratio and algal concentration ($P < 0.001$). The interaction plot shown in Figure 4-10b shows a similar interactive effect to that of $O_{2,\%,BM}$.

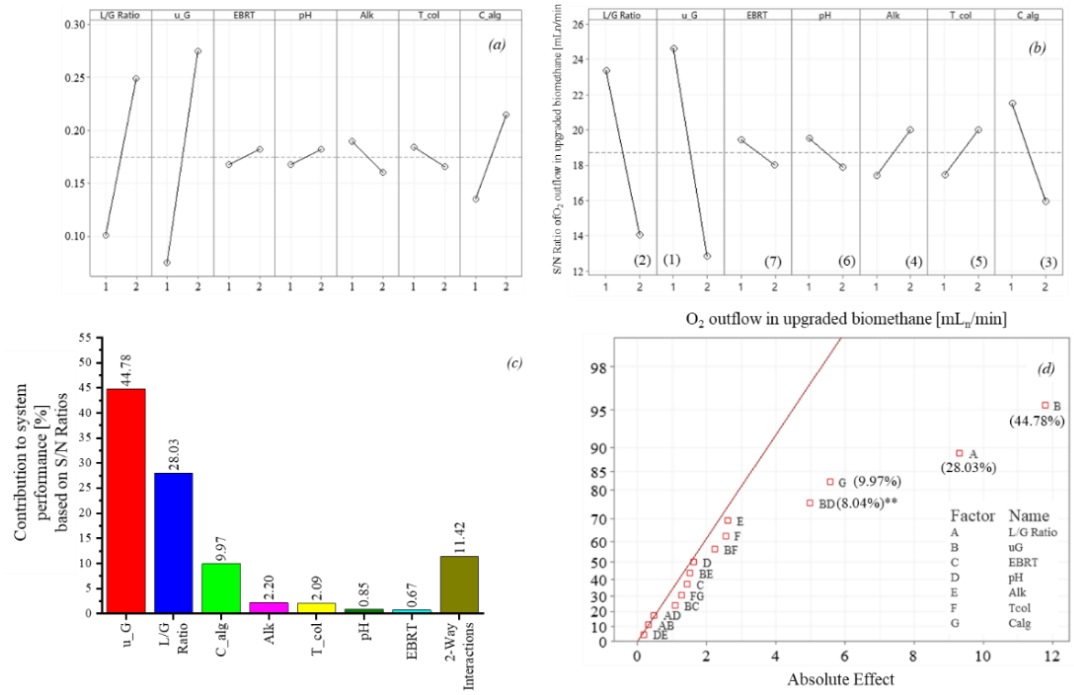


Figure 4-11 Analysis plots for the relative influence of design factors on O_2 flow rate in biomethane: (a) Main effects plot with mean; (b) Main effects plots with S/N ratio. The rank of each design factor is included in parenthesis; (c)Contribution of each design factor and interactions on the overall system outcome; and (d) Half normal probability plot with the relative contribution of major effects highlighted in brackets.

*Table 4-10 Results of ANOVA assessment for O_2 outflow with biomethane with main effects and interaction contributing over 90% towards the output response. *Denotes the statistically significant ($P < 0.05$) source (factors).*

Source	DF	Adj SS	Adj MS	F-Value	P-Value	Contribution
u_G*	1	555.55	555.547	88.46	<0.001	44.78%
L/G Ratio*	1	347.78	347.778	55.38	<0.001	28.03%
C_{alg}*	1	123.65	123.646	19.69	0.002	9.97%
u_G vs pH*	1	99.78	99.78	15.89	0.004	8.04%
Alk	1	27.29	27.29	4.35	0.071	2.20%
T_{col}	1	25.89	25.893	4.12	0.077	2.09%
pH	1	10.55	10.551	1.68	0.231	0.85%
Pooled Error	8	50.24	6.28			4.05%
Cumulative Total	15	1240.72				100.00%

4.3.4 Comparison between design factors and significant interactions

4.3.4.1 Main effects

Grid quality biomethane requires simultaneous maximisation of CO_2 removal and minimisation of O_2 stripping. As can be seen from Table 4-11, the L/G ratio is a critical design factor, having a major influence (within the top 3 factors) on each

studied response. While a higher L/G ratio is desirable for better CO_2 removal, a lower L/G ratio would minimise both oxygen stripping and corresponding concentration in upgraded biomethane. This trend is similar to those reported in multiple sources of literature [4,11]. pH is another critical design factor, a high pH would improve both the CO_2 absorption hydrodynamics and reaction rates, resulting in a consistent and robust CO_2 removal. However, although a higher pH did not have any statistically significant effect on O_2 stripping ($P = 0.231$), a slight increase in O_2 concentration in biomethane was observed ($P = 0.014$). Thus, optimisation of the bubble column (not included in this work) must be performed with pH and L/G ratio as the most significant factors.

Higher algal concentration has a major influence on the $O_{2,\%,BM}$. It could be both due to the improved hydrodynamics and/or the transfer of a considerable amount of O_2 produced by photosynthesising microalgae into the biomethane. On the contrary, the hydrodynamics of CO_2 absorption showed no statistically significant ($P > 0.05$) correlation with increasing algal concentration. However, the increased algal concentration resulted in a significant drop in the performance of the CO_2 removal efficiency of the bubble column. This could be because of non-uniform mixing due to the presence of filamentous microalgae (*Spirulina platensis*), as well as from increased foaming and clogging observed at operations with higher algal concentrations. A similar drop in CO_2 removal efficiencies from increased algal concentration has also been reported by Rodero et al., (2020b) [13], although it was not statistically significant. Alkalinity was a major factor in $R_{eff,\,CO_2}$ both increasing CO_2 removal and providing operation robustness when alkalinity was increased. A similar improvement in the consistency of $R_{eff,\,CO_2}$ was reported by Rodero et al., (2020b) [13] by increasing the alkalinity from 1.3 gIC/L to 2.4 gIC/L and above. However, it had no major contribution to either the kinetics or the hydrodynamics of CO_2 absorption, as well as on oxygen stripping.

Although superficial gas velocity plays a major role in defining the system hydrodynamics, it had a minor impact on the overall biomethane composition. In agreement with existing literature [75], superficial gas velocity had the highest influence on increasing the volume of O_2 stripped into the biogas. However, as the bubble column diameter was fixed, an increase in the superficial gas velocity was

accompanied by a proportional increase in the gas flow rate. This ensured that there was no significant change in $O_{2,\%,BM}$ with the variation in the superficial gas velocity. From the perspective of CO_2 removal, a higher superficial gas velocity would not only increase bubble diameter but also increase the bubble rise velocity [74], decreasing the gas-liquid contact time irrespective of EBRT. Expectedly, a significant drop in CO_2 removal efficiency on increasing the superficial gas velocity was observed. However, it must be remembered that to increase the throughput of the bubble column with regards to biogas upgraded, the superficial gas velocity must be increased. Thus, to counter the drop in CO_2 removal performance with regards to increasing the superficial gas velocity, the operating pH, L/G ratio and alkalinity must be included in process control and optimisation.

Table 4-11 Comparison and primary conclusions about the design factors affecting the studied process responses to assess the performance of the bubble column in photosynthetic biogas upgrading for both CO_2 removal and O_2 stripping. The values in brackets indicate the rank of the design factors based on S/N ratios for the respective response.

Design Factors	**Performance of CO_2 removal**			**O_2 stripping**		**Inference**
	$R_{eff,\,CO_2}$ [%]	**$R_{abs,\,CO_2}$ [$\times 10^{-4}$ mol/L/s]**	**$k_{G_{CO_2}}a$ [hr^{-1}]**	**O_2 in biomethane [%]**	**O_2 outflow in biomethane [mL_n/min]**	
L/G Ratio	(2)*	(3)*	(3)*	(1)*	(2)*	Critical influence
Superficial Gas Velocity	(5)*	(6)	(2)*	(7)	(1)*	Minor influence
Empty Bed Residence Time	(7)	(1)*	(4)*	(6)	(6)	Negligible influence
pH of inlet liquid	(1)*	(2)*	(1)*	(3)*	(7)	Critical influence
Alkalinity of inlet liquid	(3)*	(4)	(5)	(5)	(4)	Major influence on CO_2 removal only
Temperature	(6)	(6)	(7)	(4)*	(5)	Negligible influence
Algal Concentration	(4)*	(5)	(6)	(2)*	(3)*	Major influence on O_2 stripping only

*indicates the statistically significant main effects ($P < 0.05$)

Compared to other design factors, the influence of temperature was minimal. Although $O_{2,\%,BM}$ had a statistically significant ($P = 0.044$) decrease upon the increase in the temperature, the net contribution of temperature towards the overall variation in

the response was only around 2% (Table 4-10). Thus, the influence of temperature on the bubble column operations and controls can generally be neglected. Finally, beyond indicating a drop in reaction rates and hydrodynamic performance along the length of the reactor, which is expected from its co-current flow configuration, EBRT had no statistically significant contribution towards the upgraded biomethane composition and can hence be regarded as a minor factor when varied between 6 and 15 minutes.

4.3.4.2 Interactions

A few interactive effects between the design factors were also found to have a major and statistically significant ($P < 0.05$) effect on the performance of CO_2 removal from biogas and O_2 stripping from the alkaline algal medium. For the former, the largest interaction was between pH and L/G ratio, affecting the rate of CO_2 absorption, and hence the overall efficiency of CO_2 removal. The implications of the interactive effects between the superficial gas velocity and pH and L/G ratio implies the necessity to control both pH and L/G ratio at higher levels to enable the increase of the throughput of the bubble column (a higher gas superficial velocity for constant diameter). This is especially important, as the higher setting (factor level "2") of superficial gas velocity was limited by the practicality of the experimental setup. For O_2 stripping, the only statistically significant ($P < 0.05$) interaction was between algal concentration and L/G ratio. The results indicated the important influence of the algal concentration on increasing $O_{2,\%,BM}$ especially at a lower L/G ratio; however, at a higher L/G ratio, the $O_{2,\%,BM}$ was found to be independent of the algal concentration.

Of the interactive effects that were not statistically significant ($P > 0.05$), the interaction between temperature and algal concentration bears importance in that it provides conclusive evidence that photosynthesising *Spirulina platensis* would not play a significant role in catalysing CO_2 removal. By this, it can also be confirmed that the absorption of CO_2 is chemically driven by the carbonate/ bicarbonate present in the solution.

4.3.4.3 Prediction of bubble column operation and confirmatory experiment

Using the statistically significant ($P < 0.05$) main effects and interactions derived in Section 4.3.3, Eq. 4.15 and Eq. 4.16 were used to predict the CO_2 removal efficiency ($(S/N)_{R_{eff,\,CO_2}}$) and the oxygen outflow within biomethane ($(S/N)_{O_{2,BM}}$) in terms of the

S/N ratio. For physical interpretation, the obtained values could be converted back into practical units using Eq. 4.10 and Eq. 4.11 respectively.

$$(S/N)_{R_{eff,\,CO_2}} = -53.25 + 56.69L/G - 164.5u_G + 5.04pH + 1.1Alk - 2.07C_{alg} + 28.01L/G{\cdot}u_G - 5.63L/G{\cdot}pH + 14.1u_G{\cdot}pH \quad (4.15)$$

$$(S/N)_{O_{2,BM}} = 44.13 - 18.79L/G - 84.2u_G - 18.65C_{alg} + 17.84L/G{\cdot}C_{alg} \quad (4.16)$$

To assess the performance of the derived regression models, their statistical characteristics were calculated and compared. As can be seen from the results summarised in Table 4-12, both the regression equations for $R_{eff,\,CO_2}$ and $O_{2,BM}$ have a much higher F_{model} value (27.96 and 27.19 respectively) than critical values (3.725 and 3.36 respectively) with a P-value of less than 0.001 in both cases. This confirms the statistical significance of the proposed regression models for a confidence interval of 95%. Simultaneously, the R^2 values of the models were also above 0.9, indicating a good linear agreement between the observed and the predicted data [40].

Table 4-12 Statistical characteristics of the models for predicting CO_2 removal efficiency and O_2 flow rate in upgraded biomethane to predict the biomethane composition.

Model	**Model Characteristics**					
	DoF	**R^2**	**S**	**F_{model}**	**$F_{critical}$**	**P-value**
CO_2 removal efficiency	7	0.969	1.11%	27.96	3.725 ($F_{0.05(8,7)}$)	<0.001
O_2 flow in biomethane	4	0.908	3.22%	27.19	3.36 ($F_{0.05(5,10)}$)	<0.001

A study of the S value, which represents the average deviation of the predicted model from the observed data, shows that the model for $R_{eff,\,CO_2}$ would be able to predict the performance based on the S/N ratio with an average error of ± 1.11%; the corresponding average error in prediction of $O_{2,BM}$ is ± 3.22%. Graphical representation of this argument is presented in Figure 4-12 which reveals a good agreement between the experimental and the predicted values for both S/N ratios of $R_{eff,\,CO_2}$ and $O_{2,BM}$. All the experimental values were found to lie within the 95% prediction interval, confirming the adequacy of the simplified model with the chosen main effects and interactions.

A confirmatory experiment, separate from the sixteen Taguchi trials was performed with pH 10.5 (to maximise CO_2 removal), L/G ratio 0.2 (to minimise O_2 stripping) and alkalinity 2.5 gIC/L (to maximise CO_2 removal efficiency) while the superficial gas velocity was set at 0.2cm/s (to maximise throughput). The constant settings were selected as follows: Temperature 20°C, algal concentration 0.05 gDW/L and EBRT 6 mins. Grid quality biomethane with a CO_2 and O_2 concentration of 0.19% ± 0.17% and 0.2% ± 0.01% respectively was obtained. The corresponding S/N ratio for CO_2 removal efficiency of -0.0613 fell within the 95% CI of -2.28 and 1.66; while that for O_2 (20.77) matched closely with the predicted value of 22.78 while also being within the 95% CI (18.82, 23.74).

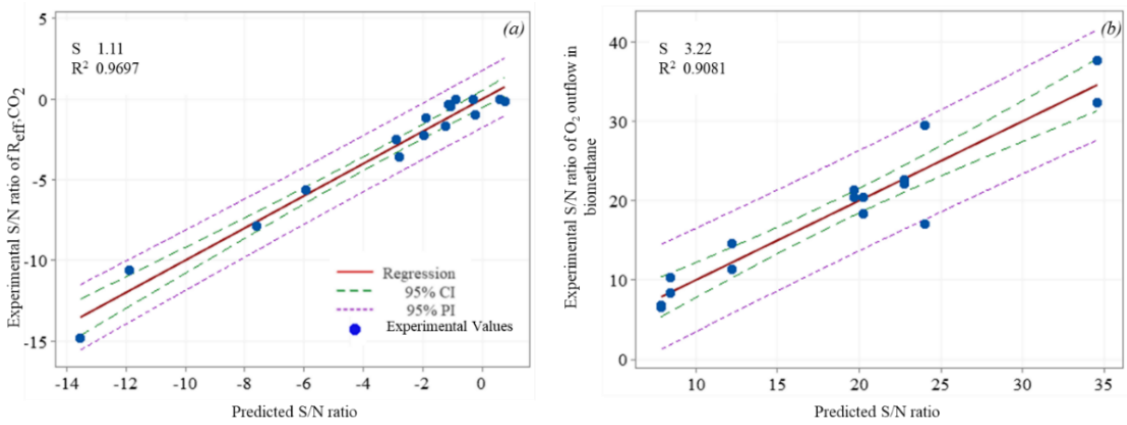


Figure 4-12 Comparison of regression model and experimental data along with 95% Confidence Interval and 95% Prediction Interval for the S/N ratios of (a) $R_{eff,\,CO_2}$ and (b) $O_{2,BM}$

Following the predictive regression equations, Figure 4-13a and Figure 4-13b represent the variation in biomethane composition between a pH 9 and pH 10.5 and an L/G ratio 0.2 and 1 for a superficial gas velocity of 0.06 cm/s (factor level "1") and 0.2 cm/s (factor level "2") respectively. EBRT and temperature were set at the lowest ranges while alkalinity was set at 2.5 gIC/L. Algal concentration was considered fixed at 0.05 gDW/L. As can be seen, with the increase in superficial gas velocity, the allowable range of operation to produce grid quality biomethane narrows significantly, especially with respect to CO_2 removal. This can be understood from the interactive effect between superficial gas velocity and both pH and L/G ratio alike, whereby, an increase in pH and L/G ratio was necessary at higher superficial gas velocity (throughput rates) to achieve grid quality biomethane, all other conditions being fixed.

Figure 4-13 must however be studied with caution as it is not an optimised plot, nor can it be extrapolated above the studied range of superficial gas velocity 0.2 cm/s. Indeed, this graph provides an indication and estimation of the profiles of biomethane composition to be expected while working with photosynthetic biogas upgrading. More accurate predictive models and contour plots must be generated with detailed optimisation experiments, which is beyond the scope of the present work.

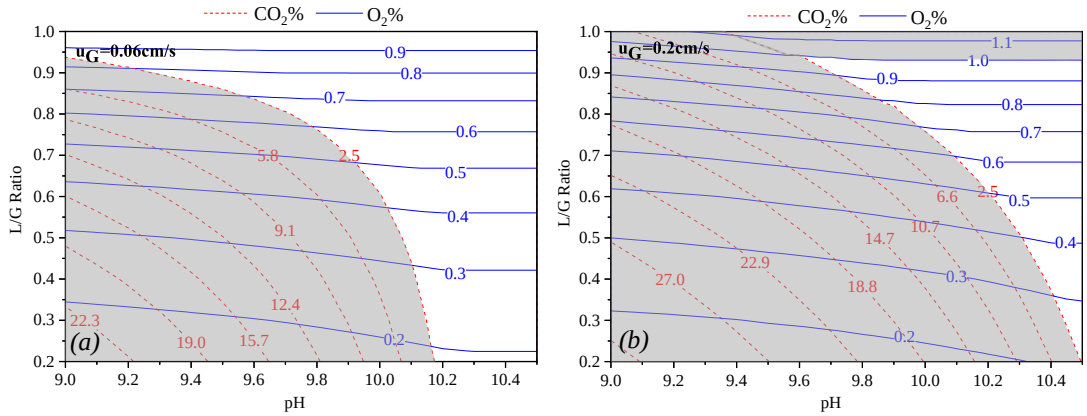


Figure 4-13 Prediction of biomethane composition at (a) u_G 0.06 cm/s (c. 0.98 L/hr) and (b) u_G 0.2 cm/s (c. 3.29 L/hr). The constant setting of other design factors are as follows: Alk 2.5gIC/L; T_{col} 20°C; C_{alg} 0.05gDW/L; and EBRT 6 mins. The acceptable region of operation is indicated in white

4.3.5 Significance of results

Similar global hydrodynamic parameters, such as the gas hold-up (i.e., the ratio of the gassed volume to the static liquid volume in the bubble column) is necessary and sufficient to achieve dynamic similarity upon scale-up [76]. For low superficial gas velocities below 1 cm/s, a minimal gas hold-up together with a negligible impact of pressure on the same allows scale-up of results with minimal errors [48]. Accordingly, the current results would remain valid for industrial-scale bubble columns operated under similar superficial gas velocities irrespective of the bubble column dimensions. The following sections, therefore, focus on the significance of the results on the industrial scale design, operation and costs of the bubble column, together with its integration with photobioreactors for the continuous operation of photosynthetic biogas upgrading system producing grid quality biomethane.

4.3.5.1 On bubble column design, operations and costs

To ensure robust and repetitive operation of the bubble column, against uncontrollable factors or noise such as DO in the algal liquid or seasonal and diurnal

cycles, process control strategies for bubble column operation must include L/G ratio and pH as critical factors along with alkalinity. The compelling evidence of the benefits of operation with a low algal concentration and the minor influence of temperature between 20 °C and 35 °C would further ease the design and operations of the bubble column. Not only does a lower algal concentration signify that light would not play a significant role in bubble column operations, but also that temperature and pressure are not crucial elements to its operation and control. From the bubble column design aspect, the relatively minor influence of EBRT as it varied between 6 and 15 minutes, indicates the possibility to reduce the height of the bubble column from that currently employed in literature for photosynthetic biogas upgrading. On the other hand, for a fixed bubble column diameter, to ensure a constant EBRT, the bubble column height would increase proportionally with the superficial gas velocity. Indeed, within the present experiments, this resulted in the aspect ratio (the ratio of the height of the bubble column to the diameter) varying from 9 to 22.5 at superficial gas velocities of 0.06 cm/s and 0.2 cm/s respectively and an EBRT of 6 minutes. Thus, it can be concluded with confidence ($P < 0.05$) that biomethane production in photosynthetic biogas upgrading would be possible in industrial bubble columns with their aspect ratios typically varying between 3 and 10 [31]. Traditional materials such as stainless steel could be used for bubble column construction without the need for specialised design and materials. However, to further increase the superficial gas velocity without having to build a considerably tall bubble column, the investigation into lowering the EBRT further can be made in future studies. pH and alkalinity should be increased towards their maximum setting (10.5 and 2.5 gIC/L corresponding to factor level "2" in the present study) with the L/G being adjusted accordingly to ensure generation of grid quality biomethane.

4.3.5.2 On the operation of algae cultivation and harvesting system

From mass balance, the CO_2 removed from the biogas in the bubble column would be added into the alkaline algal liquid, increasing its alkalinity and producing bicarbonates from carbonates (Eq. 4.1). Based on the CO_2 removal efficiency, Table 4-13 indicates the predicted effective amount of inorganic carbon added into the algal liquid from biogas in terms of alkalinity [gIC/L]. Operation at two extremes of pH and L/G ratios when the superficial gas velocity is 0.2 cm/s is considered as a representative case. A high pH and low L/G ratio, ensuring 96.5% CO_2 removal

(predicted) would maximise the inorganic carbon addition per litre of alkaline solution. However, when the L/G ratio is increased to 1, IC added would drop to 0.2 gIC/L at a CO_2 removal efficiency of 100%.

Table 4-13 Impact of pH and L/G ratio on the inorganic carbon added to the algal liquid from biogas with the corresponding CO_2 removal efficiency in brackets. CO_2 removal efficiencies are based on the predicted values obtained using Eq. 4.15 and Eq. 4.10 in order.

pH	LG ratio	
	0.2	**1**
9	0.30 (30.1%)	0.17 (87.7%)
10.5	0.96 (96.5%)	0.20 (100%)

To ensure a continuous cycle, the added carbon must account for that consumed by the algae and also meet system losses. Carbon losses in closed and open pond photobioreactors have been reported to be similar [4], often increasing at higher alkalinity [13]. Assuming the average productivity of *Spirulina platensis* in inorganic media to be around 0.175 g/L/day at 30 °C [14], and that *Spirulina platensis* comprises 50% carbon per dry weight [77], the daily carbon assimilation rate would be 0.088 g/L. Also, considering a carbon loss of 24% at an alkalinity of 2.5 gIC/L [13] the cultivation of *Spirulina platensis* at 30 °C, connected to a bubble column operating at pH 10.5 and L/G 0.2 would require an estimated 8 days of hydraulic retention time (HRT) to assimilate the added carbon. However, when the L/G ratio is increased to 1, the HRT could be reduced to 2 days only. The corresponding algal concentrations generated would vary between 2.8 gDW/L and 0.35 gDW/L respectively. Sufficient year-round CO_2 uptake could be ensured by temperature-controlled microalgae cultivation, either in closed photobioreactors [4] or open ponds within greenhouses [16]. A higher algal concentration is always desired, as it greatly simplifies the harvesting system design and cost.

4.4 Conclusions and future directions

In this work, a quantitative comparison among seven design factors affecting bubble column performance in photosynthetic biogas upgrading has been developed. The L_{16} Taguchi orthogonal array as a screening design of experiment was selected as the statistical tool. Experiments were conducted in a lab-scale bubble column reactor. Assessments regarding the performance of CO_2 removal and O_2 stripping into biomethane were performed using the signal to noise (S/N) ratio statistic derived from

the experimental data. The output of the four objectives as described in the introduction along with future research needs are synthesised as below:

i. pH and L/G ratio are the most critical design factors affecting CO_2 removal and O_2 stripping alike. For CO_2 removal in a specific bubble column, besides pH and L/G ratio, alkalinity, followed by algal concentration and superficial gas velocity are statistically significant ($P < 0.05$) design factors. On the other hand, over 85% of the variations in O_2 concentration in biomethane were explained by the main effects of the L/G ratio and algal concentration (in descending order of importance) and the interaction between the two.

ii. The interactive effect between pH and L/G ratio was the most impactful on the efficiency of CO_2 removal. Although superficial gas velocity had limited contribution to CO_2 removal, its interactions with both L/G ratio and pH caused statistically significant ($P < 0.05$) variation in the CO_2 composition in biomethane. For O_2 stripping, algal concentration had a diminishing role in increasing the O_2 concentration in biomethane as the L/G ratio increased. At higher L/G ratios, similar O_2 concentration in biomethane was observed irrespective of the algal concentration in the circulating algal medium.

iii. A higher alkalinity (2.5 gIC/L) is required to ensure consistent CO_2 removal while a lower algal concentration (0.05 gDW/L) would minimise O_2 stripping into biomethane, and also maximise and stabilise CO_2 removal. Although a high pH and L/G ratio improve CO_2 removal, it increases O_2 content in the biomethane. A higher superficial gas velocity on the other hand reduces the CO_2 removal efficiency without affecting the O_2 concentration in biomethane. Thus, future studies aiming to increase the throughput of the system and optimise the bubble column would require pH, L/G ratio and superficial gas velocity as mandatory design factors.

iv. Using only the statistically significant main effects and interactions, the biomethane composition (CO_2% and O_2%) was predicted with fair confidence for superficial gas velocities up to 0.2 cm/s using regression equations derived from the ANOVA analysis. To achieve grid quality biomethane, operations at pH between 10.3 and 10.5 and L/G ratio between 0.5 and 0.8, with alkalinity of 2.5 gIC/L and algal concentration of 0.05 gDW/L would ensure robust operations. However, to generate

more accurate predictive models, detailed optimisation experiments with the selected critical design factors must be conducted that was beyond the scope of the present work. The minimal impact of temperature and gas residence times on the system performance further indicates the possibility to use state-of-the-art bubble column designs and operational strategies for photosynthetic biogas upgrading.

Based on the results of the current work, the need to perform further research towards increasing the superficial gas velocities and lowering the EBRT can be established. This would be essential to increase the throughput of the bubble columns, without requiring them to be considerably tall. In all cases, however, pH, L/G ratio and alkalinity must be varied taking into account the feasibility of integration with the photobioreactor for microalgae cultivation to achieve the optimal design and operating conditions of the bubble column.

4.5 Acknowledgement

This work acknowledges the support from Science Foundation Ireland (SFI) through the Centre for Marine and Renewable Energy (MaREI) under Grant No. 12/RC/2302_P2 and 16/SP/3829, with industrial funding from Gas Networks Ireland through The Green Gas Innovation Group and by ERVIA and IDL Pernod Ricard. This work was also supported by the Environmental Protection Agency – Ireland (2018-RE-MS-13).

4.6 References

[1] Rajendran K, O'Gallachoir B, Murphy JD. The combined role of policy and incentives in promoting cost efficient decarbonisation of energy: A case study for biomethane. J Clean Prod 2019;219:278–90. doi:10.1016/j.jclepro.2019.01.298.

[2] Wall DM, McDonagh S, Murphy JD. Cascading biomethane energy systems for sustainable green gas production in a circular economy. Bioresour Technol 2017;243:1207–15. doi:10.1016/j.biortech.2017.07.115.

[3] Angelidaki I, Treu L, Tsapekos P, Luo G, Campanaro S, Wenzel H, et al. Biogas upgrading and utilization: Current status and perspectives. Biotechnol Adv 2018;36:452–66. doi:10.1016/j.biotechadv.2018.01.011.

[4] Bose A, Lin R, Rajendran K, Xia A, O'Shea R, Murphy JD. How to optimise photosynthetic biogas upgrading: A perspective on system design and microalgae selection. Biotechnol Adv 2019;37. doi:10.1016/j.biotechadv.2019.107444.

[5] Meier L, Pérez R, Azócar L, Rivas M, Jeison D. Photosynthetic CO_2 uptake by microalgae: An attractive tool for biogas upgrading. Biomass and Bioenergy 2015;73:102–9. doi:10.1016/j.biombioe.2014.10.032.

[6] Bose A, O'Shea R, Lin R, Murphy JD. A perspective on novel cascading algal biomethane biorefinery systems. Bioresour Technol 2020;304:123027. doi:10.1016/j.biortech.2020.123027.

[7] Meier L, Barros P, Torres A, Vilchez C, Jeison D. Photosynthetic biogas upgrading using microalgae: Effect of light/dark photoperiod. Renew Energy 2017;106:17–23. doi:10.1016/j.renene.2017.01.009.

[8] Gas Networks Ireland. Code of Operations, Part G. 2018.

[9] Bahr M, Díaz I, Dominguez A, González Sánchez A, Muñoz R. Microalgal-biotechnology as a platform for an integral biogas upgrading and nutrient removal from anaerobic effluents. Environ Sci Technol 2014;48:573–81. doi:10.1021/es403596m.

[10] Meier L, Martínez C, Vílchez C, Bernard O, Jeison D. Evaluation of the feasibility of photosynthetic biogas upgrading: Simulation of a large-scale system. Energy 2019;189:116313. doi:10.1016/j.energy.2019.116313.

[11] Toledo-Cervantes A, Madrid-Chirinos C, Cantera S, Lebrero R, Muñoz R. Influence of the gas-liquid flow configuration in the absorption column on photosynthetic biogas upgrading in algal-bacterial photobioreactors. Bioresour Technol 2017;225:336–42. doi:10.1016/j.biortech.2016.11.087.

[12] Rodero M del R, Posadas E, Toledo-Cervantes A, Lebrero R, Muñoz R. Influence of alkalinity and temperature on photosynthetic biogas upgrading efficiency in high rate algal ponds. Algal Res 2018;33:284–90. doi:10.1016/j.algal.2018.06.001.

[13] Rodero M del R, Severi CA, Rocher-Rivas R, Quijano G, Muñoz R. Long-term influence of high alkalinity on the performance of photosynthetic biogas upgrading. Fuel 2020;281:118804. doi:10.1016/j.fuel.2020.118804.

[14] de Oliveira MACL, Monteiro MPC, Robbs PG, Leite SGF. Growth and chemical composition of *Spirulina maxima* and *Spirulina platensis* biomass at different temperatures. Aquac Int 1999;7:261–75. doi:10.1023/A:1009233230706.

[15] Knuutila H, Juliussen O, Svendsen HF. Kinetics of the reaction of carbon dioxide with aqueous sodium and potassium carbonate solutions. Chem Eng Sci 2010;65:6077–88. doi:10.1016/j.ces.2010.07.018.

[16] Marín D, Carmona-Martínez AA, Blanco S, Lebrero R, Muñoz R. Innovative operational strategies in photosynthetic biogas upgrading in an outdoors pilot scale algal-bacterial photobioreactor. Chemosphere 2021;264. doi:10.1016/j.chemosphere.2020.128470.

[17] Sun Z, Liu J, Zhou Z-G. Algae for biofuels: An emerging feedstock. In: Luque R, Lin CSK, Wilson K, Clark J, editors. Handb. Biofuels Prod. 2nd ed., Elsevier B.V.; 2016, p. 673–98.

[18] Rodero M del R, Carvajal A, Arbib Z, Lara E, de Prada C, Lebrero R, et al. Performance evaluation of a control strategy for photosynthetic biogas upgrading in a

semi-industrial scale photobioreactor. Bioresour Technol 2020;307:123207. doi:10.1016/j.biortech.2020.123207.

[19] Marín D, Posadas E, Cano P, Pérez V, Blanco S, Lebrero R, et al. Seasonal variation of biogas upgrading coupled with digestate treatment in an outdoors pilot scale algal-bacterial photobioreactor. Bioresour Technol 2018;263:58–66. doi:10.1016/j.biortech.2018.04.117.

[20] Hu G, Nicholas NJ, Smith KH, Mumford KA, Kentish SE, Stevens GW. Carbon dioxide absorption into promoted potassium carbonate solutions: A review. Int J Greenh Gas Control 2016;53:28–40. doi:10.1016/j.ijggc.2016.07.020.

[21] Huang Q, Jiang F, Wang L, Yang C. Design of photobioreactors for mass cultivation of photosynthetic organisms. Engineering 2017;3:318–29. doi:10.1016/J.ENG.2017.03.020.

[22] Vasumathi KK, Premalatha M, Subramanian P. Parameters influencing the design of photobioreactor for the growth of microalgae. Renew Sustain Energy Rev 2012;16:5443–50. doi:10.1016/j.rser.2012.06.013.

[23] Barros AI, Gonçalves AL, Simões M, Pires JCM. Harvesting techniques applied to microalgae: A review. Renew Sustain Energy Rev 2015;41:1489–500. doi:10.1016/j.rser.2014.09.037.

[24] Singh G, Patidar SK. Microalgae harvesting techniques: A review. J Environ Manage 2018;217:499–508. doi:10.1016/j.jenvman.2018.04.010.

[25] Rodero M del R, Carvajal A, Castro V, Navia D, de Prada C, Lebrero R, et al. Development of a control strategy to cope with biogas flowrate variations during photosynthetic biogas upgrading. Biomass and Bioenergy 2019;131. doi:10.1016/j.biombioe.2019.105414.

[26] Franco-Morgado M, Alcántara C, Noyola A, Muñoz R, González-Sánchez A. A study of photosynthetic biogas upgrading based on a high rate algal pond under alkaline conditions: Influence of the illumination regime. Sci Total Environ 2017;592:419–25. doi:10.1016/j.scitotenv.2017.03.077.

[27] Posadas E, Morales M del M, Gomez C, Acién FG, Muñoz R. Influence of pH and CO_2 source on the performance of microalgae-based secondary domestic wastewater treatment in outdoors pilot raceways. Chem Eng J 2015;265:239–48. doi:10.1016/j.cej.2014.12.059.

[28] Posadas E, Serejo ML, Blanco S, Pérez R, García-Encina PA, Muñoz R. Minimization of biomethane oxygen concentration during biogas upgrading in algal-bacterial photobioreactors. Algal Res 2015;12:221–9. doi:10.1016/j.algal.2015.09.002.

[29] Rodero M del R, Lebrero R, Serrano E, Lara E, Arbib Z. Technology validation of photosynthetic biogas upgrading in a semi- industrial scale algal-bacterial photobioreactor. Bioresour Technol 2019;279:43–9. doi:10.1016/j.biortech.2019.01.110.

[30] Rodero M del R, Posadas E, Toledo-cervantes A, Lebrero R. Influence of alkalinity and temperature on photosynthetic biogas upgrading efficiency in high rate algal ponds. Algal Res 2018;33:284–90. doi:10.1016/j.algal.2018.06.001.

[31] Jakobsen HA. Bubble Column Reactors. Chem. React. Model. Multiph. React. Flows, Trondheim: Springer Berlin Heidelberg; 2009, p. 335–501.

[32] Molina E, Fernández J, Acién FG, Chisti Y. Tubular photobioreactor design for algal cultures. J Biotechnol 2001;92:113–31. doi:10.1016/S0168-1656(01)00353-4.

[33] Madkour FF, Kamil AEW, Nasr HS. Production and nutritive value of *Spirulina platensis* in reduced cost media. Egypt J Aquat Res 2012;38:51–7. doi:10.1016/j.ejar.2012.09.003.

[34] Kaye, G W.C., Laby TH. Tables of physical and chemical constants. 15th Edition. United States: N. p., 1986. Web. 15th ed. United States: Longman; 1986.

[35] Krishnaiah K, Shahabudeen P. Applied design of experiments and Taguchi methods. New Delhi: PHI Learning Private Limited; 2012.

[36] Montgomery DC. Design and analysis of experiments. 8th ed. John Wiley & Sons, Inc.; 2012.

[37] Awty-Carroll D, Ravella S, Clifton-Brown J, Robson P. Using a Taguchi DOE to investigate factors and interactions affecting germination in *Miscanthus sinensis*. Sci Rep 2020;10:1–11. doi:10.1038/s41598-020-58322-x.

[38] Chiranjeevi P, Mohan SV. Critical parametric influence on microalgae cultivation towards maximizing biomass growth with simultaneous lipid productivity. Renew Energy 2016;98:64–71. doi:10.1016/j.renene.2016.03.063.

[39] Rao RS, Kumar CG, Prakasham RS, Hobbs PJ. The Taguchi methodology as a statistical tool for biotechnological applications: A critical appraisal. Biotechnol J 2008;3:510–23. doi:10.1002/biot.200700201.

[40] Smith ZD, Keller JR, Bello M, Cordes NL, Welch CF, Torres JA, et al. Plackett-Burman experimental design to facilitate syntactic foam development. J Appl Polym Sci 2016;133:1–9. doi:10.1002/app.42892.

[41] Roy RK. A Primer on the Taguchi Method, Second Edition. 2010.

[42] Chen P, Huang C, Su T, Chen H, Yang M, Tsao J. Optimum conditions for the capture of carbon dioxide with a bubble-column scrubber. Int J Greenh Gas Control 2015;35:47–55. doi:10.1016/j.ijggc.2015.01.011.

[43] Clark KN. The effect of high pressure and temperature on phase distributions in a bubble column. Chem Eng Sci 1990;45:2301–7. doi:10.1016/0009-2509(90)80109-R.

[44] Deckwer WD, Louisi Y, Zaidi A, Ralek M. Hydrodynamic properties of the Fischer-Tropsch slurry process. Ind Eng Chem Process Des Dev 1980;19:699–708. doi:10.1021/i260076a032.

[45] Chen PC, Lin S. Optimisation in the absorption and desorption of CO_2 using sodium glycinate solution. Appl Sci 2018;8:2041. doi:10.3390/app8112041.

[46] Fernández I, Guzmán JL, Berenguel M, Acién FG. Dynamic modeling of microalgal production in photobioreactors. In: Tripathi, Bhumi Nath, Kumar D, editor.

Prospect. Challenges Algal Biotechnol., Springer; 2017, p. 49–86. doi:10.1007/978-981-10-1950-0.

[47] Borhani TNG, Azarpour A, Akbari V, Wan Alwi SR, Manan ZA. CO_2 capture with potassium carbonate solutions: A state-of-the-art review. Int J Greenh Gas Control 2015;41:142–62. doi:10.1016/j.ijggc.2015.06.026.

[48] Bose A, O'Shea R, Lin R, Murphy JD. Design, commissioning and performance assessment of a lab-scale bubble column reactor for photosynthetic biogas upgrading with *Spirulina platensis*. Ind Eng Chem Res 2021. doi:10.1021/acs.iecr.0c05974.

[49] Costa JAV, Colla LM, Filho PD. *Spirulina platensis* growth in open raceway ponds using freshwater supplemented with carbon, nitrogen and metal ions. Zeitschrift Fur Naturforsch - Sect C J Biosci 2003;58:76–80. doi:10.1515/znc-2003-1-214.

[50] Hu Q, Guterman H, Richmond A. A flat inclined modular photobioreactor for outdoor mass cultivation of photoautotrophs. Biotechnol Bioeng 1996;51:51–60. doi:10.1002/(sici)1097-0290(19960705)51:1<51::aid-bit6>3.0.co;2-%23.

[51] Mehta PD. Control Variable in Research. Int. Encycl. Soc. Behav. Sci., 2001, p. 2727–30. doi:10.1016/b0-08-043076-7/00734-8.

[52] Kishore RA, Kumar P, Priya S. A comprehensive optimisation study on Bi2 Te3-based thermoelectric generators using the Taguchi method. Sustain Energy Fuels 2018;2:175–90. doi:10.1039/c7se00437k.

[53] Priyadarshi D, Paul KK. Optimisation of biodiesel production using Taguchi model. Waste and Biomass Valorization 2019;10:1547–59. doi:10.1007/s12649-017-0158-9.

[54] Davis R, John P. Application of Taguchi-based design of experiments for industrial chemical processes. In: Silva V, editor. Stat. Approaches With Emphas. Des. Exp. Appl. to Chem. Process. Montgomery, IntechOpen; 2018. doi:10.5772/intechopen.69501.

[55] Myers RH, Montgomery DC, Anderson-Cook CM. Response Surface Methodology: process and product optimisation using designed experiments. 4th ed. New Jersey: John Wiley & Sons Inc; 2017.

[56] Antony J. A systematic methodology for design of experiments. Second Edi. Elsevier Ltd; 2014. doi:10.1016/b978-0-08-099417-8.00004-3.

[57] Ganapathy T, Murugesan K, Gakkhar RP. Performance optimisation of Jatropha biodiesel engine model using Taguchi approach. Appl Energy 2009;86:2476–86. doi:10.1016/j.apenergy.2009.02.008.

[58] Jones B. 21st century screening experiments: What, why, and how. Qual Eng 2016;28:98–106. doi:10.1080/08982112.2015.1100462.

[59] Mohsin I, He K, Li Z, Zhang F, Du R. Optimisation of the polishing efficiency and torque by using Taguchi method and ANOVA in robotic polishing. Appl Sci 2020;10. doi:10.3390/app10030824.

[60] Kim H. Statistical notes for clinical researchers : Chi-squared test and Fisher's exact test. Open Lect Stat 2017:152–5. doi:10.5395/rde.2017.42.2.152.

[61] Kitchin J. 6. Basic statistical inference. vol. 28. Elsevier Masson SAS; 1994. doi:10.1016/S0076-695X(08)60256-2.

[62] American Public Health Association (APHA). APHA Method 2320. Stand. Methods Exam. Water Wastewater. 18th ed., Washington, DC: American Public Health Association (APHA); 1992.

[63] Yang J, Cui X, Feng Y, Jing G, Kang L, Luo M. Experimental study on microalgae cultivation in novel photobioreactor of concentric double tubes with aeration pores along tube length direction. Int J Green Energy 2017;14:1269–76. doi:10.1080/15435075.2017.1402772.

[64] Di Leo G, Sardanelli F. Statistical significance: P-value, 0.05 threshold, and applications to radiomics—reasons for a conservative approach. Eur Radiol Exp 2020;4. doi:10.1186/s41747-020-0145-y.

[65] Zhu W. P < 0.05, < 0.01, < 0.001, < 0.0001, < 0.00001, < 0.000001, or t... J Sport Heal Sci 2016;5:77–9. doi:10.1016/j.jshs.2016.01.019.

[66] Dahiru T. P-Value, a true test of statistical significance? A cautionary note. Ann Ibadan Postgrad Med 2011;6:21–6. doi:10.4314/aipm.v6i1.64038.

[67] Krueger JI, Heck PR. Putting the P-Value in its place. Am Stat 2019;73:122–8. doi:10.1080/00031305.2018.1470033.

[68] Lakens D. The practical alternative to the P-value is the correctly used P-value. Perspect Psychol Sci 2021;16:639–48. doi:10.1177/1745691620958012.

[69] Lee S, Lee DK. What is the proper way to apply the multiple comparison test? Korean J Anesthesiol 2018;71:353–60. doi:10.4097/kja.d.18.00242.

[70] Schlattmann P, Dirnagl U. Statistics in experimental cerebrovascular research: Comparison of more than two groups with a continuous outcome variable. J Cereb Blood Flow Metab 2010;30:1558–63. doi:10.1038/jcbfm.2010.95.

[71] Ruxton GD, Beauchamp G. Time for some a priori thinking about post hoc testing. Behav Ecol 2008;19:690–3. doi:10.1093/beheco/arn020.

[72] Hikita H, Asai S, Takatsuka T. Absorption of carbon dioxide into aqueous sodium hydroxide and sodium carbonate-bicarbonate solutions. Chem Eng J 1976;11:131–41. doi:10.1016/S0300-9467(76)80035-4.

[73] Shah SR, Parikh RH, Chavda JR, Sheth NR. Application of Plackett-Burman screening design for preparing glibenclamide nanoparticles for dissolution enhancement. Powder Technol 2013;235:405–11. doi:10.1016/j.powtec.2012.10.055.

[74] Kulkarni AA, Joshi JB. Bubble formation and bubble rise velocity in gas-liquid systems: A review. Ind Eng Chem Res 2005;44:5873–931. doi:10.1021/ie049131p.

[75] Zedníková M, Orvalho S, Fialová M, Ruzicka MC. Measurement of volumetric mass transfer coefficient in bubble columns. ChemEngineering 2018;2:1–14. doi:10.3390/chemengineering2020019.

[76] Shaikh A, Al-Dahhan M. A new methodology for hydraulic similarity in bubble columns. Can J Chem Eng 2010;88:503–17. doi:10.1002/cjce.20357.

[77] Binaghi L, Del Borghi A, Lodi A, Converti A, Del Borghi M. Batch and fed-batch uptake of carbon dioxide by *Spirulina platensis*. Process Biochem 2003;38:1341–6. doi:10.1016/S0032-9592(03)00003-7.

5 Optimisation and performance prediction of photosynthetic biogas upgrading using a bubble column

Optimisation and performance prediction of photosynthetic biogas upgrading using a bubble column

Archishman Bose[a,b,†], Richard O'Shea[a,b,*,†], Richen Lin[a,b,†], Jerry D Murphy[a,b,†]

[a]Environmental Research Institute, MaREI Centre, University College Cork, Cork, T23 XE10, Ireland

[b]Department of Civil, Structural and Environmental Engineering, School of Engineering and Architecture, University College Cork, Cork, T12 K8AF, Ireland.

Abstract

Optimising the upgrading of biogas with microalgae in a combined bubble column-photobioreactor setup is currently at a low technology readiness. Alternative to most studies, targeted at optimising the overall bubble column photobioreactor system, optimising the individual components of the system to achieve definitive conclusions on the overall integrated process performance could be beneficial. In this work, performance prediction and optimisation of the least optimised component of photosynthetic biogas upgrading, the bubble column, has been conducted. The liquid inlet pH, liquid inlet alkalinity, superficial gas velocity and liquid to gas flow rate (L/G) ratio were varied using the response surface methodology. Bubble column operations were sufficiently predicted via quadratic models for liquid inlet pHs between 9.4 and 10.2; liquid inlet alkalinities between 1.3 g-inorganic carbon (IC)/L and 2.1 gIC/L; superficial gas velocities between 0.3 cm/s and 0.6 cm/s; and L/G ratios between 0.3 and 0.8. To achieve optimal operations while producing grid quality biomethane (CO_2 < 2.5%$_v$ and O_2 < 1%$_v$) the analysis found that the following conditions must be met: liquid inlet pH between 10 and 10.2; alkalinity between 1.7 gIC/L and 2.1 gIC/L; superficial gas velocities between 0.5 cm/s and 0.6 cm/s; and L/G ratio between 0.6 and 0.7. Based on these results, a perspective on the industrial-scale operation of the integrated bubble column photobioreactor system was developed by estimating the required number of bubble columns and the areal requirement of photobioreactors to upgrade 478 Nm^3/hr of biogas (equivalent to a 1 MW_e biogas plant).

Nomenclature

Symbols	Descriptions
Adj	Adjusted
Alk	Alkalinity [g-IC/L]
ANOVA	Analysis of Variance
CI	Confidence Interval
$C_{O_2,BM}$	Volumetric concentration of O_2 in outlet biomethane [%]
DoF	Degree of Freedom
DW	Dry weight
EBRT	Empty bed residence time [mins]
$Eff_{RE_CO_2}$	Efficiency of CO_2 removal from biogas [%]
G	Biogas flow rate [mL_n/s]
hr	hour
IC	Inorganic carbon
k	kilo
$K_{CO_2}a$	Mean gaseous side mass transfer coefficient [hr^{-1}]
L/G	Liquid to gas flow rate (L/G) ratio
mL_n	Milli-litres normal
MS	Mean squares
N	Molar flow rate (mol/s)
PI	Prediction Interval
s	Seconds
S/N	Signal to noise
SS	Sum of squares
SSE	Sum of square errors
TRL	Technology readiness level
u_G	Superficial gas velocity [cm/s]
Subscripts	
BC	Bubble column
BG	Biogas
BM	Biomethane
in	At the inlet of the bubble column
out	At the outlet of the bubble column

5.1 Introduction

5.1.1 Photosynthetic (microalgal) biogas upgrading

Sustainable and economic substitutes for natural gas are urgently sought to reduce greenhouse gas emissions in hard to abate sectors such as freight transport and heavy industry in the proposed low carbon economy. Biomethane obtained by removing the CO_2 and H_2S from biogas generated by anaerobic digestion (AD) of organic matter is one such alternative [1,2]. However, conventional biogas upgrading techniques using physicochemical methods such as pressure swing absorption and chemical scrubbing require considerable cost and energy [3]. To overcome these challenges, novel technologies such as photosynthetic biogas upgrading are currently being developed [4,5]. In this two-step process, a carbonate-bicarbonate cycle is used to remove CO_2 from biogas and then utilised to grow microalgae [6,7]. The high-value microalgae can improve both the economic and the environmental benefits of the biomethane produced via photosynthetic biogas upgrading [2,4].

A concept diagram of photosynthetic biogas upgrading is shown in Figure 5-1. In the first step, which occurs within a bubble column, CO_2 is absorbed in a carbonate-rich sodium carbonate-bicarbonate buffer solution (pH 9 and above). During this absorption process, bicarbonates are formed via Eq. 5.1 [8] along with a simultaneous drop in the liquid pH. In the following step, the bicarbonate is uptaken by a suitable microalgae species such as *Spirulina platensis* [6] in a connected photobioreactor. During this bicarbonate uptake step, carbonates are also regenerated (Eq. 5.2 [8]) along with a corresponding rise in the pH of the alkaline algal medium. The regenerated carbonate-rich medium can then be recirculated in the bubble column to continue the photosynthetic upgrading process.

Bubble Column: $$CO_2 + H_2O + CO_3^{2-} \rightarrow 2HCO_3^- \quad (5.1)$$

Photobioreactor: $$\left\{ \begin{array}{l} HCO_3^- \xrightarrow{Algae} CO_2 + OH^- \\ HCO_3^- + OH^- \xrightarrow{Medium} CO_3^{2-} + H_2O \end{array} \right\} \quad (5.2)$$

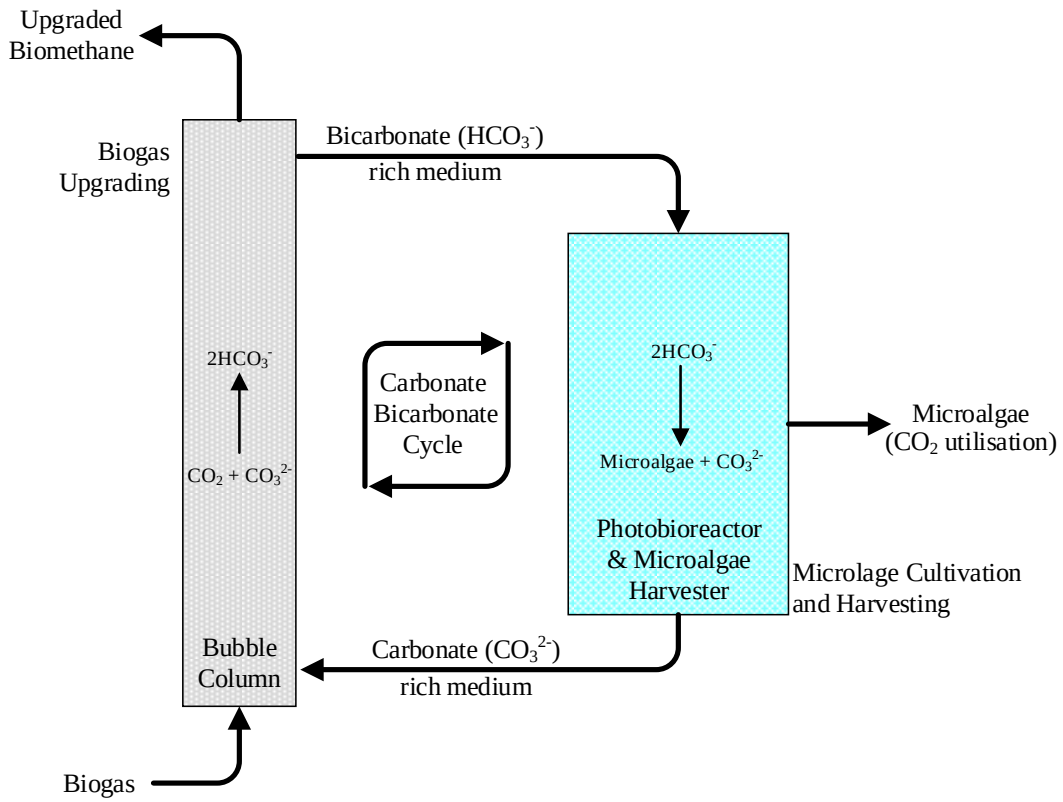


Figure 5-1 Concept diagram of the two-step bubble column-photobioreactor photosynthetic biogas upgrading system using the carbonate bicarbonate cycle for the production of biomethane and microalgae.

5.1.2 Need for optimisation of biogas upgrading in the bubble column

An optimal photosynthetic biogas upgrading system must ensure stable and continuous production of biomethane (volumetric CO_2 and O_2 content less than 2.5% and 1% respectively [9,10]) suitable for injection into a gas grid. In addition, it should also allow for efficient carbon uptake by the microalgae to maximise the desired economic and environmental sustainability of the upgrading system. Most of the current research has focussed on optimising the combined bubble column photobioreactor system. However, a major challenge in this regard is the influence of a large number of operational factors such as pH, the liquid to gas flow rate ratio, the superficial gas velocity, alkalinity, temperature, algal concentration, as well as the type and the cultivation condition of the selected microalgae species [6,8,9,11–13]. The simultaneous impact of such a large number of variables makes the optimisation of the overall system difficult and can lead to sub-optimal operations of either or both of the bubble column or the photobioreactor [8]. In addition, it can lead to variable

conclusions derived from the literature depending on the value of the input variables. For example, although Toledo Cervantes et al. (2017) [13] and Marín et al., (2021) [14] achieved grid quality biomethane (CO_2 < 2.5% and O_2 < 1%) at liquid to gas flow rate (L/G) ratios of 1 and below, Rodero et al. (2020) [15] employing an L/G ratio of 0.8 in a similar setup reported 14.1% CO_2 concentration in upgraded biomethane. Fluctuations due to seasonal [12] and diurnal [9] variations have also been found to significantly impact the results.

To overcome such variability in the research conclusions, a focused approach towards understanding the performance and optimisation of individual sub-systems would be beneficial. This would enable a better selection of the ideal operating conditions of the individual systems while also increasing the effectiveness and robustness of the operation of the overall system. Photosynthetic biogas upgrading allows microalgae to be cultivated and harvested using optimised technologies and conditions. Details of such optimisations are widely available in the literature [16–19]. In contrast, research on optimising bubble columns for CO_2 absorption in carbonate-bicarbonate solutions has primarily focused on performance improvement in either uncatalysed solutions or in solutions using additives (for example methanolamine (MEA) and glycine) without the presence of microalgae [20–22]. These conditions are significantly different from those which would be permissible in the presence of microalgae. For example, based on the tolerable limits of one of the most favourable species for photosynthetic biogas upgrading, *Spirulina platensis* [6], the maximum pH of the algal medium and the working temperature must be below 11 and 40°C respectively [23]. However, as established by Chen et al. (2015) [21], pH values around 12 and 13, along with temperatures above 50°C provide ideal conditions for biogas absorption in an alkaline algal medium. Thus, optimisation of the bubble column for CO_2 absorption in photosynthetic biogas upgrading is a significant research gap.

5.1.3 Objective and novelty

For effective optimisation of the bubble column, both the main and the interactive effects of each of the influential parameters should be understood together with their relative importance on the process outcomes. In this regard, the authors have previously published screening experiments to identify the most critical parameters

affecting bubble column operation for biogas upgrading [8]. Four parameters were identified as the most critical factors in CO_2 removal from biogas: pH and alkalinity of the inlet liquid, superficial gas velocity and L/G ratio. Except for superficial gas velocity, a higher operational value for each of the other factors was found to improve the efficiency of CO_2 removal. However, an increasing L/G ratio also resulted in the highest increase in O_2 stripping from the microalgal solution into the upgraded biomethane. This would make the upgraded biomethane unsuitable for grid injection purposes (O_2 > 1% by volume) at L/G ratios of 1 and above. The work also established that operation with lower algal concentrations (0.05 g-dry weight (DW)/L) is highly desirable as it not only results in an improved CO_2 removal performance and a lower O_2 stripping from the bubble column but also ensures a consistent and robust operation of the bubble column [8].

In the present study, based on the results of the screening experiments, optimisation of the bubble column has been performed to maximise CO_2 removal from biogas together with minimising the O_2 content in the upgraded biomethane. Central Composite Design (CCD) within the Response Surface Methodology (RSM) framework was used as the statistical tool for experimental design and analysis. Experiments were performed on a lab-scale bubble column setup, details of which are provided later. The results, obtained in the form of regression equations, were used to predict and optimise the performance of the bubble column within the design space. Through these results, the authors believe that the significant knowledge gap in the optimisation of the bubble column operations for photosynthetic biogas upgrading, as mentioned above can be overcome. Accordingly, the four primary objectives of the paper have been defined as follows:

i. Analyse the performance of the bubble column for photosynthetic biogas upgrading using statistical design of experiments methods;

ii. Obtain predictive regression equations to describe the bubble column performance;

iii. Optimise the bubble column operations to enable maximum CO_2 removal while minimising the O_2 content in the upgraded biomethane; and

iv. Provide a perspective on the combined operation of the bubble column-photobioreactor setup for effective photosynthetic biogas upgrading.

5.2 Materials and methods

5.2.1 Microorganisms and culture conditions

All experiments were performed with microalgae *Arthrospira* (*Spirulina*) *platensis* SAG 85.79, from Sammlung von Algenkulturen Goettingen (SAG), Germany. The microalgae were grown in 3-litre batches within 5 L Erlenmeyer Flasks with continuous bubbling of air. Temperature and, light were maintained at 20 ± 1°C and 4,000 ± 500 lux with a 16:8 light/dark cycle, respectively. Modified Zarrouk's medium was used as the nutrient medium, the detailed composition of which can be found elsewhere [24]. Cultures were maintained by transferring them into a new medium every three to four weeks to continue cultivation. The microalgae strains were maintained in 100 mL Erlenmeyer flasks, at pHs between 9 and 10.

5.2.2 Experimental setup

Experiments were conducted in a 2 m high, 24 mm diameter absorption (bubble) column made from a clear acrylic tube. The liquid outlet was fixed at a height of 54 cm above the top of the air-stone diffuser used for biogas sparging, based on the results of the screening experiments [8]. Accordingly, the height to diameter (aspect) ratio of the bubble column remained fixed at 22.5. A separate 24 mm diameter, 300 mm high gas-liquid separator was installed at the liquid outlet to minimise the loss of trapped gas bubbles through the outlet liquid. The entire setup was housed in a cabinet capable of maintaining temperature and light intensities between 20 to 40 °C and 2,000 to 6,000 lux respectively. As suggested by Toledo Cervantes et al. (2017) [13], the bubble column was operated under co-current configurations. For this, both biogas and the microalgae solution were supplied to the bottom of the bubble column. A schematic representation of the experimental setup has been provided in Figure 5-2.

In the present study, synthetic biogas consisting of 40% CO_2 and the remainder N_2 without any H_2S was chosen owing to safety considerations [25]. Following previously published research [8,24,26], a low concentration algal solution, measuring 0.1 ± 0.05 gDW/L was used. The algal solution was prepared by diluting 2-3 gDW/L

live microalgae culture with distilled water [8]. The dissolved oxygen (DO) content of the prepared algal solution ranged between 6 to 10 mgO_2/L similar to the values obtained during *Spirulina platensis* cultivation in photobioreactors [27].

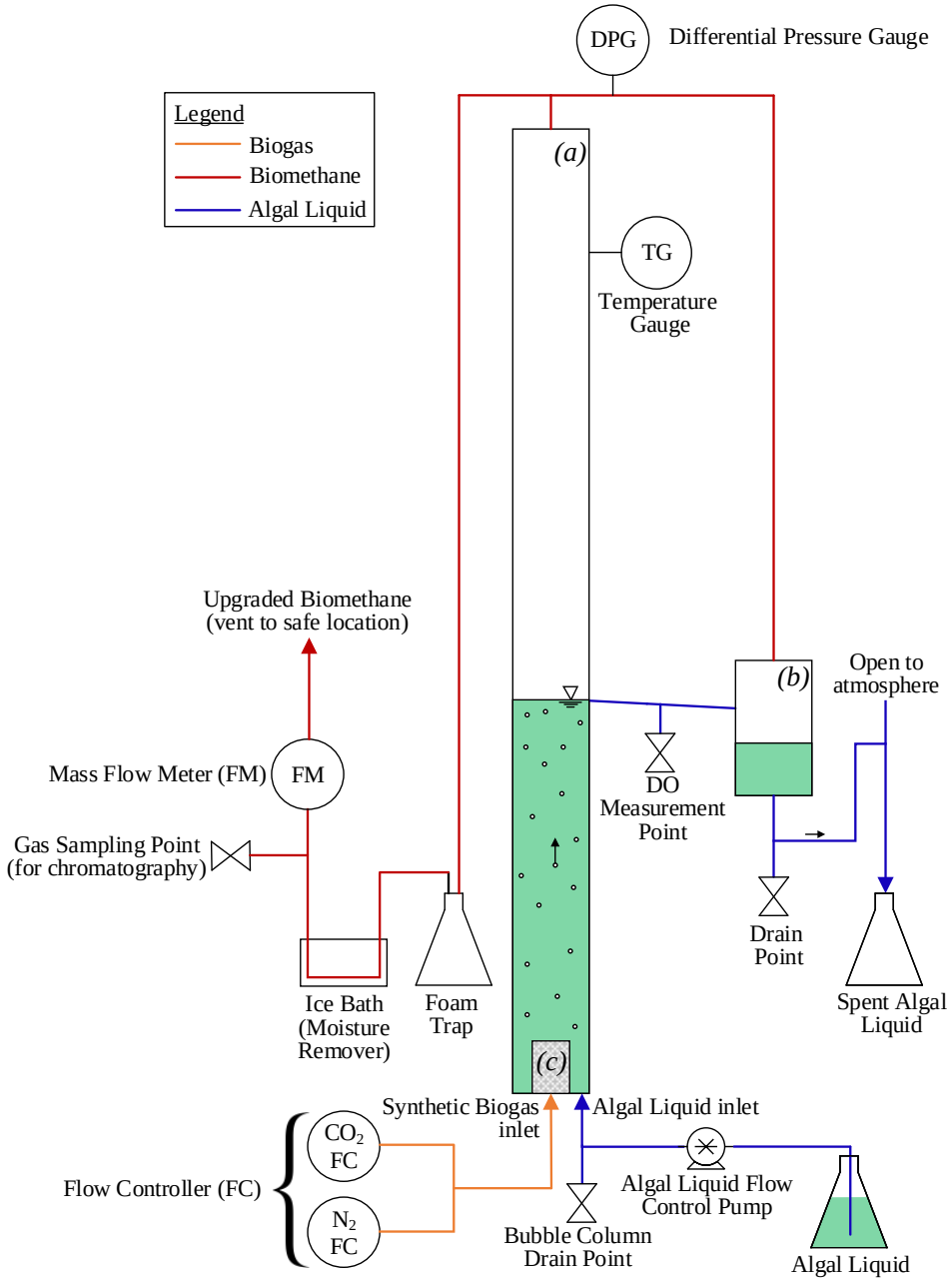


Figure 5-2 Schematic representation of the experimental setup for the optimisation of the bubble column performance (not to scale) in which (a) represents the bubble column, (b) represents the gas-liquid separator and (c) represents the gas diffuser. Adapted from Bose et al. (2021)[8]

The upgraded biomethane, comprising the gases from the bubble column and the gas-liquid separator was first passed through a condensate trap placed in an ice bath to remove excess moisture; flow rate and composition were then measured on a

dry gas basis. The liquid at the outlet of the bubble column was monitored for its pH and subsequently discarded. Further details regarding the lab-scale bubble column setup and its operation can be read from previously published literature [24].

5.2.3 Process responses for optimisation of bubble column

The bubble column should enable a robust and continuous production of grid quality biomethane (CO_2 < 2.5% and O_2 < 1%) irrespective of the fluctuations in the biogas flow rates, the circulating microalgal medium and other uncontrollable environmental factors such as pressure and temperature. Accordingly, O_2 concentration in the upgraded biomethane ($C_{O_2,BM}$) [%] was studied as a process response. CO_2 removal efficiency ($Eff_{RE_CO_2}$) [%] and the overall mass transfer coefficient for CO_2 ($K_{CO_2}a$) [hr^{-1}] were used to assess the performance of CO_2 removal [24,28] given by Eq. 5.3 and Eq. 5.4 respectively where $N_{CO_2,BG}$ is the molar flow rate of CO_2 in the inlet biogas [mol/min], $N_{CO_2,BM}$ is the molar flow rate of CO_2 in the outlet biomethane [mol/min], G is the biogas flow rate [litres/min] and V_{BC} is the undisturbed liquid volume in the bubble column [litres]. While $Eff_{RE_CO_2}$provides a measure of the efficiency of CO_2 removal, the $K_{CO_2}a$ determines the hydrodynamic performance of the bubble column concerning the absorption of CO_2. Optimised biogas upgrading should ensure a high CO_2 removal and maximise the hydrodynamic performance of the bubble column. In addition, to understand and hence predict the overall performance of CO_2 removal from biogas, the pH of the outlet liquid was also assessed as a process response.

$$Eff_{RE_CO_2} = \frac{N_{CO_2,BG} - N_{CO_2,BM}}{N_{CO_2,BG}} \times 100 \quad (5.3)$$

$$K_{CO_2}a = \frac{G}{V_{BC}} \cdot \ln \frac{N_{CO_2,BG}}{N_{CO_2,BM}} \quad (5.4)$$

5.2.4 Experimental design and assessment

5.2.4.1 Design of experiment with Response Surface Method (RSM)

Central Composite Design (CCD), a widely used class of the Response Surface Methodology (RSM) was used to design the optimisation experiments [29–31]. Following discussions in the Introduction, the influence of four independent factors

(design factors), namely, liquid inlet pH (X_1), superficial gas velocity [cm/s] (X_2), L/G ratio (X_3) and alkalinity [gIC/L] (X_4) were studied. The upper and lower limits of pH, L/G ratio and alkalinity are indicated in Table 5-1, with values chosen based on the previous research [8]. An upper limit of 0.75 cm/s for superficial gas velocity was selected in the present study to investigate a larger design space within the operational limits of the bubble column setup [24].

Table 5-1 Ranges and experimental levels of the independent variables for optimising the bubble column performance of photosynthetic biogas upgrading

Factor code	Independent variables	Notation	Ranges and levels				
			Lowest (-2)	Low (-1)	Centre (0)	High (1)	Highest (2)
X_1	Inlet pH	pH	9	9.4	9.8	10.2	10.6
X_2	Superficial Gas Velocity [cm/s]	u_G	0.15	0.30	0.45	0.60	0.75
X_3	L/G Ratio	L/G	0.05	0.3	0.55	0.8	1.05
X_4	Inlet Alkalinity [gIC/L]	Alk	0.9	1.3	1.7	2.1	2.5

Utilising the CCD approach, the design space of each factor was divided into five equally placed levels namely -2 (lowest), -1 (low), 0 (centre), 1 (high) and 2 (highest) [32] as shown in Table 5-1. Following this, a rotatable and orthogonal spherical experimental space was defined to comprise 16 (2^4) factorial points, eight axial points and six replicates of the central point [29]. Thus, a total of thirty experimental trials as compiled in Table S5-1 were conducted. Such an orthogonal and rotatable design not only ensures that the errors equidistant from the centre of the experimental domain are identical [29,33], but also allows the prediction error around the centre point to be reduced [34]. Each trial was replicated three times and all the runs including the replicates were randomised. This allowed the determination of the repeatability and the error of the experiments with minimum systematic bias [35]. Further details about RSM and CCD design can be found in the literature [29,33,36].

5.2.4.2 Model development for prediction of process responses

For each process response ($Eff_{RE_CO_2}$, $K_{CO_2}a$, $C_{O_2,BM}$ and pH_{out}) the experimental data were used to fit regression equations to describe the dependant variables in terms of the independent design factors. In the present work, using the traditional approach, a quadratic (second-order) model was fitted, taking into account the main, quadratic and first-order interactive effects between the design factors

[32,37]. The terms of the model were obtained using sequential backward elimination [29,38], by which, all terms having a statistical significance lesser than 90% ($P > 0.1$) were eliminated from the regression model [29]. The generic form of the quadratic model is given in the following Eq. 5.5.

$$\hat{Y}=B_0+\sum_{i=1}^{4} B_i X_i + \sum_{i=1}^{4} B_{ii} X_i^2 + \sum_{i=1}^{3} \sum_{j=i+1}^{4} B_{ij} X_i X_j + \varepsilon \qquad (5.5)$$

where $\hat{Y}$ indicates the predicted responses (for example $Eff_{RE_CO_2}$), B_0 is the constant of the regression equation, B_i, B_{ii}, and B_{ij} are the coefficients of the linear, quadratic, and two-way interaction terms respectively and ε is the residual error of the fitted model.

One of the fundamental assumptions during such classical model fitting is that the data is normally distributed [39,40]. However, in practice, a completely normal distribution may not be obtained, lowering the goodness of fit of the regression models. For this, in the present study, the quadratic model fitted directly over the experimental data was compared with the quadratic model fit over the transformed responses obtained using the Box Cox power transformation [40]. Using this particular set of transformations given by Eq. 5.6 [41], the process responses (Y) were normalised to Y_T by selecting the optimal transformation exponent λ. The optimal "λ" varying between -3 and 3 corresponded to the lowest standard deviation of the transformed response and were obtained using commercially available statistical software [42].

$$Y_T=\begin{cases}(Y^{\lambda}-1)/\lambda \quad \text{for } \lambda \neq 0 \\ Log_{10}(Y) \quad \text{for } \lambda=0\end{cases} \qquad (5.6)$$

The most appropriate regression model was selected based on assessing multiple statistical comparators. The coefficient of variation (CV) as a measure of the model reproducibility [32] was compared. The model F-values (signifying the predictability of the model in comparison to a model that contains no independent variables), along with the corresponding P-values (indicating the probability of obtaining the F-value by random chance [33,43]) were also evaluated. These values were obtained via a pooled ANOVA, whereby all the terms having statistical significance $P > 0.1$, were pooled into a single error term. An adequate model should not only exhibit a P-value

less than 0.05, but the corresponding F value should also be significantly higher than the critical F value (F_{cr}), where, F_{cr} represents the minimum value of the F-statistic below which the probability of falsely rejecting a true null hypothesis (i.e., the two variances are equal) is α [44]. For k number of predictors in a model and N number of experimental trials, F_{cr} was obtained in the form of $F_{\alpha(k-1,N-k)}$ from standard statistical handbooks using an α of 0.05 (95% confidence level). The robustness of each model was investigated by R^2 (a measure of the agreement between predicted and actual values), adjusted R^2 (a similar measure of the agreement between predicted and actual values, however, adjusted for the number of terms in the model), predicted R^2 (a measure of goodness of prediction) and adequate precision [32,45]. Adequate precision, calculated as the ratio between the range of predicted values in the designed space to the average prediction error provides a measure of the signal to noise ratio of the model and must be higher than 4 [32]. Further model diagnosis via the normal plot of residuals was performed to identify the necessary linearity between the observed residuals and the theoretical percentiles of the normal distribution, essential for an appropriate model.

After the selection of the appropriate model, a pooled ANOVA was constructed. Following best practice, the pooled ANOVA was further utilised to estimate the '*Lack of Fit*' of the simplified model. A '*Lack of Fit*' F value with a corresponding P statistic was evaluated. Models with a '*Lack of Fit*' P-value of more than 0.05 are desired as it indicates no statistically significant lack of fit at the 95% confidence level. The pooled ANOVA was also utilised to identify the statistical significance of each term in the model, while their respective relative importance was obtained via the half-normal probability plot [46].

5.2.4.3 Confirmatory trials for model validation

Confirmatory experiments were performed in triplicate at two chosen levels of the control factors (different from the 30 RSM experimental runs) based on the outcomes of the experimental trials. The mean process response from the confirmatory experiment (Y_{exp}) was compared with the predicted output ($\widehat{Y}$) with the following consideration (Eq. 5.7) [33,47].

$$\widehat{Y} - PI_{95\%} \leq Y_{exp} \leq \widehat{Y} + PI_{95\%} \quad (5.7)$$

where $PI_{95\%}$ represents the prediction interval of the obtained predictions at a 95% confidence level. The detailed equations to calculate the 95% prediction intervals are widely standardised and available in the literature [33,48] and hence have not been elaborated further in the present work.

5.2.4.4 Performance prediction and optimisation

The fitted regression models, following assessment using confirmatory trials, were used to predict the behaviour of each process response against the variations in the independent design factors. The main effects plot was used to study the individual impact of each design factor on the mean outcome of each process response. Statistically significant ($P < 0.05$) interactive effects between two design factors were studied using interactive plots.

The optimisation was performed using contour plots, where the variation in each process response was demonstrated against each pair of statistically significant ($P < 0.05$) independent design variables. The results of the individual optimisation were combined using the overlaid contour plot to obtain the most suitable operating regime of the bubble column, which include: *i)* a CO_2 removal efficiency above 97% to conform to the grid injection standards of less than 2.5% CO_2 in biomethane; *ii)* a simultaneous maximisation of the $K_{CO_2}a$, i.e., the hydrodynamic performance of the bubble column, and *iii)* O_2 concentration in the biomethane less than 0.8%. Although the permitted O_2 concentration in biomethane is 1%, the conservative value of 0.8% was selected to account for the uncertainties of experimentation and hence obtain a more robust research outcome. To develop the overlaid contour plots, superficial gas velocity and L/G ratio were used as the independent design factors while the liquid inlet pH and alkalinity were fixed at the optimal conditions. This was affected since the L/G ratio can be more easily controlled with respect to actual operation by valves and flow controllers in contrast to the liquid inlet pH and alkalinity which are most often influenced by the performance of the photobioreactor (Eq. 5.2). The results were further used to develop a perspective on the control strategies of the bubble column operations in photosynthetic biogas upgrading for consistent and efficient production of grid quality biomethane overcoming system fluctuations.

5.2.4.5 Perspective on integration with photobioreactors for combined operations

A hypothetical photosynthetic biogas upgrading system was considered to develop a perspective on the significance of the results in terms of integrating photobioreactors with the optimised bubble column for combined operation. A biogas flow of 478 Nm^3/hr was considered, equivalent to the scale of a 1 MW_e biogas based electric plant [6]. The biogas was assumed to contain 40% CO_2 and a flat plate photobioreactor configuration was considered as per previous research [6]. The potential number and size of the bubble columns when operating under normal temperature and pressure (20°C and 1 atm), the hydraulic retention time (HRT) within the photobioreactor and the areal footprint of the photobioreactor were evaluated.

5.2.5 Analytical procedures

All measurements were conducted under steady-state conditions characterised by both a constant gas flow rate and a constant pH of the liquid at the outlet of the gas-liquid separator (5% or less average variation) for a minimum of 120 seconds each. The upgraded biomethane was collected from the gas line located between the condensate trap and mass flow meter (Bronkhorst® F101D Low-ΔP-Flow Thermal Mass Meter) to minimise errors in measurements [24]. Biomethane composition was subsequently analysed using a gas chromatograph (GC; Agilent® 7890B, USA) equipped with a thermal conductivity detector and a 5A column. As the mass flow rate of the upgraded biomethane was measured in terms of equivalent nitrogen, [mL_nN_2/min], an online gas converter tool by Fluidat® (Bronkhorst®) was used to convert the recorded flow to the volumetric flow in terms of the gas composition measured by chromatography. To account for a noticeable air (N_2 and O_2) ingression by diffusion through the gas tubing, a further three-point correction step was employed [24]. Accordingly, N_2 was blown through the experimental setup at three different flow rates (25, 50 and 100 mL_n/min) corresponding to the N_2 flow within synthetic biogas used in the experiments and the respective outlet gas composition and flow rates were measured. The additional O_2 and N_2 flow rates obtained were then subtracted from the respective biomethane component flow rates to calculate the actual biomethane composition and flow rate.

pH and DO were measured using a handheld pH meter (VWR® MD 8000H Multi-Parameter Meter) fitted with respective interchangeable probes (pHenomenal VWR® pH / ORP sensor/ pHenomenal VWR® OPOX 11-3 sensor). Alkalinity was measured by titrating up to pH 4.5 in a Titronic® Universal Titrator using Method No. 2320 B of APHA [49].

5.2.6 Statistical analysis

Minitab® software version 19 (Minitab LLC., Pennsylvania, USA) was used to design, replicate and randomise the Central Composite Design. The results obtained were analysed using Design Expert (Stat-Ease® Inc, Minneapolis, USA) statistical software. Similar to that discussed in the previous chapter Section 4.2.3.4, a confidence level of 95% ($P < 0.05$) was selected for asserting statistical significance. However, following similar arguments, all P-values were reported to prevent biased interpretation and misuse of the experimental data in the future [50,51].

5.3 Results and discussions

5.3.1 Validation of the bubble column operations

Table 5-2 records the outcomes for CO_2 removal efficiency ($Eff_{RE_CO_2}$), CO_2 mass transfer coefficient ($K_{CO_2}a$), O_2 concentration in biomethane ($C_{O_2,BM}$) and liquid outlet pH (pH_{Out}) corresponding to each of the thirty experimental runs. Within the experimental domain, $Eff_{RE_CO_2}$ varied between 17.69% and 99.64% while the $K_{CO_2}a$ ranged between 5.90 hr^{-1} to 165.65 hr^{-1}. These values are in close agreement with previously published results [8,52]. Varying pH, L/G ratio and alkalinity between 9 and 10.5, 0.2 and 1 and 1 gIC/L and 2.5 gIC/L respectively, Bose et al. (2021) [8] reported a similar range of CO_2 removal efficiencies varying between 19.29% and 100%. Within that domain, the highest CO_2 mass transfer coefficient was 97.64 hr^{-1}. The results also match well with those reported by Chen et al., (2015) [28], who observed that the CO_2 mass transfer coefficient ranged between 54hr^{-1} and 154.8hr^{-1} as the liquid inlet pH and L/G ratio varied between 9 and 10.5 and 0.05 and 0.16 respectively. As discussed in other literature [24], such comparisons with sodium hydroxide are appropriate as the CO_2 absorption reaction is primarily driven by $[OH]^-$ ions in solution irrespective of the chemical species from which they are derived [21,53]. On the other hand, as can be seen from Table 5-2, O_2 concentrations above

0.9% in the upgraded gas were consistently obtained for L/G ratios above 0.8. Indeed, when compared with previously published work by the authors [8] which obtained consistent O_2 concentration above 0.8% at L/G ratios of 1, a close agreement between the results can be concluded. The results also match the outcomes of Toledo-Cervantes et al. (2017) [13], who recorded similar consistent O_2 concentrations above 1% for L/G ratios higher than 1. These comparisons thus provided sufficient evidence to validate both the experimental setup and the results obtained therefrom allowing for further statistical assessments of the system to be conducted.

5.3.2 Model fitting and statistical assessments

Quadratic models developed using stepwise backward elimination of factors having P values greater than 0.1 with and without data transformation were studied for their goodness of fit to the experimental data. The selected quadratic models for $Eff_{RE_CO_2}$, $K_{CO_2}a$, $C_{O_2,BM}$ and pH_{out} are given by Eq. 5.8-5.11 respectively. To ensure hierarchy, the main effects of each statistically significant interaction were also included in the model.

$$Eff_{RE_CO_2} = [-6.393\cdot10^7 + 1.125\cdot10^7 pH - 2.601\cdot10^5 u_G + 1.6\cdot10^7 L/G + 3.057\cdot10^6 Alk - 1.354\cdot10^6 pH\cdot L/G - 2.234\cdot10^5 pH\cdot Alk - 4.90\cdot10^5 pH^2 - 1.825\cdot10^6 L/G^2 - 2.135\cdot10^5 Alk^2]^{(1/3)} \quad (5.8)$$

$$K_{CO_2}a = [-389.189 + 68.726pH + 17.124u_G + 94.707L/G + 8.058Alk - 7.099pH\cdot L/G - 3.076pH^2 - 11.985u_G^2 - 17.459L/G^2 - 1.912Alk^2]^2 \quad (5.9)$$

$$C_{O_2,BM} = -13.497 + 2.532pH - 1.328u_G + 1.918L/G + 1.641Alk - 0.188pH\cdot Alk + 0.396u_G\cdot Alk - 0.112pH^2 - 0.908L/G^2 \quad (5.10)$$

$$pH_{out} = [-16{,}639.963 + 2{,}946.005pH + 931.105L/G + 890.589Alk - 132.128pH^2 - 539.139L/G^2 - 215.672Alk^2]^{(1/3)} \quad (5.11)$$

Table 5-2 Results of the process responses against each setting of operating condition designed using the central composite design for optimisation and prediction of bubble column operations in photosynthetic biogas upgrading

Experiment Order	Uncoded Variables				CO_2 removal efficiency ($Eff_{RE_CO_2}$) [%]	Mean mass transfer coefficient for CO_2 ($K_{CO_2}a$) [hr^{-1}]	O_2 concentration in biomethane ($C_{O_2,BM}$) [%]	Liquid outlet pH (pH_{OW})
	pH (X_1)	u_G (X_2)	L/G (X_3)	Alk(X_4)				
1	9.8	0.45	0.55	0.9	85.39% ± 0.87%	58.34 ± 1.83	0.78% ± 0.10%	7.77 ± 0.08
2	9.8	0.75	0.55	1.7	94.20% ± 0.97%	144.57 ± 9.00	0.51% ± 0.02%	9.21 ± 0.02
3	10.6	0.45	0.55	1.7	99.55% ± 0.15%	165.65 ± 10.98	0.62% ± 0.07%	9.82 ± 0.03
4	9.8	0.45	1.05	1.7	98.38% ± 0.23%	125.22 ± 4.47	0.94% ± 0.05%	9.45 ± 0.04
5	9.8	0.45	0.55	1.7	98.27% ± 0.47%	123.95 ± 7.73	0.66% ± 0.08%	9.10 ± 0.02
6	9.8	0.15	0.55	1.7	99.64% ± 0.34%	66.72 ± 18.17	0.94% ± 0.03%	9.17 ± 0.06
7	9.8	0.45	0.55	2.5	99.14% ± 0.56%	150.39 ± 18.91	0.71% ± 0.01%	9.33 ± 0.05
8	9.8	0.45	0.05	1.7	17.69% ± 0.89%	5.90 ± 0.33	0.05% ± 0.01%	7.64 ± 0.02
9	9.8	0.45	0.55	1.7	97.84% ± 0.18%	116.31 ± 2.53	0.67% ± 0.04%	9.18 ± 0.06
10	9	0.45	0.55	1.7	63.54% ± 3.45%	30.71 ± 2.97	0.68% ± 0.06%	7.62 ± 0.03
11	10.2	0.6	0.3	1.3	94.99% ± 0.30%	120.99 ± 2.46	0.35% ± 0.01%	8.96 0.02
12	9.8	0.45	0.55	1.7	97.83% ± 0.32%	116.43 ± 4.26	0.68% ± 0.01%	9.25 ± 0.03
13	10.2	0.3	0.8	1.3	99.02% ± 0.33%	94.59 ± 7.03	0.98% ± 0.06%	9.32 ± 0.57
14	10.2	0.6	0.8	2.1	97.57% ± 0.13%	150.24 ± 2.15	0.73% ± 0.01%	9.87 ± 0.01
15	9.4	0.3	0.8	2.1	97.52% ± 0.16%	74.69 ± 1.35	0.97% ± 0.07%	8.85 ± 0.02
16	10.2	0.3	0.3	2.1	98.15% ± 0.15%	80.64 ± 1.70	0.42% ± 0.03%	9.38 ± 0.06
17	9.4	0.6	0.8	1.3	83.61% ± 0.29%	73.07 ± 0.72	0.62% ± 0.01%	8.23 ± 0.00
18	9.8	0.45	0.55	1.7	97.63% ± 0.11%	113.43 ± 1.46	0.61% ± 0.01%	9.40 ± 0.38
19	9.4	0.6	0.3	2.1	63.63% ± 1.12%	40.88 ± 1.26	0.29% ± 0.02%	7.90 ± 0.12
20	9.4	0.3	0.3	1.3	49.68% ± 0.88%	13.87 ± 0.35	0.46% ± 0.08%	7.55 ± 0.01
21	9.4	0.6	0.3	1.3	49.91% ± 0.48%	27.93 ± 0.39	0.20% ± 0.03%	7.48 ± 0.02
22	9.4	0.3	0.3	2.1	64.59% ± 0.55%	20.97 ± 0.31	0.38% ± 0.04%	7.83 ± 0.11
23	9.8	0.45	0.55	1.7	97.23% ± 0.16%	108.76 ± 1.82	0.72% ± 0.10%	9.17 ± 0.05
24	10.2	0.3	0.8	2.1	99.01% ± 0.26%	94.04 ± 5.79	0.87% ± 0.08%	9.85 ± 0.04
25	9.4	0.3	0.8	1.3	92.80% ± 0.60%	53.22 ± 1.74	0.92% ± 0.07%	8.21 ± 0.03
26	9.8	0.45	0.55	1.7	98.38% ± 0.32%	125.47 ± 5.65	0.84% ± 0.09%	9.18 ± 0.05
27	10.2	0.6	0.3	2.1	95.53% ± 0.27%	125.64 ± 2.47	0.28% ± 0.05%	9.43 ± 0.05
28	10.2	0.6	0.8	1.3	96.75% ± 0.30%	138.63 ± 3.93	0.74% ± 0.03%	9.73 ± 0.03
29	9.4	0.6	0.8	2.1	92.39% ± 0.33%	104.12 ± 1.78	0.78% ± 0.03%	8.91 ± 0.01
30	10.2	0.3	0.3	1.3	98.05% ± 0.08%	79.54 ± 0.83	0.49% ± 0.04%	8.95 ± 0.02

The detailed statistical comparators for both the selected and the rejected models, along with the Box Cox power transform plots to obtain the optimal exponent of transformation, λ, are provided in Table S5-2 and Figure S5-1 respectively. The statistical characteristics of only the selected models are summarised in Table 5-3. As can be followed from Eq. 5.8 – Eq. 5.11 and the degrees of freedom listed in Table 5-3, the models for describing both $Eff_{RE_CO_2}$ and $K_{CO_2}a$ consists of ten terms (nine involving design factors and one constant). The corresponding number of terms in the models for $C_{O_2,BM}$ and pH_{out} are eight and seven respectively.

Table 5-3 Statistical summaries of the models chosen to describe the behaviour of the four process responses selected to describe the performance of the bubble column operations in photosynthetic biogas upgrading.

Process Response	Quadratic Regression Model	Statistical Comparators							
		DoF*	CV† [%]	F value	P value	R^2	Adjusted R^2	Predicted R^2	Adequate Prediction
$Eff_{RE_CO_2}$	with tnf$^{\Delta}$ (λ = 3)	9	8.14	81.54[a]	<0.001	0.974	0.962	0.899	27.8841
$K_{CO_2}a$	with tnf (λ = 0.5)	9	8.77	35.35[a]	<0.001	0.941	0.914	0.771	20.9106
$C_{O_2,BM}$	without tnf	7	8.11	78.77[b]	<0.001	0.968	0.956	0.921	36.2248
pH_{out}	with tnf (λ = 3)	6	4.85	114.85[c]	<0.001	0.968	0.959	0.915	34.863

*DoF: Degrees of freedom; †CV: Coefficient of Variance; $^{\Delta}$tnf: data transformation
Critical F (F_{cr}) values: [a]$F_{0.05(9,20)}$ = 2.393; [b]$F_{0.05(7,22)}$ = 2.464; [c]$F_{0.05(6,23)}$ = 2.528

For each selected model, the coefficient of variance (CV) [%] is below 10% indicating their acceptable reproducibility of results [54]. The F values for each model are also much higher than the critical F values (Table 5-3) This, along with the respective P values of less than 0.001 verifies the statistical significance of each of the selected regression models. Simultaneously, R^2 values above 0.9 for each model also indicates a good linear agreement between the observed and the predicted data [55]. Additionally, the adjusted R^2 values are fairly high with a close agreement with the predicted R^2 values (less than 0.2 difference). This shows that the models are acceptable and are not cluttered by too many terms that are not statistically significant ($P > 0.05$) [56]. The adequate precision value larger than 4 for each model also confirms the resilience of the models against the average prediction error. A fairly linear normal plot of residuals obtained by plotting the observed residuals against the

theoretical percentiles of the normal distribution (Figure S52) further indicates model acceptability.

Table 5-4 Summary of the pooled ANOVA assessment of the fitted quadratic models for the four process responses selected to describe the bubble column performance for photosynthetic biogas upgrading

$Eff_{RE_CO_2}$					
Source	**DoF†**	**Sum of Squares (10^{11})**	**Mean Square (10^{11})**	**F value**	**Pvalue**
Model	9	27.5	3.05	81.54	< 0.001
pH*	1	2.32	2.32	62.06	< 0.001
u_G*	1	0.37	0.37	9.77	0.0053
L/G*	1	4.19	4.19	111.97	< 0.001
Alk*	1	0.37	0.37	9.96	0.005
pH vs L/G*	1	2.93	2.93	78.45	< 0.001
pH vs Alk*	1	0.21	0.21	5.47	0.0299
pH^{2*}	1	1.72	1.72	46.03	< 0.001
L/G^{2*}	1	3.64	3.64	97.43	< 0.001
Alk^{2*}	1	0.33	0.33	8.74	0.0078
Residual	20	0.75	0.04		
Lack of Fit	15	0.74	0.05	19.18	0.0021
Pure Error	5	0.013	0.003		
Corrected Total	29	28.2			
$K_{CO_2}a$					
Source	**DoF**	**Sum of Squares**	**Mean Square**	**F value**	**P value**
Model	9	207.07	23.01	35.35	< 0.001
pH*	1	79.01	79.01	121.39	< 0.001
u_G*	1	21.69	21.69	33.33	< 0.001
L/G*	1	52.73	52.73	81.02	< 0.001
Alk*	1	9.3	9.3	14.29	0.0012
pH vs L/G *	1	8.06	8.06	12.39	0.0022
pH^{2*}	1	6.64	6.64	10.21	0.0046
u_G^2	1	1.99	1.99	3.06	0.0954
L/G^{2*}	1	32.66	32.66	50.18	< 0.001
Alk^2	1	2.57	2.57	3.95	0.0609
Residual	20	13.02	0.6509		
Lack of Fit	15	12.08	0.8055	4.31	0.0576
Pure Error	5	0.9354	0.1871		
Corrected Total	29	220.08			

$C_{O_2,BM}$					
Source	**DoF**	**Sum of Squares**	**Mean Square**	**F value**	**P value**
Model	8	1.62	0.2028	78.77	< 0.0001
pH	1	0.0006	0.0006	0.233	0.6343
u_G *	1	0.2321	0.2321	90.13	< 0.0001
L/G*	1	1.27	1.27	493.11	< 0.0001
Alk	1	0.0013	0.0013	0.5243	0.477
pH vs Alk*	1	0.0144	0.0144	5.59	0.0277
u_G vs Alk	1	0.009	0.009	3.51	0.0752
pH^2	1	0.0092	0.0092	3.57	0.0728
L/G^2	1	0.0915	0.0915	35.54	< 0.001
Residual	21	0.0541	0.0026		
Lack of Fit	16	0.0455	0.0028	1.67	0.299
Pure Error	5	0.0085	0.0017		
Corrected Total	29	1.68			

pH_{out}					
Source	**DoF**	**Sum of Squares (10^5)**	**Mean Square (10^5)**	**F value**	**P value**
Model	6	8.17	1.36	114.85	< 0.001
pH*	1	4.88	4.88	411.1	< 0.001
L/G*	1	1.71	1.71	144.56	< 0.001
Alk*	1	0.95	0.95	80.13	< 0.001
pH^{2*}	1	0.12	0.12	10.55	0.0035
L/G^{2*}	1	0.32	0.32	26.81	< 0.001
Alk^{2*}	1	0.33	0.33	28.12	< 0.001
Residual	23	0.27	0.01		
Lack of Fit	18	0.24	0.01	1.91	0.2447
Pure Error	5	0.03	0.007		
Corrected Total	29	8.44			

* Denotes the statistically significant ($P < 0.05$) sources (design factors).
† DoF signifies Degrees of Freedom

The '*Lack of Fit*' statistic for each model was obtained from the pooled ANOVA presented in Table 5-4. As can be noticed, except for the regression equation for CO_2 removal efficiency, none of the models shows a significant lack of fit ($P > 0.05$), confirming their statistical adequacy in predicting the design space. On the other hand, the '*Lack of Fit*' for the model predicting CO_2 removal efficiency is significant ($P = 0.002$). This signifies either the lack of a significant term in the model or false detection of a significant '*Lack of Fit*' due to an extremely small pure error (error due

to variability in experimentation) [57]. Upon further investigation into the pooled ANOVA of the model for $Eff_{RE_CO_2}$ an extremely small pure error relative to the error due to the '*Lack of Fit*' was observed. To investigate if a false detection is indeed the case in the present context, a plot of predicted versus the experimental values was used to verify the physical significance of the model and hence to confirm its goodness of fit in the designed space.

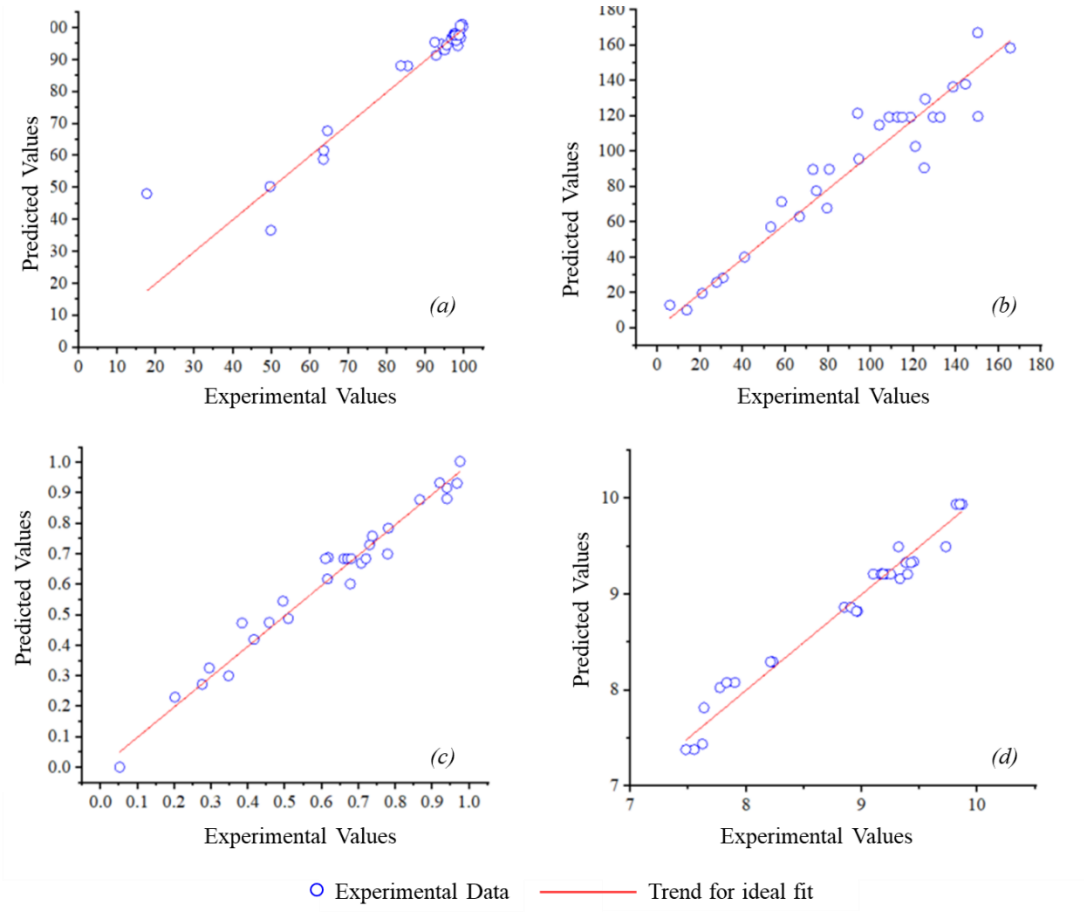


Figure 5-3 Predicted vs actual plot of the regression models for (a) $Eff_{RE_CO_2}$; (b) $K_{CO_2}a$; (c) $C_{O_2,BM}$; and (d) pHout. The circular dots indicate the experimental data while the lines indicate the trend for ideally fit data.

As can be seen from Figure 5-3a, the model for $Eff_{RE_CO_2}$ deviates significantly from the actual results at lower values of CO_2 removal efficiencies. From Table 5-2, this region could be identified to be those which are characterised by the lowest (-2) setting of pH and L/G ratio (9 and 0.05 respectively). A closer survey also shows that the model somewhat underpredicts at the highest (+2) settings of the design space, especially for the factors pH and L/G ratio (10.6 and 1.05 respectively). However, for the remainder of the design space bounded between the low (-1) and high (+1) settings

of each design factor, the prediction remains fairly accurate. Interestingly, this also contains the region of interest characterised by $Eff_{RE_CO_2}$ greater than 90% and $C_{O_2,BM}$ less than 0.8%. Indeed, then, as all other measures of goodness of fit were satisfied by the selected regression model of $Eff_{RE_CO_2}$ (Eq. 5.7), it was considered adequate and worthy of further investigation.

An investigation into the plot of predicted versus experimental values for each of the other process responses revealed a fair match between the two (Figure 5-3b-d). However, to ensure uniformity in prediction and optimisation between all the process responses, in the present study, the design space bounded by the coded values of -1(low) and +1 (high) of the design variables was considered henceforth. This corresponds to the region between a pH of 9.4 and 10.2, 0.3 cm/s and 0.6 cm/s of superficial gas velocity, 0.3 and 0.8 for L/G ratio and 1.3 gIC/L and 2.1 gIC/L for alkalinity. Beyond these limits, further experimentation would be required to develop more accurate predictive models.

5.3.3 Verification of response surface models

The regression models for each process response were verified using confirmatory trials at pH, superficial gas velocity and alkalinity of 10.1, 0.3 cm/s and 2 gIC/L respectively. The L/G ratio was varied at two points, namely 0.4 and 0.6. These settings are different from the thirty experimental trials developed using RSM.

The results from the confirmatory trials are shown in Table 5-5. A good agreement between the predicted and the observed values could be seen as most of the observed process responses had a mean value similar to the predicted outcome. The output being a continuous variable, a higher than 100% CO_2 removal efficiency was predicted for the L/G ratio of 0.6, which in effect indicates a complete CO_2 removal. Indeed, the observed CO_2 removal efficiency of 99.93% confirmed this prediction. Although the predicted $K_{CO_2}a$ for L/G ratio 0.6 was considerably lower than the mean observed response, it was still contained within the 95% prediction interval. As described in Section 5.2.4.3, this was sufficient to signify the suitability of the model in predicting the process responses in the selected design space.

Table 5-5 Results of the confirmatory experiments and their comparison with the predicted values at two different L/G ratios for a liquid inlet pH of 10.1, superficial gas velocity of 0.3 cm/s and, alkalinity of 2 gIC/L.

Experimental condition	**Data type**	**$Eff_{RE_CO_2}$**	**$K_{CO_2}a$**	**$C_{O_2,BM}$**	**pH_{out}**
L/G 0.4	Observed	99.41 ± 0.001	103.87 ± 1.88	0.54 ± 0.000	9.50 ± 0.02
	Predicted*	99.83 (95.01,104.31)	102.408 (68.97,142.43)	0.58 (0.46,0.69)	9.44 (9.15,9.71)
L/G 0.6	Observed	99.93 ± 0.001	166.16 ± 28.88	0.75 ± 0.000	9.79 ± 0.02
	Predicted*	103.15 (92.62,107.31)	126.085 (88.76,169.94)	0.78 (0.66,0.89)	9.72 (9.45,9.98)

*The values in the parenthesis indicate the upper and lower bound of the Prediction Interval with 95% confidence.

5.3.4 Analysis of design factors

5.3.4.1 Main effects

Based on the models developed using the response surface method, the main effects of the design factors on each process have been compiled in Figure 5-4. The statistical significance of each variation was obtained from the pooled ANOVA in Table 5-4, while their relative importance was evaluated through a half-normal probability plot in Figure S5-3. The L/G ratio was obtained as the most influential design factor followed by pH and alkalinity. This is in contrast to the previously published screening experiments, whereby pH was shown to be the most impactful factor and as such more impactful than the L/G ratio [8]. This could be due to the fact, that in the present study, a wider range of L/G ratios (0.05 to 1.05) was evaluated in comparison to the range investigated in the previous work (0.2 to 1). Indeed, as can be seen from the results of the individual runs in Table 5-2, the lowest L/G ratio (setting of 0.05) also caused the lowest CO_2 removal efficiency from biogas ($Eff_{RE_CO_2}$ of 17.29%). Following Figure 5-4, it can be observed that for both pH and alkalinity, a higher setting led to a diminished relative improvement in $Eff_{RE_CO_2}$. However, increasing the L/G ratio beyond 0.7 was found to lead to a slight drop in the CO_2 removal efficiencies. To explain this outcome, it must be understood that under co-current configuration, an increase in the superficial liquid velocity tends to accelerate the rising gas bubbles. Under relatively low superficial liquid velocities, this effect is often negligible [58,59]. However, in the current operations, a high L/G ratio (of the order of 1) indicates similar gas and liquid superficial velocities, which would make

the latter have a significant influence on the hydrodynamics of the bubble column [24,59]. Indeed, then, greater bubble accelerations under higher L/G ratios would tend to decrease the gas-liquid contact time. This, in turn, would cause a drop in the amount of CO_2 removed from biogas and hence a decrease in the corresponding $Eff_{RE_CO_2}$. This effect of the decrease in $Eff_{RE_CO_2}$ from diminished gas-liquid contact time can also be seen from the impact of superficial gas velocity, whereby a higher superficial gas velocity, leading to a lower gas residence time within the bubble column (also given by the empty bed residence time or EBRT) results in an almost linear drop in $Eff_{RE_CO_2}$ (Figure 5-4).

Similar profiles to that of $Eff_{RE_CO_2}$ were obtained for pH, L/G ratio and alkalinity for the CO_2 mass transfer coefficient ($K_{CO_2}a$). As can be visualised from Figure 5-4, while a diminishing improvement in $K_{CO_2}a$ occurs for both pH and alkalinity, a drop in the response beyond an L/G ratio of 0.7 takes place. The higher liquid flow rate leading to greater acceleration of the gas bubbles and less gas-liquid contact time could be considered a reason for this observation. In contrast to $Eff_{RE_CO_2}$ however, the increase in superficial gas velocity can be seen to increase $K_{CO_2}a$, indicating a better hydrodynamic performance at higher gas flow rates. The trends match well to those reported by Chen et al. (2015) [28] and Besagni et al. (2019) [60]. However, this is in contrast to the earlier work by the authors [8], where, with an increase in superficial gas velocity, a decrease in $K_{CO_2}a$ was observed. This could be explained by the different superficial gas velocities studied in the two works, resulting in different hydrodynamic conditions existing between the bubble column. However, since the aim of the technology is to increase the superficial gas velocity, the current results indicate the operations of the bubble column under more practical scenarios.

An increase in all of the following variables (pH, L/G ratio and alkalinity) results in a higher liquid outlet pH from the bubble column (Figure 5-4). However, as confirmed from the half-normal probability plot (Figure S5-3), the liquid inlet pH impacts it the highest, followed by the L/G ratio and alkalinity. Interestingly, these trends are similar to those obtained for the CO_2 removal efficiency. This indicates, that a higher liquid outlet pH, resulting in a higher average pH within the bubble column would enable better and more efficient removal of CO_2 from biogas. Similar results have been previously been described in the literature [24].

L/G ratio followed by superficial gas velocity are the two most statistically significant ($P < 0.05$) design factors to affect the $C_{O_2,BM}$ derived by O_2 stripping from the microalgal medium. Similar to those observed in multiple earlier works [6,8,13,61], a higher L/G ratio generally increases $C_{O_2,BM}$. The current results indicate an almost linear trend in this increase. Although an increase in superficial gas velocity in a co-current configuration leads to an increase in the volume of oxygen stripped into biomethane [62], a fixed bubble column diameter ensures a proportional increase in the gas flow rate through the bubble column. These combined effects can be used to explain the almost linear decrease in $C_{O_2,BM}$, with an increase in the superficial gas velocity.

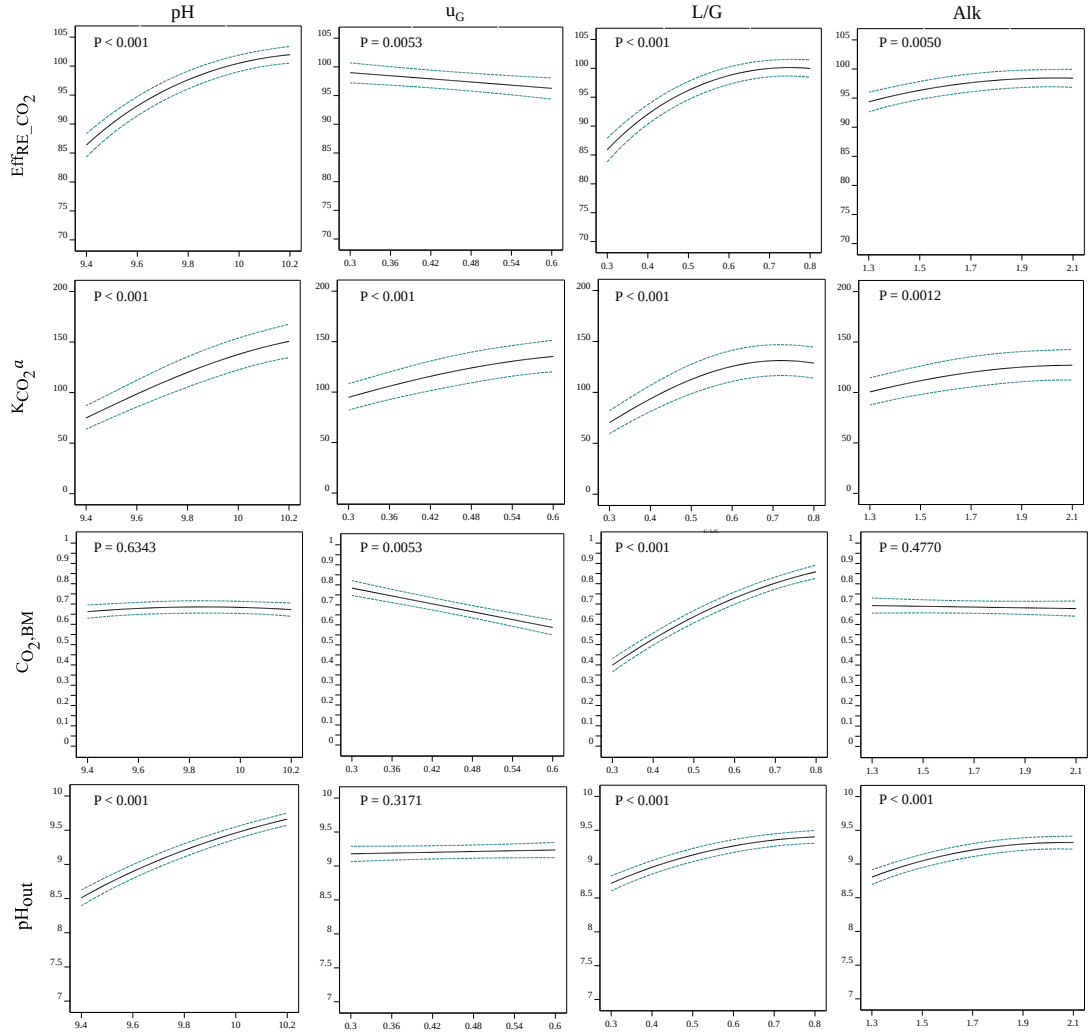


Figure 5-4 Main effects plot of the mean responses of $Eff_{RE_CO_2}$, $K_{CO_2}a$, $C_{O_2,BM}$ and pH_{out} against the four independent design factors, namely, liquid inlet pH, superficial gas velocity, L/G ratio and liquid inlet alkalinity. Except for the factor that is being varied, all the other factors are placed at their centre points, namely, pH at 9.8; u_G at 0.45 cm/s, L/G at 0.55 and Alk at 1.7 gIC/L

5.3.4.2 Interactions

The interactions between pH and L/G ratio and pH and alkalinity were found to have a statistically significant ($P < 0.05$) impact on $Eff_{RE_CO_2}$. As can be seen from Figure 5-5, at lower pH levels (pH 9.4, factor level of "-1"), a higher L/G ratio is required to ensure greater $Eff_{RE_CO_2}$. However, at higher pH levels (pH 10.2, factor level of "+1"), a consistently high $Eff_{RE_CO_2}$ greater than 90% can be achieved irrespective of the L/G ratios. Thus, increased flexibility in operation could be envisaged at a higher inlet pH setting**.** However, unlike the former, its location near the 45° line in the half-normal probability plot indicates a minor interaction between pH and alkalinity (Figure S5-3). This can also be visualised from Figure 5-5b, whereby a much small variation in the $Eff_{RE_CO_2}$could be visualised from the changes between pH and alkalinity. Nonetheless, at lower pH levels, similar to the L/G ratio, higher alkalinity would be required to ensure better removal of CO_2. However, when operated at pH levels of 10.2 (factor level of "+1"**)**, efficient removal of CO_2 can be obtained irrespective of the variations in alkalinity between 1.3 gIC/L and 2.1 gIC/L.

Inspecting the statistically significant interactive effect of pH and L/G ratio on the CO_2 mass transfer coefficient ($P = 0.002$), a similar argument with regards to the interactive effect between pH and L/G ratio for $Eff_{RE_CO_2}$can be made. However, unlike that of $Eff_{RE_CO_2}$ even at a higher pH, a high L/G ratio would play a significant role in determining $K_{CO_2}a$. Although neither pH nor alkalinity has a significant main effect on $C_{O_2,BM}$, a statistically significant ($P = 0.028$) crossover interaction was noticed between the two [63]. For lower alkalinity (alkalinity 1.3 gIC/L, factor level "-1"), $C_{O_2,BM}$ would increase with a corresponding increase in the pH. However, for a higher setting of alkalinity (alkalinity 2.1 gIC/L, factor level "+1"), a reverse effect of pH on $C_{O_2,BM}$ is seen, whereby the O_2 concentration in biomethane decreased with an increase in the pH of the inlet liquid. These effects further confirm the necessity to optimise the bubble column operations by simultaneously varying multiple design factors.

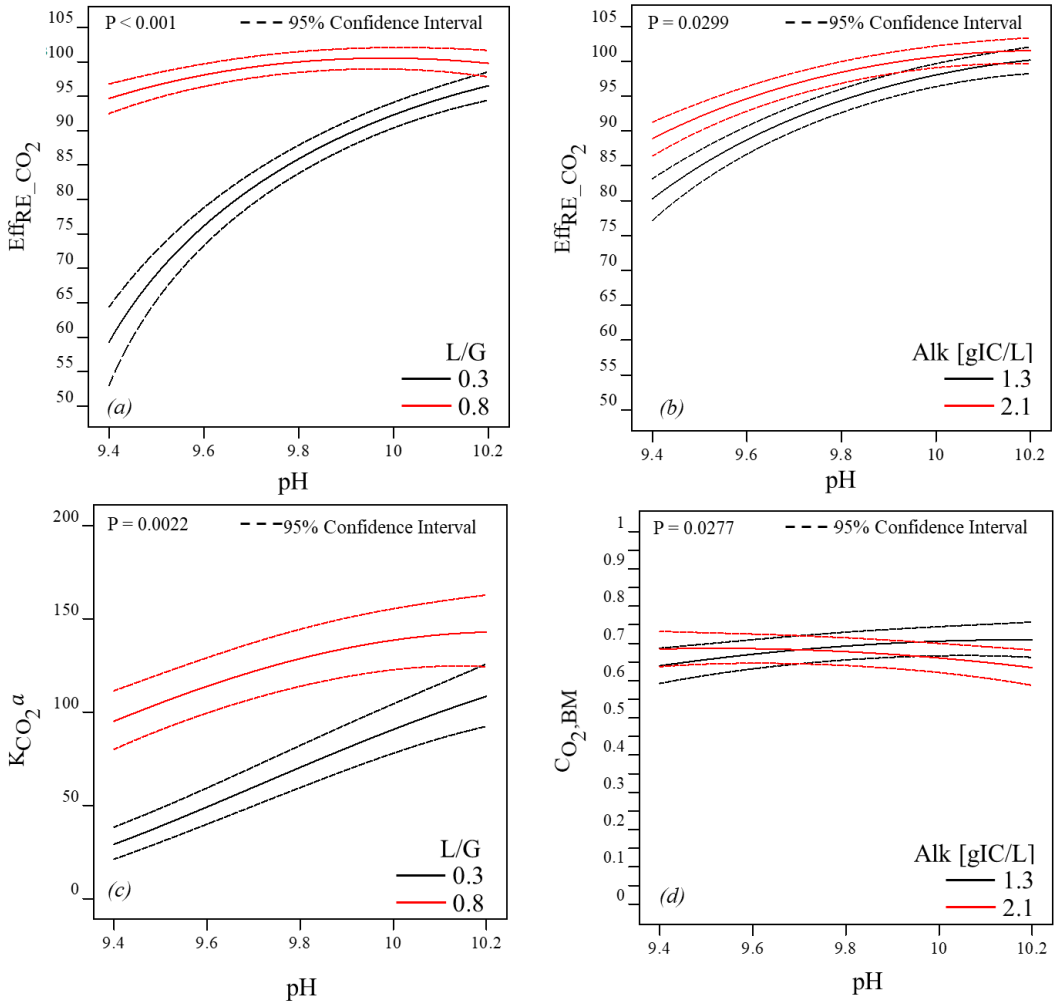


Figure 5-5 Interactive effects between (a) pH and L/G ratio on $Eff_{RE_CO_2}$; (b) pH and alkalinity on $Eff_{RE_CO_2}$; (c) pH and L/G ratio on $K_{CO_2}a$; and (d) pH and alkalinity on $C_{O_2,BM}$. Except for the factors that are being varied, all the other factors are placed at their centre points, namely, pH at 9.8; u_G at 0.45 cm/s, L/G at 0.55 and Alk at 1.7 gIC/L

5.3.5 Optimisation of bubble column operations

5.3.5.1 Optimal conditions for CO_2 removal from biogas

Performance prediction and optimisation of each process response were performed by varying only the statistically significant ($P < 0.05$) design factors for the respective process responses. Accordingly, contour plots for $Eff_{RE_CO_2}$, $K_{CO_2}a$ and pH_{out}, are plotted in Figure 5-6 to Figure 5-8 respectively within the design space bounded by factor settings of low (-1) and high (+1). Following the discussions in Section 5.2.4.4, greater than 97% CO_2 removal efficiency should be obtained with simultaneous maximisation of the hydrodynamic performance of the bubble column. Studying Figure 5-6 and Figure 5-8 in conjunction, it can be concluded that to ensure the desired CO_2 removal efficiency, the liquid pH at the bubble column outlet (pH_{out})

should preferably remain above 9.2. As can be observed from Figure 5-8, this is primarily achieved by ensuring both a higher bubble column inlet pH above 10, alkalinity above 1.7 gIC/L and L/G ratio above 0.4. To achieve a high $K_{CO_2}a$ at the same time, as can be seen from Figure 5-7, the bubble column for photosynthetic biogas upgrading should also be operated at higher superficial gas velocities. $K_{CO_2}a$ values higher than 150 hr^{-1}, similar to those for a traditional CO_2 absorption in NaOH below a pH of 11 and a temperature of 35°C [28], can be achieved only with superficial gas velocities between 0.45 cm/s and 0.6 cm/s (EBRTs of 2 minutes and 1.5 minutes respectively). Although as discussed before in Section 5.3.4.1, the increase in superficial gas velocity results in a drop in CO_2 removal efficiency (understood by a smaller area bounded by the contour corresponding to $Eff_{RE_CO_2}$ of 97% at a constant pH and L/G ratio upon an increase in superficial gas velocity (Figure 5-6), the selection of high pH and alkalinity above 10 and 1.7 gIC/L respectively would ensure that such a condition can only result when the L/G ratio is not optimised. Indeed, as revealed by both Figure 5-6 and Figure 5-7, for higher pH (above 10) and alkalinity (above 1.7 gIC/L) an L/G ratio between 0.6 and 0.7 would generally ensure a high CO_2 removal efficiency and a high CO_2 mass transfer coefficient irrespective of superficial gas velocity. Of course, the higher the pH and alkalinity, the wider would be the favourable operating ranges of the L/G ratio.

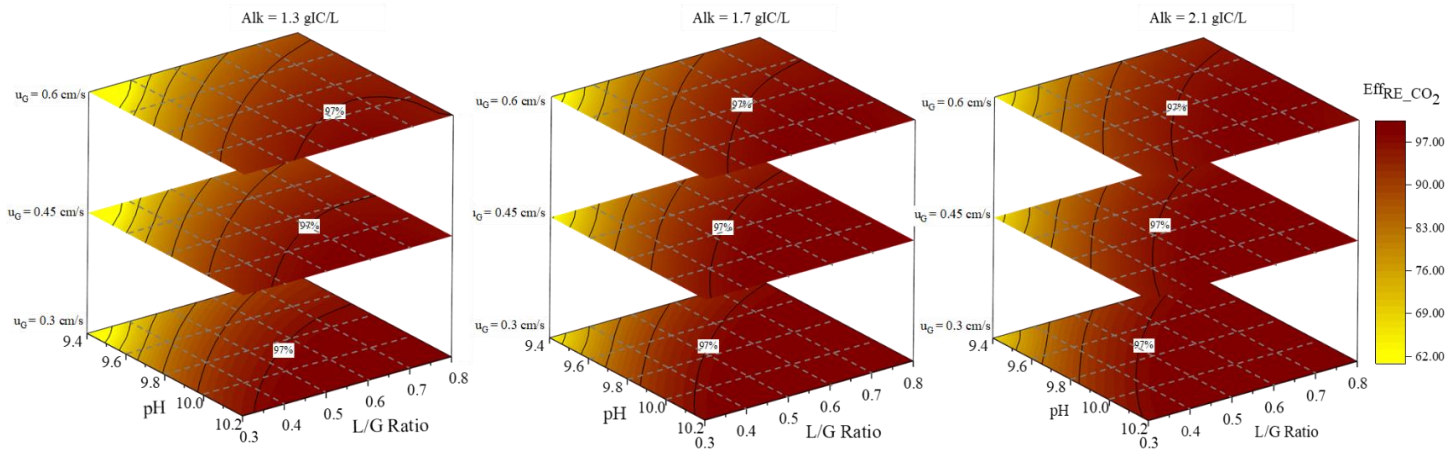


Figure 5-6 Two dimensional contour plots of CO_2 removal efficiency ($Eff_{RE_CO_2}$) versus pH and L/G ratio at different superficial gas velocities and alkalinity. The contour lines correspond to the values indicated in the legend.

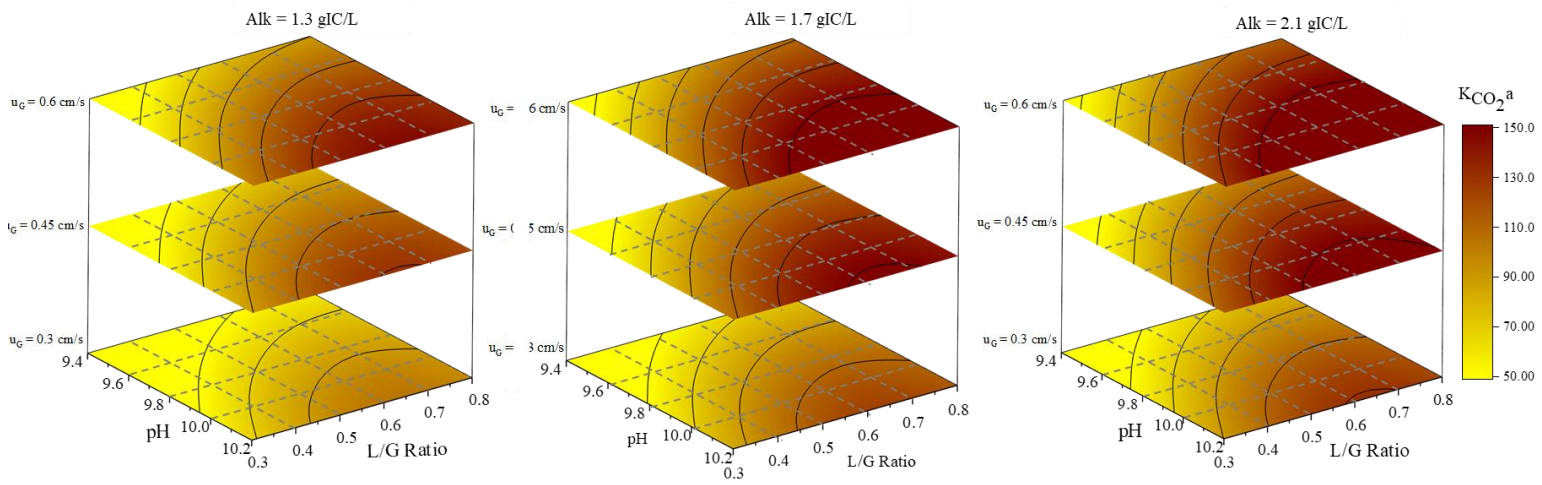


Figure 5-7 Two dimensional contour plots of mass transfer coefficient of CO_2 ($K_{CO_2}a$) a) versus pH and L/G ratio for at different superficial gas velocities and alkalinity. The contour lines correspond to the values indicated in the legend.

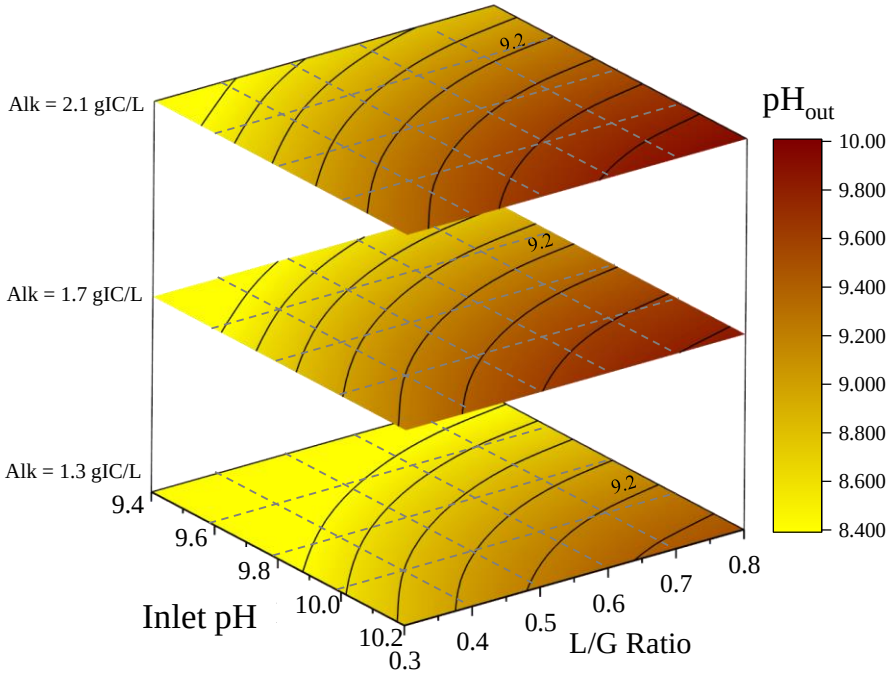


Figure 5-8 Two dimensional contour plots of the impact of inlet pH and L/G ratio on liquid outlet pH from the bubble column (pH_{out}) at different alkalinity. The effect of superficial gas velocity has been omitted due to its low statistical significance on pH_{out} ($P > 0.05$). The contour lines correspond to the values indicated in the legend.

5.3.5.2 Minimisation of O_2 concentration in upgraded biomethane

Higher superficial gas velocities lower the O_2 concentration in the upgraded biomethane ($C_{O_2,BM}$). On the contrary, as has been described in Section 5.3.4.1, a rise in the L/G ratio leads to an increase in $C_{O_2,BM}$. The contour plot, shown in Figure 5-9 reveals the combined effect of these two independent and statistically significant design factors on $C_{O_2,BM}$. As can be seen, to achieve a constant level of O_2 in the upgraded biomethane, a simultaneous increase in both the L/G ratio and the superficial gas velocity would be necessary. To cite an example, it can be seen that 0.5% O_2 would be present in the biomethane at a superficial gas velocity of 0.3 cm/s and L/G ratio of 0.3. However, to ensure a similar O_2 content in biomethane at a higher L/G ratio of around 0.45, the superficial gas velocity must be increased to 0.6 cm/s. Within the design space, a high $C_{O_2,BM}$ of more than 0.8% was obtained mostly above L/G ratios of 0.6 and below a superficial gas velocity of 0.5 cm/s. However, when considering the optimal design space for CO_2 removal (superficial gas velocity within 0.45 cm/s and 0.6 cm/s and L/G ratio between 0.6 and 0.7), it can be concluded that the O_2 content in the biomethane would usually vary between 0.7% and 0.9%. Thus, even

without the presence of H_2S in biogas, the O_2 concentration can be limited to the gas-grid suitability levels, while ensuring optimal CO_2 removal.

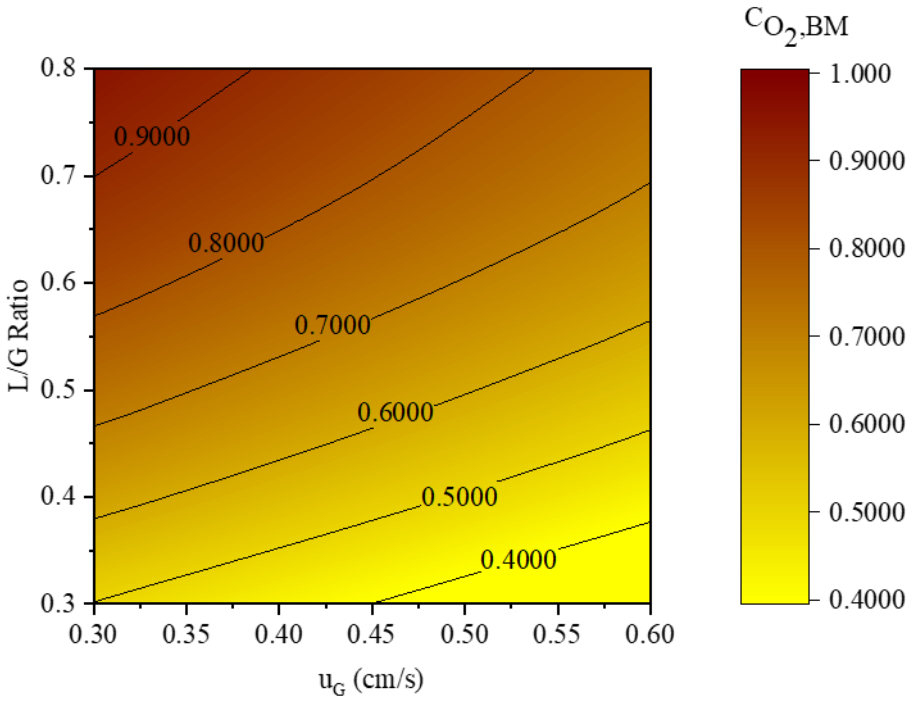


Figure 5-9 Two dimensional contour plot of superficial gas velocity (u_G) versus L/G ratio on O_2 concentration in the bubble column ($C_{O_2,BM}$). The effects of pH and alkalinity have not been depicted due to their low statistical significance on $C_{O_2,BM}$ ($P > 0.05$). The contour lines correspond to the values indicated in the legend.

5.3.5.3 Optimisation of overall bubble column operation

Optimisation results of the individual process responses were combined via overlaid contour plots to identify the most suitable operating regime. As per the previous discussion, this regime is characterised by CO_2 removal efficiency greater than 97% with a bubble column outlet pH of 9.2, CO_2 mass transfer coefficient greater than 150 hr^{-1} and less than 0.8% O_2 in the upgraded biomethane. As discussed in Section 5.2.4.4, the contour plots were plotted with superficial gas velocity and L/G ratio as the design factors. Based on the individual optimisation results, the liquid inlet pH and alkalinity were considered to vary between 10 and 10.2 and 1.7 gIC/L and 2.1 gIC/L respectively. Four different combinations of pH and alkalinity were studied and the results are presented in Figure 5-10.

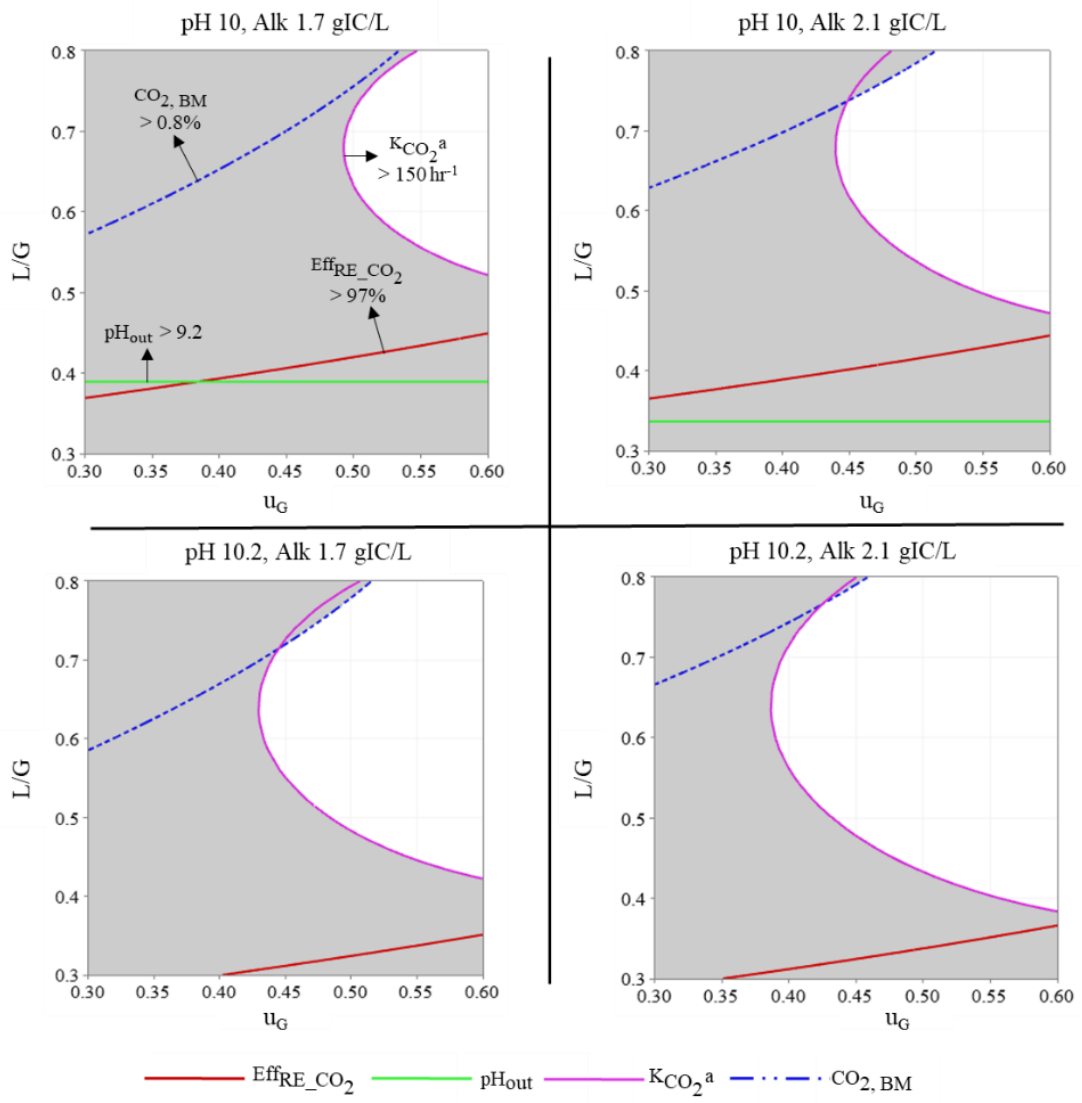


Figure 5-10 Overlaid contour plots to identify the optimal operating region of the bubble column for photosynthetic biogas upgrading for liquid inlet pH and alkalinity (Alk) ranging between 10 and 10.2 and 1.7 gIC/L and 2.1 gIC/L respectively. The un-shaded area indicates the optimal operating regions to achieve a CO_2 removal efficiency above 97% and oxygen concentration in biomethane less than 0.8%.

For the lowest optimal pH (10) and alkalinity (1.7 gIC/L), to operate the bubble column under favourable conditions, the superficial gas velocity should vary between 0.5 cm/s and 0.6 cm/s. The corresponding L/G ratio must be controlled within 0.6 and 0.8 with the optimal value being around 0.65. For each of the other combinations of pH and alkalinity, the optimal L/G ratio can be seen to be fairly constant between 0.6 and 0.65, although the allowable range of operation would increase. Similarly, as can be seen from Figure 5-10, the increase in either or both pH and alkalinity would also lead to increased flexibility in operation with respect to the superficial gas velocity. Indeed, at the highest optimal pH (10.2) and alkalinity (2.1 gIC/L), the favourable superficial gas velocity and L/G ratio could be as low as 0.4 cm/s and greater than 0.4

respectively. However, as an increased throughput is always desired, operations with higher superficial gas velocities between 0.5 cm/s and 0.6 cm/s would provide robust operation irrespective of any fluctuation in other design factors.

5.3.6 Significance of results

5.3.6.1 On bubble column design, costs and control strategy

Results from the optimisation experiments revealed the possibility to operate the bubble column optimally under superficial gas velocities of 0.5-0.6 cm/s with an optimal L/G ratio varying between 0.6 and 0.7. The high superficial gas velocities correspond to empty bed residence times (EBRTs) between 1.8 and 1.5 minutes, well below the typical industrial values of 3-6 minutes for chemical applications [64]. The results within the experimental domain being scalable [24] further signifies the possibility to utilise larger state-of-the-art bubble columns with height to diameter ratios between 3 and 10 [65].

The hypothetical biogas plant described in Section 5.2.4.5, generating 478 Nm^3/hr of biogas was used to estimate the size and number of bubble column reactors necessary to upgrade biomethane under optimised conditions. Bubble columns across multiple scales between 5-200 m^3 were investigated in which the upper limit corresponds to a very large bubble column [65]. The bubble column diameter was estimated from the volume assuming a height to diameter ratio (aspect ratio) of 5 [59]. An example calculation is included in *Box 5-1*.

As can be seen from Table 5-6, for a 5 m^3 bubble column with an approximate diameter of 1.08 m and operating at 20°C and 1 atm pressure, a superficial gas velocity of 0.4 cm/s would necessitate the requirement of an impractical number of 36 bubble columns (*Box 5.1*). Although an increase in superficial gas velocity to 0.6 cm/s would decrease the number of bubble columns to 24, it would still be a substantial setup. Increasing the bubble column volume on the other hand would significantly reduce the number of columns required. For instance, only four large 100m^3 bubble column reactors having an approximately 3-metre diameter and 15-metre height would allow operations to be carried out at superficial gas velocities between 0.5 cm/s and 0.6 cm/s. A further increase in the bubble column volume to 150 or 200 m^3, however, would not have a significant reduction in the number of columns.

BOX 5.1: Calculation of number of bubble columns to upgrade 478 Nm^3/hr of biogas in photosynthetic biogas upgrading

A perspective on upgrading 478 Nm^3/hr of biogas comprising 40% CO_2 was considered. The biogas was assumed to be supplied to the bubble column NTP (20 °C and 1 atm). Assuming 50 m^3 bubble columns with a height to diameter ratio of 5, the diameter of the bubble column (D_{BC}) can be evaluated as follows:

➔ D_{BC} [m] = $[50/(\pi/4\times5)]^{\frac{1}{3}} \approx 2.34$ m.

Accordingly, the bubble column cross section area (A_{BC}) and height (H_{BC}) are calculated as

➔ A_{BC} [m^2] = $\pi/4\times2.34^2 \approx 4.29$ m^2

➔ H_{BC} [m] = $5 \times 2.34 \approx 11.68$ m.

Considering a superficial gas velocity of 0.6 cm/s (0.006 m/s) for the biogas, the overall area required for the biogas flow (A_{ov}) and hence, the number of bubble columns can be evaluated as

➔ A_{ov} [m^2] = $\left(\frac{478}{3600}\right)/0.006 \approx 22.130$ m^2

➔ Number of bubble columns [nos.] = $\frac{A_{ov}}{A_{BC}} = 22.130/4.298 \approx 5.149 \approx 6$

Table 5-6 Estimation of the number of bubble columns required to upgrade 478 Nm^3/hr of biogas (equivalent to 1MW_e biogas based electric plant) based on the bubble column size between 5-200 m^3 and superficial gas velocities between 0.4-0.6 cm/s. The bubble column is assumed to operate at NTP (20 °C and 1 atm)

Bubble column dimensions	**Volume [m^3]**	5	25	50	100	150	200
	Diameter [m]*	1.08	1.85	2.34	2.94	3.37	3.71
	Height [m]	5.4	9.25	11.7	14.7	16.85	18.55
Superficial gas velocity [cm/s]		**Number of bubble columns**					
0.4		36	13	8	5	4	4
0.5		29	10	7	4	3	3
0.6		24	9	6	4	3	3

* *The bubble column diameter was calculated using the height to diameter ratio of 5.*

The ideal operating pH and alkalinity varying between 10 and 10.2 and 1.7 gIC/L and 2.1 gIC/L respectively fall well within the widely used operating levels of

the respective factors for photosynthetic biogas upgrading [8,14,66], as well as those used in traditional CO_2 removal columns using an alkaline medium [28]. These optimal pH ranges (10 - 10.2) and alkalinities (1.7 gIC/L – 2.1 gIC/L) would also aid in the robust and consistent operations against uncontrollable variables such as pressure, temperature, varying DO and algal concentrations [8]. In this regard, controlling the gas and liquid flow rates in the bubble column to control the superficial gas velocity and the L/G ratio would be the simplest control strategy to ensure the continuous production of grid quality biomethane. Thus, the results confirm the possibility of using traditional bubble columns with conventional materials such as stainless steel and operating them utilising control techniques and strategies widely used in the chemical industry. This would not only reduce costs but also accelerate the technology readiness level (TRL) of the overall photosynthetic biogas upgrading technology.

5.3.6.2 On integrated operations of photosynthetic biogas upgrading

Using the hypothetical plant producing 478 Nm^3/hr of biogas (Section 5.2.4.5), a perspective of a flat plate photobioreactor integrated with the optimised bubble column was developed. The influence of algal productivity was assessed at two different daily productivity rates of *Spirulina platensis* of 0.175 gDW/L/day [23] and 0.29 gDW/L/day [67]. *Spirulina platensis* was assumed to comprise 50% carbon per dry weight [68]. The daily carbon assimilation rate for the two growth rates would therefore be half of the dry weight or 0.088 gIC/L and 0.145 gIC/L respectively. A 15% overall carbon loss was considered as the present system would operate at lower alkalinities than 2.5gIC/L in which, 24% carbon loss was observed by Rodero et al. (2020) [26]. The areal footprint of the photobioreactor was assumed as a tenth of the photobioreactor surface area [69] with a surface to volume ratio of 28.57 m^2/m^3 [45].

To achieve a continuous carbonate bicarbonate cycle, the carbon added by absorption from biogas in the bubble column ($M_{C_{abs}}$) must account for both the carbon uptaken by the microalgae ($M_{C_{algae}}$) and the carbon lost through stripping ($M_{C_{stripping}}$) or as effluents ($M_{C_{effluent}}$) as per Eq. 5.12. Using this simple mass balance further elaborated in *Box 5.2*, for each L/G ratio of 0.5, 0.6 and 0.7 and with a 100% CO_2 removal, Table 5-7 shows the amount of inorganic carbon added by absorption into the algal medium in terms of alkalinity [g-IC/L].

$$M_{C_{abs}} = M_{C_{algae}} + M_{C_{stripping}} + M_{C_{effluent}} \quad (5.12)$$

As can be seen from Table 5-7, an increased L/G ratio resulting in lower addition of carbon per unit liquid flow would result in a drop in the HRT of the bubble column. However, having a higher liquid flow rate would result in a similar volume requirement for the photobioreactors, irrespective of the L/G ratio. Thus, at a constant CO_2 removal efficiency, the L/G ratio would not affect the size of the photobioreactor, which would be 6.35 hectares for algal productivity of 0.175 gDW/L/day. However, higher algal productivity of 0.29 gDW/L/day would significantly reduce the overall areal footprint to only 3.83 ha. The overall microalgae production considering 10% production losses would be around 170 kgDW/hr (*Box 5.2*). For annual operational hours of 8,000, this would thus translate to the production of almost 1,360 metric tonnes of microalgae per annum.

Table 5-7 Influence of L/G ratio and algal productivity on the design and sizing of a flat plate photobioreactor system under optimal operations of the bubble column for upgrading 478 Nm^3/hr of biogas (equivalent to that produced in a 1MW_e biogas based electricity plant [6])

Output characteristics	**Algal productivity [gDW/L/day]**	**L/G ratio**		
		0.5	**0.6**	**0.7**
$Eff_{RE_CO_2}$	NA	100%	100%	100%
Liquid flow [Nm^3/hr]	NA	239	286.8	334.6
Carbon added [gIC/L]	NA	0.39	0.33	0.28
Hydraulic retention time [days]	0.175 [23]	3.88	3.23	2.77
	0.29 [67]	2.34	1.95	1.67
Volume of PBR [m^3]	0.175	22,238.63	22,238.63	22,238.63
	0.29	13,419.86	13,419.86	13,419.86
Areal footprint [ha]	0.175	6.35	6.35	6.35
	0.29	3.83	3.83	3.83

BOX 5.2: *calculation for integration of bubble column with photobioreactor (PBR) for photosynthetic biogas upgrading*

A perspective on upgrading 478 Nm^3/hr of biogas comprising 40% CO_2 was considered. Assuming an optimal L/G ratio of 0.6 at a liquid inlet pH of 10 and alkalinity of 1.7 gIC/L to enable a 100% CO_2 removal work

➔ Algal broth circulated (L) = $478 \times 0.6 = 286.8$ m^3/hr = 6883.2 m^3/day

➔ Inorganic carbon (IC) added = $478 \times 0.4 \times \frac{101325 \times 10^{-6}}{8.314 \times 293.15} \times 12 = 93{,}478.54$ gIC/hr, where 101325 pascal is the atmospheric pressure, 8.314 J/kg/K is the universal gas constant and 293.15 K is the atmospheric temperature (20°C). Thus,

➔ Inorganic carbon added per unit liquid flow = $\frac{93{,}478.54}{286.8 \times 1000} = 0.33$ gIC/L

Algae Cultivation System

Assuming *Spirulina platensis* productivity of 0.175 g-dry weight (DW)/L [23] and that 50% of the algal dry weight is carbon [68], the effective carbon uptake rate can be calculated as

➔ Inorganic carbon uptake rate by Spirulina platensis = $0.175 \times 0.5 = 0.088$ gIC/L

Thus, the hydraulic retention time (HRT) and PBR volume can be calculated as

➔ HRT = $0.33 / 0.088 = 3.23$ days

➔ Reactor volume = $286.8 \times 24 \times 3.23 = 22{,}238.63$ m^3

To calculate the areal footprint of the connected flat plate photobioreactor system, a surface to volume ratio of 28.57 m^2/m^3 was assumed [6]. Additionally, the total land area required for the photobioreactor was considered to be a tenth of the effective overall photobioreactor surface after Placzek et al. (2017) [69]. Thus, the area required to cultivate microalgae is

➔ Photobioreactor area = $22{,}238.63 \times 28.57 \times 0.1 / 10{,}000 = 6.35$ hectare

Algae Production

Assuming 10% loss during the production of *Spirulina platensis* and an annual operating time of 8000 hours, the hourly and annual production of microalgae can be estimated as

➔ Hourly rate of algae production = $0.33 / 0.5 \times (1 - 0.1) \times 286.8 = 170.36$ kgDW/hr

➔ Annual rate of algae production = $170.36 \times 8000 / 1000 = 1362.88$ t-DW/yr

Following previous discussions, optimal L/G ratios between 0.6 and 0.7 would allow operating the overall system between a pH of 9.2 and 10 and alkalinity between 1.7 gIC/L and 2.1 gIC/L. Similar low variations in pH and alkalinity before and after the bubble column at L/G ratios between 0.5 and 0.6 have been previously described in the literature studying the combined bubble column photobioreactor operations [9,11]. During continuous operations, due to the photoperiod in the microalgae cultivation medium, a ± 0.5 and 5% variation in the bubble column inlet pH and alkalinity respectively would occur [9,12,66]. However, operating at a liquid inlet pH above 9.8 with a superficial gas velocity of 0.6 cm/s, and L/G ratios between 0.6 and 0.7 would allow a consistent CO_2 removal efficiency of over 97%. A similar consistent CO_2 removal of c. 96% during continuous operations at pHs of 9.5 ± 0.2 and L/G ratio of 1 has been previously reported in the literature [12]. The observations also show that the variation in oxygen concentration in biomethane between the light and dark phases would be low. This is supported by the results of Meier et al. (2017) [9], who obtained a fairly constant O_2 concentration in biomethane irrespective of the variations due to photoperiods in microalgae cultivation. Thus, it can be said that the current results would sufficiently describe continuous operations of a combined bubble column photobioreactor system, provided the pH and alkalinity values during photoperiods fluctuate within those included in the design phase(which, most often, would be the case).

The optimal operating conditions would minimise carbon loss from the algal solution by stripping [6,70]. In addition, the possibility to operate optimally at a bubble column inlet pH of 10 would also allow the selection of a wider variety of microalgae and minimise the negative impacts of high pH such as ammonia loss through stripping and phosphorus deposition through precipitation as inorganic salts [71]. This pH regime (optimal for growing *Spirulina platensis*) would also aid rapid carbon uptake by the microalgae, minimising both size and costs of the photobioreactor. Although the cost of setup of the microalgae cultivation, harvesting and processing systems would be significant, the possibility to sell the microalgae above 10 €/kg would thus add significant economic benefits to the biomethane plant. Incentives from carbon savings could also significantly add to the revenue. However, legislation, policies and local by-laws must be critically assessed, as products aimed for food and/or feed purposes must adhere to stringent quality control and process specifications [2].

5.3.6.3 Limitations and future research

The present work has achieved in obtaining the optimal operating pH (10 – 10.2), L/G ratio (0.6 - 0.7) and the alkalinity (1.7 – 2.1 gIC/L) to ensure effective biogas upgrading using the photosynthetic biogas upgrading technology. Although a maximum superficial gas velocity of 4 cm/s could be aimed for [8], the present setup investigated here limited it to 0.75 cm/s only. The regression equations developed for optimisation further provided fair predictions up to 0.6 cm/s, which, however, is much higher than superficial gas velocities currently employed in literature for photosynthetic biogas upgrading [8]. The possibility to increase the superficial gas velocity lies in the fact that in larger diameter industrial bubble columns higher EBRTs would be achievable. For example, for the 100 m^3 bubble column with an aspect ratio of 5, the bubble column height of 15 metres would result in an EBRT of 12.5 minutes, even if the superficial gas velocity is increased to 2 cm/s. A high EBRT, leading to higher gas-liquid contact time could hence allow greater CO_2 removal even under higher superficial gas velocities. On the other hand, while the current research shows that a higher superficial gas velocity decreases O_2 concentration in biomethane, a higher EBRT on the contrary was found to increase O_2 concentration in biomethane due to increased gas-liquid contact time [8]. Thus, extending the results of the current research to accurately study the effect of increasing the superficial gas velocities under industrial conditions would be critical to further advance the TRL of photosynthetic biogas upgrading.

5.4 Conclusions

In this research, optimisation of the bubble column for photosynthetic biogas upgrading was performed using the central composite design (CCD) within the response surface methodology (RSM). Developed regression models adequately predicted the bubble column performance for liquid inlet pHs between 9.4 and 10.2, superficial gas velocities between 0.3 cm/s and 0.6 cm/s, L/G ratios of 0.3 and 0.8 and liquid inlet alkalinities of 1.3 gIC/L and 2.1 gIC/L. A minimum pH and alkalinity of 10 and 1.7 gIC/L was found sufficient to ensure over 97% CO_2 removal and a CO_2 mass transfer coefficient above 150 hr^{-1}. The corresponding optimal L/G ratio was between 0.6 and 0.7. Increasing the superficial gas velocity was found to reduce CO_2 removal efficiency and O_2 concentration in biomethane while improving the

hydrodynamic performance of the bubble column with regard to CO_2 removal. To ensure over 97% CO_2 removal from biogas while limiting the O_2 concentration in the biomethane below 0.8%, the ideal operating superficial gas velocities and L/G ratios were found to vary between 0.5 cm/s and 0.6 cm/s and 0.6 and 0.7 respectively. The results further confirmed the possibility to use traditional well-engineered bubble columns and conventional control techniques for biogas upgrading with microalgae. Extending the results to explore its significance on commercial-scale operations, it was found that, to upgrade 478 Nm^3/hr of biogas (equivalent to a 1 MW_e biogas based electricity plant) at NTP, four 100 m^3 bubble columns with 3-metre diameter each would be required. The corresponding areal footprint of the connected flat plate photobioreactor was found to vary between 3.83 and 6.35 hectares depending on the daily algal productivity of 0.29 gDW/L or 0.175 gDW/L respectively.

5.5 Acknowledgement

This work acknowledges the support from Science Foundation Ireland (SFI) through the Centre for Marine and Renewable Energy (MaREI) under Grant No. 12/RC/2302_P2 and 16/SP/3829, with industrial funding from Gas Networks Ireland through The Green Gas Innovation Group and by ERVIA and IDL Pernod Ricard. This work was also supported by the Environmental Protection Agency – Ireland (2018-RE-MS-13).

5.6 Supplementary to Chapter 5

Table S5-1 Summary of the thirty experimental trials developed using the central composite design (CCD) to study the impact of inlet liquid pH (pH), superficial gas velocity (u_G), liquid to gas flow rate ratio (L/G) and inlet liquid alkalinity (Alk) on the process responses of a bubble column for photosynthetic biogas upgrading

Experimental Trials	Coded Variables				Uncoded Variables			
	pH (X_1)	u_G (X_2)	L/G (X_3)	Alk(X_4)	pH (X_1)	u_G (X_2)	L/G (X_3)	Alk(X_4)
1	0	0	0	-2	9.8	0.45	0.55	0.9
2	0	2	0	0	9.8	0.75	0.55	1.7
3	2	0	0	0	10.6	0.45	0.55	1.7
4	0	0	2	0	9.8	0.45	1.05	1.7
5	0	0	0	0	9.8	0.45	0.55	1.7
6	0	-2	0	0	9.8	0.15	0.55	1.7
7	0	0	0	2	9.8	0.45	0.55	2.5
8	0	0	-2	0	9.8	0.45	0.05	1.7
9	0	0	0	0	9.8	0.45	0.55	1.7
10	-2	0	0	0	9	0.45	0.55	1.7
11	1	1	-1	-1	10.2	0.6	0.3	1.3
12	0	0	0	0	9.8	0.45	0.55	1.7
13	1	-1	1	-1	10.2	0.3	0.8	1.3
14	1	1	1	1	10.2	0.6	0.8	2.1
15	-1	-1	1	1	9.4	0.3	0.8	2.1
16	1	-1	-1	1	10.2	0.3	0.3	2.1
17	-1	1	1	-1	9.4	0.6	0.8	1.3
18	0	0	0	0	9.8	0.45	0.55	1.7
19	-1	1	-1	1	9.4	0.6	0.3	2.1
20	-1	-1	-1	-1	9.4	0.3	0.3	1.3
21	-1	1	-1	-1	9.4	0.6	0.3	1.3
22	-1	-1	-1	1	9.4	0.3	0.3	2.1
23	0	0	0	0	9.8	0.45	0.55	1.7
24	1	-1	1	1	10.2	0.3	0.8	2.1
25	-1	-1	1	-1	9.4	0.3	0.8	1.3
26	0	0	0	0	9.8	0.45	0.55	1.7
27	1	1	-1	1	10.2	0.6	0.3	2.1
28	1	1	1	-1	10.2	0.6	0.8	1.3
29	-1	1	1	1	9.4	0.6	0.8	2.1
30	1	-1	-1	-1	10.2	0.3	0.3	1.3

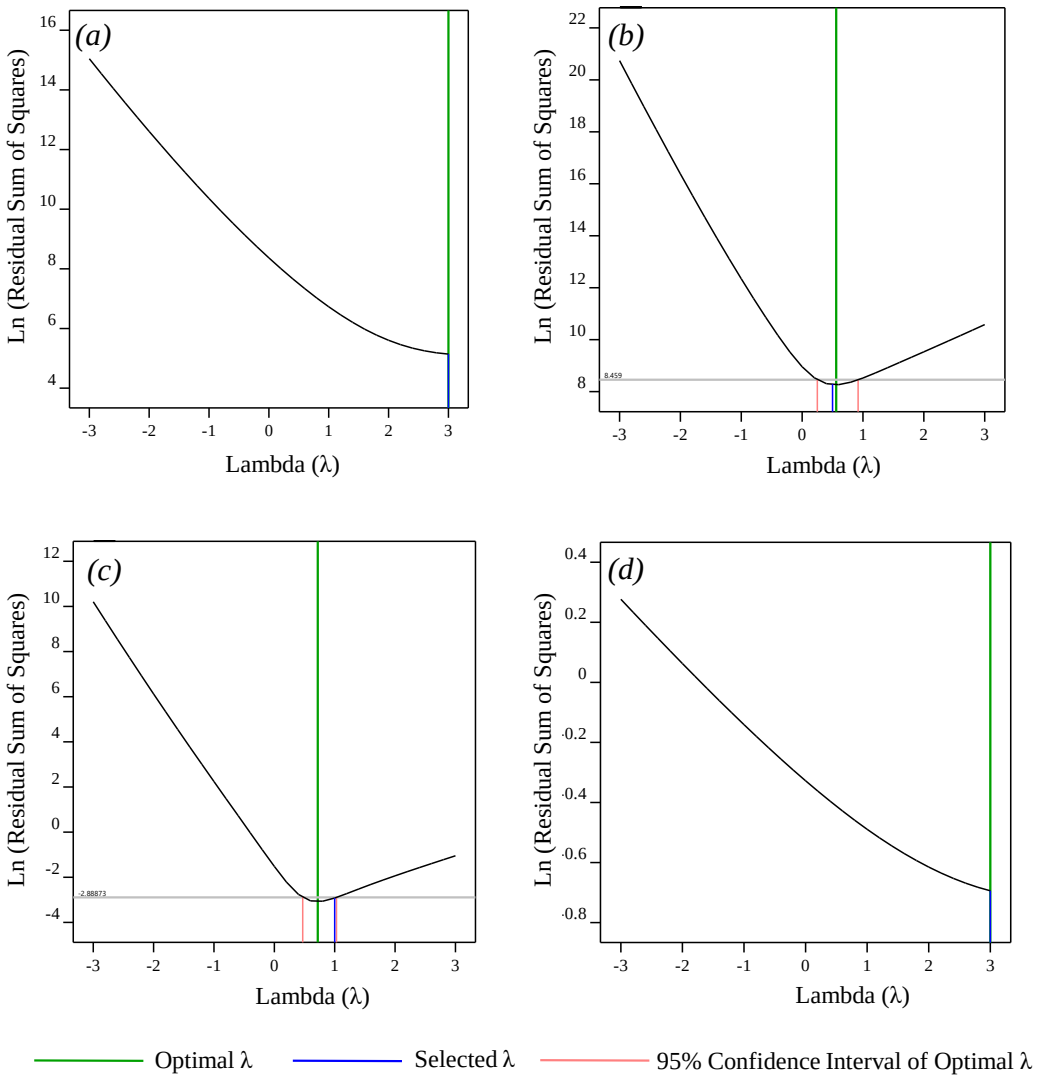


Figure S5-1 Box Cox Power Transformation plot for (a) $Eff_{RE_CO_2}$; (b) $K_{CO_2}a$; (c) $C_{O_2,BM}$; and (d) pH_{out}

Table S5-2 Statistical summary of the models chosen to describe the behaviour of the four process responses selected to describe the performance of the bubble column operations in photosynthetic biogas upgrading.

Process Response	Quadratic Regression Model	Statistical Comparators							
		DoF*	CV† [%]	F value	P value	R^2	Adjusted R^2	Predicted R^2	Adequate Prediction
$Eff_{RE_CO_2}$	without tnf$^{\Delta}$	6	7.60	40.07[a]	<0.001	0.913	0.889	0.7060	21.956
	with tnf ($\lambda = 3$)	9	8.14	81.54[b]	<0.001	0.974	0.962	0.899	27.884
$K_{CO_2}a$	without tnf	9	17.28	23.61[b]	<0.001	0.941	0.8753	0.6887	17.772
	with tnf ($\lambda = 0.5$)	9	8.77	35.35[b]	<0.001	0.941	0.914	0.771	20.911
$C_{O_2,BM}$	without tnf	7	8.11	78.77[c]	<0.001	0.968	0.956	0.921	36.225
	with tnf ($\lambda = 0.5$)	8	4.48	105.02[d]	<0.001	0.971	0.962	0.932	44.323
pH_{out}	without tnf	7	1.69	103.58[c]	<0.001	0.971	0.961	0.909	33.395
	with tnf ($\lambda = 3$)	6	4.85	114.85[a]	<0.001	0.968	0.959	0.915	34.863

*DoF: Degrees of freedom; †CV: Coefficient of Variance; $^{\Delta}$tnf: data transformation

Critical F (F_{cr}) values: [a]$F_{0.05(9,23)} = 2.528$; [b]$F_{0.05(9,20)} = 2.393$; [c]$F_{0.05(7,22)} = 2.464$; [d]$F_{0.05(8,21)} = 2.420$

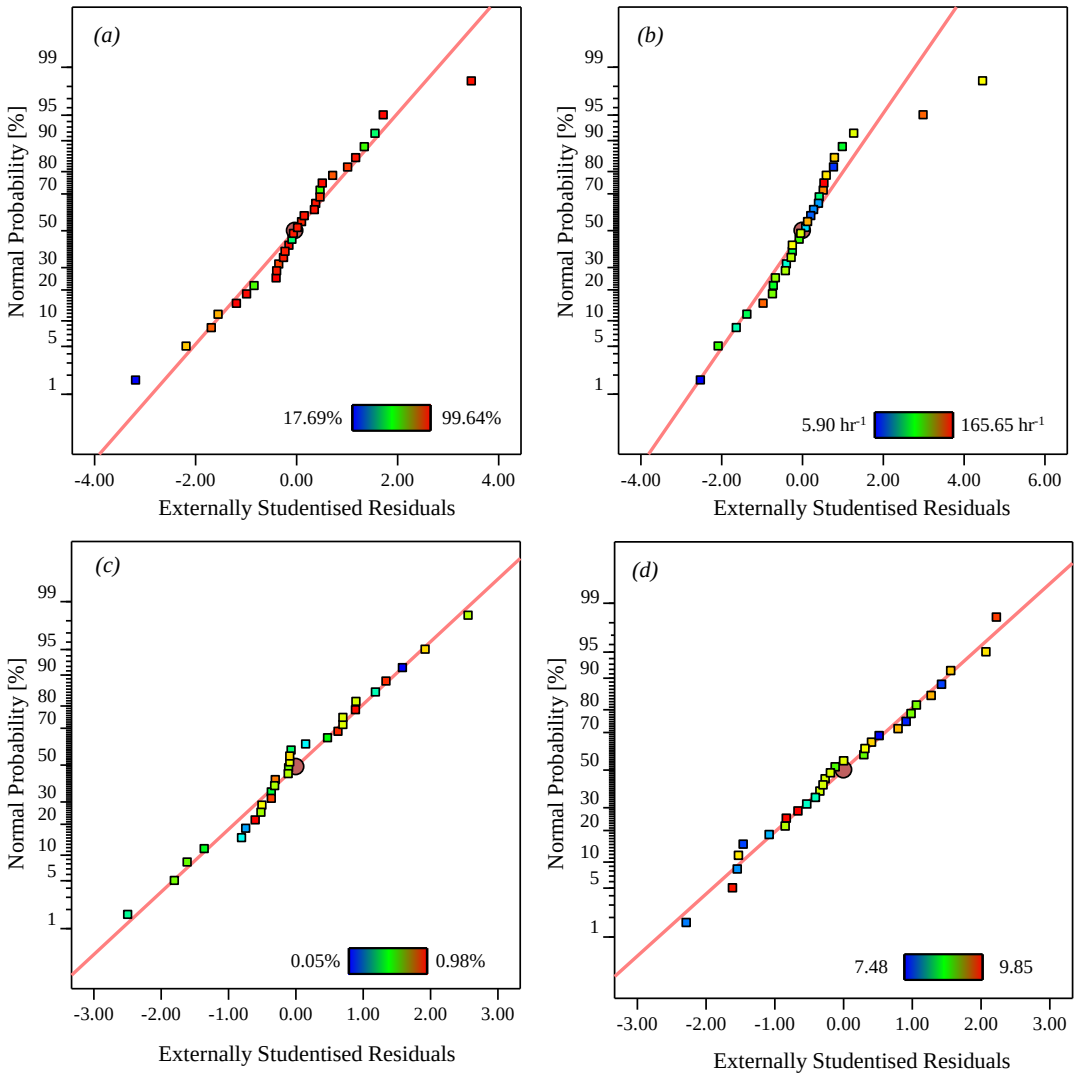


Figure S5-2 Normal probability plot of residuals for the selected regression models developed for (a) $Eff_{RE_CO_2}$; (b) $K_{CO_2}a$; (c) $C_{O_2,BM}$; and (d) pH_{out}. The colour code indicates the maximum and minimum value of the respective process response.

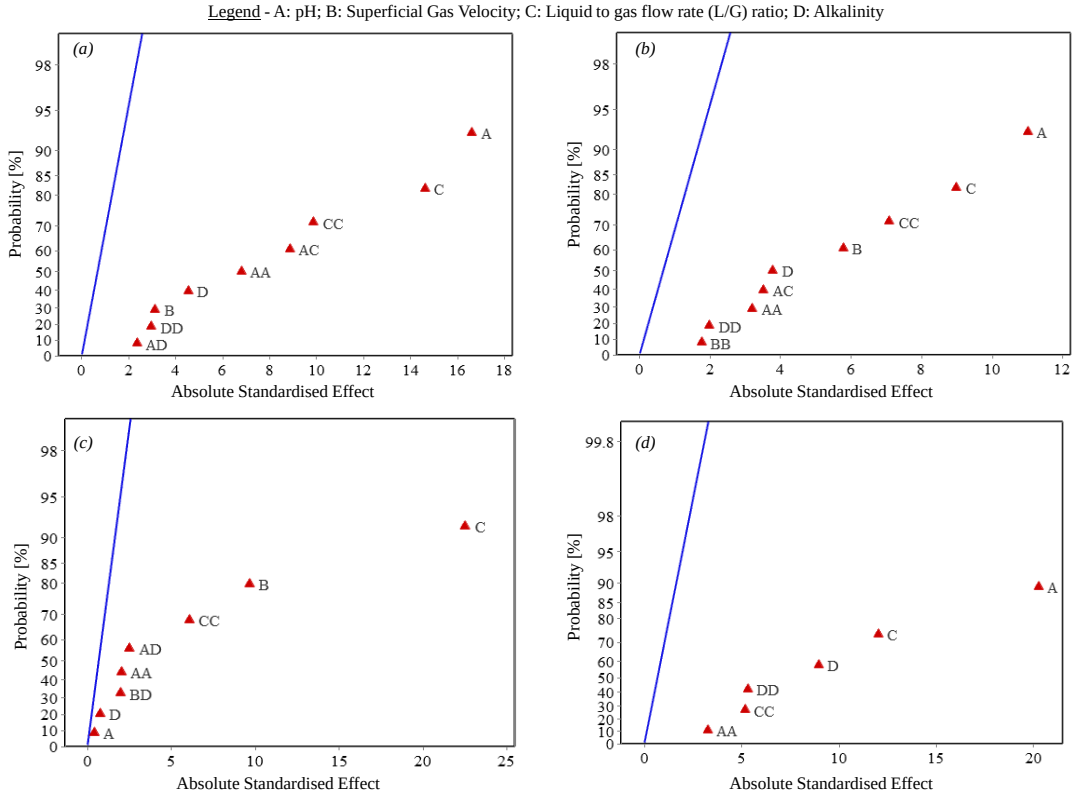


Figure S5-3 Half-Normal probability plot of the terms included in the selected regression models developed for (a) $Eff_{RE_CO_2}$; (b) $K_{CO_2}a$; (c) $C_{O_2,BM}$; and (d) pH_{out}. The points farthest away from the straight (45°) line has the highest influence on the process response.

5.7 References

[1] Wall DM, McDonagh S, Murphy JD. Cascading biomethane energy systems for sustainable green gas production in a circular economy. Bioresour Technol 2017;243:1207–15. doi:10.1016/j.biortech.2017.07.115.

[2] Bose A, O'Shea R, Lin R, Murphy JD. A perspective on novel cascading algal biomethane biorefinery systems. Bioresour Technol 2020;304:123027. doi:10.1016/j.biortech.2020.123027.

[3] Angelidaki I, Treu L, Tsapekos P, Luo G, Campanaro S, Wenzel H, et al. Biogas upgrading and utilization: Current status and perspectives. Biotechnol Adv 2018;36:452–66. doi:10.1016/j.biotechadv.2018.01.011.

[4] Toledo-Cervantes A, Estrada JM, Lebrero R, Muñoz R. A comparative analysis of biogas upgrading technologies: Photosynthetic vs physical/chemical processes. Algal Res 2017;25:237–43. doi:10.1016/j.algal.2017.05.006.

[5] Meier L, Pérez R, Azócar L, Rivas M, Jeison D. Photosynthetic CO_2 uptake by microalgae: An attractive tool for biogas upgrading. Biomass and Bioenergy 2015;73:102–9. doi:10.1016/j.biombioe.2014.10.032.

[6] Bose A, Lin R, Rajendran K, Xia A, O'Shea R, Murphy JD. How to optimise photosynthetic biogas upgrading: a perspective on system design and microalgae selection. Biotechnol Adv 2019;37. doi:10.1016/j.biotechadv.2019.107444.

[7] Xia A, Cheng J, Murphy JD. Innovation in biological production and upgrading of methane and hydrogen for use as gaseous transport biofuel. Biotechnol Adv 2016;34:451–72. doi:10.1016/j.biotechadv.2015.12.009.

[8] Bose A, O'Shea R, Lin R, Murphy JD. A comparative evaluation of design factors on bubble column operation in photosynthetic biogas upgrading. Biofuel Res J 2021;8. doi:10.18331/BRJ2021.8.2.2.

[9] Meier L, Barros P, Torres A, Vilchez C, Jeison D. Photosynthetic biogas upgrading using microalgae: Effect of light/dark photoperiod. Renew Energy 2017;106:17–23. doi:10.1016/j.renene.2017.01.009.

[10] Gas Networks Ireland. Code of Operations, Part G. 2018.

[11] Rodero M del R, Posadas E, Toledo-Cervantes A, Lebrero R, Muñoz R. Influence of alkalinity and temperature on photosynthetic biogas upgrading efficiency in high rate algal ponds. Algal Res 2018;33:284–90. doi:10.1016/j.algal.2018.06.001.

[12] Marín D, Posadas E, Cano P, Pérez V, Blanco S, Lebrero R, et al. Seasonal variation of biogas upgrading coupled with digestate treatment in an outdoors pilot scale algal-bacterial photobioreactor. Bioresour Technol 2018;263:58–66. doi:10.1016/j.biortech.2018.04.117.

[13] Toledo-Cervantes A, Madrid-Chirinos C, Cantera S, Lebrero R, Muñoz R. Influence of the gas-liquid flow configuration in the absorption column on photosynthetic biogas upgrading in algal-bacterial photobioreactors. Bioresour Technol 2017;225:336–42. doi:10.1016/j.biortech.2016.11.087.

[14] Marín D, Carmona-Martínez AA, Blanco S, Lebrero R, Muñoz R. Innovative operational strategies in photosynthetic biogas upgrading in an outdoors pilot scale algal-bacterial photobioreactor. Chemosphere 2021;264. doi:10.1016/j.chemosphere.2020.128470.

[15] Rodero M del R, Carvajal A, Arbib Z, Lara E, de Prada C, Lebrero R, et al. Performance evaluation of a control strategy for photosynthetic biogas upgrading in a semi-industrial scale photobioreactor. Bioresour Technol 2020;307:123207. doi:10.1016/j.biortech.2020.123207.

[16] Huang Q, Jiang F, Wang L, Yang C. Design of photobioreactors for mass cultivation of photosynthetic organisms. Engineering 2017;3:318–29. doi:10.1016/J.ENG.2017.03.020.

[17] Vasumathi KK, Premalatha M, Subramanian P. Parameters influencing the design of photobioreactor for the growth of microalgae. Renew Sustain Energy Rev 2012;16:5443–50. doi:10.1016/j.rser.2012.06.013.

[18] Barros AI, Gonçalves AL, Simões M, Pires JCM. Harvesting techniques applied to microalgae: A review. Renew Sustain Energy Rev 2015;41:1489–500. doi:10.1016/j.rser.2014.09.037.

[19] Singh G, Patidar SK. Microalgae harvesting techniques: A review. J Environ Manage 2018;217:499–508. doi:10.1016/j.jenvman.2018.04.010.

[20] Hu G, Nicholas NJ, Smith KH, Mumford KA, Kentish SE, Stevens GW. Carbon dioxide absorption into promoted potassium carbonate solutions: A review. Int J Greenh Gas Control 2016;53:28–40. doi:10.1016/j.ijggc.2016.07.020.

[21] Knuutila H, Juliussen O, Svendsen HF. Kinetics of the reaction of carbon dioxide with aqueous sodium and potassium carbonate solutions. Chem Eng Sci 2010;65:6077–88. doi:10.1016/j.ces.2010.07.018.

[22] Imle M, Kumelan J, Speyer D, Mccann N, Maurer G, Hasse H. Solubility of carbon dioxide in activated potash solutions in the low and high gas loading regions. Ind Eng Chem Res 2013; 52(37):13477–13489. doi:10.1021/ie401835x

[23] de Oliveira MACL, Monteiro MPC, Robbs PG, Leite SGF. Growth and chemical composition of *Spirulina maxima* and *Spirulina platensis* biomass at different temperatures. Aquac Int 1999;7:261–75. doi:10.1023/A:1009233230706.

[24] Bose A, O'Shea R, Lin R, Murphy JD. Design, commissioning and performance assessment of a lab-scale bubble column reactor for photosynthetic biogas upgrading with Spirulina platensis. Ind Eng Chem Res 2021. doi:10.1021/acs.iecr.0c05974.

[25] Posadas E, Serejo ML, Blanco S, Pérez R, García-Encina PA, Muñoz R. Minimization of biomethane oxygen concentration during biogas upgrading in algal-bacterial photobioreactors. Algal Res 2015;12:221–9. doi:10.1016/j.algal.2015.09.002.

[26] Rodero M del R, Severi CA, Rocher-Rivas R, Quijano G, Muñoz R. Long-term influence of high alkalinity on the performance of photosynthetic biogas upgrading. Fuel 2020;281:118804. doi:10.1016/j.fuel.2020.118804.

[27] Yang J, Cui X, Feng Y, Jing G, Kang L, Luo M. Experimental study on microalgae cultivation in novel photobioreactor of concentric double tubes with aeration pores along tube length direction. Int J Green Energy 2017;14:1269–76. doi:10.1080/15435075.2017.1402772.

[28] Chen P, Huang C, Su T, Chen H, Yang M, Tsao J. Optimum conditions for the capture of carbon dioxide with a bubble-column scrubber. Int J Greenh Gas Control 2015;35:47–55. doi:10.1016/j.ijggc.2015.01.011.

[29] Myers RH, Montgomery DC, Anderson-Cook CM. Response Surface Methodology: Process and product optimisation using designed experiments. Fourth. Hoboken, New Jersey: John Wiley & Sons, Ltd; 2016.

[30] Cherubini F. The biorefinery concept: Using biomass instead of oil for producing energy and chemicals. Energy Convers Manag 2010;51:1412–21. doi:10.1016/j.enconman.2010.01.015.

[31] Nazari L, Yuan Z, Ray MB, Xu CC. Co-conversion of waste activated sludge and sawdust through hydrothermal liquefaction : Optimization of reaction parameters using response surface methodology. Appl Energy 2017;203:1–10. doi:10.1016/j.apenergy.2017.06.009.

[32] Asfaram A, Ghaedi M, Dashtian K, Ghezelbash GR. Preparation and characterization of Mn0.4Zn0.6Fe2O4 nanoparticles supported on dead cells of *Yarrowia Llipolytica* as a novel and efficient adsorbent/biosorbent composite for the removal of azo food dyes: Central Composite Design optimization study. ACS Sustain Chem Eng 2018;6:4549–63. doi:10.1021/acssuschemeng.7b03205.

[33] Montgomery DC. Design and Analysis of Experiments. 8th ed. John Wiley & Sons, Inc.; 2012.

[34] Ait-Amir B, Pougnet P, El Hami A. Meta-model development. In: Hami A El, Pougnet P, editors. Embed. Mechatron. Syst. 2, vol. 2, 2015, p. 151–79. doi:10.1016/b978-1-78548-014-0.50006-2.

[35] Mehta PD. Control Variable in Research. Int. Encycl. Soc. Behav. Sci., 2001, p. 2727–30. doi:10.1016/b0-08-043076-7/00734-8.

[36] Kumar T, Mohsin R, Majid ZA, Ghafir MFA, Wash AM. Experimental study of the anti-knock efficiency of high-octane fuels in spark ignited aircraft engine using response surface methodology. Appl Energy 2020;259:114150. doi:10.1016/j.apenergy.2019.114150.

[37] Zhang Y, Prawang P, Li C, Meng X, Zhao Y, Wang H, et al. Ultrasonic assisted extraction of artemisinin from Artemisia Annua L. using monoether-based solvents. Green Chem 2018;20:713–23. doi:10.1039/c7gc03191b.

[38] Fàbrega C, Parcerisa D, Rossell JM, Gurenko A, Franke C. Predicting instrumental mass fractionation (IMF) of stable isotope SIMS analyses by response surface methodology (RSM). J Anal At Spectrom 2017;32:731–48. doi:10.1039/c6ja00397d.

[39] Khuri AI, Mukhopadhyay S. Response surface methodology. Wiley Interdiscip Rev Comput Stat 2010;2:128–49. doi:10.1002/wics.73.

[40] Bhardwaj B, Kumar R, Singh PK. An improved surface roughness prediction model using Box Cox transformation with RSM in end milling of EN 353. J Mech Sci Technol 2014;28:5149–57. doi:10.1007/s12206-014-0837-4.

[41] Sakia RM. The Box Cox transformation technique: a review. J R Stat Soc Ser D (The Stat 1992;41:169–78. doi:https://doi.org/10.2307/2348250.

[42] Stat-Ease. Design Expert 2021.

[43] Mohsin I, He K, Li Z, Zhang F, Du R. Optimization of the polishing efficiency and torque by using Taguchi method and ANOVA in robotic polishing. Appl Sci 2020;10. doi:10.3390/app10030824.

[44] Kim H. Statistical notes for clinical researchers : Chi-squared test and Fisher's exact test. Open Lect Stat 2017:152–5. doi:10.5395/rde.2017.42.2.152.

[45] Lin S, Bediako JK, Song MH, Kim JA, Cho CW, Zhao Y, et al. Effective recovery of Pt(IV) from acidic solution by a defective metal-organic framework using central composite design for synthesis. ACS Sustain Chem Eng 2019;7:7510–8. doi:10.1021/acssuschemeng.8b04637.

[46] Ganapathy T, Murugesan K, Gakkhar RP. Performance optimization of Jatropha biodiesel engine model using Taguchi approach. Appl Energy 2009;86:2476–86. doi:10.1016/j.apenergy.2009.02.008.

[47] Noordin MY, Venkatesh VC, Sharif S, Elting S, Abdullah A. Application of response surface methodology in describing the performance of coated carbide tools when turning AISI 1045 steel. J Mater Process Technol 2004;145:46–58. doi:10.1016/S0924-0136(03)00861-6.

[48] Kitchin J. 6. Basic statistical inference. vol. 28. Elsevier Masson SAS; 1994. doi:10.1016/S0076-695X(08)60256-2.

[49] American Public Health Association (APHA). APHA Method 2320. Stand. Methods Exam. Water Wastewater. 18th ed., Washington, DC: American Public Health Association (APHA); 1992.

[50] Chen PC, Huang CH, Su T, Chen HW, Yang MW, Tsao JM. Optimum conditions for the capture of carbon dioxide with a bubble-column scrubber. Int J Greenh Gas Control 2015;35:47–55. doi:10.1016/j.ijggc.2015.01.011.

[50] Di Leo G, Sardanelli F. Statistical significance: P-value, 0.05 threshold, and applications to radiomics—reasons for a conservative approach. Eur Radiol Exp 2020;4. doi:10.1186/s41747-020-0145-y.

[51] Lakens D. The practical alternative to the P-value is the correctly used P-value. Perspect Psychol Sci 2021;16:639–48. doi:10.1177/1745691620958012.

[53] Hikita H, Asai S, Takatsuka T. Absorption of carbon dioxide into aqueous sodium hydroxide and sodium carbonate-bicarbonate solutions. Chem Eng J 1976;11:131–41. doi:10.1016/S0300-9467(76)80035-4.

[54] Singh KP, Gupta S, Singh AK, Sinha S. Experimental design and response surface modelling for optimization of Rhodamine B removal from water by magnetic nanocomposite. Chem Eng J 2010;165:151–60. doi:10.1016/j.cej.2010.09.010.

[55] Smith ZD, Keller JR, Bello M, Cordes NL, Welch CF, Torres JA, et al. Plackett-Burman experimental design to facilitate syntactic foam development. J Appl Polym Sci 2016;133:1–9. doi:10.1002/app.42892.

[56] Liu J, Wang J, Leung C, Gao F. A multi-parameter optimization model for the evaluation of shale gas recovery enhancement. Energies 2018;11. doi:10.3390/en11030654.

[57] Coleman DE, Vanatta LE. Lack-of-fit testing of ion chromatographic calibration curves with inexact replicates. J Chromatogr A 1999;850:43–51. doi:10.1016/S0021-9673(99)00369-6.

[58] Rollbusch P, Becker M, Ludwig M, Bieberle A, Grünewald M, Hampel U, et al. Experimental investigation of the influence of column scale, gas density and liquid properties on gas holdup in bubble columns. Int J Multiph Flow 2015;75:88–106. doi:10.1016/j.ijmultiphaseflow.2015.05.009.

[59] Besagni G, Inzoli F, Ziegenhein T, Milano P, Lambruschini V. Two-phase bubble columns : A comprehensive review. ChemEngineering 2018;2(2):13. doi:10.3390/chemengineering2020013.

[60] Besagni G, Gallazzini L, Inzoli F. On the scale-up criteria for bubble columns. Petroleum 2019;5:114–22. doi:10.1016/j.petlm.2017.12.005.

[61] Posadas E, Serejo ML, Blanco S, Pérez R, García-Encina PA, Muñoz R. Minimization of biomethane oxygen concentration during biogas upgrading in algal-bacterial photobioreactors. Algal Res 2015;12:221–9. doi:10.1016/j.algal.2015.09.002.

[62] Zedníková M, Orvalho S, Fialová M, Ruzicka MC. Measurement of volumetric mass transfer coefficient in bubble columns. ChemEngineering 2018;2:1–14. doi:10.3390/chemengineering2020019.

[63] Loftus GR. On interpretation of interactions. Mem Cognit 1978;6:312–9. doi:10.3758/BF03197461.

[64] Bahr M, Díaz I, Dominguez A, González Sánchez A, Muñoz R. Microalgal-biotechnology as a platform for an integral biogas upgrading and nutrient removal from anaerobic effluents. Environ Sci Technol 2014;48:573–81. doi:10.1021/es403596m.

[65] Jakobsen HA. Bubble Column Reactors. Chem. React. Model. Multiph. React. Flows, Trondheim: Springer Berlin Heidelberg; 2009, p. 335–501.

[66] Rodero M del R, Lebrero R, Serrano E, Lara E, Arbib Z, García-Encina PA, et al. Technology validation of photosynthetic biogas upgrading in a semi-industrial scale algal-bacterial photobioreactor. Bioresour Technol 2019;279:43–9. doi:10.1016/j.biortech.2019.01.110.

[67] A. Converti, A. Lodi, A. Del Borghi, C. Solisio, Cultivation of *Spirulina platensis* in a combined airlift-tubular reactor system, Biochem. Eng. J. 32 (2006) 13–18. doi:10.1016/j.bej.2006.08.013.

[68] L. Binaghi, A. Del Borghi, A. Lodi, A. Converti, M. Del Borghi, Batch and fed-batch uptake of carbon dioxide by *Spirulina platensis*, Process Biochem. 38 (2003) 1341–1346. doi:10.1016/S0032-9592(03)00003-7.

[69] M. Płaczek, A. Patyna, S. Witczak, Technical evaluation of photobioreactors for microalgae cultivation, E3S Web Conf. 19 (2017) 1–10. doi:10.1051/e3sconf/20171902032.

[70] A. Xia, C. Herrmann, J.D. Murphy, How do we optimize third-generation algal biofuels ?, Biofuels, Bioprod. Biorefining. 9 (2015) 358–367. doi:10.1002/bbb.1550.

[71] L. Delgadillo-mirquez, F. Lopes, B. Taidi, D. Pareau, Nitrogen and phosphate removal from wastewater with a mixed microalgae and bacteria culture, Biotechnol. Reports. 11 (2016) 18–26. doi:10.1016/j.btre.2016.04.003.

6 A perspective on novel cascading algal biomethane biorefinery systems

A perspective on novel cascading algal biomethane biorefinery systems

Archishman Bose[a,b,†], Richard O'Shea[a,b,*,†], Richen Lin[a,b,†], Jerry D Murphy[a,b,†]

[a]Environmental Research Institute, MaREI Centre, University College Cork, Cork, T23 XE10, Ireland

[b]Department of Civil, Structural and Environmental Engineering, School of Engineering and Architecture, University College Cork, Cork, T12 K8AF, Ireland.

Abstract

Synergistic opportunities to combine biomethane production via anaerobic digestion whilst cultivating microalgae have been previously suggested in the literature. While biomethane is a promising and flexible renewable energy vector, microalgae are increasingly gaining importance as an alternate source of food and/or feed, chemicals and energy for advanced biofuels. However, simultaneously achieving, grid quality biomethane, effective microalgal digestate treatment, high microalgae growth rate, and the most sustainable use of the algal biomass is a major challenge. In this regard, the present paper proposes multiple configurations of an innovative Cascading Algal Biomethane-Biorefinery System (CABBS) using a novel two-step bubble column-photobioreactor photosynthetic biogas upgrading technology. To overcome the limitations in the choice of microalgae for optimal system operation, a microalgae composition based biorefinery decision tree has also been conceptualised to maximise profitability. Techno-economic, environmental and practical aspects have been discussed to provide a comprehensive perspective of the proposed systems.

6.1 Introduction

6.1.1 Biofuels in the future bioeconomy

Transitioning from a fossil-based economy to a renewable biological resource-based bioeconomy is required to reduce environmental impacts including greenhouse gas (GHG) emissions in food, energy and material production [1]. Within the future bioeconomy, biofuels will play a significant role in energy systems including advanced transport biofuels and agriculture [1]. To maximise profitability and sustainability, biofuels can benefit from revenues associated with co-products generated in a biorefinery system, and by the optimal choices of resources, methods of production and processing, and use of co-products.

6.1.2 Biomethane: a renewable biofuel

Gaseous biofuels, particularly biogas produced via anaerobic digestion (AD), present significant benefits including; *1)* the possibility for use in electricity, heat and /or transport; *2)* lower capital and operational costs compared to other advanced bioenergy technologies like gasification and pyrolysis; *3)* ability to incorporate a wide variety of feedstock; and *4)* scope for nutrient recycling [2]. Biomethane (over 92% CH_4 following the removal of CO_2 from biogas) can therefore be a versatile renewable biofuel that can effectively substitute natural gas in complex energy systems, viz., transport and agriculture [3]. This enables biomethane to play a significant role in decreasing emissions from energy sectors including electricity, heating and cooling, heavy industries and transport [3].

6.1.3 Advances in biogas upgrading to biomethane using microalgae

By 2026, in the EU, biomethane must effect a GHG emissions reduction of 65% as compared to the fossil fuel comparator (FFC) to be deemed sustainable as a biofuel in the transport sector [4]. Therefore, innovations in both feedstock and biogas upgrading technologies are urgently needed. Besides the choice of feedstock (the primary contributor towards the overall emissions), emissions associated with energy used in biogas upgrading are significant [5]. Traditional upgrading technologies employing physicochemical techniques, viz., membrane separation, chemical adsorption and pressure swing adsorption have a significant energy penalty (3-6% of

the energy content of biogas processed) and a high cost [6]. Photosynthetic biogas upgrading using microalgae could overcome the economic and environmental drawbacks associated with traditional biogas upgrading [7]. In this process, CO_2 is removed from biogas by a carbonate-rich solution generating bicarbonate. The bicarbonate rich solution is used as an inorganic carbon source for microalgae cultivation at a relatively high pH [8]. High areal productivity of microalgae, rapid CO_2 fixation, and ability to grow in a wide range of environments [9] would increase the sustainability of photosynthetic biogas upgrading. Although a two-step bubble-column and microalgae cultivation using a circulating algal solution have been found to be effective [10], being a novel technology, the choice of operational parameters and the microalgae species for optimal performance is still under research.

6.1.4 Cascading algal biomethane biorefinery system (CABBS) in a circular bioeconomy

Effective utilisation of highly efficient natural microalgae "bio-factories" [11] is imperative to ensure the economic and environmental sustainability of photosynthetic biogas upgrading. Indeed, without effective resource management through principles of input reduction, eco-design, minimisation and recycling of waste, a bioeconomy system often fails to achieve its objective benefits [12]. This mandates a shift from the traditional "take-make-dispose" linear economic model towards a circular economy through the integration of different sectors and technologies.

Simultaneous production of biofuels and high-value products for food, feed, and chemicals, often referred to as a microalgae biorefinery is currently receiving significant research attention to maximise the use of microalgae [11,13]. Integrating a microalgae biorefinery and AD system for biomethane production via CABBS presents an interesting opportunity for a circular bioeconomy system as shown in Figure 6-1. In addition to simultaneous biogas upgrading and CO_2 supply for microalgae growth, digestate (residue from AD) can be used as a fertiliser or as a nutrient source to grow microalgae [14]. However, to maximise the benefit of such combined systems, an assessment of each implementation possibility is required. To the best of the authors' knowledge, the present literature focuses on the microalgae strain selection based on the targeted product (such as biodiesel, biogas and protein). However, due to the considerable variation in microalgae composition from the

growing conditions, determining the use of microalgae, based on its final composition would amplify the positive impact of the integrated systems with microalgae.

In this paper, possibilities for AD based circular biomethane-biorefinery systems have been explored with an emphasis on the following:

1. Establish the state of the art of microalgae use in AD, including; *biogas generation*, *biogas upgrading* and *digestate treatment*.

2. Develop a decision tree for an effective microalgae biorefinery with a focus on AD from the perspective of microalgae composition.

3. Explore and illustrate possible configurations of the proposed CABBS layout.

4. Provide a perspective on the corresponding economic, sustainability and practical challenges of such integrated systems.

6.2 Microalgae in biogas and biomethane systems

Producing biomethane via AD entails three fundamental steps: *1)* biogas generation; *2)* biogas upgrading to biomethane; and *3)* digestate treatment and re-use. Herein, the synergies and limitations of applying microalgae in each of these steps have been reviewed focusing on the benefits to both microalgae cultivation and utilisation.

6.2.1 Biogas generation from microalgae

Theoretical specific methane yields (SMY_{PCL}) of any biomass can be estimated from its chemical composition, as described in Eq. 6.1 [15]. The SMY of 1.014 L/gVS, 0.415 L/g VS and 0.446 L/gVS from lipids (L), carbohydrates(C) and proteins(P) were found to adequately predict biogas generation from the AD of microalgae [16]. The chemical oxygen demand (COD) of the biomass can also be used to estimate the theoretical SMY (SMY_{COD}) under mesophilic conditions as described in Eq. 6.2 [17].

$$SMY_{PCL} = 0.446 \times P + 0.451 \times C + 1.014 \times L \quad (6.1)$$

$$SMY_{COD} = 0.380 mLCH_4\ g^{-1}COD \times (CODg^{-1}VS) \quad (6.2)$$

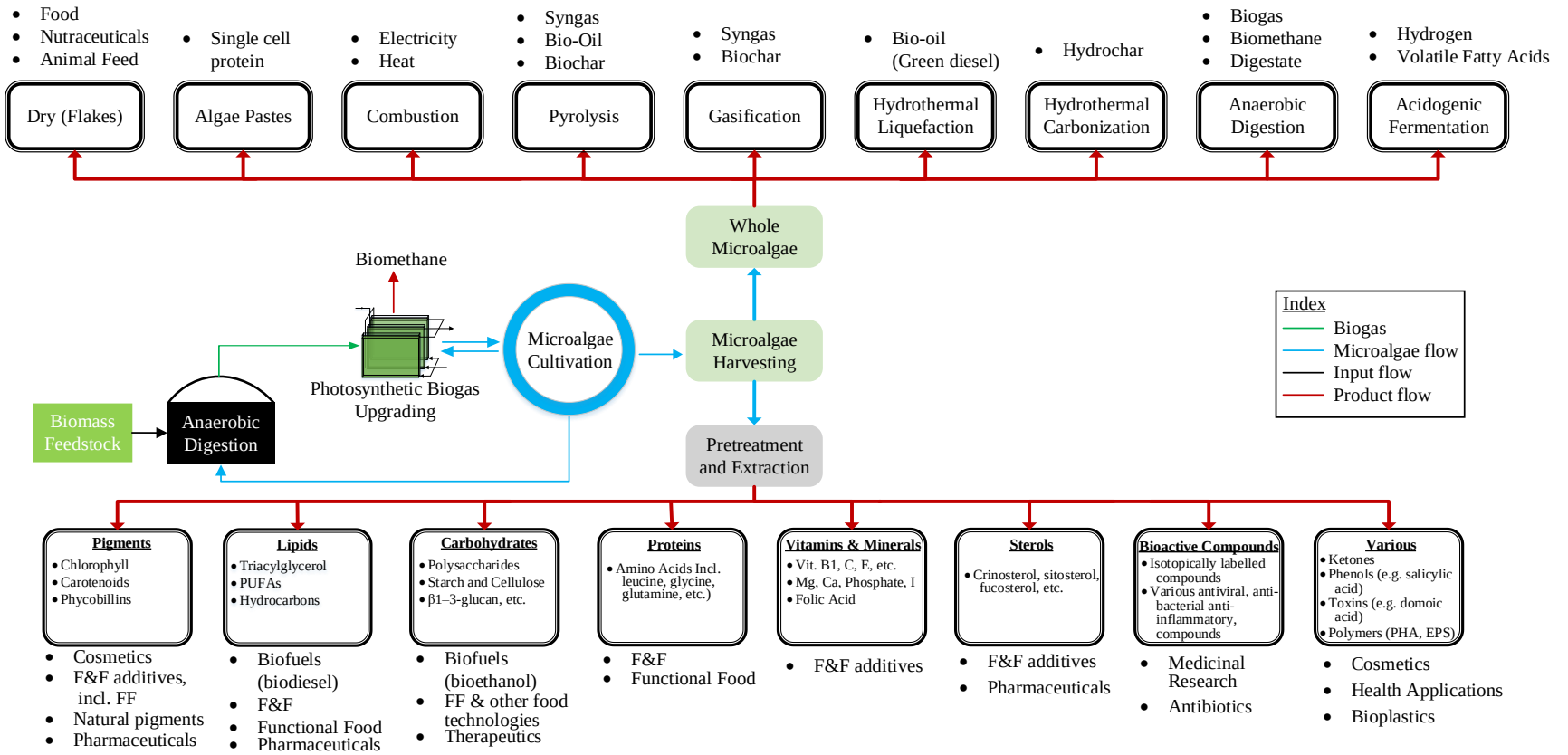


Figure 6-1 Schematic representation of a cascading algae biomethane biorefinery system with a summary of different microalgae bio-products and possible applications in food, feed and energy; F&F: Food and Feed; FF: Functional Food

Table 6-1 Theoretical and actual specific methane yield (SMY) in batch tests without pre-treatment, after pre-treatment and following fraction (lipid and protein) extraction of multiple microalgae species reported in the literature

Microalgae	Theoretical SMY [g/L-VS]	Experimental SMY, Batch [g/L-VS]				Reference
		Without pre-treatment	After pre-treatment	After lipid Extraction	After protein Extraction	
Chlamydomonas reinhardtii 6145	0.399	0.351				(Fernández-Rodríguez et al., 2019) [18]
C. reinhardtii cw15	0.433	0.381				
Chlorella vulgaris	0.465	0.046***	0.242			(Mahdy et al., 2016) [19]
Chlorella vulgaris	0.479	0.24				
Aphanizomenon ovalisporum	0.532	0.2877				(Mendez et al., 2015) [20]
Synechocystis sp.	0.476	0.38				
Borzia trilocularis	0.482	0.2842				
Chlorella vulgaris 211/11B	0.543*	0.24				(Ras et al., 2011) [17]
Chlorella vulgaris UTEX 395	0.604	0.337		0.314		
Nannochloropsis sp.	0.682	0.357		0.399		
Nannochloropsis salina	0.749	0.557		0.383		(Zhao et al., 2014) [21]
Nanofrustulum sp.	0.882	0.507		0.304		
Phaeodactylum tricornatum CCMP 632	0.629	0.337		0.339		
Nannochloropsis gaditana	1.568	0.17		0.203		
Isochrysis T-ISO	0.866	0.188		0.215		(Hernández et al., 2014) [22]
Scenedesmus almeriensis	0.646	0.165		0.203		
Tetraselmis maculata	0.738	0.205		0.236		

Microalgae	Theoretical SMY [g/L-VS]	Experimental SMY, Batch [g/L-VS]				Reference
		Without pre-treatment	After pre-treatment	After lipid Extraction	After protein Extraction	
Scenedesmus sp.	0.35	0.084	0.133			(González-Fernández et al., 2012b) [23]
Scenedesmus sp.	0.417	0.14		0.212	0.273	(Ramos-suárez and Carreras, 2014) [24]
Spirulina platensis	0.569	0.357				(Herrmann et al., 2016) [25]
Spirulina platensis	0.422**	0.37				(Aramrueang et al., 2016) [26]
Spirulina platensis	0.558	0.254	0.254		0.163	(Parimi et al., 2015b) [27]
Spirulina platensis	0.488	0.298	0.298			(Du et al., 2018) [28]
Hydrodictyon reticulatum	0.574	0.17	0.384			(Lee et al., 2014) [29]

SMY: Specific methane yield. The full names of microalgae species listed are as follows: C. reinhardtii - Chlamydomonas reinhardtii; P. tricornatum - Phaeodactylum tricornatum; H. reticulatum- Hydrodictyon reticulatum; A. ovalisporum - Aphanizomenon ovalisporum;
** Calculated based on the reported COD content in biomass using Eq. 6.2*
*** Calculated based on the reported protein, carbohydrate and lipid fractions using Eq 6.1*
**** Results from continuous 1 L Continuous Stirred Reactor (CSTR)*

The presence of a broad range of carbohydrates (7 to 69% volatile solids (VS)), lipids (1 to 63% VS) and proteins (15 to 84% VS) makes microalgae an attractive substrate for AD, either directly or after the extraction of specific fractions [30]. In practice, however, ideal biogas generation is seldom achieved. Although non-structural carbohydrates such as starch are readily digestible, high concentrations could lead to a build-up of volatile fatty acids (VFAs) in the digester and inhibit AD [31]. Sub-optimal C: N ratios owing to the presence of proteins (levels of around 6-9) [32], lead to increased NH_3^+ accumulation, accelerating digester failure through inhibition of methanogenesis and VFA accumulation [31,33]. The presence of long-chain fatty acids in lipids can cause severe inhibition to AD, requiring long retention times to achieve biodegradation [34]. In addition, the presence of complex structural carbohydrates, viz., cellulose and hemicellulose in the microalgal cell walls limit their practical methane yield by encapsulating the more readily digestible fractions [30]. For un-treated microalgae, especially freshwater species like *Scenedesmus obliquus*, therefore, biodegradability is often below 50% (Table 6-1). In contrast, due to the presence of less complex cell walls, most un-treated cyanobacteria such as *Spirulina platensis* show biodegradability of above 60%. However, a higher yield from the AD of untreated cyanobacteria is hindered due to their high protein content.

Pre-treatment of microalgae to rupture cell walls and increase the availability of digestible fractions is one of the most promising techniques to enhance SMY from microalgae, clearly observed from the data in Table 6-1. Several methods including physical (mechanical and thermal); chemical, (acidic and alkaline); and biological (aerobic digestion and enzymatic) pre-treatments have been proposed [9,30], each with its own merits and disadvantages. For example, ultra-sonic pre-treatment was reported to increase the SMY by 128 MJ/kg total solid (TS) or 90% but required 128.9 MJ/kg-TS of input energy for *Scenedesmus* sp. [32]. In contrast, a 15% increase in SMY was reported by enzymatic pre-treatment with much lower energy expenditure [35]. Co-digestion of microalgae with suitable feedstock having a high C: N ratio can optimise the C: N ratio and improve digestion conditions [30]. A 46% increase in the SMY was observed by mixing a microalgae culture dominated by *Microcystis* spp. with corn straw to ensure a C: N ratio of 20 [36]. Herrmann et al., (2016) [23] co-digested *Spirulina platensis* with barley straw, beet silage, and *Laminaria digitata* respectively at a C: N ratio of 25. Improvements in biomethane yield (22.5% as

compared to mono-digestion of *Spirulina platensis*) at a higher organic loading rate of 2 g/VS/L/day, were obtained with 55% beet silage as co-substrate (VS basis). Alternatively, changing the microalgae growth environment for a more favourable biochemical composition for AD has also been proposed to improve biogas yield [9].

Residual biomass, after extraction of valuable fractions, is also an effective substrate for biogas generation. AD of lipid extracted *Chlorella vulgaris*, *Nannochloropsis salina* and *Nannochloropsis gaditana* yielded above 0.3 L/g-VS of biogas [19]. Amino acid extracted *Scenedesmus* sp. produced 272.8 ± 7.3 $mLCH_4$/g-VS, a two-fold increase in CH_4 yield compared to untreated biomass [22]. Protein extracted *Spirluna platensis* was shown to improve the CH_4 yield by 30.4% to 236.1 $mLCH_4$/g-VS as compared to untreated biomass [37]. However, the yield was 18 mL/g-VS lower than that of pre-treated *Spirulina platensis* under high pressure without any extraction. The type of pre-treatment for fraction extraction is also crucial for the effective digestion of residues. For example, thermal pre-treatment of microalgae during lipid extraction resulted in a 40% increase in SMY compared to that from microalgae residue after lipid extraction without pre-treatment. However, the use of chloroform for lipid extraction suppressed biogas production from the residue biomass by inhibiting methanogenesis [38].

6.2.2 Biogas upgrading by microalgae

Bubbling biogas in an absorption (bubble) column connected to a photobioreactor with a circulating algal solution has been established as an effective configuration to optimise biogas upgrading using microalgae [8,39]. In this process, CO_2 is first absorbed by an alkaline solution with carbonate medium (97% CO_2 removal at pH 9.8 and above), which also ensures a total H_2S removal [7,40]. As shown in Figure 6-2, microalgae could be cultivated using bicarbonate as the inorganic carbon for photosynthesis, re-generating carbonate in return. Thus, both, a carbonate/bicarbonate cycle and the pH of the circulating medium can be maintained naturally [8]. Oxygen generated during photosynthesis, leading to elevated levels of O_2 (>1%) in the upgraded biomethane is a major challenge to meet gas grid specifications using this process without process optimisation. Besides process optimisation and expertise presented in previous chapters, the opportune choice of microalgae species could lead to further optimisation of system operations [8]. Highly

alkaliphilic cyanobacteria such as *Spirulina platensis* is one of the most promising species satisfying all criteria [8]. The ability to grow mixotrophically would further allow *Spirulina* sp. to be integrated with digestate cleaning whilst upgrading biogas. *Anabaena* sp. and *Synechococcus* sp. have similar properties, although the latter would require expensive harvesting techniques due to its unicellular structure. Among the unicellular green algae species, *Scenedesmus obliquus*, *Chlorella sorokiniana* SLA-04; a mutant strain of *Chlorella* sp. AT1 and *Dunaliella salina* NIES-2257 are suitable [8]. When simultaneous digestate treatment is not desired, alkaliphilic cyanobacteria including *Rhabdoderma* sp. and *Geitlerinema* sp. could also be effectively utilised.

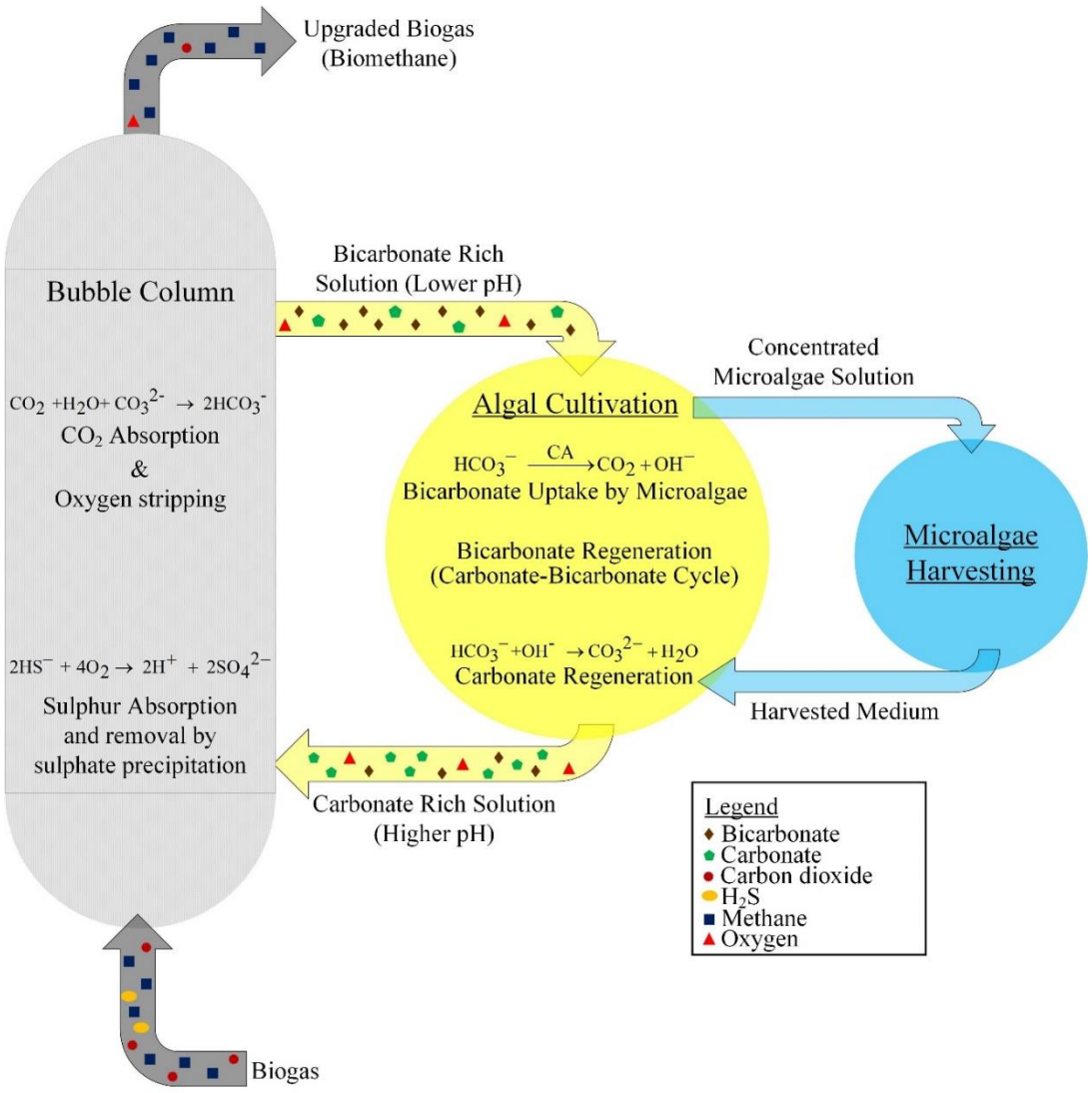


Figure 6-2 Schematic of photosynthetic biogas upgrading in an alkaline (carbonate) algal solution via carbonate/bicarbonate cycle followed by microalgae harvesting (The number of markings of each chemical species are indicative only to their relative quantity and not in absolute terms) [8]

6.2.3 Digestate treatment by microalgae

Digestate from anaerobic digestion comprises solid (10 to 20%) and liquid (80 to 90% by mass) fractions [41]. Harmful emissions to air, water and soil through contamination of the un-treated liquid fraction is a major challenge for the biogas industry [41]. However, most of the hazardous chemicals in the liquid digestate, including heavy metals are essential for microalgae growth [41]. Therefore, the use of liquid digestate as a nutrient source for microalgae cultivation has been advocated to be advantageous for digestate treatment.

Growing microalgae in liquid digestate, however, has its challenges. High turbidity; high total ammonium nitrogen (TAN) content between 1,000-3,000 mgNH_4^+/L; and high COD of 7,000 mg/L in the digestate are some inhibitory factors towards algal growth. These would thus limit direct use of digestate for microalgae cultivation [41]. Therefore, dilution of the digestate is necessary, often performed using wastewater or seawater to increase sustainability [41]. Furthermore, microalgae cultivated in digestate are prone to biological contamination from bacteria, viruses, and other foreign species [42]). This directs the current trend in treating digestate with microalgae to use robust chlorophyte species such as *Chlorella* sp. and *Scenedesmus* sp. [41,43].

6.2.4 Combined biogas upgrading and digestate treatment by microalgae

Simultaneous biogas upgrading and digestate treatment have been studied quite frequently in the literature. However, maximising the effectiveness of both strategies has seldom been reached at the same time. While the favourable pH range for digestate treatment varies between pH 7 and 8 [41], that for biogas upgrading should be preferably above pH 9.5. As Bahr et al., (2014) [40] reported during biogas upgrading, a decrease in pH from 9.4 to 7 led to a drop in both the CO_2 removal efficiency and biomass productivity when diluted digestate was added replacing mineral salt for *Spirulina platensis* growth. This inherently limits the selection of microalgae species that can simultaneously be favourable for both conditions. *Scenedesmus obliquus*, as well as moderately alkaliphilic cyanobacteria including *Anabaena* sp. and *Synechococcus* sp., able to grow favourably between pH of 7 and 9.5, could be

potential candidates. Other mutant species or species cultivated via adaptation could also be effective. Alternately, developing parallel processes for digestate treatment and biogas upgrading with separate microalgae species could be an effective solution. This might complicate the supply of CO_2 and nutrients from the biogas to ensure ideal growth conditions for the species raising both installation and operational costs. No such configurations have yet been reported in the literature.

6.3 Further opportunities from microalgae bioresource

6.3.1 Bioproducts from microalgae

Opportune use of microalgae, especially after biogas upgrading and/ or digestate treatment is essential to maximise the economic and environmental benefit of the overall process. The use of whole microalgal biomass offers the simplest practical application. Liquid and gaseous biofuels, solids such as biochar, as well as renewable heat and electricity are obtained via thermochemical conversion of whole biomass [13]. Alternatively, based on composition, specific microalgae species can be used either as food (e.g. *Nostoc* and *Spirulina*) [44] or, as soil additives and fertilizers for soil restoration against desertification [45,46]. Although direct photolysis of microalgae could generate biohydrogen, a process efficiency below 1% limits the commercialisation of this technology [47] and hence it is not described in Figure 6-1. Alternatively, hydrogen can also be generated alongside VFAs via acidogenic fermentation (AF) [48]. High protein-containing microalgae, which naturally inhibits AD due to VFA accumulation, could be advantageous in this regard. Unlike AD, the effluents from AF are rich in VFAs, considered as essential platform chemicals that could widely replace traditional petrochemicals in future biorefineries [49]. In addition, as VFAs have also been found to enhance microalgae growth, residues from AF could potentially be more advantageous for microalgae cultivation than digestate from AD [14]. Enhancement of hydrogen and VFA yield through pre-treatment and co-digestion [49] could allow attractive integration of AF into the overall biomethane biorefinery with microalgae.

Considering the utilisation of individual fractions, as can be seen in Figure 6-1, bioethanol, biobutanol, biohydrogen and organic acids can be obtained from anaerobic fermentation of the carbohydrates in microalgae including polysaccharides [50].

Polysaccharides can also be used in a variety of industries including personal care products [45]. Algal oils from lipids can substitute traditional fish or vegetable oils or can be processed to synthesize biodiesel [51]. Glycerol is a valuable chemical from biodiesel production (10% weight/weight of biodiesel) by transesterification [52]. Proteins including essential amino acids (e.g. lysine) can be widely applied in nutritional and health supplements post-extraction and purification. Carotenoids, chlorophylls and xanthophyll can be extracted for use as additives for both human and animal feed, cosmetics, pharmaceuticals, colouring agents and biomaterials [13]. Phycobiliproteins and astaxanthin from microalgae are already commercialised high-value products for use in food and feed and medicines [13,44]. Microalgae can also produce limited quantities of other valuable products including polyunsaturated fatty acids (PUFAs), phytosterols, bioactive peptides, toxins, as well as polyketides and antibiotic substances, as summarised in Figure 6-1.

6.3.2 Economic considerations of microalgae bio-products

In general, nutraceutical products attract the highest market prices followed by items for human consumption and personal care, bulk chemicals, animal feed, and biofuels [45,53]. Prices for biofuels are primarily driven by fossil fuel prices [54]. Average market prices are typically: 0.4 €/litre to 0.6 €/litre for bioethanol; 0.5 €/litre to 0.7 €/litre for biodiesel [54,55]; and 0.12 €/m^3 to 0.2 €/m^3 for biogas [45,56]. The production of electricity or heat from biogas, or the injection of biomethane into the gas grid are increasingly incentivised in many countries as advanced forms of renewable energy. In the EU, electricity rates from biogas typically vary between 4 ct€/kWh_e in Hungary to 28 ct€/kWh_e in Germany according to feed-in-tariffs (FiT) [57]. On the contrary, renewable heat is mostly characterised either by low feed-in tariff (e.g. 2.95 ct€/kWh in Ireland) [58] or variable local demands and negotiations at largely fluctuating prices between 1.2 ct€/kWh and 12 ct€/kWh [59]. Grid injection of biomethane is increasingly being incentivised within the EU. Tariffs vary between 5.5 ct€/kWh in the UK [60] to 9.5 ct€/kWh in France [61]. Considering the assumptions summarised in *Box 6.1*, the effective price per m^3 of biogas within the EU would then increase to 0.64 €/m^3 for electricity; 0.7 €/m^3 for heat; and 0.48 €/m^3 for biomethane. Despite the relatively low prices, encouraging national (in countries such as those within the EU and the USA) and international policies (such as by the Organisation for Economic Cooperation and Development) could set the biofuel sector to rapidly

increase at an average compound annual growth rate of over 5% (Figure 6-3a). Indeed, as can be visualised from the data in Figure 6-3a, electricity production presents the biggest market opportunity for bioenergy. This is followed by biomethane, with the potential to be valued at over 5 billion-€ globally by 2025 [62].

The combined health and wellness, food, and animal feed market forms the largest global bulk market for microalgae bio-products, to be worth over a trillion euro by 2025. As evident from Figure 6-3a, a significant variation in these prices results from the type of application and purity. As an example, while the price of whole microalgae for animal feed is less than 0.3 €/kg in the EU [63], dried whole *Spirulina*, cultivated in China is being sold for human consumption at 44 €/kg within the EU [64]. On the other hand, C-phycocyanin, a protein pigment, sells between 180 €/kg and 2 million €/kg based on purity [65]. In addition, as can be seen within Figure 6-3a, market growth opportunities for an individual product varies significantly. For example, high-value chemicals such as isotopically labelled compounds and astaxanthin are already commercially produced from microalgae; and thus have limited market growth potential. In contrast, ω-3 fatty acids could see a growth of over 14% in the near future.

6.3.3 The dilemma of microalgal use

Most of the low market value products from microalgae including biofuels account for either high market volume or represent significant growth opportunities in future. Products such as whole microalgae for human consumption or essential fatty acids are unique, representing both, a high selling price of around 50 €/kg and a fast-growing global market. However, compared to biofuels, they would continue to represent a considerably lower overall market volume in the future. In addition, most often, these high-value products are present in limited quantities in microalgae. To account for the varying usable fraction of microalgae and to analyse the corresponding financial benefits/drawbacks, the equivalent selling price (ESP) per dry weight of whole microalgae for each algal bio-product was evaluated (see *Box 6.1* with respective assumptions).

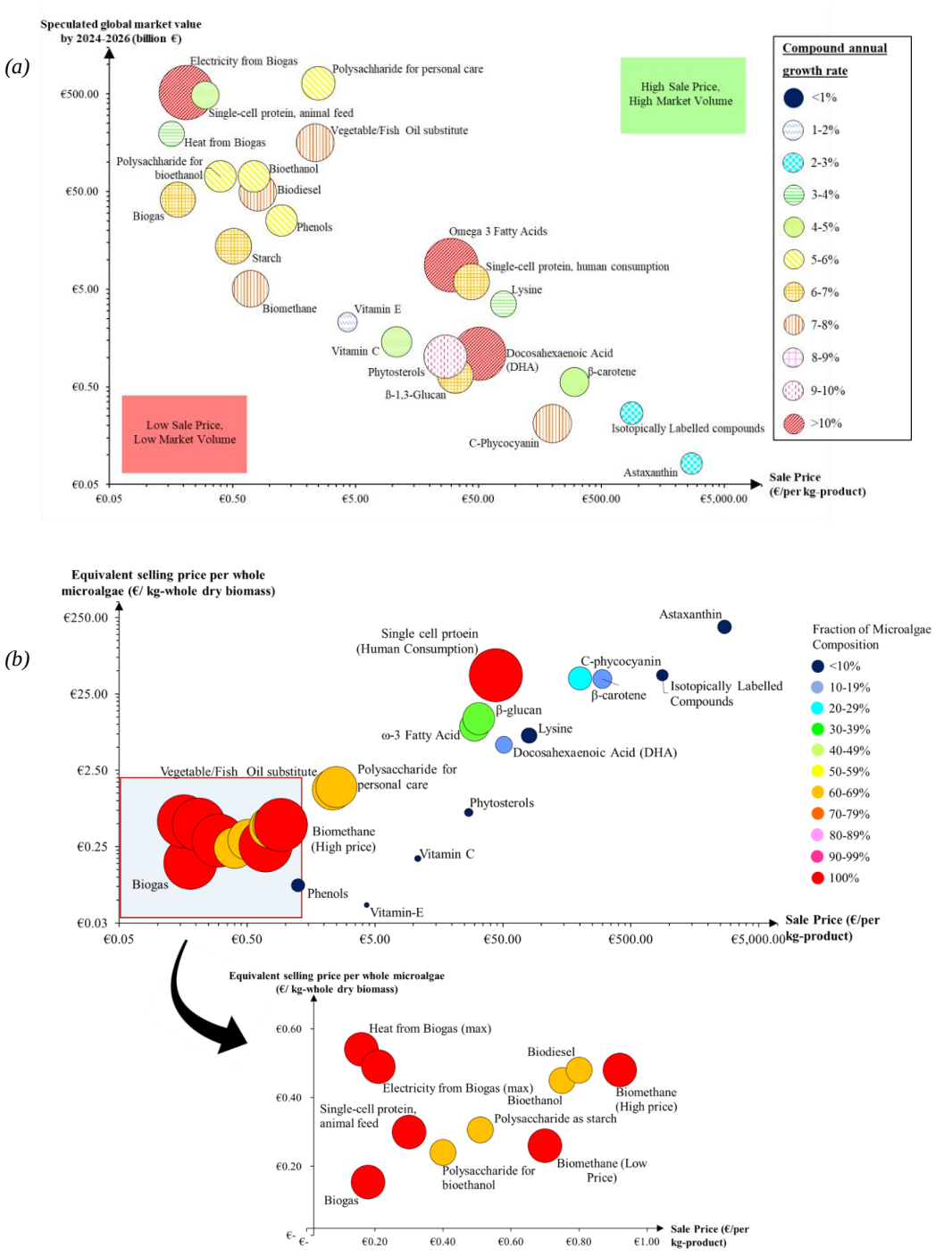


Figure 6-3 Evaluation of market opportunity and economic possibilities with respect to the current market sale price of some common bio-products from microalgae, considering (a) the speculated global market value and market growth up to 2024-26, in which, the bubble size and hatching style represents the compound annual growth rate (CAGR) of each product and (b) the equivalent selling price of corresponding bio-products respectively. The bubble sizes in (b) indicate the maximum fraction of microalgae utilisable for the corresponding bio-product considering maximum conversion. All references are explained and included in detail in Table A6.1 in the appendix.

BOX 6. 1: Example calculation for equivalent selling price per whole microalgae of algal bio-products

For all products except biodiesel, bioethanol and biogas

➔ Maximum fraction of C-phycocyanin in microalgae = 20% db* [65]

➔ Current sale price of C-phycocyanin with minimum purity = 200 €/kg [65]

➔ Equivalent sell price (ESP) of C-phycocyanin = 200 ×20% = 40 €/kg-db

For biodiesel

➔ Maximum lipid content in microalgae = 60% [53]

➔ Current sale price of biodiesel = 0.7 €/litre [55]

Assuming the density of biodiesel as 0.88 kg/L [66]

➔ ESP of biodiesel, considering entire lipid fraction to be converted to biodiesel, = (0.7 × 60%) / 0.88 = 0.48 €/kg-db

➔ ESP of biodiesel, for a partial conversion of 80% from lipid to biodiesel [67] = (0.7 × 60%) / 0.88 × 80% = 0.38 €/kg-db

For bioethanol

➔ Maximum carbohydrate content in microalgae = 60% [68]

➔ Current sale price of bioethanol = 0.6 €/litre [55]

Assuming the density of bioethanol as 0.8 kg/L [66]

➔ ESP of bioethanol, considering entire carbohydrate fraction to be converted to bioethanol = (0.6 × 60%) / 0.88 = 0.45 €/kg-db

➔ ESP of bioethanol, for a partial conversion of 64% of carbohydrate fraction [69] = (0.6 × 60%) / 0.8 × 64% = 0.29 €/kg-db

For biogas as direct commodity

➔ Maximum utilisable fraction of microalgae = 100%

➔ Current sale price of biogas = 0.2 €/m^3 [70]

From Table 6-1, assuming; 0.5 L-CH_4/g-VS, 60% CH_4, VS content of 92% in the microalgae [25,37], density of biogas as 1.1 kg/m^3 [71]:

➔ Biogas price per kg =(0.2) / 1.1 = 0.18 €/kg

➔ Biogas generated per dry biomass = (0.5 × 0.92) / 0.6 = 0.77 L-biogas/ g-db

➔ ESP of biogas = 0.7 × 0.2 = 0.154 €/kg-db

For biogas as electricity

➔ Maximum tariff for electricity = 28 ct€/kWh [72]

➔ Minimum tariff for electricity = 4 ct€/kWh [72]

Assuming biogas with a lower calorific value of 6.5 kWh/Nm^3 [73]; electricity conversion efficiency of 35%; and that biogas being sold for electricity production is priced according to an average electricity tariff of 10 ct€/kWh

➔ Average price of biogas when sold for electricity = (0.1 × 6.5 × 0.35) / 1.1 = 0.21 €/kg-biogas

➔ Highest ESP of electricity = 0.28 × 6.5 × 0.77 × 0.35 = 0.49 €/kg-db

➔ Lowest ESP of electricity = 0.04 × 6.5 × 0.77 × 0.35 = 0.07 €/kg-db

For biogas as heat

➔ Maximum tariff for heat = 12 ct€/kWh [73]

➔ Minimum tariff for heat = 1.2 ct€/kWh [73]

Assuming biogas lower calorific value of 6.5 kWh/Nm^3; heat conversion efficiency of 90%; and that biogas being sold for heat production is priced as per an average tariff of 3 ct/kWh for heat,

➔ Average price of biogas when sold for heat = (0.03 × 6.5 × 0.9) / 1.1 = 0.16 €/kg-biogas

➔ Highest ESP of heat from biogas = 0.12 × 6.5 × 0.77 × 0.9 = 0.54 €/kg-db

➔ Lowest ESP of heat from biogas = 0.012 × 6.5 × 0.77 = 0.05 €/kg-db

For biogas as biomethane

➔ Maximum tariff for biomethane = 9.5 ct€/kWh [74]

➔ Minimum tariff for biomethane = 5.3 ct€/kWh [75]

Assuming biogas lower calorific value of 6.5 kWh/Nm^3 [71], 0.77 L-biogas is generated per g-db

➔ Highest ESP of biomethane = 0.095 × 6.5 × 0.77 = 0.48 €/kg-db

➔ Lowest ESP of biomethane from biogas = 0.053 × 6.5 × 0.77 = 0.26 €/kg-db

** db represents dry biomass*

Figure 6-3b reflects the financial benefits of common microalgae bio-products based on ESP with maximum possible product content. For products making up only a minor fraction of microalgae, such as vitamins C&E or phytosterols, their ESP would

drop below that of biofuels. Thus, their extraction would not be rational without the co-production of other chemicals or biofuels for added financial benefit. Additionally, for species grown at conditions suboptimal for product accumulation, or those unable to accumulate a significant amount of the desired product, the ESP can drop significantly. For instance, β-carotene content of 0.01% in *Nannochloropsis oculata* [76] would drop its ESP to 0.04 €/$kg_{dry\ algae}$ compared to 39 €/$kg_{dry\ algae}$ for *Dunaliella salina* with 13% β-carotene content [77].

The current ESP of microalgal biodiesel and bioethanol would be limited to 0.48 and 0.45 €/$kg_{dry\ algae}$, respectively considering complete conversion (*Box 6.1*). However, these could significantly drop to 0.38 and 0.29 €/$kg_{dry\ algae}$ respectively, considering practical conversion rates (*Box 6.1*). As for the use of biogas in electricity, heat, or biomethane, individual country policies would alter the optimal use of microalgae for energy production. For instance, in Germany typical electricity, heat, and biomethane FiTs are 13 ct€/kWh [57], 2.1 ct€/kWh [59] and 7 ct€/kWh [78] respectively. Therefore, with an ESP of electricity, heat and biomethane of 0.09, 0.23 and 0.35 €/$kg_{dry\ algae}$, biomethane injection to the gas grid appears to be the most effective use of biogas from microalgae in Germany.

Microalgae composition, local incentives, and policies, as well as the possibility for considerable CO_2 mitigation, could allow biofuel production to be more attractive than food/feed and high-value compounds. With a fundamental repricing of energy in our society, biofuels could shift from being a high-volume, low-value product to being a high-value, high-volume product with a high compound annual growth rate. Such possibilities and advantages of microalgae biofuels, together with limited market growth opportunities for several high-value algal products have led some researchers to raise concerns about shrinkage in the innovation and development of traditional high-value microalgal industries [79]. Two fundamental dilemmas can be raised regarding the use of microalgae: i) Low priced biofuels (high market size or market growth) vs. high priced products (low market size and market growth); and *ii)* advanced (biofuels) vs traditional (food and pharmaceutical) bio-products.

6.3.4 Decision tree for selecting microalgae biorefinery pathway

A strategy to address the dilemma of microalgae bio-products, together with improving the economics of low-value products is the co-production of multiple products in a biorefinery [79]. Multiple studies have proposed and developed mathematical algorithms for choosing the ideal pathway for processing and utilisation of microalgae, however, focussing on biodiesel production [80,81]. In contrast, for photosynthetic biogas upgrading with or without digestate treatment, the choice of species is often governed by the upstream process(es). Therefore, the strain and the composition of microalgae should be fundamental in defining the target product(s) and corresponding pre-treatment techniques such as cell wall rupturing, if necessary. Figure 6-4 summarizes the decision-making algorithm proposed for selecting the most suitable biorefinery pathway from a microalgae strain perspective.

As an effective first step for the selection of the most preferable bio-product, the ranking of each possible product based on the ESP per kilogram is proposed. Following this, each option could then be ranked in terms of profitability, based on production costs. Practical limitations (conforming to national and international food and drug safety regulations) must also be considered, a discussion of which is presented in Section 6.5.3. Except for the direct application of whole microalgae (such as in AD, and thermochemical conversion processes) all other products including biodiesel and bioethanol must be obtained from the processing and purification of the extracted fractions of microalgae in a primary biorefinery [79]. This would necessitate a costly primary biorefinery step, estimated to be 3-12.7 €/kg of whole dry biomass [11,82]. Cost can significantly increase depending on the level of purity. In such cases, profitability from by-products should also be accounted for on a case-by-case basis. In comparison, a cost of only 1-2 €/kg is needed for processing whole biomass for bulk products (such as biogas and animal feed) [45].

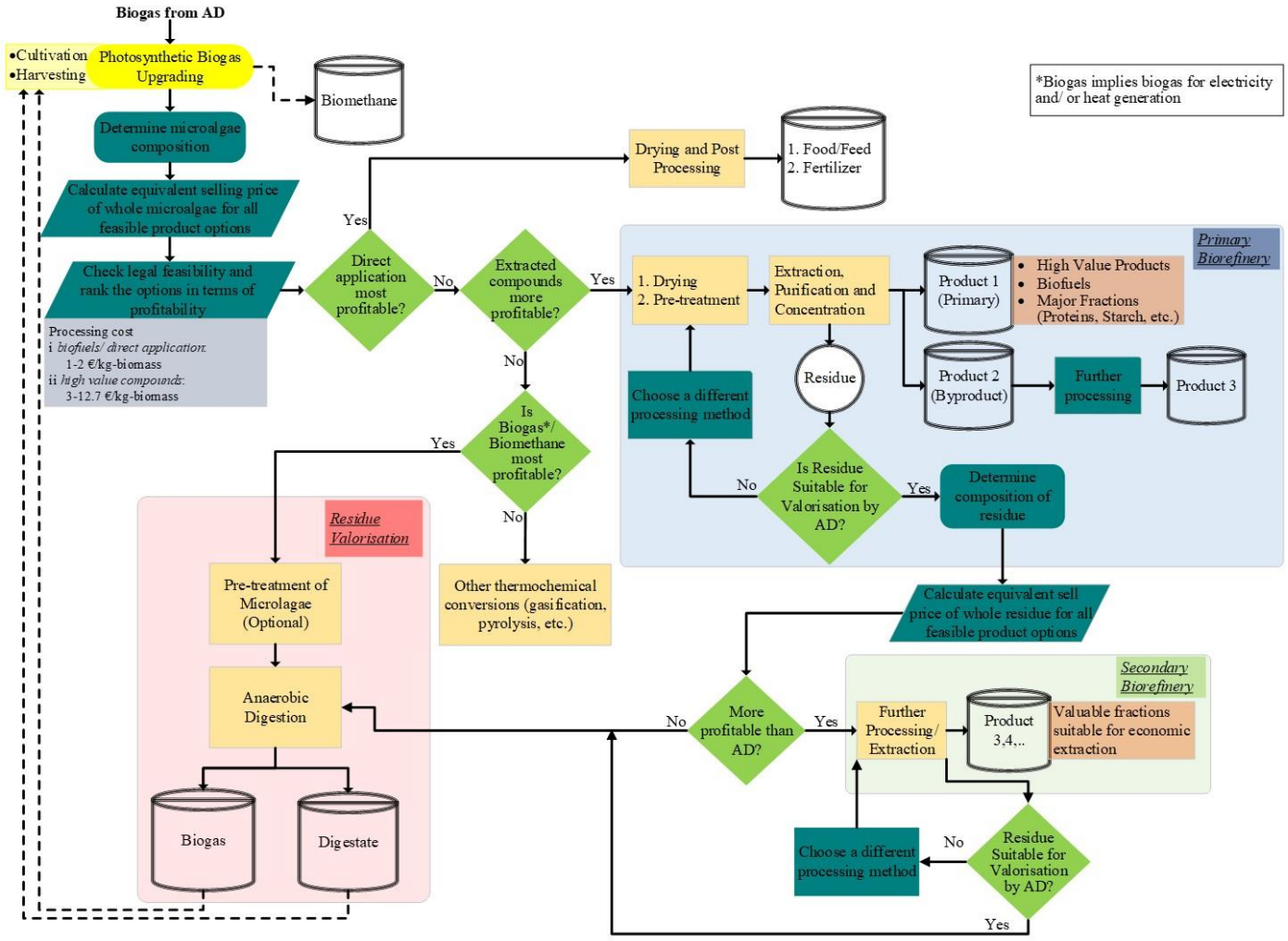


Figure 6-4 Decision-making algorithm for microalgae application in a biorefinery approach from the perspective of microalgae composition.

Residues from a primary biorefinery can be valorised either as waste or in a secondary biorefinery step. A similar decision-making step, considering residue composition and net profitability from its processing must be performed to assess the economic viability of a secondary biorefinery step. On the other hand, AD provides an attractive low-cost pathway for residue valorisation due to the multiple advantages described earlier. Additionally, the potential for coupling of AD and microalgae cultivation, while assisting biomethane production, allows AD to potentially be an integral part of a microalgae biorefinery [84].

6.4 Cascading Algal Biomethane Biorefinery System (CABBS)

Process optimisation, together with the selection of an effective microalgae strain and corresponding biorefinery pathway would be essential for the continuous generation of grid quality biomethane and chemicals, food and/or feed, and other biofuels. Considering the microalgae suitable for photosynthetic biogas upgrading, as identified in Section 6.2.2, in conjunction with the decision tree developed for the associated biorefinery pathway, three possible circular biomethane-biorefinery energy systems have been proposed.

6.4.1 Composition-based biorefinery

6.4.1.1 CABBS with protein-rich microalgae

Spirulina, *Anabaena*, *Synechococcus* and *Scenedesmus* comprise between 40% and 63% protein [15,84]. Unlike *Scenedesmus* sp. leaner cell walls in cyanobacteria make their direct application in AD technically feasible without the need for energy-intensive and costly cell-disruption techniques. However, considering the opportunities for extraction of valuable compounds from protein, as well as the disadvantages of high protein content in AD, extraction of protein in a primary biorefinery step is an attractive alternative. As shown in Figure 6-5a, further purification and concentration then lead to chemically and pharmaceutically valuable pigments such as phycobiliproteins and lectins [65]. Based on the lipid content of the microalgae species, the residual biomass can either be extracted in a secondary biorefinery step or used as an effective substrate to generate biogas. However, a detailed economic justification would then be necessary. High protein microalgae can

also be utilised directly for food and feed applications without extraction of target fractions, subject to food safety regulations.

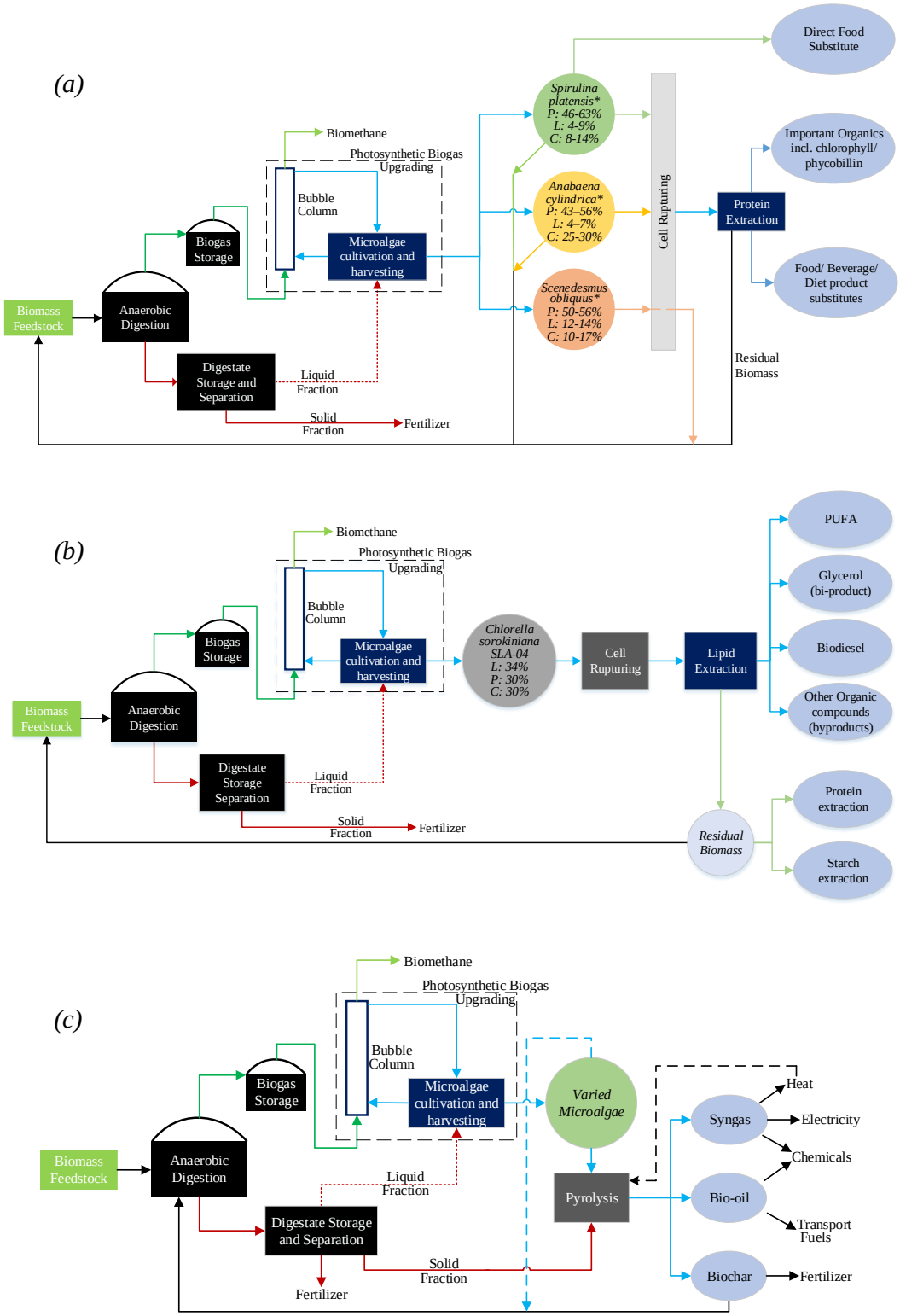


Figure 6-5 Cascading Algal Biomethane Biorefinery System (CABBS) (a) with protein-rich microalgae for photosynthetic biogas upgrading; (b) with lipid-rich microalgae for photosynthetic biogas upgrading; (c) integrating pyrolysis with AD systems and photosynthetic biogas upgrading
**Microalgae composition obtained from Becker (2007) [85] and Lizzul et al., (2018) [86], where, P is protein, L is lipid and C is carbohydrate*

6.4.1.2 CABBS with lipid-rich microalgae

Chlorella sorokiniana SLA-04 can accumulate a lipid content of up to 34% [87], therefore lipid extraction for biodiesel production could be an effective primary biorefinery. Based on the lipid upgrading technique used, glycerol, PUFAs and other organic compounds can also be extracted as by-products, as shown in Figure 6-5b. Glycerol can be subsequently utilised as a raw material for the production of chemicals/fuels including hydrogen, ethanol and biogas [52]. Interestingly, other strains of the same species can also accumulate around 30% protein or carbohydrates [86]. These can thus be extracted via protein extraction techniques in a secondary biorefinery step or co-digested with other feedstock in an AD system. Although the former is a costlier alternative, the possibility to produce high-value products would require a detailed cost-benefit assessment to assess the preferred microalgae utilisation.

6.4.1.3 CABBS utilising Pyrolysis

Production of biofuels or bio-chemicals by pyrolysis (decomposition of biomass between 400°C and 600°C in the absence of oxygen), in contrast to fraction extraction, is a feasible alternative [88]. The favourable carbon and hydrogen content in microalgae, required for pyrolysis, lack of a need for costly pre-processing, the ability to modify process parameters for effective generation of liquid biofuels, and the similarity of microalgal bio-oil compared to fossil fuels are all advantageous [88,89]. In addition, the potential to co-pyrolyse microalgae and digestate to enhance both liquid and solid yield could provide a major synergistic benefit to the proposed pyrolysis-AD system, shown in Figure 6-5c. A major by-product of pyrolysis, biochar could be widely applied as an effective soil additive and bio-adsorbent material due to its considerable carbon offset potential [90]; as well as in AD to enhance methane yield [91]. Biochar for biogas upgrading has also been recently investigated by Linville et al., (2017) [92]. Additionally, the gaseous fraction of pyrolysis can be utilised to meet the system thermal demands, used for electricity production, or processed into chemicals through thermochemical pathways including Fischer-Tropsch processes [93]. Therefore, a sustainable, flexible, and multi-product system can be envisaged. However, being a developing technology, pyrolysis faces several challenges. The presence of excess water in microalgae, requiring energy-intensive

and costly drying to make the harvested biomass suitable for pyrolysis is a major drawback [88]. Furthermore, bio-oil from pyrolysis of microalgae is acidic, unstable, and contains significant solid and water fractions [88]. Therefore, considerable technological advancements and process optimisation are necessary to achieve practical integration of the AD and pyrolysis through CABBS.

6.5 Environmental, economic and practical challenges and prospects

Techno-Economic Assessment (TEA) and Life Cycle Assessment (LCA) are two widely used tools for evaluating and optimising the financial feasibility and the environmental impacts of products/ processes respectively [13,45]. Using a systematic assessment, these tools could provide significant insights into the energetic, environmental and economic benefits of CABBS and identify effective strategies towards its potential commercialisation.

6.5.1 Environmental perspectives

LCA studies reveal that biomethane from mono-digestion of *Chlorella vulgaris* may only reduce emissions by 25% in transport, compared to the fossil fuel comparator [94]. However, as can be seen from Table 6-1, *Nannochloropsis salina* or *Spirulina platensis* with a higher biogas yield could provide greater benefits. Alternatively, co-digestion, boosting biomethane yield could also allow higher environmental benefits. Renewable energy generated per fossil energy spent (net energy ratio (NER)) was found to increase from 2.7 to 4.5 when *Chlorella* sp. was co-digested with sewage sludge due to an increased biogas production of 65% than that of mono-digestion of microalgae [97]. Toledo-Cervantes et al., (2017) [96] calculated $CO_{2\text{-eq}}$ emissions 45 times lower than traditional water-scrubber upgrading owing to reduced energy demand, and CO_2 utilisation by the microalgae. Emission benefits from microalgal treatment of digestate, enabling nutrient recycling and preventing the release of toxic compounds, have seldom been quantified in the literature. Nonetheless, significant indirect emission savings from using recycled nutrient media for microalgae growth can be achieved by substitution of inorganic fertilisers, mostly manufactured by expending fossil energy and finite natural resources [97]. Therefore, coupling microalgae cultivation with AD in a circular bioeconomy system to provide

CO_2 and nutrients, together with the use of renewable energy during microalgae cultivation, harvesting and processing could be environmentally beneficial [98].

Co-production of multiple products from a single system in a circular economy framework adds to $CO_{2\text{-eq}}$ savings due to the substitution of traditional energy-intensive individual production chains [99]. This could considerably enhance the overall emission reduction potential of biomethane generated by the CABBS layout. Further assessments of bio-product choice, suitable extraction pathways, limitations of scale and geographical location are critical as well. For example, energy requirements for drying in pyrolysis without the use of renewable energy can raise the specific emission from bio-oil to above 200 $gCO_{2\text{-eq}}$/MJ [100]. Un-optimised transesterification of microalgae has been shown to potentially raise the specific emissions from biodiesel to as high as 1,000 $gCO_{2\text{-eq}}$/MJ [101]. Often, additional $CO_{2\text{-eq}}$ savings from the valorisation of lipid extracted residue may not be sufficient to significantly improve environmental performance [101]. In a possible alternative, extracted lipid from *Nannochloropsis* sp. and *Scenedesmus* sp. was used as a substitute for vegetable oil [51]. When the remaining oil-free cake was used as a fish meal, a greater $CO_{2\text{-eq}}$ reduction potential was attained compared to combined biodiesel and biogas production [51]. This was due to the higher emission savings from the substitution of vegetable oil and fish meal than replacement of fossil diesel by microalgae biodiesel.

Presently, negative emission technologies are also being investigated to achieve an effective removal of atmospheric CO_2 with biofuel production. As different alternatives, the burial of whole or fraction extracted microalgae [102], production of long-lived potentially carbon negative chemicals like construction materials [103] or biochar for fertilisers [102] are effective routes for long-term carbon sequestration by microalgae. Indeed, if used as feedstock for chemical production, rather than a direct application for energy generation to release the captured CO_2, the proposed CABBS can lead to significant capture of atmospheric CO_2 with simultaneous biomethane generation. Such meticulous selection of microalgae usage could therefore allow the proposed CABBS configuration to be potentially referred to as a Bioenergy with Carbon Capture and Storage (BECCS) system, speculatively sequestering the CO_2 from biogas over long geological time intervals, as shown in Figure 6-6.

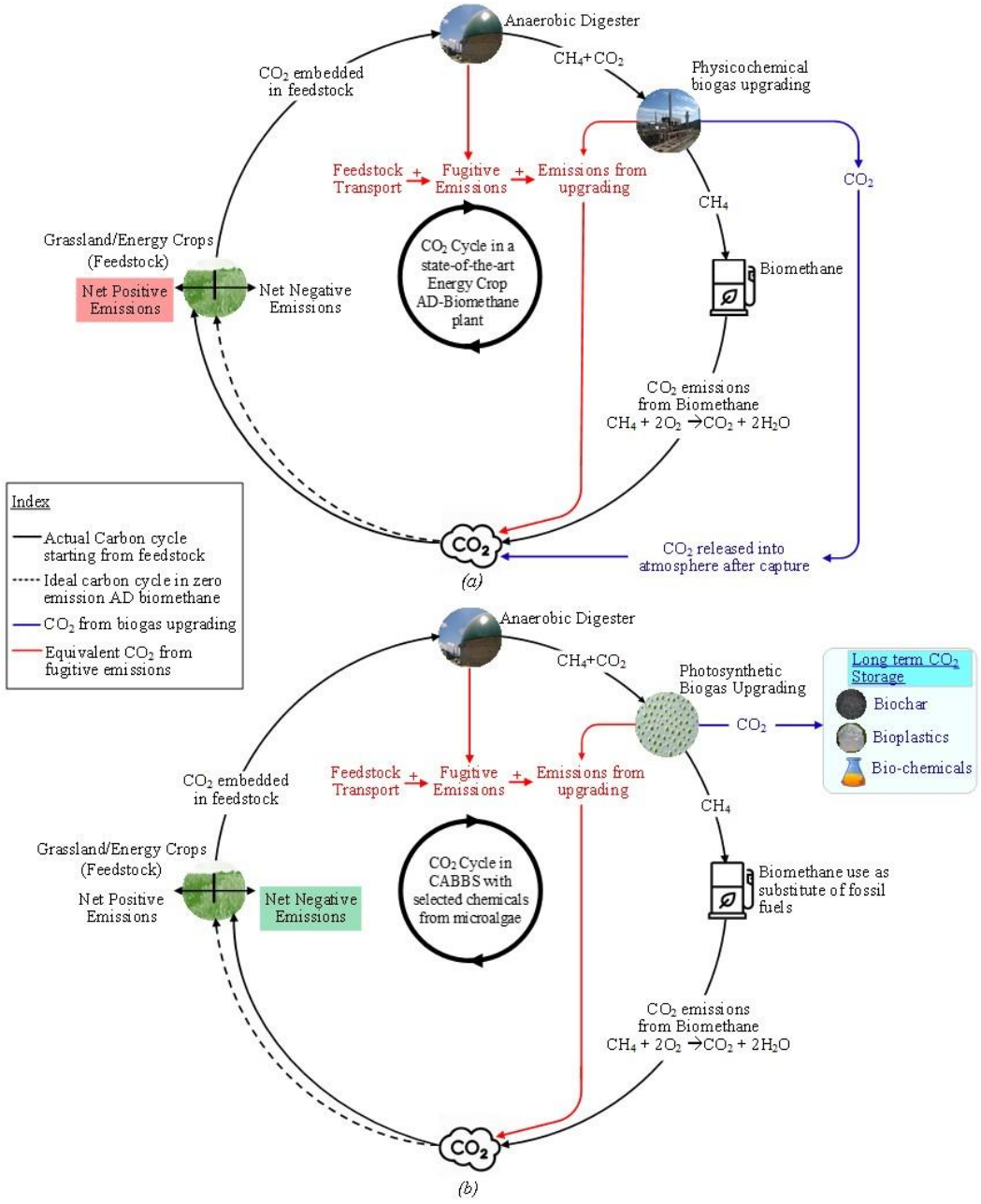


Figure 6-6 Comparison of net CO_2 flow in (a) state-of-the-art grass/energy crop based AD plant with physicochemical biogas upgrading and (b) proposed CABBS layout with the production of selected chemicals from microalgae to be regarded as a potential Bioenergy with Carbon Capture and storage (BECCS) system.

The increased requirement of water and land is, however, a major disadvantage of photosynthetic biogas upgrading as compared to conventional upgrading technologies. Nevertheless, by careful choice of algal products significant overall environmental benefits can be obtained. For example, locally sourced proteins from microalgae grown on marginal lands would have a much lower emissions and resource footprint in Europe than protein imported from commercial facilities in South America [104].

6.5.2 Techno-economic perspectives

Production of biomethane from microalgae is still not commercially viable without incentives [105]. For the proposed CABBS configuration, the capital cost would increase significantly as compared to traditional biogas upgrading facilities [96]. For yearlong operations, although a closed photobioreactor would be beneficial; this is currently limited by high cost and economic scalability [8]. Furthermore, the generation of additional revenue from microalgal bioproducts would considerably increase the economic benefit of photosynthetic biogas upgrading. Toledo-Cervantes et al., (2017) [96] predicted a payback of 5 years for a 300 Nm^3 biogas/hr photosynthetic biogas upgrading system with 20 g/m^2/day microalgae productivity in an open pond, while selling biomethane at natural gas prices of 0.3 €/Nm^3. No incentives were required as the added revenue generated from microalgae sale as fertiliser at 0.08 €/kg was highly profitable.

Direct production of biomethane and electricity from the mesophilic AD of *Cyanothece* sp. BG0011 was estimated at 6.7 ct€/kWh and 11.7 ct€/kWh respectively when grown at a scale of almost 300 tonnes per year of microalgae [106]. Based on the individual country FiT, therefore, either electricity or biomethane production could also yield considerable economic returns. Low purity C-phycocyanin was produced at 249 €/kg product or 21.5 €/kg dry biomass; the opportunity to sell it at 500 €/kg (43.3 €/kg dry biomass ESP) was found economically advantageous [107]. Conversely, the cost of protein production at 12.7 €/kg dry biomass would be too high for economic benefit. Extraction of high-value protein isolates (>2,000 €/kg) by further purification steps could be beneficial [82]. Indeed, co-production of high value and bulk compounds including biofuels, with waste valorisation for added biomethane production could increase the economic benefits further. Nonetheless, such opportunities are yet to be explored in detail.

6.5.3 Practical challenges and perspectives

Integration of a microalgae biorefinery, together with photosynthetic biogas upgrading via CABBS could accelerate the commercialisation of both technologies. To ensure rapid uptake of the photosynthetic biogas upgrading technology, the choice of bioproducts would be critical. Selecting microalgal bioproducts that are already

commercialised as co-product of biomethane would allow each co-product to be brought in line simultaneously, vastly improving the economic proposition of the photosynthetic biogas upgrading technology. However, besides economic and environmental benefits, several practical challenges must be overcome to increase the choice of product from microalgae. To use microalgae for food/feed and nutraceutical applications, it must adhere to both local and global rules regarding food safety and human health [13]. This is because the microalgae composition can vary significantly based on the growth environment, leading to the accumulation of toxins, heavy metals, allergens, pathogens and pesticides [108,109]. To cite instances, the growth of microalgae without adequate quality control, under non-standard conditions has shown to result in toxin concentrations above tolerable daily intake values [110]. Lead accumulation, up to 100 times above the safety limit for specific human consumption of 0.05 mg/kg wet weight has been reported for *Chlorella* PY-ZU1 when grown using undiluted digestate from swine manure [111].

The impact of trace compounds in biogas such as volatile organic compounds on microalgae composition is yet to be determined by the scientific community. Therefore, microalgae growth conditions within CABBS, especially when using digestate for microalgae cultivation is essentially non-standardised. Choice of specific microalgae species, together with assessment of its chemical properties within the proposed system is therefore urgently required to assess the complete potential for the simultaneous production of food/feed, chemicals and biomethane in a future circular bioeconomy.

6.6 Conclusions

In this paper, three alternate configurations have been proposed for cascading algal biomethane biorefinery systems for simultaneous production of biomethane and/or biofuels, food/feed and chemicals. In a novel approach as compared to recent review literature (Table 6-2), all significant factors necessary for developing a comprehensive perspective have been holistically identified and reviewed together with practical limitations and legislative challenges. In addition, a decision-making strategy was developed to facilitate the maximisation of the financial sustainability of the proposed CABBS layout. It is postulated that the system could be considered a carbon capture system and be an element of a negative emission technology.

6.7 Acknowledgement

This work acknowledges the support from Science Foundation Ireland (SFI) through the Centre for Marine and Renewable Energy (MaREI) under Grant No. 12/RC/2302_P2 and 16/SP/3829, with industrial funding from Gas Networks Ireland through The Green Gas Innovation Group and by ERVIA and IDL Pernod Ricard. This work was also supported by the Environmental Protection Agency – Ireland (2018-RE-MS-13).

Table 6-2 Comparison of the present review article and recent review papers (since 2015) focussing on the use of microalgae in AD systems and the development of microalgae biorefinery

Reference	Microalgae in AD systems				Microalgae biorefinery				Proposals of comprehensive biorefinery systems	
	Biogas production*	Photosynthetic biogas upgrading	Digestate treatment	Microalgae processing**	Bio-products***	Life Cycle perspectives	Dilemma of biorefinery	Decision-making strategies	Layout development	Practical & legislative consideration
This Study	✓	✓	✓	✖	✓	✓	✓	✓	✓	✓
(Bose et al., 2019) [8]	✖	✓	✖	✓	✖	✖	✖	✖	✖	✖
(Koutra et al., 2018) [43]	✓	✖	✓	✓	✓	✖	✖	✖	✖	✓
(Gifuni et al., 2018) [112]	✖	✖	✖	✓	✓	✖	✖	✖	✖	✖
('t Lam et al., 2018) [11]	✖	✖	✖	✓	✓	✖	✖	✖	✖	✖
(Saratale et al., 2018) [30]	✓	✖	✖	✖	✖	✖	✖	✖	✖	✖
(Chen et al., 2018) [14]	✓	✓	✓	✓	✓	✖	✖	✖	✓	✖
(Chew et al., 2017) [13]	✖	✖	✖	✓	✓	✓	✖	✖	✖	✓
(Jankowska et al., 2017) [9]	✓	✖	✖	✓	✓	✖	✖	✖	✓	✖
(Kothari et al., 2017) [53]	✖	✖	✖	✓	✓	✓	✖	✖	✖	✖
(Xia and Murphy, 2016) [41]	✖	✖	✓	✖	✓	✖	✖	✖	✓	✓
(Neves et al., 2016) [113]	✓	✖	✖	✓	✓	✖	✖	✖	✖	✖
(Posada et al., 2016) [51]	✖	✖	✖	✓	✓	✓	✓	✖	✓	✖
(Zhu, 2015) [80]	✖	✖	✖	✓	✓	✖	✓	✓	✖	✓

Reference	Microalgae in AD systems				Microalgae biorefinery				Proposals of comprehensive biorefinery systems	
	Biogas production*	Photosynthetic biogas upgrading	Digestate treatment	Microalgae processing**	Bio-products***	Life Cycle perspectives	Dilemma of biorefinery	Decision-making strategies	Layout development	Practical & legislative consideration
(Muñoz et al., 2015) [114]	✖	✓	✖	✖	✖	✖	✖	✖	✖	✖

Includes review on pre-treatment of microalgae

**Includes cultivation, harvesting and extraction of useable fractions from microalgae*

***Including both technological and economic aspects of microalgal bio-product*

6.8 Appendix for Chapter 6

Table A6-1 References for product content in microalgae and economics (sale price, compound annual growth rate and speculated market value) of bio-products

Product	Sale price	Product (% dry weight)	Compound annual growth rate (CAGR) and speculated market value (billion Euros)			
	Reference	Reference	Keyword[1]	News Source[2]	Date[3]	Reference[4]
Biogas	Calculated in Box 6.1	Assumed 100%	Global Biogas Market	PR Newswire	16/01/2017	
Biodiesel	Calculated in Box 6.1	(Kothari et al., 2017) [53]	Global biodiesel market	Business Wire - BZX	25/08/2017	(MarketWatch Inc, n.d.) [115]
Bioethanol	Calculated in Box 6.1	(Brányiková et al., 2011) [116]	Bioethanol	Zion Market Research	13/12/2018	
Biomethane	Calculated in Box 6.1	Assumed 100%	-		Dec 2018	(Transparency Market Research (TMR), 2018) [62]
Biogas for Electricity	Calculated in Box 6.1	Assumed 100%	Distributed Energy market	PR Newswire	21/05/2019	(MarketWatch Inc, n.d.) [115]
Biogas for Heat	Calculated in Box 6.1	Assumed 100%	Global District Heating	Zion Market Research	19/03/2018	(Globenewswire, n.d.) [117]
SCP* (Feed)	(Spruijt et al., 2016) [63]	Assumed 100%	Compound Feed	Market Research Future	07/05/2019	
SCP (Human food)	(BuyWholefoodOnline.eu, 2019) [64]	Assumed 100%	Neutral Alternative Protein Market	ACPS**	08/03/2019	(MarketWatch Inc, n.d.) [115]
Oil (human consumption)	(Xue et al., 2018) [118]	(Kothari et al., 2017) [53]			2018	(Value Market Research, 2018) [117]
Starch			Modified Starch	Business Wire	02/08/2019	

Product	Sale price	Product (% dry weight)	Compound annual growth rate (CAGR) and speculated market value (billion Euros)			
	Reference	Reference	Keyword[1]	News Source[2]	Date[3]	Reference[4]
Personal care products	(Barsanti and Gualtieri, 2018) [45]	(Bránykiková et al., 2011) [116]	Beauty & Personal Care Products	PR Newswire	22/11/2018	(MarketWatch Inc, n.d.) [115]
Lysine	(Bulk Powders, 2019) [120]	(Koyande et al., 2019) [121]	Lysine	All Company Press Releases	29/03/2019	
Vitamin E	(FeedInfo News service, 2017) [122]	(Kothari et al., 2017) [53]	Global Vitamin E Market	Zion Market Research	23/01/2019	(Globenewswire, n.d.) [117]
Astaxanthin	(Li et al., 2011) [123]	(Sathasivam, 2018) [77]	Astaxanthin	Orbis Research	19/06/2019	
Vitamin C	(Tay, 2017) [124]	(Miller and Brown, 1992) [125]	Vitamin C	ACPS	22/03/2019	
Beta-Carotene	(DEINOVE, 2015) [126]	(Sathasivam, 2018) [77]	Beta Carotene	PR Newswire	18/10/2018	(MarketWatch Inc, n.d.) [115]
Isotopically Labelled Compounds	(Kothari et al., 2017) [53]	(Kothari et al., 2017) [53]	Stable Isotope Labelled Compounds	ACPS	13/08/2018	
C-phycocyanin	(Stanic-Vucinic et al., 2018) [65]	(Stanic-Vucinic et al., 2018) [65]	Phycocyanin	Future Market Insights	29/08/2019	(Globenewswire, n.d.) [117]
Ω-3 Fatty acids	(Barsanti and Gualtieri, 2018) [45]	(Sahin et al., 2018) [127]			Nov 2018	(Verified market Research, 2018) [128]
DHA	(Pharmacompass, n.d.) [129]		Global Algal DHA	Coherent Market Insights	10/12/2018	(Globenewswire, n.d.) [117]
ß-1,3-Glucan		(Schulze et al., 2016) [130]	Beta-glucan Market Size	PR Newswire	09/01/201	(MarketWatch Inc, n.d.) [115]

Product	Sale price	Product (% dry weight)	Compound annual growth rate (CAGR) and speculated market value (billion Euros)			
	Reference	Reference	Keyword[1]	News Source[2]	Date[3]	Reference[4]
Phytosterols		(Stonik and Stonik, 2018) [131]	Phytosterols	ACUMEN Research and Consulting	09/04/2019	(Globenewswire, n.d.) [117]
Phenols	(Argus Media Group, 2018) [132]	(Li et al., 2007) [31]	-	-	Feb 2019	(imarc, 2018) [133]

[1]Keyword indicates the keyword to be entered to search for the news release cited in the present work; [2]News source indicates the name of the organisation that must be selected to obtain the news release cited in the present work;[3]Date indicates the date of news release; [4]All data accessed before 31.08.2019;
[*]SCP: Single Cell protein;
[**]ACPS: All Company Press releases

6.9 References

[1] Sanz-Hernández A, Esteban E, Garrido P. Transition to a bioeconomy: Perspectives from social sciences. J Clean Prod 2019;224:107–19. doi:10.1016/j.jclepro.2019.03.168.

[2] Bohutskyi P, Chow S, Ketter B, Betenbaugh MJ, Bouwer EJ. Prospects for methane production and nutrient recycling from lipid extracted residues and whole Nannochloropsis salina using anaerobic digestion. Appl Energy 2015;154:718–31. doi:10.1016/j.apenergy.2015.05.069.

[3] Wall DM, McDonagh S, Murphy JD. Cascading biomethane energy systems for sustainable green gas production in a circular economy. Bioresour Technol 2017;243:1207–15. doi:10.1016/j.biortech.2017.07.115.

[4] European Commission. Commission Implementing Regulation (EU) 2017/2470. Off J Eur Union 2017;351:72–201.

[5] Valli L, Rossi L, Fabbri C, Sibilla F, Gattoni P, Dale BE, et al. Greenhouse gas emissions of electricity and biomethane produced using the Biogas done right ™ system: four case studies from Italy. Biofuels, Bioprod Biorefining 2017;11:847–60. doi:10.1002/bbb.1789.

[6] Angelidaki I, Treu L, Tsapekos P, Luo G, Campanaro S, Wenzel H, et al. Biogas upgrading and utilization: Current status and perspectives. Biotechnol Adv 2018;36:452–66. doi:10.1016/j.biotechadv.2018.01.011.

[7] Marín D, Posadas E, Cano P, Pérez V, Blanco S, Lebrero R, et al. Seasonal variation of biogas upgrading coupled with digestate treatment in an outdoors pilot scale algal-bacterial photobioreactor. Bioresour Technol 2018;263:58–66. doi:10.1016/j.biortech.2018.04.117.

[8] Bose A, Lin R, Rajendran K, Xia A, O'Shea R, Murphy JD. How to optimise photosynthetic biogas upgrading: a perspective on system design and microalgae selection. Biotechnol Adv 2019;37. doi:10.1016/j.biotechadv.2019.107444.

[9] Jankowska E, Sahu AK, Oleskowicz-Popiel P. Biogas from microalgae: Review on microalgae's cultivation, harvesting and pretreatment for anaerobic digestion. Renew Sustain Energy Rev 2017;75:692–709. doi:10.1016/j.rser.2016.11.045.

[10] Meier L, Pérez R, Azócar L, Rivas M, Jeison D. Photosynthetic CO_2 uptake by microalgae: An attractive tool for biogas upgrading. Biomass and Bioenergy 2015;73:102–9. doi:10.1016/j.biombioe.2014.10.032.

[11] 't Lam GP, Vermuë MH, Eppink MHM, Wijffels RH, van den Berg C. Multi-product microalgae biorefineries: From concept towards reality. Trends Biotechnol 2018;36:216–27. doi:10.1016/j.tibtech.2017.10.011.

[12] D'Amato D, Veijonaho S, Toppinen A. Towards sustainability? Forest-based circular bioeconomy business models in Finnish SMEs. For Policy Econ 2020;110:101848. doi:10.1016/j.forpol.2018.12.004.

[13] Chew KW, Yap JY, Show PL, Suan NH, Juan JC, Ling TC, et al. Microalgae biorefinery: High value products perspectives. Bioresour Technol 2017;229:53–62. doi:10.1016/j.biortech.2017.01.006.

[14] Chen Y di, Ho SH, Nagarajan D, Ren N qi, Chang JS. Waste biorefineries — integrating anaerobic digestion and microalgae cultivation for bioenergy production. Curr Opin Biotechnol 2018;50:101–10. doi:10.1016/j.copbio.2017.11.017.

[15] Sialve B, Bernet N, Bernard O. Anaerobic digestion of microalgae as a necessary step to make microalgal biodiesel sustainable. Biotechnol Adv 2009;27:409–16. doi:10.1016/j.biotechadv.2009.03.001.

[16] Heaven S, Milledge J, Zhang Y. Comments on "Anaerobic digestion of microalgae as a necessary step to make microalgal biodiesel sustainable." Biotechnol Adv 2011;29:164–7. doi:10.1016/j.biotechadv.2010.10.005.

[17] Ras M, Lardon L, Bruno S, Bernet N, Steyer JP. Experimental study on a coupled process of production and anaerobic digestion of *Chlorella vulgaris*. Bioresour Technol 2011;102:200–6. doi:10.1016/j.biortech.2010.06.146.

[18] Fernández-Rodríguez MJ, de la Lama-Calvente D, Jiménez-Rodríguez A, Borja R, Rincón-Llorente B. Influence of the cell wall of *Chlamydomonas reinhardtii* on anaerobic digestion yield and on its anaerobic co-digestion with a carbon-rich substrate. Process Saf Environ Prot 2019;128:167–75. doi:10.1016/j.psep.2019.05.041.

[19] Mahdy A, Ballesteros M, González-Fernández C. Enzymatic pretreatment of *Chlorella vulgaris* for biogas production: Influence of urban wastewater as a sole nutrient source on macromolecular profile and biocatalyst efficiency. Bioresour Technol 2016;199:319–25. doi:10.1016/j.biortech.2015.08.080.

[20] Mendez L, Mahdy A, Ballesteros M, González-Fernández C. *Chlorella vulgaris* vs cyanobacterial biomasses: Comparison in terms of biomass productivity and biogas yield. Energy Convers Manag 2015;92:137–42. doi:10.1016/j.enconman.2014.11.050.

[21] Zhao B, Ma J, Zhao Q, Laurens L, Jarvis E, Chen S, et al. Efficient anaerobic digestion of whole microalgae and lipid-extracted microalgae residues for methane energy production. Bioresour Technol 2014;161:423–30. doi:10.1016/j.biortech.2014.03.079.

[22] Hernández D, Solana M, Riaño B, García-González MC, Bertucco A. Biofuels from microalgae: Lipid extraction and methane production from the residual biomass in a biorefinery approach. Bioresour Technol 2014;170:370–8. doi:10.1016/j.biortech.2014.07.109.

[23] González-Fernández C, Sialve B, Bernet N, Steyer JP. Thermal pretreatment to improve methane production of *Scenedesmus* biomass. Biomass and Bioenergy 2012;40:105–11. doi:10.1016/j.biombioe.2012.02.008.

[24] Ramos-Suárez JL, Carreras N. Use of microalgae residues for biogas production. Chem Eng J 2014;242:86–95. doi:10.1016/j.cej.2013.12.053.

[25] Herrmann C, Kalita N, Wall D, Xia A, Murphy JD. Optimised biogas production from microalgae through co-digestion with carbon-rich co-substrates. Bioresour Technol 2016;214:328–37. doi:10.1016/j.biortech.2016.04.119.

[26] Aramrueang N, Rapport J, Zhang R. Effects of hydraulic retention time and organic loading rate on performance and stability of anaerobic digestion of *Spirulina platensis*. Biosyst Eng 2016;147:174–82. doi:10.1016/j.biosystemseng.2016.04.006.

[27] Parimi NS, Singh M, Kastner JR, Das KC, Forsberg LS, Azadi P. Optimization of protein extraction from *Spirulina platensis* to generate a potential co-product and a biofuel feedstock with reduced nitrogen content. Front Energy Res 2015;3:1–9. doi:10.3389/fenrg.2015.00030.

[28] Du X, Tao Y, Liu Y, Li H. Stimulating methane production from microalgae by alkaline pretreatment and co-digestion with sludge. Environ Technol (United Kingdom) 2020;41:1546–53. doi:10.1080/09593330.2018.1540665.

[29] Lee K, Chantrasakdakul P, Kim D, Kong M, Park KY. Ultrasound pretreatment of filamentous algal biomass for enhanced biogas production. Waste Manag 2014;34:1035–40. doi:10.1016/j.wasman.2013.10.012.

[30] Ganesh Saratale R, Kumar G, Banu R, Xia A, Periyasamy S, Dattatraya Saratale G. A critical review on anaerobic digestion of microalgae and macroalgae and co-digestion of biomass for enhanced methane generation. Bioresour Technol 2018;262:319–32. doi:10.1016/j.biortech.2018.03.030.

[31] Li Y, Jin Y, Borrion A, Li H, Li J. Effects of organic composition on the anaerobic biodegradability of food waste. Bioresour Technol 2017;243:836–45. doi:10.1016/j.biortech.2017.07.028.

[32] González-Fernández C, Sialve B, Bernet N, Steyer JP. Impact of microalgae characteristics on their conversion to biofuel. Part II: Focus on biomethane production. Biofuels, Bioprod Biorefining 2012;6:205–18. doi:10.1002/bbb.337.

[33] Magdalena JA, Ballesteros M, González-Fernandez C. Efficient anaerobic digestion of microalgae biomass: Proteins as a key macromolecule. Molecules 2018;23:1–16. doi:10.3390/molecules23051098.

[34] Rasit N, Idris A, Harun R, Wan Ab Karim Ghani WA. Effects of lipid inhibition on biogas production of anaerobic digestion from oily effluents and sludges:

An overview. Renew Sustain Energy Rev 2015;45:351–8. doi:10.1016/j.rser.2015.01.066.

[35] Passos F, Hom-Diaz A, Blanquez P, Vicent T, Ferrer I. Improving biogas production from microalgae by enzymatic pretreatment. Bioresour Technol 2016;199:347–51. doi:10.1016/j.biortech.2015.08.084.

[36] Zhong W, Chi L, Luo Y, Zhang Z, Zhang Z, Wu WM. Enhanced methane production from Taihu Lake blue algae by anaerobic co-digestion with corn straw in continuous feed digesters. Bioresour Technol 2013;134:264–70. doi:10.1016/j.biortech.2013.02.060.

[37] Parimi NS, Singh M, Kastner JR, Das KC. Biomethane and biocrude oil production from protein extracted residual *Spirulina platensis*. Energy 2015;93:697–704. doi:10.1016/j.energy.2015.09.041.

[38] Passos F, Uggetti E, Carrère H, Ferrer I. Pretreatment of microalgae to improve biogas production: A review. Bioresour Technol 2014;172:403–12. doi:10.1016/j.biortech.2014.08.114.

[39] Meier L, Pérez R, Azócar L, Rivas M, Jeison D. Photosynthetic CO_2 uptake by microalgae: An attractive tool for biogas upgrading. Biomass and Bioenergy 2015;73:102–9. doi:10.1016/j.biombioe.2014.10.032.

[40] Bahr M, Díaz I, Dominguez A, González Sánchez A, Muñoz R. Microalgal-biotechnology as a platform for an integral biogas upgrading and nutrient removal from anaerobic effluents. Environ Sci Technol 2014;48:573–81. doi:10.1021/es403596m.

[41] Xia A, Murphy JD. Microalgal Cultivation in Treating Liquid Digestate from Biogas Systems. Trends Biotechnol 2016;34:264–75. doi:10.1016/j.tibtech.2015.12.010.

[42] Yan C, Zhang Q, Xue S, Sun Z, Wu X, Wang Z, et al. A novel low-cost thin-film flat plate photobioreactor for microalgae cultivation. Biotechnol Bioprocess Eng 2016;21:103–9. doi:10.1007/s12257-015-0327-2.

[43] Koutra E, Economou CN, Tsafrakidou P, Kornaros M. Bio-based products from microalgae cultivated in digestates. Trends Biotechnol 2018;36:819–33. doi:10.1016/j.tibtech.2018.02.015.

[44] Spolaore P, Joannis-Cassan C, Duran E, Isambert A. Commercial applications of microalgae. J Biosci Bioeng 2006;101:87–96. doi:10.1263/jbb.101.87.

[45] Barsanti L, Gualtieri P. Is exploitation of microalgae economically and energetically sustainable? Algal Res 2018;31:107–15. doi:10.1016/j.algal.2018.02.001.

[46] Lababpour A. Potentials of the microalgae inoculant in restoration of biological soil crusts to combat desertification. Int J Environ Sci Technol 2016;13:2521–32. doi:10.1007/s13762-016-1074-4.

[47] Nagarajan D, Lee DJ, Kondo A, Chang JS. Recent insights into biohydrogen production by microalgae – From biophotolysis to dark fermentation. Bioresour Technol 2017;227:373–87. doi:10.1016/j.biortech.2016.12.104.

[48] Lin S, Bediako JK, Song MH, Kim JA, Cho CW, Zhao Y, et al. Effective recovery of Pt(IV) from acidic solution by a defective metal-organic framework using central composite design for synthesis. ACS Sustain Chem Eng 2019;7:7510–8. doi:10.1021/acssuschemeng.8b04637.

[49] Sun C, Xia A, Liao Q, Fu Q, Huang Y, Zhu X, et al. Improving production of volatile fatty acids and hydrogen from microalgae and rice residue: Effects of physicochemical characteristics and mix ratios. Appl Energy 2018;230:1082–92. doi:10.1016/j.apenergy.2018.09.066.

[50] De Farias Silva CE, Grisa B, Sforza E, Rocca N La, Bertucco A. Effects of sodium bicarbonate on biomass and carbohydrate production in *Synechococcus* PCC 7002. Chem Eng Trans 2016;49:241–6. doi:10.3303/CET1649041.

[51] Posada JA, Brentner LB, Ramirez A, Patel MK. Conceptual design of sustainable integrated microalgae biorefineries: Parametric analysis of energy use, greenhouse gas emissions and techno-economics. Algal Res 2016;17:113–31. doi:10.1016/j.algal.2016.04.022.

[52] Fan X, Burton R, Zhou Y. Glycerol (byproduct of biodiesel production) as a source for fuels and chemicals - Mini review. Open Fuels Energy Sci J 2010;3:17–22. doi:10.2174/1876973X01003010017.

[53] Kothari R, Pandey A, Ahmad S, Kumar A, Pathak V V., Tyagi V V. Microalgal cultivation for value-added products: a critical enviro-economical assessment. 3 Biotech 2017;7:1–15. doi:10.1007/s13205-017-0812-8.

[54] van der Voort M, Vulsteke E, Vulsteke E, Visser CLM de. Report WP2A7.02: Macro-economics of algae products. Swansea: 2015.

[55] Debnath D, Whistance J, Westhoff P, Binfield J, Thompson W. International Biofuels Baseline Briefing Book. Columbia: Food and Agricultural Policy Research Institute (FAPRI); 2018.

[56] Rajendran K, Browne JD, Murphy JD. What is the level of incentivisation required for biomethane upgrading technologies with carbon capture and reuse? Renew Energy 2019;133:951–63. doi:10.1016/j.renene.2018.10.091.

[57] Pablo-Romero M del P, Sánchez-Braza A, Salvador-Ponce J, Sánchez-Labrador N. An overview of feed-in tariffs, premiums and tenders to promote electricity from biogas in the EU-28. Renew Sustain Energy Rev 2017;73:1366–79. doi:10.1016/j.rser.2017.01.132.

[58] Department of Communications Climate Action and Environment. Support Scheme for Renewable Heat - Scheme Overview 2017:1–6.

[59] Herbes C, Halbherr V, Braun L. Factors influencing prices for heat from biogas plants. Appl Energy 2018;221:308–18. doi:10.1016/j.apenergy.2018.03.188.

[60] Ofgem. Non-Domestic RHI tariff table, Q2 - 2019/20 2019. https://www.ofgem.gov.uk/publications/non-domestic-rhi-tariff-table.

[61] Blaisonneau L, El Fadili S, Faure M, Gondel A, Julien E, Rakotojaona L. Overview of the biomethane sector in France 2017:1–55.

[62] Transparency Market Research (TMR). Biomethane market - Global industry analysis, size, share, growth, trends, and forecast, 2018–2026 2019.

https://www.transparencymarketresearch.com/pressrelease/bio-methane-market-2018-2026.htm.

[63] Spruijt J, Rommie van der Weide P, Marinus van Krimpen P. Opportunities for micro algae as ingredient in animal diets 2016:12–45.

[64] BuyWholefoodOnline.eu. Organic *Spirulina* Powder 1kg 2019. https://www.buywholefoodsonline.eu/organic-spirulina-powder-1kg.html.

[65] Stanic-Vucinic D, Minic S, Nikolic MR, Velickovic TC. *Spirulina* phycobiliproteins as food components and complements. In: Jacob-Lopes E, Zepka LQ, Queiroz MI, editors. Microalgal Biotechnol., IntechOpen; 2018. doi:10.5772/intechopen.73791.

[66] Sustainable Energy Authority of Ireland (SEAI). Conversion Factors n.d.

[67] Posada JA, Brentner LB, Ramirez A, Patel MK. Conceptual design of sustainable integrated microalgae biorefineries: Parametric analysis of energy use, greenhouse gas emissions and techno-economics. Algal Res 2016;17:113–31. doi:10.1016/j.algal.2016.04.022.

[68] Brányiková I, Maršálková B, Doucha J, Brányik T, Bišová K, Zachleder V, et al. Microalgae - novel highly efficient starch producers. Biotechnol Bioeng 2011;108:766–76. doi:10.1002/bit.23016.

[69] de Farias Silva CE, Bertucco A. Bioethanol from microalgae and cyanobacteria: A review and technological outlook. Process Biochem 2016;51:1833–42. doi:10.1016/j.procbio.2016.02.016.

[70] Barsanti L, Gualtieri P. Is exploitation of microalgae economically and energetically sustainable? Algal Res 2018;31:107–15. doi:10.1016/j.algal.2018.02.001.

[71] Swedish Gas Technology Centre Ltd (SGC). Basic data on Biogas. Malmo: 2012. doi:10.1016/0140-7007(80)90028-6.

[72] Pablo-Romero M del P, Sánchez-Braza A, Salvador-Ponce J, Sánchez-Labrador N. An overview of feed-in tariffs, premiums and tenders to promote

electricity from biogas in the EU-28. Renew Sustain Energy Rev 2017;73:1366–79. doi:10.1016/j.rser.2017.01.132.

[73] Herbes C, Halbherr V, Braun L. Factors influencing prices for heat from biogas plants. Appl Energy 2018;221:308–18. doi:10.1016/j.apenergy.2018.03.188.

[74] Blaisonneau L, El Fadili S, Faure M, Gondel A, Julien E, Rakotojaona L. Overview of the biomethane sector in France. 2017.

[75] Ofgem. Non-Domestic RHI tariff table, Q2 - 2019/20 2019.

[76] Faé Neto WA, Borges Mendes CR, Abreu PC. Carotenoid production by the marine microalgae Nannochloropsis oculata in different low-cost culture media. Aquac Res 2018;49:2527–35. doi:10.1111/are.13715.

[77] Sathasivam R, Ki JS. A review of the biological activities of microalgal carotenoids and their potential use in healthcare and cosmetic industries. Mar Drugs 2018;16. doi:10.3390/md16010026.

[79] Zhu L. Biorefinery as a promising approach to promote microalgae industry: An innovative framework. Renew Sustain Energy Rev 2015;41:1376–84. doi:10.1016/j.rser.2014.09.040.

[80] Gong J, You F. Optimal design and synthesis of algal biorefinery processes for biological carbon sequestration and utilization with zero direct greenhouse gas emissions: MINLP model and global optimization algorithm. Ind Eng Chem Res 2014;53:1563–79. doi:10.1021/ie403459m.

[81] Sen Gupta S, Shastri Y, Bhartiya S. Integrated microalgae biorefinery : Impact of product demand profile. Biofuels, Bioprod Biorefining 2017;11:1065–76. doi:10.1002/bbb.1815.

[82] Lupatini AL, Colla LM, Canan C, Colla E. Potential application of microalga *Spirulina platensis* as a protein source. J Sci Food Agric 2017;97:724–32. doi:10.1002/jsfa.7987.

[83] Thi Nguyen ML, Lin CY, Lay CH. Microalgae cultivation using biogas and digestate carbon sources. Biomass and Bioenergy 2019;122:426–32. doi:10.1016/j.biombioe.2019.01.050.

[84] Becker EW. Micro-algae as a source of protein. Biotechnol Adv 2007;25:207–10. doi:10.1016/j.biotechadv.2006.11.002.

[85] Buchmann L, Bertsch P, Böcker L, Krähenmann U, Fischer P, Mathys A. Adsorption kinetics and foaming properties of soluble microalgae fractions at the air/water interface. Food Hydrocoll 2019;97:105182. doi:10.1016/j.foodhyd.2019.105182.

[86] Lizzul AM, Lekuona-Amundarain A, Purton S, Campos LC. Characterization of *Chlorella sorokiniana*, UTEX 1230. Biology (Basel) 2018;7:1–12. doi:10.3390/biology7020025.

[87] Vadlamani A, Viamajala S, Pendyala B, Varanasi S. Cultivation of microalgae at extreme alkaline pH conditions: A novel approach for biofuel production. ACS Sustain Chem Eng 2017;5:7284–94. doi:10.1021/acssuschemeng.7b01534.

[88] Azizi K, Keshavarz Moraveji M, Abedini Najafabadi H. A review on biofuel production from microalgal biomass by using pyrolysis method. Renew Sustain Energy Rev 2018;82:3046–59. doi:10.1016/j.rser.2017.10.033.

[89] Fermoso J, Coronado JM, Serrano DP, Pizarro P. Pyrolysis of microalgae for fuel production. Elsevier Ltd.; 2017. doi:10.1016/B978-0-08-101023-5.00011-X.

[90] Mumme J, Srocke F, Heeg K, Werner M. Use of biochars in anaerobic digestion. Bioresour Technol 2014;164:189–97. doi:10.1016/j.biortech.2014.05.008.

[91] Shanmugam SR, Adhikari S, Nam H, Kar Sajib S. Effect of biochar on methane generation from glucose and aqueous phase of algae liquefaction using mixed anaerobic cultures. Biomass and Bioenergy 2018;108:479–86. doi:10.1016/j.biombioe.2017.10.034.

[92] Linville JL, Shen Y, Ignacio-de Leon PA, Schoene RP, Urgun-Demirtas M. In-situ biogas upgrading during anaerobic digestion of food waste amended with

walnut shell biochar at bench scale. Waste Manag Res 2017;35:669–79. doi:10.1177/0734242X17704716.

[93] Speight JG. Production of syngas, synfuel, bio-oils, and biogas from coal, biomass, and opportunity fuels. Elsevier Ltd; 2016. doi:10.1016/B978-1-78242-378-2.00006-7.

[94] Collet P, Hélias Arnaud A, Lardon L, Ras M, Goy RA, Steyer JP. Life-cycle assessment of microalgae culture coupled to biogas production. Bioresour Technol 2011;102:207–14. doi:10.1016/j.biortech.2010.06.154.

[95] Solé-Bundó M, Garfí M, Matamoros V, Ferrer I. Co-digestion of microalgae and primary sludge: Effect on biogas production and microcontaminants removal. Sci Total Environ 2019;660:974–81. doi:10.1016/j.scitotenv.2019.01.011.

[96] Toledo-Cervantes A, Estrada JM, Lebrero R, Muñoz R. A comparative analysis of biogas upgrading technologies: Photosynthetic vs physical/chemical processes. Algal Res 2017;25:237–43. doi:10.1016/j.algal.2017.05.006.

[97] Collet P, Lardon L, Hélias A, Bricout S, Lombaert-Valot I, Perrier B, et al. Biodiesel from microalgae - Life cycle assessment and recommendations for potential improvements. Renew Energy 2014;71:525–33. doi:10.1016/j.renene.2014.06.009.

[98] Togarcheti SC, Mediboyina M Kumar, Chauhan VS, Mukherji S, Ravi S, Mudliar SN. Life cycle assessment of microalgae based biodiesel production to evaluate the impact of biomass productivity and energy source. Resour Conserv Recycl 2017;122:286–94. doi:10.1016/j.resconrec.2017.01.008.

[99] D'Amato D, Korhonen J, Toppinen A. Circular, green, and bio Economy: How do companies in land-use intensive sectors align with sustainability concepts? Ecol Econ 2019;158:116–33. doi:10.1016/j.ecolecon.2018.12.026.

[100] Bennion EP, Ginosar DM, Moses J, Agblevor F, Quinn JC. Lifecycle assessment of microalgae to biofuel: Comparison of thermochemical processing pathways. Appl Energy 2015;154:1062–71. doi:10.1016/j.apenergy.2014.12.009.

[101] Rocca S, Agostini A, Giuntoli J, Marelli L. Biofuels from algae: technology options, energy balance and GHG emissions. 2015. doi:10.2790/125847.

[102] Sayre R. Microalgae: The potential for carbon capture. Bioscience 2010;60:722–7. doi:10.1525/bio.2010.60.9.9.

[103] Greene CH, Huntley ME, Archibald I, Gerber LN, Sills DL, Granados J, et al. Geoengineering, marine microalgae, and climate stabilization in the 21st century. Earth's Futur 2017;5:278–84. doi:10.1002/2016EF000486.

[104] Rösch C, Roßmann M, Weickert S. Microalgae for integrated food and fuel production. GCB Bioenergy 2019;11:326–34. doi:10.1111/gcbb.12579.

[105] Rajendran K, O'Gallachoir B, Murphy JD. The combined role of policy and incentives in promoting cost efficient decarbonisation of energy: A case study for biomethane. J Clean Prod 2019;219:278–90. doi:10.1016/j.jclepro.2019.01.298.

[106] Wu Y, Xie H, Liu T, Wang Y, Wang F, Gao X, et al. Soda ash production with low energy consumption using proton cycled membrane electrolysis. Ind Eng Chem Res 2019;58:3450–8. doi:10.1021/acs.iecr.8b05371.

[107] Chaiklahan R, Chirasuwan N, Loha V, Tia S, Bunnaga B. Stepwise extraction of high-value chemicals from *Arthrospira* (*Spirulina*) and an economic feasibility study. Biotechnol Reports 2018;20:e00280.

[108] García JL, de Vicente M, Galán B. Microalgae, old sustainable food and fashion nutraceuticals. Microb Biotechnol 2017;10:1017–24. doi:10.1111/1751-7915.12800.

[109] van der Spiegel M, Noordam MY, van der Fels-Klerx HJ. Safety of novel protein sources (insects, microalgae, seaweed, duckweed, and rapeseed) and legislative aspects for their application in food and feed production. Compr Rev Food Sci Food Saf 2013;12:662–78. doi:10.1111/1541-4337.12032.

[110] Roy-Lachapelle A, Solliec M, Bouchard MF, Sauvé S. Detection of cyanotoxins in algae dietary supplements. Toxins (Basel) 2017;9:1–17. doi:10.3390/toxins9030076.

[111] Cheng J, Xu J, Huang Y, Li Y, Zhou J, Cen K. Growth optimisation of microalga mutant at high CO_2 concentration to purify undiluted anaerobic digestion effluent of swine manure. Bioresour Technol 2015;177:240–6. doi:10.1016/j.biortech.2014.11.099.

[112] Gifuni I, Pollio A, Safi C, Marzocchella A, Olivieri G. Current bottlenecks and challenges of the microalgal biorefinery. Trends Biotechnol 2019;37:242–52. doi:10.1016/j.tibtech.2018.09.006.

[113] Neves VTDC, Sales EA, Perelo LW. Influence of lipid extraction methods as pre-treatment of microalgal biomass for biogas production. Renew Sustain Energy Rev 2016;59:160–5. doi:10.1016/j.rser.2015.12.303.

[114] Muñoz R, Meier L, Diaz I, Jeison D. A review on the state-of-the-art of physical/chemical and biological technologies for biogas upgrading. Rev Environ Sci Biotechnol 2015;14:727–59. doi:10.1007/s11157-015-9379-1.

[115] MarketWatch Inc. MarketWatch All Company Press Releases n.d. https://www.marketwatch.com/search?q=&m=Keyword&rpp=15&mp=2007&bd=true&bd=false&bdv=06%2F01%2F2018&rs=true (accessed 7.30.19.).%0AGoogle Scholar.

[116] Brányiková I, Maršálková B, Doucha J, Brányik T, Bišová K, Zachleder V, et al. Microalgae-novel highly efficient starch producers. Biotechnol Bioeng 2011;108:766–76. doi:10.1002/bit.23016.

[117] Globenewswire. GlobeNewswire Press Releases n.d. https://www.globenewswire.com/NewsRoom.

[118] Xue Z, Wan F, Yu W, Liu J, Zhang Z, Kou X. Edible oil production from microalgae: A review. Eur J Lipid Sci Technol 2018;120. doi:10.1002/ejlt.201700428.

[119] Value Market Research. Food And Beverages. Glob edible oil fat mark rep by type (vegetable seed oil, spreadable oil fats, olive oil, cook fats others), by source (animal plant), by form (liquid-solid), by distrib channel (supermarket, hypermarket, Conv Sto 2018. https://www.valuemarketresearch.com/report/edible-oil-and-fat-market (accessed August 2, 2019).

[120] Bulk Powders. L-Lysine 2019. https://www.bulk.com/ie/l-lysine.html (accessed August 1, 2019).

[121] Koyande AK, Chew KW, Rambabu K, Tao Y, Chu DT, Show PL. Microalgae: A potential alternative to health supplementation for humans. Food Sci Hum Wellness 2019;8:16–24. doi:10.1016/j.fshw.2019.03.001.

[122] FeedInfo News service. Feed additive price overview – 21 September 2017 2017. https://marketing.feedinfo.com/feed-additive-price-overview-21-september-2017/.

[123] Li J, Zhu D, Niu J, Shen S, Wang G. An economic assessment of astaxanthin production by large scale cultivation of Haematococcus pluvialis. Biotechnol Adv 2011;29:568–74. doi:10.1016/j.biotechadv.2011.04.001.

[124] Tay C. China's pollution clampdown triples vitamin C prices within one year 2017. https://www.nutraingredients-asia.com/Article/2017/11/22/China-s-pollution-clampdown-triples-vitamin-C-prices-within-one-year.

[125] Miller K a., Brown MR. The ascorbic acid content of eleven species of microalgae used in mariculture. J Appl Phycol 1992;4:205–15.

[126] DEINOVE. Natural carotenoids meeting consumer needs. Carotenoids Mark 2015. https://www.deinove.com/en/profile/strategy-and-markets/carotenoids-market.

[127] Sahin D, Tas E, Altindag UH. Enhancement of docosahexaenoic acid (DHA) production from *Schizochytrium* sp. S31 using different growth medium conditions. AMB Express 2018;8. doi:10.1186/s13568-018-0540-4.

[128] Verified Market Research. Omega 3 Market Size And Forecast. Glob Omega 3 Mark Size By Type, By Source, By Appl By Geogr Scope Forecast 2018. https://www.verifiedmarketresearch.com/product/global-omega-3-market-size-and-forecast-to-2025/ (accessed September 2, 2019).

[129] Pharmacompass. Pharmacompass price n.d. https://www.pharmacompass.com/price (accessed July 15, 2019).

[130] Schulze C, Wetzel M, Reinhardt J, Schmidt M, Felten L, Mundt S. Screening of microalgae for primary metabolites including β-glucans and the influence of nitrate starvation and irradiance on β-glucan production. J Appl Phycol 2016;28:2719–25. doi:10.1007/s10811-016-0812-9.

[131] Stonik VA, Stonik I V. Sterol and sphingoid glycoconjugates from microalgae. Mar Drugs 2018;16:1–20. doi:10.3390/md16120514.

[132] Argus Media Group. Argus benzene and derivatives 2018.

[133] imarc. Phenol Market: Global Industry Trends, Share, Size, Growth, Opportunity and Forecast 2019–2024. Glob Phenol Mark Oppor Forecast 2018. https://www.imarcgroup.com/phenol-technical-material-market-report-3 (accessed August 2, 2019).

7 Producing biofuel with food and biofertiliser in a circular economy system

Producing biofuel with food and biofertiliser in a circular economy system

Archishman Bose[a,b], Richard O'Shea[a,b], Richen Lin[a,b], Aoife Long[a,b], Karthik Rajendran[c], David Wall[a,b], Sudipta De[d], Jerry D Murphy[a,b*]

[a]MaREI Centre, Environmental Research Institute, University College Cork, T23 XE10, Ireland

[b]Department of Civil, Structural and Environmental Engineering, School of Engineering and Architecture, University College Cork, T12 K8AF, Ireland.

[c]Department of Environmental Science, SRM University-AP, Andhra Pradesh, 522 240, India

[d]Department of Mechanical Engineering, Jadavpur University, West Bengal, 700 032, India

Abstract

Biomethane is a viable alternative to natural gas and diesel for decarbonising hard to abate sectors such as agriculture, industry and heavy transport. Unlike conventional biogas upgrading, photosynthetic biogas upgrading cogenerates biomethane, biofertiliser and microalgal bioproducts with the potential to improve resource utilisation and process performance in a circular economy. In this paper, a photosynthetic biogas upgrading based polygeneration process is proposed and analysed to co-produce biofuel (biomethane), bio-fertiliser (digestate) and food (*Spirulina* powder, protein supplement) using agricultural feedstock. Based on a multi-criteria performance assessment, the economic and environmental benefits of the process are demonstrated; reducing the energy for greenhouse heating to cultivate microalgae will enable a higher energy output than input. Using economic allocation, a carbon footprint of biomethane less than 10 $gCO_{2\text{-}eq}$/MJ (lower than 32.9 $gCO_{2\text{-}eq}$/MJ for sustainable biomethane use in transport in the EU Renewable Energy Directive (RED-II)); *Spirulina* protein of 0.8 $kgCO_{2\text{-}eq}$/100 grams protein (compared to 50 $kgCO_{2\text{-}eq}$/100 grams protein for beef); and digestate of 0.4 $kgCO_{2\text{-}eq}$/kgN (comparing positively to 1.5-3 $kgCO_{2\text{-}eq}$/kgN for synthetic nitrogenous fertiliser) was achieved. Unlike the current RED-II mandated methodology of using energy allocation, the analysis established that the energy, CO_2 emissions, land and water footprints of each

co-product are best represented using an economic allocation principle. With an extended nutrition profile, *Spirulina* as a complete food would ensure its superiority of CO_2 emissions, land and water footprints over most meat and plant-based protein alternatives.

7.1 Introduction

Agriculture, food and heavy transport contribute to over 40% of the global anthropogenic greenhouse gas (GHG) emissions [1–3]. Anaerobic digestion (AD) of agricultural residues for the production of biogas has multiple benefits that can reduce the climate impact of agriculture and heavy transport with additional environmental benefits including nutrient recycling, waste management, improved water quality and reduced odours [4–6]. In a circular economy system, the substitution of natural gas and diesel with upgraded biogas (biomethane) from agricultural feedstock is particularly beneficial in hard to abate sectors which rely heavily on fossil fuels [4,5]. However, energy-intensive physicochemical biogas upgrading techniques currently lead to emissions often above those mandated for sustainability (for example 32.9 $gCO_{2\text{-}eq}/MJ$ for biomethane for use in transport in the EU [7]) and require incentives for financial viability [8,9]. The two-step bubble column photobioreactor photosynthetic biogas upgrading system using microalgae (of which *Spirulina platensis* is an optimal choice [10]) is currently under research as an alternative to conventional biogas upgrading technologies [11,12]. By integrating anaerobic digestion (AD) with a microalgae biorefinery (Figure 7-1), within a circular economy system, the ambition is to improve the carbon footprint and add value beyond biomethane (energy) production [12]. In this process, CO_2 is cyclically absorbed and uptaken as bicarbonates by the microalgae via a carbonate-bicarbonate cycle (Eq. 7.1 and Eq. 7.2 respectively). Hydrogen sulphide (H_2S) in biogas can simultaneously be removed, producing sulphates with dissolved oxygen [13]. Even though photosynthetic biogas upgrading is at a low Technology Readiness Level (TRL), significant advancements have been made in both lab-scale experiments [14,15] and semi-industrial scale operations [16].

$$CO_2 + CO_3^{2-} + H_2O \rightarrow 2HCO_3^- \quad (7.1)$$

$$2HCO_3^- \xrightarrow{\text{Light}} \text{Algae} + CO_3^{2-} + H_2O \quad (7.2)$$

Producing multiple outputs from a single integrated system can improve resource utilisation, process performance and flexibility of operation over standalone facilities [17]. However, no detailed assessment on the performance of a polygeneration system using photosynthetic biogas upgrading, to the best of the

authors' knowledge, is available in the literature. Toledo-Cervantes et al. (2017) [18] focussed on the photosynthetic biogas upgrading process rather than a complete polygeneration system. To overcome this research gap, this study has been developed to provide a comprehensive performance assessment of a photosynthetic biogas upgrading based polygeneration plant co-producing fuel (biomethane), food (*Spirulina* powder) and biofertiliser (digestate) (Figure 7-2). With no unanimity regarding process performance metrics for polygeneration systems [17,19], a multi-criteria performance assessment was adopted. To avoid the uncertainty in a detailed life cycle assessment of a low TRL technology [20], only GHG emissions were estimated using the methodology proposed by the EU Renewable Energy Directive (Recast) (RED-II) [21]. However, the authors critique the validity of this methodology to assess the complete performance of polygeneration systems [22], and therefore suggest and evaluate possible modifications to the RED-II method; in particular, economic allocation and inclusion of digestate as a valuable product.

Accordingly, this study, in a first-of-its-kind work, provides a comprehensive evaluation of an as yet uncommercialised photosynthetic biogas upgrading system, whilst posing the following questions:

Q1. How does the proposed process perform in thermodynamic, economic and environmental aspects in a multi-criteria performance assessment?
Q2. How can the product and process performance be enhanced going forward?

Based on answers to the above, the following hypotheses were tested to assert the benefits from the proposed polygeneration process.

H1. The economic allocation provides a better product performance assessment compared to the RED-II mandated energy allocation methodology for a polygeneration system coproducing energy and non-energy bioproducts.
H2. The inclusion of digestate as a valuable product reduces specific emissions from *biomethane* and *Spirulina* powder.
H3. The co-products generated fare better in terms of energy, emission and water footprints than current market-available commodities.

H4. *Spirulina* as a complete food provides better performance than when considered just as a protein supplement.

H5. The land footprint is a major challenge, however, can be significantly reduced by increasing the productivity of the microalgae.

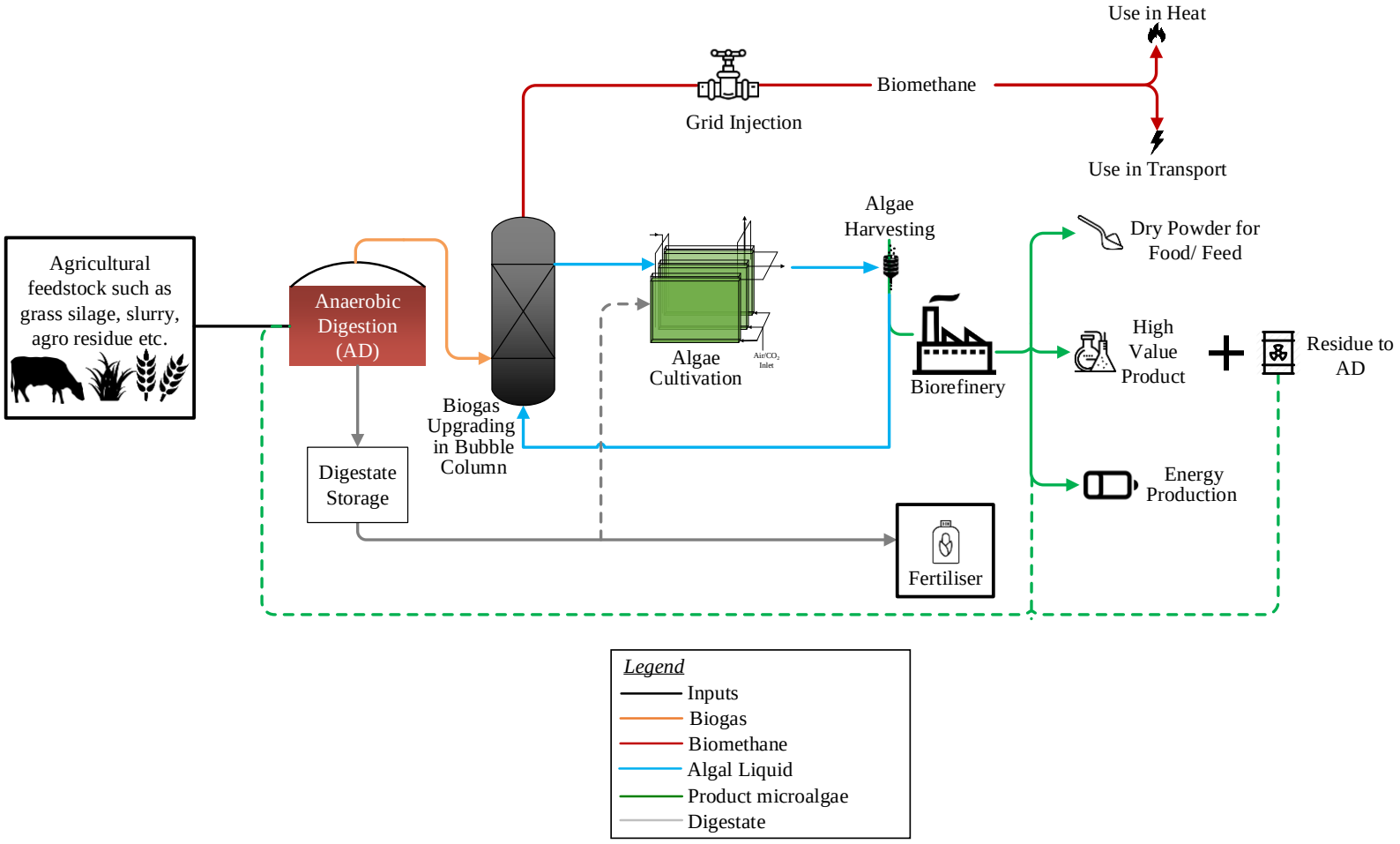


Figure 7-1 Concept layout of cascading algal biomethane-biorefinery systems (CABBS) with agricultural wastes using anaerobic digestion and photosynthetic biogas upgrading

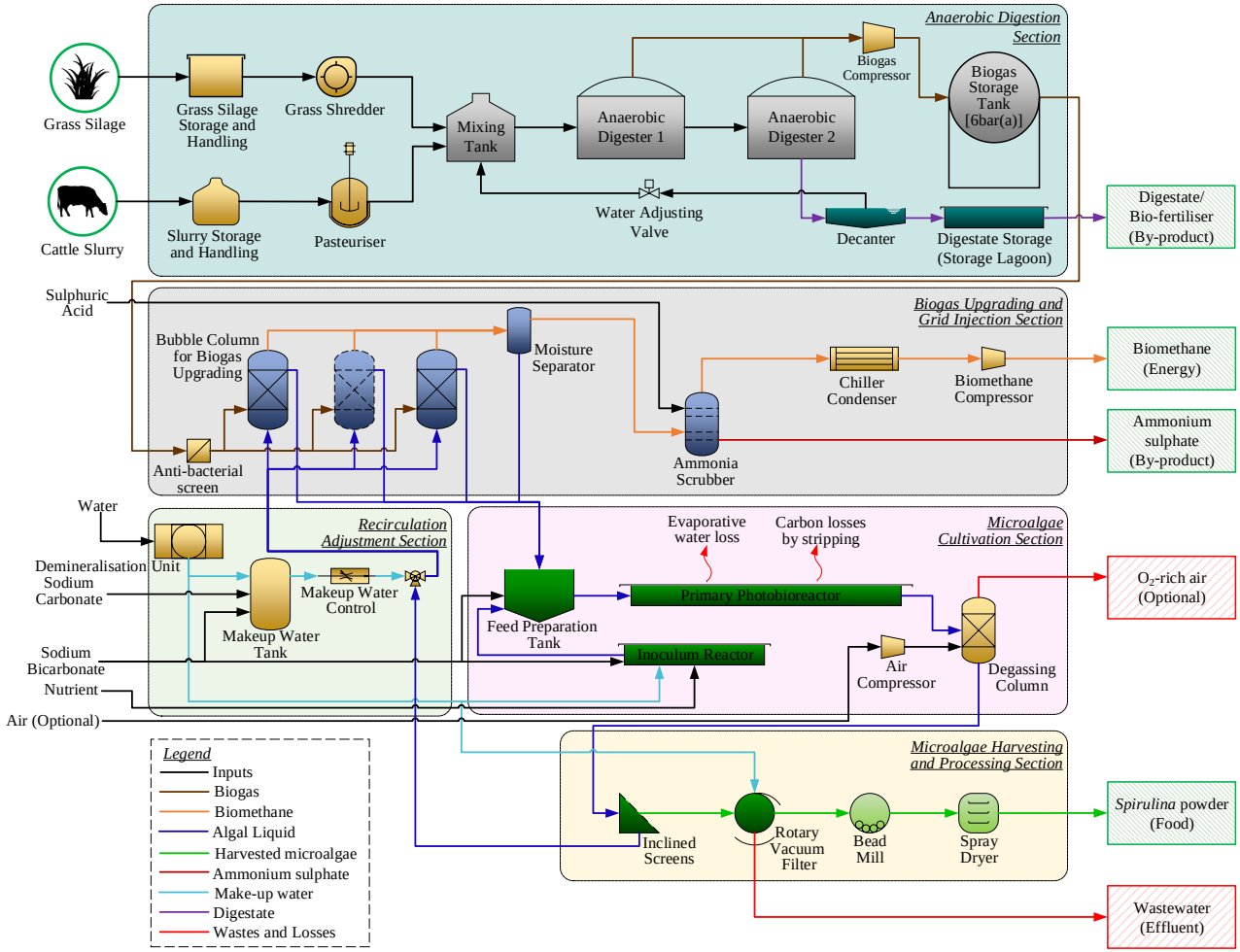


Figure 7-2 General process flow diagram of biomethane and dietary protein production as food-grade Spirulina platensis alongside biofertiliser as digestate using agricultural feedstock and photosynthetic biogas upgrading

7.2 Methods

7.2.1 Feedstock, resources and process outputs

The proposed polygeneration plant was modelled in a temperate oceanic climatic zone, typical of north-western and western Europe, Japan, Pacific Northwest of America (Washington, Idaho and northern California), parts of southern America (coastal regions of Chile and Argentina), south-eastern parts of Australia (Victoria and Tasmania) and New-Zealand. As an abundant agricultural resource in this climatic zone, grass silage (produced from first cut perennial ryegrass) and cattle slurry (Table 7-1) were selected as co-digestion feedstock to maximise the applicability of the results [23,24]. An 80:20 ratio of grass silage and cattle slurry (on a volatile solid (VS) basis) was considered as the optimal feed mix [25]. While the grass silage was procured at a cost, the slurry was obtained free, requiring only transportation charges [9]. The other major inputs to the process included sodium carbonate and sodium bicarbonate for the carbonate-bicarbonate buffer, Zarrouk's media for *Spirulina platensis* cultivation [26], makeup water, electricity from the grid and natural gas for heating. A small quantity of sulphuric acid would also be required for ammonia scrubbing [27] (Table 7-2).

Table 7-1 Characteristics of co-digestion substrates used in this study along with their respective costs as adapted from multiple literature [30–35]

Description	Grass	Slurry
Chemical Formula	$C_{28.4}H_{44.5}O_{17.7}N$	$C_{22}H_{34.8}O_{9.7}N_{1.7}S_{0.06}$
Moisture content when harvested [% FW[a]]	82	-
Moisture content at plant [% FW[a]]	70	91.2
Dry Solids (DS) [%]	30	8.8
Volatile Solids [%DS]	93.3	76.1
C:N ratio	24:1	13:1
Cost of procurement [€/tonne]	27	4 (transport costs only)

[a]*fresh weight*

Biomethane (sold to the gas-grid at 7 c€/kWh [12]) and *Spirulina* powder (sold at plant gate as protein supplement at 10 €/kg [28]) were the intended process outputs (Table S7-1). Digestate from AD (sold as a biofertiliser at 4 €/tonne [29]) was the major by-product of the process on a mass basis with a minor quantity of ammonium sulphate. The nitrogen-depleted sludge from the microalgae harvesting and washing

effluent was the only waste generated from the process and was sent for end-of-life treatments at 100 €/tonne (Table S7-1).

Table 7-2 Summary of the major inputs to the process and their corresponding costs

Component	Unit cost	Reference
Grass silage	27 €/tonne*	Rajendran et al. (2019) [9]
Cattle slurry (Transport costs only)	4 €/tonne*	
Sodium carbonate	184 €/tonne*	Hyun et al. (2018) [36]
Sodium bicarbonate (commercial grade)†	234 €/tonne*	Lee et al. (2019) [37]
Zarrouk's media (without sodium bicarbonate)	2,653 €/tonne	See *Box S7.1*
Sulphuric acid	100 €/tonne	Adapted from Hemphill (2020) [38]
Water	1.21 €/m^3	Adapted from CRU (2019) for large scale industrial processes [39]
Air	-	
Electricity	12.5 c€/kWh	Adapted from Eurostat (2021) [40]
Natural gas for heating	3 c€/kWh	Rajendran et al. (2019) [9]

*USD to Euro conversion factor was selected as 0.8
†Commercial grade Sodium bicarbonate was found to suitably replace costly lab-grade sodium bicarbonate [41,42]

7.2.2 Process description and scenarios for performance assessment

7.2.2.1 Process description

The proposed polygeneration plant has been divided into several sections, the conceptual layout of which is shown in Figure 7-2. A mesophilic (37°C) anaerobic co-digestion of grass silage and cattle slurry generated biogas in the *anaerobic digestion section*. Grass silage was shredded in a shredder and the cattle slurry was pasteurised before AD [43,44]. Two digesters in series provided the optimal configuration for biogas generation [9,30]. The biogas was compressed and stored in a biogas buffer tank to provide a constant gas flow for biogas upgrading. The digestate was stored in a lagoon and distributed for use as a fertiliser. The biogas was upgraded in one or more co-current bubble column reactors based on the biogas flow rate in the *biogas upgrading section*. As the biogas would be in direct contact with the microalgae cultivation media, antibacterial filters [45] were provided to condition the biogas before upgrading. Post upgrading, biomethane was further conditioned through

sulphuric acid scrubbing for ammonia removal and dehumidification before being compressed and transported via pipelines for gas grid injection.

Microalgae were cultivated in the bicarbonate-rich medium exiting the bubble column in the *microalgae cultivation section*. Before entering the main cultivation unit, the medium was adjusted for nutrients and initial microalgae concentration to allow uniform cultivation conditions in each cycle. The entire cultivation unit including the inoculum reactor and the harvesting facility were housed within a greenhouse maintained at 25 °C to allow yearlong cultivation of microalgae and requiring 1,000 MJ/m^2/year of heat [46]. Inclined screens and rotary vacuum filters respectively harvested and concentrated [47] the cultivated microalgae in the *microalgae harvesting and processing section*. The concentrated microalgae were then washed, milled and dried to produce powdered food-grade *Spirulina* [48]. The harvested algal media thus formed the recirculation media. However, before being pumped to the bubble column, it was adjusted with makeup water at a specific pH and alkalinity in the *recirculation adjustment section* to continue the carbonate-bicarbonate cycle.

The biogas production and the methane content were estimated assuming an organic loading rate (OLR) of 3.5 kgVS/m^3/day and using the results and recommendations of Wall et al. (2014) [49] and Vo et al. (2018) [30]. The concentration of H_2S and ammonia impurities within the biogas were assumed at 200 ppm respectively. Co-current bubble columns upgraded the biogas at a liquid to gas flow (L/G) ratio of 0.6. During upgrading, a maximum of 100% CO_2 and H_2S removal was assumed based on previous works by Bose et al. (2021) [15] and Meier et al. (2018) [13] respectively. Microalgae production was estimated as per Eq. 7.3 assuming a *Spirulina platensis* composition of $C_{20}H_{34.8}O_{7.8}N_{3.7}S_{0.1}$ [50] (molecular mass 22.72). The Zarrouk's media and spent salts were adjusted before and after the cultivation of algae (Eq. 7.3) respectively to achieve the required mass balance. The efficiency of microalgae harvesting was adjusted to ensure an algal concentration between 0.08 and 0.09 gDW/L in the recirculation medium. Makeup water was supplied at a constant pH and alkalinity of 10.2 and 1.5 g-Inorganic Carbon (IC)/L respectively by adjusting the input amounts of sodium carbonate and bicarbonate.

$$2NaHCO_3 \xrightarrow{\text{Zarrouk's Medium}} Na_2CO_3 + Spirulina + 1.24O_2 + 0.13H_2O + Salts \qquad (7.3)$$

7.2.2.2 Process assessment through multiple scenarios

The effect of allocation principles, current policy mandates and the type of photobioreactor (PBR) on the process and product performance of the proposed polygeneration system was studied using five scenarios (Figure 7-3). For the baseline scenario (*BASE-EC*), microalgae were cultivated in open pond photobioreactors (OPPBR) and digestate was included as a valuable output from the process. An economic (revenue-based) allocation was considered using the prices of biomethane, *Spirulina* powder and digestate as 7 c€/kWh, 10 €/kg and 4 €/tonne respectively (Section 7.2.1). Scenario *RED-EN* was defined to replicate the current RED-II guidelines (excluding digestate as a product and using embodied energy-based allocation [51]). Scenario *RED-EC* analysed the influence of economic allocation excluding digestate as a product. Separately, the influence of the energy allocation method whilst considering digestate as a valuable product was assessed by the scenario *ALLOC-EN*. Lastly, Flat plate PBRs (FPPBR) for microalgae cultivation was assessed using scenario *FPCULT-EC*. The *Spirulina* productivity in OPPBR and FPPBR were assumed to be 0.15 g-dry weight (DW)/L/day [52] and 0.2 gDW/L/day respectively; the slightly higher productivity was assumed to match the superior efficiency of the FPPBR system.

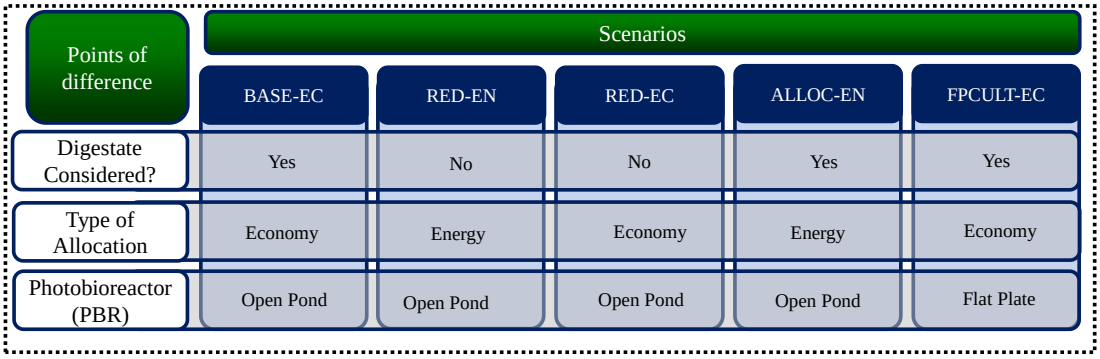


Figure 7-3 Graphical representation of the scenarios assessed to study its performance. The acronyms EC and EN refer to economic and energy allocation respectively. BASE represents the Base case scenario, RED refers to the scenario replicating the recommendations of the EU Renewable Energy Directive (Recast) (RED-II), i.e., excluding digestate as a valuable product, ALLOC-EN allows for an energy allocation method whilst considering digestate as a valuable product and FPCULT refers to the scenario where flat plate photobioreactors were used to cultivate the microalgae.

7.2.3 Process modelling

The following section provides a detailed description of the process model simulated using SuperPro software V10.03, Intelligen Inc.®. The general assumptions used for modelling and process assessment are compiled as follows:

- A simple mass and energy balance under steady-state operations were assumed and therefore all reactions were considered to be at chemical equilibrium.
- The atmospheric temperature and pressure were chosen as 20 °C and 1.013 bar respectively (normal conditions of temperature and pressure).
- A cultivation system housed within a greenhouse set at an average temperature of 25 °C was considered to ensure a sufficient growth rate of *Spirulina platensis* [52].
- Biomethane with less than 2.5% CO_2 and 1% O_2 respectively and compressed to 65 bars was considered to suffice for grid injection requirements [53,54].
- The pH between 9.2 and 10.6 and alkalinity [gIC/L] were evaluated based on the relative concentration of sodium carbonate and bicarbonate in water [55]. A simple linear interpolation was used in situations for which no value could be obtained directly.
- The efficiencies of pumps and compressors were assumed to be 70% and 80% respectively.
- No additional heat loss and inefficiencies were considered between components.
- Except for microalgae drying and pasteurisation, a conventional air source heat pump with a Coefficient of Performance (COP) of 3.5 [56] was considered to supply all the heating requirements of the proposed plant including the greenhouse.

Besides these, the other assumptions specific to each section of the polygeneration layout have been included in each subsection detailed below (Sections 7.2.3.1-7.2.3.5). Except otherwise stated, all components were modelled using the default SuperPro Designer library.

7.2.3.1 Anaerobic digestion section

Figure 7-4 describes the model of a mesophilic anaerobic digestion unit. The grass silage was handled by an initial storage unit (S1-101), followed by a grass shredder (SR-1001) before being mixed with the slurry. A pasteurisation unit (PZ-101) was employed to homogenise the slurry that may be obtained from multiple farms and also to minimise pathogens [43,44]. The slurry, after being treated at 72 °C for 1 hour, was pumped and mixed with the shredded grass silage before being temporarily stored in a feed storage unit (V-105) [9]. The water content in the combined feed was adjusted to 18% dry solids (DS) [30] using recycled water from digestate before being loaded into the digester at an OLR of 3.5 kgVS/m^3/day as described previously in Section 7.2. Two anaerobic digesters (AD-101 and AD-102) in series generated biogas by reducing 84% of the VS [30], further details of which are provided in Table 7-3. The generated biogas was assumed to comprise CH_4, CO_2 and traces of NH_3 and H_2S. The theoretical concentrations of CH_4 and CO_2 were obtained via Eq. 7.4 [57]. As photosynthetic biogas upgrading has been shown to simultaneously remove CO_2 and H_2S [58], no additional H_2S removal unit was necessary for the present plant configuration.

$$C_xH_yO_z + \left(x - \frac{y}{4} - \frac{z}{2} +\right) H_2O \rightarrow \left(\frac{x}{2} + \frac{y}{8} - \frac{z}{4}\right) CH_4 + \left(\frac{x}{2} - \frac{y}{8} + \frac{z}{4}\right) CO_2 \qquad (7.4)$$

The combined biogas from both the reactors was first passed through a moisture trap (CSP-101) to remove excess moisture and then compressed to 6 bars for storage for a maximum of two days in a gas storage (V-101) [59,60]. The medium pressure storage was selected to act as a buffer and allow a continuous supply of biogas for photosynthetic biogas upgrading (described in the following Section 7.2.3.2). For simplicity, the dry biogas was assumed to contain negligible moisture. The amount of digestate was calculated using a simple mass balance, whereby, of the total feed entering the system, the output was divided among biogas and digestate only. While a fraction of the decanted digestate (in decanter CL-101) was recirculated to adjust for the dry solids content in the digester inlet feed, the rest was stored in a digestate storage lagoon (V-102) for further use or distribution (not modelled in this work).

Table 7-3 Process parameters utilised to simulate the Anaerobic Digestion section in SuperPro

Process parameter	Unit	Value	Comment/ Reference
Dry solid content in the combined feedstock	%	18	Vo et al. (2018) [30]
Temperature of digester	°C	37	Wall et al. (2014) [25]
Organic loading rate (OLR)	kgVS/m^3/day	3.5	Adapted from Wall et al. (2014) [25]
Hydraulic retention time of AD-1	days	30	Adapted to match overall organic loading rate (OLR)
Hydraulic retention time of AD-2	days	25	
AD working volume	% of total volume	90	Assumed
VS reduction	%	84	Vo et al. (2018) [30]
Yield from AD-1	% of total biogas	80	Adapted from Vo et al. (2018) [30]
Yield from AD-2	% of total biogas	20	
AD hot water inlet and outlet temperature	°C	60/40	Calise et al. (2020) [61]
Methane loss	%	1	Assumed from Liebetrau et al. (2017) [62]

In the model, the heat required to bring the feedstock up to the digestion temperature was provided by the heat exchanger (HX-101) before the first digester (AD-101). To calculate the heat requirement in the digester, the heat of reaction for anaerobic digestion was assumed to be -58 kJ/kg [63] while the heat loss in the digesters was modelled by an additional heat exchanger (HX-102) placed between the two digesters and set to an outlet temperature of 25 °C. The specific electrical and heat demands of each of the individual units comprising the anaerobic digestion section such as the grass shredder and the pasteuriser are further summarised in Table 7-4. A 1% methane loss was assumed [62] and was included in the model as a by-stream at the output of the biogas storage vessel.

Table 7-4 Specific energy consumption of the individual components of the Anaerobic Digestion section, the Biogas Upgrading section, the Microalgae Cultivation section and the Microalgae Harvesting and Processing Section. The values without references are default values of the components in the SuperPro Designer library.

Component	Unit	Electricity	Heat
Grass Silage Storage Unit	kWh/t-grass	0.085 [64]	-
Grass Conveyer	kW/(m^3/hr)/m-conveyer length	0.02	-
Gras Shredder	kW/(kg/hr)	0.02 [9]	
Cattle Slurry Storage Unit	kW/(t-slurry/hr)	0.085 [64]	-
Pasteuriser	kW/(t-slurry/hr)	6.28 (Half of the heat demand) [65]	12.56
Slurry Pump	W/(t-slurry/hr)	40	-
Feed storage Tank	-	-	-
Anaerobic Digester	Wh/m^3-digester volume	10	-
Biogas Compressor	W/(Nm^3-biogas/hr)	76.3	
Digestate Decanter	W/(t-slurry/hr)	100	
Digestate Lagoon	Wh/t-digestate stored	-	-
Clarified liquid circulating pump	W/(m^3-water/hr)	40	-
Biomethane compressor (up to 65 bars)	W/(Nm^3-biomethane/hr)	250	
Microalgae circulating pump	W/(m^3/hr)	40	-
Open Pond Photobioreactor	kWh/ha/day	55.1 [66]	-
Flat Plate Photobioreactor	W/(m^3/hr)	53 [67]	
Inoculum Reactor	kWh/ha/day	55.1 [66]	-
Greenhouse	MJ/m^2/year	-	1,000* [46]
Microalgae Harvesting Screens	-	-	-
Rotary Vacuum Filter	Wh/m^2-filter area	461.8	-
Bead Mill	kW/(t/hr)	35.7	
Spray Dryer	kW/(t/hr)	24** [68]	645

*To be supplied by a heat pump as electricity
**Estimated as 0.037 times the heat consumption during drying [68]

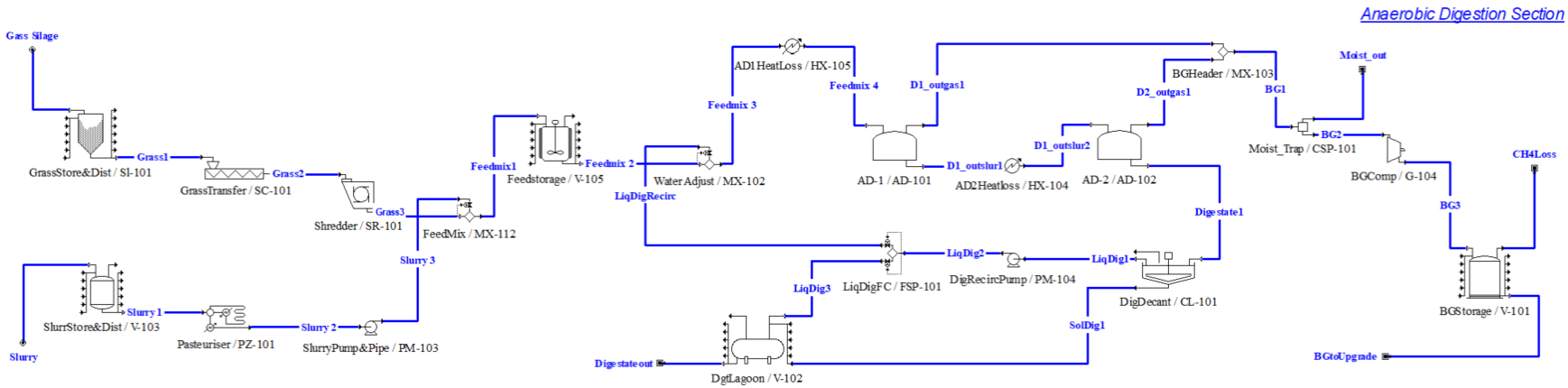


Figure 7-4 Simulated model details of the anaerobic digestion section

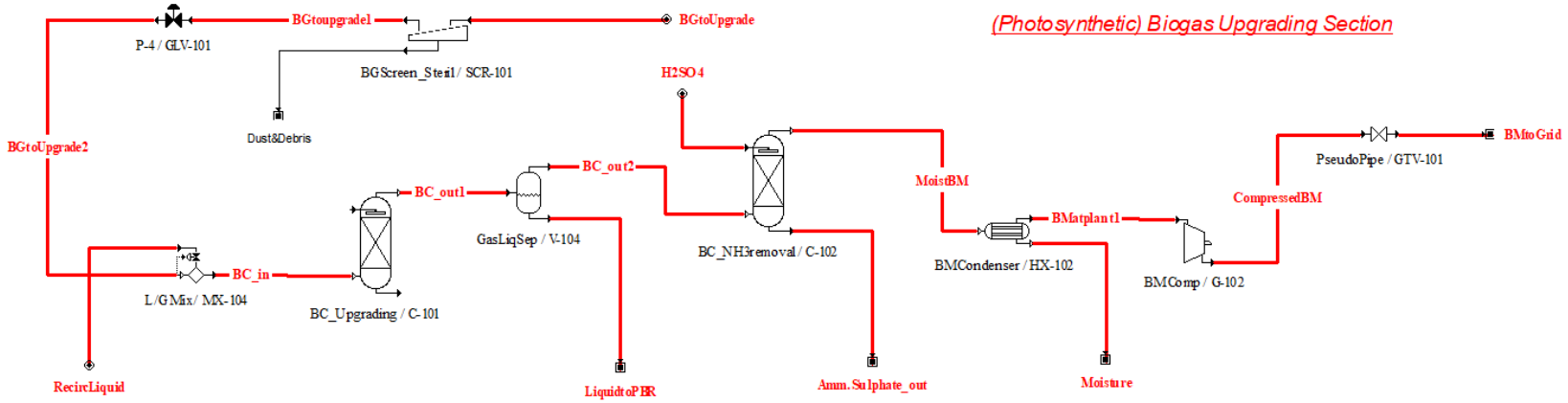


Figure 7-5 Simulated model details of the photosynthetic biogas upgrading section including biomethane injection into the gas grid

7.2.3.2 Photosynthetic biogas upgrading section

The biogas from the gas storage in anaerobic digestion was first passed through an antibacterial screen (SCR-101) to condition it for use in food production processes. The pressure before the bubble column inlet was also adjusted to 2 bars to account for pressure drops in the bubble columns and downstream processing such as ammonia scrubbing. In the current simulation within SuperPro Designer (Figure 7-5), the bubble column (C-101) was assumed as a simple stoichiometric reactor capable of removing a maximum of 100% of both CO_2 and H_2S alike while utilising a liquid to gas flow (L/G) ratio of 0.6 [13,69] (calculated at normal pressure and temperature (NTP)). While the CO_2 absorption reaction can be given using Eq. 7.1, Eq. 7.5 describes the absorption of H_2S in Na_2CO_3 at a pH below 11 [13,70]. The absorbed H_2S in the form of NaHS would then react with the dissolved oxygen (DO) in the solution to produce sulphates of Sodium (Eq. 7.6). The conversion of NaHS was assumed to be 100% based on the availability of DO; 90% of the dissolved oxygen and nitrogen (if any) were considered to be stripped into the biomethane during biogas upgrading.

$$H_2S + Na_2CO_3 = NaHS + NaHCO_3 \quad (7.5)$$

$$Na_2CO_3 + NaHS + 2O_2 = Na_2SO_4 + NaHCO_3 \quad (7.6)$$

As can be seen from Figure 7-5, the outlet of the bubble column is routed to a gas-liquid separator modelled using a Flash Chamber (V-104). The liquid from the outlet of the gas-liquid separator (LiqtoPBR), rich in bicarbonates formed the cultivation media of the microalgae. The ensuing moist biomethane, on the other hand, containing an assumed concentration of 5% moisture by volume was directed into a packed column (C-102) for ammonia scrubbing using sulphuric acid [27]. The ammonia scrubbing was modelled using a stoichiometric reactor; 90% NH_3 removal was considered. The outlet gas, cleaned of CO_2, NH_3 and H_2S was passed through a chilled water condenser (HX-102) operating at 4 °C to remove excess moisture. The ensuing biomethane, meeting grid emission standards (less than 2.5% and 1% CO_2 and O_2 respectively) was finally compressed to 65 bar in the compressor G-102 and sent to the gas grid injection point via pipelines. The specific energy demands of the individual units comprising the biogas upgrading section are compiled in Table 7-4.

7.2.3.3 Microalgae Cultivation Section

The liquid output from the gas-liquid separator of the bubble column (LiqtoPBR) was first adjusted for the necessary nutrient and algal concentration. Modified Zarrouk's media comprising 16.8 g/L of $NaHCO_3$ and the remaining 5.33 g/L of other nutrients including nitrate, phosphate, and sulphate were used as the most suitable nutrient for *Spirulina platensis* production [26,70]. However, to simplify the analysis, instead of inputting each chemical separately, Zarrouk's medium without $NaHCO_3$ was considered as one component. Accordingly, its concentration at the inlet to the primary photobioreactor (RP-101) was adjusted to 5.33 g/L for optimal operations. The sodium carbonate on the other hand was left to vary as per the alkalinity of the circulating liquid. The initial algal concentration was adjusted to 0.1 gDW/L using microalgae from the inoculum reactor (RP-102) to ensure steady and constant operations.

To estimate the hydraulic retention time [days] and specific growth [day^{-1}] the average volumetric productivity (P_{alg}) [gDW/L/day] was used [52]. Eq. 7.7 and Eq. 7.8 were used to evaluate the hydraulic retention time and specific growth rate respectively.

$$\text{Hydraulic retention time (HRT)} = \frac{C_{alg_{t2}} - C_{alg_{t1}}}{P_{alg}} \quad (7.7)$$

$$\text{Specific Growth } (\mu) = \frac{\ln C_{alg_{t2}} - \ln C_{alg_{t1}}}{t2 - t1} \quad (7.8)$$

where $C_{alg_{t2}}$ and $C_{alg_{t1}}$ are the algal concentration [gDW/L] at the time intervals t2 and t1 [days] respectively. To evaluate the volume of each PBR, the HRT was multiplied by the volumetric flow of the liquid assuming a 90% occupancy in the photobioreactor. The PBR dimensions and hence the areal footprint of each reactor was evaluated considering the following: *i)* the depth of OPPBR is 0.3 m [71], and *ii)* the surface to volume ratio of the FPPBR is 28.57 m^2/m^3 [67] with an aerial footprint to surface area ratio of 0.1 [72]. While the OPPBR required no aeration, average aeration of 0.17 vvm was considered for mixing in the FPPBR [73]. For both of these PBRs, no separate oxygen stripping column was considered necessary at the end of the PBR. As can be seen from Figure 7-6, the greenhouse was included in the model as a separate custom unit (GBX-106) to enable heat requirement calculations. The specific energy demand

of each PBR, as well as the other components comprising the microalgae cultivation section, are compiled in Table 7-4.

Carbon loss by stripping [14] and water loss through evaporation [74] were modelled separate to the photobioreactor to ensure the simplicity of the model. The carbon loss was attributed to the sodium bicarbonate fraction (10%), while no stripping of the carbon from sodium carbonate was assumed to occur. Based on the temperate climate maintained inside the greenhouse, 0.003% water loss via evaporation was assumed for open ponds; the model results were verified with respect to annual evaporation data [meters/year] obtained by Béchet (2018) [74]. Being a closed photobioreactor, the water loss from the FPPBR was neglected [75,76]. The outlet concentration of microalgae from the inoculum reactor was considered constant at 2 gDW/L to ensure adequate availability of microalgae for adjusting the input algal concentration of the primary PBR. The remaining microalgae medium was partly circulated back into the inoculum reactor through a flow controller (FSP-102). This allowed the adjustment of the inflow of the medium into the inoculum reactor to ensure continuity of the cycle. The excess flow (if any) was harvested along with the microalgae obtained from the primary PBR. The inoculum reactor was modelled similar to the main PBR for all scenarios analysed with its inlet algal concentration being 0.1 gDW/L upon adjustment with water. Zarrouk's media and $NaHCO_3$ were adjusted to 5.33 g/L and 16.8 g/L respectively to maintain optimal operating conditions in the inoculum reactor. Similar models of carbon and water loss were also included.

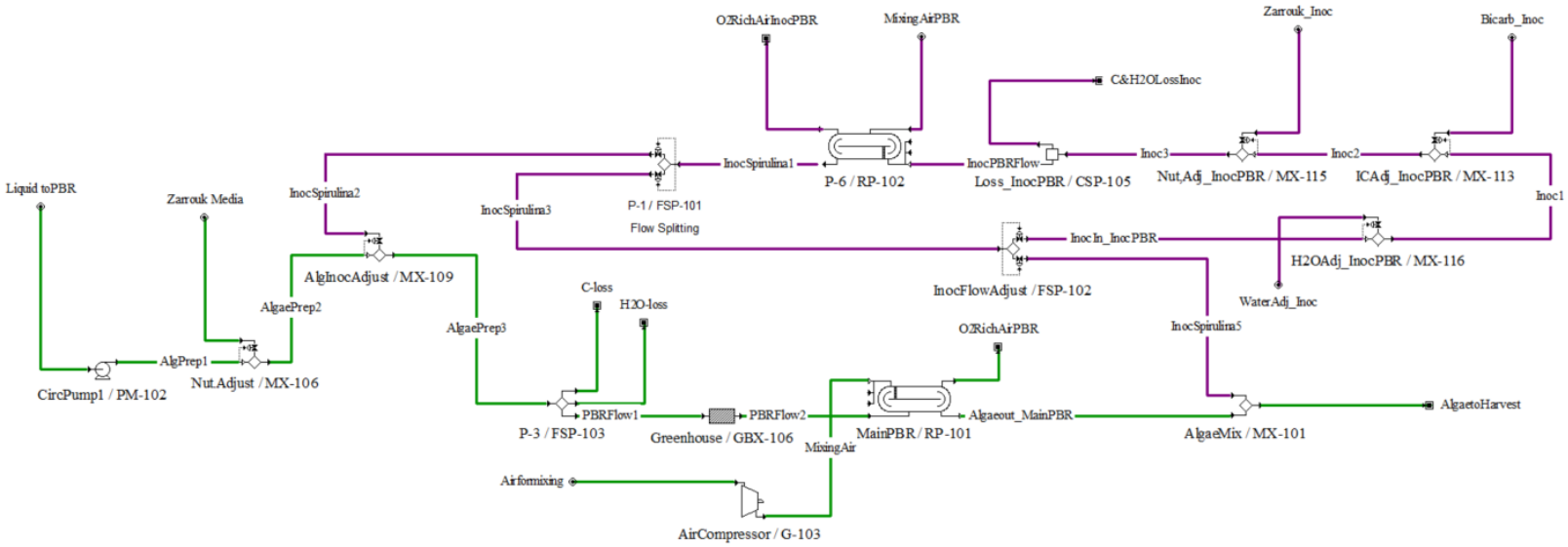


Figure 7-6 Simulated model of the microalgae cultivation section including the inoculum reactor and accessories. The air compressor for circulating air would be necessary only when closed photobioreactors are concerned. However, it has been included in the general model to maintain generality.

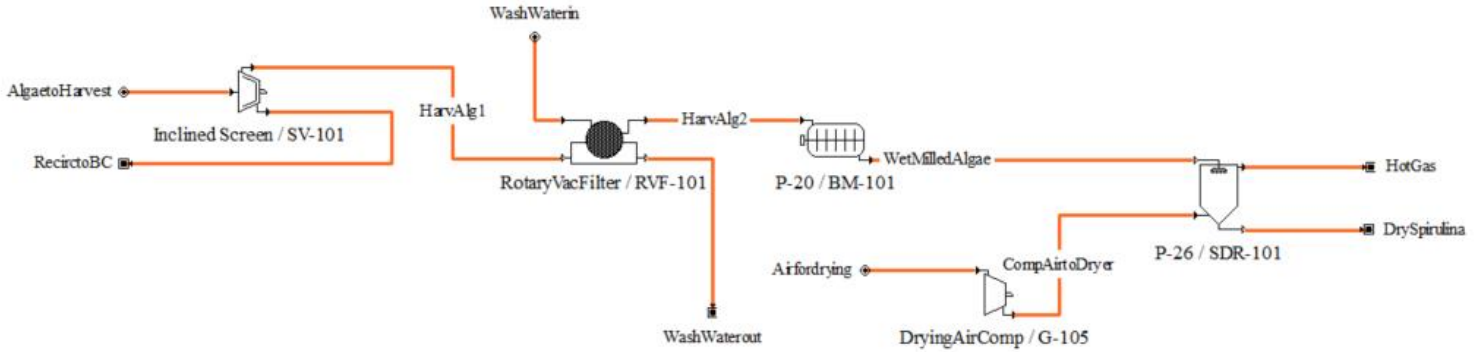


Figure 7-7 Simulated model of the microalgae harvesting and processing section towards obtaining dry Spirulina.

7.2.3.4 Microalgae harvesting and processing section

As shown in Figure 7-7, the microalgae were harvested using inclined screens (SV-101) to ensure a concentration between 0.08 and 0.09 gDW/L in the post-harvested culture medium. The resulting harvested slurry was further concentrated from 9% to 25% solids in a rotary vacuum filtration unit (RVF-101) [47]. A wash-water stream (WashWaterin) was used to wash the harvested algae after filtration to remove the residual salts. The output from the rotary vacuum filter was first milled in a bead milling unit (BM-101) before being dried in a spray drier (SDR-101) [48,77] using steam at 242 °C to produce 97% dry *Spirulina* powder. The exiting product temperature was set to 50 °C to enable heat recovery and improve the efficiency of operation. The individual electricity and heat demands are included in Table 7 4.

7.2.3.5 Recirculation Adjustment Section

The liquid exiting the inclined screen harvesters (SV-101 in Figure 7-8) forms the recirculating medium. In the simulated model, photosynthetic biogas upgrading was continued by adjusting the makeup water to allow operation at the selected L/G ratio. Fresh water and recycled water from the wastewater treatment plant was first demineralised in a demineralisation (DM) unit and then adjusted for pH and alkalinity before entering the process via a flow control valve (FAD-101). As can be seen from Figure 7-8, the pH and alkalinity were adjusted by varying the carbonate and bicarbonate concentrations. Besides the DM unit, the liquid circulating pump (PM-101) was the only energy-consuming component of the section having a specific electricity consumption of 20 W/m^3.

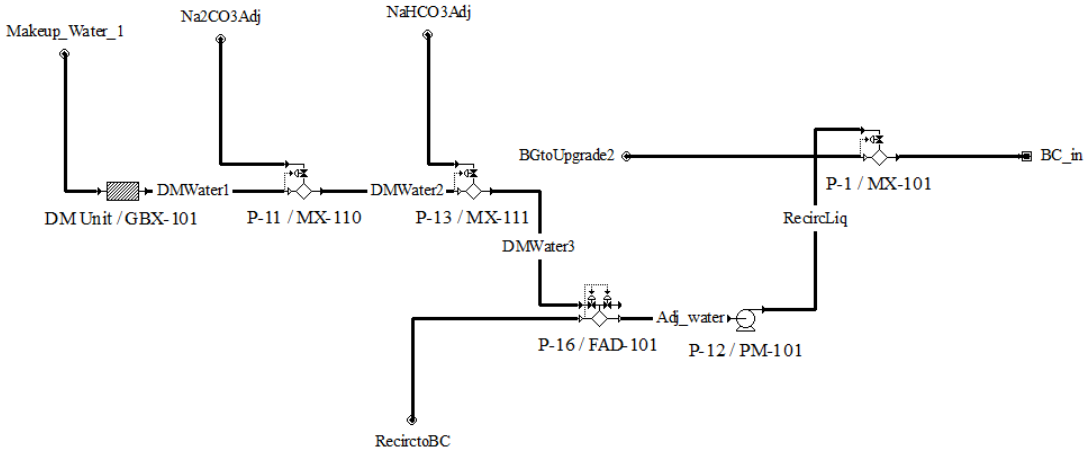


Figure 7-8 Simulated model of the recirculation adjustment section

7.2.3.6 Auxiliary Units

The demineralisation unit, along with the other auxiliary units such as the wastewater treatment plant were not modelled in detail. However, they were included in the assessment using their specific energy consumptions (Table 7-5). The sludge exiting the wastewater treatment plant was assumed to contain 20% solids [78]. However, it was assumed to be dried to around 60% solids before being sent for tertiary end-of-life treatments.

Table 7-5 Energy consumption details of the demineralisation plant and other auxiliary units considered within the system boundary of the proposed polygeneration unit

Auxiliary facility	Unit	Electricity	Heat
Demineralisation unit (using reverse osmosis)	kWh/m^3-water	6 [79]	-
Cooling tower	kWh/m^3-water	0.05 [80]	-
Wastewater treatment plant	kWh/m^3-water	2 [78]	
Chiller for condenser	kW/ton of refrigeration*	1 [81]	-
Sludge drier	kWh/tonne-evaporated water	-	600** [82]
Other auxiliary units including space heating by heat pumps	kW	2% of the energy contained in biomethane (assumed)	5% of the total heat demand (assumed)

*1 ton of refrigeration = 3.5 kW
** Assumed that raw sludge entering the drier had 20% water content after secondary treatment [78].

7.2.4 Process performance assessment

Multi-criteria performance assessments of the proposed polygeneration plant were performed using thermodynamic, economic and environmental metrics. The **standard energy return on investment (S-EROI)** was used as the thermodynamic measure. By this, the energy within the output products, namely, biomethane, *Spirulina* powder and digestate (except under RED-II framework) was compared with the energy input to the system in terms of both direct and indirect energies as per Eq. 7.9 [83]. The direct energy was obtained by considering both the electrical and the heat energy requirements of all the primary and auxiliary units considered within the process boundary. The total indirect energy input to the system is described by Eq. 7.10 as the summation of the energy required for farming (both grass and slurry) (E_{farm}), for transportation of input materials and resources ($E_{trans,\ in}$), for transportation of products ($E_{trans,\ out}$) and production of the chemicals used in the system (E_{chem}) [84].

$$\text{S-EROI}= \frac{\text{Energy within output products } (E_{out})}{\text{Direct Energy Input } (E_{dir}) + \text{Indirect Energy Input } (E_{indir})} \quad (7.9)$$

$$E_{indir}=E_{farm}+E_{trans,in}+E_{trans,out}+E_{chem} \quad (7.10)$$

Assuming an average energy consumption of 2,975.3 MJ/ha for farming grass (including ploughing, sowing, harrowing, rolling, fertiliser and herbicide, spreading, transport, harvesting and ensiling) [85] and an annual grass production of 65 t-FW/ha with 18% dry solid when cut [34], E_{farm} for the grass was estimated as 71.67 MJ/t-FW grass entering the facility (30% dry solid). Since cattle slurry is obtained as a by-product of agricultural activities, E_{farm} for slurry was assumed as 0. Grass and slurry were assumed to be obtained from an average distance of 10.5 km and 6.4 km respectively [86] using a truck consuming energy at 2 MJ/t-km [87]. For digestate, a similar truck was assumed to distribute it to nearby fields from where the grass has been sourced. The indirect chemical energies for the major chemicals listed in Table 7-2 were assumed as follows: 14.9 GJ/tonne Na_2CO_3 [88]; 7.5 GJ/tonne $NaHCO_3$ [89]; 6.1 GJ/tonne Zarrouk's Media [90].

The economic performance was studied using the **cost utilization factor (CUF)** [19] with a minimum desired value of 1. Eq. 7.11 was used to calculate CUF, where, both the input and output utilities and materials were calculated specifically to one Nm^3/hr of biogas flow using respective costs and market prices compiled in Table 7-2. The cost of sludge disposal (end of life process) was included as a negative price to the numerator to account for the cost to the plant.

$$\text{CUF}= \frac{\text{Market Price of output products}}{\text{Total Cost of input utilities and materials}} \quad (7.11)$$

The **Carbon Emission Factor (CEF)** [19] was used to measure the environmental performance of the proposed polygeneration plant. As shown in Eq. 7.12, the net GHG emissions from the proposed process (detailed in Section 7.2.8) were compared with the emissions from individual systems producing similar quantities of each output (or equivalent). For the reference standalone biomethane production, both water and amine scrubbing technologies for biogas upgrading were considered for comparison. Using a similar feedstock, the respective emissions from those systems were 17.3 $gCO_{2\text{-eq}}$/MJ-biomethane [91] and 34 $gCO_{2\text{-eq}}$/MJ-biomethane respectively [49]. A *Spirulina* production facility housed in a greenhouse in western

France [92] was selected as the reference standalone process to produce *Spirulina*. The corresponding GHG emissions were 15.5 $kgCO_{2\text{-}eq}$/kg-Spirulina [92]. For simplicity, the reference GHG emissions from inorganic fertiliser production were considered as 2 $kgCO_{2\text{-}eq}$ /kg equivalent N as an EU average value [93].

$$CEF=\frac{\text{Overall GHG emissions from the polygeneration plant}}{\text{GHG emissions from individual units delivering the same utilities}} \quad (7.12)$$

7.2.5 Estimation of energy, land and water footprints

7.2.5.1 Process energy demand

The overall energy demand (En_{plant}) of the proposed polygeneration unit was obtained as the sum of all the direct final energies consumed by the plant (Eq. 7.13), in which, En_{AD} refers to the energy consumed in the AD section including biogas compression, $En_{BG\&BM}$ is the energy required to upgrade the biomethane, dehumidify the upgraded biomethane and compress it for grid injection purposes, En_{PBR} is the energy required to cultivate the microalgae, $En_{harv\&proc}$ is the energy required to harvest, mill and spray dry the produced *Spirulina*, $En_{liqcirc}$ is the energy required to recirculate the water and in make-up water supply and En_{aux} is the energy associated with the operations of the auxiliary units (Table 7-5). It must be noted that all energies take into account both electrical and thermal energy inputs separately (final energy basis).

$$En_{plant}=En_{AD}+ En_{BG\&BM}+ En_{PBR} +En_{harv\&proc} +En_{liqcirc}+En_{aux} \quad (7.13)$$

7.2.5.2 Land footprint estimation

The land requirement for the anaerobic digestion facility was assumed as 86 m^2/Nm^3 biomethane generated [94,95]. The total land required for biogas upgrading in the bubble column was estimated considering four meters distance between each column. The areal footprint of the microalgae cultivation and harvesting system, as the area under the greenhouse cover, was calculated as 1.43 times the area of the primary PBR [73]. Since no specific laws or norms are available to evaluate the land footprint of a polygeneration plant, the summation of the above three land requirements was used to estimate the overall land footprint of the proposed system. To account for the lands required to process microalgae, strip ammonia and compress

biomethane as well as accommodate auxiliary facilities, an additional 20% land was considered.

7.2.5.3 Water footprint estimation

Eq. 7.14 was used to evaluate the overall water required [m^3/hr] for operating the proposed system in terms of the water entering the bubble column (L_{BC}), the makeup water accounting for the water lost both within the process (L_{mu}) and within the utilities (L_{ut}), the water added to the inoculum reactor (L_{inoc}) and the water required to wash the microalgae after harvesting (L_{wash}). The process of water loss was evaluated during the simulation taking into account the water losses by evaporation and as effluents. The water for washing the microalgae was also obtained from the simulation assuming an equal volume of wash water is required for each m^3 of harvested algal cake.

$$L_{FP}=L_{BC}+L_{mu}+L_{ut}+L_{Inoc}+L_{wash} \quad (7.14)$$

The water flows for heating of the anaerobic digester as well as the greenhouse was obtained assuming a 20 °C temperature differential between the hot and cold waters. For steam drying, a temperature drop of 88 °C between the inlet and the outlet steam was assumed according to the default steam drying unit in the SuperPro Designer library. The water required in the chiller condenser was directly evaluated from the simulation. For all of these systems, a 0.1% water loss was considered assuming an advanced system. Cooling water for biogas and biomethane compressors, and the algae dryer after moisture removal was obtained from the SuperPro model. Assuming a wet cooling tower for the cooling system, a 1% water loss was assumed [96]. Accordingly, the utility water requirement (L_{ut}) [m^3/hr] was estimated as per Eq. 7.15, where, $L_{heating}$ is the total water flow for all heating purposes within the plant, L_{steam} is the steam required in the spray drier, L_{chil} is the water circulated in the condenser and $L_{cooling}$ is the overall cooling water flow within the entire plant.

$$L_{ut}=0.001\times L_{heating}+0.001\times L_{steam}+0.001\times L_{chil}+0.01\times L_{cooling} \quad (7.15)$$

7.2.6 Allocation principles

Energy and economic methods were selected as appropriate allocation principles [64] for resources (energy, land and water requirements) and emission distribution among the co-products. This is necessary as the contribution of emissions and resources towards each co-product were overlapped in the polygeneration system. For example, the energy input into the PBR is as important for biogas upgrading as it is for microalgae production. For energy allocation (Eq. 7.16), the energy within biomethane and *Spirulina* powder were estimated as 50 MJ/kg-CH_4 [97]; and 17 MJ/kg [98] respectively. The energy in digestate was based on the LHV of dry digestate (15 MJ/kg-dry [99,100]). For the economic allocation (Eq. 7.17), the revenues were calculated using the material flows obtained from simulation and the corresponding selling prices compiled in Table S7-1.

$$Alloc_{Ener,i} = \frac{En_{i,yr}}{\sum_i En_{i,yr}} \quad (7.16)$$

$$Alloc_{Econ,i} = \frac{Rev_{i,yr}}{\sum_i Rev_{i,yr}} \quad (7.17)$$

where, $En_{i,yr}$ and $Rev_{i,yr}$ are the annual energy and revenue generated respectively by the i^{th} product, *i* being either of biomethane, *Spirulina* powder and digestate.

7.2.7 Product performance assessment and functional units

Either the energy or the economic allocation was used to allocate the energy, land and water requirements, as well as the GHG emissions to the individual co-products. As an example, the methodology to evaluate the energy consumption in the production of biomethane (En_{spec,BM_k}), *Spirulina* powder ($En_{spec,Spirul_k}$) and digestate ($En_{spec,DigN_k}$) and are shown below (Eq. 7.18 – Eq. 7.20 respectively), where k represents either the energetic or the economic allocation.

$$En_{spec,BM_k} = Alloc_{k,BM} \times En_{plant} \quad (7.18)$$

$$En_{spec,Spirul_k} = Alloc_{k,Spirul} \times En_{plant} \quad (7.19)$$

$$En_{spec,DigN_k} = \frac{Alloc_{k,Dig} \times En_{plant}}{0.39} \times 100 \quad (7.20)$$

where $Alloc_{k,BM}$, $Alloc_{k,Spirul}$ and $Alloc_{k,Dig}$ are the allocations for biomethane, *Spirulina* and digestate on k (energy or economy) respectively.

The specific energy consumption, water and land footprints of each co-product along with their corresponding GHG emissions were hence evaluated to assess the product performances from the proposed polygeneration process and allow effective comparison with market-available alternatives. For this, appropriate functional unit(s) for each coproduct was selected [101]. Biomethane was evaluated using both 1 Nm^3/hr of biogas flow under normal conditions (NTP) and 1MJ of fuel. The selected functional units of *Spirulina* powder were 1 kg of dry powdered *Spirulina*, 100 grams of protein (gp) and 100 nutrient density score (NDS). Each gram of *Spirulina* was considered to contain 0.6 grams of protein [102]. The functional unit of digestate was taken as 1 kg-N to compare with standard inorganic nitrogenous fertilisers. To obtain the specific energy of digestate as equivalent nitrogen, the digestate was considered to contain 0.39% Nitrogen on a wet weight basis [49].

The Nutrient-Rich Foods Index version 9.3 ($NRF_{9.3}$) method [103,104] was adopted to calculate the NDS of *Spirulina* as a complete food and compare it with other alternatives. *Spirulina* contains all essential amino acids [105] and as such it is a suitable meat substitute and is also considered a superfood [105]. Accordingly, the equation to estimate NDS per 100 kcal of energy from *Spirulina* powder was given by Eq. 7.21 [104] where, N_{sp_i} is the content of the i^{th} nutrient within 100 kcal of the edible fraction. The amount of each nutrient in *Spirulina platensis* powder, together with their corresponding recommended daily values (RDV) and maximum daily values (MDV) necessary for this calculation are compiled in Table 7-6. Based on these values, the $NDS_{NRF9.3}$ score of *Spirulina* was obtained as 191.8/100 kCal. The corresponding values of other protein alternatives studied in this work are compiled in Table S7-2.

$$NDS_{NRF9.3}=\left(\sum_{i=1}^{9}\frac{N_{sp_i}}{RDV_i}-\sum_{i=1}^{3}\frac{N_{sp_i}}{MDV_i}\right)\times 100 \qquad (7.21)$$

Table 7-6 Nutrient value in Spirulina powder along with the recommended and the maximum daily values of each of the corresponding nutrients. The nutrient values in Spirulina were obtained from [102,106], while the recommended daily value (RDV) and the maximum daily value (MDV) were compiled from [104,107,108].

Nutrient	Value in *Spirulina* [g/100 g]	Recommended daily value (RDV) [g]	Maximum daily value (MDV) [g]
Protein	60	57	-
Dietary Fibre	3.6	25	-
Vitamin A	570 IU[a]	5000 IU	
Vitamin C	0.0085	0.08	-
Vitamin E	5 mg	12 mg	
Calcium	0.12	0.8	-
Iron	28.5 mg	14 mg	
Potassium	1.36	2	-
Magnesium	195 mg	375 mg	-
Saturated Fat	2.7	-	20
Sodium	0.5	-	2.4
Added Sugar	0	-	90
Energy	336 kcal/100 g	-	-

[a]IU: International Unit

7.2.8 Estimation of GHG emissions

Net hourly GHG emissions ($GHG_{net,nd}$) [$gCO_{2\text{-}eq}$/hr] without accounting for digestate was estimated using Eq. 7.22. When digestate was included, however, Eq.7.23 was employed.

$$GHG_{net,nd} = \sum_i S_i\left(e_{ec,i}+e_{td,fs,i}+e_{l,i}-e_{sca,i}\right) + e_p + \sum_j e_{td,prod,j} + e_u - e_{ccs} - e_{ccr} \quad (7.22)$$

$$GHG_{net,d} = \sum_i S_i\left(e_{ec,i}+e_{td,fs,i}+e_{l,i}-e_{sca,i}\right) + e_p + \sum_j e_{td,prod,j} + e_u - e_{ccs} - e_{ccr} - e_{dig} \quad (7.23)$$

where S_i is the share of the feedstock i (i being grass silage and slurry); $e_{ec,i}$ is the emissions from the cultivation of raw wet feedstock, i; $e_{td,fs,i}$ is the emissions from the transportation of the feedstock i to the digester; $e_{l,i}$ defines the annualised emissions from land-use change caused by feedstock i; $e_{sca,i}$ is the emission savings from improved agricultural management of feedstock i; e_p denotes the emissions from processing; $e_{td,prod,j}$ is the emissions from the transport of the j^{th} product (j being either of biomethane and *Spirulina* powder); e_u is the emissions from fuel use, i.e., greenhouse gas emitted during the combustion of the biofuel produced; e_{ccs} refers to

the emission savings from CO_2 capture and storage in geological formations; and e_{ccr} is the emission savings for CO_2 capture and replacement and e_{dig} is the emission savings from the application of digestate as a fertiliser replacing traditional inorganic fertilisers.

The share of each feedstock i (S_i) was evaluated using Eq. 7.24 and Eq 7.25 where P_i is the energy yield [MJ] per kg of wet feedstock i; I_i is the annual input of the feedstock i into the digester [t-FW], and AM_i and SM_i are the annual averages and standard moisture content of the substrate [kg water/kg fresh weight] i respectively [21,109]. In the present study, AM was assumed to be similar to SM for simplicity and hence Eq. 7.24 may be further simplified to $W_i = \frac{I_i}{\sum_i I_i}$. P_{slurry} was assumed as mandated by the RED-II, as 0.5 MJ/kg slurry (90% moisture). However, as there is considerable variability in the result of the biogas yield from grass, the LHV of grass (17 MJ/kg-dry [35]) was used to evaluate P_{grass} (5.1 MJ/kg-grass (70% moisture)).

$$S_i = \frac{P_i \times W_i}{\sum_i (P_i \times W_i)} \tag{7.24}$$

$$W_i = \frac{I_i}{\sum_i I_i} \left(\frac{1 - AM_i}{1 - SM_i}\right) \tag{7.25}$$

GHG emissions from the feedstock cultivation ($e_{ec,i}$), transport ($e_{td,fs,i}$) and land-use change ($e_{l,k}$) are compiled in Table 7-7. A round trip was considered to evaluate the emissions from transporting grass silage and cattle slurry. The specific emissions from a truck, similar to the one adopted for evaluating the energy requirement in transport was assumed as 50g CO_{2eq}/tonne-km [87]. As recommended by RED-II, the benefits from using cattle slurry as a renewable energy source were accounted as carbon credits of 54 $kgCO_{2\text{-}eq}$/tonne of fresh slurry [21] for year-round housing of cattle. On the other hand, assuming a typical soil carbon sequestration value of 2.2 tCO_2/ha/yr [85] and an annual grass yield of 65 t-FW/ha/yr with 18% moisture content [34], the net carbon credits from grass silage at the plant gate was obtained to be around 56.4 $kgCO_{2\text{-}eq}$/tonne of fresh grass (70% moisture content); this value can vary depending on site-specific conditions.

Emissions from indirect land-use change or ILUC is typically considered, when crop for biofuel is grown on food crop sites, forcing the latter into high carbon storage

sites such as rainforests or grasslands. In the temperate oceanic climatic, while grass silage is an abundant naturally occurring resource, cattle slurry is usually available as a by-product of beef and dairy farms. Thus, both feedstock was assumed to have an ILUC of zero, supported further by the RED-II [21]. The uniqueness of photosynthetic biogas upgrading is, however, the requirement of land for biogas processing. As substantial land is required for microalgae cultivation and harvesting, if the cultivated microalgae are used for biofuel production, then ILUC from microalgae cultivation is most likely to be associated with the evaluation of the overall GHG emissions. However, in the process proposed, the intended use of microalgae is for food production, and thus would not require ILUC to be included in the assessment of emissions from microalgae cultivation. In addition, it is to be understood that this process proposes microalgae as a replacement of beef as either food or protein. Thus, the process already has considered the concept of substitution of an existing resource, limiting the expansion of land requirements for the production of additional sellable goods.

The emissions from processing (e_p) included both the direct emissions from electricity and heat consumption, as well as those embodied in the chemicals used within the process [21]. In a decarbonised world electricity could be associated directly with a wind turbine or a PV array and heat with wood chips. However in this work, to be conservative, the emission factors for grid electricity and natural gas were considered (Table 7-7). Methane losses of 2% (1% each during anaerobic digestion and biogas upgrading) were assumed as process emissions alongside inorganic carbon losses via stripping from the PBR and through the effluents during harvesting. As nitrates were used as the nitrogen source of the microalgae and the photobioreactors were considered to operate under high DO levels (above 9 mgO_2/L), no N_2O emissions were considered from the cultivation of *Spirulina* [110]. No emissions from the sludge of the nitrogen replete wastewater were considered. The specific emissions from the major chemicals used in the process are listed in Table 7-7.

The emissions from the distribution of biomethane were accounted for by the electrical emissions during compression of the biomethane within the process emissions. As such, it was not separately evaluated under the category of emissions from product distribution. As *Spirulina* was proposed to be sold at the gate, no

distribution would be required. Biofertiliser (digestate) when considered was assumed to be used in the fields from where the grass is procured. Therefore, emissions similar to the transportation of grass were used for biofertiliser as well. Dried sludge containing 60% solids was assumed to be sent for tertiary end-of-life treatment, 50 km from the site; 20% of the dissolved solids were assumed to be removed during wastewater treatment. Within the plant, no additional fuel use was considered. As the carbon captured from the biogas would be used for food production via microalgae, no emission savings from carbon capture and storage (CCS) was considered.

In a traditional standalone *Spirulina* production facility, bicarbonates are separately supplied as the carbon source [102]. Conventional sodium bicarbonate production requires large amounts of fossil fuels for lime kilns [111] thus adding a significant emission penalty to microalgae production [102,112]. In the present plant, however, photosynthetic biogas upgrading allowed biogenic CO_2 to directly produce bicarbonate for *Spirulina* production. It would therefore replace fossil-derived CO_2 in the production of commercial $NaHCO_3$. Thus, e_{ccr} was considered as 660 gCO_2 for every kg of commercial $NaHCO_3$ replaced, similar to the emissions from market-bought $NaHCO_3$. For the scenarios considering digestate use, emission savings of 12 $kgCO_{2\text{-eq}}$/tonne digestate was assumed after Capponi et al. (2012) [113], who obtained CO_2 savings of 168.1 $tCO_{2\text{-eq}}$ from the use of 13,932 tonnes of digestate as a replacement of conventional fertilisers.

Table 7-7 Specific emissions under the different emission categories required to evaluate the overall GHG emissions of the proposed polygeneration plant as per the RED-II

Emission Category	Emission components	Unit	Value	Comments and Reference
$e_{ec,i}$	Emission from cultivation (grass silage, 70% moisture)	$gCO_{2\text{-eq}}$/tonne-FW[a]	50,948	Adapted from Long and Murphy (2019) [7] assuming 65 t-FW/ha/yr grass yield with 82% moisture content at the time of harvest [85]
	Emission from field N_2O (grass silage, 70% moisture)	$gCO_{2\text{-eq}}$/tonne-FW	41,282	
	Emission from cultivation (cattle slurry)	$gCO_{2\text{-eq}}$/tonne-FW	0	RED-II [21]
$e_{td,fs,i}$	Distance travelled by truck handling grass silage (both ways)	km	10.5	O'Shea et al. (2017) [86]
	Distance travelled by truck handling slurry (both ways	km	6.4	O'Shea et al. (2017) [86]

Emission Category	Emission components	Unit	Value	Comments and Reference
	Specific emissions from a truck	$gCO_{2\text{-eq}}$/tonne-km	50	Dünnebeil and Lambrecht (2012) [87]
$e_{l,i}$	Emissions from land-use change from the cultivation of grass	$gCO_{2\text{-eq}}$/ tonne-FW	0	-
	Emissions from land-use change from slurry	$gCO_{2\text{-eq}}$/ tonne-FW	0	-
$e_{sca,i}$	Emission savings from improved cultivation of grass	$gCO_{2\text{-eq}}$/ tonne-FW	-56,400	Adapted from Korres et al. (2010) [85]
	Emission savings from improved handling of slurry	$gCO_{2\text{-eq}}$/ tonne-FW	-54,000	RED-II [21]
	Specific emissions from electricity	$gCO_{2\text{-eq}}$/kWh	255	EU average electricity grid emission factor 2020 [114]
	Specific emissions from heat	$gCO_{2\text{-eq}}$/kWh	204	SEAI (2020) [115]
	Specific emissions from methane loss	$gCO_{2\text{-eq}}/gCH_4$	25	RED-II [21]
	Specific emissions from Sodium carbonate	$gCO_{2\text{-eq}}$/kg	300	Adapted from Bonfim-Rocha et al. (2020) [116]
e_p	Specific emissions from Sodium bicarbonate	$gCO_{2\text{-eq}}$/kg	660	Bonfim-Rocha et al. (2020) [116] & Barsoumian (2013) [89]
	Specific emissions from Zarrouk's medium (without sodium bicarbonate)	$gCO_{2\text{-eq}}$/kg	566	Adapted from Frank et al. (2011) [90]
	Specific emissions from CO_2 stripping	$gCO_{2\text{-eq}}/gCO_2$	1	-
	Specific emissions from sludge	$gCO_{2\text{-eq}}$/kg	0	No emission assumed from nitrogen replete wastewater sludge
	Distance travelled by truck for sludge disposal (both ways)	km	100	Assumed
$e_{td,prod,j}$	Emissions from the transport of biomethane	$gCO_{2\text{-eq}}$/MJ-biomethane	-	Included as emissions during biomethane compression
	Emissions from the transport of *Spirulina* powder	$gCO_{2\text{-eq}}$/kg-*Spirulina*	0	Assumed at the gate as per system boundary definition
	Distance travelled by truck for distributing digestate (both ways)	km	10.5	Same distance as the that travelled during procurement of grass.
e_u	Emissions from fuel use	$gCO_{2\text{-eq}}$/MJ-biomethane	0	-
e_{ccs}	Emission savings from carbon capture and storage	$gCO_{2\text{-eq}}$/MJ-biomethane	0	-

Emission Category	Emission components	Unit	Value	Comments and Reference
e_{ccr}	Emission savings from CO_2 capture and replacement	$gCO_{2\text{-}eq}$/kg-$NHCO_3$	-660	Replacing emissions from fossil fuels used in commercial $NaHCO_3$ production [111].
e_{dig}	Emission savings from the application of digestate as a replacement for conventional fertilisers	$kgCO_{2\text{-}eq}$/tonne	-12	Adapted from Capponi et al. (2012) [113]

7.2.9 Sensitivity analysis

As the technology enabler, the different input process parameters of photosynthetic biogas upgrading were investigated for their impact on the overall process and product performance. Sensitivity assessments were performed on the base case scenario by varying the input process parameters (such as makeup water, pH, L/G ratio and alkalinity). Other sensitivity studies varying process variables were performed wherever appropriate. All variables were varied by +/-10% from their base values unless otherwise mentioned.

Monte Carlo simulation was used to identify the uncertainty and variability of the obtained results. The Monte Carlo method was selected due to its wide usage as a comprehensive statistical tool to assess the sensitivity of complex mathematical models and process simulations [117,118]. For the present analysis, the uncertainty was assessed by conducting 1,000 randomised iterations, as used in previous literature [117,118]. The random samples were generated based on the probabilistic density function of each process variable. As limited data was available to fit any actual distribution, a symmetric triangular distribution was assumed [119,120]. The base or the most probable value was selected as the mode and +/- 10% was considered to make up the extremities of the triangular distribution [121].

7.3 Results

7.3.1 Mass balance and model validation

7.3.1.1 Mass balance

The simulated model was validated on the base case scenario (BASE-EC) both with respect to the mass balance assessment and based on a comparison of the simulation outputs to that published in the literature. For every 3 tonne/hr (t/hr) of grass silage inlet (70% moisture) and 3.13 t/hr of cattle slurry (91.2% moisture), 670.8 Nm^3/hr of biogas was produced. A small recycling stream of decanted liquid was used to adjust the water content of the digester feed, resulting in a net raw digestate production of 5.4 t/hr with 5.94% solids. Biogas upgrading, followed by ammonia scrubbing and excess moisture removal by condensation, generated grid quality biomethane at 229.6 kg/hr or 361.5 Nm^3/hr. The equivalent power rating of the plant was therefore 3.19 MW-biomethane at 8.8 kWh/Nm^3-biomethane (*Box S7.2*). 382 t/hr of algal liquid was circulated through the bubble column for photosynthetic biogas upgrading. The exiting liquid, rich in bicarbonate was adjusted with 2.8 t/hr of higher density (2 gDW/L or 0.2% dry solids concentration) algal culture from the inoculum reactor to ensure a consistent algal concentration of 0.1 gDW/L at the inlet to the primary photobioreactor. Within the main OPPBR, water and carbon losses occurred, together with oxygen released from the photosynthesising microalgae. After harvesting using inclined screens, 8.14 t/hr (9% solids content) of microalgae slurry was further concentrated to 25% solids content and washed with 0.92 t/hr of water in the vacuum filtration facility. Following bead milling and drying, around 241.5 kg/hr of *Spirulina* powder was produced at a moisture content of 3%, with a loss of 0.7 t/hr of water from drying. Around 7.5 m^3/hr of wastewater was generated, which was subsequently treated to regenerate and recycle water required by the process while generating 206 kg/hr of sludge with 60% solids (following drying). For each cycle, 4.2 t/hr of makeup water was necessary, together with 243.3 kg/hr of Na_2CO_3 and 168 kg/hr $NaHCO_3$ as replenishment to the water and inorganic carbon lost within the process. Since a major part of the water is recycled after treatment, only 1.5 t/hr of fresh water was required to be supplemented for each cycle. A detailed mass flow diagram for the base case scenario of the proposed polygeneration plant is provided in Figure 7-9.

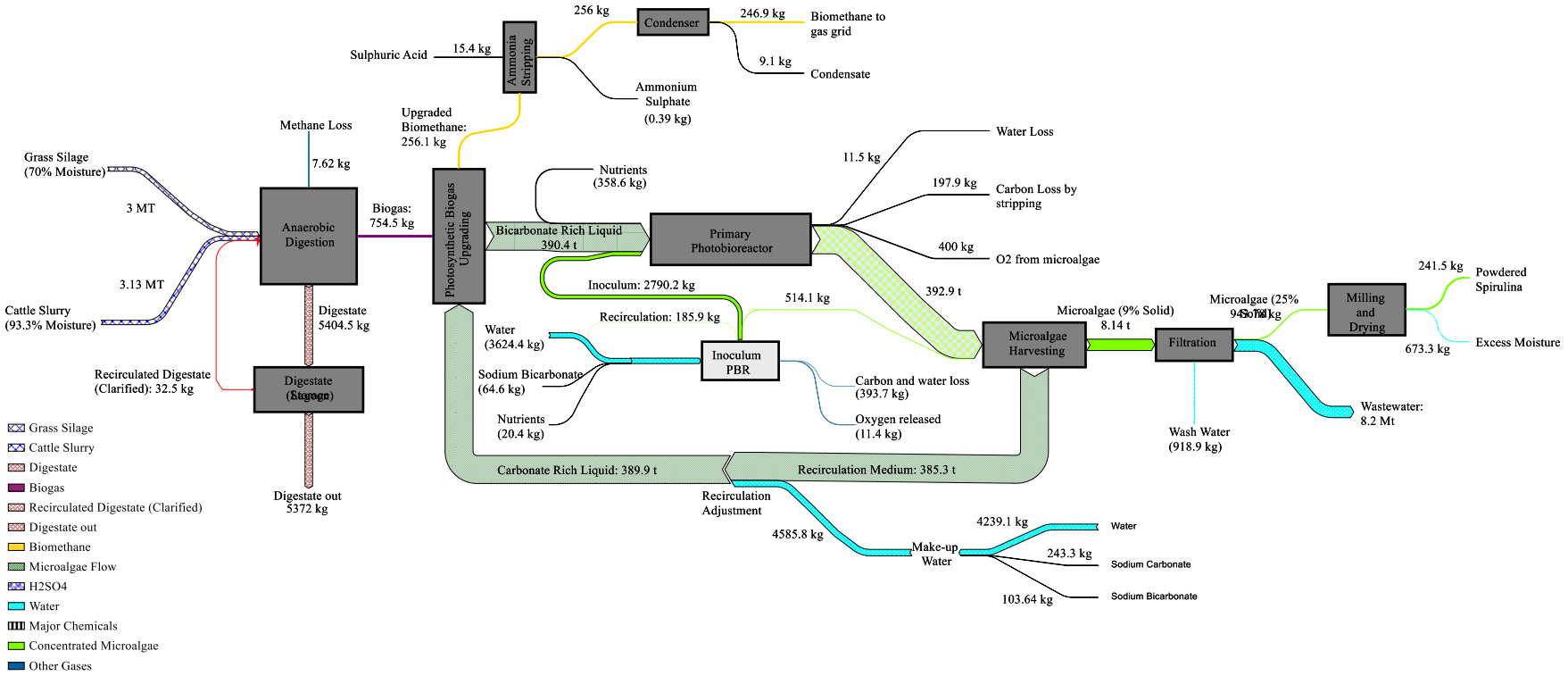


Figure 7-9 Mass flow diagram for co-generation of biomethane and Spirulina powder in a cascading polygeneration system utilising photosynthetic biogas upgrading for the base case scenario (BASE-EC)

7.3.1.2 Model validation

As can be seen from Table 7-8, the simulation results of biogas production obtained in the present study match well with the experimental results of Wall et al. (2014) [25] and simulation results of Vo et al. (2018) [30]. A net yield of 0.366 Nm^3 of methane per kg of VS was obtained, similar to the methane yields previously reported in the literature [25,30]. The obtained biogas contained 54.5% CH_4, 45.4% CO_2 and 220 ppm each of NH_3 and H_2S. The digestate produced had a solids content of 5.9%, within the usual range of 1.1% and 7.5% [122]. Considering a 1% methane loss, the net energy generated in the form of biogas was thus 520 kWh/t-fresh feed. The overall digestate generation per unit feedstock also matched well with literature studying the co-digestion of grass silage and cattle slurry [9,30].

Table 7-8 Model validation of biogas production via anaerobic co-digestion of grass silage and cattle slurry

Description	Unit	This Study	Literature
Methane Production	Nm^3-CH_4/kgVS[a]	366	366 [25]; 369 [30]
Biogas Production	m^3/ t-FW[b]	109	122 [30]
Volumetric Biogas Composition	$\%CH_4$	54.5%	55% [25]; 51.1% [30]
	$\%CO_2$	45.4%	48.9% [30]
	NH_3 (ppm)	212	Maximum ammonia in biogas generated from maize silage and pig manure co-digestion is 332 ppm [118]
	H_2S (ppm)	212	
Energy generated	kWh/t-FW	519.9	
Digestate Generation	t/t-FW	876.9	839.3 [30]; 871.4 [9]
Solid fraction of Digestate	%	5.9%	1.1% - 7.5% [122]

[a] VS: Volatile solids; [b] FW: Fresh weight

The performance of biogas upgrading was compared with the predictive models published by Bose et al. (2021) [69]. Although the pH of the makeup water and the liquid entering the bubble column remained the same at 10.2, the alkalinity at the bubble column inlet was higher (2 gIC/L) than that supplied through the makeup water (1.5 gIC/L). Such a rise in the alkalinity has been previously reported in photosynthetic biogas upgrading experiments by Rodero et al. (2020) [14] and Marin et al. (2018) [124], especially under long-term operation. Under these conditions, the CO_2 and H_2S removal efficiencies of 100% match well with the values obtained via predictive

models and those reported in the literature [13,69]. The upgraded biomethane after scrubbing of ammonia and removal of excess water contained 95.2% CH_4, 0.71% O_2, 1.8% N_2, 2.29% water and traces of ammonia (7 ppm) (Table 7-9), matching grid injection guidelines. The pH of the liquid exiting the bubble column outlet was 9.75 and matched closely with the predicted value of 9.80 [69].

Table 7-9 Model validation of biogas upgrading in photosynthetic biogas upgrading

Description	**Unit**	**This Study**	**Literature**
pH of liquid entering bubble column		10.2	
Alkalinity of liquid entering bubble column	gIC/L	2.0	
Dissolved oxygen of liquid entering bubble column	mgO_2/L	11.5	
L/G ratio		0.6	
CO_2 removal efficiency	%	100	100* [69]
H_2S removal	%	100	100 [13]
	$\%CH_4$	95.2	
	$\%CO_2$	0.0	
	$\%O_2$	0.7	0.63* [69]
Upgraded biomethane composition	% N_2	1.80	
	NH_3 (ppm)	7.0	
	H_2S (ppm)	0.00	
	$\%H_2O$	2.3	
pH of liquid exiting the bubble column		9.75	9.80* [69]
Alkalinity of liquid exiting the bubble column	gIC/L	2.4	
Dissolved oxygen of liquid exiting bubble column	mgO_2/L	1.0	

*Predicted using the model developed by Bose et al. (2021) [69]

The final microalgae at the end of the cultivated period of almost 4 days (hydraulic retention time) was 0.69 gDW/L yielding a specific growth rate of 0.50 day^{-1} and average aerial productivity of 10 $gDW/m^2/day$. Both these values matched well with the literature (Table 7-10) confirming a sufficiently accurate model. For the flat plate PBR, the areal productivity increased by over two times to 23.5 $gDW/m^2/day$. Considering the *Spirulina* carbon concentration to be 52.8% of the dry weight, the effective carbon utilisation was 25% of the total utilisable carbon in the form of bicarbonates. This matches well with the previous work by Binaghi et al. (2003) [125] who observed around 20% carbon uptake by *Spirulina platensis* after the first four days of cultivation. A rise in pH during cultivation, from 9.75 at the exit of the bubble column (Table 7-9) to 10.2 at the outlet from the open pond was also noticed (Table

7-10). The corresponding alkalinity dropped from 2.4 gIC/L to 1.9 gIC/L respectively, partly due to consumption by the microalgae and partly from loss due to stripping. The adopted evaporation model for the OPPBR also yielded favourable results in comparison to the literature. The specific microalgae production of 0.36 kg per Nm^3 biogas flow was found to closely relate to the value of 0.37 reported by Toledo-Cervantes et al. (2017) [18], thus suggesting the adequacy of modelling of the harvesting and processing units.

Table 7-10 Model validation of microalgae cultivation and harvesting in photosynthetic biogas upgrading

Description	Unit	This Study	Literature
Concentration of cultivated microalgae concentration	gDW/L	0.7	
Hydraulic Retention Time	days	3.8	
Specific growth rate	day^{-1}	0.5	0.46-0.58 [52]
Areal productivity	$g/m^2/day$	10.0	9 (spring/autumn) – 13.5 (summer) in open ponds in Spain [126] 14.47 ± 0.16 in open ponds in Italy [127]
Carbon sequestered	% of C as bicarbonates	25.0	c. 20% in a carbonate bicarbonate buffer after 4 days of cultivation at a pH of 9.6 [125]
pH after cultivation		10.2	
Alkalinity after cultivation	gIC/L	1.9	
Dissolved oxygen at outlet	mgO_2/L	10.5 (c. 140%)[§]	< 160% saturation in Open pond with sump [128,129]
Evaporation	m/year	0.8	0.7-0.9 in Temperature Climate [74]; 1.1 [18]
Microalgae production	kg/Nm^3-biogas	0.36	0.37 [18]

[§] Assuming an average salinity of 20 [125] and using the USGS Water tables [131]

Based on the loss models adopted in the present study, the overall methane loss was assessed as 2% including for both biogas generation and biogas upgrading sections (Table 7-11). Each cycle required the addition of 2.1% of the water flowing through the system due to the losses from evaporation, biomass harvesting, drying and wastewater treatment and recycling. The net inorganic carbon loss per cycle was obtained as 7.5%, close to the value observed by Toro-Huertas et al. (2019) [132]. As such 5.4% and 5.6% of fresh sodium carbonate and sodium bicarbonate were required

to be added in each cycle to ensure continuous operation of the proposed polygeneration plant. These proximities of the results for the base case scenario (BASE-EC) with data and prediction models published in the literature were considered sufficient to validate the process model. Following model validation, the overall mass balance of each scenario was assessed, the results are shown in Figure 7-10.

Table 7-11 Validation of methane, carbon and water losses for the proposed polygeneration system

Description	Unit	This Study	Literature
Overall methane loss	%	2	Liebetrau et al. (2017) [62]
Carbonate Recirculation	%	5.4	
Bicarbonate Recirculation	%	5.6	
Inorganic carbonate Recirculation	%	5.5	10%-15% [9]
Overall Carbon Loss	%	7.5	5% for alkaline algal medium with pH > 9.3 [132]
Water Recirculation	%	2.1	

7.3.2 Energy balance and GHG emissions

7.3.2.1 Energy Balance

Under the proposed configuration, the energy generated as biomethane (4.8 kWh/Nm^3-biogas) was lower than the direct energy consumed (4.9 kWh/Nm^3-biogas while using the OPPBR and 6.1 kWh/Nm^3-biogas using the FPPBR, final energy basis (Figure 7-11a)). Although the OPPBR consumed low electricity, over half of the total energy consumed were for the electricity required to heat the greenhouse, which housed the microalgae cultivation and harvesting units (Figure 7-11b). When the microalgae were cultivated using FPPBRs, the electricity consumed in the PBRs increased significantly (Figure 7-11a & b). Nonetheless, when the embodied energies of all the products were included, the energy produced (c. 6.2 kWh/Nm^3-biogas) was higher than the direct energy consumed under all scenarios.

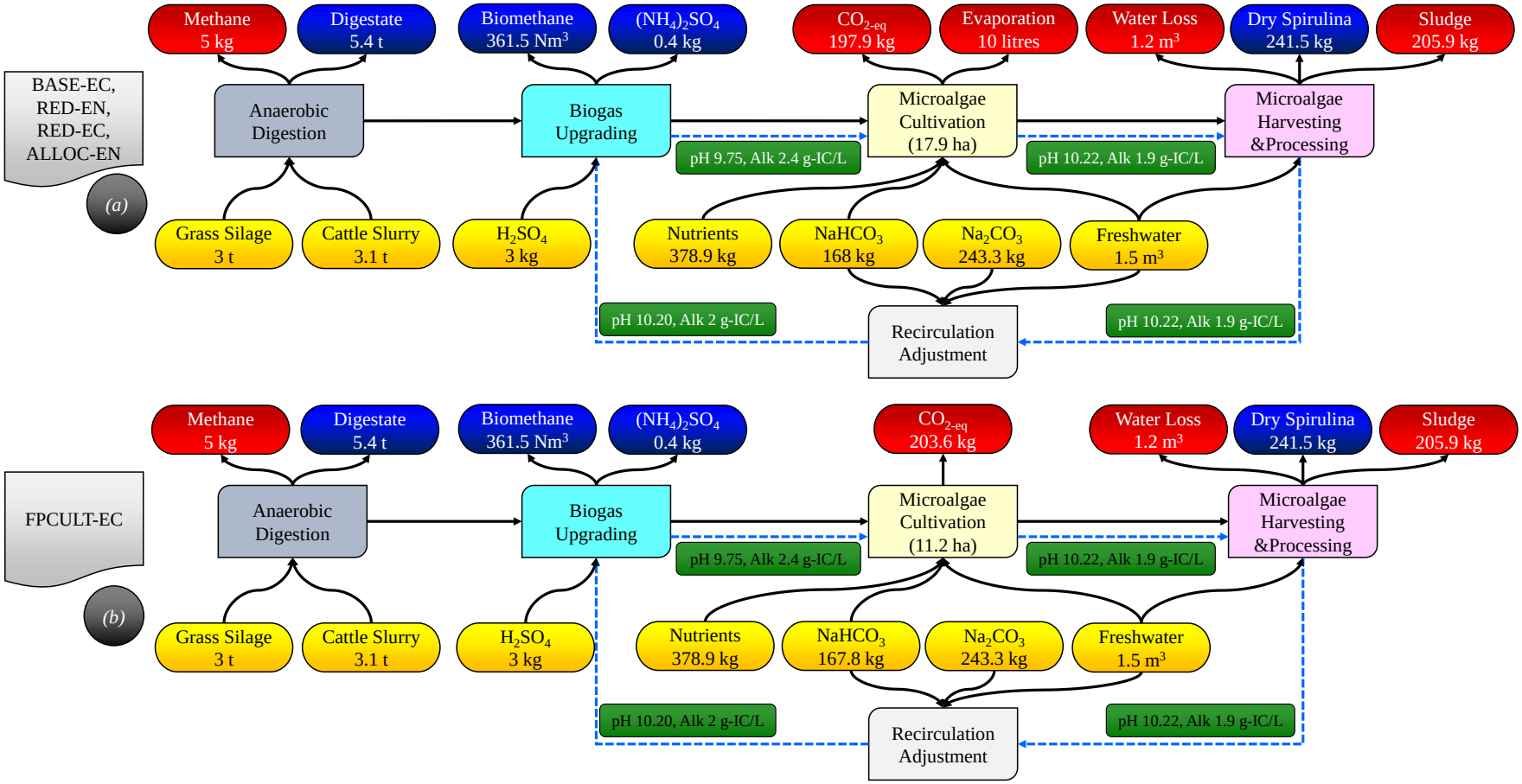


Figure 7-10 Hourly mass balance of the proposed polygeneration plant producing biomethane, Spirulina powder and digestate for (a) scenarios BASE-EC, RED-EN, RED-EC and ALLOC-EN, (b) scenario FPCULT-EC

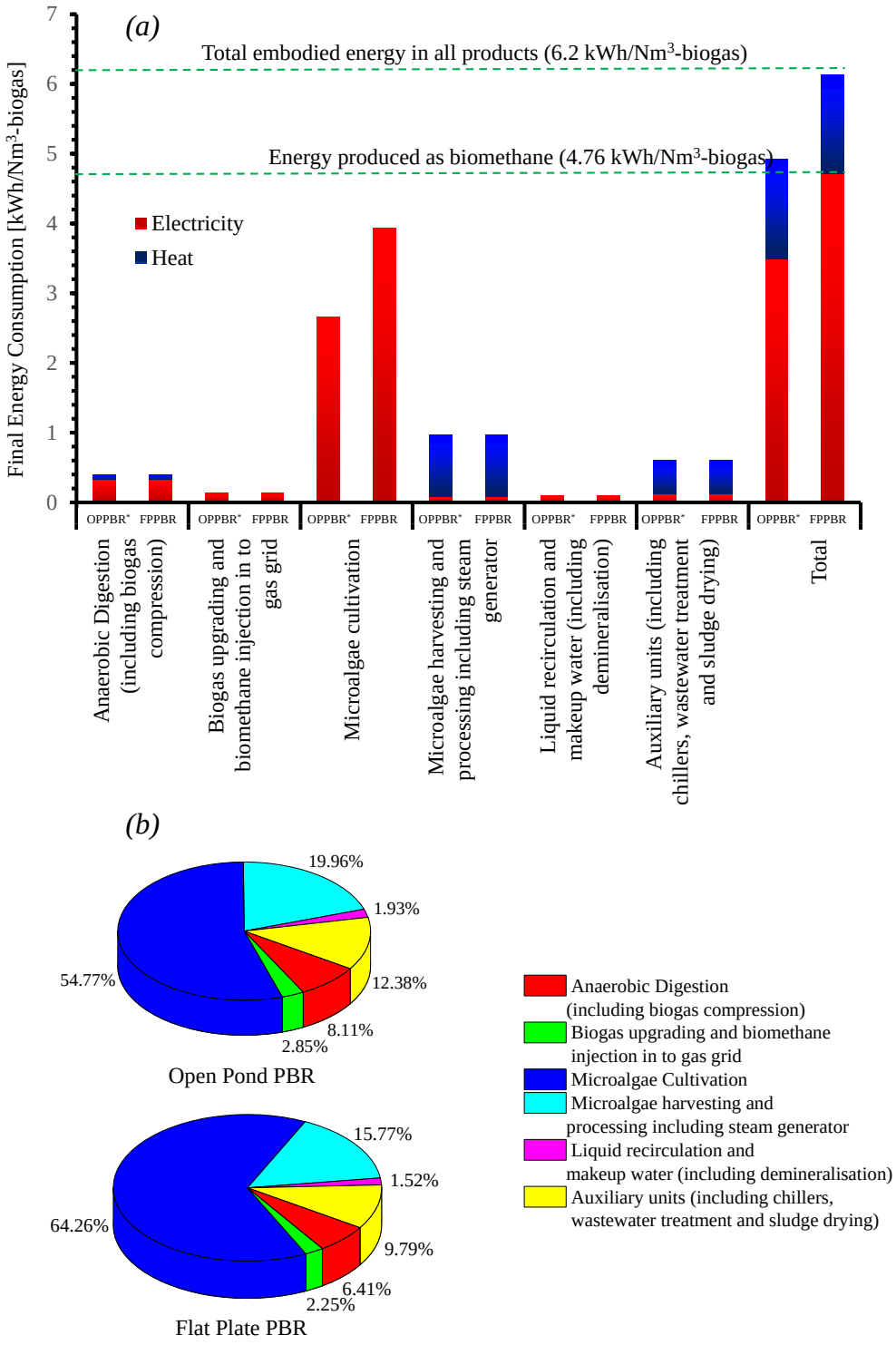


Figure 7-11 Energy balance of the proposed polygeneration plant producing biomethane, Spirulina powder and digestate for each scenario where (a) represents the overall direct energy consumption of the plant (final energy basis), (b) represents the contribution of the different plant components towards the overall energy consumption of the plant when either an open pond or a flat plate photobioreactor (PBR) is used.

7.3.2.2 Process greenhouse gas emissions

Figure 7-12a shows the net GHG emissions from the proposed polygeneration plant under each scenario assessed. For the scenarios using OPPBR (BASE-EC, RED-

EN, RED-EC and ALLOC-EN), the highest fraction of GHG emissions (24.4%, Figure 7-12b) resulted from grid electricity use (carbon intensity 255 $gCO_{2\text{-}eq}/kWh_e$ [114]) for heating the greenhouse. A higher energy requirement of operating the FPPBR increased the emissions from the cultivation of microalgae under the FPCULT-EC scenario (c. 39% including greenhouse heating, Figure 7-12b). Irrespective of the type of cultivation system, however, the chemicals required for microalgae cultivation accounted for over 20% of the total emissions, with the Zarrouk's media accounting for over 50% of those emissions. Such high emissions from chemicals in *Spirulina* cultivation have been previously reported in the literature [92,112].

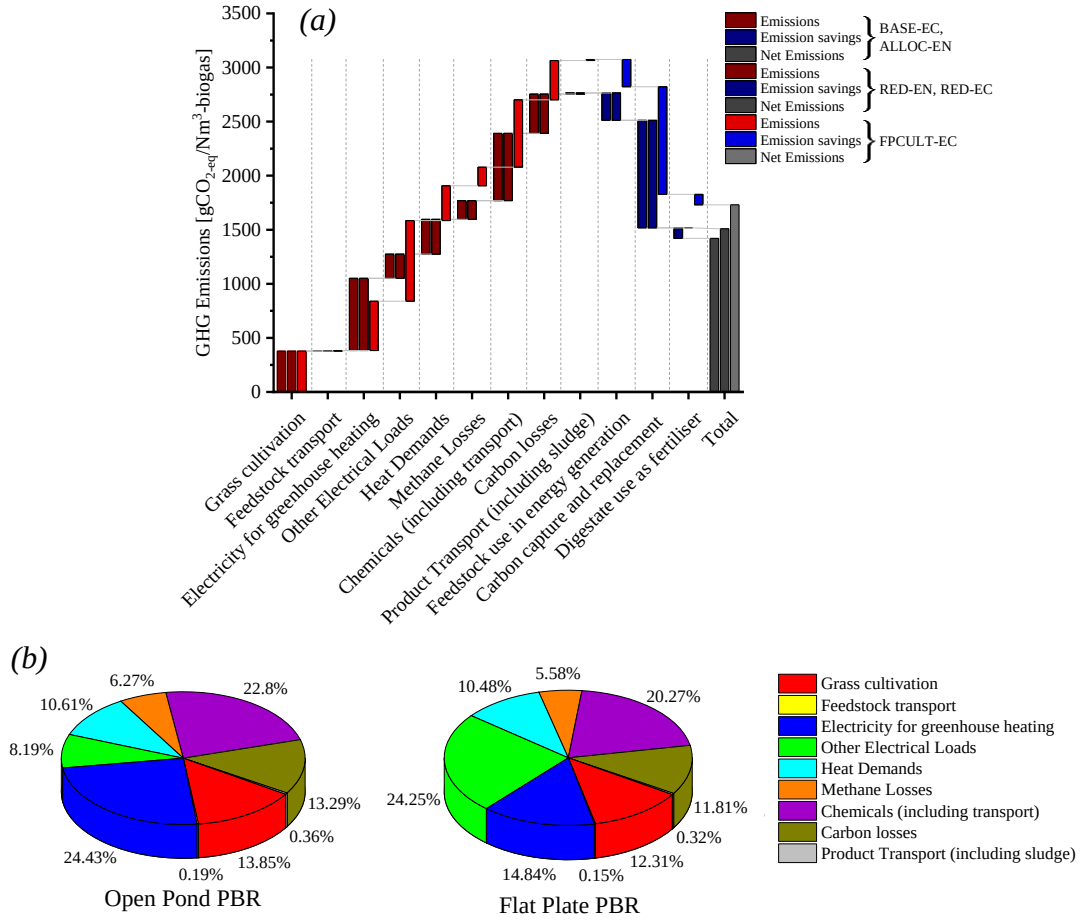


Figure 7-12 (a) GHG emissions and emission savings per Nm^3 biogas produced from the proposed polygeneration process under each scenario assessed; (b) the contribution to emissions when either an open pond or a flat plate photobioreactor (PBR) is used.

.

Box 7.1: Estimation of emissions from carbon loss for the base case scenario (BASE-EC)

197.9 kg/hr of CO_2 was stripped from the open pond PBR. Biogas generated from AD was 670.8 Nm^3/hr. Accordingly,

➔ Equivalent emissions from CO_2 stripping = $\frac{197.9}{670.8} \cong 0.295$ $kgCO_{2\text{-}eq}/Nm^3$-biogas

Based on the simulations, 81.8 kg/hr of Na_2CO_3 and 32.1 kg/hr of $NaHCO_3$ was lost with the effluent during harvesting of microalgae. Considering the GHG burdens of Na_2CO_3 and $NaHCO_3$ as 300 $kgCO_{2\text{-}eq}$/tonne [116] and 660 $kgCO_{2\text{-}eq}$/tonne [89,116] respectively, the effective emissions from the lost inorganic carbon sources can be estimated as:

➔ Equivalent emissions from lost Na_2CO_3 = $\frac{81.8\times300}{670.8} \cong 36.6$ $gCO_{2\text{-}eq}/Nm^3$-biogas

➔ Equivalent emissions from lost $NaHCO_3$ = $\frac{32.1\times660}{670.8} \cong 31.6$ $gCO_{2\text{-}eq}/Nm^3$-biogas

Thus, the equivalent emissions from the carbon loss from the system can be evaluated as:

➔ Equivalent emissions from C loss = 295 + 36.6 +31.6

= 363.2 $gCO_{2\text{-}eq}/Nm^3$-biogas

The emissions from carbon loss, evaluated as shown in *Box 7.1* were also significant, accounting for over 10% of the total process emissions. Considerable GHGs would also be emitted during grass silage production (cultivation and field N_2O), amounting to net GHG emissions of 378.4 $gCO_{2\text{-}eq}/Nm^3$-biogas. Of the emissions mitigated during the process, the highest saving of 995.3 $gCO_{2\text{-}eq}/Nm^3$-biogas was obtained from the replacement of conventionally sourced $NaHCO_3$ with the $NaHCO_3$ directly produced during photosynthetic biogas upgrading (e_{ccr}). The example calculation for the base case scenario is shown in *Box 7.2*. As can be seen from Figure 7-11c, soil carbon sequestration also added considerable carbon credits to the proposed polygeneration system. Considering the benefits of emission savings from the digestate, the overall GHG emissions from the proposed system under the

BASE-EC scenario amounted to 1,420.6 $gCO_{2\text{-}eq}/Nm^3$-biogas (Figure 7-11c). However, under the purview of RED-II (scenarios RED-EN and RED-EC), when the digestate was excluded as a product, the overall emissions increased by around 7% to 1,508.1 $gCO_{2\text{-}eq}/Nm^3$-biogas. Due to the increased energy demand of cultivating microalgae in an FPPBR, the net emissions from the FPCULT-EN scenario of 1,730.3 $gCO_{2\text{-}eq}/Nm^3$-biogas was substantially larger than the emissions generated while using an OPPBR.

Box 7.2: Estimation of carbon capture and replacement (e_{ccr})

The emissions from each tonne of $NaHCO_3$ accounts for 660 $kgCO_{2eq}$, primarily of fossil origin [89,116]. Therefore, $NaHCO_3$ produced during biogas upgrading would save an equivalent emission of 660 $kgCO_{2eq}$/tonne of $NaHCO_3$ replaced.

$$CO_2 + Na_2CO_3 + H_2O = 2NaHCO_3 \quad (7.1)$$

$$2NaHCO_3 \xrightarrow{\text{Light}} \text{Algae} + Na_2CO_3 + H_2O \quad (7.2)$$

Using mass balance, 529.9 kg/hr (12.04 kmol/hr) of CO_2 was found to be generated within biogas. For the base case scenario, considering a 100% CO_2 removal efficiency and using equation (7.1)

➔ Net $NaHCO_3$ generated: 12.04 ×2 = 24.08 kmol/hr, or, 2,023.25 kg/hr.

Following equation (7.2), half of the $NaHCO_3$ must be converted back to carbonate, while the other half is available to the microalgae for uptake of inorganic carbon. Therefore,

➔ Net effective bicarbonate added to system = 2,023.25 /2 = 1,011.6 kg/hr.

Thus, effective CO_2 savings from carbon capture and replacement (e_{ccr}) can be evaluated as:

➔ $e_{ccr} = \frac{1011.6 \times 660}{1000}$ =667.7 $kgCO_{2\text{-}eq}$/hr or, $\frac{667.7}{670.8} \cong 995.3$ $gCO_{2\text{-}eq}/Nm^3$-biogas

7.3.3 Process performance

Multi-criteria performance assessments of the proposed polygeneration process were performed using thermodynamic, economic and environmental metrics.

The highest S-EROI (thermodynamic metric) was 0.97 for the BASE-EC and ALLOC-EN scenarios (Figure 7-13a). This energy deficit of the proposed process can be explained by the high electricity consumption, primarily for greenhouse heating. The high electricity consumption also contributed the most to the process energetic uncertainties (Figure 7-13b). However, it also needs to be understood that energy generation is not the only intended outcome of the process and that the majority of the energy is expended to produce food as *Spirulina* powder. Indeed, when compared with the current EROI of beef production (chemical energy basis), which usually varies from as low as 0.016 in the USA [133] to around 0.36 in New Zealand [134], the S-EROI value of 0.97 seems to be extremely promising. Thus, a traditional interpretation of S-EROI with a primary interest in the energy return on energy invested of the fuel generated (biomethane) would not suit well the proposed process. In that case, a comparison of the specific energy demands of the individual co-products (detailed further in Section 7.3.4) with market-available alternatives would provide a further evaluation of the thermodynamic performance of the proposed process. Nonetheless, lowering the energy consumption by improving the energy efficiency of components such as using a heat pump with a higher coefficient of performance or COP (4 and above with ground and water-source heat pumps [56]) could increase the S-EROI above 1. All other scenarios resulted in lower S-EROI (Figure 7-13a).

According to CUF (economic metric) shown in Figure 7-13c, for all scenarios, the cumulative values of the products were almost twice the cumulative value of the input utilities and materials (Table 7-2). CUF was most sensitive to the *Spirulina* selling prices followed by the costs of the microalgae nutrient medium and electricity (Figure 7-13d).

As observed from Figure 7-13e, a similar GHG reduction (c. 4 fold or a CEF c. 0.23-0.26), when compared to individual systems (see Methods Section 7.2.4) was obtained for all scenarios. Of the different variables, the CEF had the highest sensitivity to the reference emissions of standalone *Spirulina* production systems

(Figure 7-13f). The grid electricity emission factor also had a high influence on CEF (Figure 7-13f); the use of green electricity (carbon intensity 0 $gCO_{2\text{-}eq}/KWh_e$) would reduce CEF to below 0.1.

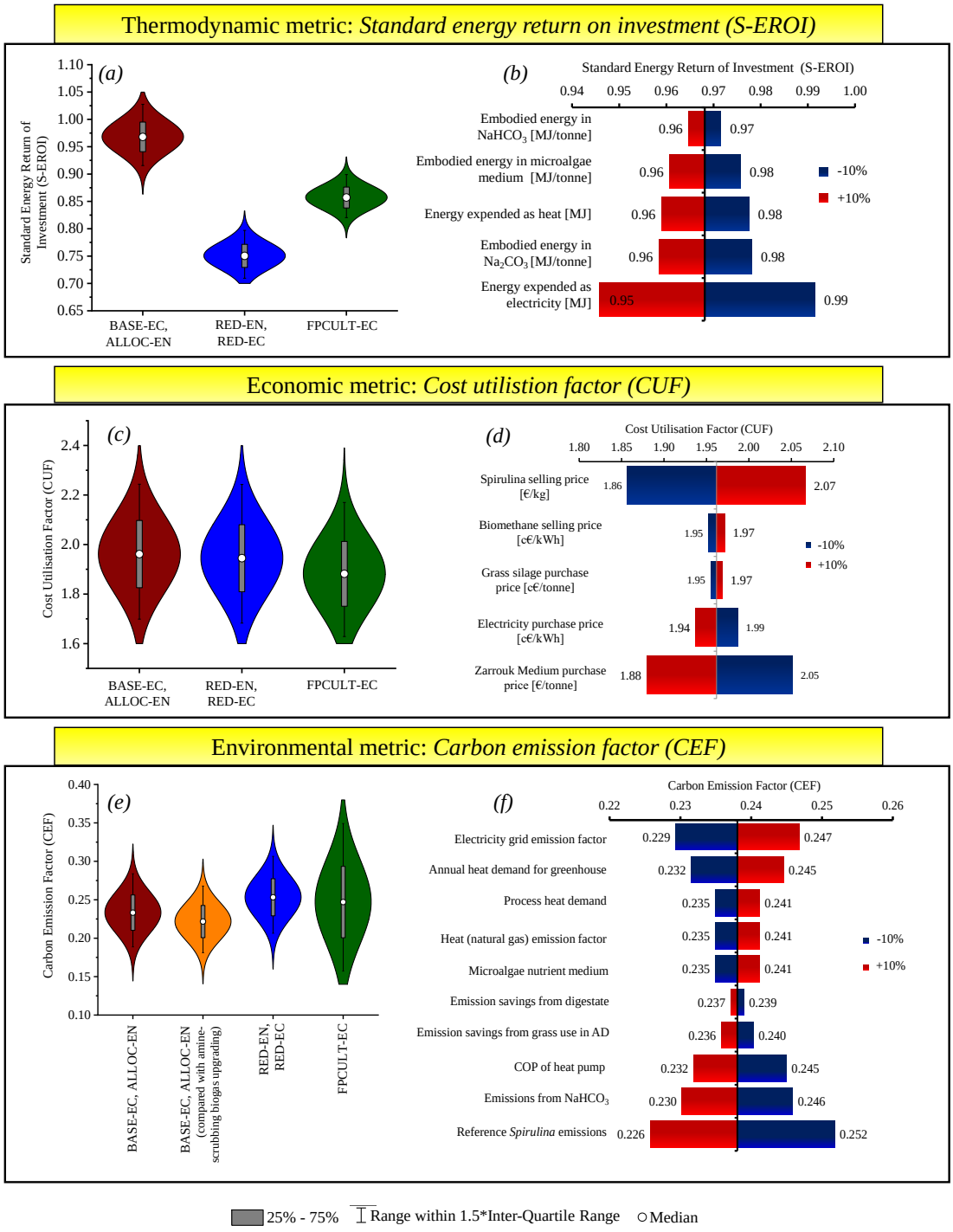


Figure 7-13 Results and sensitivities of (a & b) standard energy return on investment (S-EROI); (c & d) cost utilization factor (CUF); (e & f) carbon emission factor (CEF) of the proposed polygeneration process. The "curve" lines in figures (a), (c) and (e) signify the uncertainty distribution of S-EROI, CUF and CEF respectively. For details of the uncertainty assessment, refer to section 7.2.9.

7.3.4 Product performance

7.3.4.1 Allocation of resources and emissions for each scenario

Based on the mass and energy balances obtained from the simulation studies along with the selling price of the co-products, the allocations to the products for each scenario are compiled in Table 7-12. As a fuel, the energy content in biomethane is the highest among the co-products. Therefore, upon the use of energetic allocation, the majority of the energy consumption or the environmental impacts would be allocated to biomethane irrespective of the consideration of digestate as a co-product. However, when based on the economic criteria, the high-value *Spirulina* powder would attract the maximum allocation due to its high share of revenue among the co-products (over 90%).

Table 7-12 Summary of allocation of resources and emissions to the co-products under each scenario.

Co-Product	**Scenarios***				
	BASE-EC	**RED-EN**	**RED-EC**	**ALLOC-EN**	**FPCULT-EC**
Biomethane	8.40%	73.68%	8.88%	54.48%	8.81%
Spirulina powder	90.79%	26.32%	91.12%	19.47%	90.38%
Digestate	0.78%	-	-	26.06%	0.81%

* EC indicates economic allocation and EN indicates energetic allocation.

7.3.4.2 Biomethane

The highest specific energy consumption of 6.7 kWh/Nm^3-biomethane or c. 76% of the energy in biomethane (*Box S7.2*) was obtained in the RED-EN scenario. Inclusion of the digestate lowered the specific energy consumption to c. 5 kWh/Nm^3-biomethane (scenario ALLOC-EN). In contrast, using economic allocation (scenarios BASE-EC, RED-EC and FPCULT-EC), specific energy consumption in biomethane generation was less than 0.9 kWh/Nm^3-biogas (less than 10.2% of the energy in biomethane). Although this value is higher than the energy required to produce biomethane via water scrubbing (0.3 kWh/Nm^3-biomethane [91]), it is significantly lower than the energy required when biogas is upgraded using amine scrubbing (2.5 kWh/Nm^3- biomethane [30], Figure 7-14b).

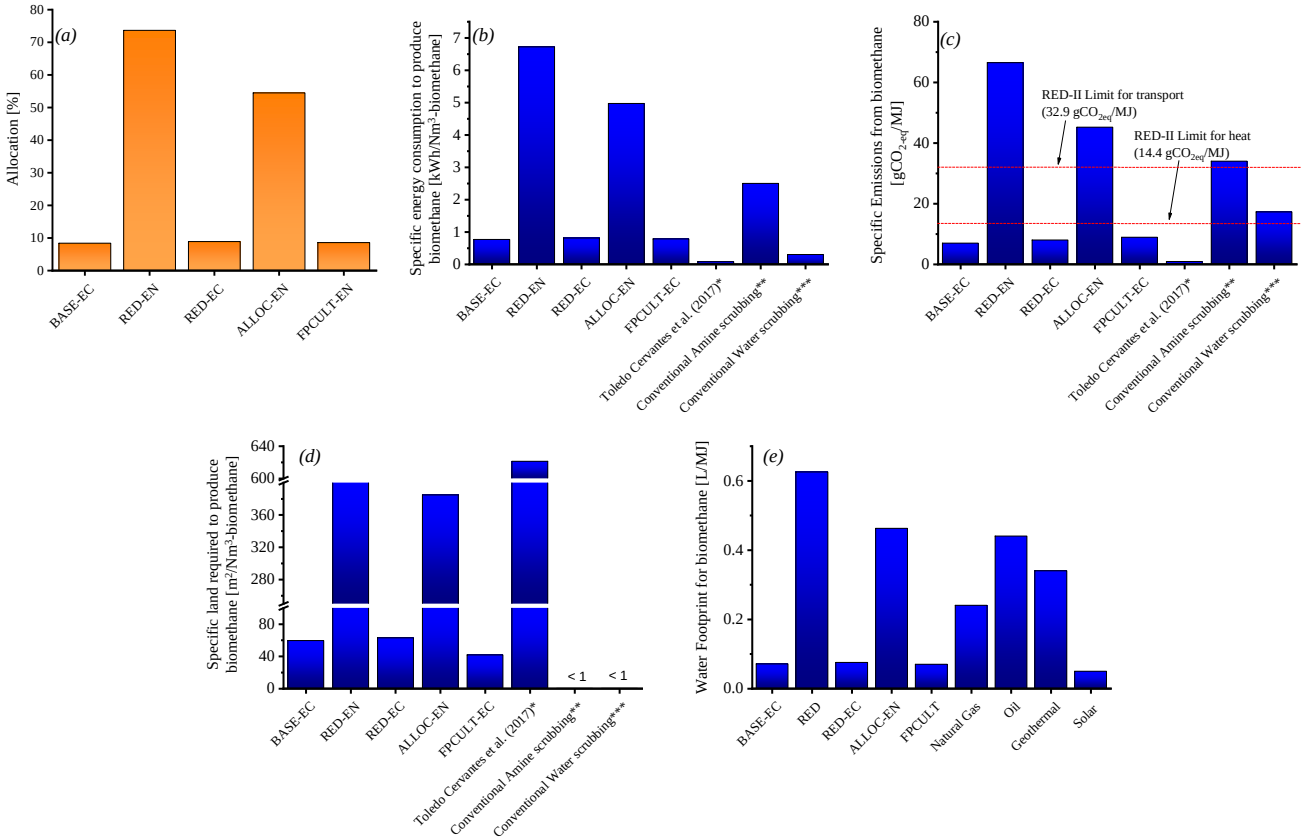


Figure 7-14 (a) Allocation and performance of biomethane based on (b) Specific energy consumed [kWh/Nm^3-biomethane]; (c) Specific GHG emissions [gCO$_{2\text{-}eq}$/MJ]; (d) Specific land footprint [m^2/Nm^3-biomethane]; and (e) Specific water footprint [L/MJ]. The values of specific water footprint for the production of conventional and renewable energies shown in (e) were compiled from Mekonnen et al. (2015) [135].

* *Values for photosynthetic biogas upgrading without biogas generation [18]*

** *Values from Vo et al. (2018a) [30] and Vo et al. (2018b) [49];*

*** *Referenced from Rotunno et al. (2017) [136]*

As under the RED-II guidelines (RED-EN scenario), the majority of the emissions occurring during microalgae cultivation, harvesting and processing were allocated to biomethane using energy allocation (Figure 7-14a), the GHG emissions from the corresponding biomethane remained above 60 $gCO_{2\text{-}eq}$/MJ (Figure 7-14c). However, economic allocation resulted in biomethane emissions to be less than 10 $gCO_{2\text{-}eq}$/MJ, lower than that from commercial upgrading processes (Figure 7-14c). The lowest specific land footprint of 41.6 m^2/Nm^3hr^{-1}-biomethane resulted in the FPCULT-EC scenario (Figure 7-14d). However, this was still substantially higher than the land footprint of biomethane from conventional technologies (< 1 m^2/Nm^3hr^{-1} biomethane). Biomethane water footprint levels using the economic allocation was 0.07 L/MJ, similar to those of other renewable energy systems such as solar (0.05 MJ/L [128]) (Figure 7-14e). Energy allocation, however, increased the biomethane water footprint above its non-renewable substitute, natural gas (0.24 L/MJ [135]).

7.3.4.3 *Spirulina* powder

Due to its high economic value, over 90% of the resources and emissions were allocated to *Spirulina* powder when using economic allocation (Figure 7-15a). Therefore for the BASE-EC and RED-EC scenarios, 1.9 kWh/100-grams protein (gp) was expended (final energy basis), similar to the energy consumption to produce chicken protein (1.85 kWh, Figure 7-15b). The specific energy to produce *Spirulina* powder using FPPBRs was 2.6 kWh/100-gp (FPCULT-EC scenario).

The GHG emissions from *Spirulina* protein using economic allocation (0.6-0.8 $kgCO_{2\text{-}eq}$/100-gp) were higher than the emissions from plant-based proteins (0.44 $kgCO_{2\text{-}eq}$/100-gp from pulses and lentils, Figure 7-15c). On the contrary, *Spirulina* powder demonstrated a low GHG impact under all the scenarios on a comprehensive nutrition basis (less than 0.07 $kgCO_{2\text{-}eq}$/100 $NDS_{NRF9.3}$). A high $NDS_{NRF9.3}$ score of 191.8 per 100 kCal of *Spirulina* (Section 7.2.7) could be used to explain the results. As a comparison beef and fish would emit 11.3 $kgCO_{2\text{-}eq}$/100 $NDS_{NRF9.3}$ and 0.77 $kgCO_{2\text{-}eq}$/100 $NDS_{NRF9.3}$ respectively (Table S7-2).

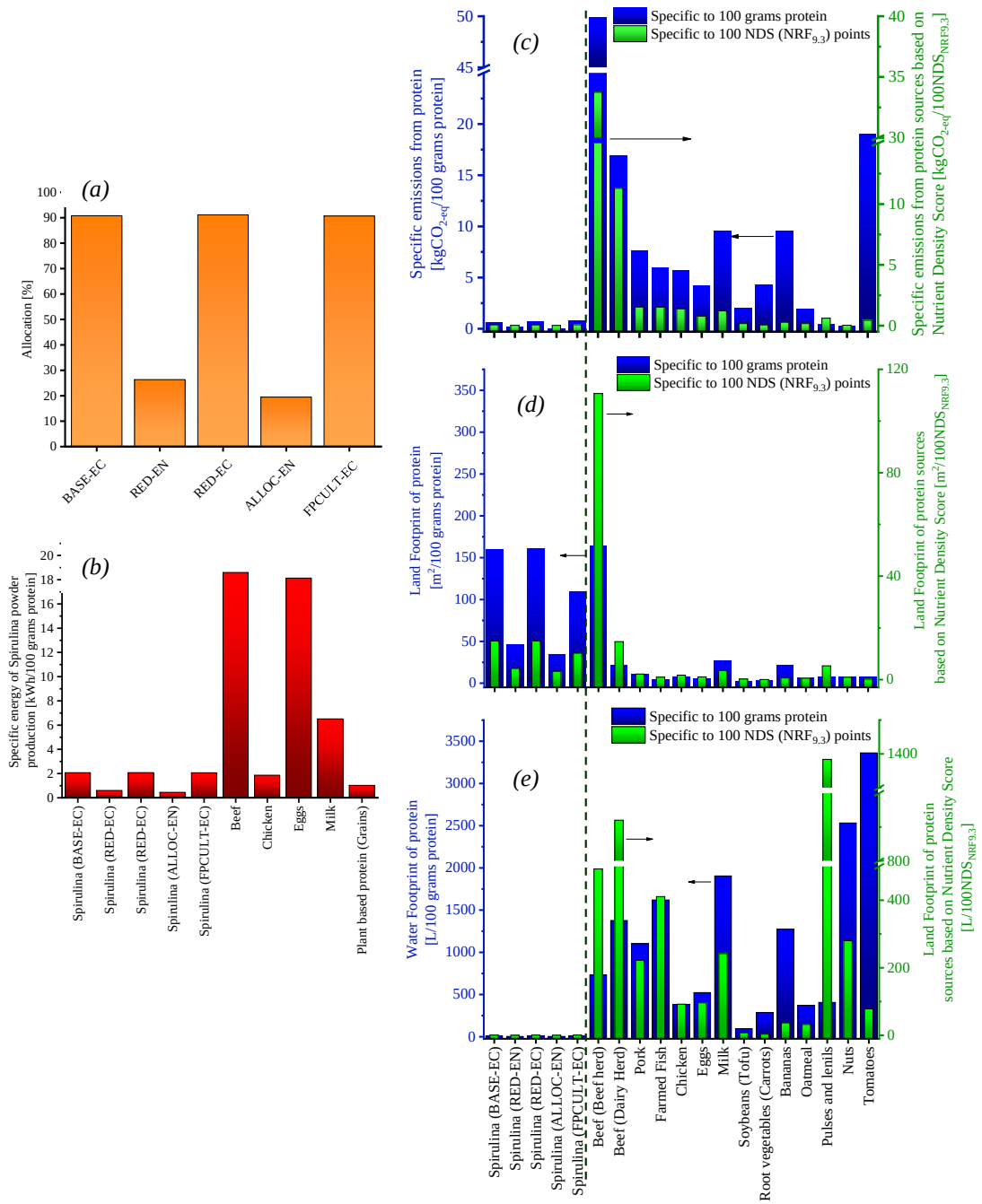


Figure 7-15 (a) Allocation and performance of dietary protein (Spirulina powder) based on (b) Specific energy consumed [kWh/100 grams protein]; (c) Specific GHG emissions [$kgCO_{2\text{-}eq}$/100 grams protein and $kgCO_{2\text{-}eq}$/100 $NDS_{NRF9.3}$ score]; (d) Specific land footprint [m^2/100 grams protein and m^2/100 $NDS_{NRF9.3}$ score]; and (e) Specific water footprint [L/100 grams protein and L/100 $NDS_{NRF9.3}$ score]. The specific energy consumption of protein from conventional sources has been compiled from Pimentel et al. (2003) [137]. The $NDS_{NRF9.3}$ values, together with the GHG Emissions, land and water footprints of the conventional protein sources are compiled in Table S7-2.

When considering only the protein content, the specific land footprint of *Spirulina* powder remained high irrespective of the type of allocation and PBR used. The least land requirement was obtained using energy allocation (34 m^2/100-gp, ALLOC-EN scenario). This was only exceeded by the land required by beef protein

(Figure 7-15d). However, when compared as a complete food, the specific land footprint of *Spirulina* using economic allocation (<15 m^2/100 $NDS_{NRF9.3}$) became comparable to chicken (15.9 m^2/100 $NDS_{NRF9.3}$) and pork (14.5 m^2/100 $NDS_{NRF9.3}$). *Spirulina* protein had a lower specific water footprint than most plant or meat-based protein sources for all types of allocation and photobioreactor used and the nutrient profile considered (Figure 7-15e).

7.3.4.4 Biofertiliser or digestate (Equivalent Nitrogen)

As per RED-II guidelines, no allocation was made towards the digestate for the RED-EN and RED-EC scenarios. The specific energy to produce a kilogram of equivalent nitrogen as fertiliser was the highest for the ALLOC-EN scenario (41 kWh/kgN, Figure 7-16b). This corresponded to the highest emissions as well (11.9 $kgCO_{2\text{-}eq}$/kgN, Figure 7-16a) amongst all scenarios. In contrast, an economic allocation made the production of biofertiliser beneficial with much lower specific energy consumption (1.2 kWh/kgN) and GHG emissions (0.4 $kgCO_{2\text{-}eq}$/kgN). Although the impact under the FPCULT-EC scenario would be higher (0.5 $kgCO_{2\text{-}eq}$/kgN), it would remain lower than all of the other conventional nitrogenous fertilisers (1.5-3 $kgCO_{2\text{-}eq}$/kgN [93]). Both the lowest land and water footprints of c. 68 m^2/kgN and 3.6 L/kgN respectively were achieved under the FPCULT-EC scenario (Figure 7-16b).

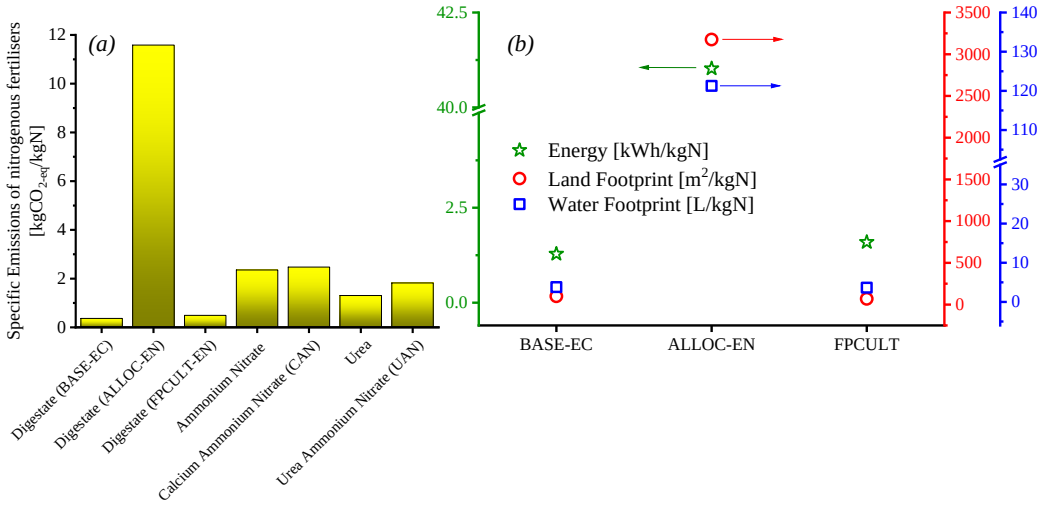


Figure 7-16 Performance of biofertiliser or digestate production (equivalent N) based on (a) Specific GHG emissions; (b) Specific energy consumption, land and water footprints. The GHG emissions in the production of conventional fertilisers have been compiled from Hoxha and Christensen (2018) for the EU average scenario [93]

7.3.4.5 Sensitivity and uncertainty of specific emissions of each co-product

Sensitivity assessments performed using the BASE-EC scenario showed that the specific emissions of biomethane and digestate varied considerably with their respective selling prices and the selling price of *Spirulina (*Figure 7-17a & e respectively). The electricity emissions factor, the performance of the heat pump and the heat required in the greenhouse also affected the specific emissions of each co-product.

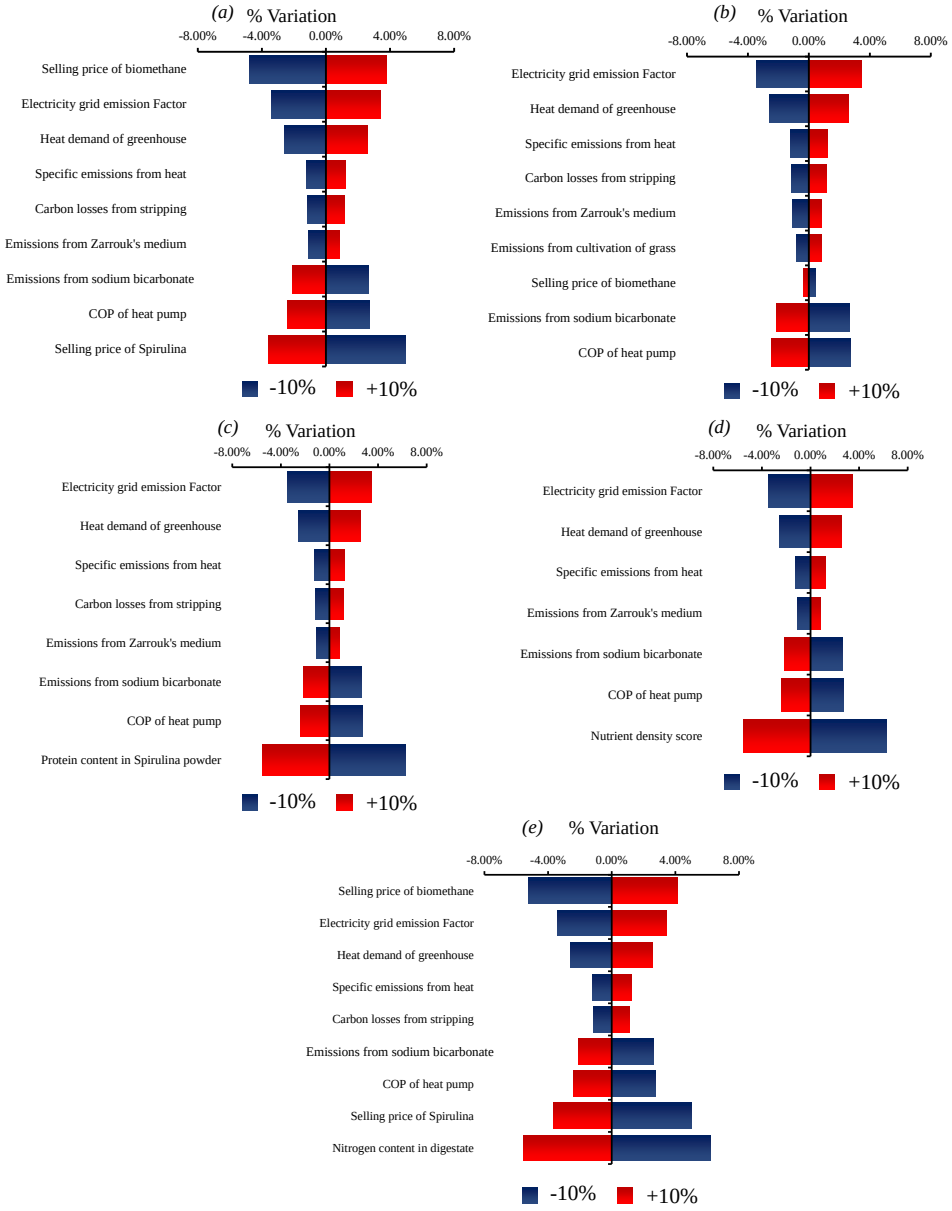


Figure 7-17 Sensitivity Analysis of process variables and product selling prices on the specific GHG emissions of (a) Biomethane, (b) Spirulina powder, (c) Spirulina powder as a protein supplement, (d) Spirulina powder as a complete food using the $NRF_{9.3}$ nutrient profile and (e) digestate (equivalent N) as a substitute of inorganic nitrogenous fertilisers.

The nitrogen and the protein content of the digestate and the *Spirulina* powder showed considerable influence in their respective specific emissions (Figure 7-17e & c respectively). The emissions from sodium bicarbonate caused the specific emissions of each co-product to also vary considerably. Accordingly, for the BASE-EC scenario, the most probable specific emissions of biomethane and digestate would be of the order of 7.5 $gCO_{2\text{-eq}}$/MJ and 0.4 $kgCO_{2\text{-eq}}$/kgN respectively (Figure 7-18). The emissions from *Spirulina* would be 4 $kgCO_{2\text{-eq}}$/kg-*Spirulina*, lower than most literature values [92,102] resulting in 0.7 $kgCO_{2\text{-eq}}$/100-gp and 0.06 $kgCO_{2\text{-eq}}$/100 $NDS_{NRF9.3}$.

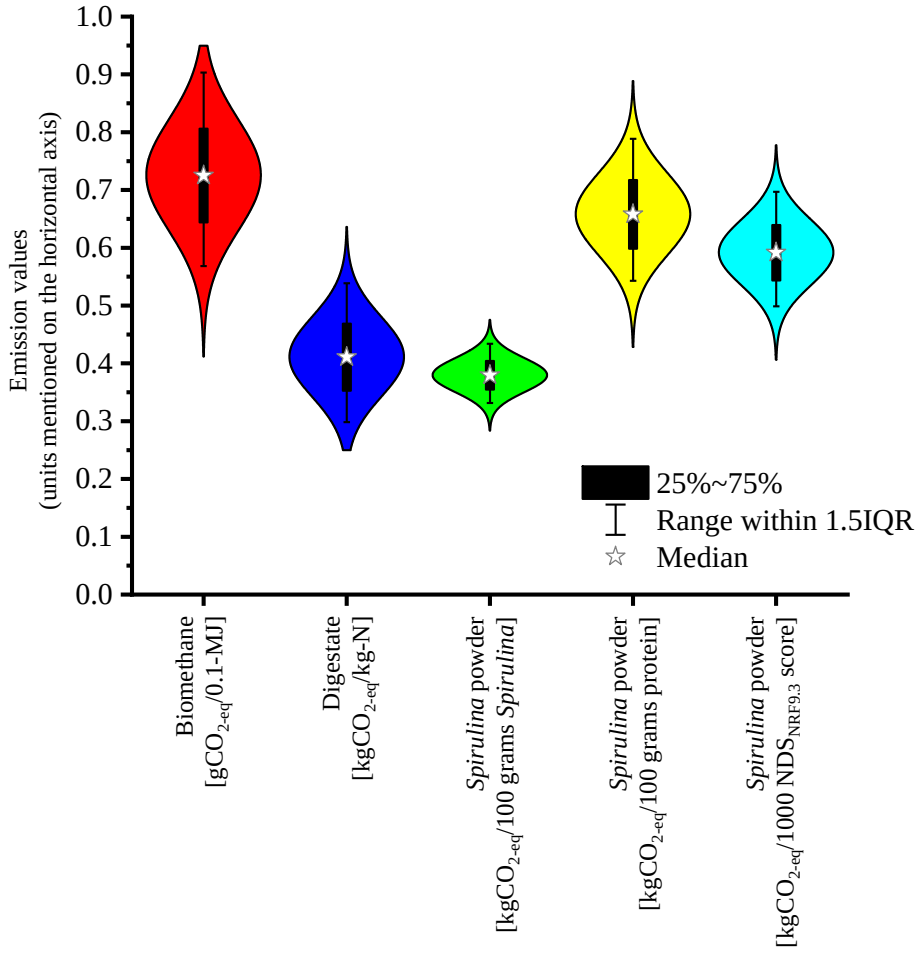


Figure 7-18 Results of the Monte Carlo uncertainty assessment on the specific GHG emissions of each co-product from the proposed integrated polygeneration process. IQR signifies the interquartile range.

7.3.5 Sensitivity analysis of process parameters of photosynthetic biogas upgrading

The impact of the variations of the makeup water pH and alkalinity, the L/G ratio and the microalgae productivity have been studied. While all the other process input parameters were varied within a range of +/- 10% of their base values, the pH was only varied between +/- 3% from the limitation of the producing grid quality biomethane. All the variations in the process and product performances have been normalised with respect to the values obtained in the BASE-EC scenario.

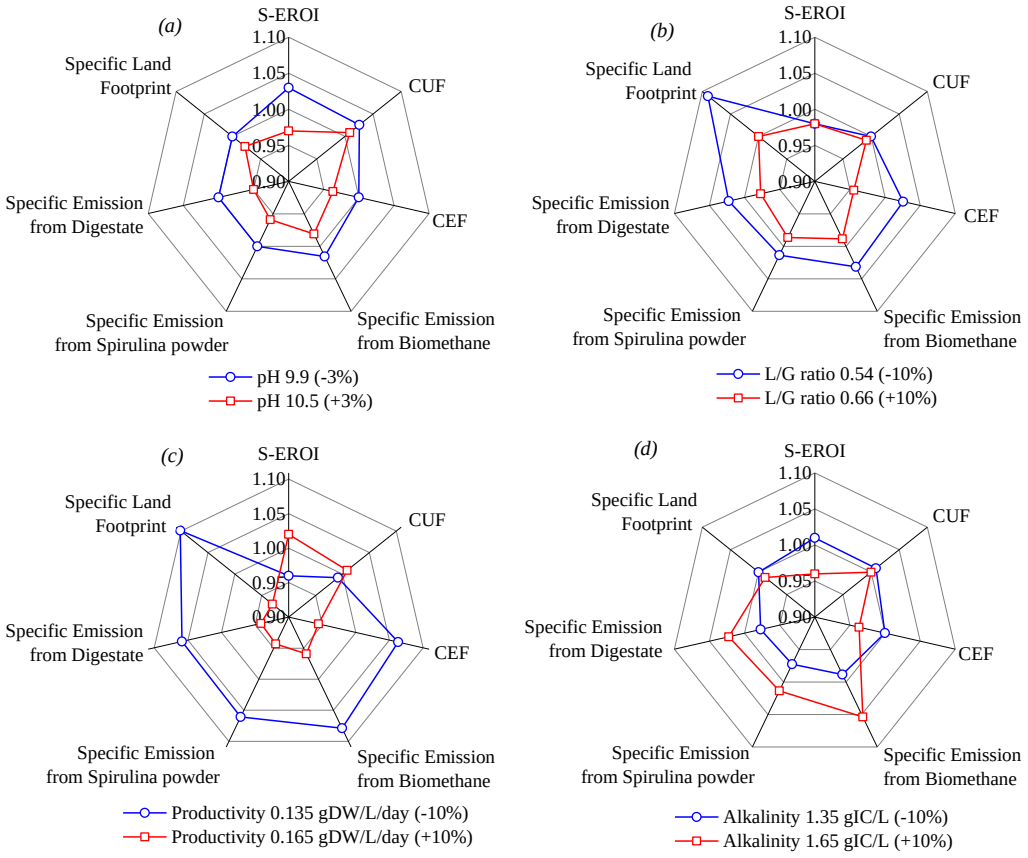


Figure 7-19 Sensitivity of the process and product performance from the variations of (a) makeup water pH; (b) L/G ratio; (c) microalgae productivity; and (d) makeup water alkalinity.

As the pH increased, the S-EROI decreased, as did the CEF and the specific emissions of each co-product (Figure 7-19a). A lower L/G ratio resulted in a much larger areal footprint of the plant and increased the CEF of the process and the specific emissions of all the co-products (Figure 7-19b). A 10% decrease in productivity led to a 7% increase in the specific GHG emissions of the co-products and vice versa (Figure 7-19c). The land footprint increased substantially and the CUF decreased, making the

system economically unviable. Lowering the alkalinity decreased the specific emissions of the co-products while increasing the S-EROI. However, CUF was not affected (Figure 7-19d). Therefore, lower pH and alkalinity, along with higher L/G ratio and algal productivity were desirable (as long as grid quality biomethane of CO_2 < 2.5% and O_2 < 1% is ensured).

7.4 Legislative challenges and implications of economic allocation

Under the RED-II guidelines (scenario RED-EN), biomethane from the proposed polygeneration process (specific emission above 36.2 $gCO_{2\text{-}eq}$/MJ, Figure 7-20a) would fail to meet the EU sustainability criteria for biofuels. The lack of circularity by not considering digestate as a valuable product and mandating the use of energy allocation, limit the applicability of RED-II, especially for polygeneration systems with non-energy co-products (such as *Spirulina* powder) [22]. Including digestate as a valuable product, and using economic allocation can better represent the actual benefits of the proposed polygeneration plant (BASE-EC scenario).

Fluctuations in pricing and incentives, however, pose challenges for economic allocation. For example, for the BASE-EC scenario, biomethane priced at 7 c€/kWh, would qualify as a heat and transport fuel in most European countries (<25 $gCO_{2\text{-}eq}$/MJ, Figure 7-20b). Contrarily, if priced at 15 c€/kWh (similar to diesel with taxes), depending on the climatic conditions and electricity grid emission factors, biomethane might fail to qualify as a sustainable biofuel (for example in Poland and Estonia, Figure 7-20c). In other words, a higher selling price of biomethane (Figure 7-21) would demand a proportionally higher price of *Spirulina* to ensure the minimisation of emission allocations to biomethane. Indeed, as the energy required to heat the greenhouse or the emission factor from grid electricity increases, the difference in revenue between *Spirulina* powder and biomethane must increase as well to allow biomethane to be produced sustainably and conform to the sustainability criteria of RED-II (Figure 7-21a and b). The higher sustainability criteria associated with transport fuel allows a carbon footprint of 32.9 $gCO_{2\text{-}eq}$/MJ (as opposed to 14.4 $gCO_{2\text{-}eq}$/MJ for heat) and as such the allocation of emissions towards biomethane can be higher. Accordingly, when biomethane would be used for transport (Figure 7-21b),

Spirulina could be sold at a lower rate irrespective of the grid emission factor. However, when intended for use in heat, the majority of the emissions must be allocated to *Spirulina*, which would increase under both an increasing heat requirement in the greenhouse and grid emission factor (Figure 7-21a).

Irrespective of biomethane usage, the pricing of the co-products must ensure the economic viability of the system. In this regard, a study of the plot in Figure 7-21c revealed that to maintain a CUF greater than 1, *Spirulina* must be sold at above 4 €/kg irrespective of the heat demand of the greenhouse and the price of biomethane. Comparing with Figure 7-21a and b, this result implies that for most price variations, an economic allocation would favour the use of biomethane in transport. However, to use biomethane in the heating sector (<14.4 $gCO_{2\text{-}eq}$/MJ) either greening of the electricity grid is necessary (Figure 7-20c) or a higher selling price of *Spirulina* powder would be required to lower the emissions burden on biomethane.

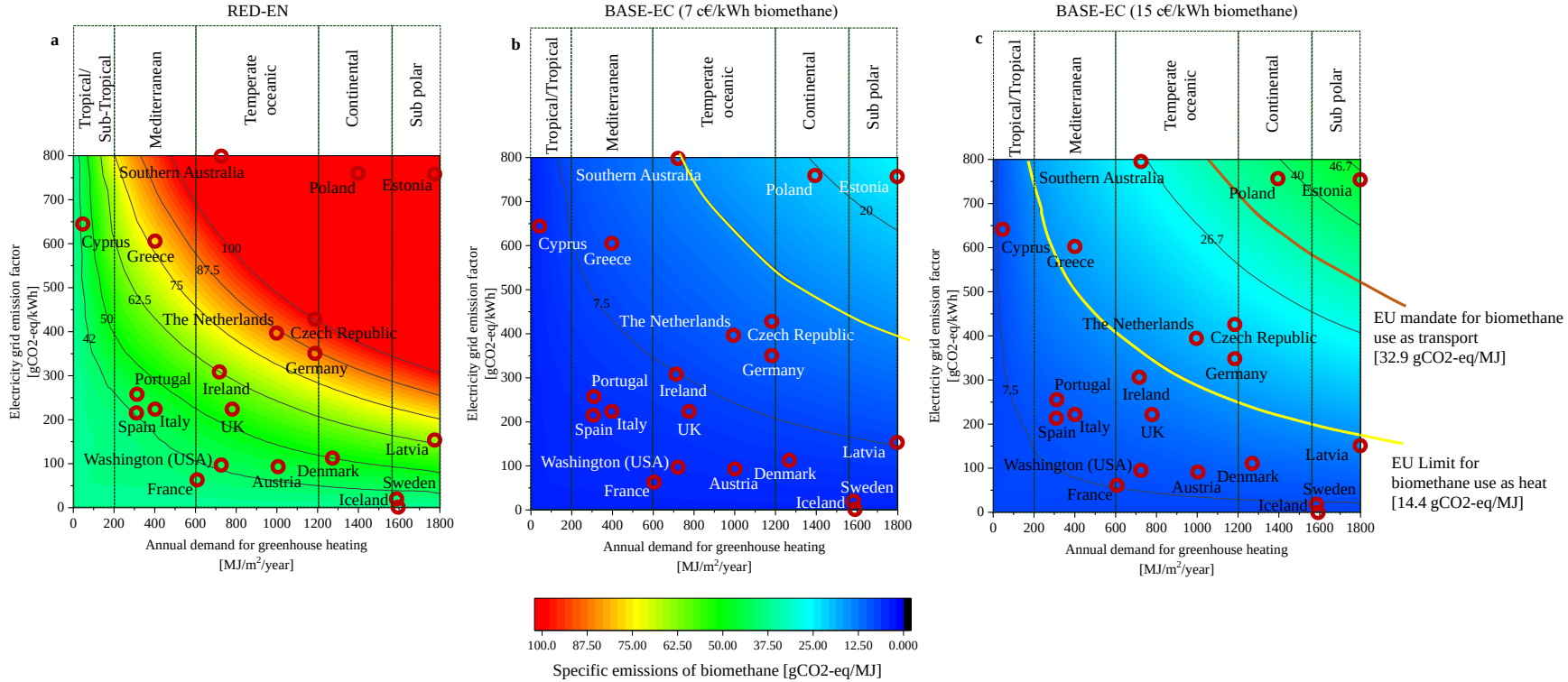


Figure 7-20 Specific emissions of biomethane from the proposed process with the annual energy demand for heating the greenhouse (climatic conditions) and the electricity emission factors (grid electricity) for the following scenarios (a) RED-EN, (b) BASE-EC with the biomethane selling price of 7 c€/kWh and (c) BASE-EC with the biomethane selling price of 15 c€/kWh. The country-specific electricity grid emission factors were obtained from multiple pieces of literature [114,138] while the annual energy demands were estimated from the results of Mariani et al. (2016) [46]. It is to be noted that the country-specific energy requirements have been based on the average climatic conditions of a country. The results might vary based on location-specific climatic fluctuations.

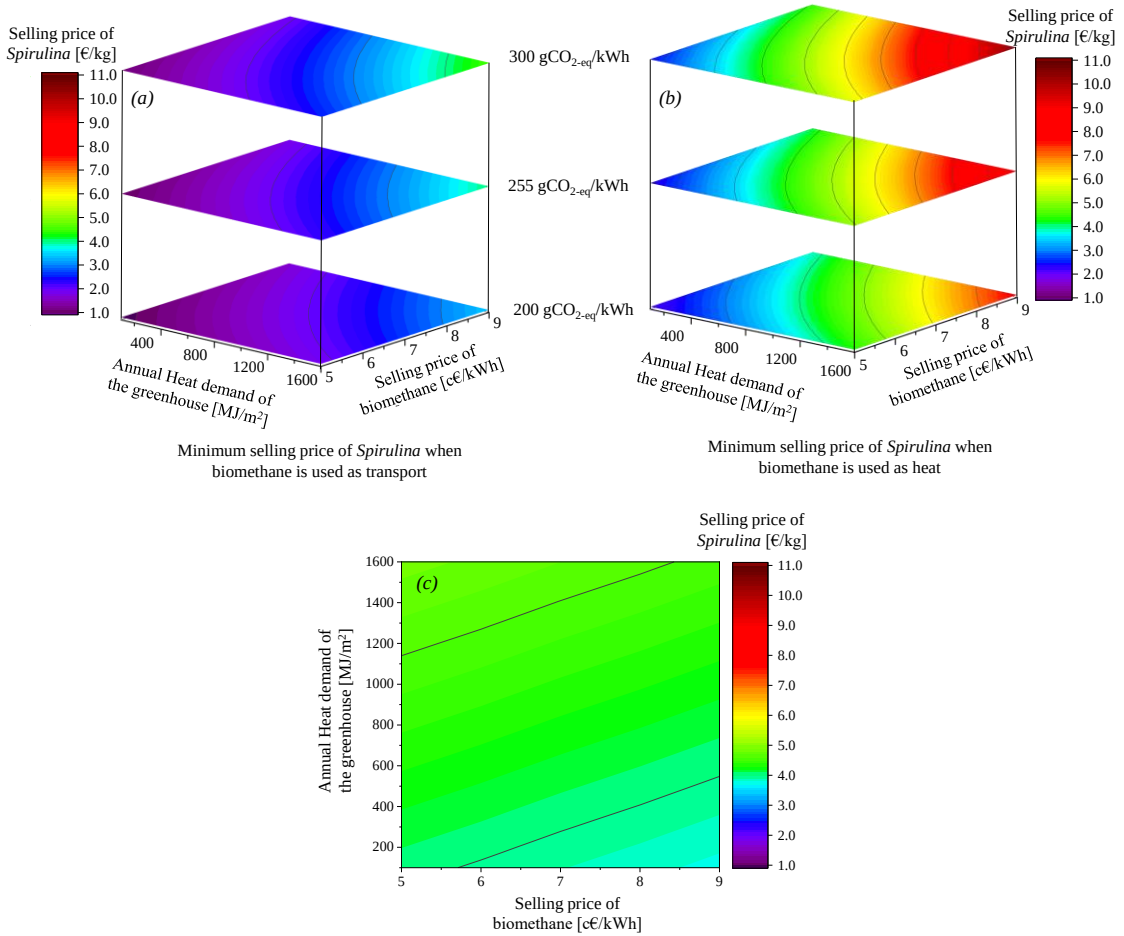


Figure 7-21 Variation of the selling prices of Spirulina powder required to produce biomethane which satisfies the sustainable criteria for (a) transport and (b) heat according to RED-II from the proposed polygeneration system with variation in the heat demand of the greenhouse, electricity grid emission factor and the biomethane selling price while (c) shows the minimum selling price of Spirulina powder against the biomethane selling price and the heat required in the greenhouse to ensure a Cost Utilisation Factor (CUF) greater than 1.

7.5 Conclusions and strategies to improve process performance

The answers to the questions posed in the introduction are summarised as follows:

Q1. How does the proposed process perform in thermodynamic, economic and environmental aspects in a multi-criteria performance assessment?

Currently, the energy for greenhouse heating to cultivate microalgae presented one of the primary challenges to a positive ratio of energy output to energy input (S-EROI > 1). In economic terms, the plant was able to double the value of the inputs while quartering GHG emissions compared to reported standalone facilities producing the same (or similar) products. The emission savings from carbon capture in the production of sodium bicarbonate during biogas upgrading was found to be critical and an essential bridge to low carbon micro-algae cultivation using photosynthetic biogas upgrading.

Q2. How can the product and process performance be enhanced going forward?

In the future, the product and process carbon footprints can be substantially enhanced by the use of renewable electricity and heat. The use of open pond photobioreactors along with improved algal productivity together and emission reduction from chemicals are crucial to ensure process viability and generate further GHG savings. For flat plate PBRs to be viable, the volumetric productivity of microalgae must be more than doubled as that of open pond PBRs through technological optimisation. Although the replacement of inorganic nutrient medium by liquid digestate [18,139] or wastewater [140] is technically feasible, their use must be carefully studied to meet local and international food safety regulations [141].

Building on the knowledge from the above questions, the conclusions against each hypothesis were drawn as follows:

H1, H2 and H3. The economic allocation provides a better product performance assessment compared to the RED-II mandated energy allocation

methodology for a polygeneration system producing energy and non-energy bioproducts. The inclusion of digestate as a valuable product will reduce specific emissions from *biomethane* and *Spirulina powder*. The co-products generated fare better in terms of energy, emission and water footprints than current market-available commodities.

The allocation methodology is crucial and the RED-II is limited in assessing the complexity of the polygeneration system. Inclusion of digestate as a product and the use of economic allocation instead of energy allocation models resulted in biomethane with a carbon footprint of below 10 $gCO_{2\text{-}eq}$/MJ (meeting the most stringent sustainability criteria of RED-II); digestate with a carbon intensity of 0.4 $kgCO_{2\text{-}eq}$/kgN (less than mineral fertiliser at 1.5 to 3 $kgCO_{2\text{-}eq}$/kgN); and *Spirulina* protein below 0.8 $kgCO_{2\text{-}eq}$/100-gp (lower than meat proteins at 50 $kgCO_{2\text{-}eq}$/100-gp).

H4 and H5. *Spirulina* as a complete food provides better performance than when considered just as a protein supplement. The land footprint is a major challenge, however, can be significantly reduced by increasing the productivity of the microalgae.

On a complete food basis and using economic allocation, *Spirulina* had less than 0.07 $kgCO_{2\text{-}eq}$ emissions per100 $NDS_{NRF9.3}$ points (over 150 times lower than the CO_2 emissions from beef). Contrarily the CO_2 emission difference between *Spirulina* and beef proteins is around 60 times. On a complete food basis and using economic allocation, *Spirulina* demonstrated a specific land footprint of less than 15 m^2/100 $NDS_{NRF9.3}$ (comparable to chicken at 15.9 m^2/100 $NDS_{NRF9.3}$) as opposed to over 150 m^2/100-gp, surpassed only by beef protein. Increasing the productivity of the associated microalgae species through improving growth conditions or identifying fast-growing species would be essential to reduce the technological bottleneck in terms of land requirement of photosynthetic biogas upgrading.

7.6 Acknowledgement

This work acknowledges the support from Science Foundation Ireland (SFI) through the Centre for Marine and Renewable Energy (MaREI) under Grant No. 12/RC/2302_P2 and 16/SP/3829, with industrial funding from Gas Networks Ireland

through The Green Gas Innovation Group and by ERVIA and IDL Pernod Ricard. This work was also supported by the Environmental Protection Agency – Ireland (2018-RE-MS-13).

7.7 Supplementary to Chapter 7

Box S7.1: Calculation of the cost of Zarrouk's medium (without sodium bicarbonate)

Cost of Zarrouk's Medium: 80 USD/1000 L [26,41] c. 64 €/1000 L

Based on Zarrouk's media composition, each litre of media comprises 16.8 grams $NaHCO_3$ and the remaining 5.33 grams of other nutrients. Thus,

➔ Unit Cost of Zarrouk's medium = 64/(16.8+5.13) = 2.89 €/kg or 2,892 €/tonne

Conventional Zarrouk's medium comprises high-cost analytical grade sodium bicarbonate[42], typically costing around 3,000 €/tonne[142]. Thus,

➔ Cost of analytical grade bicarbonate in one tonne of Zarrouk media
= 16.83/22.13×3,000 = 2,277 €

Therefore,

➔ Cost of nutrients in one tonne of Zarrouk's media = 2,892 – 2,277 = 615 €

➔ Unit Cost of Zarrouk's media (without bicarbonates) = 615/(5.13/22.13) ≈ 2,653 €/tonne

Table S7-1 Summary of the major outputs to the process and their corresponding unit prices/ costs

Component	Unit price/cost	Reference
Biomethane	7 c€/kWh	Average grid injection price (feed-in tariff) [12]
Spirulina platensis powder (protein supplement)	10 €/kg	Similar to the current production prices of *Spirulina* [28,143]
Digestate from anaerobic digestion	4 €/tonne	Murphy et al. (2011) [29]
Ammonium Sulphate	3600 €/tonne	Obtained from Glanbiaconnect (2021) [144]
Wastewater Sludge (Disposal Fee)	-100 €/tonne[ζ]	Adapted from IES (2021) [145]

[ζ] Negative sign indicates the disposal cost of the product that must be borne by the plant.

Table S7-2 $NRF_{9.3}$ scores and specific emissions of other protein-based foods compared with Spirulina. The data has been compiled from multiple literature [104,108,146–149]

Protein Type	$NRF_{9.3}$ [value/ 100 kCal]	Specific Emissions			Specific Land Footprint			Specific Water Footprint		
		$kgCO_{2\text{-eq}}$/ 100 grams protein (gp)	$kgCO_{2\text{-eq}}$/ 1,000 kCal	$kgCO_{2\text{-eq}}$/1,000 $NRF_{9.3}$ points	m^2/kg-protein	m^2/ 1,000 kCal	m^2/1,000 $NRF_{9.3}$ points	L/kg-protein	L/1,000 kCal	L/1,000 $NRF_{9.3}$ points
Beef (Beef Herd)	10.8	49.9	36.4	337.4	1,636	119.5	1,106.4	7,280	532	4,925.9
Beef (Dairy Herd)	10.8	16.9	12.2	112.9	219	15.8	146.7	13,750	994	9,203.7
Pork	33.8	7.6	5.2	15.2	107	7.3	21.5	11,000	751	2,221.9
Farmed Fish	50.2	5.9	7.6	15.2	37	4.7	9.4	16,190	2,062	4,107.6
Chicken	38.7	5.7	5.3	13.8	71	6.6	17.1	3,810	357	922.5
Eggs	41.6	4.2	3.2	7.8	57	4.4	10.5	5,210	401	963.9
Milk	43.3	9.5	5.2	12.1	271	14.9	34.5	19,040	1,047	2,418
Soybeans (Tofu)	69.4	1.9	1.2	1.7	22	1.3	1.9	930	55	79.3
Root vegetables (Carrots)	234.9	4.3	1.2	0.5	33	0.9	0.4	2,840	77	32.8
Bananas	51.8	9.6	1.4	2.8	214	3.2	6.2	12,720	191	368.7
Oatmeal	57	1.9	0.95	1.7	58	2.9	5.1	3,710	184	322.8
Pulses and lenils	8.6	0.4	0.5	6.1	73	4.6	53.1	4,055	1,190	13,837.2

Protein Type	$NRF_{9.3}$ [value/ 100 kCal]	Specific Emissions			Specific Land Footprint			Specific Water Footprint		
		$kgCO_{2\text{-}eq}$/ 100 grams protein (gp)	$kgCO_{2\text{-}eq}$/ 1,000 kCal	$kgCO_{2\text{-}eq}$/1,000 $NRF_{9.3}$ points	m^2/kg-protein	m^2/ 1,000 kCal	m^2/1,000 $NRF_{9.3}$ points	L/kg-protein	L/1,000 kCal	L/1,000 $NRF_{9.3}$ points
Nuts	24	0.26	0.07	0.29	79	2.1	8.8	25,310	672	2,800
Tomatoes	248.9	19	11	4.42	73	4.2	1.7	33,620	1,946	781.8

Box S7.2: Calculation of the specific energy of biomethane

Assumed calorific value of methane: 50 MJ/kg [97]

Methane density is assumed as 0.668 kg/m^3 at NTP (20°C, 1 atm) [150] or 0.717 at STP (0°C, 1 bar) [150]

LHV methane on volume basis is therefore

➔ 50 × 0.668 = 33.36 MJ/Nm^3, or,

➔ 50 × 0.717 = 35.85 MJ/Sm^3

Based on biomethane composition (95.2% methane), therefore,

➔ LHV of biomethane produced = 33.36 × 0.952 = 31.8 MJ/Nm^3
= 31.8/3.6 ≈ 8.83 kWh/Nm^3 biomethane, or,

➔ LHV of biomethane produced = 35.85 × 0.952 = 34.08 MJ/Sm^3
= 34.08/3.6 ≈ 9.47 kWh/Sm^3 biomethane

Accordingly, for the 361.5 Nm^3/hr of biomethane generated,

➔ the energy produced as biomethane = 361.5 × 8.83 ≈ 3,192 kWh

Thus,

➔ Power rating of the proposed polygeneration plant = 3.19 MW-biomethane

7.8 References

[1] Crippa M, Solazzo E, Guizzardi D, Tubiello FN, Leip A. Food systems are responsible for a third of global anthropogenic GHG emissions. Nat Food 2021;2. doi:10.1038/s43016-021-00225-9.

[2] Ritchie H. Cars, planes, trains: where do CO_2 emissions from transport come from? Our World Data 2020. https://ourworldindata.org/co2-emissions-from-transport (accessed July 5, 2021).

[3] Fuelling transport. Nat Clim Chang 2020;10:793. doi:10.1038/s41558-020-00912-8.

[4] Wall DM, McDonagh S, Murphy JD. Cascading biomethane energy systems for sustainable green gas production in a circular economy. Bioresour Technol 2017;243:1207–15. doi:10.1016/j.biortech.2017.07.115.

[5] Wall DM, Dumont M, Murphy JD. Green gas. 2018.

[6] Tonini D, Saveyn HGM, Huygens D. Environmental and health co-benefits for advanced phosphorus recovery. Nat Sustain 2019;2:1051–61. doi:10.1038/s41893-019-0416-x.

[7] Long A, Murphy JD. Can green gas certificates allow for the accurate quantification of the energy supply and sustainability of biomethane from a range of sources for renewable heat and or transport ? Renew Sustain Energy Rev 2019;115:109347. doi:10.1016/j.rser.2019.109347.

[8] Rajendran K, O'Gallachoir B, Murphy JD. The combined role of policy and incentives in promoting cost efficient decarbonisation of energy: A case study for biomethane. J Clean Prod 2019;219:278–90. doi:10.1016/j.jclepro.2019.01.298.

[9] Rajendran K, Browne JD, Murphy JD. What is the level of incentivisation required for biomethane upgrading technologies with carbon capture and reuse? Renew Energy 2019;133:951–63. doi:10.1016/j.renene.2018.10.091.

[10] Bose A, Lin R, Rajendran K, Xia A, O'Shea R, Murphy JD. How to optimise photosynthetic biogas upgrading: a perspective on system design and microalgae selection. Biotechnol Adv 2019;37. doi:10.1016/j.biotechadv.2019.107444.

[11] Meier L, Pérez R, Azócar L, Rivas M, Jeison D. Photosynthetic CO_2 uptake by microalgae: An attractive tool for biogas upgrading. Biomass and Bioenergy 2015;73:102–9. doi:10.1016/j.biombioe.2014.10.032.

[12] Bose A, O'Shea R, Lin R, Murphy JD. A perspective on novel cascading algal biomethane biorefinery systems. Bioresour Technol 2020;304:123027. doi:10.1016/j.biortech.2020.123027.

[13] Meier L, Stará D, Bartacek J, Jeison D. Removal of H_2S by a continuous microalgae-based photosynthetic biogas upgrading process. Process Saf Environ Prot 2018;119:65–8. doi:10.1016/j.psep.2018.07.014.

[14] Rodero M del R, Severi CA, Rocher-Rivas R, Quijano G, Muñoz R. Long-term influence of high alkalinity on the performance of photosynthetic biogas upgrading. Fuel 2020;281:118804. doi:10.1016/j.fuel.2020.118804.

[15] Bose A, O'Shea R, Lin R, Murphy JD. A comparative evaluation of design factors on bubble column operation in photosynthetic biogas upgrading. Biofuel Res J 2021;8. doi:10.18331/BRJ2021.8.2.2.

[16] Rodero M del R, Lebrero R, Serrano E, Lara E, Arbib Z, García-Encina PA, et al. Technology validation of photosynthetic biogas upgrading in a semi-industrial scale algal-bacterial photobioreactor. Bioresour Technol 2019;279:43–9. doi:10.1016/j.biortech.2019.01.110.

[17] Jana K, Ray A, Mansouri M, Assadi M, De S. Polygeneration as a future sustainable energy solution – A comprehensive review. Appl Energy 2017;202:88–111. doi:10.1016/j.apenergy.2017.05.129.

[18] Toledo-Cervantes A, Estrada JM, Lebrero R, Muñoz R. A comparative analysis of biogas upgrading technologies: Photosynthetic vs physical/chemical processes. Algal Res 2017;25:237–43. doi:10.1016/j.algal.2017.05.006.

[19] Jana K, De S. Polygeneration performance assessments: Multi-dimensional viewpoint. Clean Technol Environ Policy 2015;17:1547–61. doi:10.1007/s10098-014-0885-6.

[20] Moni SM, Mahmud R, High K, Carbajales-dale M. Life cycle assessment of emerging technologies : A review Sheikh Moniruzzaman Moni 1. J Ind Ecol 2019:1–12. doi:10.1111/jiec.12965.

[21] European Parliament and the Council of the European Union. Directive (EU) 2018/2001 of the European Parliament and of the Council on the promotion of the use of energy from renewable sources. 2018.

[22] Maes D, Van Dael M, Vanheusden B, Goovaerts L, Reumerman P, Márquez Luzardo N, et al. Assessment of the sustainability guidelines of EU Renewable Energy Directive: The case of biorefineries. J Clean Prod 2015;88:61–70. doi:10.1016/j.jclepro.2014.04.051.

[23] Bedoić R, Ćosić B, Duić N. Technical potential and geographic distribution of agricultural residues, co-products and by-products in the European Union. Sci Total Environ 2019;686:568–79. doi:10.1016/j.scitotenv.2019.05.219.

[24] Bolaric S, Barth S, Melchinger AE, Posselt UK. Molecular genetic diversity within and among German ecotypes in comparison to European perennial ryegrass cultivars. Plant Breed 2005;124:257–62. doi:10.1111/j.1439-0523.2005.01108.x.

[25] Wall DM, Allen E, Straccialini B, Kiely PO, Murphy JD. Optimisation of digester performance with increasing organic loading rate for mono- and co-digestion of grass silage and dairy slurry. Bioresour Technol 2014;173:422–8. doi:10.1016/j.biortech.2014.09.126.

[26] Madkour FF, Kamil AEW, Nasr HS. Production and nutritive value of *Spirulina platensis* in reduced cost media. Egypt J Aquat Res 2012;38:51–7. doi:10.1016/j.ejar.2012.09.003.

[27] Khakharia P, Huizinga A, Jurado Lopez C, Sanchez Sanchez C, De Miguel Mercader F, Vlugt TJH, et al. Acid wash scrubbing as a countermeasure for ammonia

emissions from a postcombustion CO_2 Capture Plant. Ind Eng Chem Res 2014;53:13195–204. doi:10.1021/ie502045c.

[28] Grahl S. Food product development with spirulina (*Arthrospira platensis*) – Sensory profiling, product perception and consumer acceptance. Georg-August-Universität Göttingen, 2019.

[29] Murphy JD, Korres NE, Singh A, Smyth B, Nizami A-S, Thamsiriroj T. The potential for grass biomethane as a biofuel compressed biomethane generated from grass, utilised as a transport biofuel. CCRP Report. 2011.

[30] Vo TTQ, Wall DM, Ring D, Rajendran K, Murphy JD. Techno-economic analysis of biogas upgrading via amine scrubber, carbon capture and ex-situ methanation. Appl Energy 2018;212:1191–202. doi:10.1016/j.apenergy.2017.12.099.

[31] Nizami AS, Korres NE, Murphy JD. Review of the integrated process for the production of grass biomethane. Environ Sci Technol 2009;43:8496–508. doi:10.1021/es901533j.

[32] Banks CJ, Zhang Y. Technical Report: Optimising inputs and outputs from anaerobic digestion processes. 2010..

[33] Germinal Ireland Limited. The value of grass introduction : Thurles, Tipperary: 2015.

[34] Smyth BM, Murphy JD, Brien CMO. What is the energy balance of grass biomethane in Ireland and other temperate northern European climates ? Renew Sustain Energy Rev 2009;13:2349–60. doi:10.1016/j.rser.2009.04.003.

[35] TNO. Grass (#613). Phyllyis2 1997. https://phyllis.nl/Browse/Standard/ECN-Phyllis (accessed June 5, 2021).

[36] Hyun J, Lee JH, Kee I, Hyun C. Techno-economic and environmental evaluation of CO_2 mineralization technology based on bench-scale experiments. J CO2 Util 2018;26:522–36. doi:10.1016/j.jcou.2018.06.007.

[37] Lee JH, Lee DW, Kwak C, Kang K, Lee JH. Technoeconomic and environmental evaluation of sodium bicarbonate production using CO_2 from flue gas

of a coal-fired power plant. Ind Eng Chem Res 2019;58:15533–41. doi:10.1021/acs.iecr.9b02253.

[38] Hemphill A. OUTLOOK ’20: Sulphuric acid market begins 2020 on bearish note. ICIS n.d. https://www.icis.com/explore/resources/news/2020/01/10/10458518/outlook-20-sulphuric-acid-market-begins-2020-on-bearish-note (accessed May 4, 2021).

[39] Commission for Regulation of Utilities (CRU). Irish Water’s Non -Domestic Tariff Framework CRU Decision Paper. 2019.

[40] Eurostat. Electricity price statistics. 2021 n.d. https://ec.europa.eu/eurostat/statistics-explained/index.php?title=Electricity_price_statistics#Electricity_prices_for_non-household_consumers (accessed May 18, 2021).

[41] Costa JAV, Freitas BCB, Rosa GM, Moraes L, Morais MG, Mitchell BG. Operational and economic aspects of *Spirulina*-based biorefinery. Bioresour Technol 2019;292:121946. doi:10.1016/j.biortech.2019.121946.

[42] Raoof B, Kaushik BD, Prasanna R. Formulation of a low-cost medium for mass production of *Spirulina*. Biomass and Bioenergy 2006;30:537–42. doi:10.1016/j.biombioe.2005.09.006.

[43] Rajendran K, Gallachóir BÓ, Murphy JD. The role of incentivising biomethane in Ireland using anaerobic digestion (2016-RE-DS-6) - EPA Research Report. 2019.

[44] Nolan S, Thorn CE, Ashekuzzaman SM, Kavanagh I, Nag R, Bolton D, et al. Landspreading with co-digested cattle slurry, with or without pasteurisation, as a mitigation strategy against pathogen, nutrient and metal contamination associated with untreated slurry. Sci Total Environ 2020;744:140841. doi:10.1016/j.scitotenv.2020.140841.

[45] Pall Corporation. Sterile or Final Compressed Air and Gas Filtration 2020. https://www.pall.com/en/food-beverage/compressed-air-gas/sterile-filtration.html (accessed May 5, 2021).

[46] Mariani L, Cola G, Bulgari R, Ferrante A, Martinetti L. Space and time variability of heating requirements for greenhouse tomato production in the Euro-Mediterranean area. Sci Total Environ 2016;562:834–44. doi:10.1016/j.scitotenv.2016.04.057.

[47] Vonshak A, Richmond A. Mass production of the blue-green alga *Spirulina*: An overview. Biomass 1988;15:233–47. doi:10.1016/0144-4565(88)90059-5.

[48] Gao W, Chen F, Wang X, Meng Q. Recent advances in processing food powders by using superfine grinding techniques : A review. Compr Rev Food Sci Food Saf 2020;19:2222–55. doi:10.1111/1541-4337.12580.

[49] Vo TTQ, Rajendran K, Murphy JD. Can power to methane systems be sustainable and can they improve the carbon intensity of renewable methane when used to upgrade biogas produced from grass and slurry? Appl Energy 2018;228:1046–56. doi:10.1016/j.apenergy.2018.06.139.

[50] Ortega-Calvo JJ, Mazuelos C, Hermosin B, Saiz-Jimenez C. Chemical composition of *Spirulina* and eukaryotic algae food products marketed in Spain. J Appl Phycol 1993;5:425–35. doi:10.1007/BF02182735.

[51] European Commission. Commission Implementing Regulation (EU) 2017/2470. Off J Eur Union 2017;351:72–201.

[52] de Oliveira MACL, Monteiro MPC, Robbs PG, Leite SGF. Growth and chemical composition of *Spirulina maxima* and *Spirulina platensis* biomass at different temperatures. Aquac Int 1999;7:261–75. doi:10.1023/A:1009233230706.

[53] Bord Gais. The Natural Gas Network. n.d.

[54] Meier L, Barros P, Torres A, Vilchez C, Jeison D. Photosynthetic biogas upgrading using microalgae: Effect of light/dark photoperiod. Renew Energy 2017;106:17–23. doi:10.1016/j.renene.2017.01.009.

[55] AAT Bioquest Inc. Carbonate-bicarbonate buffer (pH 9.2 to 10.6) preparation 2016. https://www.aatbio.com/resources/buffer-preparations-and-recipes/carbonate-bicarbonate-buffer-ph-9-2-to-10-6 (accessed May 6, 2021).

[56] Teagasc. Heat pumps in agriculture (Fact sheet Energy 09). 2020.

[57] Achinas S, Euverink GJW. Theoretical analysis of biogas potential prediction from agricultural waste. Resour Technol 2016;2:143–7. doi:10.1016/j.reffit.2016.08.001.

[58] Meier L, Stará D, Bartacek J, Jeison D. Removal of H_2S by a continuous microalgae-based photosynthetic biogas upgrading process. Process Saf Environ Prot 2018;119:65–8. doi:10.1016/j.psep.2018.07.014.

[59] Bachmann N. Design and engineering of biogas plants. In: Wellinger A, Murphy J, Baxter D, editors. Biogas Handb. Sci. Prod. Appl. 1st ed., Woodhead Publishing Limited; 2013, p. 191–211. doi:10.1533/9780857097415.2.191.

[60] al Seadi T, Rutz D, Prassl H, Kottner M, Finsterwalder T, Volk S, et al. Biogas Handbook. Esbjerg: University of Southern Denmark Esbjerg,; 2008.

[61] Calise F, Cappiello FL, D'Accadia MD, Infante A, Vicidomini M. Modelling of the anaerobic digestion of organic wastes: Integration of heat transfer and biochemical aspects. Energies 2020;13. doi:10.3390/en13112702.

[62] Liebetrau J, Reinelt T, Agostini A, Linke B. Methane emissions from biogas plants. IEA Bioenergy; 2017.

[63] Scholwin F, Nelles M. Energy flows in biogas plants: Analysis and implications for plant design. Biogas Handb. Sci. Prod. Appl., 2013, p. 212–27. doi:10.1533/9780857097415.2.212.

[64] Timonen K, Sinkko T, Luostarinen S, Tampio E, Joensuu K. LCA of anaerobic digestion: Emission allocation for energy and digestate. J Clean Prod 2019;235:1567–79. doi:10.1016/j.jclepro.2019.06.085.

[65] FAO. Energy Requirements in milk and milk processing n.d. http://www.fao.org/3/T0515E/T0515E03.htm (accessed June 16, 2021).

[66] Slade R, Bauen A. Micro-algae cultivation for biofuels : Cost, energy balance, environmental impacts and future prospects. Biomass and Bioenergy 2013;53:29–38. doi:10.1016/j.biombioe.2012.12.019.

[67] Sierra E, Acién FG, Fernández JM, García JL, González C, Molina E. Characterization of a flat plate photobioreactor for the production of microalgae. Chem Eng J 2008;138:136–47. doi:10.1016/j.cej.2007.06.004.

[68] Baker CGJ, Mckenzie KA. Energy consumption of industrial spray dryers. Drying Technology 2005; 23(1-5):365-386. doi: 10.1081/DRT-200047665.

[69] Bose A, O'Shea R, Lin R, Murphy JD. Optimisation and performance prediction of photosynthetic biogas upgrading using a bubble column. Under Rev 2021.

[70] Bose A, O'Shea R, Lin R, Murphy JD. Design, commissioning and performance assessment of a lab-scale bubble column reactor for photosynthetic biogas upgrading with *Spirulina platensis*. Ind Eng Chem Res 2021. doi:10.1021/acs.iecr.0c05974.

[71] Huang Q, Jiang F, Wang L, Yang C. Design of photobioreactors for mass cultivation of photosynthetic organisms. Engineering 2017;3:318–29. doi:10.1016/J.ENG.2017.03.020.

[72] Płaczek M, Patyna A, Witczak S. Technical evaluation of photobioreactors for microalgae cultivation. E3S Web Conf 2017;19:1–10. doi:10.1051/e3sconf/20171902032.

[73] Clippinger J, Davis R. Techno-economic analysis for the production of algal biomass via closed photobioreactors : Future cost potential evaluated across a range of cultivation system designs techno-economic analysis for the production of algal biomass via closed photobioreactor. 2019.

[74] Béchet Q, Sialve B, Steyer JP, Shilton A, Guieysse B. Comparative assessment of evaporation models in algal ponds. Algal Res 2018;35:283–91. doi:10.1016/j.algal.2018.08.022.

[75] Goetz V, Le Borgne F, Pruvost J, Plantard G, Legrand J. A generic temperature model for solar photobioreactors. Chem Eng J 2011;175:443–9. doi:10.1016/j.cej.2011.09.052.

[76] Markou G. Overview of microalgal cultivation, biomass processing and application. In: Konur O, editor. Handb. Algal Sci. Technol. Med., Academic Press; 2020. doi:https://doi.org/10.1016/B978-0-12-818305-2.00021-8.

[77] Togarcheti SC, Mediboyina M kumar, Chauhan VS, Mukherji S, Ravi S, Mudliar SN. Life cycle assessment of microalgae based biodiesel production to evaluate the impact of biomass productivity and energy source. Resour Conserv Recycl 2017;122:286–94. doi:10.1016/j.resconrec.2017.01.008.

[78] Christoforidou P, Bariamis G, Iosifidou M, Nikolaidou E, Samaras P. Energy benchmarking and optimization of wastewater treatment plants in Greece. Environ Sci Proc 2020;2:36. doi:10.3390/environsciproc2020002036.

[79] Stillwell AS, Webber ME. Predicting the specific energy consumption of reverse osmosis desalination. Water (Switzerland) 2016;8:1–18. doi:10.3390/w8120601.

[80] Marques CAX, Fontes CH, Embiruçu M, Kalid RA. Energy efficiency in an industrial wet cooling tower through improved control. Comput Aided Chem Eng 2009;27:1449–54. doi:10.1016/S1570-7946(09)70632-7.

[81] Al-Bassam E, Maheshwari GP, Al-Hadban Y, Rasquinha J. Energy-efficient production of chilled water in industry. Energy 1997;22:1183–8. doi:10.1016/S0360-5442(97)00035-2.

[82] SUEZ. Drying unit energy consumption. Suez Degremont® Water Handb 2021. https://www.suezwaterhandbook.com/processes-and-technologies/dewatered-sludge-treatment/drying/drying-unit-energy-consumption (accessed June 1, 2021).

[83] Hall CAS, Lambert JG, Balogh SB. EROI of different fuels and the implications for society. Energy Policy 2014;64:141–52. doi:10.1016/j.enpol.2013.05.049.

[84] Chiriboga G, De La Rosa A, Molina C, Velarde S, Carvajal C G. Energy Return on Investment (EROI) and Life Cycle Analysis (LCA) of biofuels in Ecuador. Heliyon 2020;6. doi:10.1016/j.heliyon.2020.e04213.

[85] Korres NE, Singh A, Nizami A, Murphy JD. Is grass biomethane a sustainable transport biofuel ? Biofuels, Bioprod Biorefining 2010;4:310–25. doi:10.1002/bbb.228.

[86] O'Shea R, Wall DM, Kilgallon I, Browne JD, Murphy JD. Assessing the total theoretical, and financially viable, resource of biomethane for injection to a natural gas network in a region. Appl Energy 2017;188:237–56. doi:10.1016/j.apenergy.2016.11.121.

[87] Dünnebeil F, Lambrecht U. Fuel efficiency and emissions of trucks in Germany An overview. Heidelberg: 2012.

[88] Wu Y, Xie H, Liu T, Wang Y, Wang F, Gao X, et al. Soda ash production with low energy consumption using proton cycled membrane electrolysis. Ind Eng Chem Res 2019;58:3450–8. doi:10.1021/acs.iecr.8b05371.

[89] Yablonsky A, Barsoumian S, Legere D. SkyMine® carbon mineralization pilot project: Decision point 1 topical report. Austin, Texas: 2013.

[90] Frank ED, Han J, Palou-Rivera I, Elgowainy A, Wang MQ. Life cycle analysis of algal lipid fuels with the GREET Model. 2011.

[91] Beausang C, Mcdonnell K, Murphy F. Assessing the environmental sustainability of grass silage and cattle slurry for biogas production. J Clean Prod 2021;298:126838. doi:10.1016/j.jclepro.2021.126838.

[92] Duran Quintero C, Ventura A, Lépine O, Pruvost J. Eco-design of *Spirulina* solar cultivation: Key aspects to reduce environmental impacts using Life Cycle Assessment. J Clean Prod 2021;299. doi:10.1016/j.jclepro.2021.126741.

[93] Hoxha A, Christensen B. The carbon footprint on fertiliser production: regional reference values. Int Fertil Soc 2018;1:1–21.

[94] World Biogas Association. 8. Case study 3: Nature Energy 2020. https://www.worldbiogasassociation.org/8-case-study-3-nature-energy/ (accessed May 18, 2021).

[95] Kumar P. Largest Biogas Plants 2017. https://www.nsenergybusiness.com/news/newslargest-biogas-plants-061017-5943061/ (accessed May 18, 2021).

[96] Vengateson U. Cooling Towers: Estimate Evaporation Loss and Makeup Water Requirements 2017. https://www.chemengonline.com/cooling-towers-estimate-evaporation-loss-and-makeup-water-requirements/?printmode=1 (assessed May 25, 2021).

[97] Sforza PM. Theory of aerospace propulsion. Butterworth-Heinemann; 2012. doi:10.1016/C2009-0-61051-5.

[98] TNO. Microalgae, *Spirulina* (#1450). ECN Phyllis2 1999. https://phyllis.nl/Biomass/View/1450 (accessed June 5, 2021).

[99] Kratzeisen M, Starcevic N, Martinov M, Maurer C, Müller J. Applicability of biogas digestate as solid fuel. Fuel 2010;89:2544–8. doi:10.1016/j.fuel.2010.02.008.

[100] Deng C, Lin R, Kang X, Wu B, O'Shea R, Murphy JD. Improving gaseous biofuel yield from seaweed through a cascading circular bioenergy system integrating anaerobic digestion and pyrolysis. Renew Sustain Energy Rev 2020;128:109895. doi:10.1016/j.rser.2020.109895.

[101] Sills DL, Gerber L, Doren V, Beal C, Raynor E. The effect of functional unit and co-product handling methods on life cycle assessment of an algal biorefinery. Algal Res 2020;46:101770. doi:10.1016/j.algal.2019.101770.

[102] Ye C, Mu D, Horowitz N, Xue Z, Chen J, Xue M, et al. Life cycle assessment of industrial scale production of *Spirulina* tablets. Algal Res 2018;34:154–63. doi:10.1016/j.algal.2018.07.013.

[103] Drewnowski A. The Nutrient Rich Foods Index helps to identify healthy, affordable. Am J Clin Nutr 2010;91:1095–101. doi:10.3945/ajcn.2010.28450D.Am.

[104] Sluik D, Streppel MT, Lee L van, Geelen A, Feskens EJM. Evaluation of a nutrient-rich food index score in the Netherlands. J Nutr Sci (2015), 2015;4:1–9. doi:10.1017/jns.2015.4.

[105] Liestianty D, Rodianawati I, Arfah RA, Assa A. Nutritional analysis of *Spirulina sp* to promote as superfood candidate. IOP Conf Ser Mater Sci Eng 2019;509:012031. doi:10.1088/1757-899X/509/1/012031.

[106] Agriculture UD of. Food-Data Central 2021. https://fdc.nal.usda.gov/index.html.

[107] Schwalfenberg GK, Genuis SJ. The Importance of Magnesium in clinical healthcare. Scientifica (Cairo) 2017:4179326. doi:10.1155/2017/4179326.

[108] Fulgoni III VL, Keast DR, Drewnowski A. Development and validation of the Nutrient-Rich Foods Index : A tool to measure nutritional quality of foods 1 – 3. J Nutr 2009;139:1549–54. doi:10.3945/jn.108.101360.1549.

[109] Giuntoli J, Agostini A, Edwards R, Marelli L. Solid and gaseous bioenergy pathways : Input values and GHG emissions. Ispra: 2017. doi:10.2790/27486.All.

[110] Bauer SK, Grotz LS, Connelly EB, Colosi LM. Reevaluation of the global warming impacts of algae-derived biofuels to account for possible contributions of nitrous oxide. Bioresour Technol 2016;218:196–201. doi:10.1016/j.biortech.2016.06.058.

[111] Huttenhuis P, Roeloffzen A, Versteeg G. CO_2 capture and re-use at a waste incinerator. Energy Procedia 2016;86:47–55. doi:10.1016/j.egypro.2016.01.006.

[112] Braud L, McDonnell K, Murphy F. Improving LCI data collection methodologies for novel food systems: A case study on microalgae cultivation for phycocyanin production. In: Eberle U, Smetana S, Bos U, editors. 12th Int. Conf. Life Cycle Assess. Food LCA - Food2020, Berlin: 2020, p. 186–9.

[113] Capponi S, Fazio S, Barbanti L. CO_2 savings affect the break-even distance of feedstock supply and digestate placement in biogas production. Renew Energy 2012;37:45–52. doi:10.1016/j.renene.2011.05.005.

[114] European Environment Agency. Greenhouse gas emission intensity of electricity generation 2020. https://www.eea.europa.eu/data-and-maps/daviz/co2-emission-intensity-6#tab-

googlechartid_googlechartid_googlechartid_googlechartid_chart_11111 (accessed May 5, 2021).

[115] Sustainable Energy Authority of Ireland (SEAI). Conversion factors. Ireland's energy stat 2019. https://www.seai.ie/data-and-insights/seai-statistics/conversion-factors/ (accessed June 1, 2021).

[116] Bonfim-Rocha L, Silva AB, de Faria SHB, Vieira MF, de Souza M. Production of sodium bicarbonate from CO_2 reuse processes : A brief review. Int J Chem React Eng 2019;2019:20180318. doi:10.1515/ijcre-2018-0318.

[117] Turgut SS, Feyissa AH, Küçüköner E, Karacabey E. Uncertainty and sensitivity analysis by Monte Carlo simulation: Recovery of trans-resveratrol from grape cane by pressurised low polarity water system. J Food Eng 2021;292. doi:10.1016/j.jfoodeng.2020.110366.

[118] Al Garni HZ, Awasthi A. A Monte Carlo approach applied to sensitivity analysis of criteria impacts on solar PV site selection. In: Samui P, Bui DT, Chakraborty S, Deo RC, editors. Handb. Probabilistic Model., Elsevier Inc.; 2019, p. 489–504. doi:10.1016/B978-0-12-816514-0.00020-5.

[119] Salling KB, Banister D. Feasibility risk assessment of transport infrastructure projects: The CBA-DK decision support model. Eur J Transp Infrastruct Res 2010;10:103–20. https://doi.org/10.18757/ejtir.2010.10.1.2871.

[120] Subramanyan K, Diwekar UM. User manual for stochastic simulation capability in GREET. Illinois: 2005.

[121] Górecki J, Díaz-Madroñero M. Who risks and wins?-Simulated cost variance in sustainable construction projects. Sustain 2020;12:1–31. doi:10.3390/SU12083370.

[122] Risberg K, Sun L, Levén L, Horn SJ, Schnürer A. Biogas production from wheat straw and manure - Impact of pretreatment and process operating parameters. Bioresour Technol 2013;149:232–7. doi:10.1016/j.biortech.2013.09.054.

[123] Strik DPBTB, Domnanovich AM, Holubar P. A pH-based control of ammonia in biogas during anaerobic digestion of artificial pig manure and maize silage. Process Biochem 2006;41:1235–8. doi:10.1016/j.procbio.2005.12.008.

[124] Marín D, Posadas E, Cano P, Pérez V, Blanco S, Lebrero R, et al. Seasonal variation of biogas upgrading coupled with digestate treatment in an outdoors pilot scale algal-bacterial photobioreactor. Bioresour Technol 2018;263:58–66. doi:10.1016/j.biortech.2018.04.117.

[125] Binaghi L, Del Borghi A, Lodi A, Converti A, Del Borghi M. Batch and fed-batch uptake of carbon dioxide by *Spirulina platensis*. Process Biochem 2003;38:1341–6. doi:10.1016/S0032-9592(03)00003-7.

[126] Jiménez C, Cossío BR, Niell FX. Relationship between physicochemical variables and productivity in open ponds for the production of *Spirulina*: A predictive model of algal yield. Aquaculture 2003;221:331–45. doi:10.1016/S0044-8486(03)00123-6.

[127] Pushparaj B, Pelosi E, Tredici MR, Pinzani E, Materassi R. An integrated culture system for outdoor production of microalgae and cyanobacteria. J Appl Phycol 1997;9:113–9. doi:10.1023/A:1007988924153.

[128] De Vree JH, Bosma R, Janssen M, Barbosa MJ, Wijffels RH. Comparison of four outdoor pilot-scale photobioreactors. Biotechnol Biofuels 2015;8:1–12. doi:10.1186/s13068-015-0400-2.

[129] Acién FG, Molina E, Reis A, Torzillo G, Zittelli GC, Sepúlveda C, et al. Photobioreactors for the production of microalgae. In: Gonzalez-Fernandez C, Muñoz R, editors. Microalgae-based biofuels and bioproducts; From feedstock cultivation to end-products, Woodhead Publishing; 2017, p. 1–44. doi:10.1016/B978-0-08-101023-5.00001-7.

[130] Kebede E. Response *of Spirulina platensis* (*Arthrospira fusiformis*) from Lake Chitu, Ethiopia, to salinity stress from sodium salts. J Appl Phycol 1997;9:551–8. doi:10.1023/A:1007949021786.

[131] U.S. Department of the Interior and U.S. Geological Survey. Water resources of the United States - DOTABLES Result 2018. https://water.usgs.gov/cgi-bin/dotables (accessed May 20, 2021).

[132] Toro-Huertas EI, Franco-Morgado M, de los Cobos Vasconcelos D, González-Sánchez A. Photorespiration in an outdoor alkaline open-photobioreactor used for biogas upgrading. Sci Total Environ 2019;667:613–21. doi:10.1016/j.scitotenv.2019.02.374.

[133] Pelletier N, Audsley E, Brodt S, Garnett T, Henriksson P, Kendall A, et al. Energy intensity of agriculture and food systems. Annu Rev Environ Resour 2011;36:233–46 doi:10.1146/annurev-environ-081710-161014.

[134] Norton S. Energy use in New Zealand's primary food production chains and a transition to lower emissions. 2019.

[135] Mekonnen MM, Gerbens-Leenes PW, Hoekstra AY. The consumptive water footprint of electricity and heat: a global assessment. Environ Sci Water Res Technol 2015;1:285–97. doi:10.1039/C5EW00026B.

[136] Rotunno P, Lanzini A, Leone P. Energy and economic analysis of a water scrubbing based biogas upgrading process for biomethane injection into the gas grid or use as transportation fuel. Renew Energy 2017;102:417–32. doi:10.1016/j.renene.2016.10.062.

[137] Pimentel D, Pimentel M. Sustainability of meat-based and plant-based diets and the. Am J Clin Nutr 2003;78:660–3. doi:10.1093/ajcn/78.3.660S.

[138] Carbon Footprint Ltd. Country specific electricity grid greenhouse gas emission factors. 2019.

[139] Thi Nguyen ML, Lin CY, Lay CH. Microalgae cultivation using biogas and digestate carbon sources. Biomass and Bioenergy 2019;122:426–32. doi:10.1016/j.biombioe.2019.01.050.

[140] El-Kassas HY, Heneash AMM, Hussein NR. Cultivation of *Arthrospira* (*Spirulina*) *platensis* using confectionary wastes for aquaculture feeding. J Genet Eng Biotechnol 2015;13:145–55. doi:10.1016/j.jgeb.2015.08.003.

[141] van der Spiegel M, Noordam MY, van der Fels-Klerx HJ. Safety of novel protein sources (insects, microalgae, seaweed, duckweed, and rapeseed) and legislative aspects for their application in food and feed production. Compr Rev Food Sci Food Saf 2013;12:662–78. doi:10.1111/1541-4337.12032.

[142] Amazon. Amazon UK cost for Sodium Bicarbonate 2021. https://www.amazon.co.uk/s?k=sodium+bicarbonate&crid=19LI9D0ILT1A2&currency=EUR&sprefix=sodium+bic%2Caps%2C155&ref=nb_sb_ss_ts-doa-p_1_10 (accessed June 20, 2021).

[143] Benemann JR, Woertz I, Lundquist T. Autotrophic microalgae biomass production: From niche markets to commodities 1 1. Ind Biotechnol 2018;14:3–10. doi:10.1089/ind.2018.29118.jrb.

[144] Glanbia Ingredients. Sulphate of Ammonia 1.25kg n.d. https://www.glanbiaconnect.com/shop/product/Sulphate-of-Ammonia-1-25kg/9087158 (accessed June 16, 2021).

[145] International Energy Agency (IEA). Waste disposal costs and share of EfW in selected countries 2020. https://www.iea.org/data-and-statistics/charts/waste-disposal-costs-and-share-of-efw-in-selected-countries (accessed May 18, 2021).

[146] Ritchie H, Roser M. Environmental impacts of food production. Our World Data 2020. https://ourworldindata.org/environmental-impacts-of-food.

[147] Mekonnen MM, Hoekstra AY. The water footprint of livestock and livestock products. vol. 2. Delft: 2010.

[148] Streppel MT, Sluik D, Yperen JF Van, Geelen A, Hofman A, Franco OH, et al. Nutrient-rich foods, cardiovascular diseases and all-cause mortality : the Rotterdam study. Eur J Clin Nutr 2014;68:741–7. doi:10.1038/ejcn.2014.35.

[149] Hess JM, Slavin JL. Healthy snacks : Using nutrient profiling to evaluate the nutrient-density of common snacks in the United States. J Food Sci 2017;00:1–8. doi:10.1111/1750-3841.13819.

[150] Engineering Toolbox. Gases-Densities 2003. https://www.engineeringtoolbox.com/gas-density-d_158.html (accessed June 1, 2021).

8 A profitable low carbon process to co-produce biomethane, food and biofertiliser

A profitable low carbon process to co-produce biomethane, food and biofertiliser

Archishman Bose[a,b], Richard O'Shea[a,b], Richen Lin[a,b], Aoife Long[a,b], Karthik Rajendran[c], David Wall[a,b], Sudipta De[d], Jerry D Murphy[a,b*]

[a] MaREI Centre, Environmental Research Institute, University College Cork, T23 XE10, Ireland

[b] Department of Civil, Structural and Environmental Engineering, School of Engineering and Architecture, University College Cork, T12 K8AF, Ireland.

[c] Department of Environmental Science, SRM University-AP, Andhra Pradesh, 522 240, India

[d] Department of Mechanical Engineering, Jadavpur University, West Bengal, 700 032, India

Abstract

Biomethane from anaerobic digestion of agricultural feedstock is a versatile energy vector for decarbonising agriculture, heavy transport and heat. To lower costs and increase the emission-saving potential, photosynthetic biogas upgrading, cogenerating microalgae with biomethane is currently under research. Although considerable focus has been given to advancing the upgrading technology, a detailed enviro-economic assessment of the complete process is a significant gap in the literature. Accordingly, in a first-of-its-kind work, this paper reports the enviro-economic performance and the marginal (CO_2) abatement cost (MAC) of a polygeneration plant co-producing energy (biomethane), food (*Spirulina* powder) and bio-fertiliser (digestate) from agricultural feedstock using photosynthetic biogas upgrading. Unlike at medium and small scale, the process was shown to be profitable (net present value > 0) at an industrial scale (3 MW biomethane) while selling biomethane at the price of natural gas (3 c€/kWh). The OPEX, including the cost of the *Spirulina* cultivation medium and the plant capacity factor had the highest influence on its profitability. Replacing beef as a complete food with *Spirulina* powder maximised the emission savings rather than replacing beef protein with *Spirulina* protein. A negative MAC at the industrial scale highlighted the enviro-economic benefit as a low carbon technology over conventional biomethane production

processes. Using economic allocation as opposed to energy allocation, each co-product generated low levels of specific GHG emissions while showing cost-competitiveness with market-available alternatives. Trading of biomethane in the EU emission trading scheme should allow financial viability of smaller scale processes by 2030.

8.1 Introduction

Decarbonising hard to abate sectors (such as food processing and agricultural sectors [1,2] and the heavy transport sector [3]), heavily reliant on fossil fuel and difficult to electrify is crucial to tackle climate change. Renewable biomethane produced by upgrading biogas from the anaerobic digestion (AD) of biodegradable materials is an effective substitute for fossil natural gas [4]. Biomethane produced from the AD of food and agricultural residues could therefore potentially decarbonise heat, haulage and heavy machinery (such as tractors and excavators) [5–7] while also reducing the carbon footprint of the food and agriculture sectors [1,2,4,6]. Digestate, the residue of AD could further add to the sustainability of these systems by its use as a low carbon biofertiliser [5] or for the production of biochar in advanced energy systems [5,8].

Current state-of-the-art physicochemical biogas upgrading techniques are, however, costly and energy-intensive [9]. This lowers the emission reduction potential of biomethane from AD and often requires incentivisation for its financial viability. For example, biomethane from the co-digestion of grass silage and cattle slurry upgraded using amine scrubbing was found to have a net GHG emission reduction of 63% when substituting natural gas; this is lower than the EU mandated decrease of 65% and 80% by replacing natural gas in transport and heat respectively [10]. In other works, Rajendran et al. (2019a and 2019b) [11,12] concluded that current biomethane production would not be economically viable without subsidy or other incentives to the scale given to other renewable technologies especially, electric vehicles.

To overcome the energetic and economic challenges of conventional biogas upgrading technologies, the two-step bubble column-photobioreactor photosynthetic biogas upgrading is currently a topic of research [13,14]. In this process, CO_2 and H_2S in biogas are first removed by absorption (Eq. 8.1 and Eq. 8.2 respectively) in a carbonate-rich, high pH alkaline microalgal medium within a bubble column [15,16]. Following this, the absorbed CO_2 in the form of bicarbonates is used as the carbon source by the microalgae [13,14] while also regenerating carbonates (Eq. 8.3), establishing a functional carbonate-bicarbonate cycle [15]. At a pH above 9, and in the presence of abundant dissolved oxygen, the absorbed H_2S (NaHS) is converted into sulphates (Eq. 8.4) providing a fraction of the necessary sulphates required for

microalgae growth [17]. Due to the cogeneration of microalgae with biomethane, the process economics could potentially improve, while also reducing energy consumption and GHG emissions associated with biogas upgrading [18].

$$CO_2 + H_2O + CO_3^{2-} \rightarrow 2HCO_3^- \quad (8.1)$$

$$H_2S + Na_2CO_3 = NaHS + NaHCO_3 \quad (8.2)$$

$$\left\{ \begin{array}{l} HCO_3^- \xrightarrow{Algae} CO_2 + OH^- \\ HCO_3^- + OH^- \xrightarrow{Medium} CO_3^{2-} + H_2O \end{array} \right\} \quad (8.3)$$

$$Na_2CO_3 + NaHS + 2O_2 = Na_2SO_4 + NaHCO_3 \quad (8.4)$$

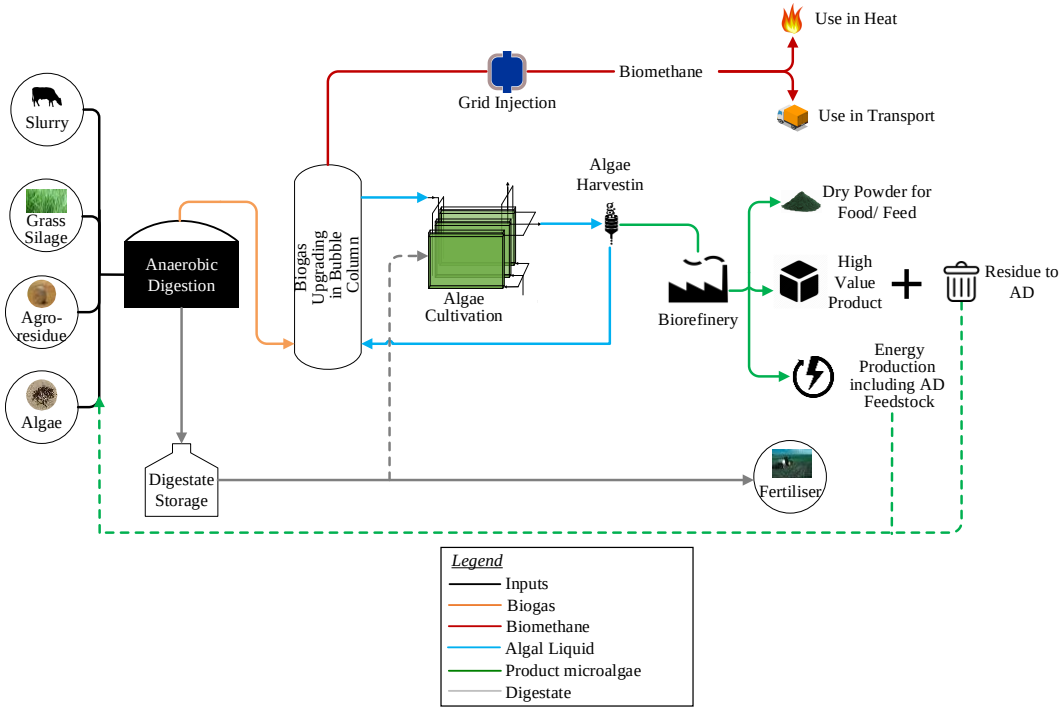


Figure 8-1 Concept layout of cascading biomethane-biorefinery with agricultural feedstock using anaerobic digestion and photosynthetic biogas upgrading.

Due to significant variation in reported results, photosynthetic biogas upgrading is still at a low Technology Readiness Level (TRL). However, recent advances have shown promising results in both laboratory [19–21] and semi-industrial scale experiments [22]. Microalgae species capable of rapid and efficient CO_2 uptake under alkaline conditions such as *Spirulina platensis* have also been identified for their suitability in photosynthetic biogas upgrading [15]. A perspective on a cascading polygeneration system by suitably combining biomethane production with microalgae

biorefinery (Figure 8-1) was also developed by Bose et al. (2020) [14]. The possibility to maximise economic and environmental benefits from biomethane generation by suitably selecting microalgae bio-products and the corresponding conversion pathways was shown. However, no detailed techno-economic or environmental assessment of such systems has as yet been reported in the literature. Toledo-Cervantes et al. (2017) [18], calculated the economic and environmental performance of the photosynthetic biogas upgrading step including for microalgae cultivation and harvesting sections only. As such a detailed enviro-economic assessment of the complete polygeneration system to assess the viability of such systems is a significant gap in the literature.

The present paper, in a first-of-its-kind work, details the profitability and the enviro-economic performance of a polygeneration plant co-producing energy (biomethane), food (*Spirulina* powder) and biofertiliser (digestate) from agricultural feedstock using photosynthetic biogas upgrading. The economic performance of the plant was assessed using a techno-economic assessment (TEA) [23]. The overall GHG emissions were evaluated using the methodology outlined in the EU Renewable Energy Directive (Recast) (RED-II) [24] with modifications for the inclusion of digestate as a sellable by-product [25]. Product-specific costs and emissions were obtained by either the energy allocation (suggested by RED-II) [24] or the economic allocation [25] methods. Combining the economic and environmental outcomes, the levelised cost of carbon abatement (LCOA), also known as marginal (CO_2) abatement cost (MAC) [26,27] was evaluated. The impact of scale, the type of product being replaced, the composition of feedstock to the AD plant and the allocation strategy were studied simultaneously through multiple scenarios and sensitivity and uncertainty assessments. Accordingly, the novelty of the work provided herein offers vital knowledge regarding the enviro-economic benefits of photosynthetic biogas upgrading based AD systems. The results would also indicate the need for incentives and subsidies to accelerate the TRL of photosynthetic biogas upgrading [26]. Accordingly, the following four key questions were raised and answered:

1. Does scale impact the profitability of the polygeneration process?

2. Are the co-products cost-competitive with market-available alternatives?

3. How can the GHG abatement potential of the plant be maximised?

4. How does the plant's LCOA/MAC compare with other renewable technologies?

8.2 Methods

8.2.1 Feedstock, resources and process outputs

The polygeneration plant was modelled as situated in Ireland, a country in the northwest of Europe with a temperate oceanic climate. It experiences a favourable climate for agriculture and is also representative of other regions globally including most of north-western Europe, Japan, the Pacific Northwest of America (including states of Washington and Idaho and parts of northern California), parts of southern America (coastal regions of Chile and Argentina), south-eastern parts of Australia (Victoria and Tasmania) and New-Zealand. In addition, the ease of access to data was also a priority factor while selecting the study location.

Table 8-1 Characteristics of co-digestion substrates used in this study along with their respective costs as adapted from [~~10,~~28–33]

Description	Grass	Slurry
Chemical formula	$C_{28.4}H_{44.5}O_{17.7}N$	$C_{22}H_{34.8}O_{9.7}N_{1.7}S_{0.06}$
Moisture content when harvested [% FW[a]]	82	-
Moisture content at plant [% FW[a]]	70	91.2
Dry solids (DS) [%]	30	8.8
Volatile solids [%DS]	93.3	76.1
C:N ratio	24:1	13:1
Cost of procurement [€/tonne]	27	4 (transport costs only)

[a] *FW: fresh weight*

The co-digestion of cattle slurry and grass silage produced from first cut perennial ryegrass (the two most abundant agricultural feedstocks within the studied zone) were selected to maximise the generality of the results [34,35]. The detailed composition of grass silage and cattle slurry, together with their procurement costs are compiled in Table 7-1. Besides grass silage and slurry, the other major inputs to the system included sodium carbonate and sodium bicarbonate for the carbonate-bicarbonate buffer, Zarrouk's media as the nutrient media for *Spirulina platensis* [36],

makeup water, electricity from the grid and heat as natural gas Table 7-2. A small quantity of sulphuric acid was also required for ammonia scrubbing [37].

Table 8-2 Summary of the major inputs to the process and their corresponding costs

Component	Unit Cost	Reference
Grass silage	27 €/tonne*	Rajendran et al. (2019) [12]
Cattle slurry (Transport costs only)	4 €/tonne*	
Sodium carbonate	184 €/tonne*	Hyun et al. (2018) [38]
Sodium bicarbonate (commercial grade)†	234 €/tonne*	Lee et al. (2019) [39]
Zarrouk's media (without sodium bicarbonate)	2,653 €/tonne	See *Box S8.1*
Sulphuric Acid	100 €/tonne	Adapted from Hemphill (2020) [40]
Water	1.21 €/m^3 (Large-scale**)	Adapted from CRU (2019) [41]
	1.3 €/m^3 (Medium-scale**)	
	1.87 €/m^3 (Small-scale**)	
Air	-	
Electricity	12.5 c€/kWh	Adapted from Eurostat (2021) [42]
Natural gas for heating	3 c€/kWh	Rajendran et al. (2019) [12]

*USD to Euro conversion factor was selected as 0.8

† Commercial grade Sodium bicarbonate was found to suitably replace costly lab-grade sodium bicarbonate [43,44]

**For the definition of scales, refer to Section 8.2.2.2.

Biomethane and *Spirulina* powder as a protein supplement for human consumption are the modelled process outputs. Digestate from AD was a major by-product from the process, available to be sold as a biofertiliser. Minor quantities of ammonium sulphate were also generated during ammonia scrubbing. The wastewater from microalgae harvesting and processing was the only effluent from the system. Based on the plant scale (discussed in Section 8.2.3), the wastewater was either directly disposed of at a cost to the plant or was treated in an in-house on-site wastewater treatment plant. For an on-site wastewater treatment facility, the treated water was recycled and the nitrogen-depleted sludge following drying was sent for end-of-life treatments at 100 €/tonne [45]. The outputs and effluents from the proposed process are summarised in Table S8-1.

8.2.2 Process description

The proposed polygeneration plant has been divided into several sections, the conceptual layout of which is shown in Figure 8-2. A mesophilic (37°C) anaerobic co-digestion of grass silage and cattle slurry generated biogas in the *anaerobic digestion section*. Grass silage was shredded in a shredder and the cattle slurry was pasteurised before AD [46,47]. Two digesters in series provided the optimal configuration for biogas generation [12,28]. The biogas was compressed and stored in a biogas buffer tank to provide a constant gas flow for biogas upgrading. The digestate was stored in a lagoon and distributed for use as a fertiliser. The biogas was upgraded in one or more co-current bubble column reactors based on the biogas flow rate in the *biogas upgrading section*. As the biogas would be in direct contact with the microalgae cultivation media, antibacterial filters [48] were provided to condition the biogas before upgrading. Post upgrading, biomethane was further conditioned through sulphuric acid scrubbing for ammonia removal and dehumidification before being compressed and transported via pipelines for gas grid injection.

Microalgae were cultivated in the bicarbonate-rich medium exiting the bubble column in the *microalgae cultivation section*. Before entering the main cultivation unit, the medium was adjusted for nutrients and initial microalgae concentration to allow uniform cultivation conditions in each cycle. The entire cultivation unit including the inoculum reactor and the harvesting facility were housed within a greenhouse maintained at 25 °C to allow yearlong cultivation of microalgae and requiring 800 MJ/m^2/year of heat [49]. Inclined screens and rotary vacuum filters respectively harvested and concentrated [50] the cultivated microalgae in the *microalgae harvesting and processing section*. The concentrated microalgae were then washed, milled and dried to produce powdered food-grade *Spirulina* [51]. The harvested algal media thus formed the recirculation media. However, before being pumped to the bubble column, it was adjusted with makeup water at a specific pH and alkalinity in the *recirculation adjustment section* to continue the carbonate-bicarbonate cycle.

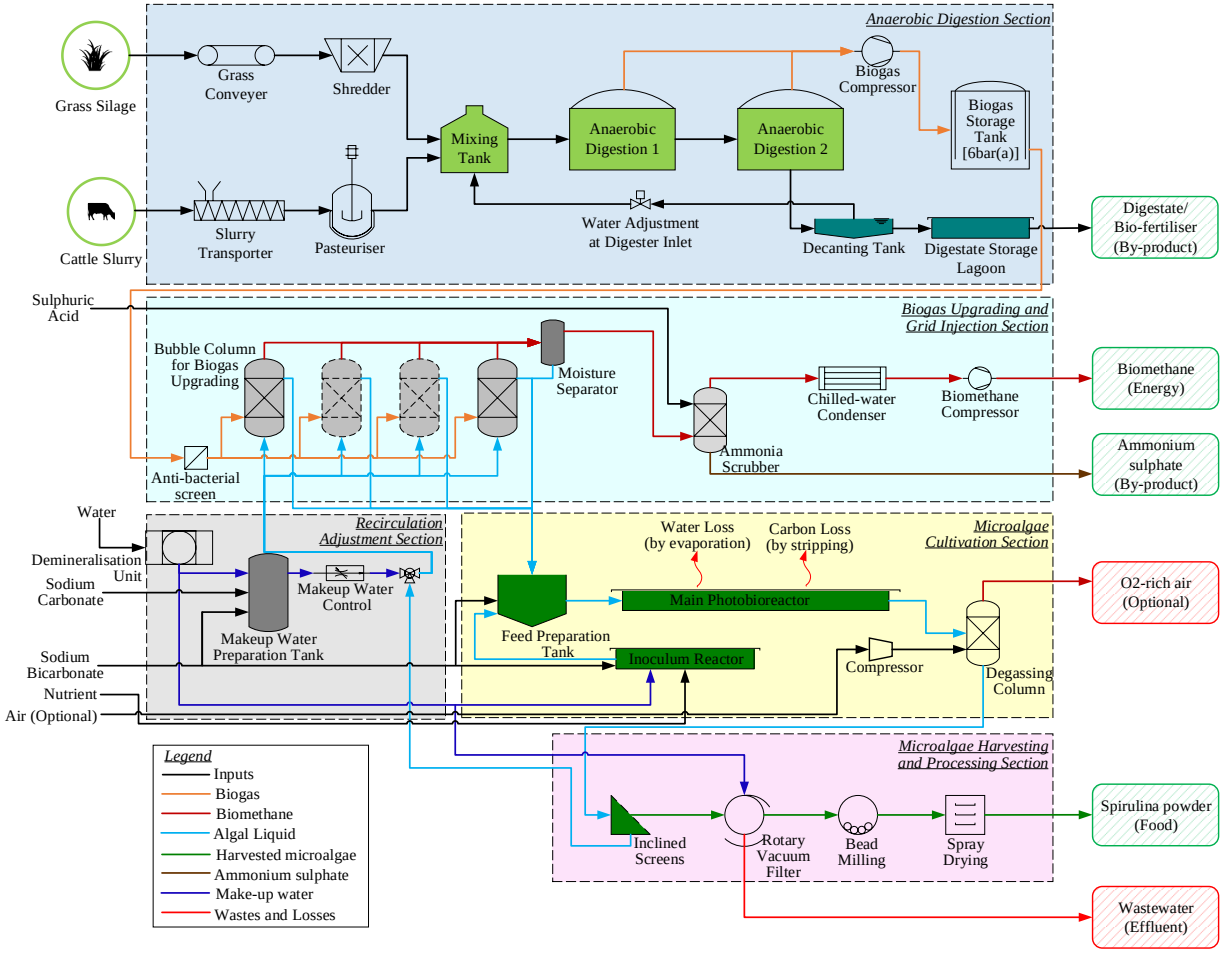


Figure 8-2 General process flow diagram of biomethane and dietary protein production as food-grade Spirulina platensis using agricultural feedstock and photosynthetic biogas upgrading

The biogas production and the methane content were estimated assuming an organic loading rate (OLR) of 3.5 kgVS/m^3/day and using the results and recommendations of Wall et al. (2014) [52] and Vo et al. (2018) [28]. The concentration of H_2S and ammonia impurities within the biogas were assumed at 200 ppm respectively. Co-current bubble columns upgraded the biogas at a liquid to gas flow (L/G) ratio of 0.6. During upgrading, a maximum of 100% CO_2 and H_2S removal was assumed based on previous works by Bose et al. (2021) [21] and Meier et al. (2018) [17] respectively. Microalgae production was estimated as per Eq. 8.5 assuming a *Spirulina platensis* composition of $C_{20}H_{34.8}O_{7.8}N_{3.7}S_{0.1}$ [53] (molecular mass 22.72). The Zarrouk's media and spent salts were adjusted before and after the cultivation of algae (Eq. 8.5) respectively to achieve the required mass balance. The efficiency of microalgae harvesting was adjusted to ensure an algal concentration between 0.08 and 0.09 gDW/L in the recirculation medium. Makeup water was supplied at a constant pH and alkalinity of 10.2 and 1.5 g-Inorganic Carbon (IC)/L respectively by adjusting the input amounts of sodium carbonate and bicarbonate. The process model developed using SuperPro Designer, together with necessary assumptions have been detailed previously in Chapter 7 and are hence not repeated.

$$2NaHCO_3 \xrightarrow{\text{Zarrouk's Medium}} Na_2CO_3 + \text{Spirulina} + 1.24O_2 + 0.13H_2O + \text{Salts} \qquad (8.5)$$

8.2.3 Scenarios for process assessment

Fifteen different scenarios were selected to study the enviro-economic benefits of the plant and its co-products. To assess the feasibility of producing biomethane in the absence of financial incentives, subsidies, or feed-in tariffs, or increased purchase price of natural gas to the customer, biomethane was modelled as sold to the gas grid at 3 c€/kWh, the same price as that of natural gas. However, cognizant of the financial benefits in place for biomethane in most advanced economies, a sensitivity analysis was later conducted to study the influence of the biomethane price on the process feasibility and economics (Section 8.3.5). *Spirulina* powder and digestate were sold at the plant gate at 10 €/kg [54,55] and 4 €/tonne [56] respectively.

Table 8-3 Description of the scenarios assessed towards studying the techno-economic and the LCOA (MAC) of the polygeneration system coproducing biomethane and Spirulina powder as a protein supplement.

Scenario Code*	Scenario Description	Specific Assumptions/ Considerations
82IBP	Base Case Scenario with 80% grass and 20% slurry on a VS basis at industrial-scale considering benefits of beef protein replacement	
82IBF	Base case but replacing beef with *Spirulina* as a complete functional food.	
82MBP	Base case but a medium-scale plant (community-based)	Compiled in Table 8-4
82MBF	Base case but a medium-scale plant with *Spirulina* as a substitute for beef as a complete food	
82SBP	Base case but a Small-scale plant (Farm based)	
82SBF	Base case but a Small-scale plant with *Spirulina* as a substitute of beef as a complete food	
64IBP	Grass: Slurry ratio – 60:40 (VS basis) industrial-scale replacing beef protein	
82IMP	Base case but with *Spirulina* as a substitute for milk protein	
82IMF	Base case but with *Spirulina* as a substitute for milk as a complete food	
82ICP	Base case but with *Spirulina* as a substitute for chicken protein	Same as Base Case Scenario
82ICF	Base case but with *Spirulina* as a substitute for chicken as a complete food	
82ITP	Base case but with *Spirulina* as a substitute for protein from tofu	
82ITF	Base case but with *Spirulina* as a substitute for tofu as a complete food	
82IBP-R	Performance of different feedstock combinations under RED-II framework	Digestate was not accounted as a process output and energy allocation was used for all assessments
64IBP-R		

* The first two digits indicate the grass: slurry ratio in the feedstock (VS basis), divided by 10 (e.g., 8 implies 80% grass content in the AD feedstock); the second letter indicates the scale of the system (I – Industrial, M - medium and S - small); the third letter indicates the type of protein replaced (B – beef, M - milk, C – chicken and T- tofu); the fourth letter stands for the type of food replaced (P – protein only F – complete food replacement); - R represents the scenarios considering RED-II recommendations.

The influence of the process scalability was studied using scenarios 82IBP, 82MBP and 82SBP and 82IBF, 82MBF and 82SBF, as described in Table 8-3. For the base case scenario (82IBP), an industrial-scale plant was assumed, handling

around 1,000 kg-volatile solid (VS)/hr (power rating c. 3MW of biomethane output). *Spirulina* was assumed as a replacement of protein from beef. As compiled in Table 8-4, the AD feedstock, grass silage and cattle slurry were obtained from within 10.5 km and 6.4 km radii respectively [57]. An 80:20 grass and slurry mix (VS basis) was considered [58]. Biogas was upgraded in 50 m^3 bubble columns at a liquid to gas flow (L/G) ratio of 0.6 [59]. The number of columns was estimated considering the superficial gas velocity of 0.6 cm/s [59] and an inlet gas pressure of 2 bars to account for pressure drop in the bubble column and subsequent downstream processes. The upgraded biomethane was injected into the high-pressure transmission grid at 65 bar(absolute), located 2 km off-site. Although a flat plate PBR would require less space and provide several operational benefits [15], an open pond PBR was considered due to its lower costs [60] and proven scalability [61]. Demineralised water for process and utility purposes was supplied by an on-site demineralisation plant. A wastewater treatment plant also operated under the scope of the proposed plant removing 100% of the undissolved solids and 20% of the dissolved salts. The exiting sludge comprising 20% solids [62] was dried to 60% solids content using natural gas before being subjected to end of life treatment, 50 km off-site. Although the medium (82MBP) and small-scale (82SBP) scenarios were similar in layout (Table 8-3), no wastewater treatment or sludge drying facility were considered for these scales of production (Table 8-4). For these scales, wastewater was disposed of at a cost to the plant to be treated at a centralised wastewater treatment facility.

The LCOA/MAC of each scenario was estimated by replacing natural gas with biomethane, beef protein with *Spirulina* protein and inorganic nitrogenous fertiliser with digestate (refer Section 8.2.5). To understand the impact of the replacement of beef with *Spirulina* as a complete food, scenarios 82IBF, 82MBF and 82SBF were used (Table 8-3). The nutrient-rich food index $NRF_{9.3}$ was adopted, which comprises 12 essential micro and macronutrients in the daily diet of a typical human adult [63,64]. Accordingly, the equation to estimate NDS per 100 kcal of energy from *Spirulina* powder was given by Eq. 8.6 [65] where, N_{sp_i} is the content of the i^{th} nutrient within 100 kcal of edible fraction. The amount of each nutrient in *Spirulina platensis* powder, together with their corresponding recommended daily values (RDV) and maximum daily values (MDV) necessary for this calculation are compiled in Table S8-2. Based on these values, the $NDS_{NRF9.3}$ score of *Spirulina* was obtained as 191.8,

much higher than the $NDS_{NRF9.3}$ values of conventional sources of protein such as beef, milk or chicken (Table S8-3).

$$NDS_{NRF9.3} = \left(\sum_{i=1}^{9} \frac{N_{sp_i}}{RDV_i} - \sum_{i=1}^{3} \frac{N_{sp_i}}{MDV_i} \right) \times 100 \quad (8.6)$$

Table 8-4 Values of process variables assumed for different scenarios. † Similar assumptions to be used for scenarios 82IBF, 82IMP, 82IMF, 82ICP, 82ICF, 82ITP, 82ITF, 82IBP-R and 64IBP-R

Description	**Unit**	**Values**		
		Scenarios 82IBP, 64IBP †	**Scenarios 82MBP, 82MBF**	**Scenarios 82SBP, 82SBF**
Grass: Slurry Ratio	Volatile solids basis		80:20	
Volatile solids (VS) input	kgVS/hr[a]	1,000	100	10
Grass silage input	t-FW/hr[b]	3/2.37[¥]	0.3	0.03
Cattle slurry input	t-FW/hr	3.13/6.65[¥]	0.313	0.0313
Grass silage procurement radius	km	10.5 [57]	4[**]	1[**]
Cattle slurry procurement radius	km	6.4 [57]	3[**]	1[**]
Organic loading rate (OLR)	$kgVS/m^3/day$		3.5 [58]	
Hydraulic Retention Time (1st digester)	days		30	
Hydraulic Retention Time (2nd digester)	days		20	
Pressure of biogas storage	bar (absolute)		6	
Digestate holding capacity	months		6 [66]	
Inlet pressure of biogas to bubble column	bar (absolute)		2	
Liquid to gas flow (L/G) ratio	-		0.6 [59]	
Superficial gas velocity	cm/s		0.6 [59]	
Bubble Column Volume	m^3	50	5	1
Bubble Column height to diameter ratio	-		5	
Bubble Column diameter	m	2.34	1.08	0.63
Bubble Column height	m	11.68	5.42	3.17
Grid Injection pressure	Bar (absolute)	65	4	4
Distance of grid from site	km	2	1	1
Type of pipe for transmission	-		Stainless steel	
Type of photobioreactor	-		Open Pond housed within a greenhouse	
Dimension of each module of open pond photobioreactor	m	250*20*0.3	25*2*0.3	

Covered area by the greenhouse	m^2	1.43 times the area of the open pond modules (adopted from Clippinger and Davis (2019) [67])		
Annual heat requirement of the greenhouse	$MJ/m^2/year$	800 [49]		
Algal productivity	gDW/L/day[c]	0.15 [68]		
Algal concentration in the recirculation medium	gDW/L	0.08-0.09		
pH of make-up water	-	10.2		
Alkalinity of make-up water	g-IC/L[d]	1.5		
Digestate distribution	km (radius)	10.5*	4*	1*
Distance travelled by chemicals during procurement	km	500		
Emission allocations	-	Economic allocation (revenue basis)***		
Wastewater treatment	-	Included	Disposed at cost	
Sludge disposal	-	Disposed by plant	Not applicable	
Cooling tower type	-	Wet Industrial	Small cooling towers	
Chillers	-	Included		
Demineralisation unit	-	Included		
Steam generator	-	Included		

*assumed to be distributed to the fields from where the grass is procured; **assumed values as per scale

***for scenarios 82IBP-R and 64IBP-R, energy allocation was used.

[a] t-FW: tonne fresh weight; [b] VS: Volatile solid; [c] DW: Dry weight; [d] IC: Inorganic Carbon

¥ Value of feedstock the 64IBP and 64IBP-R scenarios

To evaluate the impact of altering the feedstock mix on the enviro-economic performance of the system, the 64IBP scenario was defined by using a grass silage and cattle slurry feed ratio of 60:40 (VS basis) [58], all other factors being constant. The impacts of the type of protein replaced were studied using scenarios 82IMP, 82ICP and 82ITP respectively (Table 8-3). While milk and chicken are widely consumed animal-based proteins [69,70], tofu is being increasingly consumed as an effective plant-based protein alternative [71]. Accordingly, scenarios 82IMF, 82ICF and 82ITF were used to evaluate the effect of complete replacement of milk, chicken and tofu respectively as functional food using the corresponding $NRF_{9.3}$ scores (Table S8-3). Finally, scenarios 82IBP-R and 64IBP-R used RED-II guidelines which omits digestate from both the economic and environmental considerations (Table 8-3). All corresponding allocations were based on the energy content in the products. For this, the energy content in methane and *Spirulina* powder were assumed as 50 MJ/kg [72]

and 17 MJ/kg respectively [73]. Further details of the specific inputs, constants and constraints of each scenario are compiled in Table 8-4.

8.2.4 Economic analysis

8.2.4.1 Total capital expenditure (CAPEX)

In this work, a bottom-up approach for technoeconomic analysis was adopted [74,75]. Preference was given to obtain the bare erected costs of each module (BEC) from the literature. When not available, the bare module cost (BMC) was used. All the reference costs were converted to 2020 Euro value ($BMC_{i,2020,ref}$ or $BEC_{i,2020,ref}$) wherever necessary using the SuperPro economic module. Each cost was scaled to the actual value using a scaling factor (M) according to Eq. 8.7 and Eq. 8.8 for the bare module costs and the bare erected costs respectively [76].

$$BMC_i = BMC_{i,2020,ref}\left(\frac{J_i}{J_{ref}}\right)^M \quad (8.7)$$

$$EMC_i = EMC_{i,2020,ref}\left(\frac{J_i}{J_{ref}}\right)^M \quad (8.8)$$

where BMC_i and BEC_i represent the bare module cost or the bare erected cost of the actual equipment having a capacity J_i. J_{ref} represents the capacity of the reference equipment. The scaled erected costs for each bare module was then obtained by assuming an additional 49% of the BMC_i for its erection, steel structuring and painting [77]. In case of non-availability of data, the bare module costs available in the SuperPro designer was used. The reference cost of each piece of equipment, together with its corresponding reference size, reference year and the scaling factor is compiled in Table 8-5.

Table 8-5 Reference capital cost of each equipment included in the model of the proposed polygeneration plant.

Section included in	Equipment	Cost type	Reference unit	Reference size	Reference price	Reference year	Scaling factor	Reference	Scenarios included in
Anaerobic Digestion Section	Grass silage & Cattle slurry reception infrastructure	Bare Module Cost	tonne-substrate/day	1	1,284 €	2017	1	Dennehy et al. (2017) [66]	All
	Grass shredder		tonne-grass/day	3	18,000 €	2020	N/A	SuperPro Cost Model	
	Pasteurizer and pasteurizer heat exchangers		tonne/day	1	2,125 €	2017	1	Dennehy et al. (2017) [66]	
	Manure pipework and pumps		ad-hoc	1	8,000 €		1	Dennehy et al. (2017) [66]	
	Feed storage tank		m^3-tank volume	1	1,040 €	2019	0.37	Cost from Rajendran et al. (2019) [12]; Scaling Factor from Loh et al. (2002) [78]	
	Digesters (including heat exchangers)		m^3-digester	1	200 €	2017	1	Dennehy et al. (2017) [66]	
	Biogas storage tank		m^3-tank volume	1	56.60 €	2012	0.6	Nolan et al. (2012) [79]	
	Flare		m^3-digester	1,526	5,000 €		0.6	Nolan et al. (2012) [79]	
	Decanter		m^3	1	6,647 €	2019	0.6	Rajendran et al. (2019) [12]	

Section included in	Equipment	Cost type	Reference unit	Reference size	Reference price	Reference year	Scaling factor	Reference	Scenarios included in
Biogas Upgrading Section	Digestate storage lagoon		m^3	1510	46,800 €	2017	0.54	Dennehy et al. (2017) [66] Scaling Factor for tanks from Loh et al. (2002) [78]	
	Biogas bacterial screen		number of units	1	1,100 €	2020	1	Flomax (2021) [80]	20 nos. for scenarios S1, S1A, S4-S9; 5 nos. for S2 & S2A; 2 nos. for S3 & S3A.
	Absorption column with all accessories		m^3-column volume	200	350,200 €	2014	0.67	Starr et al. (2015) [81]	
	Moisture separator/ flash chamber		m^3-tank volume	1	3,143 €	2001	0.67	Rotunno et al. (2017) [82]	
	Ammonia scrubber column		Nm^3/h-gas flow	1	250 €	2014	0.67	Starr et al. (2015) [81]	
	Ammonia scrubber packing		Nm^3/h-gas flow	1	250 €	2014	1	Starr et al. (2015) [81]	All
	Biomethane chiller condenser		kW-cooling load	100	103,572 €	1989	0.73	Cost from cesenergy (2010) [83]. Scaling factor from Garret et al. (1989) [84]	
	Biomethane pipeline for grid injection		inch-km	1	151,300 €	2016	1	Fremont Government (2016) [85]	

Section included in	Equipment	Cost type	Reference unit	Reference size	Reference price	Reference year	Scaling factor	Reference	Scenarios included in
Microalgae Cultivation Section	Main cultivation unit including inoculum reactor	Bare erected cost	Acres of cultivation (main)	1	13,791 €	2014	0.85	Clippinger et al. (2019) [67]	
	Field equipment for microalgae cultivation			1	4815 €	2014	0.85		
	Liner for initial installation			1	2,040 €	2014	0.85		
	Greenhouse		m^2-cover area	1	280 €	2019	0.48	Cost from Nupponen (2019) [86]. The scaling factor was calculated from Allied Ltd. (2021) [87]	
Microalgae Harvesting and Processing Section	Inclined screen	Bare module cost	m^3/h-culture flow	401.7	47,000 €	2020	0.185	SuperPro Cost Model	
	Vacuum filter		m^2-filter area	50	240,00 €	2018	0.6	Fasaei et al. (2018) [88]	
	Bead mill		ha of main cultivation	1	60,000 €	2016	0.85	Panis et al. (2016) [89]	
	Spray dryer		ha of main cultivation	1	60,000 €	2016	0.85	Panis et al. (2016) [89]	
Recirculation Adjustment Section	Demineralisation plant		m^3/h-water treated	4.54	80,000 €	2020	0.6	Samco Technologies (2020) [90]	
	Water storage tank		m^3-tank volume	1	1,040 €	2019	0.37	Cost from Rajendran et al. (2019) [12]; Scaling	

Section included in	Equipment	Cost type	Reference unit	Reference size	Reference price	Reference year	Scaling factor	Reference	Scenarios included in
								Factor from Loh et al. (2002) [78]	
	Compressor		Nm^3/h-gas flow	1	462 €		0.93	Carlson et al. (2017) [91]	
	Centrifugal pump		kW_e-motor rating	7.5	8,202 €	2008	0.33	James et al. (2009) [92] & Peters et al. (2003) [93]	
	Air source heat pump		kW_e-rating	1	483 €	2010	0.7	Edberg et al. (2011) [94] & Caduff et al. (2014) [95]	
	Steam generator		kW-heating	100	20,000 €	2002	0.4	Peters et al. (2003) [93]	
Various	Wastewater treatment plant		m^3/h-water flow	7.89	391,850 €	1998	0.4	Foess et al. (1998) [96]	
	Sludge dryer	Bare erected cost	kg/hr-sludge	2000	1.1 M€	2015	0.46	Cost from Murashko et al. (2018) [97]. Scaling factor calculated from Mininni et al. (2000) [98]	S1, S1A, S4-S9
	Cooling tower	Bare module cost	m^3/h-water flow	1	21,543 €	1998	0.2	Adapted from data reported by Loh et al. (2002) [99]	All

The total bare erected cost (TBEC) was obtained as the sum of the erected cost of each unit of the plant with an additional 5% cost considered for all other unaccounted equipment. The total direct plant cost (TDPC) was evaluated by adding 20% of the TBEC towards piping, electrical ancillaries and instrumentation [28] (Eq. 8.7). The engineering, procurement and construction cost (EPCC) was estimated as 15% of TDPC, accounting for the costs of detailed design, contractor permitting and project management services [77]. To this, 10% contingency cost was added to obtain the Total Project Cost (TPC) [66]. To improve the robustness of the financial assessments, the owners' cost and contingencies were assumed to be 15% of the TPC [100] providing the total overnight project cost (TOPC). The procedures used to estimate EPCC, TPC and TOPC are summarised in Eq. 8.9.

$$\begin{aligned} TOPC &= 1.15 \times TPC = 1.15 \times 1.1 \times EPCC \\ &= 1.15 \times 1.1 \times 1.15 \times TDPC \\ &= 1.15 \times 1.1 \times 1.15 \times 1.2 \times TBEC \end{aligned} \quad (8.9)$$

8.2.4.2 Operational expenditure (OPEX)

According to standard practice, the plant operation and maintenance costs (OPEX) were divided between fixed and variable costs [28,101]. The fixed OPEX comprised property tax and insurance as 0.7% of the TOPC [28]; plant annual maintenance cost as 3% of TBEC [28]; additional administrative costs as 1% of TOPC (assumed). To establish a realistic estimate, the labour type and amount were assumed to significantly differ according to plant size [102], as summarised in Table 8-6. The variable operation costs on the other hand comprised the cost of electricity and heat to operate the plant, cost of chemicals, cost of the feedstock, supply water charges and waste disposal costs in terms of the sludge disposal fee or the wastewater disposal charges (Table 7-2 and Table S8-1). An additional cost of 4 €/tonne was considered as transport charges for chemicals and sludge. The water charges were evaluated by determining the total amount of water required in the system as the makeup water, the water added to the inoculum reactor, the water required for washing the harvested microalgae and the water to replenish the lost utility water. Except for the utility water, the remaining water requirements were obtained directly from the SuperPro model. The methodology to estimate the utility water has been previously described in Chapter 7.2.5.3 and hence is not repeated further in this chapter.

Table 8-6 Annual labour costs for each scale of operation

Description	Scenario Scales		
	Industrial	**Medium**	**Small**
Plant operators for microalgae cultivation (annual salary 40,000 €[§])	10	2	1
Plant operator for other facilities (annual salary 40,000 €[§])	8[*]	2	1
Quality control manager (annual salary 36,000 €[§])	2	1	0
Plant supervisor (annual salary 45,000 €[§])	1	0	0
Plant manager (annual salary 75,000 €[§])	1	1	0
Total annual labour charges ('000 €)	912	271	80

[*]2 operators each for anaerobic digestion section, biogas upgrading and biomethane injection section, microalgae processing and for operating other accessory facilities and general plant operations.
[§] Estimated using the online PayScale website [103]

As part of the expenditure, a 12.5% tax on the profit generated was assumed [12]. To repay the debt, an interest of 2% on the TOPC [104] was also considered, assumed to be paid equally over the first 10 years of the project life. Yearly inflation of 2% [105] was added to both the OPEX and the revenues to estimate the year-by-year earnings and expenditures. Further general economic assumptions are compiled in Table 8-7.

Table 8-7 Generalised assumptions for techno-economic analysis

Description	Assumptions
Annual operating hours [hours]	8,000
Project lifetime [years]	20 (after construction and start-up)
Calculation year	2020
Discount Rate [%]	10 (average for biomass facilities [106])
Depreciation	Straight line over plant life [107,108] (20 years)
Depreciation rate [%]	5
Income Tax in profit [%]	12.5 [12]
Debt Ratio [%]	40
Loan Period [years]	10
Interest on debt [%]	2 [104]
Inflation rate (on OPEX and product pricing) [%]	2 [105]
Year-on-year decrease in production [%]	2

8.2.4.3 Economic indicators

The levelised cost (LC_{prod}) was calculated to estimate the "break-even" costs of each co-product [77] as per Eq. 8.10 using the discounted annual production (P_T) of the respective co-product in the year T [109]. For all scenarios except 82IBP-R and 64IBP-R (using RED-II), cost allocation (Alloc) between the products was based on the respective revenues earned between biomethane, *Spirulina* powder and biofertiliser (economic allocation). The levelised cost of biomethane was evaluated per kWh of energy. To estimate the levelised cost of protein, *Spirulina* was assumed to contain 60% protein [110]. The levelised cost of biofertiliser in terms of equivalent nitrogen was estimated assuming 0.39% total nitrogen content in the digestate (wet basis) [52].

$$LC_{prod} = \frac{Alloc \times \sum_{i=1}^{T} \frac{CAPEX_T + OPEX_T}{(1+i)^T}}{\sum_{i=1}^{T} \frac{P_T}{(1+i)^T}} \quad (8.10)$$

The net present value (NPV) was evaluated as the summation of all future positive (revenues) and negative (CAPEX, OPEX and depreciation costs) cash flows discounted over the entire lifetime of the plant [66,74] (Eq. 8.11). Straight-line depreciation of the plant assets was assumed, resulting in a uniform depreciation throughout the 20 years of the project life [107,108]. The internal rate of return (IRR) was assessed to evaluate the discount rate at which the NPV of the project became zero (Eq. 8.12) [111]. The discounted payback period (DPBP) [years] was assessed as the time required by the project to turn its cumulative cash flow from negative to positive. Microsoft Excel 2016 was used to perform all financial assessments.

$$NPV = -TOPC + \sum_{i=1}^{T} \frac{Revenues_T - OPEX_T - Depr_T}{(1+i)^T} \quad (8.11)$$

$$TOPC = \sum_{i=1}^{T} \frac{Revenues_T - OPEX_T - Depr_T}{(1+IRR)^T} \quad (8.12)$$

where T represents the year of plant operation, i represents the discount rate of the plant (Table 8-7) and $Depr_T$ represents the depreciated or salvage value of the pant in its T^{th} year of operation.

8.2.5 LCOA or MAC

As the first step to estimate the LCOA (MAC), the overall GHG emissions of the polygeneration plant (GHG_{plant}) were assessed. The methodology proposed by RED-II for anaerobic co-digestion of feedstock [10] was used, to which a saving of 12 $kgCO_{2\text{-}eq}$/tonne of digestate (e_{dig}) [112] was added (Eq. 8.13) for all scenarios except scenarios 82IBP-R and 64IBP-R. GHG emissions from cultivation of feedstock ($e_{ec,k}$), transport ($e_{td,fs,k}$) and land-use change ($e_{l,k}$), as well as the GHG savings (carbon credits) from their utilisation ($e_{sca,k}$) were evaluated as per the literature (Table 8-8). The emissions from processing (e_p) included both the direct emissions from electricity and heat consumption, as well as those embodied in the chemicals used within the process [10]. Methane losses of 2% (1% each during AD and biogas upgrading) were assumed as process emissions. Additionally, the inorganic carbon losses via stripping from the PBR and through the effluents during harvesting also contributed to the GHG emissions of the plant. No separate emissions from the distribution of products ($e_{td,prod,w}$) were considered, except that for the digestate, which depended on the plant scale (Table 8-4). Irrespective of the scenario, no additional emissions from fuel use (e_u) occurred within the plant. No emissions were saved by carbon capture and storage (e_{ccs}). Bicarbonates, produced during photosynthetic biogas upgrading allowed the replacement of conventional sodium bicarbonate, which is essential to operate a standalone *Spirulina* production facility [110]. Thus, emission savings from carbon capture and replacement (e_{ccr}) were considered as 660 $gCO_{2\text{-}eq}$ (fossil origin) for each kg of conventional $NaHCO_3$ replaced [113]. As details of GHG assessment including evaluation of e_{ccr} and methodology to determine the share of each feedstock (S_k) have been previously detailed in Chapter 7, it is not further elaborated in this chapter.

$$GHG_{plant} = \sum_k S_k \left(e_{ec,k} + e_{td,fs,k} + e_{l,k} - e_{sca,k}\right) + e_p + \sum_j e_{td,prod,w} + e_u - e_{ccs} - e_{ccr} - e_{dig} \quad (8.13)$$

where, k is either grass or slurry and w represents any of biomethane, *Spirulina* powder or digestate.

Table 8-8 Specific emissions under the different emission categories required to evaluate the overall GHG emissions of the proposed polygeneration plant as per the EU Renewable Energy Directive II (Recast) (RED-II)

Emission Category	Emission components	Unit	Value	Comments and Reference
$e_{ec,i}$	Emission from cultivation (grass silage, 70% moisture)	$gCO_{2\text{-}eq}$/tonne-FW[a]	50,948	Adapted from Long and Murphy 2019 [114] assuming 65 t-FW/ha/yr grass yield with 82% moisture content at the time of harvest [115]
	Emission from field N_2O (grass silage, 70% moisture)	$gCO_{2\text{-}eq}$/tonne-FW	41,282	
	Emission from cultivation (Cattle slurry)	$gCO_{2\text{-}eq}$/tonne-FW	0	EU RED (Recast) (2018) [10]
$e_{td,fs,i}$	Distance travelled by truck handling grass silage (both ways)	km	Varied	Based on scenario, compiled in Table 8-3 of the main text
	Distance travelled by truck handling cattle slurry (both ways	km	Varied	O'Shea et al. (2017) [57]
	Specific emissions from a truck	$gCO_{2\text{-}eq}$/tonne-km	50	Dünnebeil and Lambrecht (2012) [116]
$e_{l,i}$	Emissions from land-use change from the cultivation of grass	$gCO_{2\text{-}eq}$/ tonne-FW	0	-
	Emissions from land-use change from cattle slurry	$gCO_{2\text{-}eq}$/ tonne-FW	0	-
$e_{sca,i}$	Emission savings from improved cultivation of grass	$gCO_{2\text{-}eq}$/ tonne-FW	-56,400	Adapted from Korres et al. (2010) [85]
	Emission savings from improved handling of slurry	$gCO_{2\text{-}eq}$/ tonne-FW	-54,000	RED-II [21]
e_p	Specific emissions from electricity	$gCO_{2\text{-}eq}$/kWh	325	Irish electricity grid emission factor for 2019 [117]
	Specific emissions from heat	$gCO_{2\text{-}eq}$/kWh	204	SEAI (2020) [118]
	Specific emissions from methane loss	$gCO_{2\text{-}eq}/gCH_4$	25	RED-II [10]
	Specific emissions from Sodium carbonate	$gCO_{2\text{-}eq}$/kg	300	Adapted from Bonfim-Rocha et al. (2020) [119]
	Specific emissions from Sodium bicarbonate	$gCO_{2\text{-}eq}$/kg	660	Bonfim-Rocha et al. (2020) [119] & Barsoumian (2013) [120]
	Specific emissions from Zarrouk's medium (without sodium bicarbonate)	$gCO_{2\text{-}eq}$/kg	566	Adapted from Frank et al. (2011) [121]
	Specific emissions from CO_2 stripping	$gCO_{2\text{-}eq}/gCO_2$	1	-

Emission Category	Emission components	Unit	Value	Comments and Reference
	Specific emissions from sludge	$gCO_{2\text{-eq}}$/kg	0	No emission assumed from nitrogen replete wastewater sludge
	Distance travelled by truck for sludge disposal (both ways)	km	100	Distances based on scenario, compiled in Table 8-4
	Emissions from the transport of biomethane	$gCO_{2\text{-eq}}$/MJ-biomethane	-	Included as emissions during biomethane compression
$e_{td,prod,j}$	Emissions from the transport of *Spirulina* powder	$gCO_{2\text{-eq}}$/kg-Spirulina	0	Assumed at the gate as per system boundary definition
	Distance travelled by truck for distributing digestate (both ways)	km	Varied	Based on scenario, compiled in Table 8-3 of the main text
e_u	Emissions from fuel use	$gCO_{2\text{-eq}}/MJ_{product}$	0	-
e_{ccs}	Emission savings from carbon capture and storage	$gCO_{2\text{-eq}}/MJ_{product}$	0	-
e_{ccr}	Emission savings from CO_2 capture and replacement	$gCO_{2\text{-eq}}$/kg-$NHCO_3$	-660	Replacing emissions from fossil fuels used in commercial $NaHCO_3$ production [113].
e_{dig}	Emission savings from the application of digestate as a replacement for conventional fertilisers	$kgCO_{2eq}$/tonne	-12	Adapted from Capponi et al. (2012) [112]

The overall GHG emission saving from the polygeneration plant was estimated as the sum of the emissions saved by each of the individual co-products. Accordingly, Table 8-9 provides the commodities and their reference emissions that each of the co-products replaced. The annual GHG emissions saved by *Spirulina* as a complete food replacement ($GHG_{abat,Spirul_{NRF9.3}}$) was estimated using Eq. 8.14, utilising the annual $NRF_{9.3}$ points produced as *Spirulina* ($Spirul_{NRF9.3,yr}$), the reference emissions per $NRF_{9.3}$ score of the protein source replaced ($GHG_{prot_{NRF9.3}}$) and the annual emissions allocated to *Spirulina* ($GHG_{Spirul,yr}$).

$$GHG_{abat,Spirul_{NRF9.3}} = Spirul_{NRF9.3,yr} \times GHG_{prot_{NRF9.3}} - GHG_{Spirul,yr} \quad (8.14)$$

From the net GHG emissions saved by the overall plant (GHG_{abat}), the LCOA (MAC) was evaluated according to Eq. 8.15, using discounted CO_2 savings, as suggested by the IPCC [122]. In congruence to the annual 2% drop in production, a

2% net increase in the specific emission of each co-product year-on-year per year was considered.

$$\text{LCOA (MAC)} = \frac{-\text{NPV}}{\sum_{i=1}^{T} \frac{GHG_{abat}}{(1+i)^T}} \quad (8.15)$$

Table 8-9 Specific emissions from reference components to be replaced by the co-products produced in the proposed polygeneration plant

Reference Product to be replaced	Reference Specific Emissions	Replaced by
Natural gas	56.9 $gCO_{2\text{-}eq}$/MJ [123]	Biomethane
Beef protein†	168.7 $kgCO_{2\text{-}eq}$/kg-protein [124]	*Spirulina* protein
Milk protein	95 $kgCO_{2\text{-}eq}$/kg-protein [124]	
Chicken protein	57 $kgCO_{2\text{-}eq}$/kg-protein [124]	
Tofu protein (Soy protein)	19.8 $kgCO_{2\text{-}eq}$/kg-protein [124]	
Beef as a complete food*	113** $kgCO_{2\text{-}eq}$/1000 $NRF_{9.3}$-points	*Spirulina* (as a complete food)
Milk as a complete food*	12.1** $kgCO_{2\text{-}eq}$/1000 $NRF_{9.3}$-points	
Chicken as a complete food*	13.2** $kgCO_{2\text{-}eq}$/1000 $NRF_{9.3}$-points	
Tofu as a complete food*	1.7** $kgCO_{2\text{-}eq}$/1000 $NRF_{9.3}$-points	
Inorganic nitrogenous fertiliser (production emissions only)	2 $kgCO_{2\text{-}eq}$/kg-N [125]	Digestate

† Beef from retired dairy cows
* Evaluated as $CO_{2\text{-}eq}$ emissions per 1000 $NRF_{9.3}$-points
** Detailed data in Table S8-3

8.2.6 Sensitivity Assessment

Sensitivity assessments were performed to determine the influence of CAPEX, OPEX and other economic assumptions on the NPV, IRR, DPBP, levelised costs and LCOA or MAC. Variations of ± 10% were considered for all sensitivity assessments. Based on the results, Monte Carlo uncertainty assessments with 1,000 iterations were conducted to obtain the most likely value of the LCOA/MAC at the assumed selling prices of the co-products. A triangular distribution was assumed with the base value as the mode and +/- 10% making up the extremities of the distribution. In addition, to study the performance of the process under a more practical scenario, the enviro-economic outcomes of each of the 82IBP, 82MBP and 82SBP scenarios were further evaluated at a biomethane selling price between 4 and 10 c€/kWh.

8.3 Results

8.3.1 Technical analyses

As per Figure 8-3, for the industrial-scale plants with 20% slurry in the feedstock (VS basis), (scenarios 82IBP, 82IBF, 82IMP, 82IMF, 82ICP, 82ICF, 82ITP and 82ITF), 2.89 MNm^3 of grid quality biomethane (95.2% CH_4, 0.7% O_2 1.8% N_2 and 2.3% H_2O) was generated annually (25,536 MWh, *Box S8.2*). Four 50m^3 bubble columns in parallel were required to upgrade the biogas (Table 8-10). Microalgae were cultivated in 12.5 ha of open ponds, yielding almost 2,000 tonnes of *Spirulina* powder each year. The corresponding area under the greenhouse was 17.9 ha. Over 1,570 tonnes of CO_2 was lost by stripping; while 100 m^3 of water was lost by evaporation from the cultivation ponds. Approximately 43,000 tonnes of digestate and 1,650 tonnes of sludge were generated as the major by-product and effluent respectively. Over 12,000 m^3 of fresh water was required each year to operate the plant. As the slurry concentration in the feedstock increased to 40% (VS basis) (scenario 64IBP), due to a lower biogas generation, the annual biomethane and *Spirulina* productions dropped to 2.66 MNm^3 and 1,870 tonnes respectively. Although the number of bubble columns required was the same, the areal footprint of the greenhouse decreased to 17.2 ha. However, the digestate yield increased significantly to over 66,000 tonnes, increasing the volume of the digestate storage (Table 8-10). The medium and small scale plants (scenarios 82MBP (&F) and 82SBP (&F)), fed using 10 and 100 times less feedstock than that of the industrial-scale plant, showed a proportional decrease in the outputs. Accordingly, the number of bubble columns required were two 5-m^3 and one 1-m^3 column respectively. As evident from Table 8-10, only 0.2 ha of land was required to cultivate and harvest microalgae for the small-scale system making the technology technically acceptable for implementation across the scale. The recommended system boundary by RED-II meant that digestate was not accounted as a system output, indicated by the mass balance of scenario 82IBP-R in Figure 8-3.

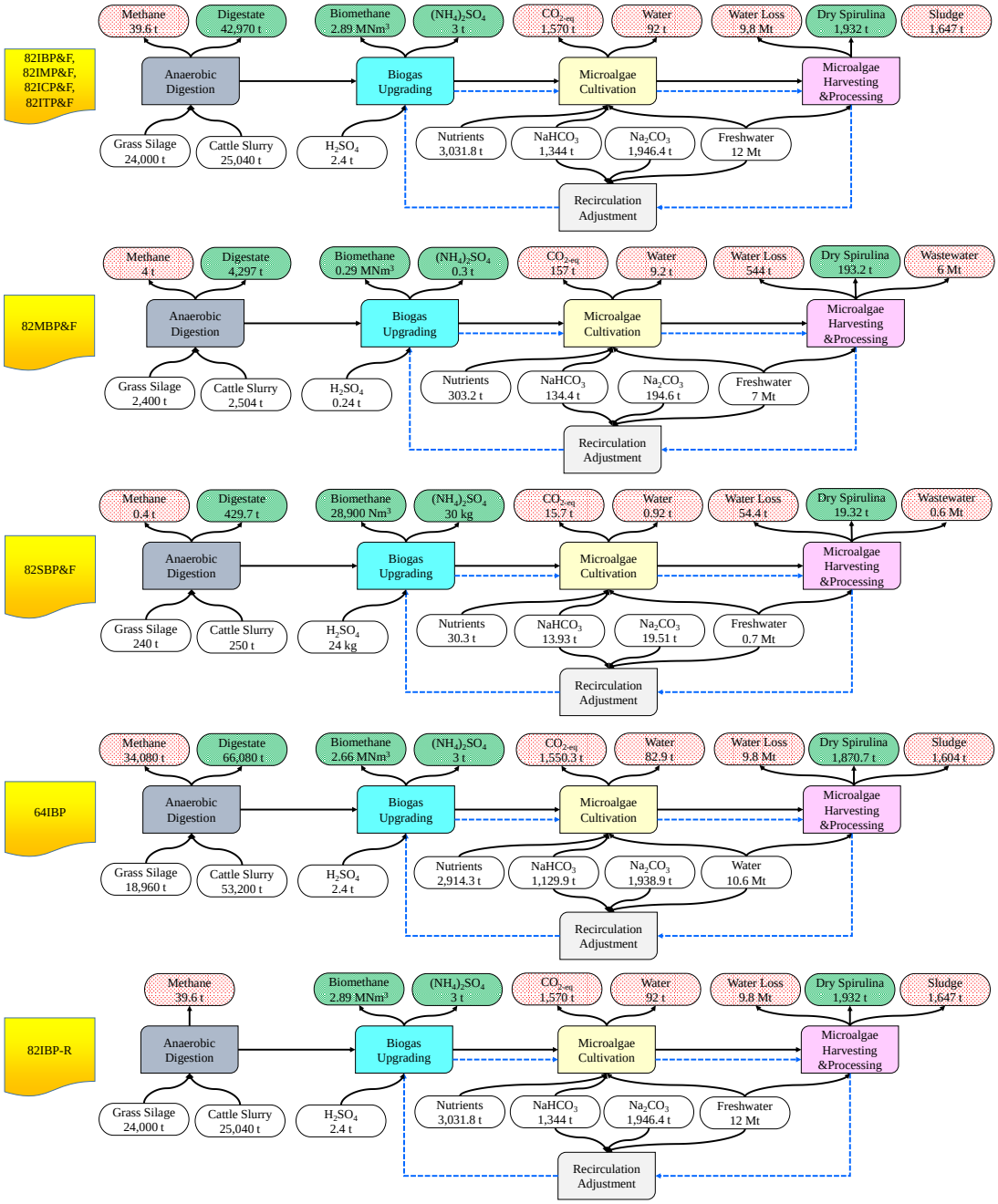


Figure 8-3 Annual mass balances of the polygeneration process under each of the scenarios assessed. Scenario 64IBP-R was not shown, as it is similar to 64IBP without the digestate as per RED-II guidelines.

The electricity and heat demands of each scenario are shown in Figure 8-4. Based on the biogas generated (Table 8-10), the specific energy demand of the 64IBP scenario was the highest, 4.83 kWh/(Nm^3/hr-biogas), just lower than the specific energy yield of biomethane (4.85 kWh/(Nm^3/hr-biogas). In contrast, the specific energy demand of the 82IBP scenario (4.21 kWh/(Nm^3/hr-biogas)), was significantly lower than the energy generated as biomethane (4.76 kWh/(Nm^3/hr-biogas)). The energetic benefits of operating the AD system with a higher grass content in the

feedstock are evident. Due to the absence of the wastewater treatment plant and the sludge drying facility, the medium and small-scale plants (scenarios 82MBP (&F) and 82SBP (&F)) had lower specific energy requirements of 3.79 kWh/(Nm^3/hr-biogas). For these systems, over 85% of the heating demand was for microalgae drying while over 50% of the electricity demand was towards microalgae cultivation. Of the latter, almost 97% was required to heat the greenhouse at a rate of 800 MJ/m^2/yr [49].

Table 8-10 Technical parameters of the polygeneration plant under different scenarios

Technical Characteristics	**Scenario(s)**			
	82IBP&F, 82IMP&F, 82ICP&F, 82ITP&F, 82IBP-R	**82MBP&F**	**82SBP&F**	**64IBP, 64IBP-R**
Hydraulic Retention Time of AD [days]	30 days in AD 1 and 25 days in AD 2			20 days in AD 1 and 15 days in AD 2
Volume of AD reactors [m^3]	AD 1 - 4423.5 AD 2 - 3270	AD 1 – 442.4 AD 2 - 327	AD 1 – 44.2 AD 2 – 32.7	AD 1 - 4423.5 AD 2 - 3270
Hourly biogas generated [Nm^3/hr]	670.8	67.1	6.7	603.9
Specific Biogas generation [Nm^3/tonne-VS]	366	366	366	321
Volume of biogas storage tank [m^3]	7,000	700	70	7,000
Volume of digestate storage [m^3]	4,258	426	43	4,883
No. of bubble columns for biogas upgrading	4 X 50 m^3	2 X 5 m^3	1 X 1m^3	4 X 50 m^3
Power rating (biomethane) [kW] *(Box S2)*	3,192	319	32	2,933
Specific energy generated as biomethane [kWh/Nm^3-biogas]	4.76	4.76	4.76	4.85
Areal footprint of photobioreactors (PBRs) [ha]	12.5	1.25	0.13	12
Total Areal footprint of microalgae cultivation and harvesting [ha]	17.9	1.8	0.2	17.2
pH of water entering the bubble column	10.22	10.22	10.22	10.15
Alkalinity of water entering the bubble column [g-IC/L]	2.0	2.0	2.0	1.93

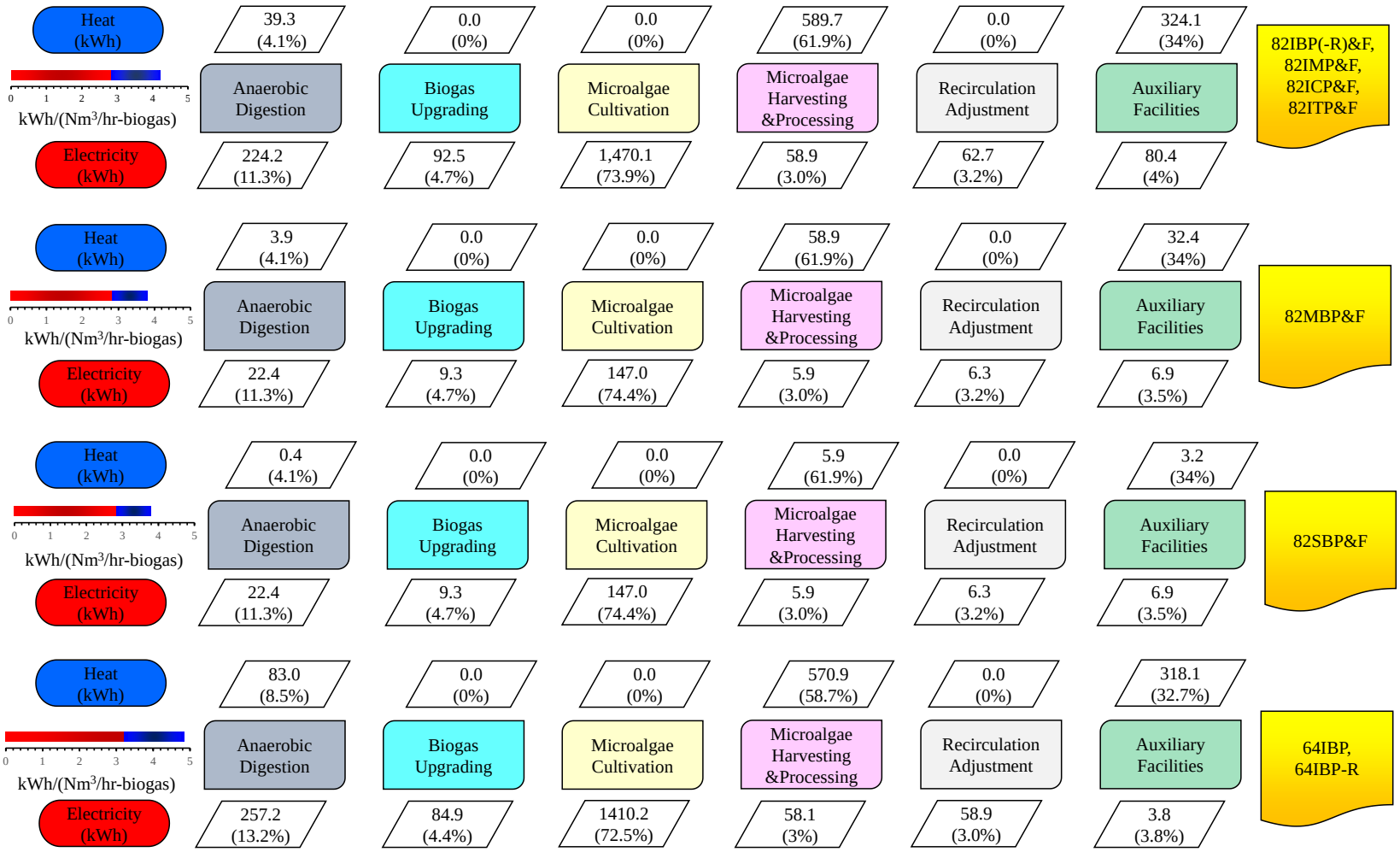


Figure 8-4 Overall and specific energy demand of the proposed polygeneration process under the fifteen scenarios.

8.3.2 Economic assessments

8.3.2.1 Costs and revenues

The annualised costs and revenues of the process, specific to one Nm^3/hr of biogas flow are plotted in Figure 8-5. The 82IBP scenario resulted in the lowest specific CAPEX of 28,380 €/(Nm^3/hr-biogas). Due to a drop in biogas production, the specific CAPEX was over 31,000 €/(Nm^3/hr-biogas) for the 64IBP scenario. In comparison, the costs for conventional upgrading systems at a similar scale are around 2,000 €/(Nm^3/hr-biogas) [28]. However, the specific CAPEX of the proposed plant is similar to the specific CAPEX of 28,500 €/(Nm^3/hr-biogas) (300 €/tonne-feedstock) of a power-to-gas bio-methanation plant of similar scale and running with similar feedstock [12]. As can be seen from Figure 8-6a, for the industrial-scale facilities, irrespective of the feedstock composition, the microalgae cultivation, harvesting and processing system, together with the wastewater treatment and sludge drying unit added significantly (over 30%) to the costs to the proposed plant. These costs, along with the high cost of the biogas upgrading columns and grid connection pipeline (Table S8-4) contributed substantially to the high overall capital expenses of the industrial-scale system. The AD system was also expensive, accounting for over 35% of the plant equipment costs. When the slurry content in the feedstock mix was higher (scenarios 64IBP & 64IBP-R) the requirement of larger pasteurisers and digestate storage resulted in the AD system contributing to over 40% of the total equipment costs.

For the medium and small-scale scenarios, the absence of the wastewater treatment plant reduced plant costs. Thus, the medium-scale plant had a specific CAPEX of 35,200 €/(Nm^3/hr-biogas), 6,700 €/(Nm^3/hr-biogas) greater than the industrial-scale facility, all other parameters being constant. The small scale unit (82SBP (&F) scenario) cost over 1.05 M€/(Nm^3/hr-biogas). As the system size reduced, the cost of grid connection became a significant element of the CAPEX, up from 10% in the medium-scale plant to over 19% for the small-scale facility (Figure 8-6a). The auxiliary units also added significantly (over 29%) to the cost of the facility for the small-scale scenario, followed by the equipment for microalgae cultivation, harvesting and processing (over 24%).

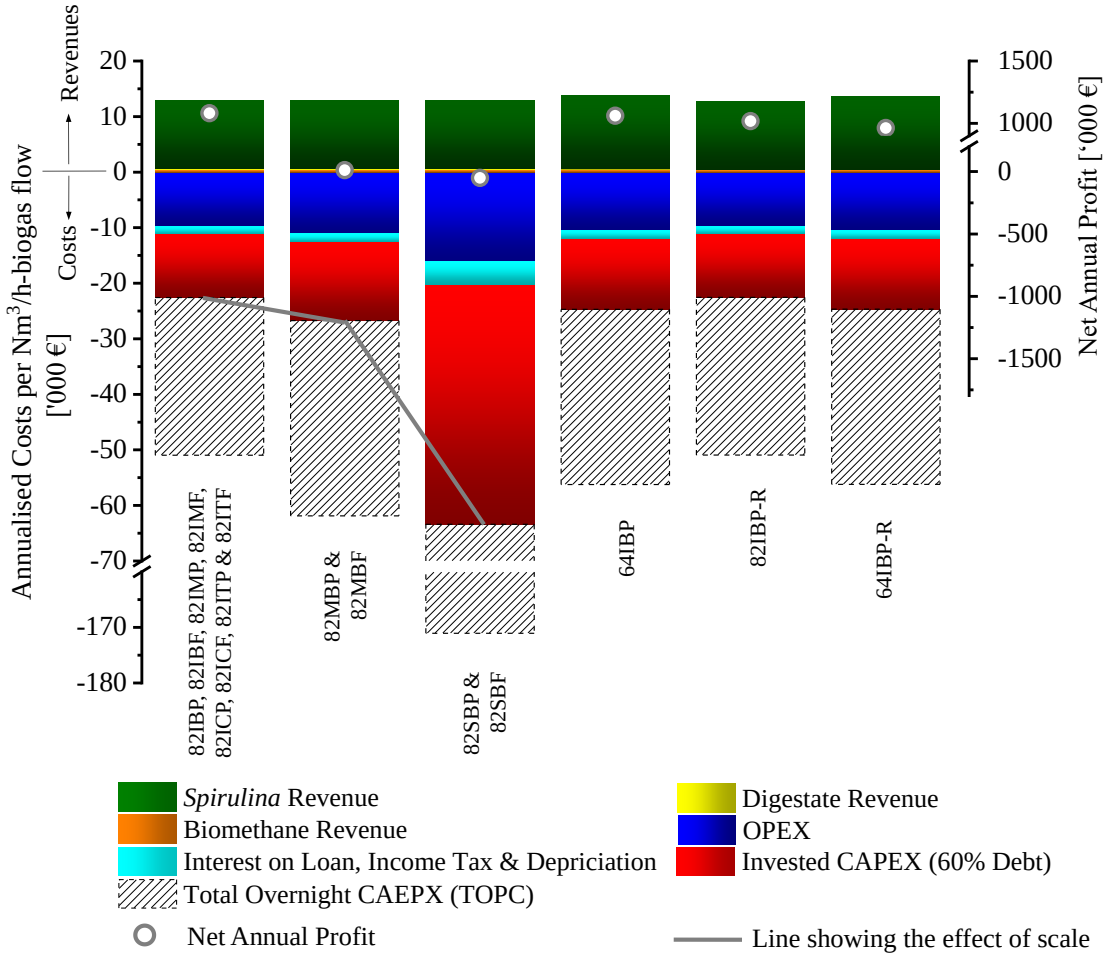


Figure 8-5 Annualised discounted costs, revenues, and net profit from the proposed polygeneration system without any incentives or subsidies towards the process or the products specific to 1 Nm^3/hr of biogas flow.

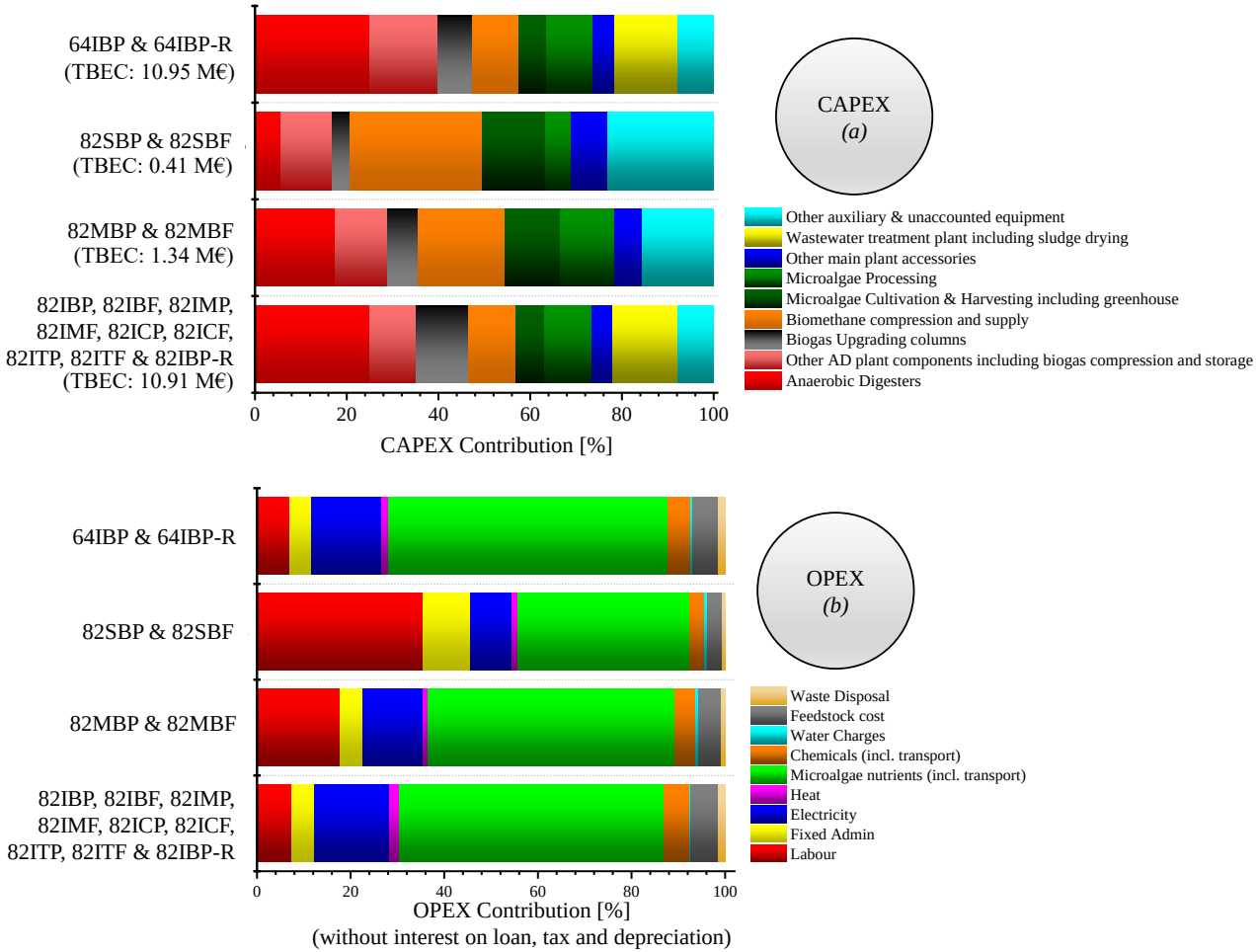


Figure 8-6 Breakdown of (a) CAPEX and (b) OPEX of the proposed polygeneration process for each scenario assessed

The lowest specific OPEX of 9,760 €/(Nm^3/hr-biogas) was obtained for the scenarios 82IBP (&F) and similar others (such as 82IMP (&F), Figure 8-5). The microalgae nutrient contributed to almost 56% of the annual expenditure of the plant. This was followed by the electricity cost (16%), the cost of labour (7.3%) and feedstock (6%) (Figure 8-6b). Although for the 64IBP scenario the overall OPEX was lower than that for the 82IBP scenario (Table S8-5), a lower biogas production increased the specific OPEX of the 64IBP scenario by 1,000 €/(Nm^3/hr-biogas). With a reduction in system size for the medium and small-scale scenarios, the specific OPEX increased from 11,120 €/(Nm^3/hr-biogas) for 82MBP (&F) scenarios to over 16,000 €/(Nm^3/hr-biogas) for the 82SBP (&F) scenarios. As can be seen from Figure 8-6b, labour became the highest contributor to the OPEX for smaller plants, increasing from 17.3% for the medium-scale plant to over 35% for the small-scale facility. The nutrient costs remained a major challenge irrespective of scale. The fixed administration charges also rose above 10% for the small-scale scenario.

Of all scenarios, the 82IBP (&F) scenarios were the most profitable, generating a net annual profit of over 1 M€ from a gross specific annual revenue of 12,800 €/(Nm^3/hr-biogas) (8.6 M€ overall). As can be concluded from Figure 8-5, *Spirulina* powder contributed over 95%, of the gross annual revenue while biomethane without incentives accounted for 3.8%. Digestate accounted for less than 1% of the annual revenue. Nonetheless, the gross annual revenue from the plant dropped by almost 60,000 € as digestate was not awarded an economic value under the 82IBP-R scenario. Although the specific annual revenue of 12,800 €/(Nm^3/hr-biogas) remained constant across scale (scenarios 82IBP (&F), 82MBP (&F) and 82SBP (&F)), the net profit margin decreased as the size of the plant reduced. Accordingly, a net annualised profit of only 10,000 € was obtained for scenarios 82MBP (&F), while the 82SBP (&F) scenarios resulted in an annual loss of c. 50,000 €.

A lower biogas production led to a drop in net gross revenue for the 64IBP scenario. Nonetheless, this lower biogas production resulted in the increase of the specific gross revenue to 13,830 €/(Nm^3/hr-biogas). The corresponding share of the annual revenue from digestate increased to about 1.3%, while the revenue from biomethane dropped below 3.6%. However, a higher specific CAPEX and OPEX caused the net annual profit of the plant to drop by almost 20,000 € when compared

to the 82IBP scenario. Due to a higher contribution from digestate, the revenue drop between scenarios 64IBP-R and 64IBP was 190 €/(Nm^3/hr-biogas) while the corresponding net annual profit decreased by 100,000 € (Figure 8-5).

8.3.2.2 Process economic indicators

Based on the discounted cash flows (Figure 8-7), the industrial-scale systems were highly profitable without any incentives. The highest net profit-generating scenarios (82IBP and similar) had the highest NPV of 14 M€ with a corresponding IRR of 46% and DPBP of 3 years (Figure 8-8). Without selling digestate, IRR reduced by 2.3%, and the NPV reduced to 12.7 M€ (82IBP-R scenario). For the 64IBP scenario, an NPV of 13.6 M€ was generated with an IRR of 44.6%; the DPBP was 3 years. As the quantity of digestate produced was higher, not accounting digestate as a product resulted in a larger drop in the IRR. Accordingly, the 64IBP-R scenario had an NPV and IRR of 11.6 M€ and 41% respectively, the lowest among the industrial-scale plants. The minimal net annual profit for the 82MBP (&F) scenarios of 11,600 € was not enough to overcome the expenses and hence resulted in a negative NPV of -737,000 €. The small-scale plant running at a loss had an unattractive NPV of -1.3 M€ without any incentives.

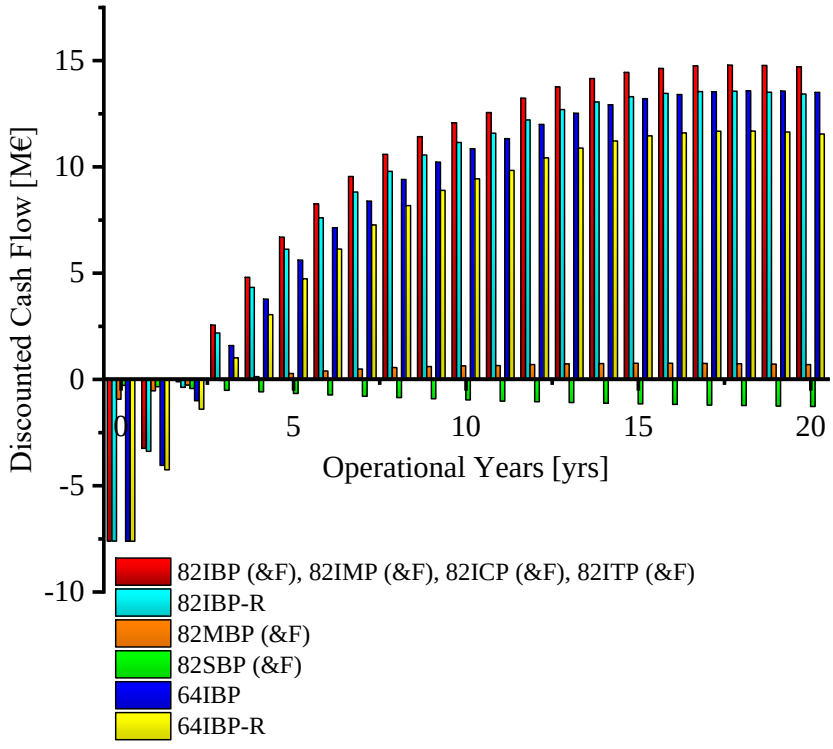


Figure 8-7 Discounted cash flow of each of the fifteen scenarios of the proposed polygeneration plant studied in this work.

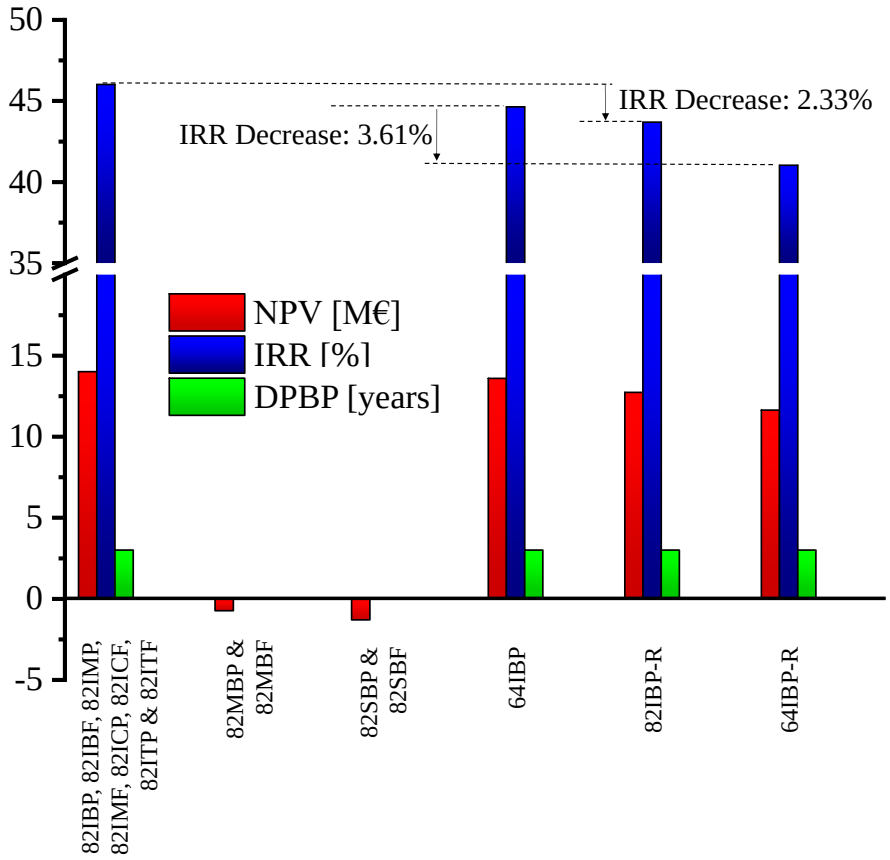


Figure 8-8 Net present value (NPV), internal rate of return (IRR) and discounted payback (DPBP) of the proposed polygeneration plant under each scenario assessed.

8.3.2.3 Levelised costs

Industrial-scale operations with an economic allocation of the expenses (scenarios 82IBP and similar and 64IBP) generated biomethane at the lowest levelised cost of 2.73 c€/kWh (0.31 €/Nm^3 or 464 €/tonne biomethane) irrespective of the feedstock composition (Figure 8-9a). The levelised cost of biomethane increased from 3.13 c€/kWh for the 82MBP (&F) scenario to over 4.84 c€/kWh for the 82SBP (&F) scenarios. Irrespective of scale, the prices remained much lower than the current costs of biomethane production of 6 to 12 c€/kWh [11,28,107] (equivalent to 0.68-1.36 €/Nm^3). As can be seen from Figure 8-9a, the levelised cost of biomethane was also lower than the feed-in tariffs (FiTs) typically provided to grid injected biomethane. In contrast, when the costs were allocated based on the product energy contents (scenarios 82IBP-R and 64IBP-R), the levelised cost of biomethane increased to above 57.5 c€/kWh or 6.55 €/m^3, making it absolutely uneconomical as compared to most renewable fuels. Energy allocation, therefore, would not favour biomethane produced by the polygeneration system.

Spirulina powder was produced at a levelised cost of 9.13 €/kg from the 82IBP and 64IBP scenarios, generating around 90 c€ profit from each kilogram of *Spirulina* powder sold. The results match well to the conventional prices of *Spirulina* production (up to 10 €/kg at plant gate [54,55]), in facilities without greenhouses [54]. The corresponding price of protein was around 15.1 €/kg-protein, similar to the cost of protein from beef (16.16 €/kg-protein [126]). However, *Spirulina* powder remained a more costly source of protein than chicken or milk (Figure 8-9b). The break-even cost of production further increased to 17.38 €/kg-protein and 26.80 €/kg-protein when produced from the medium or a small-scale facility respectively. Assuming a four-times increase in price from the farm gate to the retail market [127], the minimum wholesale price of *Spirulina* from the 82SBP (&F) scenarios would thus be c. 68 €/kg, competitive with the current retail prices of *Spirulina* powder (30-70 €/kg, Figure 8-9b). As *Spirulina* powder has a lower energetic value than biomethane, energy allocation resulted in a low levelised cost of c. 2 €/kg-product or 3.33 €/kg-protein.

The levelised cost of digestate was the lowest for the 82IBP (&F) scenarios (3.11 €/tonne or 795 €/tonne-N). The price increased to 3.63 €/tonne (931 €/tonne-N) under the 64IBP scenario when a greater quantity of digestate was produced. These prices correspond well to the cost of conventional fertilisers that usually range between 700 and 800 €/tonne-N (Figure 8-9c). The highest levelised cost of digestate as a bio-fertiliser resulted from the small-scale facility (scenarios 82SBP (&F)) at 5.56 €/tonne (1,426 €/tonne-N), higher than the assumed selling price of 4 €/tonne. Nevertheless, it was still lower than the price of solid manure as a fertiliser at c. 8 €/tonne [128] (5,710 €/tonne-N with a lower nitrogen content of 0.14% (wet basis) [128]). Digestate had no monetary value in the 82IBP-R and 64IBP-R scenarios.

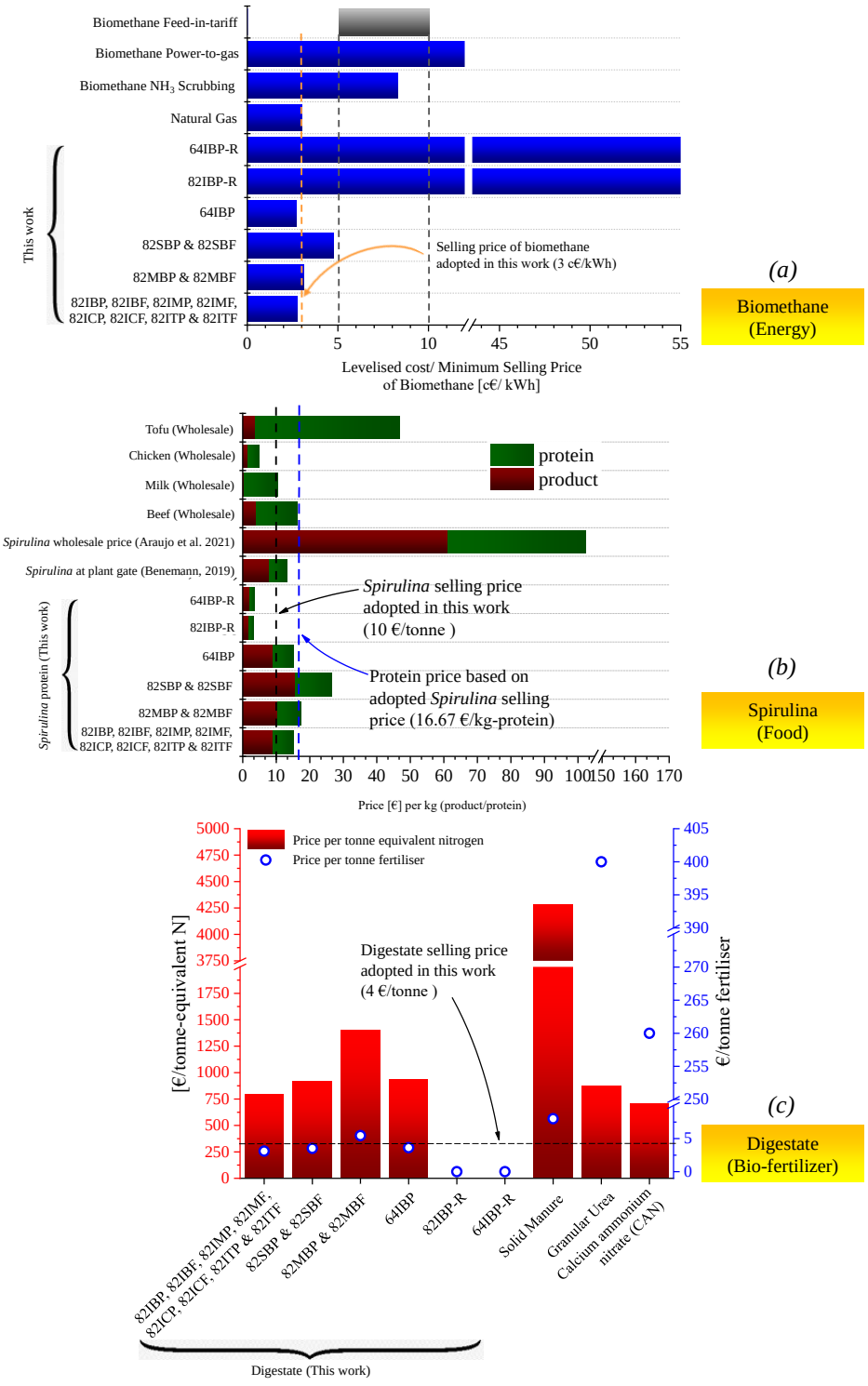


Figure 8-9 Levelised cost of (a) biomethane; (b) Spirulina powder and Spirulina protein; (c) digestate from the proposed polygeneration plant under each scenario. The levelised cost of biomethane from other technologies was obtained from Vo et al. (2018) [28]. The feed-in tariffs were compiled from various literature [14,129,130]. The Spirulina price at the plant gate was obtained from Benemann et al. (2019) [54], while the wholesale price of Spirulina was sourced from Araujo et al. (2021) [131]. Wholesale prices of other protein sources are compiled in Table S8-3 in the supplementary. The price of solid manure was sourced from Teagasc (2021) [128] while the prices of inorganic fertilisers were obtained from Walsh (2021) [132]. The nitrogen content of the inorganic fertilisers was evaluated using the results in Hoxha and Christensen (2018) [125]

8.3.3 LCOA (Marginal abatement cost)

8.3.3.1 Specific emissions and emission savings

The greenhouse gas emissions from the proposed plant in each scenario are shown in Figure 8-10. The highest hourly emissions of 1.01 tonnes$CO_{2\text{-eq}}$ were from the 82IBP and similar scenarios, operating with 20% slurry in the feedstock. When the emission savings from digestate application was not accounted for, as in the 82IBP-R scenario, the emissions from the process increased to around 1.07 tonnes$CO_{2\text{-eq}}$. The highest emissions (0.65 tonnes$CO_{2\text{-eq}}$) occurred from grid electricity (carbon intensity 325 g$CO_{2\text{-eq}}$/kWh$_e$ for the Irish grid), mostly consumed to heat the greenhouse for microalgae cultivation (Figure 8-4). Emissions from chemicals use were also substantial (over 0.4 tonnes$CO_{2\text{-eq}}$), followed by emissions from cultivation of grass (0.26 tonnes$CO_{2\text{-eq}}$) and emissions as a result of carbon losses (0.24 tonnes$CO_{2\text{-eq}}$). Carbon capture and replacement enabled a major emission saving of over 0.65 tonnes$CO_{2\text{-eq}}$. The use of agricultural residue as feedstock provided GHG benefits of 0.17 tonnes$CO_{2\text{-eq}}$ while around 0.06 tonnes of $CO_{2\text{-eq}}$ was saved from applying digestate as a fertiliser. As the sizes of the system dropped between scenarios 82IBP, 82MBP and 82SBP, the emissions were also reduced proportionally (Figure 8-10). When a higher slurry content was used in the feedstock, as in the case of scenario 64IBP, the net hourly emissions from the plant were significantly lower by over 0.15 tonnes$CO_{2\text{-eq}}$. Not only were the emissions lower, but also increased emission savings from a higher slurry content and digestate produced were beneficial. However, because a higher emission saving was enabled from a greater digestate content, its absence resulted in a greater rise in emissions from the process. Accordingly, emissions from the 64IBP-R scenario had an emission of almost 0.95 tonnes$CO_{2\text{-eq}}$, almost 0.1 tonnes$CO_{2\text{-eq}}$ higher than the corresponding 64IBP scenario.

Economic allocation of emissions ensured sustainability compliance of biomethane in both heat and transport (32.9 g$CO_{2\text{-eq}}$/MJ and 14.4 g$CO_{2\text{-eq}}$/MJ sustainability criteria in RED-II for transport and heat respectively [114]). However, energy allocation increased the specific biomethane emissions to similar and above emissions of natural gas (56.9 g$CO_{2\text{-eq}}$/MJ) as in scenarios 82IBP-R and 64IBP-R (Table 8-11). Thus, the current RED-II guidelines would not suit biomethane generation from the proposed polygeneration system.

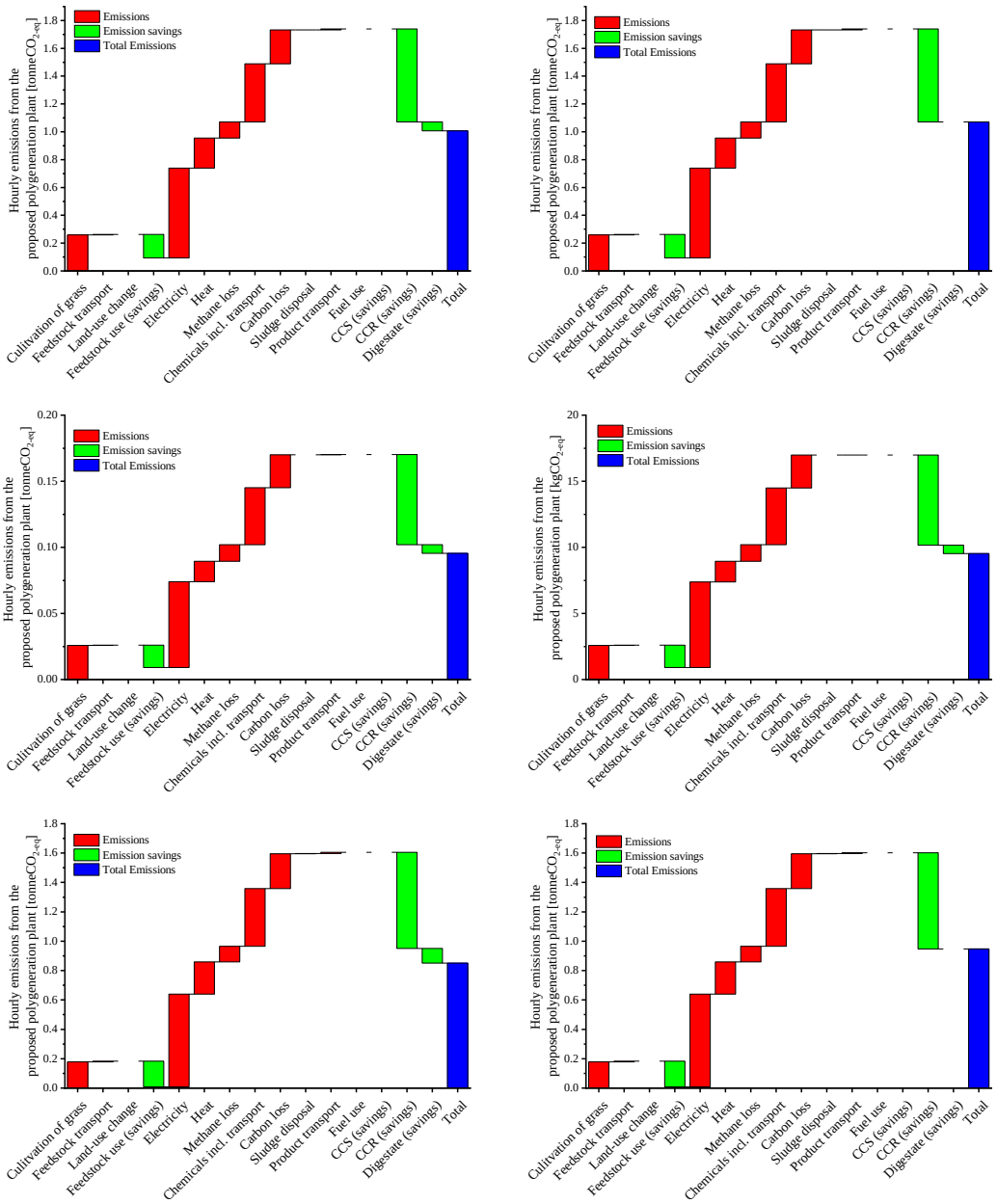


Figure 8-10 Greenhouse emissions and savings from the proposed polygeneration plant for (a) scenarios 82IBP, 82IBF, 82IMP, 82IMF, 82ICP, 82ICF, 82ITP and 82ITF, (b) 82IBP-R, (c) 82MBP and 82MBF, (d) 82SBP and 82SBF, (e) 64IBP and (f) 64IBP-R. In the figures, CCS refers to carbon capture and storage, CCR refers to carbon capture and replacement.

The highest emissions from *Spirulina* powder production were obtained for the 82IBP (&F) scenarios. At 3.98 $kgCO_{2\text{-eq}}$/kg-product, this was lower than the emissions of 6 $kgCO_{2\text{-eq}}$ reported by Ye et al. (2018) [110] and 15.5 $kgCO_{2eq}$ reported by Quintero et al. (2021) [133] per kg of *Spirulina* powder in standalone facilities. The emissions from *Spirulina* were also significantly lower both as protein and as a complete food than the alternative protein sources considered (Table 8-9). The lowest specific emission of 1.11 $kgCO_{2\text{-eq}}$/kg-product (1.91 $kgCO_{2\text{-eq}}$/kg-protein) was recorded for the

64IBP-R scenario as most of the allocation was shifted to biomethane using embodied energy. Specific emissions from digestate as a biofertiliser was the lowest under the 64IBP scenario (0.34 $kgCO_{2\text{-}eq}$/kg-N), while the highest was for the 82IBP scenario (0.40 $kgCO_{2\text{-}eq}$/kg-N). Both of the emissions were lower than the typical emissions from the production of conventional nitrogenous fertilisers of around 2 $kgCO_{2\text{-}eq}$/kg-N [125].

Table 8-11 Specific GHG emissions from each co-product and the overall lifetime GHG emission savings of the proposed polygeneration plant for each of the fifteen scenarios assessed.

Scenario code	Specific emissions (Base year)					Net Discounted Lifetime GHG savings [ktonnes-$CO_{2\text{-}eq}$]
	Biomethane [$gCO_{2\text{-}eq}$/MJ]	*Spirulina* (product) [$kgCO_{2\text{-}eq}$/kg-product]	*Spirulina* (protein) [$kgCO_{2\text{-}eq}$/kg-protein]	*Spirulina* ($NRF_{9.3}$ points) [$kgCO_{2\text{-}eq}$/ 1000 $NRF_{9.3}$ points]	Digestate [$kgCO_{2\text{-}eq}$/ kg-N]	
82IBP	3.32	3.98	6.83	0.62	0.41	1,451.42
82IBF	3.32	3.98	6.83	0.62	0.41	6,327.78
82MBP	3.05	3.65	6.28	0.57	0.38	145.70
82MBF	3.05	3.65	6.28	0.57	0.38	633.26
82SBP	3.04	3.64	6.26	0.57	0.38	15.05
82SBF	3.04	3.64	6.26	0.57	0.38	65.36
64IBP	3.10	3.35	5.58	0.50	0.34	1,443.85
82IMP	3.32	3.98	6.83	0.62	0.41	810.10
82IMF	3.32	3.98	6.83	0.62	0.41	672.95
82ICP	3.32	3.98	6.83	0.62	0.41	479.43
82ICF	3.32	3.98	6.83	0.62	0.41	766.81
82ITP	3.32	3.98	6.83	0.62	0.41	155.73
82ITF	3.32	3.98	6.83	0.62	0.41	87.56
82IBP-R	68.36*	1.16	2.01	0.18	-	1,420.32
64IBP-R	56.89*	1.11	1.91	0.17	-	1,538.32

* equal or higher than the specific emission of natural gas being replaced (56.9 $gCO_{2\text{-}eq}$/MJ)

As can be seen in Table 8-11, the highest emission savings of over 6.3 $MtonnesCO_{2\text{-}eq}$ over the project lifetime was achieved in the 82IBF scenario. Over 99% of these GHG savings occurred from the replacement of beef with *Spirulina* powder as a complete food (Figure 8-11). Biomethane enabled an emission savings of 36,670 $tonnesCO_{2}$-eq, while digestate contributed to around 14,000 tonnes CO_{2}-eq. On the contrary, when only protein from beef was replaced with protein from *Spirulina* powder, the emission savings dropped to 1.45 $MtonnesCO_{2\text{-}eq.}$ As the specific emissions from the protein source being replaced by *Spirulina* dropped, the overall GHG savings from the proposed process were reduced simultaneously. For an industrial scale plant, the lowest emission reductions were obtained when *Spirulina*

was considered as a replacement of tofu as a complete food (87,560 tonnes$CO_{2\text{-eq}}$, scenario 82ITF). Indeed, this was lower than the emission savings when only tofu protein was replaced (155,730 tonnes$CO_{2\text{-eq}}$, scenario 82ITP). This is since, unlike beef, tofu (and milk) are more nutritious as a complete food, than just as a protein source. Although the specific emissions of each co-product were lower for the 64IBP scenario, due to a lower biomethane production, emission savings decreased by 7,570 tonnes$CO_{2\text{-eq}}$ as compared to the 82IBP scenario. Without accounting for savings from digestate (biofertiliser) and using energy allocation, a drop of around 31,000 tonnes$CO_{2\text{-eq}}$ occurred between the 82IBP and 82IBP-R scenarios respectively. However, when compared to the 64IBP scenario, the 64IBP-R scenario had higher emission savings by c. 94,000 tonnes$CO_{2\text{-eq}}$. Although digestate was not accounted for, allowing greater emission savings from *Spirulina* by using the energy allocation method proved beneficial. As the specific emissions from biomethane were higher than natural gas being replaced for 82IBP-R and 64IBP-R scenarios, biomethane resulted in a net positive emission by replacing natural gas, indicating no contribution to emission savings (Figure 8-11).

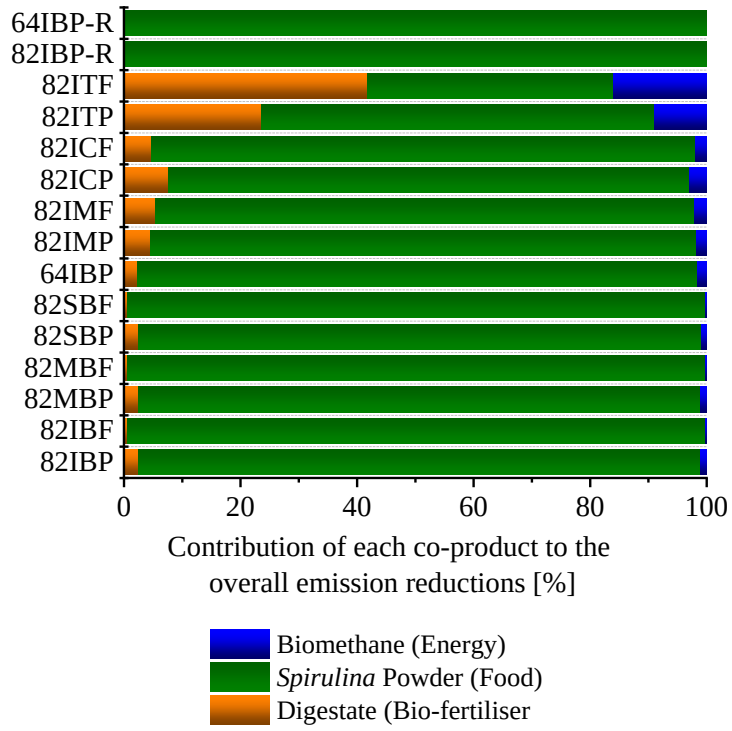


Figure 8-11 Contribution of the co-products towards the overall emissions in each of the fifteen scenarios.

8.3.3.2 LCOA/MAC

The highest annual GHG savings of 316,389 tonne$CO_{2\text{-eq}}$ was achieved at an LCOA of minus 2 €/tonne$CO_{2\text{-eq}}$ under the 82IBF scenario with *Spirulina* replacing beef as a complete food (Figure 8-12). When only protein substitution was considered (82IBP), a profit of 9.7 €/tonne$CO_{2\text{-eq}}$ was generated, however, with an annual GHG saving of only 72,571 tonne$CO_{2\text{-eq}}$. For a higher slurry content in the feedstock (64IBP scenario), although the annual GHG savings were lower by 400 tonne$CO_{2\text{-eq}}$ as compared to the 82IBP scenario, a minimal variation in LCOA was observed. Replacing protein from tofu with *Spirulina* protein yielded the highest profitability of GHG mitigation (lowest LCOA of -159.9 €/tonne$CO_{2\text{-eq}}$). However, the corresponding annual GHG savings was also nominal (4,378 tonne$CO_{2\text{-eq}}$). Due to increasing LCOAs, the proposed system became less enviro-economically attractive under the RED-II guidelines.

These results are encouraging as most current literature has priced biomethane at over 60 €/tonne$CO_{2\text{-eq}}$ (positive LCOA), higher than the current price of CO_2 (Figure 8-12). Other renewable technologies and fuels such as energy from biomass gasification, biodiesel and hydrogen from renewable resources had MACs of over 100 €/tonne$CO_{2\text{-eq}}$ (Figure 8-12), higher than the highest LCOA of 87.1 €/tonne$CO_{2\text{-eq}}$ obtained for the 82SBP scenario (farm-scale plant operating with 20% slurry in the feedstock). By selecting the appropriate food replacement, the emission savings and potential cost of CO_2 abatement could however be further minimised. For example, the LCOA decreased to 20.1 €/tonne$CO_{2\text{-eq}}$ for the 82SBF scenario, when a complete replacement of beef by *Spirulina* powder was assumed, lower than the 2020 carbon price in Ireland (26 €/tonne$CO_{2\text{-eq}}$) [134].

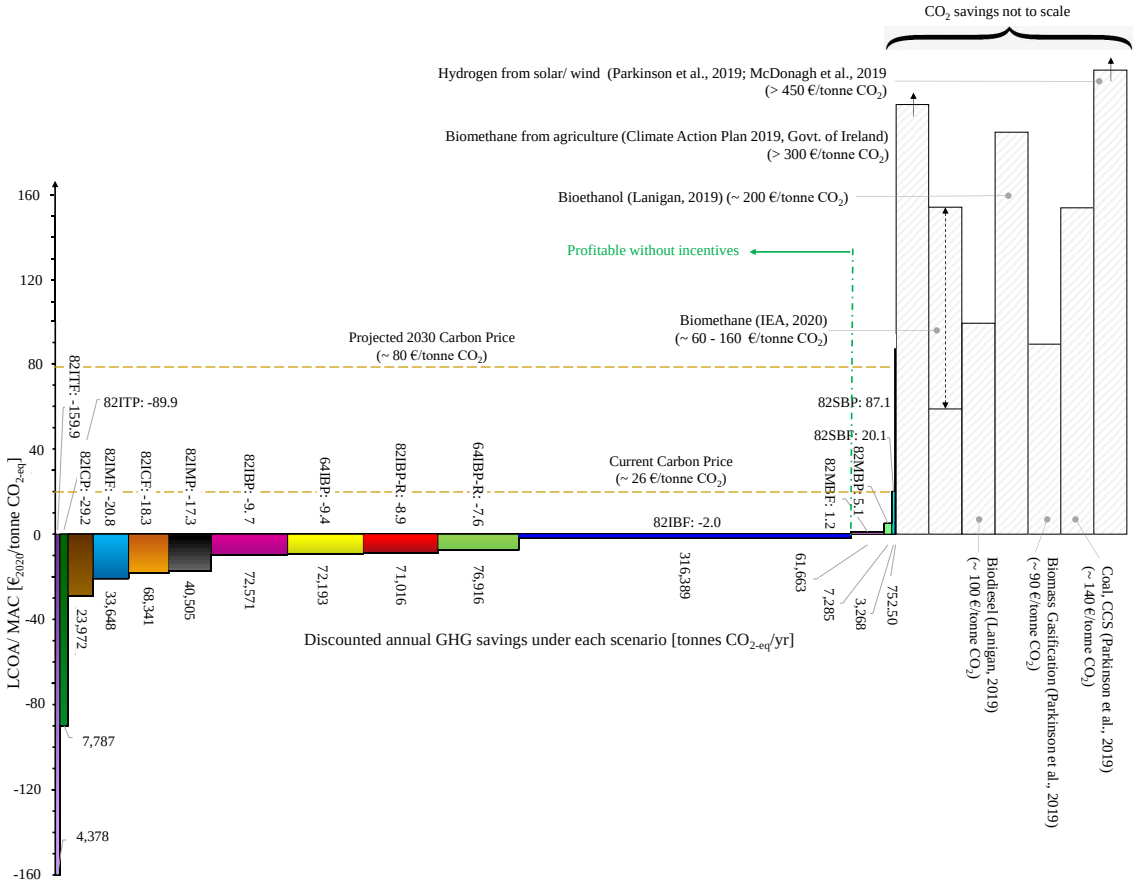


Figure 8-12 Levelised cost of GHG abatement (LCOA) or marginal abatement cost (MAC) of the proposed polygeneration plant under each of the fifteen scenarios assessed along with the current cost CO_2 and the MACs of a few alternatives to biomethane. The current (2020) and the future prices of CO_2 were obtained from data from the Government of Ireland [134] and projections of Ireland's GHG emissions by EPA (2021) [135] respectively. The MACs of the alternative technologies were obtained from various sources of literature [136–139]

8.3.4 Sensitivity assessment

The sensitivity assessments of the enviro-economic performance of the proposed polygeneration plant were performed on the base case scenario (scenario 82IBP). As can be seen from the results in Figure 8-13, *Spirulina* pricing had the highest influence on the system economics. For a 10% drop in the selling price of *Spirulina* to 9 €/kg, the system became unprofitable (negative NPV and a positive LCOA). Although the levelised cost of *Spirulina* remained similar, the levelised costs of biomethane and digestate increased by over 10% due to a greater allocation of costs towards them. The price variation in biomethane, however, generated minimal impact on the process economics and GHG savings. However, the levelised costs of biomethane increased linearly with an increase in the biomethane selling price and vice-versa. A 10% increase in the OPEX lowered the NPV by over 80%, while the corresponding LCOA increased by a similar amount. The IRR was reduced by almost 50%. The levelised costs of each co-product increased by over 9%. A similar drop in costs and increase in profitability was observed when the OPEX decreased by 10%. The process economics were also sensitive to the capacity factor, whereby a higher capacity factor improved the plant economics significantly. For a 10% variation in the capacity factor, NPV varied over 30%, IRR and LCOA by over 20%. However, a minimum influence of the capacity factor on the levelised costs of the co-products was observed. As can be observed from Figure 8-13, a 10% increase in CAPEX was found to decrease the NPV and IRR by around 16%, while the LCOA increased by the same amount.

Based on the results of the sensitivity assessment, a Monte Carlo simulation was performed using triangular distribution to assess the uncertainties in the NPV and the LCOA from an economic standpoint. The most probable NPV lay between 10 and 20 M€ while the LCOA varied between -10 and -8 €/tonne$CO_{2\text{-eq}}$ (Figure 8-14) indicating the profitability of the system at the assumed selling price of the co-products. The interquartile range of the NPV remained between 7.5 and 20 M€ with the corresponding LCOA around -14 and -6 €/tonne$CO_{2\text{-eq}}$ respectively. None of the scenarios simulated predicted an NPV below zero or LCOA above zero, establishing the robust economic performance of the process for the base case scenario (82IBP).

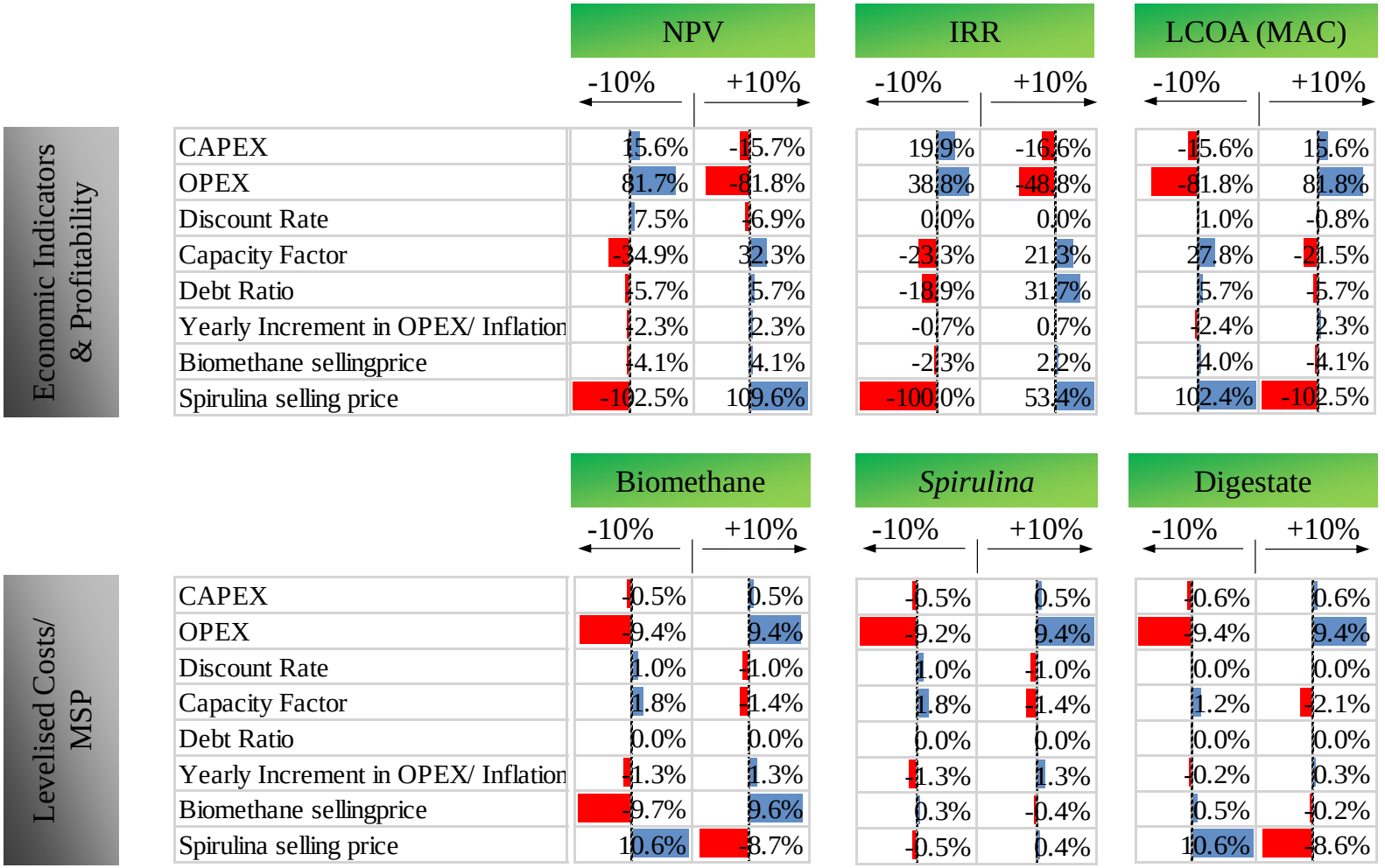


Figure 8-13 Sensitivity assessments of the different variables including the prices of biomethane and Spirulina powder on the NPV, IRR, LCOA and the levelised cost of each co-product for the base case scenario (scenario 82IBP)

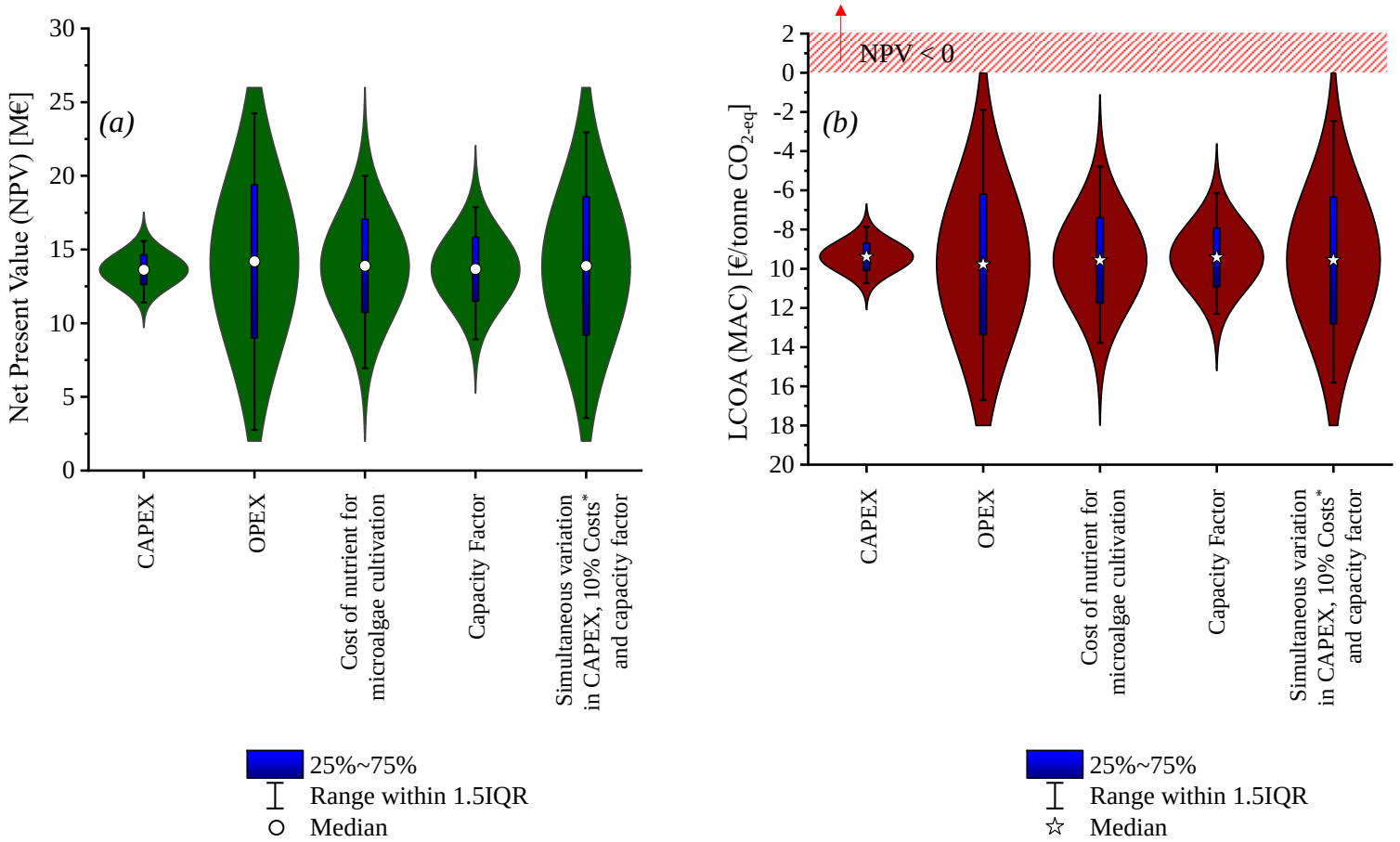


Figure 8-14Monte Carlo simulations to determine the most probable (a) NPV and (b) LCOA or marginal abatement cost of the proposed technology for the base case scenario (82IBP).

** 10% cost variation indicates a variation of ± 10% of the individual cost components of the OPEX including the cost for the nutrient medium for microalgae cultivation.*

8.3.5 Operations with financial benefits to biomethane

Although the analyses were performed considering no financial support, under most circumstances, biomethane can command a higher price than natural gas either through feed-in tariffs or premiums or through auctions [14,129,140]. Alternatively, as the price of natural gas is increased through carbon tax such as in Ireland and Switzerland [129,134], paying more for biomethane (renewable gas) seems justifiable. Accordingly, the enviro-economic performance of the proposed system was studied for a biomethane price between 4 c€/kWh and 10 c€/kWh. The scenarios 82IBP, 82MBP and 82SBP were considered for comparative evaluation. The price of natural gas was raised to 4 c€/kWh including carbon tax [134]. Figure 8-15 shows the results.

A selling price of biomethane greater than 7 c€/kWh made the medium scale plant profitable (Figure 8-15b). Thus, in the UK, with mostly a similar climate as that of Ireland and where biomethane for transport use is paid almost 9.5 c€/kWh (8.2 p£/kWh [130]), the 82BMP (&F) scenarios would be economically viable. However, if used for heat, the tariff for biomethane of 5.8 c€/kWh (c. 5 p£/kWh [130]) would not be high enough to generate a sufficient profit. Even a feed-in-tariff of 10 c€/kWh was not high enough to generate a profit for the small-scale system and hence is not shown in Figure 8-15. An increasing biomethane price also lowered the levelised cost of *Spirulina* powder through a lower allocation of costs. As can be seen from Figure 8-15c, the minimum price of *Spirulina* powder of 8.43 €/kg was obtained when biomethane was sold at 10 c€/kWh from the industrial scale system (scenario 82IBP). The corresponding cost of *Spirulina* powder from the medium and small-scale plants was 9.59 €/kg and 14.84 €/kg respectively.

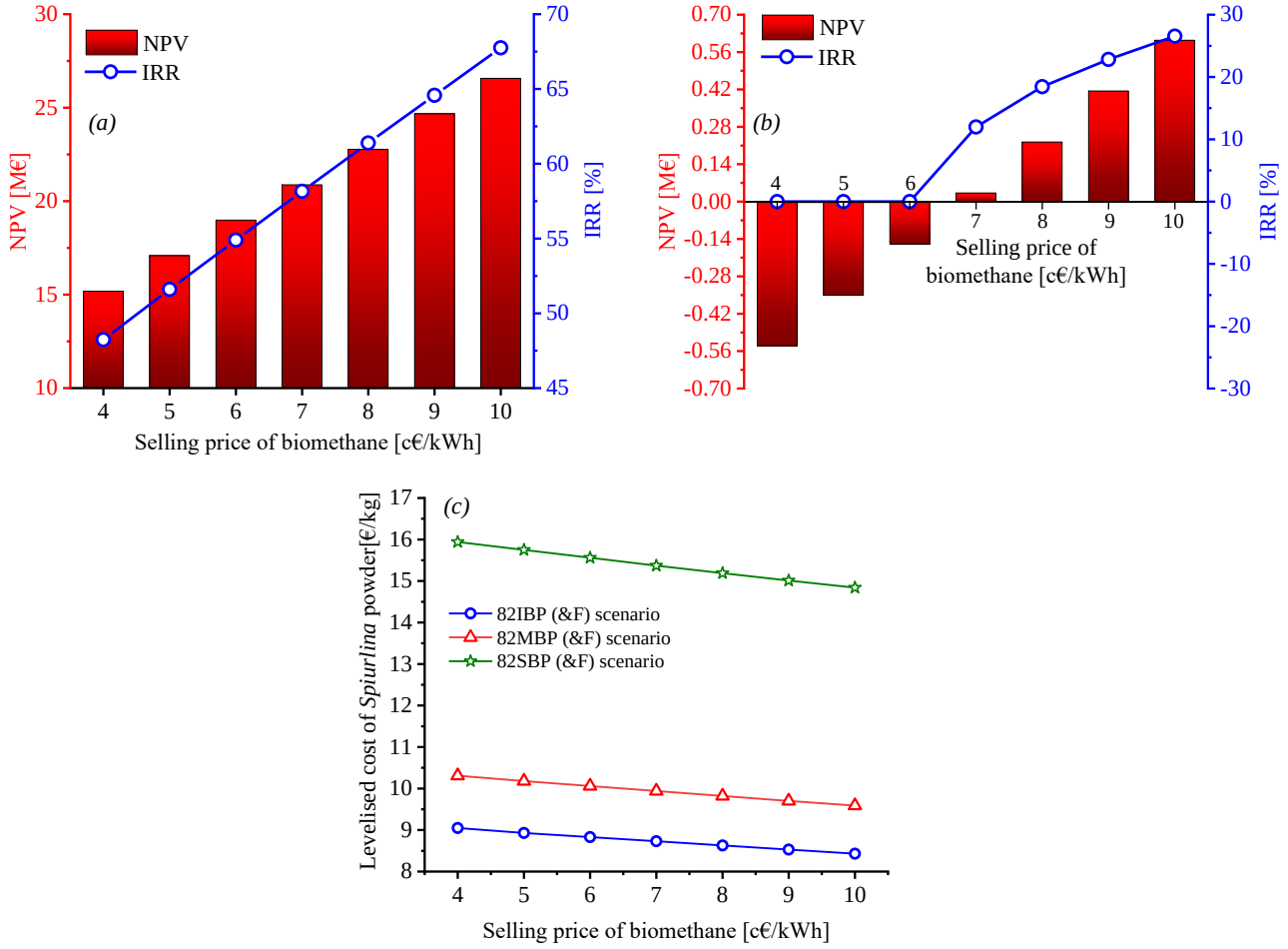


Figure 8-15 Impact of selling price of biomethane on (a) NPV and IRR of the 82IBP (&F) scenarios, (b) NPV and IRR of the 82MBP (&F) scenarios and (c) levelised cost of Spirulina powder of the 82IBP (&F), 82MBP (&F) and 82SBP (&F) scenarios.

8.4 Discussion

8.4.1.1 Verdict on the technology and future outlook

On-site co-production of *Spirulina* powder with biomethane utilising CO_2 from biogas via photosynthetic biogas upgrading added significant value to a conventional AD plant generating biogas. Although this increased the cost of the plant by a factor of ten compared to a conventional biomethane production facility, the revenues earned from *Spirulina* recuperated the investments in just three years, all while selling biomethane at only 3 c€/kWh. Using digestate as a biofertiliser also added to the revenue streams while generating emission savings through the replacement of conventional fertilisers. When compared to current bidding prices of biomethane of around 15 c€/kWh [140], the proposed plant would thus provide a considerable economic advantage, both on an industrial and community (medium) scale. This would also allow biomethane to be cost-competitive with other renewables such as on-shore wind and solar, which are currently auctioned between 4.5 and 6.5 c€/kWh in Europe [140,141]. An added advantage, that would be gained from the proposed process and the co-products are the similar market valuations and growth rate between biomethane and *Spirulina* as a complete food. Both biomethane and *Spirulina* powder as single-cell protein are expected to be valued at around 5 billion€ between 2024 and 2026, growing at an annual rate of 7-8% and 5-6%, year-on-year basis respectively [14]. This would prevent market saturation of either of the products, giving robustness to the process economics assessed in this work.

Sodium bicarbonate, commercially produced using fossil fuels in lime kilns [113] is separately supplied as the primary inorganic carbon source in conventional standalone *Spirulina* production facilities [110]. In contrast, by employing photosynthetic biogas upgrading, the proposed process was able to produce a majority of the sodium bicarbonate from biogenic CO_2 of biogas. This resulted in significant emission reductions during *Spirulina* production in the proposed process as compared to stand-alone *Spirulina* production farms. In addition, *i)* economic allocation; *ii)* the inclusion of digestate as a sellable biofertiliser; *iii)* using a higher grass content in the AD feedstock would also ensure that each co-product is generated at either lower emission levels than most market alternatives or below those mandated by legislatures (such as RED-II).

In the future, with increased renewables in both the electricity and gas grids, GHG mitigation can be further increased. For example, by 2030, with the predicted Irish electricity and gas grid carbon intensities of 110 $gCO_{2\text{-}eq}$/kWh [142] and 160 $gCO_{2\text{-}eq}$/kWh (calculated as 20% renewable biomethane in the gas grid by 2030 [143]) respectively, a 5% additional GHG saving can be achieved from the 82IBP scenario. The corresponding LCOA would be -9 €/tonne$CO_{2\text{-}eq}$ for replacing beef protein with *Spirulina* protein; the LCOA for the small scale 82SBP scenario would be 83.2 €/tonne$CO_{2\text{-}eq.}$ However, if *Spirulina* is considered as a replacement of beef as a complete food, the LCOA for the 82SBP scenario would drop to 19.9 €/tonne$CO_{2\text{-}eq}$. When compared with the Irish government's estimate of the MAC of biomethane (from agricultural feedstocks) of more than 300 €/tonne$CO_{2\text{-}eq}$ [139], the results, therefore, indicate the versatility of biogas-based systems, seldom exploited in conventional standalone facilities. The proposed process would also better the MAC of conventional bioenergy with carbon capture and sequestration in geological storages, typically given from a minimum of c. 40 €/tonne$CO_{2\text{-}eq}$ [144] to over 500 €/tonne$CO_{2\text{-}eq}$ for 80% emission reductions [145].

8.4.1.2 Can the small-scale process be made profitable?

The profitability (NPV>0) of the small-scale system can be achieved by selling biomethane at an unrealistic price of over 67 c€/kWh without increasing the selling price of *Spirulina*. On the contrary, *Spirulina* could be sold at the farm gate at a more realistic price of 18.50 €/kg to support a biomethane price of 3 c€/kWh. If biomethane receives a price of 9 c€/kWh as a transport fuel, the *Spirulina* price could drop to around 17.70 €/kg (Figure 8-16). Although selling *Spirulina* at a higher price could be challenging, as it may be considered a vegan-friendly superfood, it could benefit from 10-20% healthy food subsidies [146–148]. Alternatively, additional revenue can be generated from accounting for CO_2 savings if biomethane is traded within the EU Emission Trading Scheme (ETS). However, it would require emissions from agriculture and transport (including haulage and shipping) to be included in the ETS as well [149]. If the GHG reduction benefits from replacing beef as a complete food are included, the LCOA (20.3 €/tonne$CO_{2\text{-}eq}$) would be lower than the 2020 EU CO_2 traded price of 25 €/tonne$CO_{2\text{-}eq}$ [150] and the process would become profitable (NPV: 0.29 M€, IRR: 31.4% and DPBP: 3 years). However, if only protein substitution from beef is considered, a higher carbon price, above 87 €/tonne$CO_{2\text{-}eq}$ would be required

to ensure the economic viability of the small-scale plant under emission trading schemes.

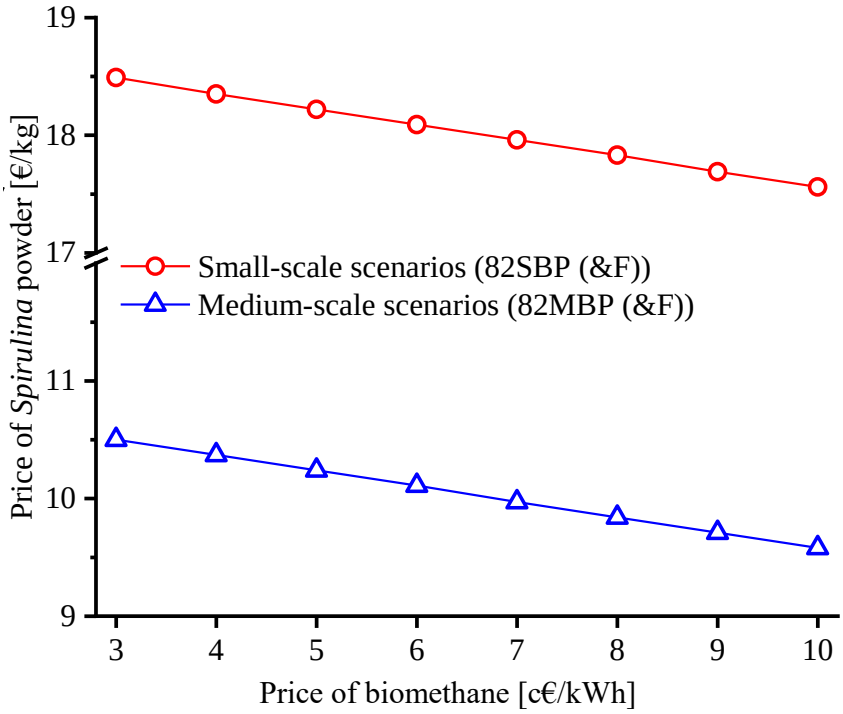


Figure 8-16 Variation in the minimum price of Spirulina powder with the price of biomethane to ensure the profitability of the medium (82MBP and 82MBF) and the small-scale (82SBP and 82SBF) scenarios (NPV > 0)

8.5 Conclusions

The answers to the questions raised in the objectives are as follows:

1. Does scale impact the profitability of the polygeneration process?: The industrial-scale plant (c. 3 MW biomethane) was profitable across scale irrespective of the type of feedstock used without any incentives. Although a 40% slurry content in the feedstock (VS basis) decreased the profitability of the plant as compared to when 20% slurry was used, the IRR was still above 40%. The medium-scale plant (300 kW biomethane) only became profitable at a biomethane price of 7 c€/kWh. However, with a specific CAPEX of over 1.05 M€/(Nm^3/hr-biogas), the small-scale plant (30 kW biomethane) was not profitable without significant policy supports and benefit mechanisms.

2. Are the co-products cost-competitive with available alternatives?: Using the proposed plant configuration and economic allocation, biomethane from an

industrial-scale plant was generated at a levelised cost of 2.73 c€/kWh, lower than the price of natural gas (3 c€/kWh). The corresponding price of *Spirulina* powder was around 9.1 €/kg, similar to the current farm-gate prices. On a nitrogen basis, digestate was also produced at a cost-competitive price to that of inorganic nitrogenous fertilisers. From less profitable smaller systems, however, the prices of commodities were higher. Exploiting the large variation in *Spirulina* market prices and possible healthy food benefits, a high price from Spirulina powder could potentially be charged to make the small-scale plants profitable.

3. How can the GHG abatement potential of the plant be maximised?: Economic allocation would ensure that each co-product is generated at either lower emission levels than most market alternatives or below those mandated by legislatures (such as RED-II). However, as the slurry content in the AD feedstock increases, energy allocation would increase the overall emission savings from the proposed process. Additionally, the inclusion of digestate as a sellable biofertiliser and replacing a more polluting and less nutritious protein source (such as beef) with *Spirulina* powder as a complete food would also add to the GHG emission savings from the polygeneration plant. For instance, the largest annual GHG emission savings for scenario 82IBP was calculated as 129 tonnes$CO_{2\text{-}eq}$/tonne-feedstock or 1.18 tonnes$CO_{2\text{-}eq}$/(Nm^3/hr-biogas) by replacing beef as a complete food with *Spirulina* while using 20% slurry in the feedstock (VS basis). Similar high emission savings could be expected by replacing other meat proteins such as lamb, mutton, or pork [124]. However, if a less environmentally polluting protein such as chicken is replaced, the net specific emission savings would drop to around 16.4 tonnes$CO_{2\text{-}eq}$/tonne-feedstock or 0.15 tonnes$CO_{2\text{-}eq}$/(Nm^3/hr-biogas). The GHG mitigation achieved by replacing plant-based protein such as soy would be much lower. Therefore, strategic marketing and policy support for *Spirulina* powder would be required to ensure the successful commercialisation and wide uptake of this alternative superfood.

4. How does the plant's LCOA/MAC compare with other renewable technologies?: Although the LCOA varied significantly for the type of protein being replaced, it was always less than 0 for the industrial-scale process. In contrast, the current LCOA for biomethane is estimated anywhere between 60 €/tonne$CO_{2\text{-}eq}$ and

above 300 €/tonne$CO_{2\text{-eq}}$. The small-scale plant had the highest LCOA of 87.1 €/tonne$CO_{2\text{-eq}}$ when the produced *Spirulina* was considered a substitute of beef protein only. However, by appropriate food substitution such as replacing beef as a complete food with *Spirulina*, the LCOA dropped to 20.3 €/tonne$CO_{2\text{-eq}}$, below the current market price of CO_2 (25 €/tonne$CO_{2\text{-eq}}$ for EU [101] and 26 €/tonne$CO_{2\text{-eq}}$ for Ireland [94]).

8.6 Acknowledgement

This work acknowledges the support from Science Foundation Ireland (SFI) through the Centre for Marine and Renewable Energy (MaREI) under Grant No. 12/RC/2302_P2 and 16/SP/3829, with industrial funding from Gas Networks Ireland through The Green Gas Innovation Group and by ERVIA and IDL Pernod Ricard. This work was also supported by the Environmental Protection Agency – Ireland (2018-RE-MS-13).

8.7 Supplementary to Chapter 8

Box S8.1: Calculation of the cost of Zarrouk's medium (without sodium bicarbonate)

Cost of Zarrouk's Medium: 80 USD/1000 L [36,43] c. 64 €/1000 L

Based on Zarrouk's media composition, each litre of media comprises 16.8 grams $NaHCO_3$ and the remaining 5.33 grams of other nutrients. Thus,

➔ Unit Cost of Zarrouk's medium = 64/(16.8+5.13) = 2.89 €/kg or 2,892 €/tonne

Conventional Zarrouk's medium comprises high-cost analytical grade sodium bicarbonate [44], typically costing around 3,000 €/tonne [151]. Thus,

➔ Cost of analytical grade bicarbonate in one tonne of Zarrouk media

= 16.83/22.13×3,000 = 2,277 €

Therefore,

➔ Cost of nutrients in one tonne of Zarrouk's media = 2,892 – 2,277 = 615 €

➔ Unit Cost of Zarrouk's media (without bicarbonates) = 615/(5.13/22.13) ≈ 2,653 €/tonne

Table S8-1 Summary of the major outputs to the process and their corresponding unit prices/ costs

Component	Unit price/cost	Reference
Biomethane	7 c€/kWh	Average grid injection price (feed-in tariff) [14]
Spirulina platensis powder (protein supplement)	10 €/kg	Similar to the current production prices of *Spirulina* [54,55]
Digestate from anaerobic digestion	4 €/tonne	Murphy et al. (2011) [56]
Ammonium sulphate	3600 €/tonne	Adapted from Glanbiaconnect (2021) [152]
Wastewater Sludge (Disposal Fee)	-100 €/tonne[ζ]	Adapted from IES (2021) [45]

[ζ] Negative sign indicates the disposal cost of the product that must be borne by the plant.

Table S8-2 Nutrient value in Spirulina powder along with the recommended and the maximum daily values of each of the corresponding nutrients. The nutrient values in Spirulina were obtained from [110,151], while the recommended daily value (RDV) and the maximum daily value (MDV) were compiled from [65,154,155].

Nutrient	**Value in *Spirulina* [g/100 g]**	**Recommended daily value (RDV) [g]**	**Maximum daily value (MDV) [g]**
Protein	60	57	-
Dietary Fibre	3.6	25	-
Vitamin A	570 IU[a]	5000 IU	
Vitamin C	0.0085	0.08	-
Vitamin E	5 mg	12 mg	
Calcium	0.12	0.8	-
Iron	28.5 mg	14 mg	
Potassium	1.36	2	-
Magnesium	195 mg	375 mg	-
Saturated Fat	2.7	-	20
Sodium	0.5	-	2.4
Added Sugar	0	-	90
Energy	336 kcal/100 g	-	-

[a]IU: International Unit

Table S8-3 $NRF_{9.3}$ scores, wholesale prices and specific emissions of the four protein-based foods compared with Spirulina, namely, beef, milk, chicken and tofu (soybeans)

Protein Type	**$NRF_{9.3}$ [value/100 kCal]**	**Wholesale price**		**Specific emissions**	
		Product [€/kg]	**Protein [€/kg-protein]**	**$kgCO_{2\text{-}eq}$/100 kCal [124]**	**$kgCO_{2\text{-}eq}$/1000 $NRF_{9.3}$ points**
Beef (Dairy Herd)	10.8 [155]	4.04 [126]	16.16 [126]	1.22	113
Milk (Whole, 2% Fat)	43.3 [155]	0.35 [126]	10 [126]	0.525	12.1
Chicken (Breast, boneless meat)	38.7 [155]	1.54 [126]	4.97 [126]	0.534	13.8
Tofu/ Soybeans	69.4 [156]	3.75 [157]	46.88 (assuming 8% protein in tofu [158])	0.17	1.7

Box S8.2: Calculation of the specific energy of biomethane

Assuming the lower heating value (LHV) of methane as 50 MJ/kg [72] and the density of methane as 0.668 0.~~668~~ kg/m^3 at NTP (20°C, 1 atm) [159] or 0.717 at STP (0°C, 1 bar) [159].

➔ LHV methane (volume basis) = 50 × 0.667 = 33.36 MJ/Nm^3, or,
= 50 × 0.716 = 35.8 MJ/Sm^3

The produced biomethane contains 95.2% CH_4 for all scenarios. Therefore,

➔ LHV of biomethane produced = 33.36 × 0.952 = 31.8 MJ/Nm^3
= 31.8/3.6 ≈ 8.83 kWh/Nm^3 biomethane, or,

➔ LHV of biomethane produced = 35.8 × 0.952 = 34.08 MJ/Sm^3
= 34.08/3.6 ≈ 9.47 kWh/Sm^3 biomethane

For AD feedstock with 80% grass silage and 20% slurry, 361.5 Nm^3/hr of biomethane was generated. Hence,

→ Energy produced as biomethane = 361.5 × 8.83 ≈ 3,192 kWh/hr
≡ 3.19 MWh/hr, or,
= 3.19 × 8,000 ≈ 25,536 MWh/yr

And,

➔ Power rating of the proposed polygeneration plant = 3.19 MW-biomethane

For AD feedstock with 60% grass silage and 40% slurry, 332.2 Nm^3/hr of biomethane was generated. Hence,

➔ Energy produced as biomethane = 332.2 × 8.83 ≈ 2,933 kWh/hr
≡ 2.93 MWh/hr, or,
= 2.93 × 8,000 ≈ 23,474 MWh/yr

And,

➔ Power rating of the proposed polygeneration plant = 2.93 MW-biomethane

Table S8-4 Bare erected cost and the corresponding sizing of each equipment within the individual scenarios assessed. All costs are in 2020 Euros.

Component	Sizing unit	82IBP, 82IBF, 82IMP, 82IMF, 82ICP, 82ICF, 82ITP, 82ITF & 82IBP-R		82MBP & 82MBF		82SBP & 82SBF		64IBP & 64IBP-R	
		Size	Erected equipment cost ('000€)	Size	Erected equipment cost ('000€)	Size	Erected equipment cost ('000€)	Size	Erected equipment cost ('000€)
Anaerobic Digestion Section - Biogas production and digestate handling									
Grass reception infrastructure	tonne / co-substrate/day	72.0	€ 141.55	7.2	€ 14.16	0.7	€ 1.42	56.9	€ 111.75
Slurry reception infrastructure		75.1	€ 147.51	7.5	€ 14.75	0.8	€ 1.48	158.9	€ 312.90
Grass shredder		72.0	€ 26.82	7.2	€ 6.71	0.7	€ 1.49	56.9	€ 23.84
Pasteurizer and pasteurizer heat exchangers		75.1	€ 244.36	7.5	€ 24.44	0.8	€ 2.98	158.9	€ 518.52
Manure pipework and pumps	unit	1.0	€ 11.90	1.0	€ 11.92	0.1	€ 11.92	1.0	€ 11.92
Feed storage tank	m^3	64.9	€ 7.45	6.5	€ 3.13	0.6	€ 1.49	47.6	€ 6.71
Digester 1	m^3	4,423.5	€ 1,583.87	442.3	€135.59	44.2	€ 13.56	4,423.5	€ 1,583.87
Digester 2	m^3	3,296.9	€ 1,145.81	329.7	€ 101.32	33.0	€ 10.13	3,296.9	€ 1,145.81
Biogas compressor	Nm^3/hr-biogas	670.8	€ 312.90	67.1	€ 37.25	6.7	€ 10.43	603.9	€ 298.00
Biogas Storage tanks (2 days storage capacity)	m^3	7,000.3	€ 16.39	700.0	€ 4.47	70.0	€ 1.19	7,000.0	€ 16.39
Flare	digester m^3	7,720.4	€ 23.84	772.0	€ 5.22	77.2	€ 3.73	7,720.4	€ 23.84

Component	Sizing unit	82IBP, 82IBF, 82IMP, 82IMF, 82ICP, 82ICF, 82ITP, 82ITF & 82IBP-R		82MBP & 82MBF		82SBP & 82SBF		64IBP & 64IBP-R	
		Size	Erected equipment cost ('000€)	Size	Erected equipment cost ('000€)	Size	Erected equipment cost ('000€)	Size	Erected equipment cost ('000€)
Decanter	m^3	12.1	€ 44.70	1.2	€ 11.18	0.1	€ 2.98	18.4	€ 58.11
Digestate storage lagoons	m^3	4,258.5	€ 125.16	425.8	€ 20.86	42.6	€ 12.66	4,916.6	€ 233.93
Biogas Upgrading Section									
Biogas bacterial screen	unit	20	€ 29.80	5	€ 7.45	0.5	€ 2.98	20	€ 29.80
Pump to recirculate water	kW_e	16.93	€ 19.37	1.7	€ 8.94	0.2	€ 3.73	15.3	€ 19.37
Absorption column with all accessories	m^3	50	€ 1,256.07	5	€ 89.40	0.5	€ 16.39	50.0	€ 837.38
Moisture separator/ flash chamber	m^3	22.31	€ 55.13	3.8	€ 16.39	0.34	€ 3.73	32.5	€ 71.52
Ammonia scrubber column	Nm^3/hr of gas	370.6	€ 20.86	37.4	€ 4.47	3.7	€ 1.49	343.3	€ 20.86
Ammonia scrubber packing	Nm^3/hr of gas	370.6	€141.55	37.4	€ 14.90	3.7	€ 1.49	343.3	€ 147.51
BM chiller condenser	kW_e	6.33	€ 9.69	0.7	€ 2.24	0.1	€ 1.86	5.6	€ 9.69
Biomethane compressors	Nm^3/hr-biogas processed	361.5	€171.35	36.2	€ 22.35	3.6	€ 2.98	332.2	€ 160.92
Biomethane pipeline	Euro/inch-km	2inch, 2km	€ 938.70	1 inch, 1km	€ 233.93	0.5 inch, 1km	€ 116.22	2inch, 2km	€ 938.70

Component	Sizing unit	82IBP, 82IBF, 82IMP, 82IMF, 82ICP, 82ICF, 82ITP, 82ITF & 82IBP-R		82MBP & 82MBF		82SBP & 82SBF		64IBP & 64IBP-R	
		Size	Erected equipment cost ('000€)	Size	Erected equipment cost ('000€)	Size	Erected equipment cost ('000€)	Size	Erected equipment cost ('000€)
Microalgae Cultivation Section									
Main cultivation unit and inoculum	ha	12.5	€ 121.00	1.25	€ 17.00	0.13	€2.50	12.00	€ 116.00
Piping, valves and fittings	ha	12.5	€ 138.00	1.25	€ 19.00	0.13	€2.85	12.00	€ 132.00
Other field equipments	ha	12.5	€ 90.00	1.25	€ 13.00	0.13	€2.00	12.00	€ 87.00
Liner for initial installation	ha	12.5	€ 38.00	1.25	€ 5.50	0.13	€1.00	12.00	€ 37.00
Cost of greenhouse	ha	17.9	€ 99.72	1.49	€ 33.02	0.15	€10.93	17.20	€ 97.78
Spirulina Harvesting and Processing Section									
Inclined screen	m^3/h	402.0	€ 70.03	40.2	€ 45.74	4.0	€ 29.87	345	€ 68.08
Vacuum filter	m^2	7.8	€ 119.20	0.8	€ 29.80	0.1	€7.45	6.98	€ 111.75
Bead milling	per hectare of cultivation	12.50	€ 795.66	1.3	€ 111.75	0.13	€16.39	12.0	€ 768.84
Spray dryer	per hectare of cultivation	12.5	€ 350.15	1.3	€ 49.17	0.13	€ 6.85	12	€ 338.23
Recirculation Adjustment Section and Other Auxiliary Equipment									
Dm water storage tank	m^3	452.81	€ 15.65	46.8	€ 6.71	4.68	€ 2.83	432.7	€ 14.90
Pump to recirculate water	kW_e	7.6	€ 13.41	0.6	€ 5.96	0.06	€ 3.73	7.25	€ 13.41

Component	Sizing unit	82IBP, 82IBF, 82IMP, 82IMF, 82ICP, 82ICF, 82ITP, 82ITF & 82IBP-R		82MBP & 82MBF		82SBP & 82SBF		64IBP & 64IBP-R	
		Size	Erected equipment cost ('000€)	Size	Erected equipment cost ('000€)	Size	Erected equipment cost ('000€)	Size	Erected equipment cost ('000€)
Heat pumps	kW_e	1,442.43	€ 117.08	161.1	€ 25.24	16.1	€ 8.30	1,417.6	€ 115.67
Dm water plant	m^3/hr	9.43	€ 184.86	1.0	€ 13.15	0.10	€ 11.89	9.01	€ 179.89
Steam generator	kW	633.3	€ 92.38	63.3	€ 37.25	6.33	€ 16.39	634.4	€ 92.38
Wastewater treatment unit	m^3/hr	7.5	€ 859.73	N/A	-	N/A	-	7.25	€ 846.32
Sludge dryer	kg/hr sludge in	655.7	€ 688.00	N/A	-	N/A	-	600.0	€ 660.00
Cooling tower	m^3/hr	39.9	€ 119.20	4.0	€ 83.44	0.40	€ 52.15	584.5	€ 128.14
Overall Equipment Costs ('000€)									
Total bare erected cost (TBEC) of all equipment of the plant (including 5% additional cost for unaccounted equipment)			€ 10,906.19		€ 1,350.23		€ 421.15		€ 10,908.16

Table S8-5 Breakdown of the operational costs of the polygeneration process for each scenario. All costs are in '000 Euros and are calculated for the base year (2020)

Cost Components	**82IBP, 82IBF, 82IMP, 82IMF, 82ICP, 82ICF, 82ITP, 82ITF & 82IBP-R**	**82MBP & 82MBF**	**82SBP & 82SBF**	**64IBP & 64IBP-R**
Labour costs	€ 912.00	€ 271.00	€ 80.00	€ 912.00
Maintenance and administrative Charges	€ 608.63	€ 74.61	€ 23.09	€ 608.74
Electricity	€ 1,988.79	€ 197.73	€ 20.08	€ 1,944.05
Heat	€ 254.22	€ 17.97	€ 2.48	€ 209.10
Process water	€ 20.81	€ 9.81	€ 1.41	€ 41.47
Wastewater disposal	-	€ 11.34	€ 1.15	-
Sodium carbonate	€ 358.13	€ 35.81	€ 3.59	€ 356.75
Sodium bicarbonate	€ 314.50	€ 31.45	€ 3.26	€ 264.38
Zarrouk's medium for microalgae cultivation	€ 8,043.47	€ 804.35	€ 83.08	€ 7,731.69
Sulphuric acid	€ 0.16	€ 0.02	€ 0.00	€ 0.16
Grass	€ 648.00	€ 64.80	€ 6.48	€ 511.92
Slurry	€ 100.16	€ 10.02	€ 1.00	€ 211.84
Sludge disposal	€ 164.70	-	-	€ 172.64
Chemical transport	€ 31.89	€ 2.53	€ 0.26	€ 30.85
Total annual OPEX (Year 1, 2020)	€ 13,445.46	€ 1,531.43	€ 225.88	€ 12,995.60

8.8 References

[1] Sagues WJ, Assis CA, Hah P, Sanchez DL, Johnson Z. Decarbonizing agriculture through the conversion of animal manure to dietary protein and ammonia fertilizer. Bioresour Technol 2020;297:122493. doi:10.1016/j.biortech.2019.122493.

[2] O'Shea R, Lin R, Wall DM, Browne JD, Murphy JD. Using biogas to reduce natural gas consumption and greenhouse gas emissions at a large distillery. Appl Energy 2020;279:115812. doi:10.1016/j.apenergy.2020.115812.

[3] Gray N, Mcdonagh S, Shea RO, Smyth B, Murphy JD. Decarbonising ships, planes and trucks : An analysis of suitable low-carbon fuels for the maritime, aviation and haulage sectors. Adv Appl Energy 2021;1:100008. doi:10.1016/j.adapen.2021.100008.

[4] Wall DM, McDonagh S, Murphy JD. Cascading biomethane energy systems for sustainable green gas production in a circular economy. Bioresour Technol 2017;243:1207–15. doi:10.1016/j.biortech.2017.07.115.

[5] Monlau F, Sambusiti C, Ficara E, Aboulkas A, Barakat A, Carrère H. New opportunities for agricultural digestate valorization: Current situation and perspectives. Energy Environ Sci 2015;8:2600–21. doi:10.1039/c5ee01633a.

[6] Lin CSK, Pfaltzgraff LA, Herrero-Davila L, Mubofu EB, Abderrahim S, Clark JH, et al. Food waste as a valuable resource for the production of chemicals, materials and fuels. Current situation and global perspective. Energy Environ Sci 2013;6:426–64. doi:10.1039/c2ee23440h.

[7] Wall DM, Dumont M, Murphy JD. Green gas. 2018.

[8] Deng C, Lin R, Kang X, Wu B, O'Shea R, Murphy JD. Improving gaseous biofuel yield from seaweed through a cascading circular bioenergy system integrating anaerobic digestion and pyrolysis. Renew Sustain Energy Rev 2020;128:109895. doi:10.1016/j.rser.2020.109895.

[9] Angelidaki I, Treu L, Tsapekos P, Luo G, Campanaro S, Wenzel H, et al. Biogas upgrading and utilization: Current status and perspectives. Biotechnol Adv 2018;36:452–66. doi:10.1016/j.biotechadv.2018.01.011.

[10] European Parliament and the Council of the European Union. Directive (EU) 2018/2001 of the European Parliament and of the Council on the promotion of the use of energy from renewable sources. 2018.

[11] Rajendran K, O'Gallachoir B, Murphy JD. The combined role of policy and incentives in promoting cost efficient decarbonisation of energy: A case study for biomethane. J Clean Prod 2019;219:278–90. doi:10.1016/j.jclepro.2019.01.298.

[12] Rajendran K, Browne JD, Murphy JD. What is the level of incentivisation required for biomethane upgrading technologies with carbon capture and reuse? Renew Energy 2019;133:951–63. doi:10.1016/j.renene.2018.10.091.

[13] Meier L, Pérez R, Azócar L, Rivas M, Jeison D. Photosynthetic CO_2 uptake by microalgae: An attractive tool for biogas upgrading. Biomass and Bioenergy 2015;73:102–9. doi:10.1016/j.biombioe.2014.10.032.

[14] Bose A, O'Shea R, Lin R, Murphy JD. A perspective on novel cascading algal biomethane biorefinery systems. Bioresour Technol 2020;304:123027. doi:10.1016/j.biortech.2020.123027.

[15] Bose A, Lin R, Rajendran K, Xia A, O'Shea R, Murphy JD. How to optimise photosynthetic biogas upgrading: a perspective on system design and microalgae selection. Biotechnol Adv 2019;37. doi:10.1016/j.biotechadv.2019.107444.

[16] Marín D, Posadas E, Cano P, Pérez V, Blanco S, Lebrero R, et al. Seasonal variation of biogas upgrading coupled with digestate treatment in an outdoors pilot scale algal-bacterial photobioreactor. Bioresour Technol 2018;263:58–66. doi:10.1016/j.biortech.2018.04.117.

[17] Meier L, Stará D, Bartacek J, Jeison D. Removal of H_2S by a continuous microalgae-based photosynthetic biogas upgrading process. Process Saf Environ Prot 2018;119:65–8. doi:10.1016/j.psep.2018.07.014.

[18] Toledo-Cervantes A, Estrada JM, Lebrero R, Muñoz R. A comparative analysis of biogas upgrading technologies: Photosynthetic vs physical/chemical processes. Algal Res 2017;25:237–43. doi:10.1016/j.algal.2017.05.006.

[19] Marin-Batista JD, Villamil JA, Rodriguez JJ, Mohedano AF, de la Rubia MA. Valorization of microalgal biomass by hydrothermal carbonization and anaerobic digestion. Bioresour Technol 2019;274:395–402. doi:10.1016/j.biortech.2018.11.103.

[20] Rodero M del R, Severi CA, Rocher-Rivas R, Quijano G, Muñoz R. Long-term influence of high alkalinity on the performance of photosynthetic biogas upgrading. Fuel 2020;281:118804. doi:10.1016/j.fuel.2020.118804.

[21] Bose A, O'Shea R, Lin R, Murphy JD. A comparative evaluation of design factors on bubble column operation in photosynthetic biogas upgrading. Biofuel Res J 2021;8. doi:10.18331/BRJ2021.8.2.2.

[22] Rodero M del R, Lebrero R, Serrano E, Lara E, Arbib Z, García-Encina PA, et al. Technology validation of photosynthetic biogas upgrading in a semi-industrial scale algal-bacterial photobioreactor. Bioresour Technol 2019;279:43–9. doi:10.1016/j.biortech.2019.01.110.

[23] Jana K, Ray A, Mansouri M, Assadi M, De S. Polygeneration as a future sustainable energy solution – A comprehensive review. Appl Energy 2017;202:88–111. doi:10.1016/j.apenergy.2017.05.129.

[24] European Commission. Commission Implementing Regulation (EU) 2017/2470. Off J Eur Union 2017;351:72–201.

[25] Timonen K, Sinkko T, Luostarinen S, Tampio E, Joensuu K. LCA of anaerobic digestion: Emission allocation for energy and digestate. J Clean Prod 2019;235:1567–79. doi:10.1016/j.jclepro.2019.06.085.

[26] Vogt-schilb A, Meunier G, Hallegatte S. When starting with the most expensive option makes sense : Optimal timing, cost and sectoral allocation of abatement investment. J Environ Econ Manage 2018;88:210–33. doi:10.1016/j.jeem.2017.12.001.

[27] Inderwildi O, Zhang C, Wang X, Kraft M. The impact of intelligent cyber-physical systems on the decarbonization of energy. Energy Environ Sci 2020;13:744–71. doi:10.1039/c9ee01919g.

[28] Vo TTQ, Wall DM, Ring D, Rajendran K, Murphy JD. Techno-economic analysis of biogas upgrading via amine scrubber, carbon capture and ex-situ methanation. Appl Energy 2018;212:1191–202. doi:10.1016/j.apenergy.2017.12.099.

[29] Nizami AS, Korres NE, Murphy JD. Review of the integrated process for the production of grass biomethane. Environ Sci Technol 2009;43:8496–508. doi:10.1021/es901533j.

[30] Banks CJ, Zhang Y. Technical Report: Optimising inputs and outputs from anaerobic digestion processes. 2010. doi:WR0212.

[31] Germinal Ireland Limited. The value of grass introduction : Thurles, Tipperary: 2015.

[32] Smyth BM, Murphy JD, Brien CMO. What is the energy balance of grass biomethane in Ireland and other temperate northern European climates ? Renew Sustain Energy Rev 2009;13:2349–60. doi:10.1016/j.rser.2009.04.003.

[33] TNO. Grass (#613). Phyllyis2 1997. https://phyllis.nl/Browse/Standard/ECN-Phyllis (accessed June 5, 2021).

[34] Bedoić R, Ćosić B, Duić N. Technical potential and geographic distribution of agricultural residues, co-products and by-products in the European Union. Sci Total Environ 2019;686:568–79. doi:10.1016/j.scitotenv.2019.05.219.

[35] Bolaric S, Barth S, Melchinger AE, Posselt UK. Molecular genetic diversity within and among German ecotypes in comparison to European perennial ryegrass cultivars. Plant Breed 2005;124:257–62. doi:10.1111/j.1439-0523.2005.01108.x.

[36] Madkour FF, Kamil AEW, Nasr HS. Production and nutritive value of Spirulina platensis in reduced cost media. Egypt J Aquat Res 2012;38:51–7. doi:10.1016/j.ejar.2012.09.003.

[37] Khakharia P, Huizinga A, Jurado Lopez C, Sanchez Sanchez C, De Miguel Mercader F, Vlugt TJH, et al. Acid wash scrubbing as a countermeasure for ammonia emissions from a postcombustion CO_2 Capture Plant. Ind Eng Chem Res 2014;53:13195–204. doi:10.1021/ie502045c.

[38] Hyun J, Lee JH, Kee I, Hyun C. Techno-economic and environmental evaluation of CO_2 mineralization technology based on bench-scale experiments. J CO2 Util 2018;26:522–36. doi:10.1016/j.jcou.2018.06.007.

[39] Lee JH, Lee DW, Kwak C, Kang K, Lee JH. Technoeconomic and environmental evaluation of sodium bicarbonate production using CO_2 from flue gas of a coal-fired power plant. Ind Eng Chem Res 2019;58:15533–41. doi:10.1021/acs.iecr.9b02253.

[40] Hemphill A. OUTLOOK ’20: Sulphuric acid market begins 2020 on bearish note. ICIS n.d. https://www.icis.com/explore/resources/news/2020/01/10/10458518/outlook-20-sulphuric-acid-market-begins-2020-on-bearish-note (accessed May 4, 2021).

[41] Commission for Regulation of Utilities (CRU). Irish Water’s Non - Domestic Tariff Framework CRU Decision Paper. 2019.

[42] Eurostat. Electricity price statistics. 2021 n.d. https://ec.europa.eu/eurostat/statistics-explained/index.php?title=Electricity_price_statistics#Electricity_prices_for_non-household_consumers (accessed May 18, 2021).

[43] Costa JAV, Freitas BCB, Rosa GM, Moraes L, Morais MG, Mitchell BG. Operational and economic aspects of *Spirulina*-based biorefinery. Bioresour Technol 2019;292:121946. doi:10.1016/j.biortech.2019.121946.

[44] Raoof B, Kaushik BD, Prasanna R. Formulation of a low-cost medium for mass production of *Spirulina*. Biomass and Bioenergy 2006;30:537–42. doi:10.1016/j.biombioe.2005.09.006.

[45] International Energy Agency (IEA). Waste disposal costs and share of EfW in selected countries 2020. https://www.iea.org/data-and-statistics/charts/waste-disposal-costs-and-share-of-efw-in-selected-countries (accessed May 18, 2021).

[46] Rajendran K, Gallachóir BÓ, Murphy JD. The role of incentivising biomethane in Ireland using anaerobic digestion (2016-RE-DS-6) - EPA Research Report. 2019.

[47] Nolan S, Thorn CE, Ashekuzzaman SM, Kavanagh I, Nag R, Bolton D, et al. Landspreading with co-digested cattle slurry, with or without pasteurisation, as a mitigation strategy against pathogen, nutrient and metal contamination associated with untreated slurry. Sci Total Environ 2020;744:140841. doi:10.1016/j.scitotenv.2020.140841.

[48] Pall Corporation. Sterile or final compressed air and gas filtration 2020. https://www.pall.com/en/food-beverage/compressed-air-gas/sterile-filtration.html (Accessed on June 02 2021).

[49] Mariani L, Cola G, Bulgari R, Ferrante A, Martinetti L. Space and time variability of heating requirements for greenhouse tomato production in the Euro-Mediterranean area. Sci Total Environ 2016;562:834–44. doi:10.1016/j.scitotenv.2016.04.057.

[50] Vonshak A, Richmond A. Mass production of the blue-green alga *Spirulina*: An overview. Biomass 1988;15:233–47. doi:10.1016/0144-4565(88)90059-5.

[51] Gao W, Chen F, Wang X, Meng Q. Recent advances in processing food powders by using superfine grinding techniques : A review. Compr Rev Food Sci Food Saf 2020;19:2222–55. doi:10.1111/1541-4337.12580.

[52] Vo TTQ, Rajendran K, Murphy JD. Can power to methane systems be sustainable and can they improve the carbon intensity of renewable methane when used to upgrade biogas produced from grass and slurry? Appl Energy 2018;228:1046–56. doi:10.1016/j.apenergy.2018.06.139.

[53] Ortega-Calvo JJ, Mazuelos C, Hermosin B, Saiz-Jimenez C. Chemical composition of *Spirulina* and eukaryotic algae food products marketed in Spain. J Appl Phycol 1993;5:425–35. doi:10.1007/BF02182735.

[54] Benemann JR, Woertz I, Lundquist T. Autotrophic microalgae biomass production: From niche markets to commodities. Ind Biotechnol 2018;14:3–10. doi:10.1089/ind.2018.29118.jrb.

[55] Grahl S. Food product development with *Spirulina* (*Arthrospira platensis*) – Sensory profiling, product perception and consumer acceptance. Georg-August-Universität Göttingen, 2019.

[56] Murphy JD, Korres NE, Singh A, Smyth B, Nizami A-S, Thamsiriroj T. The potential for grass biomethane as a biofuel compressed biomethane generated from grass, utilised as a transport biofuel. CCRP Report. 2011.

[57] O'Shea R, Wall DM, Kilgallon I, Browne JD, Murphy JD. Assessing the total theoretical, and financially viable, resource of biomethane for injection to a natural gas network in a region. Appl Energy 2017;188:237–56. doi:10.1016/j.apenergy.2016.11.121.

[58] Wall DM, Allen E, Straccialini B, Kiely PO, Murphy JD. Optimisation of digester performance with increasing organic loading rate for mono- and co-digestion of grass silage and dairy slurry. Bioresour Technol 2014;173:422–8. doi:10.1016/j.biortech.2014.09.126.

[59] Bose A, O'Shea R, Lin R, Murphy JD. Optimisation and performance prediction of photosynthetic biogas upgrading using a bubble column. Under Rev 2021.

[60] Delrue F, Alaux E, Moudjaoui L, Gaignard C, Fleury G, Perilhou A, et al. Optimization of *Arthrospira platensis* (*Spirulina*) growth: From laboratory scale to pilot scale. Fermentation 2017;3. doi:10.3390/fermentation3040059.

[61] Huang Q, Jiang F, Wang L, Yang C. Design of photobioreactors for mass cultivation of photosynthetic organisms. Engineering 2017;3:318–29. doi:10.1016/J.ENG.2017.03.020.

[62] Christoforidou P, Bariamis G, Iosifidou M, Nikolaidou E, Samaras P. Energy benchmarking and optimization of wastewater treatment plants in Greece. Environ Sci Proc 2020;2:36. doi:10.3390/environsciproc2020002036.

[63] Drewnowski A. The Nutrient Rich Foods Index helps to identify healthy, affordable. Am J Clin Nutr 2010;91:1095–101. doi:10.3945/ajcn.2010.28450D.Am.

[64] Hess JM, Slavin JL. Healthy snacks : Using nutrient profiling to evaluate the nutrient-density of common snacks in the United States. J Food Sci 2017;00:1–8. doi:10.1111/1750-3841.13819.

[65] Sluik D, Streppel MT, Lee L van, Geelen A, Feskens EJM. Evaluation of a nutrient-rich food index score in the Netherlands. J Nutr Sci (2015), 2015;4:1–9. doi:10.1017/jns.2015.4.

[66] Dennehy C, Lawlor PG, Gardiner GE, Jiang Y, Shalloo L, Zhan X. Stochastic modelling of the economic viability of on-farm co-digestion of pig manure and food waste in Ireland. Appl Energy 2017;205:1528–37. doi:10.1016/j.apenergy.2017.08.101.

[67] Clippinger J, Davis R. Techno-Economic analysis for the production of algal biomass via photobioreactors : Future cost potential evaluated across a range of cultivation system designs techno-economic analysis for the production of algal biomass via closed photobioreactor. 2019.

[68] de Oliveira MACL, Monteiro MPC, Robbs PG, Leite SGF. Growth and chemical composition of *Spirulina maxima* and *Spirulina platensis* biomass at different temperatures. Aquac Int 1999;7:261–75. doi:10.1023/A:1009233230706.

[69] BordBia. What Ireland ate last night 2021. https://www.bordbia.ie/industry/news/press-releases/what-ireland-ate-last-night/ (accessed June 9, 2021).

[70] Ritchie H, Roser M. Meat and Dairy Production. Our World Data 2017. https://ourworldindata.org/meat-production#citation (accessed June 10, 2021).

[71] Curtain F, Grafenauer S. Plant-based meat substitutes in the flexitarian age : An audit of products on supermarket shelves. Nutrients 2019;11:2603. doi:doi:10.3390/nu11112603.

[72] Sforza PM. Theory of aerospace propulsion. Butterworth-Heinemann; 2012. doi:10.1016/C2009-0-61051-5.

[73] TNO. Microalgae, *Spirulina* (#1450). ECN Phyllis2 1999. https://phyllis.nl/Biomass/View/1450 (accessed June 5, 2021).

[74] Farooqui A, Di Tomaso F, Bose A, Ferrero D, Llorca J, Santarelli M. Techno-economic and exergy analysis of polygeneration plant for power and DME production with the integration of chemical looping CO_2/H_2O splitting. Energy Convers Manag 2019;186:200–19. doi:10.1016/j.enconman.2019.02.043.

[75] Gerdes K, Summers WM, Wimer J. Cost estimation methodology for NETL assessments of power plant performance. Doe/Netl-2011/1455 2011:26.

[76] Richard Turton, Richard C. Bailie, Wallace B. Whiting JAS. Analysis, synthesis and design of chemical processes Third Edition. vol. 53. 2013. doi:10.1017/CBO9781107415324.004.

[77] Farooqui A, Bose A, Ferrero D, Llorca J, Santarelli M. Techno-economic and exergetic assessment of an oxy-fuel power plant fueled by syngas produced by chemical looping CO_2 and H_2O dissociation. J CO2 Util 2018. doi:10.1016/j.jcou.2018.09.00.

[78] Loh HP, Lyons J, White CWI. Process equipment cost estimation Final Report. 2002.

[79] Nolan T, Troy SM, Gilkinson S, Frost P, Xie S, Zhan X, et al. Economic analyses of pig manure treatment options in Ireland. Bioresour Technol 2012;105:15–23. doi:10.1016/j.biortech.2011.11.043.

[80] FloMAX. Medical Sterile Filters MS 2021. https://www.flomax.ie/Catalogue/COMPRESSED-AIR-EQUIPMENT-RING-

MAINS/Compressed-Air-Filtration-Treatment/Alpha-Series-Filters/Medical-Sterile-Filters-MS (accessed June 1, 2021).

[81] Starr K, Ramirez A, Meerman H, Villalba G, Gabarrell X. Explorative economic analysis of a novel biogas upgrading technology using carbon mineralization. A case study for Spain. Energy 2015;79:298–309. doi:10.1016/j.energy.2014.11.015.

[82] Rotunno P, Lanzini A, Leone P. Energy and economic analysis of a water scrubbing based biogas upgrading process for biomethane injection into the gas grid or use as transportation fuel. Renew Energy 2017;102:417–32. doi:10.1016/j.renene.2016.10.062.

[83] cesenergy. Energy Efficient Solutions 2010. 2010.

[84] Donald E. Garrett. Chemical engineering economics. 1st ed. Springer, Dordrecht; 1989. doi:https://doi.org/10.1007/978-94-011-6544-0.

[85] City of Fremont. Gas pipeline calculation sizing – For Steel Pipe 2019:3–6.

[86] Nupponen L. Cost of production analysis : Hightech glasshouse production in Australia. 2019.

[87] Allied Ltd. How much does it cost to build a commercial greenhouse? Green steel build constr n.d. https://www.alliedbuildings.com/commercial-greenhouse/ (accessed May 15, 2021).

[88] Fasaei F, Bitter JH, Slegers PM, van Boxtel AJB. Techno-economic evaluation of microalgae harvesting and dewatering systems. Algal Res 2018;31:347–62. doi:10.1016/j.algal.2017.11.038.

[89] Panis G, Carreon JR. Commercial astaxanthin production derived by green alga *Haematococcus pluvialis*: A microalgae process model and a techno-economic assessment all through production line. Algal Res 2016;18:175–90. doi:10.1016/j.algal.2016.06.007.

[90] Samco Technologies. An introduction to industrial water demineralization systems 2020.

[91] Carlson MD, Middleton BM, Ho CK. Techno-economic comparison of solar-driven SCO_2 Brayton cycles using component cost models baselined with vendor data and estimates. Proc. ASME 2017 Power Energy Conf., Charlotte, North Carolina: ASME; 2017, p. 1–7.

[92] James BD, Baum GN, Perez J, Baum KN. Technoeconomic boundary analysis of biological pathways to hydrogen production. 2009.

[93] Peters MS, Timmerhaus KD, West RE. Plant design and economics for chemical engineers. 5th ed. McGraw-Hill Chemical Engineering Series; 2003.

[94] Edberg O, Barker N, Stambaugh J. Review of technical information on renewable heat technologies. Oxfordshire: 2011.

[95] Caduff M, Huijbregts MAJ, Koehler A. Scaling relationships in life cycle assessment the case of heat production from biomass and heat pumps 2014;00:1–14. doi:10.1111/jiec.12122.

[96] Foess GW, Steinbrecher P, Williams K, Garrett GS, Hill CHM, West K, et al. Cost and performance evaluation of BNR processes. Florida Water Resour J 1998;1:11–6.

[97] Murashko K, Nikku M, Sermyagina E, Vauterin JJ, Hyppänen T, Vakkilainen E, et al. Techno-economic analysis of a decentralized wastewater treatment plant operating in closed-loop. A Finnish case study. J Water Process Eng 2018;25:278–94. doi:10.1016/j.jwpe.2018.08.011.

[98] Mininni G, Salera A, Rolle E, Carucci A. Critical factors for implementing sludge processing of the Rome wastewater treatment plants. Water Sci Technol 2000;41:45–52. doi:10.2166/wst.2000.0167.

[99] Praveen P, Guo Y, Kang H, Lefebvre C, Loh KC. Enhancing microalgae cultivation in anaerobic digestate through nitrification. Chem Eng J 2018;354:905–12. doi:10.1016/j.cej.2018.08.099.

[100] Rubin E, Booras G, Davison J, Ekstrom C, Matuszewski M, Mccoy S, et al. Toward a common method of cost estimation for CO_2 capture and storage at fossil fuel power plants. 2013.

[101] Huang Z, Grim RG, Schaidle JA, Tao L. The economic outlook for converting CO_2 and electrons to molecules. Energy Environ Sci 2021;2. doi:10.1039/d0ee03525d.

[102] Tredici MR, Rodolfi L, Biondi N, Bassi N, Sampietro G. Techno-economic analysis of microalgal biomass production in a 1-ha Green Wall Panel (GWP®) plant. Algal Res 2016;19:253–63. doi:10.1016/j.algal.2016.09.005.

[103] PayScale. Ireland Payscale 2021. https://www.payscale.com/research/IE/Job (accessed June 1, 2021).

[104] Commission for Regulation of Utilities. Cost of capital – CRU approach a look at how the weighted average cost of capital (WACC) has been applied in regulating the electricity. 2020.

[105] Statista. Ireland: Inflation rate from 1986 to 2026 2021. https://www.statista.com/statistics/375229/inflation-rate-in-ireland/ (accessed June 9, 2021).

[106] Grant Thornton UK LLP. Renewable energy discount rate survey results – 2018. 2019.

[107] Verbeeck K, Buelens LC, Galvita V V., Marin GB, van Geem KM, Rabaey K. Upgrading the value of anaerobic digestion via chemical production from grid injected biomethane. Energy Environ Sci 2018;11:1788–802. doi:10.1039/c8ee01059e.

[108] Festel G, Würmseher M, Rammer C, Boles E, Bellof M. Modelling production cost scenarios for biofuels and fossil fuels in Europe. J Clean Prod 2014;66:242–53. doi:10.1016/j.jclepro.2013.10.038.

[109] National Energy Technology Laboratory. Simple levelized cost of energy (LCOE) calculator documentation. Distrib Gener Energy Technol Cost Perform Data n.d.

[110] Ye C, Mu D, Horowitz N, Xue Z, Chen J, Xue M, et al. Life cycle assessment of industrial scale production of *Spirulina* tablets. Algal Res 2018;34:154–63. doi:10.1016/j.algal.2018.07.013.

[111] Aldersey-Williams J, Rubert T. Levelised cost of energy – A theoretical justification and critical assessment. Energy Policy 2019;124:169–79. doi:10.1016/j.enpol.2018.10.004.

[112] Capponi S, Fazio S, Barbanti L. CO_2 savings affect the break-even distance of feedstock supply and digestate placement in biogas production. Renew Energy 2012;37:45–52. doi:10.1016/j.renene.2011.05.005.

[113] Huttenhuis P, Roeloffzen A, Versteeg G. CO_2 Capture and re-use at a waste incinerator. Energy Procedia 2016;86:47–55. doi:10.1016/j.egypro.2016.01.006.

[114] Long A, Murphy JD. Can green gas certificates allow for the accurate quantification of the energy supply and sustainability of biomethane from a range of sources for renewable heat and or transport ? Renew Sustain Energy Rev 2019;115:109347. doi:10.1016/j.rser.2019.109347.

[115] Korres NE, Singh A, Nizami A, Murphy JD. Is grass biomethane a sustainable transport biofuel ? Biofuels, Bioprod Biorefining 2010;4:310–25. doi:10.1002/bbb.228.

[116] Dünnebeil F, Lambrecht U. Fuel efficiency and emissions of trucks in Germany An overview. Heidelberg: 2012.

[117] European Environment Agency. Greenhouse gas emission intensity of electricity generation 2020. https://www.eea.europa.eu/data-and-maps/daviz/co2-emission-intensity-6#tab-googlechartid_googlechartid_googlechartid_googlechartid_chart_11111 (accessed May 5, 2021).

[118] Koffi B, Cerutti A, Duerr M, Iancu A, Kona A, Janssens-Maenhout G. CoM default emission factors for the member states of the European Union dataset Version 2017. 2017.

[119] Bonfim-Rocha L, Silva AB, de Faria SHB, Vieira MF, de Souza M. Production of Sodium Bicarbonate from CO_2 Reuse Processes : A Brief Review. Int J Chem React Eng 2019;2019:20180318. doi:10.1515/ijcre-2018-0318.

[120] Yablonsky A, Barsoumian S, Legere D. SkyMine® carbon mineralization pilot project: Decision point 1 topical report. Austin, Texas: 2013.

[121] Frank ED, Han J, Palou-Rivera I, Elgowainy A, Wang MQ. Life cycle analysis of algal lipid fuels with the GREET Model. 2011.

[122] Krey V., O. Masera, G. Blanford, T. Bruckner, R. Cooke, K. Fisher-Vanden, H. Haberl, E. Hertwich, E. Kriegler, D. Mueller, S. Paltsev, L. Price, S. Schlömer, D. Ürge-Vorsatz, D. van Vuuren and TZ. Annex II: Metrics & Methodology. 2014.

[123] Sustainable Energy Authority of Ireland (SEAI). Conversion factors. Ireland's energy stat 2019. https://www.seai.ie/data-and-insights/seai-statistics/conversion-factors/ (accessed June 1, 2021).

[124] Ritchie H, Roser M. Environmental impacts of food production. Our World Data 2020. https://ourworldindata.org/environmental-impacts-of-food.

[125] Hoxha A, Christensen B. The carbon footprint on fertiliser production: regional reference values. Int Fertil Soc 2018;1:1–21.

[126] Ciani M, Lippolis A, Fava F, Rodolfi L, Niccolai A, Tredici MR. Microbes : Food for the Future. Food Sci Hum Wellness 2021;10:971. doi:10.3390/foods10050971.

[127] Economic Research Service (US Department of Agriculture). Price spreads from farm to consumer: Milk and dairy basket 2021. https://www.ers.usda.gov/data-products/price-spreads-from-farm-to-consumer/ (accessed July 1, 2021).

[128] Teagasc. Available Nutrient Content & Guide Value (€) of organic fertilisers 2021. vol. 2021. 2021.

[129] Decorte M, Tessens S, Fernández D, Aebig R, Mccarthy PJ, Oriordan B, et al. D6.1 Mapping the state of play of renewable gases in Europe. 2020.

[130] NNFCC Ltd. Farmers generating biomethane can claim RHI and RTFO payments. Biofuels 2018.

[131] Araújo R, Vázquez Calderón F, Sánchez López J, Azevedo IC, Bruhn A, Fluch S, et al. Current status of the algae production industry in europe: an emerging sector of the blue bioeconomy. Front Mar Sci 2021;7:1–24. doi:10.3389/fmars.2020.626389.

[132] Walsh S. Fertiliser prices jump on the back of tight supplies. Irish Farmers J 2021.

[133] Duran Quintero C, Ventura A, Lépine O, Pruvost J. Eco-design of *Spirulina* solar cultivation: Key aspects to reduce environmental impacts using Life Cycle Assessment. J Clean Prod 2021;299. doi:10.1016/j.jclepro.2021.126741.

[134] Irish Tax and Customs. Natural Gas Carbon Tax (NGCT). Excise and Licences 2021. https://www.revenue.ie/en/companies-and-charities/excise-and-licences/energy-taxes/natural-gas-carbon-tax/rate-of-tax.aspx (accessed July 2, 2021).

[135] Environmental Protection Agency (EPA). Ireland's final greenhouse gas emissions. 2021.

[136] Lanigan GJ, Donnellan T, Lanigan G, Donnellan T, Hanrahan K, Paul C, et al. An analysis of abatement potential of greenhouse gas emissions in Irish agriculture 2021-2030 prepared by the Teagasc greenhouse gas working group authors : Carlow: 2019.

[137] Parkinson B, Balcombe P, Speirs JF, Hawkes AD, Hellgardt K. Levelized cost of CO_2 mitigation from hydrogen production routes. Energy Environ Sci 2019;12:19–40. doi:10.1039/c8ee02079e.

[138] IEA. Outlook for biogas and biomethane. Prospects for organic growth. 2020.

[139] Government of Ireland. Climate Action Plan 2019: To tackle climate breakdown. 2019.

[140] Eyl-Mazzega M-A, Mathieu C, Boesgaard K, Daniel-Gromke J, Denysenko V, Liebetrau J, et al. Biogas and biomethane in Europe: Lessons from Denmark, Germany and Italy. Études de l'Ifri, Ifri; 2019.

[141] IEA. Have the prices from competitive auctions become the "new normal" prices for renewables? Paris: 2019.

[142] Daly H, Deane P. Emissions and energy system implications of increasing the ambition on the 70 % RES-E target. 2020.

[143] Ervia. Vision 2050: A net zero carbon Gas Network for Ireland. 2020.

[144] Lameh M, Al-Mohannadi DM, Linke P. Minimum marginal abatement cost curves (Mini-MAC) for CO2 emissions reduction planning. Clean Technol Environ Policy 2021. doi:10.1007/s10098-021-02095-y.

[145] Yue X, Deane JP, O'Gallachoir B, Rogan F. Identifying decarbonisation opportunities using marginal abatement cost curves and energy system scenario ensembles. Appl Energy 2020;276:115456. doi:10.1016/j.apenergy.2020.115456.

[146] Blakely T, Cleghorn C, Mizdrak A, Waterlander W, Nghiem N, Swinburn B, et al. The effect of food taxes and subsidies on population health and health costs: a modelling study. Lancet Public Heal 2020;5:e404–13. doi:10.1016/S2468-2667(20)30116-X.

[147] Harrington JM, Leydon C, Twohig C, Vandevijvere S. Policies for tackling obesity and creating healthier food environments in Ireland: Food-EPI 2020. 2020.

[148] Niebylski ML, Redburn KA, Duhaney T, Campbell NR. Healthy food subsidies and unhealthy food taxation: A systematic review of the evidence. Nutrition 2015;31:787–95. doi:10.1016/j.nut.2014.12.010.

[149] Piedra-Garcia D, Nych F, Kirchmeyr F, Majer S, Kovacs A. Guidelines for biomethane evaluation. 2017.

[150] Ember. Daily Carbon Prices n.d. https://ember-climate.org/data/carbon-price-viewer/ (accessed July 5, 2021).

[151] Amazon. Amazon UK cost for Sodium Bicarbonate 2021. https://www.amazon.co.uk/s?k=sodium+bicarbonate&crid=19LI9D0ILT1A2&currency=EUR&sprefix=sodium+bic%2Caps%2C155&ref=nb_sb_ss_ts-doa-p_1_10 (accessed June 20, 2021).

[152] Glanbia Ingredients. Sulphate of Ammonia 1.25 kg n.d. https://www.glanbiaconnect.com/shop/product/Sulphate-of-Ammonia-1-25kg/9087158 (accessed June 16, 2021).

[153] Agriculture UD of. FoodData Central 2021. https://fdc.nal.usda.gov/index.html.

[154] Schwalfenberg GK, Genuis SJ. The Importance of Magnesium in clinical healthcare. Scientifica (Cairo) 2017:4179326. doi:10.1155/2017/4179326.

[155] Fulgoni III VL, Keast DR, Drewnowski A. Development and validation of the Nutrient-Rich foods index : A tool to measure nutritional quality of foods. J Nutr 2009;139:1549–54. doi: 10.3945/jn.108.101360.

[156] Streppel MT, Sluik D, Yperen JF Van, Geelen A, Hofman A, Franco OH, et al. Nutrient-rich foods, cardiovascular diseases and all-cause mortality : the Rotterdam study. Eur J Clin Nutr 2014;68:741–7. doi:10.1038/ejcn.2014.35.

[157] Hodo Foods. Wholesale bulk Tofu (10 lbs) 2021. https://shop.hodofoods.com/products/tofu-bulk (accessed July 1, 2021).

[158] British Nutrition Foundation. Good sources of protein. Protein 2018. https://www.nutrition.org.uk/nutritionscience/nutrients-food-and-ingredients/protein.html?start=4 (accessed June 30, 2021).

[159] Engineering Toolbox. Gases-Densities 2003. https://www.engineeringtoolbox.com/gas-density-d_158.html (accessed June 1, 2021).

9 Conclusions and Recommendations

9.1 Chapter overview

This chapter concludes this thesis, aimed at exploring and advancing photosynthetic biogas upgrading as a technology and its effective integration into a circular economy system. This chapter also justifies how photosynthetic biogas upgrading can minimise emissions associated with biomethane and ensure sustainability in a future circular bioeconomy.

9.2 Conclusions to the thesis objectives

Each of the chapters 2-8 contribute to the conclusions of this thesis. A recap of the chapter contents are as follows:

- Chapter 2 reviews the technology and identifies favourable microalgae species for photosynthetic biogas upgrading.
- Chapter 3 describes the experimental setup, which was conceptualised and constructed to optimise the bubble column (the component of photosynthetic biogas upgrading that most needed optimisation).
- Chapter 4 investigates seven design factors using the L_{16} Taguchi orthogonal array as a screening design of experiment to identify the critical design factors affecting bubble column operations.
- Chapter 5 uses four critical factors identified in Chapter 4 to optimise the bubble column operations using the response surface methodology (RSM) and uses the results to provide a perspective on the integrated operations of the overall photosynthetic biogas upgrading process.
- Chapter 6 investigates the pathways to effectively integrate photosynthetic biogas upgrading in a broader circular economy framework.
- Chapter 7 uses the conclusions of both Chapter 5 and Chapter 6 to model and analyse the thermodynamic, economic, and environmental (greenhouse gas) performances of a polygeneration system and its co-products, namely, biomethane, *Spirulina* powder as human food and biofertiliser (digestate). The chapter further studies the feasibility of such a system using RED-II methodologies.

- Chapter 8 conducts a techno-economic and enviro-economic performance assessment of the polygeneration system generating biomethane, *Spirulina* powder and biofertiliser as proposed in Chapter 7.

In the following subsections, the outcomes of the individual chapters are compiled to answer each high-level objective and corresponding sub-objectives and conclude this thesis.

9.2.1 Objective 1: Identify the areas where photosynthetic biogas requires the most improvement and establish a framework for selecting suitable microalgae species.

Conclusions from Chapter 2:

→ The photosynthetic biogas upgrading technology can be divided into three fundamental sections: *1)* biogas upgrading in a bubble column, *2)* microalgae cultivation and *3)* microalgae harvesting.

→ The gas-sparged bubble absorption column coupled to flat plate photobioreactors is recommended as the most promising technological configuration for biogas upgrading and microalgae cultivation, although the open pond is the most commercially feasible technology for microalgae cultivation at present.

→ Relative and interactive effects between pH, L/G ratio, gas and liquid velocities, as well as the impact of algal concentration and microalgae photosynthetic activity during biogas upgrading in the bubble column, are critical research gaps that must be filled to ensure a robust optimisation of the photosynthetic biogas upgrading technology.

→ The five criteria required to select the optimal microalgae species for photosynthetic biogas upgrading are as follows:

a. the ability for mixotrophic growth
b. high pH tolerance
c. external carbonic anhydrase activity
d. high CO_2 tolerance

e. ease of harvesting.

→ Five common microalgae species are shown to be promising for photosynthetic biogas upgrading, namely: *Anabaena cylindrica*, *Chlorella sorokiniana*, *Scenedesmus obliquus*, *Spirulina platensis* and *Synechococcus* sp.

→ *Spirulina platensis* is chosen as the optimal microalgae species, especially due to its favourable growing conditions under high pH (pH 9-11 [1]), ease of harvesting and established commercial applications.

Conclusions from Chapter 3 that answer the objectives:

→ The bubble column is the most lacking in optimisation across the photosynthetic biogas upgrading system and is a source of significant variations in the results available in the literature.

9.2.2 Objective 2: Perform robust optimisation using a systems approach to advance the overall photosynthetic biogas upgrading technology.

Conclusions from Chapter 3:

→ The experimental setup designed to optimise the bubble column was able to treat up to 16.3 L_n/hr of biogas for scalable results corresponding to a superficial gas velocity of 1 cm/s.

→ The selection of tubing and sampling arrangements significantly impacted the results and system performance, especially with regards to an oxygen ingress in the upgraded biomethane.

→ Inlet conditions to the bubble column which generated grid quality biomethane (CO_2 below 2% and O_2 below 0.55% by volume) at L/G ratios above 0.4 and CO_2 removal efficiency of over 98% were documented as liquid pH of 9.35 ± 0.05, alkalinity of 2.8 ± 1 gIC/L; superficial gas velocity of 0.2 cm/s and algal concentrations of 0.05 gDW/L.

→ For the above conditions, the volumetric oxygen mass transfer coefficient ($k_{l_{O_2}}a$) varied between 0.0002 s^{-1} and 0.0018 s^{-1} at L/G ratios 0.1 and 0.5 respectively.

→ Algal density and photosynthetic activity were shown not to have a significant effect on the CO_2 removal performance of the bubble column under the experimental conditions assessed.

→ A higher algae concentration in the circulating liquid led to practical challenges of foaming, clogging and increased O_2 concentrations in the upgraded biomethane.

Conclusions from Chapter 4:

→ pH and L/G ratio were shown as the most critical design factors affecting CO_2 removal and O_2 stripping alike.

→ High pH and L/G ratio improved CO_2 removal while facilitating an increase in the superficial gas velocity and as such process throughput.

→ The interactive effect between pH and L/G ratio was shown as the most impactful interactive effect on the efficiency of CO_2 removal.

→ For efficient CO_2 removal, besides pH and L/G ratio, alkalinity, algal concentration and superficial gas velocity (in order of decreasing importance) were shown to be statistically significant ($P < 0.05$) design factors.

→ Higher alkalinity ensured consistent CO_2 removal while a lower algal concentration maximised and stabilised CO_2 removal.

→ No interactive effect between algal concentration and temperature was noted; hence showing that external carbonic anhydrase activity does not catalyse the biogas upgrading reaction in photosynthetic biogas upgrading.

→ O_2 concentration in biomethane was primarily influenced by the L/G ratio (over 55%), followed by algal concentration (c. 14%) and the interaction between the two (c. 17%).

→ Both lower L/G ratio and lower algal concentration favoured lowering the O_2 concentration in biomethane.

→ A high L/G ratio was shown to primarily influence O_2 concentration in biomethane irrespective of the algal concentration in the circulating liquid medium. For lower L/G ratios, however, higher algal concentration led to significantly increased O_2 concentration in the biomethane.

→ A minimal effect of temperature and empty bed residence time (EBRT) of the biogas on biogas upgrading highlights the possibility to use state-of-the-art bubble column designs and operational strategies for photosynthetic biogas upgrading.

→ Future studies aiming to increase the throughput of the system and optimise the bubble column would require pH, L/G ratio and superficial gas velocity as mandatory design factors.

→ Operating at a lower algal concentration, and circulating the algal liquid after harvesting is a preferable process configuration to produce consistent grid quality biomethane.

Conclusions from Chapter 5 that answer the objectives:

→ The bubble column performance including CO_2 removal efficiency, overall CO_2 mass transfer coefficient, O_2 concentration in biomethane and pH of the outlet algal medium were adequately predicted using regression equations within the pH range from 9.4 to 10.2, superficial gas velocities between 0.3 cm/s and 0.6 cm/s, L/G ratios of 0.3 and 0.8 and liquid inlet alkalinities of 1.3 gIC/L and 2.1 gIC/L.

→ A minimum pH of 10 and alkalinity of 1.7 gIC/L was found sufficient to ensure over 97% CO_2 removal and CO_2 mass transfer coefficient above 150 hr^{-1}.

→ The optimal L/G ratio for superficial gas velocities between 0.5 cm/s and 0.6 cm/s to ensure over 97% CO_2 removal efficiency and less than 0.8% O_2 concentration in biomethane (without H_2S in biogas) was found to lie between 0.6 and 0.7.

→ Complete CO_2 removal was achieved at empty bed residence times of as low as 1.5 minutes, confirming the possibility to use traditional well-engineered bubble columns for biogas upgrading with microalgae.

→ Although increasing the superficial gas velocity was found to reduce the CO_2 removal efficiency and O_2 concentration, a higher pH and optimal L/G ratio were found to ensure the production of grid quality biomethane.

→ Control of L/G ratio and superficial gas velocities would allow the production of grid quality biomethane against the variations of pH, alkalinity and other uncontrollable variables (noise).

→ The optimal conditions in the bubble column would allow its effective integration with the *Spirulina* cultivation unit for favourable overall operations of the photosynthetic biogas upgrading system.

→ A higher L/G ratio was found to lower the hydraulic retention time (HRT) of the microalgae cultivation unit, resulting in a lower concentration of the microalgae produced, with the same volume of the photobioreactor.

→ Higher algal productivity was shown to lower hydraulic residence times and the areal footprint of the microalgae cultivation unit and hence would be critical to decrease the land footprint of the photosynthetic biogas upgrading system.

9.2.3 Objective 3: Identify strategies to integrate photosynthetic biogas upgrading based biomethane systems in a circular bioeconomy system.

Conclusions from Chapter 6:

→ Microalgae can be effectively used in every stage of the anaerobic digestion process including biogas generation, biogas upgrading and digestate treatment.

→ Simultaneous use of microalgae in biogas upgrading and digestate treatment currently limits optimising both systems simultaneously.

→ Integrating a microalgae biorefinery with anaerobic digestion via photosynthetic biogas upgrading is an interesting alternative to improve process economy and to achieve a solution to the dilemma of microalgae use.

→ Renewable energy including electricity and heat, direct injection of biomethane in the gas grid and food and feed markets promise substantial growth in future, presenting effective opportunities for targeted microalgal bioproducts within these markets.

→ The effective selling price (ESP) per dry weight of whole microalgae or ESP for each algal bio-product provides a better route to select the most financially attractive microalgal bio-product(s). Selecting the corresponding biorefinery pathway is then crucial to maximise profitability.

→ The effective selling price further assists in evaluating the financial benefit of complete utilisation of microalgae including residue valorisation for an effective circular bioeconomy.

→ Producing whole dry microalgae such as powder for human food is one of the easiest and most profitable approaches for microalgae utilisation.

→ Based on the microalgae composition, the cascading algal biomethane biorefinery system (CABBS) can have multiple configurations.

→ CABBS utilising pyrolysis is technologically feasible, producing liquid biofuels and biochar alongside other valuable chemicals.

→ By appropriate selection of microalgae bioproducts (such as long-lived chemicals or biochar), the CABBS configuration has the potential to be a Bioenergy with Carbon Capture and Storage (BECCS) system (and as such a negative emission technology).

→ Using digestate to cultivate microalgae will limit its application in food and/ or feed applications.

9.2.4 Objective 4: Propose and apply methods to assess the energetic, environmental and economic performances of a polygeneration system using photosynthetic biogas upgrading and compare it with state-of-the-art biogas upgrading technologies.

Conclusions from Chapter 7:

→ A working model of a polygeneration process cogenerating biomethane, *Spirulina* powder (protein supplement) and biofertiliser (digestate) was developed and validated with experimental results and literature values.

→ Currently, the energy for greenhouse heating to cultivate microalgae presents a major challenge to achieve a higher energy output than input, especially in colder climates such as in central/northern/western Europe.

→ The sum of the sale prices of all co-products (including digestate) were assessed as twice the sum of the costs of all the input utilities and materials highlighting the economic potential of the process.

→ The combined polygeneration process was found to reduce GHG emissions by a factor of four as compared to reported standalone facilities producing the same (or similar) outputs.

→ The emission savings from carbon capture in the production of sodium bicarbonate during biogas upgrading was found as a critical and essential bridge to low-carbon microalgae cultivation and biomethane production using photosynthetic biogas upgrading.

→ The current RED-II methodology was judged to be limited in assessing the complexity of the polygeneration system.

→ Economic allocation was found to enable the production of each component within mandated emission levels or at levels lower than current market alternatives.

→ The inclusion of digestate as a product was found to lower the specific emissions from both biomethane and *Spirulina*.

→ Inclusion of digestate as a product and the use of economic allocation instead of energy allocation was found to generate biomethane with a carbon footprint of below 10 $gCO_{2\text{-}eq}$/MJ (meeting the most stringent sustainability criteria of the RED-II); digestate with a carbon intensity of 0.4 $kgCO_{2\text{-}eq}$/kgN (less than synthetic nitrogen fertiliser at 1.5 to 3 $kgCO_{2\text{-}eq}$/kgN); and *Spirulina* protein below 0.8 $kgCO_{2\text{-}eq}$/100-gp (lower than meat proteins at 50 $kgCO_{2\text{-}eq}$/100-gp). On a complete food basis, the corresponding *Spirulina* powder emissions were less than 0.07 $kgCO_{2\text{-}eq}$/100 $NDS_{NRF9.3}$ (lower than beef and fish, emitting 11.3 $kgCO_{2\text{-}eq}$/100 $NDS_{NRF9.3}$ and 0.77 $kgCO_{2\text{-}eq}$/100 $NDS_{NRF9.3}$ respectively).

→ Irrespective of the allocation methodology, the specific land footprint was found to be a major challenge for biomethane produced using photosynthetic biogas upgrading. Accounting for digestate and using economic allocation, the biomethane water footprint was 0.07 L/MJ, similar to those of other renewable energies such as solar.

→ The land footprint of *Spirulina* (15 m^2/100 $NDS_{NRF9.3}$) was found to be comparable to conventional protein sources such as chicken (15.9 m^2/100 $NDS_{NRF9.3}$) if assessed on a complete food basis, rather than on the basis of protein only.

→ The use of open pond photobioreactors along with improved algal productivity and emission reduction from chemicals were assessed as crucial to ensure process viability and generate further GHG savings.

→ For most price variations of biomethane, an economic allocation was found to favour the use of biomethane in transport (at less than 32.9 $gCO_{2\text{-}eq}$/MJ mandated by RED-II).

→ To use biomethane in the heating sector (with a carbon footprint of less than 14.4 $gCO_{2\text{-}eq}$/MJ mandated by RED-II) either greening of the electricity grid is necessary or a higher selling price of *Spirulina* powder would be required to lower the emissions burden on biomethane.

Conclusions from Chapter 8:

→ The process is profitable on an industrial scale (c. 3 MW biomethane) irrespective of the relative quantities of grass silage and cattle slurry in the AD feedstock without any need for incentives (biomethane sale price was assessed as the same as the natural gas price of 3 c€/kWh).

→ A greater grass silage content (on a volatile solid (VS) basis) was found to increase the profitability of the proposed plant.

→ The medium-scale plant (c. 300 kW biomethane) was found to be profitable under current feed-in tariff rates for biomethane of 7 c€/kWh and above.

→ With a specific CAPEX of over 1.05 M€/(Nm^3/hr-biogas), the small-scale plant (c. 30 kW biomethane) was found unprofitable, unless significant policy supports and benefit mechanisms are ensured.

→ Economic allocation of costs led to a levelised cost of biomethane (from the industrial-scale plant with 20% slurry and 80% grass silage as the feedstock mix (VS basis)) of 2.73 c€/kWh. The corresponding levelised cost of *Spirulina* powder was 9.1 €/kg (similar to the current farm-gate prices); while that of digestate was 795 €/tonne on an equivalent nitrogen basis (cost-competitive to that of inorganic nitrogenous fertilisers).

→ The levelised costs of commodities were found to be higher from less profitable smaller systems.

→ Based on the feedstock composition, energy or economic allocation can both maximise the overall emission savings from the proposed CABBS plant.

→ Emissions savings could be maximised by selecting the suitable food that *Spirulina* powder could replace.

→ Replacing beef as a complete food was found to provide specific emissions savings of 129 tonnes$CO_{2\text{-eq}}$/tonne-feedstock or 1.18 tonnes$CO_{2\text{-eq}}$/(Nm^3/hr-biogas) from the industrial-scale plant while using 20% slurry in the feedstock (VS basis). If a less carbon-intensive protein source such as chicken was replaced

instead of beef, the net specific emission savings drops to 16.4 tonnes$CO_{2\text{-}eq}$/tonne-feedstock or 0.15 tonnes$CO_{2\text{-}eq}$/(Nm^3/hr-biogas).

→ Levelised cost of carbon abatement (LCOA) or marginal abatement cost (MAC) of the process was found to vary significantly with the type of protein being replaced.

→ The most probable LCOA of the industrial-scale CABBS process while replacing beef as a protein with *Spirulina* protein was found to vary between -10 and -8 €/tonne$CO_{2\text{-}eq}$, irrespective of the feedstock composition. The corresponding LCOA when replacing beef as a complete food would be -2 €/tonne$CO_{2\text{-}eq.}$

→ The small-scale plant had the highest LCOA of 87.1 €/tonne$CO_{2\text{-}eq}$ when the *Spirulina* substitutes beef protein only.

→ On replacing beef as a complete food with *Spirulina*, the LCOA of the small-scale plant was found to drop to 20.3 €/tonne$CO_{2\text{-}eq}$, below the current market price of CO_2 (25 €/tonne$CO_{2\text{-}eq}$ for EU [2] and 26 €/tonne$CO_{2\text{-}eq}$ for Ireland [3]).

→ The small-scale processes would become profitable if additional revenue can be generated by trading the CO_2 savings from the process within the EU Emission Trading Scheme (ETS). However, it would require emissions from agriculture and transport (including haulage and shipping) to be included in the ETS [4].

9.3 Impact on policy, industry and society

The work in this thesis contributes to the MaREI research centre's ~~has~~ three impact priorities: (1) inform policy; (2) support industry and (3) empower society. These are discussed below:

9.3.1 Policy implications

The results of the thesis show that an optimised photosynthetic biogas upgrading process along with suitable microalgae bioproducts provides a profitable route to achieve a reduction of GHG emissions from both energy use in heat and/or transport and production of food and fertilisers. This indicates the potential of this technology

to produce low-carbon biofuels, and ***contribute to meeting the requirements of national and international climate actions plans including,***

a. ***the Paris Agreement's and the Glasgow Climate Pact's target of limiting the global temperature rise to 1.5 °C above pre-industrial levels*** [5,6]**;**
b. ***the transition of Ireland to a carbon-neutral economy by 2050 as required by the 2021 Irish Government's Climate Action plan*** [7]; and
c. ***the inclusion of 20% green gas in the Irish Gas Grid by 2030.***

To operate such systems successfully, however, favourable policies must be implemented. For example, ***suitable modification of existing legislation and policy in EU Renewable Energy Directive (Recast) must be made to allow for economic allocation and the inclusion of digestate as a valuable process outcome***. Without this, the proposed CABBS processes, co-producing non-energy products along with biomethane will be assessed as unsustainable from the specific emissions of biomethane perspective.

Additional revenue may be possible by trading CO_2 savings from biomethane within the EU Emission Trading Scheme (ETS). However, this ***would require emissions from agriculture and transport (including haulage and shipping) to be included in the ETS*** [4].

By proposing and analysing in detail a circular economy system encompassing agriculture, food/feed, energy and transport, the author believes that this research proposal can promote job creation, especially in rural areas. More workers in agri-food and dairy sectors can be employed in innovative biorefinery systems (such as CABBS), thereby ***contributing to the aims set in the Irish government's white paper on rural community: Ag Soláthar Don Todhchaí: Straitéis D'thorbairt Tuaithe in Éirinn Páipéar Bán ar Fhorbairt Tuaithe.*** By establishing the possibility of low cost and low emission energy, food and/or chemicals and fertiliser supply, ***this thesis contributes to the priority action area "enhancing the environment and securing energy" outlined in the Government paper, Building Ireland's Smart Economy.***

The thesis also provides a pathway for the effective management of agricultural feedstock and wastes via co-digestion followed by photosynthetic biogas upgrading,

assisting farmers and the agri-food industry to comply with the Nitrates Directive (91/676/EEC) and the Water Framework Directive (2000/60/EC). This work investigated grass silage and cattle slurry to produce biomethane, biofertiliser and microalgae bioproducts. However, this process can be replicated with any other biodegradable feedstock including foodwaste, seaweed and biogenic fractions of municipal solid wastes among many others. Thus, the proposed work also presents a viable method for ***meeting the requirements of the EU Landfill Directive (1999/31/EC) by providing an economic and low-carbon pathway of the diversion of biodegradable waste from landfills.***

Combining the above arguments, it can also be concluded that the thesis aligns well with several of the 17 United Nations Sustainable Development Goals (SDGs). Simultaneous production of low-carbon biomethane, food and/or chemicals and biofertilisers through photosynthetic biogas upgrading is a pathway to meeting ***SDG number 7 (affordable and clean energy for all) and SDG number 13 (urgent action to tackle climate change).*** With the potential development expected in rural areas with associated job creation from the implementation of the studied technology, this thesis aligns itself to ***both SDG numbers 8 (achieving decent work and economic growth) and 9 (ensuring resilient infrastructure, industry and innovation).*** Using anaerobic digestion to divert wastes from landfills for energy generation further ensures ***the availability of clean water and sanitary (SDG 6) while assisting in conserving life on both land (SDG number 15) and water (SDG number 14).*** In addition, a community-based biomethane plant, producing energy for heat and/or transport, food and biofertiliser and thus improving energy and food security can be considered to be a ***major contributor to SDG number 11 (making cities and communities sustainable).***

9.3.2 Industry implications

The use of commercialised components such as industrial bubble columns could enable the rapid industrialisation of the photosynthetic biogas based CABBS processes. If biogas is generated using agricultural feedstock such as grass silage and slurry, this could ***lower the emissions from agriculture*** as well, a typically hard to abate sector that contributes over 35% of the total annual anthropogenic GHG emissions in Ireland [8,9]. By generating revenue through the production of additional

high value (microalgal) products, the ***long-term stable supply and cost reduction*** of both green gas (biomethane) and fertilisers (digestate) can be achieved. This will ***benefit both local and regional consumers from the point of view of costs, stability and security of supply of energy and materials*** (fertilisers). Using biomethane produced via CABBS as a substitute for natural gas will enable the ***reduction in emissions from heat, heavy transport, and large industries*** (for example in tri-generation associated with data centres and food and beverage industries). The use of microalgae as food will ***additionally generate security of food while reducing its emissions through local manufacturing***. Indeed, it has been established that locally sourced proteins from microalgae grown on marginal lands have lower emissions and resource footprints in Europe than protein imported from commercial facilities in South America [10].

A negative LCOA or marginal abatement cost achieved by effective integration of biomethane production with microalgae biorefinery has established the ***versatility of anaerobic digestion systems, seldom exploited in conventional standalone facilities***. It also reveals that the CABBS has the potential to be ***one of the most attractive technological bridges for industrial symbiosis within an industrial ecosystem***. Thus, the ***industry can explore multiple pathways to produce innovative food/feed/chemicals for negative/low emission processes***, benefitting additionally from financial incentives available for low emission technologies. Furthermore, the thesis also provides industry with a possible approach to address the dilemma of microalgae use, namely *i)* low priced biofuels (high market size or market growth) vs. high priced products (low market size and market growth); and *ii)* advanced (biofuels) vs traditional (food and pharmaceutical) bio-products.

9.3.3 Social implications

To promote non-conventional production and use of microalgae, including its use as a ***vegan-friendly replacement of widely consumed protein sources such as animal meat*** would require specific socio-economic approaches beyond technology feasibility studies or generic life cycle assessments. The resistance to change of an established agrarian economy to producing non-conventional food through different farming techniques (such as microalgae cultivation) could be a major bottleneck. As such, ***significant advertisement campaigns, robust public awareness building***

mechanisms and government policies need to be developed with a strong collaboration between academia, industry, government and citizens. Co-design of such local systems with the local community would be of great benefit in realising this industry.

9.4 Recommendations and future research

The author believes that this thesis has played a crucial role in advancing photosynthetic biogas upgrading technology while highlighting the versatility and multiple co-benefits of biomethane production from anaerobic digestion. However, to further advance the technology towards potential commercialisation, several recommendations are made, opening up scope for future research.

1 The study of a further increase in superficial gas velocity to increase the throughput of the process should be conducted. The critical superficial velocity, marking the transition from the homogeneous phase to the heterogeneous phase of operation in the bubble column needs to be determined for photosynthetic biogas upgrading. Whether the choice of microalgae species is significant in this transition, especially from the hydrodynamic standpoint of the bubble column, is also to be determined. Hence, future research with an experimental bubble column matching Wilkinson's scalability criteria (minimum 15 cm column diameter with a minimum aspect ratio of 5 and with a sparger pore diameter greater than 1-2mm [11]) can be used for scalable results irrespective of superficial gas velocity.

2 Investigation into using possible alternative microalgae species with high commercial value and the ability to grow faster at lower temperatures of around 20 °C should be undertaken. This would reduce both the energy required in greenhouses and the land footprint of the process, improving technological viability and decreasing costs, especially when cultivated in colder climates of northern Europe. For this, the impact of temperature on the microalgae composition needs to be studied, which opens up scope for extensive laboratory work to develop and determine further suitable microalgae species for photosynthetic biogas upgrading.

3 The study of the simultaneous use of microalgae in biogas upgrading and digestate treatment is still under research for potential optimisation and is also limited by health and safety concerns, especially if the microalgae are used for food and /feed or medical applications. A detailed assessment of microalgae composition grown in different types of digestate needs to be assessed. If not viable for food application, the potential for the use of microalgae cultivated in digestate for extraction of high-grade chemicals must also be assessed from a health and safety standpoint, opening up possibilities of conducting scientific laboratory-based research.

4 Developing a semi-industrial scale prototype and upscaling it to a fully functional prototype of the photosynthetic biogas upgrading process will be required to achieve a TRL of 7. This will require considerable lab-based and semi-industrial scale experimentation, together with cooperative research between industry and academia.

5 A detailed life cycle assessment including the study of alternative allocation techniques such as the system expansion method needs to be conducted to assess the overall impact of the proposed process. TEA and LCA studies of alternative configurations with different AD feedstocks and microalgal bioproducts need to be conducted with the generation of separate MACs for each configuration. This can establish the true potential of CABBS, opening up scope for comprehensive experimental and desktop-based research in future. Producing innovative chemicals or integration with a circular economy can make the proposed process versatile and an attractive technological bridge for industrial symbiosis in industrial ecosystem.

6 Studies of the social implications of CABBS, especially when producing food and biofertilisers need to be undertaken. This could be done using desk-top based tools such as social life cycle assessment and using extensive field-based research including thorough interactions with farmers and all other players in the agri-food chain, heavy industries, transport fleet owners, consumers, i.e., the citizens and the respective governments. Interdisciplinary research would enable a robust perception and incentivise the uptake of such innovative processes and products.

9.5 Final Remarks

This work has been conducted under Gas Networks Ireland and Science Foundation Ireland co-funded project titled "*The Role of Biogas in Greening Agriculture & Industry*" (2015-SR-007). The author believes that this thesis has successfully delivered on the following deliverables mandated by the project;

1. *Peer-reviewed paper on microalgal systems for biogas upgrading*
2. *Peer-reviewed paper on Green Gas Road Map for Ireland.*

and contributed to three of the expected outcomes of the project:

1. *Optimise biogas upgrading to biomethane through photosynthetic microalgae biogas upgrading*
2. *Contribute towards Ireland's renewable energy target in heat (RES-H) and transport (RES-T) and help the EU to fulfil its commitment to GHG reductions;*
3. *Present a viable method for meeting the requirements of the Landfill EU Landfill Directive (1999/31/EC) on diversion of biodegradable waste from landfills via co-digestion of agricultural wastes and by-products;*

The results have been presented with a global outlook and can be applied in any country, of course with necessary modifications, required to meet local limitations, demands and legislations. The author sincerely hopes that this work will motivate future researchers to conduct further research into photosynthetic biogas upgrading to advance the technology to commercialisation. The author hopes for a world that maximises environmental and social benefits from integrated combined processes that will enable a cleaner, greener and sustainable environment.

9.6 References

[1] de Oliveira MACL, Monteiro MPC, Robbs PG, Leite SGF. Growth and chemical composition of *Spirulina maxima* and *Spirulina platensis* biomass at different temperatures. Aquac Int 1999;7:261–75. doi:10.1023/A:1009233230706.

[2] Ember. Daily Carbon Prices n.d. https://ember-climate.org/data/carbon-price-viewer/ (accessed July 5, 2021).

[3] Irish Tax and Customs. Natural Gas Carbon Tax (NGCT). Excise and Licences 2021. https://www.revenue.ie/en/companies-and-charities/excise-and-licences/energy-taxes/natural-gas-carbon-tax/rate-of-tax.aspx (accessed July 2, 2021).

[4] Piedra-Garcia D, Nych F, Kirchmeyr F, Majer S, Kovacs A. Guidelines for biomethane evaluation. 2017.

[5] UNFCCC. Paris Agreement. Conf Parties Its Twenty-First Sess 2015:32. doi:FCCC/CP/2015/L.9/Rev.1.

[6] United Nations Framework Convention on Climate Change (UNFCCC). Glasgow Climate Pact. Conf. Parties Serv. as Meet. Parties to Paris Agreem., Glasgow: United Nations; 2021.

[7] Department of the Environment Climate and Communications. 2021 Climate Action and Low Carbon Development (Amendment) Bill 2021. Dublin: Department of the Environment Climate and Communications; 2021.

[8] Teagasc. Agricultural Emissions – greenhouse gases and ammonia. 2020.

[9] Environmental Protection Agency (EPA). Ireland’s final greenhouse gas emissions. 2021.

10] Rösch C, Roßmann M, Weickert S. Microalgae for integrated food and fuel production. GCB Bioenergy 2019;11:326–34. doi:10.1111/gcbb.12579.

[11] Besagni G, Gallazzini L, Inzoli F. On the scale-up criteria for bubble columns. Petroleum 2019;5:114–22. doi:10.1016/j.petlm.2017.12.005.